CARDIORESPIRATORY COUPLING - NOVEL INSIGHTS FOR INTEGRATIVE BIOMEDICINE

EDITED BY: Tijana Bojić, Maurizio Acampa and Andreas Voss

PUBLISHED IN: Frontiers in Physiology and Frontiers in Neuroscience

frontiers Research Topics

ISSN 1664-8714
ISBN 978-2-88966-793-2
DOI 10.3389/978-2-88966-793-2

About Frontiers

Frontiers is more than just an open-access publisher of scholarly articles: it is a pioneering approach to the world of academia, radically improving the way scholarly research is managed. The grand vision of Frontiers is a world where all people have an equal opportunity to seek, share and generate knowledge. Frontiers provides immediate and permanent online open access to all its publications, but this alone is not enough to realize our grand goals.

Frontiers Journal Series

The Frontiers Journal Series is a multi-tier and interdisciplinary set of open-access, online journals, promising a paradigm shift from the current review, selection and dissemination processes in academic publishing. All Frontiers journals are driven by researchers for researchers; therefore, they constitute a service to the scholarly community. At the same time, the Frontiers Journal Series operates on a revolutionary invention, the tiered publishing system, initially addressing specific communities of scholars, and gradually climbing up to broader public understanding, thus serving the interests of the lay society, too.

Dedication to Quality

Each Frontiers article is a landmark of the highest quality, thanks to genuinely collaborative interactions between authors and review editors, who include some of the world's best academicians. Research must be certified by peers before entering a stream of knowledge that may eventually reach the public - and shape society; therefore, Frontiers only applies the most rigorous and unbiased reviews.
Frontiers revolutionizes research publishing by freely delivering the most outstanding research, evaluated with no bias from both the academic and social point of view. By applying the most advanced information technologies, Frontiers is catapulting scholarly publishing into a new generation.

What are Frontiers Research Topics?

Frontiers Research Topics are very popular trademarks of the Frontiers Journals Series: they are collections of at least ten articles, all centered on a particular subject. With their unique mix of varied contributions from Original Research to Review Articles, Frontiers Research Topics unify the most influential researchers, the latest key findings and historical advances in a hot research area! Find out more on how to host your own Frontiers Research Topic or contribute to one as an author by contacting the Frontiers Editorial Office: frontiersin.org/about/contact

CARDIORESPIRATORY COUPLING - NOVEL INSIGHTS FOR INTEGRATIVE BIOMEDICINE

Topic Editors:
Tijana Bojić, University of Belgrade, Serbia
Maurizio Acampa, Siena University Hospital, Italy
Andreas Voss, Technische Universität Ilmenau, Germany

Citation: Bojić, T., Acampa, M., Voss, A., eds. (2021). Cardiorespiratory Coupling - Novel Insights for Integrative Biomedicine. Lausanne: Frontiers Media SA. doi: 10.3389/978-2-88966-793-2

Table of Contents

frontiers in Neuroscience

EDITORIAL
published: 07 April 2021
doi: 10.3389/fnins.2021.671900

Editorial: Cardiorespiratory Coupling-Novel Insights for Integrative Biomedicine

Maurizio Acampa[1]*, *Andreas Voss*[2] and *Tijana Bojić*[3]

[1] Stroke Unit, Department of Emergency-Urgency and Transplants, Azienda Ospedaliera Universitaria Senese, "Santa Maria alle Scotte" General-Hospital, Siena, Italy, [2] Institut für Innovative Gesundheitstechnologien (IGHT), Jena, Germany, [3] Laboratory for Radiobiology and Molecular Genetics-080, Institute of Nuclear Sciences Vinča-National Institute of the Republic of Serbia, University of Belgrade, Belgrade, Serbia

Keywords: integrative physiology, cardiorespiratory coupling, autonomic nervous system, respiratory sinus arrhythmia, heart rate variability, arterial baroreflex, periodic repolarization dynamics, ProBNP

Editorial on the Research Topic

Cardiorespiratory Coupling-Novel Insights for Integrative Biomedicine

In recent years, integrative physiology is gaining increased attention; novel findings in the area of molecular and systemic cardiopulmonary interaction overgrow the classical opinion that the adoption and transport of oxygen and elimination of carbon dioxide are their only functions. Mechanical, molecular, endocrine, and neural subsystems of the autonomic nervous system are integrative scales of these two mutually dependent organs, providing a wider range of adaptation of the organism to the growing requirements of the environment, fitness, and pathological changes.

In the present Frontiers Research Topic, an international selection of investigators contributed original data to increase our current understanding about the complex cardiorespiratory interactions, providing novel findings about physiologic and pathogenic mechanisms and possible therapeutic advancement concerning the area of cardiorespiratory medicine.

Several contributions focused on new methods in order to properly investigate cardiorespiratory interactions, especially considering that cardiac and respiration signals have periodic oscillatory dynamics that can also be time-varying, so this increasing complexity have to take into account that frequency, coupling strength and coupling function are also varying in time.

In this view, Lukarski et al. developed a procedure for determination of the time window based on data analyses, as opposed to the previous practice of arbitrary choice. This study shows that the cardiorespiratory coupling strength and the similarity of form of coupling functions continuously change according to the breathing frequency, with greater values for slower breathing.

Cui et al. provided a further contribution in developing quantitative measures for respiratory sinus arrhythmia (RSA). RSA has profound significance in physiology and pathology and is usually evaluated by means of two techniques, the time and the frequency domain. By mathematically modeling this modulation, the authors proposed a quantitative measurement of RSA by means of the cardiopulmonary resonance function (CRF) and cardiopulmonary resonance indices (CRI) that are derived by disentanglement of the RR-intervals series into respiratory-modulation component (R-HRV), and non-respiratory component (NR-HRV), using Granger causality function. Their results suggest a superior representation ability of this technique in comparison with heart rate variability (HRV) and cardiopulmonary coupling index, with profound significance in physiology, pathology, and in possible future clinical applications.

Edited and reviewed by:
Vaughan G. Macefield, Baker Heart and Diabetes Institute, Australia

***Correspondence:**
Maurizio Acampa
m.acampa@ao-siena.toscana.it

Specialty section:
This article was submitted to Autonomic Neuroscience, a section of the journal Frontiers in Neuroscience

Received: *24 February 2021*
Accepted: *15 March 2021*
Published: *07 April 2021*

Citation:
Acampa M, Voss A and Bojić T (2021) Editorial: Cardiorespiratory Coupling-Novel Insights for Integrative Biomedicine. Front. Neurosci. 15:671900. doi: 10.3389/fnins.2021.671900

The analysis of fluctuations in blood pressure and heart period represents another parameter of clinical importance as risk marker for cardiovascular morbidity and mortality (La Rovere et al., 2011), especially in some cardiac (Malberg et al., 2002) and non-cardiac diseases (Bär et al., 2007) or after specific therapeutic procedures (Acampa et al., 2011), that are able to determine changes at different levels, including arterial vascular walls, mechanosensitive ion channels, and voltage-gated ion channels (Tu et al., 2019). However, spontaneous baroreflex indices don't clearly reflect arterial baroreflex gain (Lipman et al., 2003); for this reason, Wessel et al. tested whether the xBRS method (Wesseling et al., 2017) is suitable to quantify the baroreflex sensitivity from non-invasive, non-interventional measurements under resting conditions. According to their analysis, xBRS method seems to have a potentially large bias in characterizing the capacity of the arterial baroreflex under resting conditions and seems to be exclusively dominated by the heart rate to systolic blood pressure ratio.

In this Frontiers topic, other studies focused on the important change of different cardiopulmonary parameters in different physiologic states such as wake and sleep, exercise and rest, circadian rhythms, as well as pathologic conditions.

One of these conditions, the deep sleep, is typically associated with an increased cardio-respiratory coupling, that corresponds to a maximal RSA. Based on that assumption, Zorko et al. evaluated HRV data, quantifying the (self)similarity among shapelets (that are short chunks of HRV time series), whose "shapes" are related to the respiration cycle; their results show distinctive patterns stable across age and sex, that are not only indicative of sleep and awake, but that are able to identify one more, potentially more sensitive indicator of sleep initiation. Additional studies are necessary that would involve contemporary classic polysomnography and novel, proposed index. In case of positive results, one of the possible applications of this approach could be related to public and general safety, by developing alarm systems that are able to recognize drowsiness in the person under the observation.

Another study by Limanskaya et al. examined a specific sleeping alteration, the central sleep apnea, by evaluating electroencephalogram, ECG, eye movements, air flow, thoracic respiratory muscle movements and myoelectric activity of the stomach and the duodenum in cats with sudden arrest of breathing during sleep. Their results suggest that the stereotypic coupling of activities in various visceral systems during episodes of central sleep apnea most likely reflects a complex adaptive behavior rather than an isolated respiratory pathology.

Another study by Matić et al. explored the physiological background of the non-linear operating mode of cardiorespiratory oscillators as the fundamental question of cardiorespiratory homeodynamics and as a prerequisite for the understanding of neurocardiovascular diseases. Their results show that cardiac and respiratory short-term and long-term complexity parameters have different state-dependent patterns supporting the hypothesis of a hierarchical organization of complexity regulatory mechanisms. In particular, a specific and comprehensive cardiorespiratory regulation in standing with 0.1 Hz breathing suggests that this state could represent the potentially most beneficial maneuver for cardiorespiratory conditioning, critically important for intensive care rehabilitation of artificially ventilated patients, as most actual in this moment-COVID 19 patients.

The interaction between breathing alterations and autonomic nervous system activity is another important subject, especially considering their possible pathogenic role in the pathogenesis of ventricular arrhythmias (Lai et al., 2019; Stavrakis et al., 2020); in this view, Schüttler et al. investigated the link among hyperventilation, sympathetic activity, and periodic repolarization dynamics (evaluated by means of beat-to-beat variations of the T wave vector on ECG). Their results suggest increased PRD values after hyperventilation, providing further insights about the alteration of ventricular repolarization associated to the hyperventilation.

Other two studies focused on the cardiopulmonary interactions during physical activity. Uryumtsev et al. investigated the mechanisms of oxygen supply regulation, which involves the respiratory and cardiovascular systems, during human adaptation to intense physical activity. Their results show that highly qualified athletes enhance intersystem integration in response to hypoxia, with a decreased oxygen consumption and a higher cardiorespiratory coherence in comparison with middle level athletes. In the second study, Abreu et al. evaluated healthy cyclist during and after inspiratory muscle training (IMT), that is a technique capable of improving cardiorespiratory interactions. In particular, they observed the effect of different degrees of IMT in amateur cyclists, analyzing electrocardiograms, non-invasive arterial pressures, and thoracic respiratory movements and quantifying cardiorespiratory coupling by means of squared coherence function, and causal model-based transfer entropy. In this way the authors demonstrated that the post-training increase of cardiorespiratory coupling might be the genuine effect of some rearrangements at the level of central respiratory network and its interactions with sympathetic drive and vagal activity.

The interaction between cardiorespiratory coupling and singing is the focus of another study of this Research Topic. Previous investigations about the effects of singing together focused on the synchronization of HRV, experienced by choir singers (Pearce et al., 2015). Ruiz-Blais et al. specifically evaluated HRV (using time-frequency coherence analysis) in pairs of non-experts in different vocalizing conditions; their results show that HRV becomes more coupled when people make long (>10 s) sounds synchronously and this synchronization persists when the effect of respiration is removed: these results suggest that since autonomic physiological entrainment is observed for non-expert singing, it may be exploited as part of interventions in music therapy or social prescription programs for the general population.

In this Research Topic other clinical studies show the relevance of the complex relationships between respiratory system and neurohormonal cardiac modulation involving both neural autonomic and humoral factors (hormonal factor, inflammatory cytokines). These complex mechanisms suggest particularly important implications in some diseases and during rehabilitation treatment. An unbalanced autonomic nervous system activity associated with different diseases can represent an

important factor contributing to the occurrence of many specific cardiovascular complications (Goldberger et al., 2019). In this view, schizophrenia is a mental disorder that is associated with an increased cardiovascular mortality rate that could be determined by autonomic alterations (Laursen et al., 2014); on that basis, Schulz et al. assessed instantaneous cardiorespiratory couplings by quantifying the casual interaction between heart rate and respiration, in patients suffering from schizophrenia, compared with healthy first-degree relatives and control subjects. Their results clearly point to an underlying disease-inherent genetic component of the cardiac system for subjects with schizophrenia and first-degree relatives, while respiratory alterations seem to be only clearly present in patients with schizophrenia and correlated to their mental emotional states.

Obesity is another pathological condition that is associated with an increasing occurrence of cardiovascular complications even in childhood and adolescence: in this condition autonomic nervous system alterations can represent an important factor contributing to the initiation and progression of many cardiovascular disorders. However, the impaired parasympathetic control in obese patients seems to be associated with a different relative contribution of baroreflex and non-baroreflex (central) mechanisms underlying the origin of RSA. In particular, Javorka et al. applied a recently proposed information-theoretic methodology (partial information decomposition) to the time series of HRV, systolic blood pressure variability and respiration pattern, demonstrating that obesity is associated with blunted involvement of non-baroreflex RSA mechanisms and with a reduced response to postural stress (but not to mental stress).

The relationship between neural autonomic and humoral factors seems to be particularly important during rehabilitation of patients with chronic obstructive pulmonary disease (COPD): (Paulin et al., 2020) in a secondary analysis of a previous randomized trial (Paulin et al., 2017) point out for the first time for the relevance of Vitamin B12 on cardiovascular health in COPD subjects. Supplementation with vitamin B12 appears to lead to discrete positive effects on exercise tolerance in groups of subjects with more advanced COPD, significantly changing the time course of NT-proBNP responses during treatment. Even if their final analysis could not support a significant change in NT-proBNP levels owing to high-intensity constant work-rate exercise, the association between slower initial V'O2 adjustments toward a steady-state during rest-to-exercise transitions and more severe ventricular chamber volume/pressure stress recruitment, expressed by higher NT-proBNP secretion, suggest that vitamin B12 supplementation could modulate NT-proBNP secretion.

Furthermore, inflammatory markers can have a role in modulating autonomic nervous system in specific conditions, especially after surgery. It is well-known the association among cardiac and extracardiac surgery, inflammation and autonomic nervous system activity (Amar et al., 1998; Acampa et al., 2016). Clinical evidence shows that surgical procedures weaken the vagal tone, favoring a number of different complications such as sepsis, cardiac arrhythmias. In this view, Grote et al. demonstrated that orthopedic rehabilitation has the potential to strengthen the vagal activity and hence boost inflammatory control, also suggesting that a vagal reinforcement procedure prior to the surgery ("prehabilitation") might be a beneficial strategy against post-operative complications.

In conclusion, the high-quality contributions of this Research Topic significantly enriched our knowledge about the field of Integrative Physiology, shedding light on complex physiologic and pathogenic mechanisms, with relevant clinical implications for patients' management. These studies also provide important suggestions for further investigation in this emerging area.

AUTHOR CONTRIBUTIONS

MA and TB contributed to the conception, design, and drafting of the work. TB and AV revised the draft. TB, AV, and MA approved the final version, agreed to be accountable for all aspects of the work, ensuring that questions related to the accuracy, or integrity of any part of it are appropriately investigated and resolved. All authors contributed to the article and approved the submitted version.

FUNDING

The work of TB on this paper and the Research Topic was supported by the Grant 5537, Proof of Concept, supported by Innovation Fund of the Republic of Serbia.

REFERENCES

Acampa, M., Guideri, F., Marotta, G., Tassi, R., D'Andrea, P., Lo Giudice, G., et al. (2011). Autonomic activity and baroreflex sensitivity in patients submitted to carotid stenting. *Neurosci. Lett.* 491, 221–226. doi: 10.1016/j.neulet.2011.01.044

Acampa, M., Lazzerini, P. E., Guideri, F., Tassi, R., and Martini, G. (2016). Ischemic stroke after heart transplantation. *J. Stroke* 18, 157–168. doi: 10.5853/jos.2015.01599

Amar, D., Fleisher, M., Pantuck, C. B., Shamoon, H., Zhang, H., Roistacher, N., et al. (1998). Persistent alterations of the autonomic nervous system after noncardiac surgery. *Anesthesiology* 89, 30–42. doi: 10.1097/00000542-199807000-00008

Bär, K. J., Boettger, M. K., Berger, S., Baier, V., Sauer, H., Yeragani, V. K., et al. (2007). Decreased baroreflex sensitivity in acute schizophrenia. *J. Appl. Physiol.* 102, 1051–1056. doi: 10.1152/japplphysiol.00811.2006

Goldberger, J. J., Arora, R., Buckley, U., and Shivkumar, K. (2019). Autonomic nervous system dysfunction: JACC focus seminar. *J. Am. Coll. Cardiol.* 73, 1189–1206. doi: 10.1016/j.jacc.2018.12.064

La Rovere, M. T., Maestri, R., and Pinna, G. D. (2011). Baroreflex sensitivity assessment – latest advances and strategies. *Eur. Cardiol. Rev.* 7:89. doi: 10.15420/ecr.2011.7.2.89

Lai, Y., Yu, L., and Jiang, H. (2019). Autonomic neuromodulation for preventing and treating ventricular arrhythmias. *Front. Physiol.* 10:200. doi: 10.3389/fphys.2019.00200

Laursen, T. M., Nordentoft, M., and Mortensen, P. B. (2014). Excess early mortality in schizophrenia. *Annu. Rev. Clin. Psychol.* 10, 425–448. doi: 10.1146/annurev-clinpsy-032813-153657

Lipman, R. D., Salisbury, J. K., and Taylor, J. A. (2003). Spontaneous indices are inconsistent with arterial baroreflex gain. *Hypertension* 42, 481–487. doi: 10.1161/01.HYP.0000091370.83602.E6

Malberg, H., Wessel, N., Hasart, A., Osterziel, K. J., and Voss, A. (2002). Advanced analysis of spontaneous baroreflex sensitivity, blood pressure and heart rate variability in patients with dilated cardiomyopathy. *Clin. Sci.* 102, 465–473. doi: 10.1042/cs1020465

Paulin, F. V., Goelzer, L. S., and Müller, P. T. (2020). Vitamin B12 supplementation and NT-proBNP levels in COPD patients: a secondary analysis of a randomized and controlled study in rehabilitation. *Front. Neurosci.* 14:740. doi: 10.3389/fnins.2020.00740

Paulin, F. V., Zagatto, A. M., Chiappa, G. R., and Müller, P. T. (2017). Addition of vitamin B12 to exercise training improves cycle ergometer endurance in advanced COPD patients: a randomized and controlled study. *Respir. Med.* 122, 23–29. doi: 10.1016/j.rmed.2016.11.015

Pearce, E., Launay, J., and Dunbar, R. I. (2015). The ice-breaker effect: singing mediates fast social bonding. *Open Sci.* 2:150221. doi: 10.1098/rsos.150221

Stavrakis, S., Kulkarni, K., Singh, J. P., Katritsis, D. G., and Armoundas, A. A. (2020). Autonomic modulation of cardiac arrhythmias: methods to assess treatment and outcomes. *JACC Clin. Electrophysiol.* 6, 467–483. doi: 10.1016/j.jacep.2020.02.014

Tu, H., Zhang, D., and Li, Y. L. (2019). Cellular and molecular mechanisms underlying arterial baroreceptor remodeling in cardiovascular diseases and diabetes. *Neurosci Bull.* 35, 98–112. doi: 10.1007/s12264-018-0274-y

Wesseling, K. H., Karemaker, J. M., Castiglioni, P., Toader, E., Cividjian, A., Settels, J. J., et al. (2017). Validity and variability of xBRS: instantaneous cardiac baroreflex sensitivity. *Physiol. Rep.* 5:e13509. doi: 10.14814/phy2.13509

Conflict of Interest: The authors declare that the research was conducted in the absence of any commercial or financial relationships that could be construed as a potential conflict of interest.

frontiers in Neuroscience

ORIGINAL RESEARCH
published: 05 November 2019
doi: 10.3389/fnins.2019.01116

Dynamics of Vagal Activity Due to Surgery and Subsequent Rehabilitation

Vincent Grote[1,2,3†], Zoran Levnajić[4†], Henry Puff[2], Tanja Ohland[2], Nandu Goswami[3], Matthias Frühwirth[1] and Maximilian Moser[1,3*]*

[1] Human Research Institute, Weiz, Austria, [2] Orthopedic Rehabilitation Center, Humanomed Center Althofen, Althofen, Austria, [3] Division of Physiology, Otto Loewi Research Center for Vascular Biology, Immunology and Inflammation, Medical University of Graz, Graz, Austria, [4] Complex Systems and Data Science Lab, Faculty of Information Studies in Novo Mesto, Novo Mesto, Slovenia

Background: Vagal activity is critical for maintaining key body functions, including the stability of inflammatory control. Its weakening, such as in the aftermatch of a surgery, leaves the body vulnerable to diverse inflammatory conditions, including sepsis.

Methods: Vagal activity can be measured by the cardiorespiratory interaction known as respiratory sinus arrhythmia or high-frequency heart-rate variability (HRV). We examined the vagal dynamics before, during and after an orthopedic surgery. 39 patients had their HRV measured around the period of operation and during subsequent rehabilitation. Measurements were done during 24 h circadian cycles on ten specific days. For each patient, the circadian vagal activity was calculated from HRV data.

Results: Our results confirm the deteriorating effect of surgery on vagal activity. Patients with stronger pre-operative vagal activity suffer greater vagal withdrawal during the peri-operative phase, but benefit from stronger improvements during post-operative period, especially during the night. Rehabilitation seems not only to efficiently restore the vagal activity to pre-operative level, but in some cases to actually improve it.

Discussion: Our findings indicate that orthopedic rehabilitation has the potential to strengthen the vagal activity and hence boost inflammatory control. We conclude that providing a patient with a vagal reinforcement procedure *prior* to the surgery ("pre-habilitation") might be a beneficial strategy against post-operative complications. The study also shows the clinical usefulness of quantifying the cardiorespiratory interactions.

Keywords: circadian rythm, surgery, vagal tone, inflammatory control, rehabilitation

OPEN ACCESS

Edited by:
Andreas Voss, Institut für Innovative Gesundheitstechnologien (IGHT), Germany

Reviewed by:
Vlasta Bari, San Donato General Hospital, Italy
Steffen Schulz, Institut für Innovative Gesundheitstechnologien (IGHT), Germany

***Correspondence:**
Zoran Levnajić
zoran.levnajic@fis.unm.si
Maximilian Moser
max.moser@medunigraz.at

† These authors have contributed equally to this work

Specialty section:
This article was submitted to Autonomic Neuroscience, a section of the journal Frontiers in Neuroscience

Received: *24 April 2019*
Accepted: *02 October 2019*
Published: *05 November 2019*

Citation:
Grote V, Levnajić Z, Puff H, Ohland T, Goswami N, Frühwirth M and Moser M (2019) Dynamics of Vagal Activity Due to Surgery and Subsequent Rehabilitation. Front. Neurosci. 13:1116. doi: 10.3389/fnins.2019.01116

INTRODUCTION

Vagus nerve is the longest nerve of the autonomic nervous system (ANS) and the key component of parasympathetic nervous system. Its baseline activity, often refered to as *vagal activity*, is crucial for maintaining several body functions at rest, including heart, lungs, and digestion. Vagal activity is stronger during sleep, stabilizing the body's circadian rhythms, which are key for good general health (Mundigler et al., 2002; Moser et al., 2006a; Kastner et al., 2010; Rocha et al., 2011; Scheiermann et al., 2013; Curtis et al., 2014; Papaioannou et al., 2014; Alamili, 2015; Madrid-Navarro et al., 2015; Wright et al., 2015).

Vagal activity is also the critical factor behind the functionality of the *inflammatory reflex*, mechanism responsible for resolving the inflammation once its purpose has been served

(Tracey, 2002, 2007; Moser et al., 2008; Rosas-Ballina and Tracey, 2009; Leslie, 2014; Mayer, 2015). Actually, the vagal inflammatory reflex involves 80% vagal afferents and 20% efferents, which means that four times more information is collected by the brain than transmitted to the periphery: macrophages in the inflamed tissue produce inflammation signals such as TNF-alpha and interleukin 1 (Andersson and Tracey, 2012; Olofsson et al., 2012), which attract other monocytes from nearby blood vessels. Vagal afferents carry receptors for these signals and communicate with certain stem brain areas transmitting the information on inflammation location and strength (Andersson and Tracey, 2012). Upon processing this information, vagal efferents respond by release of acetylcholine at the location of the inflamed tissue (Olofsson et al., 2012). Nicotinergic acetylcholine receptors have been identified on the surface of the macrophages, which down-regulate their cytosine production as a response to the cholinergic stimulation (Rosas-Ballina and Tracey, 2009), thereby reducing the attraction of additional inflammatory immune cells. This inflammatory reflex loop prevents over-activity of the immune system enabling the brain to locally control the immune activity. It also represents the "first line" of inflammation control (Olofsson et al., 2012).

In addition to improving the effectiveness and usefulness of the inflammatory reflex, a strong vagal activity protects against several serious or chronic conditions. They include atherosclerosis, ulceral colitis, Hashimoto's disease, type 2 diabetes, cancer (Donchin et al., 1992; Moser et al., 2006a; Das, 2011; Huston and Tracey, 2011; Chow et al., 2014), and sepsis, which is know to be related to weakening of body's natural ability to resolve the inflammation (Tracey, 2002; Nguyen et al., 2006; Nathan and Ding, 2010). The vagus nerve can be electrically and pharmacologically stimulated, while its overall activity can be improved via acupuncture, nutritional therapies, and physical exercise (Huang et al., 2005; Moser et al., 2017).

Measuring vagal activity can be reliably done by analyzing the heart rate variability (HRV). In fact, HRV is created by the interaction between ANS and the sinus node of the heart (Moser et al., 1995). Its main component, originating in vagal activity, is respiratory modulation of the heart frequency. Through a gating process that takes place in the brainstem, vagal activity is responsible for speeding up the heart when we breath in, and slowing it down when we breath out (Langhorst et al., 1983). The amplitude of this respiratory sinus arrhythmia is proportional to the vagal activity. This cardiorespiratory interaction mediated by the vagus nerve is faster (approximately 0.25 Hz) than other influences of the ANS (0.1 Hz or slower). Actually, postsynaptic vagal activity is mediated by acetylcholine, which is rapidly degraded in the synaptic gap by its esterase, an enzyme that warrants fast decay of neurotransmitters after release. This makes the parasympathetic synapses much faster than the sympathetic ones, which use norepinephrine postsynaptically (Moser et al., 1998). Norepinephrine is eliminated mainly by presynaptic reuptake, which results in transmitters remaining longer in the synaptic gap. In short, the intensity of this cardiorespiratory interaction can be used as a reliable measure of vagal activity (Moser et al., 1994).

Surgery is a situation where it is paramount to preserve the strong vagal activity. There is aboundant evidence that surgical procedures weaken the vagal activity (Donchin et al., 1992; Munford and Tracey, 2002; Williamson et al., 2010), while surgery is a notorious trigger of sepsis. With this in mind we performed a clinical study aimed at testing the effects of surgery on patient's vagal activity. Our study relies on a longitudinal measurement and comparison of circadian dynamics (24 h recordings) of vagal activity in patients before, during and after a surgical procedure. This includes measurements during and after rehabilitation, for up to 1 year after the surgery. Vagal activity is computed from HRV data as described in Moser et al. (1994), Moser et al. (1995), Lehofer et al. (1999).[1] We report our results in what follows.

MATERIALS AND METHODS

Patients and Ethics

Thirty-nine patients (23 female of age 32–83 and 16 male of age 32–81) were recruited for our study. They were hospitalized at the Orthopedic Rehabilitation Center at Humanomed Center in Althofen, Austria for total endoprosthetic orthopedic surgery (replacement of hip or knee joints). Inclusion criteria were age 30–90 and completion of 3 week rehabilitation within 3 months after the surgery. Exclusion criteria were usage of pacemaker and clinically identified complications (thrombosis, pulmonary embolism, or wound healing disorders). Patients were informed about the nature and the purpose of the study, signed the informed consent and participated voluntarily. After the study, personal results were given to all patients with adequate expert explanation. The study was authorized by the Ethical Committee of the Carinthian Government, authorization number A 02/05, 01 February, 2005. Methods were chosen in accordance with the relevant guidelines and regulations.

Measurement Protocol

In order to investigate the behavior of vagal activity in relation to the surgery and the subsequent recovery, we divided the operation-rehabilitation process into the following four phases: immediately before the surgery (*pre-operative phase*), immediately after the surgery (*peri-operative phase*), *rehabilitation,* and long-term recovery (*post-operative phases*). On ten specific days each patient had his/her vagal activity measured over the entire day, i.e., the 24 h circadian cycle. These are referred to as "measurement days" and denoted as T1,T2,. . .T10. They are "time periods" chosen to best reflect each phase of the operation-rehabilitation process as follows.

- *Immediately before the surgery* ("*pre-operative*"; measurement days T1 and T2). Patients were measured on 2 days, sometime between 8 and 2 days prior to the surgery.
- *Immediately after the surgery* ("*peri-operative*"; measurement day T3). Patients were measured on 1 day sometime between 2nd and 4th day after the surgery, depending on their availability due to their medical state.
- *Rehabilitation* ("*post-operative*"; measurement days T4, T5, and T6). Patients were measured on 2nd, 9th, and 16th day

[1] Actually, HRV is long known as a good marker for risk stratification, early prognosis and prediction of post-operative complications.

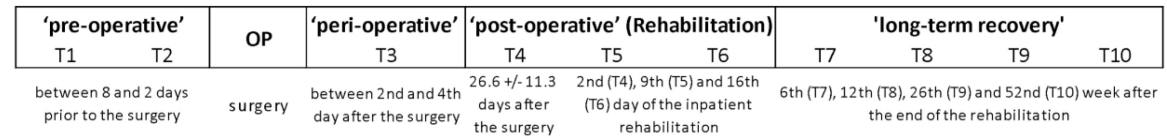

FIGURE 1 | Shematic representation of the division of operation-rehabilitation process into phases and measurement days for the purposes of our study.

of the inpatient rehabilitation process (rehabilitation started 26.6 ± 11.3 days after the surgery).

- *Long-term recovery* (measurement days T7, T8, T9, and T10). Patients were measured at the beginning of 6th, 12th, 26th, and 52nd week after the end of the rehabilitation.

For better orientation we show in **Figure 1** the schematic representation of this division.

Since previous studies found a strong cure-treatment effects to peak after 6 weeks (Moser et al., 1998; Lehofer et al., 1999), we used this time period to perform the first post-rehabilitation measurements. After this, we used approximate doubles of 6-week-intervals until the end after 1 year, which is a reasonable (almost) exponential frame for observing long-term effects. These measurements are taken on as equidistant time-points as patients compliance allowed.

HRV Measurements

On each measurement day we made precise circadian measurements of heart-rate variability (HRV) for each patient. That is to say, each patient had his/her instantaneous heart rate recorded continuously for 24 h, using a mobile 8000 Hz Holter-ECG with 16 bit A/D converter (ChronoCord, manufacturer: Joysys, Austria), developed from space medical research (Gallasch et al., 1997). The instrument was attached to a patient in a way not to interfere with his/her regular daily activities. Vagal activity was computed from these time series of around 100,000 heartbeats per patient/day as described below, and then averaged over 5 min intervals distributed evenly over 24 h. After this averaging, one circadian time series consisted of 1440 values, i.e., 1 value per each minute of the measurement day. Thus, on each measurement day we obtained for each patient a circadian time series with 1440 HRV values. We defined the *circadian time* from noon on a measurement day to noon on the following day. Our study lasted for over an entire year (408 ± 34,3 days) for each patient (not all patients participated simultaneously). 16 of them completed all the measurements (age 32–81, 11 female). For these 16 patients, some data points were still missing (13.75%). We report the data here only from these 16 patients.

Pre-processing and Computation of the Vagal Activity

Pre-processing steps included filtering and removal of the artifacts, done according to Lehofer et al. (1999). R peaks were detected from the ECG recordings by a digital filter described in Moser et al. (1994), Lehofer et al. (1999) to more than 1 ms accuracy. We then computed the vagal activity time series from the cardiorespiratory arrhythmia by the robust time-domain method named *logRSArr*. The method is described and evaluated in Moser et al. (1994), Lehofer et al. (1999) and its relaton with cardiorespiratory interactions is established in Topçu et al. (2018). In short, we used the formula:

$$\text{Vagal activity} = \log_{10}\left(median_{(5\,\text{min})}\,|RR_{i+1} - RR_i|\right),$$

where RRs are the consecutive inter-beat (RR) intervals, and the median value is taken over the 5 min interval. This logRSArr method acts as a filter emphasizing high-frequency HRV components, and reflects the vagally mediated respiratory component of HRV better than RMSSD or high frequency HRV (Topçu et al., 2018). Also, the chosen method is more robust than frequency-domain methods and allows a higher time-resolution. Robustness is here important since it prevents the results from disturbances by movement artifacts and ectopic heartbeats. Upon computation, we focused our analysis on these data, which consist of one circadian time series of vagal activity values for each patient on each measurement day.

Statistical Analysis

General linear models (GLM) were used to perform a per protocol analysis via repeated measures ANOVA. Within-subject factor is "time period" [pre-operative (individual means of T1 and T2), peri-operative (T3), rehabilitation (T4, T5, and T6), and long-term recovery (T7, T8, T9, and T10)] for three different "activity periods" of vagal activity within a day (logRSArr during "sleep," "wake," and "24 h mean"). The calculation of the used periods "sleep" and "wake" is based on visual controlled activity protocols of the patients, whereby transitions between wake and sleep, the first and last 30 min of each activity period, were not taken into account. For these statistical analyses, missings (in already aggregated values) in "time period" had to be replaced by individual means of nearby time points in 11 out of 192 cases (5.7%). Later we add pre-operative "vagal-type" as between-subject factor, computed via median split of aggregated 24 h means of logRSArr from T1 and T2 (pre-operative vagal activity) to quantify a hypothesized interaction (time course x vagal-type) for a different development in time course of subjects with a constitutional high vs. low vagal activity.

RESULTS

Overall Circadian Dynamics of Vagal Activity

We first present the overall circadian behavior of vagal activity during operation-rehabilitation process. To this end, we averaged the data over all 16 patients, obtaining one averaged circadian

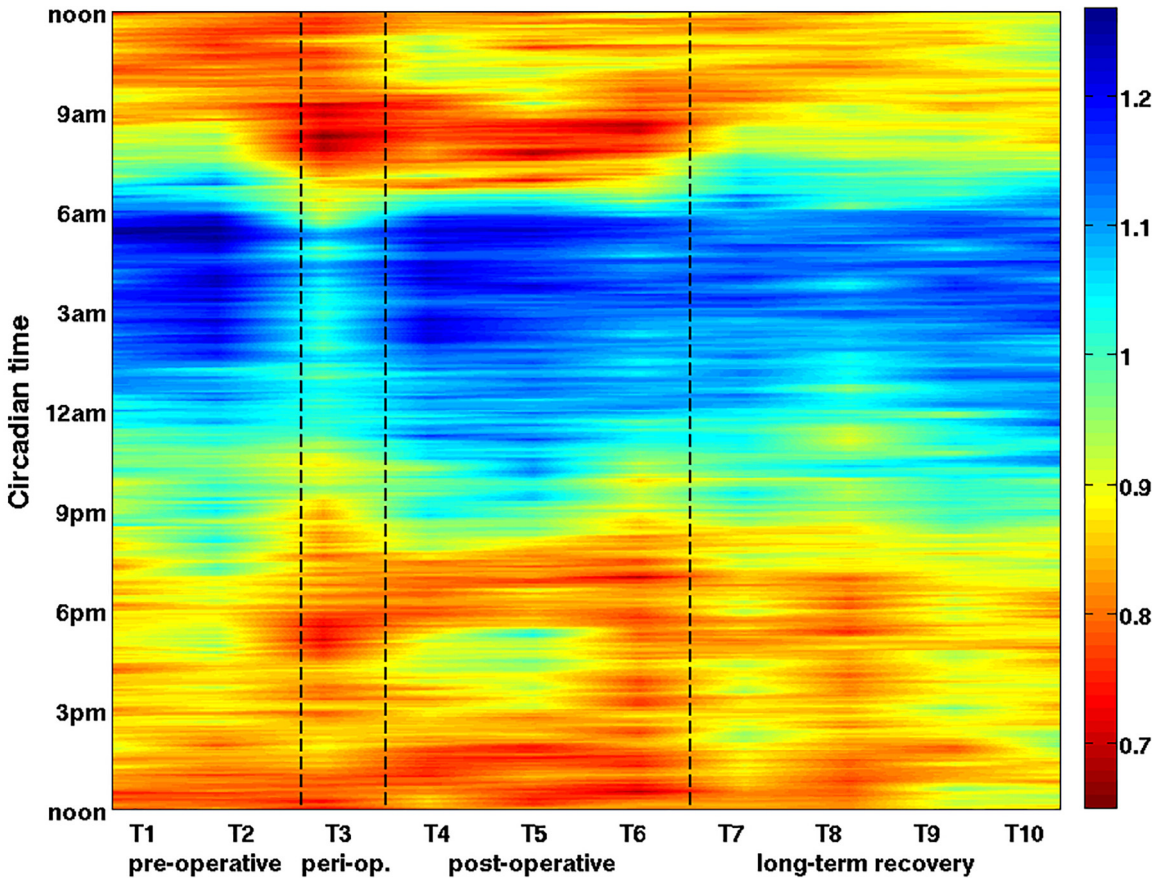

FIGURE 2 | The overall dynamics of the vagal activity during the operation-rehabilitation process. Each color represents the value of the vagal activity averaged over all 16 patients on a given measurement day (horizontal axis, T1–T10) and at a given circadian hour (vertical axis, time runs from bottom to top). Clinical phases are also indicated on the horizontal axis. Each averaged vagal activity value is represented as a color, where red means low and blue means high vagal activity (see color bar). Phases of the operation-rehabilitation process are delimited by the dashed lines. Vagal activity is reduced during peri-operative phase (T3), especially during the night. During the post-operative rehabilitation (T4–T6) original vagal activity values are gradually restored. See also our statistical analysis (**Tables 1**, **2**), which confirms the statistical significance of the vagal activity changes.

TABLE 1 | Statistical significance of vagal activity differences over time.

Repeated measures ANOVA [time (4)]† logRSArr [ms]			Mean	*SD*	*Post hoc* (LSD)	*F*	*P significance*	η_p^2
Time (vagal activity; log RSArr)	Sleep	Pre-operative	1,152	0,175	Pre- vs. Peri-operative (p = 0.004**)	4,124	0.025*	0,216
		Peri-operative	1,021	0,172				
		Rehabilitation	1,106	0,233				
		Long-term recovery	1,119	0,271				
		Overall	1,099	0,195	Square time effect	12,739	0.003**	0,459
	Wake	Pre-operative	0,887	0,182		2,189	0.102	0,127
		Peri-operative	0,808	0,183	Peri- vs. Long-term recovery (p = 020*)			
		Rehabilitation	0,841	0,244				
		Long-term recovery	0,882	0,203				
		Overall	0,854	0,185	Square time effect	7,475	0.015**	0,333
	Mean-24 h	Pre-operative	0,980	0,155	Pre- vs. Peri-operative (p = 0.028*)	3,243	0.046*	0,178
		Peri-operative	0,885	0,170				
		Rehabilitation	0,935	0,225	Peri- vs. Long-term recovery (p = 010*)			
		Long-term recovery	0,967	0,212				
		Overall	0,942	0,175	Square time effect	17,095	0.001**	0,533

†*N = 16 (13.75% replaced missing values). Marked levels of significance: *p < 0.05 and **p < 0.01.*

time series for each measurement day. The results are shown in **Figure 2**.

Natural oscillations of vagal activity from stronger (night) to weaker (day) are visible on all measurement days, indicated by a change of blue during the night to red during the day. Clearly, peri-operative vagal activity (T3) is severely weakened over the entire circadian cycle. In fact, on T3 a major decrease was observed even during the night, when the immune system is actually more active. During rehabilitation (T4–T6), vagal activity is gradually restored to its pre-operative circadian rhythm and to its usual circadian values. On T5 we observe a longer night time interval of strong vagal activity, which increases their average daily vagal activity. On T4–T6 we see a slight decrease between 7–9 am and 6–8 pm, most likely attributable to rehabilitation treatments. During long-term recovery (T7–T10), previously observed circadian pattern shifts to later in a day. This reduces the overall daily vagal activity, restoring the normal circadian oscillations and amplitudes, similar to pre-operative ones.

To confirm the statistical significance of these results, we performed standard ANOVA on these vagal changes and show the results in **Table 1**.

We find that the effect of the surgery on vagal activity is most significant during sleep (repeated ANOVA: part. Eta^2 [η^2] = 0.216; *Post hoc*$_{\text{lsd}}$: pre- vs. peri-operative p = 0.004). The vagal activity recovery after surgery is most pronounced in the 24 h mean values in the long-term recovery phase after finishing the rehabilitation (0.885 $\pm$ 0.170 peri-operative vs. 0.967 $\pm$ 0.212 long-term recovery: η^2 = 0.178; *Post hoc*$_{\text{lsd}}$: p = 0.010). The dynamics can also be observed in vagal activity while the patient is awake (η^2 = 0.127), but this is probably more confounded by various daily activities.

Scatter Plot Analysis

We next studied more closely how peri-operative, rehabilitation ("post-operative") and long-term recovery values of vagal dynamics depend on the corresponding pre-operative values. We investigated two specific time intervals: during the day from noon to 8 pm (when vagal activity is typically low) and during the night from 10 pm to 6 am (when vagal activity is usually strong). We averaged the values of vagal activity over these two intervals, but this time for each patient and on each measurement day separately. This provides an average daily and an average nightly vagal activity value for each patient and for each measurement day.

First, to examine the change of vagal activity due to surgery, the peri-operative vagal activity (measured on T3) was compared to pre-operative vagal activity (taken as the mean between measurements on T1 and T2). This comparison is shown as two scatter plots in top panels on **Figure 3** In both cases a reduction of vagal activity can be observed due to the surgery, especially in patients with larger pre-operative values. This is even more pronounced for the nightly values. Second, in the two middle panels in **Figure 3** we repeat the same analysis, but this time for post-operative values. They were taken as the mean between measurements on T5 and T6 (we exclude T4 from this averaging to allow more time for rehabilitation to make noticable effect), and scatter ploted agains pre-operative values (as above). Both plots show that during rehabilitation, the vagal activity values are gradually restored to the pre-operative ones. This effect is very clear during the night: patients with weaker pre-operative vagal activity show a very slow recovery, whereas patients with strong pre-operative vagal activity in fact show a noticable increase of vagal activity as a result of the early rehabilitation process. Note that due to the logarithmic representation of vagal activity values (see section "Materials and Methods"), nightly increase in vagal activity is actually much higher than immediately visible in these plots, and also higher

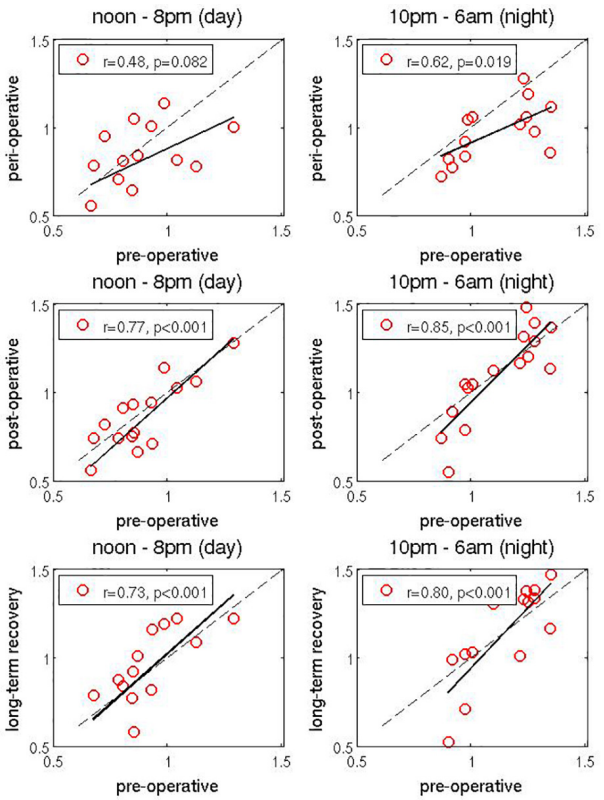

FIGURE 3 | Scatter plots of vagal activity values. Peri-operative values **(top panels)**, post-operative values **(middle panels)**, and long-term recovery values **(bottom panels)** are reported on the vertical axis, as a function of pre-operative values, which are in all panels reported on horizontal axis (each dot represents one patient). They are computed, respectively, as values on T3, average between T4 and T5, average between T9 and T10, average between T1 and T2. Changes in day-time values (measured from noon to 8 pm) are shown on the left and changes in the night-time values (measured from 10 pm to 6 am) are shown on the right. Linear regression is shown as a full black line and the line of identity is shown as a dashed black line. Correlation coefficient r is reported for each plot separately. Significances are all $p < 0.08$. While the event of surgery clearly reduces the vagal activity, the rehabilitation process gradually restores it to the original values. In fact, in some cases final vagal activity values are actually higher than the original pre-operative values. This effect is especially pronounced during the night (due to logarithmic representation of vagal activity values, real changes are actually more pronounced than it appears). See text and **Table 2**. Figures have different numbers of points, since for 16 patients that completed the study certain daily and/or nightly values are missing.

TABLE 2 | Statistical analysis for interaction (time × vagal-type) according (**Figures 2**, **3**).

Repeated measures ANOVA (*N* = 16) [4 × 2 design (time × vagal-type)]† logRSArr [ms]		**Vagal-type**				**Effects time vagal-type**	***F***	***P significance***	η_p^2
		Strong vagal activity (*n* = 8)		**Weak vagal activity (*n* = 8)**					
		mean	**SD**	**mean**	**SD**				
Sleep	Pre-operative	1281	0,088	1022	0,139				
	Peri-operativ	1,114	0,151	0,927	0,145	Time	4,203	0.022*	0,231
	Rehabilitation	1246	0,110	0,966	0,248	Vagal-type	13,803	0.002**	0,496
	Long-term recovery	1287	0,120	0,951	0,279				
	Overall	1,232	0,083	0,967	0,184	Interaction	1,287	0.292	0,084
Wake	Pre-operative	1,007	0,177	0,767	0,079				
	Peri-operativ	0,907	0,111	0,709	0,192	Time	2,224	0.099(*)	0,137
	Rehabilitation	1,007	0,155	0,675	0,201	Vagal-type	14,528	0.002**	0,509
	Long-term recovery	1,007	0,112	0,757	0,200				
	Overall	0,982	0,118	0,727	0,148	Interaction	1,234	0.306	0,082
Mean-24 h	Pre-operative†	**1,097**	**0,125**	**0,863**	**0,066**				
	Peri-operativ	0,986	0,109	0,783	0,162	Time	3,273	0.048*	0,190
	Rehabilitation	1,095	0,118	0,775	0,190	Vagal-type	17,151	0.001**	0,551
	Long-term recovery	1,089	0,111	0,844	0,222				
	Overall	1,067	0,090	0,816	0,146	Interaction	1,141	0.336	0,075
	Time					Time	4,432	0.042*	0,869
MANOVA	Vagal-typ					Vagal-type	5,208	0.016*	0,566
	Interaction (Time × vagal-type)					Interaction	5,900	0.021*	0,898

†*A median split of pre-operative vagal activity was used to classify into vagal-types with strong of weak vagal activity (cut-off value: 0.9654). This classification was also used for* ***Figure 5****. *p < 0.05 and **p < 0.01.*

than the decrease for the patients with low pre-operative vagal activity. Third, in the bottom panels of **Figure 3** we scatter plot the long-term recovery values against pre-operative values. The former were taken as the mean between T9 and T10 (again, we exclude T7 and T8 from averaging to give more time to long-term recovery). We find a generally positive slope of the regression line, indicating overall improvement of the vagal activity (recall that the logarithmic representation of vagal activity is less faithful toward larger values). Again, patients with stronger pre-operative values benefit from stronger improvement, while patients with lower pre-operative values show similar or slightly weaker values. However, we must take into account here that several months have passed since the surgery, so other life factors might have influenced the vagal activity.

Table 2 shows the results of two-way ANOVA [within-factor (time-course; 4-stage), between-factor (pre-operative-vagal activity; 2-stage)] performed to detect differences (interactions) in time course among the patients. Interestingly, while the patients suffer from larger reduction of vagal activity due to surgery (top panels of **Figure 3**), patients with strong pre-operative vagal activity exhibit larger increase of vagal activity during rehabilitation (middle panels **Figure 3** and **Table 2**: repeated MANOVA: Interaction: $p = 0.021$, $\eta^2 = 0.898$), and actually finish with vagal activity values even higher than the pre-operative ones. This is the case, at least, in some patients. The multivariate significant increase of the vagal activity ($p = 0.042$, $\eta^2 = 0.869$, see **Table 2**) after surgery is dependent on the pre-operative values (time × vagal-type: $p = 0.021$, $\eta^2 = 0.898$). This is shown for individual cases later in **Figure 4**. Due to the small and heterogeneous sample of patients, this significant dependence on initial values (pre-operative) was not seen in inference statistics via univariate testing ($p > 0.292$) for the used aggregated time points.

Effects on the Entire Circadian Dynamics

Finally, we investigated the effects of surgery and rehabilitation on the entire circadian dynamics of vagal activity. To that end we selected two patients, one with a generally strong and the other with generally weak pre-operative vagal activity (see also **Table 2**). In **Figure 4** top panel, we show three circadian time series for the first patients. Both the reduction due to surgery (red) and the improvement due to rehabilitation (green) are clearly visible over almost the entire circadian cycle. During rehabilitation, the improvement is especially pronounced during the first part of the night: vagal activity increases beyond its pre-operative values. Next we examine the same time series for the second patient (with generally weak vagal activity) in **Figure 4** bottom panel. Similar patterns are found over the circadian cycle, but the improvement due to rehabilitation is now almost entirely absent. Weak pre-operative vagal activity seem to be connected to weak vagal response during rehabilitation. This again confirms that the rehabilitation process can enhance vagal activity to values higher than normal, and particularly so for the patients with

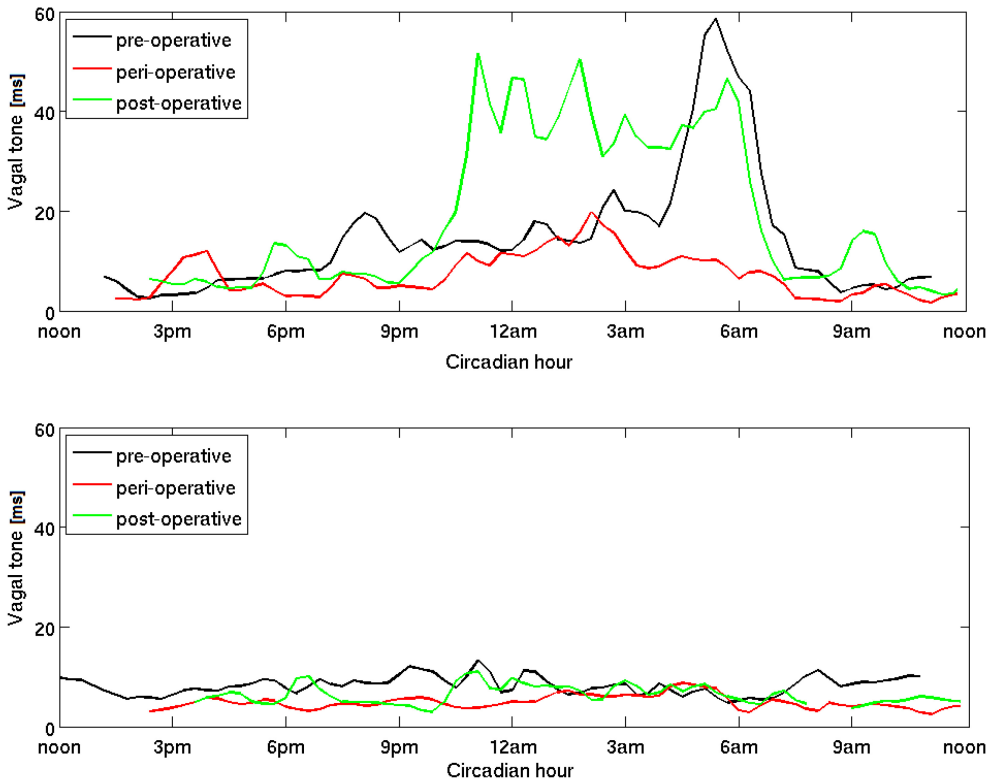

FIGURE 4 | Circadian dynamics of vagal activity (vagal tone) during the operation-rehabilitation process. A patient with a strong pre-operative vagal activity is shown in the **top panel** and another patient with a weak pre-operative vagal activity is shown in the **bottom panel**. Three circadian time series for the entire 24 h cycle are shown in each panel, measured on three specific days, pre-operative on T1, peri-operative on T3 and post-operative on T5. We remove the logarithmic scale for better clarity (see section "Materials and Methods") and use the moving average over a window of several minutes to avoid minute-to-minute fluctuation. While the patient in the **top panel** shows a clear improvement of post-operative vagal activity, especially during the night, the patient in the **bottom panel** shows very little improvement, and even during the night.

initially strong values. Our results suggest that if the patient's vagal activity could be boosted pre-operatively, this patient could realistically expect a lesser risk of peri-operative sepsis and a better outcome of rehabilitation. For completeness, we later make a clearer separation between strong and weak vagal activity.

Analysis of Other HRV Parameters

As an addition to logRSArr we next examine further HRV parameters in **Table 3** over 24 h during the examined time interval. Next to a lower vagal activity (logRSArr, $p = 0.046$) and an increased heart rate ($p = 0.072$; RR: $p = 0.011$), HRV is generally reduced immediately after surgery and it takes time to recover (only in the follow-up after rehabilitation; "long-term recovery"; all $p < 0.10$). Autonomic Balance (Ratio LF/HF) is not affected by the orthopedic surgery ($p = 0.830$).

Next we compare our patients with age and gender matched reference values from healthy controls at the pre-operative time. Results are reported in **Table 4**. Overall, patients in our clinical sample seem to have higher pre-operative heart rate ($z = 0.43$, $p = 0.096$)[2] with a slightly reduced vagal activity ($z = -0.28$, $p = 0.115$), where the other HRV values are in general similar to healthy individuals (all $p \geq 0.60$, MANOVA with HR, SDNN, TOT, LF, HF, VLF, VQ; pre-operative patients vs. healthy controls: $F = 0.674$, $p = 0.675$; see **Table 4** and **Figure 5**).[3]

Using above HRV parameters, we can now make a clearer distinction between patients with strong as opposed to weak vagal activity. To this end we perform MANOVA [calculated for HR, SDNN, TOT, LF, HF, VLF, and VQ; $F = 3.113$, $p = 0.062$, p.Eta2 = 0.675] and report the results in **Figure 5**. Patients with a pre-operative "weak vagal activity" differ markedly from patients with "strong vagal activity" in almost all HRV parameters (effect size: mean absolute z-differences[3] = 0.759, $p = 0.011$). This confirms that vagal activity (logRSArr) is a good indicator for differences in cardio-autonomic (HRV) status, as it reflects different pattern of HRV markers and thus types of cardio-autonomic profiles. It can also be useful as a marker for different reaction types, e.g., to surgery, possible complications like sepsis or different clinical courses. This also clarifies our

[2]Standard scores, also called z-values (z) are calculated by subtracting the population mean from an individual raw score and then dividing the difference by the population standard deviation (here: for healthy controls; e.g., age and gender matched reference values for autonomic (HRV) parameters see **Table 4**). Similarly, the deviations from zero or from mean-differences of z-values can interpreted as effect size as presented in **Figure 5** and **Table 4**.

[3]The data for healthy individuals were taken from a general database.

TABLE 3 | Analysis of other HRV parameters.

Heart rate variability (HRV) parameters	Overall: $n = 16$ (24 h mean)		Time course (time points; 24 h mean)				Unifactoriell GLM – time effect			Post hoc test (LSD)
	Mean ± SD	Unit	Pre-operative (1)	Peri-operative (2)	Rehabilitation (3)	Long-term recovery (4)	F	P	η_p^2	$p < 05$
vagal activity (logRSArr)	0,94 ± 0,17	log(ms)	0,98	0,88	0,93	0,97	3,24	0.046*	0,18	1 vs. 2; 2 vs. 4
Consecutive inter-beat intervals (RR)	788,67 ± 75,33	ms	790,49	760,15	794,48	809,56	4,16	0.011*	0,22	2 vs. 3, 4
Heart rate (HR)	78,69 ± 7,81	bpm	78,91	80,60	78,34	76,90	2,49	0.072(*)	0,14	2 vs. 4
Standard deviation of RR (SDNN)	45,65 ± 9,37	ms	49,49	40,22	46,26	46,61	5,00	0.016*	0,25	1 vs. 2
Total variability pow er (lnTOTrr)	7,11 ± 0,45	ln(ms^2)	7,30	6,90	7,10	7,14	3,95	0.035*	0,21	1 vs. 2, 3
Low frequency power (lnLFrr)	5,57 ± 0,51	ln(ms^2)	5,76	5,31	5,58	5,63	4,65	0.019*	0,24	1 vs. 2; 2 vs. 4
High frequency pow er (lnHFrr)	4,37 ± 0,91	ms^2	4,53	4,12	4,37	4,47	2,70	0.077(*)	0,15	1 vs. 2
Very low frequency power (lnVLFrr)	6,46 ± 0,40	ms^2	6,64	6,29	6,43	6,45	3,18	0.065(*)	0,17	1 vs. 2, 3
Ratio LF/HF	1,20 ± 0,60	[]	1,23	1,18	1,21	1,16	0,19	0.830	0,01	
Respiratory rate (ATMFrsa)	17,52 ± 1,29	fpm	17,02	17,64	17,46	17,95	3,19	0.062(*)	0,18	1 vs. 3,4; 3 vs. 4

*Marked levels of significance: (*)$p < 0.1$ and *$p < 0.05$.*

choice of two patiens with weak vs. strong vagal activity in earlier **Figure 4**.

Analysis of Results of Questionnaires

Further data relative to clinical information of patients (standardized questionnaires; Zerssen, 1976; Hobi, 1985; Grote, 2009) are shown in **Table 5**. Most patients report an improvement of subjective well-being ($p = 0.027$), already during "rehabilitation." Only in the "long-term recovery" period, the values ("well-being" and "sleep recovery") reach those of healthy reference data [0.00 ± 1.00; $(z)^3$]. General symptoms of "complaints" appear to be less affected over time ($p = 0.139$) and remain higher than in healthy controls ($z > 0.75$) throughout the whole observation period. Hence in general, no significant correlations between autonomic (HRV) parameters and questionnaire results can be observed.

DISCUSSION

Using the intensity of cardio-respiratory sinus arrhythmia for determination of vagal activity, we showed that vagal activity decreases around the time of (orthopedic) surgery, and increases during rehabilitation and long-term recovery. The former is an indicator of dangers accompanying surgical procedures, including sepsis. We found that in the wake of surgery vagal activity is impaired in essentially all patients in our sample. This impairment is present during both day and night, but is more prominent during the night. The observed decrease of vagal activity implies the breakdown of the inflammatory reflex. This hinders the ability of the body to timely resolve inflammation, thus leaving the patient considerably more vulnerable to diverse inflammatory conditions after surgery. Given that surgery and the associated tissue injury are both pro-inflammatory, preserving the inflammation resistance is paramount during this critical period. Moreover, weakening of vagal activity could be unintentionally enhanced in other ways, such as via narcotic treatments that are known to dampen ANS, including its vagal component (Shapiro et al., 2010; Tarvainen et al., 2012). Our findings suggest that caution must be observed when using such narcotics.

Our next main result is that the rehabilitation process, besides being clearly effective in restoring the vagal activity, also seems to provide a way of boosting it, as suggested by the larger than normal values observed in several patients. This vagal activity increase was particularly prominent during the night, which is normally characterized by higher vagal activity compared to the day-time values. In fact, sleep is well-known to be important for general health and helpful in many medical conditions (Reynolds et al., 2012; Moser and Kripke, 2013). Therefore, rehabilitation appears to be suited for restoring the autonomic regulation and thus the inflammatory reflex, which persist even 1 year after rehabilitation in our study.

TABLE 4 | Age and gender matched reference values for pre-operative HRV parameters.

Heart rate variability (HRV) parameters	Healthy matched sample (n = 32)† 24 h mean		Rehab sample (n = 16): "pre-operative" [normalized 24 h mean; (z)]		
	Mean ± *SD*	Unit	mean [z] ± *SD*	*T*	*P*
vagal activity (logRSArr)	1, 03 ± 0, 23	log(ms)	−0, 28 ± 0, 67	−1,67	0.115
Consecutive inter-beat intervals (RR)	827, 85 ± 99, 76	ms	−0, 37 ± 0, 89	−1,69	0.112
Heart rate (HR)	75, 08 ± 9, 02	bpm	0, 43 ± 0, 96	1,78	0.096(*)
Standard deviation of RR (SDNN)	49, 64 ± 14, 68	ms	−0, 01 ± 0, 72	−0,06	0.956
Total variability power (lnTOTrr)	7, 30 ± 0, 61	ln(ms^2)	0, 00 ± 0, 70	0,02	0.982
Low frequency power (lnLFrr)	5, 83 ± 0, 72	ln(ms^2)	−0, 10 ± 0, 72	−0,53	0.604
High frequency power (lnHFrr)	4, 55 ± 0, 92	ms^2	−0, 03 ± 0, 90	−0,11	0.911
Very low frequency power (lnVLFrr)	6, 61 ± 0, 56	ms^2	0, 06 ± 0, 71	0,37	0.719
Ratio LF/HF	1, 28 ± 0, 55	[]	−0, 08 ± 1, 00	−0,33	0.747
Respiratory rate (ATMFrsa)	16, 98 ± 2, 27	fpm	0, 02 ± 0, 57	0,15	0.884

†*Age, 59.25 ± 10.34 (68.8% female).*

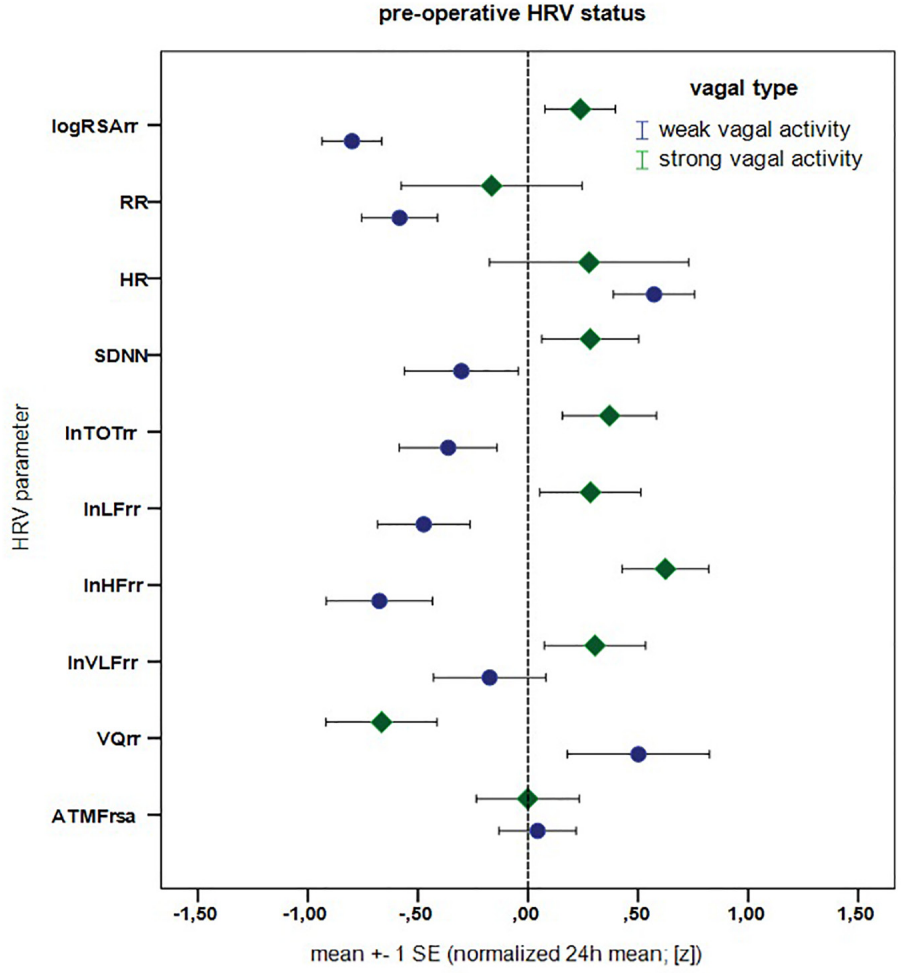

FIGURE 5 | Pre-operative cardio-autonomic status - patients with weak vs. stronge vagal activity. Mean (absolute) *z*-difference (weak vs. strong vagal activity) = 0.759, T = –2.936 (df = 14), p = 0.011* (MANOVA: F = 3.113, p = 0.062, η_p^2 = 0.675, calculated for HR, SDNN, TOT, LF, HF, VLF, and VQ).

TABLE 5 | Statistics and Questionnaires.

	Repeated measures ANOVA questionnaires – psychometric scales [z]†		Mean† ± *SD*	*Post hoc* (LSD; $p \leq 05$)	*F*	*P*	η_p^2
Time course	Well-being (n = 13) (Hobi, 1985)	Pre-operative (1)‡	−0,426 ± 0,780	1 vs. 4	4,201	0.027*	0,276
		Peri-operativ (2)	−0,771 ± 0,879	2 vs. 3, 4			
		Rehabilitation (3)	−0,155 ± 0,852				
		Long-term recovery (4)	0,033 ± 0,686				
	Complaints (n = 14) (Zerssen, 1976)	Pre-operative (1)	1,094 ± 1,147		1,949	0.139	0,140
		Peri-operativ (2)	1,094 ± 1,109				
		Rehabilitation (3)	0,811 ± 1,313				
		Long-Term recovery (4)	0,753 ± 1,278				
	Sleep recovery (n = 13) (Grote, 2009)	Pre-operative (1)	−0,253 ± 0,995	2 vs. 4	2,391	0.086(*)	0,179
		Peri-operative (2)	−0,802 ± 1,277				
		Rehabilitation (3)	−0,258 ± 1,164				
		Long-Term recovery (4)	−0,018 ± 1,085				

†*Normalized with healthy controls [z-values].* ‡*Correlation with vagal activity: r = 0.387, p = 0.155. MANOVA (n = 12) - time: F = 1.846, p-0.071(*), η_p^2 = 0.156 (Pillai). Marked levels of significance: (*)p < 0.1 and *p < 0.05.*

Vice versa of this situation has been reported. For instance, independent of the origin of inflammation, vagal activity is always reduced in inflammatory conditions (Lujan and DiCarlo, 2013). This may lead to a positive feedback loop or a vicious circle, entangling the inflammation reflex, and the accompanying pathology. Some forms of obesity are indeed known to lead to inflammation, while at the same time the chronic inflammation promotes obesity-associated diabetes (Wang et al., 2003). This indicates that besides in the development of sepsis, dysfunctional vagal control or circadian disturbance of the ANS could play a role in several key diseases of modern society, including cardiovascular diseases, metabolic syndrome and/or even development of cancer (Moser et al., 2006b; Eiró and Vizoso, 2012).

On the other hand, we realize that after surgery vagal activity is bound to increase, regardless of whether the patient undergoes rehabilitation or not. It is hard to identify which part of vagal activity increase that we observed comes as a result of rehabilitation, and which part can be attributed to natural bodily regeneration mechanisms. Yet there is extensive evidence for the positive influence of rehabilitation on a number of factors related to general well-being (Strauss-Blasche et al., 2004), many of which are directly associated with the strength of vagal activity. Our findings indicate that rehabilitation generally does have a positive effect on vagal activity, but the question of precise difference of vagal activity between patients that undergo rehabilitation and those that do not remains to be answered.

Is there a minimum value of vagal activity above which the patient is protected against diseases (such as sepsis)? While this interesting question calls for more research, we report that none of the patients contracted sepsis. This suggests that, at least for sepsis, this threshold value is below the minimums observed here.

Clinical Applications of Our Findings

We suggest that in order to reduce the chances of inflammatory conditions in the wake of surgery, it might be worthwhile to provide some activities that increase the vagal activity *prior* to the surgery ("pre-habilitation"). This would increase the patient's vagal inflammatory resistance allowing him/her to cope with the event of surgery and the associated stress more effectively (Geiss et al., 2005; Laitio et al., 2007; Mazzeo et al., 2011; Bravi et al., 2012; Bohanon et al., 2015; Ernst et al., 2017; Reimer et al., 2017; Yang et al., 2018). An additional argument in favor of this conclusion comes from our observation that patients with strong pre-surgery values make the best use of the rehabilitation in improving their vagal activity. Hence, strengthening the vagal activity of a patient during the weeks before the planned surgery appears to be a promising strategy to minimize the risk of vagal fail and hence inhibit the developement of inflammatory states. The aim of this paper was to provide more empirical evidence for these hypotheses, which if ultimately proven correct, may open new approaches, for example, in treating or preventing sepsis. This study also shows the clinical value of a quantified cardiorespiratory interactions, the respiratory sinus arrhythmia.

DATA AVAILABILITY STATEMENT

The datasets generated for this study are available on request to the corresponding author MM (max.moser@medunigraz.at).

ETHICS STATEMENT

This study involved the patients from the Orthopedic Rehabilitation Center at Humanomed Center in Althofen, Austria. Patients were informed about the nature and the purpose of the study, signed the informed consent and participated voluntarily. After the study, personal results were given to all patients with adequate explanation from a doctor. The study was authorized by the Ethical Committee of the Carinthian Government, authorization number A 02/05, 01 February, 2005. All methods used in this study are in accordance with the relevant guidelines and regulations, usual for research in medical sciences.

AUTHOR CONTRIBUTIONS

MM, VG, and HP envisaged the study. HP and TO arranged for the patient voluntary participation. VG and TO carried out the measurements. MM, MF, VG, and ZL analyzed the data and the results. ZL, NG, VG, and MM wrote the manuscript. All authors reviewed the manuscript.

FUNDING

This work was supported by the Austrian Research Promotion Society via Excellence Network Knet Water Subproject Balneology, the Slovenian Research Agency via Program P1-0383 and Project J5-8236, and the European Union's Horizon 2020 Research and Innovation Program under the Marie Skłodowska-Curie Grant Agreement No. 642563 (COSMOS). Financial assistance was also made by the Doctoral School for Lifestyle-Related Diseases of the Medical University of Graz, Austria.

ACKNOWLEDGMENTS

We most gratefully acknowledge the voluntary participation of all patients. Thanks to Alexander Avian, Jure Bon, Sylvia Farzi, Peter Köhldorfer, Helmut Lackner, Bernhard Puswald, and the employees of Humanomed GmbH for their help and useful feedback.

REFERENCES

Alamili, M. (2015). Circadian variation in endotoxaemia and modulatory effects of melatonin. *Dan. Med. J.* 62:B5096.

Andersson, U., and Tracey, K. J. (2012). Neural reflexes in inflammation and immunity. *J. Exp. Med.* 209, 1057–1068. doi: 10.1084/jem.20120571

Bohanon, F. J., Mrazek, A. A., Shabana, M. T., Mims, S., Radhakrishnan, G. L., Kramer, G. C., et al. (2015). Heart rate variability analysis is more sensitive at identifying neonatal sepsis than conventional vital signs. *Am. J. Surg.* 210, 661–667. doi: 10.1016/j.amjsurg.2015.06.002

Bravi, A., Green, G., Longtin, A., and Seely, A. J. E. (2012). Monitoring and identification of sepsis development through a composite measure of heart rate variability. *PLoS One* 7:e45666. doi: 10.1371/journal.pone.0045666

Chow, E., Iqbal, A., Bernjak, A., Ajjan, R., and Heller, S. R. (2014). Effect of hypoglycaemia on thrombosis and inflammation in patients with type 2 diabetes. *Lancet* 383:S35.

Curtis, A. M., Bellet, M. M., Sassone-Corsi, P., and O'Neill, L. A. (2014). Circadian clock proteins and immunity. *Immunity* 40, 178–186. doi: 10.1016/j.immuni.2014.02.002

Das, U. (2011). Can vagus nerve stimulation halt or ameliorate rheumatoid arthritis and lupus? *Lip. Heal. Dis.* 10:19. doi: 10.1186/1476-511x-10-19

Donchin, Y., Constantini, S., Szold, A., Byrne, E. A., and Porges, S. W. (1992). Cardiac vagal tone predicts outcome in neurosurgical patients. *Crit. Care Med.* 20, 942–949. doi: 10.1097/00003246-199207000-00008

Eiró, N., and Vizoso, F. J. (2012). Inflammation and cancer. *World J. Gastroint. Surg.* 4, 62–72.

Ernst, G., Watne, L. O., Frihagen, F., Wyller, T. B., Dominik, A., and Rostrup, M. (2017). Decreases in heart rate variability are associated with postoperative complications in hip fracture patients. *PLoS One* 12:e0180423. doi: 10.1371/journal.pone.0180423

Gallasch, E., Moser, M., Kozlovskaya, I., Kenner, T., and Noordergraaf, A. (1997). Effects of an eight-day space flight on microvibration and physiological tremor. *Am. J Physiol.* 273, R86–R92.

Geiss, A., Rohleder, N., Kirschbaum, C., Steinbach, K., Bauer, H. W., and Anton, F. (2005). Predicting the failure of disc surgery by a hypofunctional HPA axis: evidence from a prospective study on patients undergoing disc surgery. *Pain* 114, 104–117. doi: 10.1016/j.pain.2004.12.007

Grote, V. (2009). *Schlaferholung und Herzratenvariabilität als Indikatoren für Wohlbefinden und Gesundheit*. Doctoral dissertation, Karl-Franzens-Universität, Graz.

Hobi, V. (1985). *Basler Befindlichkeitsskala (BBS). Ein Self-Rating zur Verlaufsmessung der Befindlichkeit*. Weinheim: Beltz Testgesellschaft

Huang, S. T., Chen, G. Y., Lo, H. M., Lin, J. G., Lee, Y. S., and Kuo, C. D. (2005). Increase in the vagal modulation by acupuncture at neiguan point in the healthy subjects. *Am. J. Chin. Med.* 33, 157–164. doi: 10.1142/s0192415x0500276x

Huston, J. M., and Tracey, K. J. (2011). The pulse of inflammation: heart rate variability, the cholinergic anti-inflammatory pathway and implications for therapy. *J. Intern. Med.* 269, 45–53. doi: 10.1111/j.1365-2796.2010.02321.x

Kastner, L., Aksentijevich, I., and Goldbach-Mansky, R. (2010). Autoinflammatory disease reloaded: a clinical perspective. *Cell* 140, 784–90. doi: 10.1016/j.cell.2010.03.002

Laitio, T., Jalonen, J., Kuusela, T., and Scheinin, H. (2007). The role of heart rate variability in risk stratification for adverse postoperative cardiac events. *Anesthe. Analg.* 105, 1548–1560. doi: 10.1213/01.ane.0000287654.49358.3a

Langhorst, P., Schulz, B., Schulz, G., and Lambertz, M. (1983). Reticular formation of the lower brainstem. a common system for cardiorespiratory and somatomotor functions: discharge patterns of neighboring neurons influenced by cardiovascular and respiratory afferents. *J. Auton. Nerv. Syst.* 9, 411–432. doi: 10.1016/0165-1838(83)90005-x

Lehofer, M., Moser, M., Hoehn-Saric, R., McLeod, D., Hildebrandt, G., and Egner, S. (1999). Influence of age on the parasympatholytic property of tricyclic antidepressants. *Psychiatry Res.* 85, 199–207. doi: 10.1016/s0165-1781(99)00005-0

Leslie, M. (2014). Inflammation debate reignites. *Science* 345:607. doi: 10.1126/science.345.6197.607

Lujan, H. L., and DiCarlo, S. E. (2013). Physical activity, by enhancing parasympathetic tone and activating the cholinergic anti-inflammatory pathway, is a therapeutic strategy to restrain chronic inflammation and prevent many chronic diseases. *Med. Hypotheses* 80, 548–552. doi: 10.1016/j.mehy.2013.01.014

Madrid-Navarro, C. J., Sanchez-Galvez, R., Martinez-Nicolas, A., Marina, R., Garcia, J. A., Madrid, J. A., et al. (2015). Disruption of circadian rhythms and delirium, sleep impairment and sepsis in critically ill patients. potential therapeutic implications for increased light-dark contrast and melatonin therapy in an ICU environment. *Curr. Pharm. Des.* 21, 3453–3468. doi: 10.2174/1381612821666150706105602

Mayer, A. (2015). How a well-adapted immune system is organized. *Proc. Natl. Acad. Sci. U.S.A.* 112, 5950–5955. doi: 10.1073/pnas.1421827112

Mazzeo, A. T., La Monaca, E., Di Leo, R., Vita, G., and Santamaria, L. B. (2011). Heart rate variability: a diagnostic and prognostic tool in anesthesia and intensive care. *Acta Anaesthesiol. Scand.* 55, 797–811. doi: 10.1111/j.1399-6576.2011.02466.x

Moser, M., Fruhwirth, M., and Kenner, T. (2008). The symphony of life. *IEEE Eng. Med. Biol. Mal.* 27, 29–37.

Moser, M., Frühwirth, M., Messerschmidt, D., Goswami, N., Dorfer, L., Bahr, F., et al. (2017). Investigation of a micro-test for circulatory autonomic nervous system responses. *Front. Physiol.* 8:448. doi: 10.3389/fphys.2017.00448

Moser, M., Frühwirth, M., Penter, R., and Winker, R. (2006a). Why life oscillates – from topographical towards a functional chronobiology. *Cancer Cause Control* 17, 591–599. doi: 10.1007/s10552-006-0015-9

Moser, M., Schaumberger, K., Schernhammer, E., and Stevens, R. G. (2006b). Cancer and rhythm. *Cancer Cause Control* 17, 483–487. doi: 10.1007/s10552-006-0012-z

Moser, M., and Kripke, D. F. (2013). Insomnia: more trials needed to assess sleeping pills. *Nature* 493:305. doi: 10.1038/493305d

Moser, M., Lehofer, M., Hildebrandt, G., Voica, M., Egner, S., and Kenner, T. (1995). Phase- and frequency coordination of cardiac and respiratory function. *Biol. Rhythm Res.* 26, 100–111. doi: 10.1080/09291019509360328

Moser, M., Lehofer, M., Hoehn-Saric, R., McLeod, D. R., Hildebrandt, G., Steinbrenner, B., et al. (1998). Increased heart rate in depressed subjects in spite of unchanged autonomic balance? *J. Affect. Disord.* 48, 115–124. doi: 10.1016/s0165-0327(97)00164-x

Moser, M., Lehofer, M., Sedminek, A., Lux, M., Zapotoczky, H. G., Kenner, T., et al. (1994). Heart rate variability as a prognostic tool in cardiology. a contribution to the problem from a theoretical point of view. *Circulation* 90, 1078–1082. doi: 10.1161/01.cir.90.2.1078

Mundigler, G., Delle-Karth, G., Koreny, M., Zehetgruber, M., Steindl-Munda, P., and Marktl, W. (2002). Impaired circadian rhythm of melatonin secretion in sedated critically ill patients with severe sepsis. *Crit. Care Med.* 30, 536–540. doi: 10.1097/00003246-200203000-00007

Munford, R. S., and Tracey, K. J. (2002). Is severe sepsis a neuroendocrine disease? *Mol. Med.* 8, 437–442. doi: 10.1007/bf03402023

Nathan, C., and Ding, A. (2010). Nonresolving inflammation. *Cell* 140, 871–882. doi: 10.1016/j.cell.2010.02.029

Nguyen, H. B., Rivers, E. P., Abrahamian, F. M., Moran, G. J., Abraham, E., and Trzeciak, S. (2006). Emergency department sepsis education, and g. strategies to improve survival working, severe sepsis and septic shock: review of the literature and emergency department management guidelines. *Ann. Emerg. Med.* 48, 28–54.

Olofsson, P. S., Rosas-Ballina, M., Levine, Y. A., and Tracey, K. J. (2012). Rethinking inflammation: neural circuits in the regulation of immunity. *Immunol. Rev.* 248, 188–204. doi: 10.1111/j.1600-065X.2012.01138.x

Papaioannou, V., Mebazaa, A., Plaud, B., and Legrand, M. (2014). 'Chronomics' in ICU: circadian aspects of immune response and therapeutic perspectives in the critically ill. *Intensive Care Med. Exp.* 2:18. doi: 10.1186/2197-425X-2-18

Reimer, P., Máca, J., Szturz, P., Jor, O., Kula, R., Ševčík, P., et al. (2017). Role of heart-rate variability in preoperative assessment of physiological reserves in patients undergoing major abdominal surgery. *Ther. Clin. Risk Manag.* 13, 1223–1231. doi: 10.2147/TCRM.S143809

Reynolds, A. C., Dorrian, J., Liu, P. Y., Van Dongen, H. P., Wittert, G. A., Harmer, L. J., et al. (2012). Impact of five nights of sleep restriction on glucose metabolism, leptin and testosterone in young adult men. *PLoS One* 7:e41218. doi: 10.1371/journal.pone.0041218

Rocha, A. S., Araújo, M. P., Campos, A., Costa Filho, R., Mesquita, E. T., and Santos, M. V. (2011). Circadian rhythm of hospital deaths: comparison between intensive care unit and non-intensive care unit. *Rev. Assoc. Med. Bras.* 57, 519–533.

Rosas-Ballina, M., and Tracey, K. J. (2009). Cholinergic control of inflammation. *J. Intern. Med.* 265, 663–679. doi: 10.1111/j.1365-2796.2009.02098.x

Scheiermann, C., Kunisaki, Y., and Frenette, P. S. (2013). Circadian control of the immune system. *Nat. Rev. Immun.* 13, 190–198. doi: 10.1038/nri3386

Shapiro, N. I., Khankin, E. V., Van Meurs, M., Shih, S. C., Lu, S., and Yano, M. (2010). Leptin exacerbates sepsis-mediated morbidity and mortality. *J. Immunol.* 185, 517–524. doi: 10.4049/jimmunol.0903975

Strauss-Blasche, G., Muhry, F., Lehofer, M., Moser, M., and Marktl, W. (2004). Time course of well-being after a three-week resort-based respite from occupational and domestic demands: carry-over, contrast and situation effects. *J. Leis. Res.* 36, 293–309. doi: 10.1080/00222216.2004.11950025

Tarvainen, M. P., Georgiadis, S., Laitio, T., Lipponen, J. A., Karjalainen, P. A., Kaskinoro, K., et al. (2012). Heart rate variability dynamics during low-dose propofol and dexmedetomidine anesthesia. *Ann. Biomed. Eng.* 40, 1802–1813. doi: 10.1007/s10439-012-0544-1

Topçu, Ç, Fruehwirth, M., Moser, M., Rosenblum, M., and Pikovsky, A. (2018). Disentangling respiratory sinus arrhythmia in heart rate variability records. *Physiol. Meas.* 39:054002. doi: 10.1088/1361-6579/aabea4

Tracey, K. J. (2002). The inflammatory reflex. *Nature* 420, 853–859. doi: 10.1038/nature01321

Tracey, K. J. (2007). Physiology and immunology of the cholinergic antiinflammatory pathway. *J. Clin. Invest.* 117, 289–296. doi: 10.1172/jci30555

Wang, H., Yu, M., Ochani, M., Amella, C. A., Tanovic, M., and Susarla, S. (2003). Nicotinic acetylcholine receptor alpha7 subunit is an essential regulator of inflammation. *Nature* 421, 384–388.

Williamson, J. B., Lewis, G., Grippo, A. J., Lamb, D., Harden, E., Handleman, M., et al. (2010). Autonomic predictors of recovery following surgery: a comparative study. *Auton. Neurosci.* 156, 60–66. doi: 10.1016/j.autneu.2010.03.009

Wright, K. P., Drake, A. L. Jr., Frey, D. J., Fleshner, M., Desouza, C. A., Gronfier, C., et al. (2015). Influence of sleep deprivation and circadian misalignment on cortisol, inflammatory markers, and cytokine balance. *Brain Behav. Immun.* 47, 24–34. doi: 10.1016/j.bbi.2015.01.004

Yang, G.-Z., Xue, F.-S., Sun, C., Liao, X., and Liu, J.-H. (2018). Vagal nerve stimulation: a potential useful adjuvant to treatment of sepsis. *J. Anesth. Perioper. Med.* 5, 161–168. doi: 10.24015/japm.2017.0012

Zerssen, D. v. (1976). *Die Beschwerden-Liste*. Weinheim: Beltz Test GmbH.

Conflict of Interest: The authors declare that the research was conducted in the absence of any commercial or financial relationships that could be construed as a potential conflict of interest.

frontiers in Physiology

ORIGINAL RESEARCH
published: 17 January 2020
doi: 10.3389/fphys.2019.01554

Heart Rhythm Analyzed via Shapelets Distinguishes Sleep From Awake

Albert Zorko[1], Matthias Frühwirth[2], Nandu Goswami[3], Maximilian Moser[2,3†] and Zoran Levnajić[1†]*

[1] Complex Systems and Data Science Lab, Faculty of Information Studies in Novo Mesto, Novo Mesto, Slovenia, [2] Human Research Institute, Weiz, Austria, [3] Physiology Division, Otto Loewi Research Center of Vascular Biology, Immunity and Inflammation, Medical University of Graz, Graz, Austria

Automatically determining when a person falls asleep from easily available vital signals is important, not just for medical applications but also for practical ones, such as traffic safety or smart homes. Heart dynamics and respiration cycle couple differently during sleep and awake. Specifically, respiratory modulation of heart rhythm or *respiratory sinus arrhythmia (*RSA) is more prominent during sleep, as both sleep and RSA are connected to strong vagal activity. The onset of sleep can be recognized or even predicted as the increase of cardio-respiratory coupling. Here, we employ this empirical fact to design a method for detecting the change of consciousness status (sleep/awake) based only on heart rate variability (HRV) data. Our method relies on quantifying the (self)similarity among *shapelets* – short chunks of HRV time series – whose "shapes" are related to the respiration cycle. To test our method, we examine the HRV data of 75 healthy individuals recorded with microsecond precision. We find distinctive patterns stable across age and sex, that are not only indicative of sleep and awake, but allow to pinpoint the change from awake to sleep almost immediately. More systematic analysis along these lines could lead to a reliable prediction of sleep.

Keywords: respiratory sinus arrhythmia, time series analyses, shapelets, onset of sleep, heart rate variability, logRSA

OPEN ACCESS

Edited by:
Tijana Bojić,
University of Belgrade, Serbia

Reviewed by:
Ronny P. Bartsch,
Bar-Ilan University, Israel
Markus Wilhelm Abel,
University of Potsdam, Germany

***Correspondence:**
Zoran Levnajić
zoran.levnajic@fis.unm.si

† These authors have contributed equally to this work

Specialty section:
This article was submitted to Autonomic Neuroscience, a section of the journal Frontiers in Physiology

Received: *27 July 2019*
Accepted: *10 December 2019*
Published: *17 January 2020*

Citation:
Zorko A, Frühwirth M, Goswami N, Moser M and Levnajić Z (2020) Heart Rhythm Analyzed via Shapelets Distinguishes Sleep From Awake. Front. Physiol. 10:1554. doi: 10.3389/fphys.2019.01554

INTRODUCTION

Determining the status of consciousness (being awake or asleep) is usually done in a sleep lab by sophisticated polygraphic recordings (Quintana-Gallego et al., 2004). Under real life conditions it would be preferable to do this online from automated analysis of vital signs recorded with minimally obtrusive sensor systems. In fact, several approaches have already been explored (Canisius and Penzel, 2007; Romine et al., 2019; Sadek et al., 2019) to achieve this. Various medical applications are easy to imagine, but perhaps more important are practical applications in which vigilance plays an important role. An obvious example is transportation, where the driver of a bus, train or a plane must stay awake at all times. Such an algorithm could be also translated into an alarm system that activates when the algorithm 'recognizes' that the driver is at risk of falling asleep. Statistics show that a significant number of car accidents were probably due to driver falling asleep (Horne and Reyner, 1995; Royal, 2003; Ftouni et al., 2012).

Any algorithm that automatically determines whether a person is awake or asleep (awake status) needs constant access to the body's vital signals. Those signals (data) should be processed continuously, so that patterns in the data that indicate sleep (or reduced vigilance) could be spotted immediately. Of course, the practical interest is to detect the change in consciousness status as soon as possible. Even more useful would be to *predict* the onset of sleep, so that the alarm can

be triggered in a timely manner. In such a setting, false positives (alarm goes off, but the driver is awake) are far less dangerous than false negatives (the opposite).

The precision in determining consciousness status involves two aspects: (*i*) correctly recognizing the onset of sleep or reduction of vigilance and minimize the rate of false positives (accuracy), and (*ii*) recognizing the onset as quickly as possible, or even better, predicting it. Both depend on the quality of available data as well as the sophistication of data analysis. A myriad of new data analysis approaches rose in the last decades in response to increased availability and richness of datasets in varying domains of society, science, and technology. Modern methods of time series analysis are able to identify, quantify and compare virtually any pattern of interest with great accuracy and even from noisy data (Richman and Moorman, 2000; Yaffee and McGee, 2000; Bevington and Robinson, 2003; Small, 2005; Bendat and Piersol, 2010; Grote et al., 2019; Zou et al., 2019).

Besides data analysis, quality of this determination will also depend on whether any prior data of vital signs for that person are available. Ideally, an algorithm should establish the status of consciousness without prior data from the same person, which is a very challenging task given that body processes related to falling asleep differ from person to person considerably (Ogilvie, 2001). In contrast, with the prior data available, the awake status will be identifiable faster and with better precision. Another factor is the presence of noise and incompleteness in the vital sign data: fortunately, these can be significantly reduced thanks to modern measuring equipment.

Which vital signal or signals are most useful for such an algorithm? The best choices to measure vigilance are vital signals that are easy to measure with good precision and signals that change in synchrony with the sleep and awake states or at least indicate a transition between these states. One such signal is the phase and frequency coordination (synchrony) between respiratory and heart rhythm known as *respiratory sinus arrhythmia* (RSA), which is observed in the sequence of time intervals between consecutive heart beats (Moser et al., 1994, 1995; Yasuma and Hayano, 2004; Bartsch et al., 2005; Denwer et al., 2007). Modern Holter (or similar) devices can measure RSA with microsecond precision, which more than suffices for application to the problem considered here (Lynn et al., 2013; Barrett et al., 2014; American Heart Association, 2015). Measuring RSA can be done with minimal hinderance of the person's normal activities by belt or glue electrodes from a unipolar ECG taken from the chest or hands. There are also other forms of coupling related to cardio-respiratory phase synchronization and cardio-respiratory time delay stability (Bartsch et al., 2014), but these involve the high resolution and synchronized recordings of respiration, which is usually not available in clinical settings. This suggests that RSA is a more suitable choice of vital data for our study, where we choose not to quantify vagal activity via RSA, but to investigate the similarity of sequences of HRV data carrying different amounts of RSA information.

But how to precisely define sleeping vs. awake from RSA data? The gold standard for determination of being asleep including sleep staging is polygraphy, including EEG, ECG, EMG, respiration, and movement sensors (Kaplan et al., 2017; National Institute of Neurological Disorders and Stroke, 2019). On the other hand, first bodily signs of sleep are shown at the autonomic level, as brainstem activity controls the sleep stages and the brain centers for respiration and circulation are anatomically close to sleep-induction centers. Additionally, heart and respiratory cycle are coupled differently during the sleep and awake states (Moser et al., 2006). While falling asleep, the heart rhythm gets gradually more modulated by respiration, which indicates increasing vagal control of the heart (Chouchou and Desseilles, 2014; Niizeki and Saitoh, 2018). This is illustrated in a sleep onset recording done on a 10-year-old boy (**Figure 1**), measured before and after falling asleep.

During deep sleep, heart and respiratory oscillations are maximally coupled to one another, which corresponds to maximal RSA and is a reliable indicator of autonomic regulation of sleep. RSA indicates the presence of strong vagal oscillations synchronous to respiration, which regulates (speeds up or slows down) the heart rhythm (Moser et al., 1994). The increase of cardio-respiratory coupling (the increase of order of RSA) is hence the first sign that the body is falling asleep. For the purpose of this work, we identify the onset of sleep with the onset of RSA. This onset is detectable from heart rate variability (HRV) data, which is the main topic of this paper.

However, identifying the onset of RSA from HRV data alone is challenging and requires a good choice of data analysis methods. In contrast to previous studies (Billman, 2011; Billman et al., 2015), rather than considering time and frequency domain parameters of RSA, we employ shapelet analysis, which has several advantages and was revealed as useful in analyzing biomedical data (Xi et al., 2006; Ye and Keogh, 2009; Hills et al., 2013, 2014; Rakthanmanon and Keogh, 2013). Shapelets are short segments of HRV time series that are repetitively compared to prior and past parts of the original time series. Their self-similarity and pairwise distances can be precisely classified, including the similarity to any pre-selected shapelet. Using this framework, we identify the shapelet whose distances to all other time intervals generates the best distinction between sleep and awake. We examine how this self-similarity changes as the subject transits from awake to sleep, which allows us to pinpoint the onset of sleep (change of consciousness status) with good precision.

The aim of this paper is to propose a new methodology for analyzing awake-to-sleep transition and discuss its merits for a practical and useful algorithm. We construct a shapelets-based method relying on standard approaches in non-linear time series analysis. Then, using the statistics of shapelet comparison, we define a similarity threshold that we show is a reliable indicator of the change of awake status. As an intermediate step in our analysis we identify the *best shapelet* – the most self-similar shapelet in the HRV time series – and show that its length is comparable to the multiple length of a typical respiration cycle. This confirms that HRV time series at the onset of sleep are most self-similar at the RSA time-scale, as expected from the definition of RSA.

To test our methods, we use the data from 75 healthy individuals of varying age and sex whose circadian (diurnal) 24 h HRV data were recorded with microsecond precision. Our data also include the self-reported information about when the

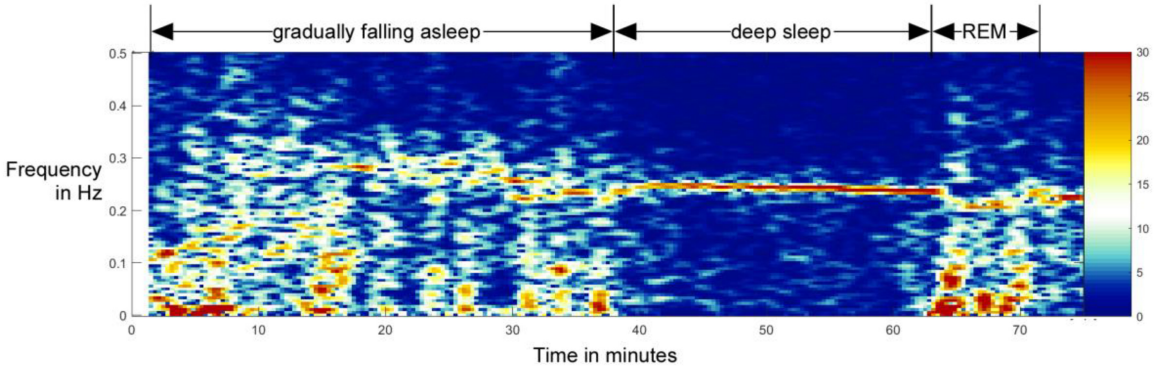

FIGURE 1 | Example of the transition from awake state to non-REM sleep and later to REM sleep in a 10-year-old boy. In this spectral analysis of HRV, one can clearly see the gradual formation and increase of RSA as a band around 0.25 Hz. Although the total activity is higher during awake state, the activity in the RSA band stands out during the non-REM sleep – falling asleep qualitatively resembles a phase transition normally studied in physics (Bartsch et al., 2012; Penzel et al., 2016). This process is reversed when entering the REM stage (from minute 63 on). This figure is not a part of the study reported in this paper, but it was done independently, as part of another study reported in Bonin et al. (2004).

subject fell asleep and when he/she woke up. This narrows our search since we look for the onset of RSA close to the time when subject declared going to sleep. We show that our method can pinpoint the change of awake status with a good precision using only HRV data – but of course, only as long as a representative sample of a person's 24 h HRV data was available. As our subject sample is relatively small, we were unable to make any substantial prediction of the onset of sleep. However, we were able to identify that a subject was asleep almost immediately after he/she fell asleep. We found that HRV self-similarity patterns relevant for this identification are fairly stable across age and sex. This suggests that a more systematic analysis with larger and more diverse sample sets could lead to automating this procedure, possibly even without prior data. Along the same lines, this is a step toward an algorithm for early-warning of falling sleep.

SUBJECTS AND MEASUREMENTS

Subjects

The data was collected within the setting of workplace-related health assessment. We made 24 h-measurements of HRV from 75 participants, 40 men (age 16–57, mean ± SD: 34.7 ± 11.0) and 35 women (age 16–56, mean ± SD: 37.0 ± 13.5). All subjects declared themselves to be in good general health, and with no prior history of cardiologic problems or other medical conditions that would influence heart or autonomic activity. Each subject agreed to wear a portable Holter monitor for an entire day, while carrying on with his/her routine activities on that day, including sleeping during the night. Subjects had given their written consent to participate in the study beforehand and received feedback on their results after completion. The study protocol complied with the guidelines of "good clinical practice" (ICH-GCP) following the declaration of Helsinki and with the regulations of the National Data Protection Act (Section 14 Abs. 1DSG 2000). Since this study involved only healthy subjects without endangering their health, and since it involved no medical diagnoses, interventions or treatments, according to the local legislation in Austria the study did not require an approval from the University's ethics committee.

Heart Rate Variability Measurements and Data

We used a single-channel high-precision ECG monitor (ChronoCord[1], 7th generation, Joysys, Weiz, Austria, sample rate: 8000 Hz, resolution: 16 bit) (Joysys, 2018) to continuously record intervals between heartbeats (Noble et al., 1990; Gallasch et al., 1996, 1997; Pinnell et al., 2007; Surawicz and Knilans, 2008). For the continuous measurements, three adhesive electrodes were applied on the trunk of the participants (sternum, 5th left intercostal space, and a reference electrode on the right side of the trunk between 11th and 12th rib) (Klabunde, 2012; Medical Training and Simulation LLC, 2017). The device was then attached to a belt or the waistband of the subject. During a 24-h period, the device assessed the intervals between heart beats with precision of several microseconds. Data have been stored on an SD card for further evaluation. The subjects were instructed to note the time of light off in the evening and light on in the morning as a best available proxy for falling asleep. Heart beats were detected from ECG by device during recording. For further analysis, they were expressed as R-wave-to-R-wave (RR) intervals (time intervals between two consecutive R waves of heart beat) (Amani et al., 2011). Smaller (respectively, larger) RR values indicate that heart works faster (respectively, slower; Hurst, 1998; Iaizzo, 2005). After the measurements were completed, we extracted for each person the time series (sequence) of RR values. Each of these 75 time series contained about 110,000 RR values. For easier interpretability and with no loss of generality we converted the data from RR intervals to heart rate, expressed in beats per minute (b/min). To reduce above described errors, we removed RR values that were smaller than the minimum ECG

[1]We confirm that we have obtained the permission from the copyright holder of this device to use the name of the device (ChronoCord) in this manuscript.

value (40 bmp) or higher than 180 bmp, in accordance with the standard procedures in medical sciences (Perski et al., 1992; Krul et al., 2013; Sarzynski et al., 2013). This resulted in removal of the 0.63% of the data (basically negligible).

Preliminary Analysis

We first show some sample results to better illustrate the data. In **Figures 2A–D** we show four examples of HRV beat-to-beat time series. The values of heart rate (in bpm) are shown as function of time during 24 h of recordings. We show two typical examples for younger subject (male and female, above) and two for middle-aged subjects (below). We indicate in each plot the part of the day when the subject slept (according to self-reported information). In general, the heart beats faster (higher bpm) when a person is awake compared to asleep. While sleeping, heart beat meta-oscillations seem steadier than while awake, especially during non-REM phases. These meta-oscillations indicate autonomic nervous system activity (Moser et al., 1994, 2008) mediated via vagal and sympathetic branches to the sinus node. All plots display quite intense fluctuations during the entire 24 h, which is somewhat more prominent for younger subjects.

In **Figures 2E,F** we show scatter plots of mean heart rate (HR, shown on y) vs. age (shown on x), for male and female subjects, respectively. Sleep and awake mean HR are calculated separately for each subject (according to self-reported information) and shown by different colors in each scatter plot. Clearly, the heart on average beats slower while asleep. This preliminary analysis shows that while there are qualitative differences in heart activity between sleep and awake, determining the status of consciousness from HRV alone is not sufficient, since none of these simple parameters discriminate it precisely. This stresses the need for more sophisticated data analysis approaches, to which we devote the rest of this paper.

SHAPELET ANALYSIS

In this section we introduce shapelet analysis as our main methodological tool (Xi et al., 2006; Ye and Keogh, 2009; Hills et al., 2013, 2014; Rakthanmanon and Keogh, 2013). In general, our approach belongs to unsupervised learning from data (James et al., 2013; Längkvist et al., 2014; Celebi and Aydin, 2016). We search for the best way to divide a time series in two parts (classes) such that self-similarity of the time series is maximal within each class, and minimal between the classes. In fact, a long-standing challenge in time series classification is how to find the most efficient measure of similarity between two (or more) time series or parts thereof. Many methods in the literature strive to meet these criteria (Kin-Pong and Wai-Chee Fu, 1999; Costa et al., 2005; Liao, 2005; Aboy et al., 2007; Ding et al., 2008; Batista et al., 2011; Yentes et al., 2013), including shapelet analysis, which we chose for its good record in recognizing physical activities from biomedical time-resolved data. In this regard, shapelet analysis is conceptually somewhat similar to wavelet analysis (Daubechies, 1992). Shapelets rely on a simple quantification of similarity/difference between time series, they are fast to compute and provide easily interpretable results with very good accuracy. We developed our own programing codes for the entire analysis that follows without resorting to any specific software.

What Are Shapelets?

We explain the concept of shapelets by referring directly to our HRV data. We take a time series of RR values (similar analysis could be done with time series of frequencies). We decompose this time series into *segments* (chunks) of 2 min in length (duration). That yields about 700 segments during 24h, depending on the subject. We assume that at least qualitatively, the heart activity does not drastically change within 2 min, i.e., that it is (relatively) stationary during each segment[2]. This is our starting resolution to detect changes of the consciousness status.

Now we consider one 2-min segment and divide it into smaller parts that we call *shapelets*. In other words, a shapelet is a short sub-interval of a 2 min segment and hence of the original 24 h time series. When dividing a segment into shapelets, we do so in three ways:

- Division into two equal halves, each 1 min long ("level 1"),
- Division into four equal quarters, each 30 s long ("level 2"),
- Division into eight equal eighths, each 15 s long ("level 3").

So, each following level is made of shapelets with half-length of the previous level. At level 1 we obtain 2 shapelets from each segment, each covering a half of the segment, without overlapping. Similarly, at levels 2 and 3 we obtain 4 and 8 shapelets, respectively, jointly covering the entire segment, without overlapping. Besides this main division, at each level we also consider an additional set of shapelets, obtained by shifting the shapelets by half-length at that level. That is to say, at level 1 we obtain one additional shapelet of 1 min length, which is centered at mid-point between the two main shapelets. Similarly, at levels 2 and 3 we obtain 3 and 7 more shapelets, respectively, centered at mid-points between the main set shapelets at each level. We clarify this scheme by illustration in **Figure 3**, where different shapelets are illustrated by varying tones of gray. We considered additional levels of division, but found them not to contribute to the results: heart activity varies too much on the time scale above 2 min, while below 15 s the resolution becomes too poor. We also examined shapelets down to 1/128 of segment and found no improvement of results.

Choosing the shapelet level defines the resolution of our analysis. For example, at average respiratory rates during sleep, one shapelet of level three will contain about 3–4 respiratory cycles of 4 s duration. Selecting one of the possible resolutions, we can divide all segments of a given time series into shapelets. We can do that also for all levels, obtaining a large ensemble of shapelets, to which we refer as *pool of shapelets*.

Measuring Distances Between Shapelets

Since we wish to construct a framework for comparing time series (or parts of them, shapelets and segments), we next introduce

[2]Choice of 2 min as the fundamental segment length is somewhat arbitrary. This choice involves two factors. Too short segments increase the computational cost, while too long segments deteriorate the resolution of analysis. By carrying out the shapelet analysis (described in rest of the manuscript) we found 2 min to be the best compromise.

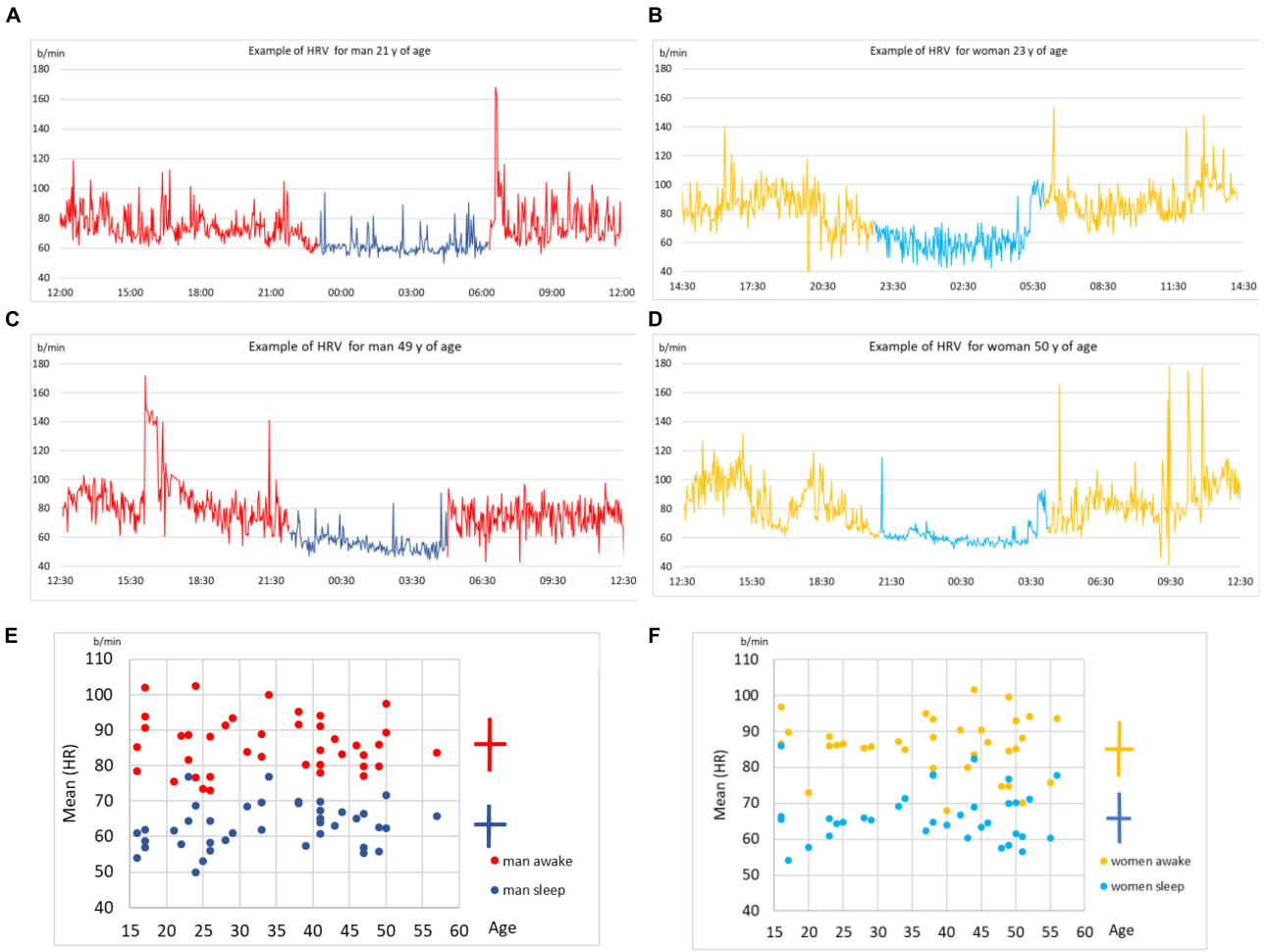

FIGURE 2 | (A) Time series of beat-to-beat HRV data (heart rate as function of time) over a day (24 h) for a male subject, 21 years of age. Part of the day when the subject slept is indicated in blue (self-reported information). **(B)** The same data but for a female subject, 23 years of age. **(C)** The same data for another male subject, 49 years of age. **(D)** The same data for another female subject, 50 years of age. **(E)** Scatter plot of age (shown on *x*) vs. mean heart rate (HR, shown on *y*) for all male subjects in our sample. Each male subject is represented as two points, one for sleep mean HR and the other of awake mean HR. Mean value and standard deviation are indicated by the cross symbol next to the scatter plot. **(F)** The same as in **(E)** but for all female subjects in our sample.

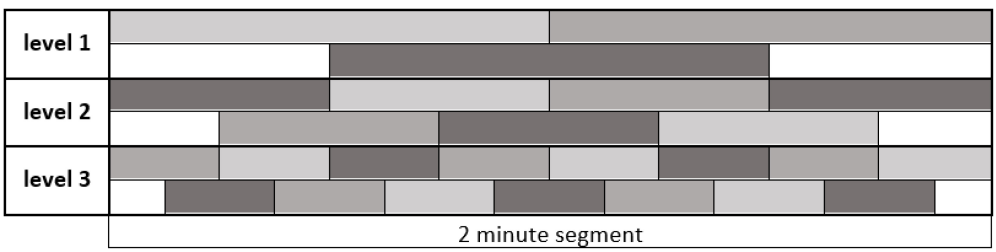

FIGURE 3 | Dividing a 2 min segment of the original 24h time series into shapelets. The length of the entire interval in figure is 2 min, as indicated. Each level contains equally sized adjacent shapelets without overlapping. The original set of shapelets is illustrated as the top sequence at each level. Additional set of shapelets obtained by shifting by half shapelet length is illustrated as bottom sequence at each level. For clarity, shapelets show different shades of gray. In later computations we consider all these shapelets equally, no matter to which level they belong. We call 'pool of shapelets' this entire ensemble of shapelets cumulatively.

a distance between a shapelet and a segment. Segments and shapelets can be seen as two time series of different length (duration): a segment is always 2 min long, while shapelet length depends on the level (15 s, 30 s, or 60 s). We first equip ourselves with a measure of similarity between a pair of time series of equal length. We adopt the general Euclidean measure and define the

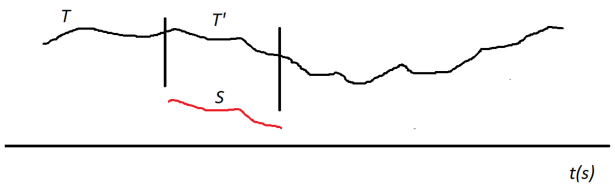

FIGURE 4 | Searching for best matching location between the shapelet *S* (red) and the segment *T* (black). Shapelet is translated (shifted) along *T* from the start to the end, step by step (point by point). At each location we measure the distance *D* between *S* and the corresponding chunk (sub-segment) of the whole segment *T*, which we generically denote with *T'*. The length of *T'* is always equal to the length of *S*. In this illustration the best matching location of *T'* is shown, where the distance *D* is minimal. This minimal distance *D* is then taken as the distance δ between *S* and *T*.

distance D between time series T_1 and T_2 as (Faloutsos et al., 1994; Goldin et al., 2004; Deza and Deza, 2009):

$$D(T_1, T_2) = \sqrt{\sum_i (x_i - y_i)^2},$$

where x_i are the values belonging to the time series T_1, and y_i to the time series T_2. The sum runs along the index i for the entire length of T_1 and T_2. Distance D is zero if the time series are identical to one another at each point. In any other case the distance is greater than zero.

Now we generalize this into a distance between a shapelet and a segment called δ. Let us (generically) denote the shapelet with S and the segment with T. Based on the above definition of D, we introduce δ by aligning the shapelet's first data point with the segment's first data point. When S and T are positioned like this, we can use D to measure the distance between S and the initial chunk (sub-segment) of T that is of the same length as S (we denote this chunk with T'). This will yield some value for the distance. Now we shift S along T by one data point (toward later time). S is now aligned with a different chunk of T (which overlaps with the previous chunk except in one point on the left and one on the right). We measure that distance and obtain a new value. We keep repeating this procedure: translate (shift) S along T point by point and measure the distance D at each step. We finish this when the end point of S aligns with the end point of T. The process is illustrated in **Figure 4**. We now define the distance δ between S and T simply as the minimal distance found during this shifting process (Xi et al., 2006; Ye and Keogh, 2009; Hills et al., 2013):

$$\delta(S, T) = \min_{T'}[D(S, T')].$$

Here, we denote with T' the consecutive chunks of the segment T, so that δ is the minimal distance D when all possible T' are considered. Thus defined δ meets the requirements for distance in the mathematical sense.

Note that this minimal distance is found when S is aligned with a specific chunk of T. In other words, the distance δ between S and T is actually the distance D between S and the chunk of T that is *most similar* to S. Therefore, there is a specific *best matching location* for S along T, at which it overlaps with chunk T' to which it has minimal distance, as illustrated in **Figure 4**. So, when some S and some T are close, it means that T includes a chunk that is very similar to S. Note that the interpretation of δ also depends on the level of shapelet S. It is easier for δ to be small when S is short.

Now, for each member in the pool of shapelets we can measure the distance to all segments in the time series. Note that the distance between a shapelet and the segment to which it belongs is always zero, for all levels. Shapelets having small distances to other segments will be more "characteristic" for that time series. For example, shapelets belonging to sleep segments will typically have small distances to other sleep segments, since many HRV patterns recur during sleep. Similarly, "awake" segments will typically be similar to other awake segments. The relevance of these distances can be tuned by varying the resolution, i.e., changing the shapelet level. This property can be used to put together all segments belonging to sleep in one class and segments belonging to awake in another class, i.e., make classification of segments.

Circadian (Diurnal) Patterns in Heart Rate Variability Data From Shapelet Distance Matrices

We next look at all-to-all distances between segments (for simplicity we call it distance between segments, even though by definition the distance is measured only between a shapelet and a segment). We create a matrix of distances between all pairs of segments as follows. We take a shapelet from the first segment of the measurement, and calculate the distance from that shapelet to all other segments in 24 h. These values fill up the first row in our matrix. Then, we take a shapelet from the second segment, and calculate the distances to all other segments in 24 h, filling up the second row in our matrix. Repeating this process, we arrive to the last segment and pick one of its shapelets, whose distances to all other segments fill up the last row in our matrix. Note that this is a square matrix and its size is the number of segments in 24 h. In our matrix, the element i-j reports the distance from a shapelet belonging to the i-th segment to the j-th segment (which we here confuse with the distance between i-th and j-th segment). Meanwhile, the element j-i will report the distance from a shapelet belonging to j-th segment to the i-th segment. Note that this matrix is not (necessarily) symmetric, since it depends on the choices of shapelets. However, in further analysis this matrix will be considered as symmetric, since our calculations indicate that this non-symmetry mismatches are negligible.

This setup depends on the choice of shapelet, specifically since we wish our distances to be interpretable as distances between pairs of segments. To this aim we consistently take an equivalently positioned shapelet in every segment. Specifically, we chose the last one in the first row of level 2 (cf. **Figure 3**). We tried several options for this analysis and this choice gave the most interpretable results (we do not report the entire choosing procedure).

Proceeding with the computations as described above, we obtain a distance matrix for each subject. We represent it as a heat-map (color-map), where the color in each matrix element

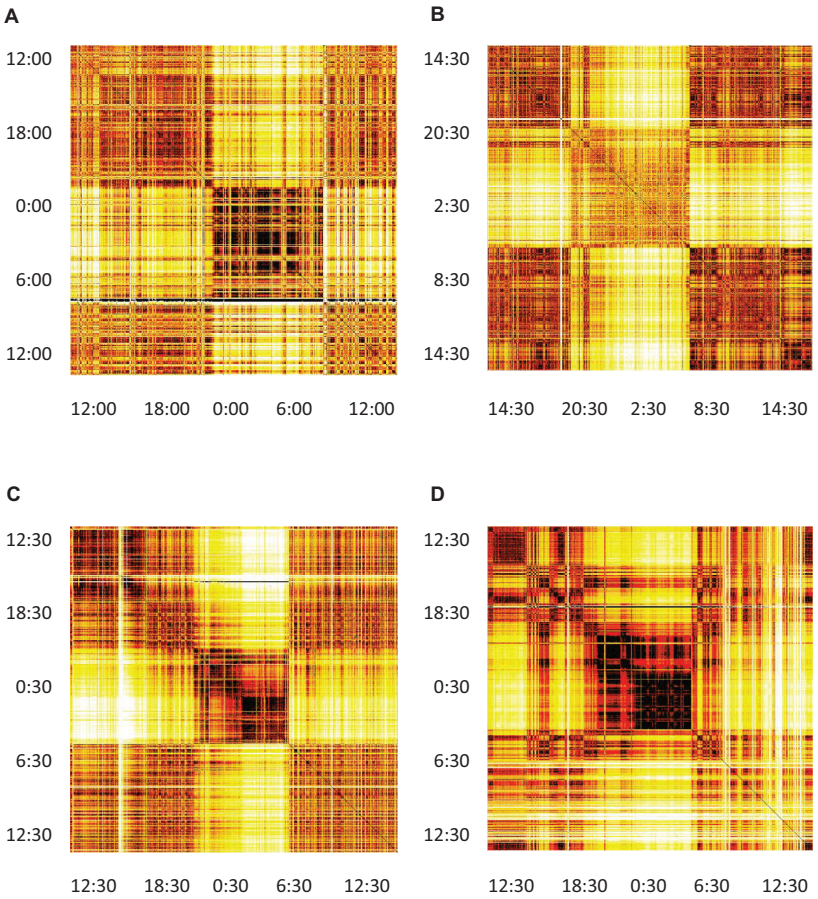

FIGURE 5 | Distance matrices for four selected subjects visualized as heat-maps. **(A)** Male subject, 21 years of age, **(B)** Female subject, 23 years of age. **(C)** Male subject, 49 years of age. **(D)** Female subject, 50 years of age. All matrices have 24 h of measurements indicated both horizontally and vertically. The color of each matrix element indicates the distance between the two segments, identifies as *x* and *y* coordinate of that matrix element (we neglect the asymmetry of this matrix, see section "Discussion" in the text). Darker colors represent shorter distances and brighter colors larger distances, so that darker cells indicate that two segments have similar heart activity, while brighter colors connect segments with different heart activity. It can be noted that sleep shows more self-similarity than awake.

i-j indicates the distance between the i-th and j-th segment. In **Figure 5** we show matrices for the same four typical subjects from **Figure 2**. All matrices offer a clear picture of sleep/awake difference: (almost) all sleep segments are similar to most other sleep segments (dark), but different from most awake segments (light), with corresponding comparisons obtaining for awake segments. The timing of falling asleep and waking up can also be identified for all four subjects and it agrees well with the self-reported information. Some qualitative patterns vary between younger subjects (top two panels) and middle-aged subjects (bottom panels). Of course, segments that are far apart have different heart activity, whereas those that are close have similar heart activity. In addition to the main sleep and awake stages, we see many short periods of opposite stage within both sleep and awake. For example, the person can relax or "take a nap" for a short period of time during the day, which is visible as different coloring within otherwise awake stage. Similarly, shallow sleep, arousals or even shortly waking up is seen in all panels. Interestingly, besides these intermittent changes of status, sleep state shows distinct patterns that might reflect various sleep phases (REM vs. deep sleep). This suggest the presence of short arousals/awakenings during sleep, possibly in relation to (Dvir et al., 2018).

DETERMINING THE ONSET OF SLEEP VIA BEST SHAPELET

We now extend the above analysis and construct a method to pinpoint precisely the onset of sleep using shapelet analysis. That amounts to finding in a time series the point (or points) during 24h where the time series (heart activity) qualitatively changes the most. We can safely claim that these points correspond to the changes of awake status. Namely, since the subjects observed their normal daily routines (refraining from sport and exercises) we do not expect these changes to reflect anything else. There are at least two such points in 24 h, one for falling asleep and one for waking up. However, as noted earlier with **Figure 5**, there could be more such points. In practice, we wish to classify all 2 min segments into two distinct groups based on the similarities of their time

series patterns quantified via shapelet analysis. These two classes should (roughly) correspond to the parts of distance matrices colored differently. Note that this information on the onset of sleep will be *independent* from the self-reported information.

Identifying the Best Split Point Between Sleep and Awake

Below we describe our procedure step by step. First, we take one shapelet, belonging to any segment and any level. We compute the distance δ from this shapelet to all segments in the time series. We put all those distances in a histogram. An example for a typical subject is shown in **Figure 6**. In such a histogram, small distances will cluster in one (or more) peaks near zero, whereas large distances will accumulate in other peak(s) away from zero. In fact, such grouping is seen in **Figure 6**, one peak around 0.03 and the other around 0.45. The reason for this grouping is clear: segments with short distances are chiefly those belonging to the same consciousness state as the chosen shapelet (sleep, for illustration), whereas segments with large distances are by and large belonging to the opposite state (awake, for illustration). What we want in our histogram, is that these two peaks are as separated as possible, so that the corresponding segments can be classified in two distinct groups as clearly as possible.

How to split the histogram into two optimally distinct parts? In formal terms we are looking for the *optimal split point*: the point on the horizontal axis at which the histogram can be most meaningfully divided into two parts. This is an optimization/classification problem that can be approached in several ways. We resort to information theory (MacKay, 2005; Cover and Thomas, 2006; Delgado-Bonal and Martín-Torres, 2016) and proceed as follows. We examine a tentative split point between two adjacent bins and compute the *information gain* (*IG*) for the corresponding division. *IG* quantifies how meaningful it was to split the histogram this way. To compute *IG* we label the two classes of segments with A and B. Segments with distances smaller than the split point belong to class A, and segments with larger distances to class B. To compute *IG*, we first define the *entropy E* of such a division as (Uğuz, 2011; Sonka et al., 2015; Shapiro, 2019):

$$E(D) = -p(A) \cdot \log_2(p(A)) - p(B) \cdot \log_2(p(B)).$$

Proportions of the segments in class *A* and B are *p(A)* and *p(B)*, respectively. We have $p(A) + p(B) = 1$. That is to say, for each division of segments into two classes, we can define the entropy *E* of such a division via the above formula. Naturally, the above defined entropy is maximal when the segments are split in two equal classes, while it is minimal when all segments are in one class and none in the other class. Entropy will be used to determine information gain.

Before proceeding further, we recall that sleeping and awake segments are not homogeneous time-wise, since subjects can briefly change their consciousness status during "formal" sleep and awake. However, we are interested in distinguishing the sleep from awake states, regardless of when and in how many pieces it occurs. That is to say, "taking a nap" during the day is to be classified as sleep. A typical situation is illustrated in **Figure 7**.

Still, our focus is determining the onset of the real sleep, when the subject intentionally fell asleep. Namely, other changes of the awake status are not intentional and it is not clear how will they be reflected in the data. Hence, our next step is to improve the way we determine the optimal split point by including the self-reported information.

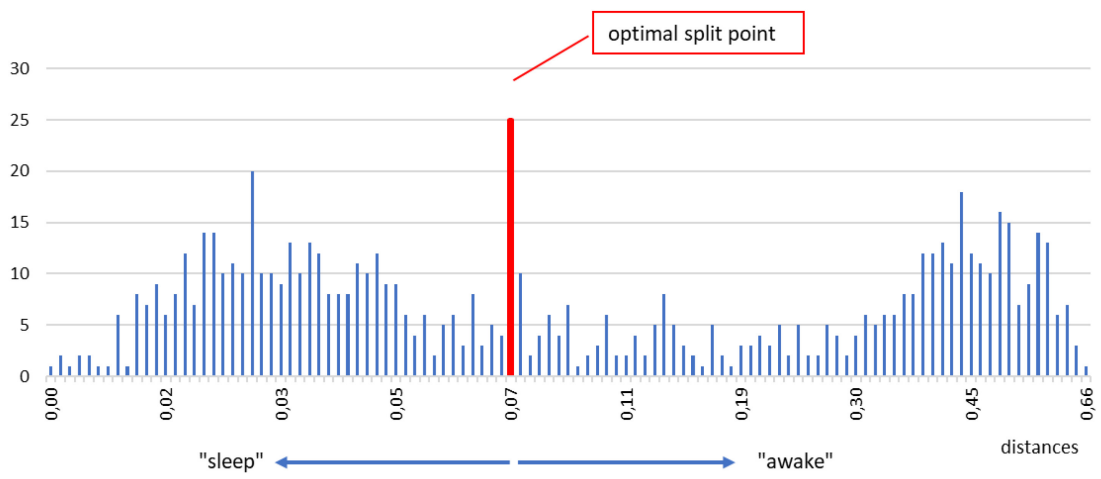

FIGURE 6 | Example of a histogram of all distances between the selected shapelet (taken from sleep, just for illustration) and all segments in a time series. Two main peaks mentioned in the text are visible, one for smaller distances, one for larger distances (denoted as "sleep" and "awake" for easier orientation). To find the optimal split point we test all tentative split points between each two histogram bins. We do so by computing the information gain corresponding to each tentative split point and choose the one that gives the best (maximal) information gain. The optimal split point for the histogram above is marked by a vertical red line. Segments whose distances are smaller (respectively, larger) than the optimal split point are defined as belonging to the first (respectively, second) class. After repeating this procedure for the entire pool of shapelets we define the best shapelet as the one, whose optimal split point gives the maximal information gain. We call this best split point and consider it the output of our method for determining the onset of sleep.

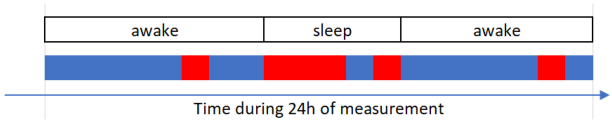

FIGURE 7 | Conceptual (illustrative) representation of the classification of segments. Red and blue lines represent sleep and awake stages, respectively, obtained via our classification. Self-reported information is indicated in boxes. Actual sleep and awake stages overlap only partially with the stages as reported by the subject.

Considering a tentative split point, most segments classified as A belong to either self-reported sleep or self-reported awake stage. Let us assume for a moment that A belong to sleep. Then, most segments classified as B will belong to self-reported awake, but not all (see **Figure 7**). Similarly, there will be some segments classified as A, which will according to self-reported information belong to awake. We wish our optimal split point to account for this as best possible. We want to minimize the number of "misclassified" segments, or at least to have them as similar as possible to "correctly" classified segments of the same kind. In other words, we want to improve the information provided by the subject. We thus define *IG* starting with the general formula (Mitchell, 1997; Carmel et al., 2002; Ye and Keogh, 2009; Rakthanmanon and Keogh, 2013):

$$IG = E(D)_{before} - E(D)_{after},$$

which states that *IG* is the difference in entropy before and after the splitting. More precisely, *IG*, as the difference of these two entropy values, is also weighted average entropy of both subsets after splitting, and can be expressed via formula:

$$IG = E(D) - \frac{n_{awake}}{n_{total}}{}^{*} E(D_{awake}) - \frac{n_{sleep}}{n_{total}}{}^{*} E(D_{sleep}).$$

Here, E(D) is calculated via previous formula, n_{total} is the total number of segments in 24h, n_{awake} and n_{sleep} are the total number of segments classified in the class where majority of segments, respectively, belong to awake and sleep according to self-reported information. Values $E(D_{awake})$ and $E(D_{sleep})$ are obtained by considering the fact that "misclassified" segments represent a splitting of its own within self-reported sleep and awake stage. Hence, we calculate them using the earlier formula for Entropy, but now considering "correctly" classified vs. "misclassified" segments.

To sum up, for any tentative split point, *IG* quantifies how much are we better off considering that split point than self-reported split point. Then, the *optimal* split point is defined as the one for which the information gain is maximal. Such split point represents the best improvement of information obtained via splitting with respect to the self-reported information. With this in mind, we try each tentative split point, calculate the *IG* associated with it, and identify the split point leading to maximal *IG* as the *optimal split point*.

Furthermore, we note that the above procedure allows us to find the optimal split point for any shapelet in the pool of shapelets. Each optimal split point comes with its own *IG*. But these values of *IG* can be compared, and in particular, the maximum among them can be identified. We call it *best split point* and the shapelet corresponding to it the *best shapelet*. It is the shapelet whose optimal split point comes with the maximal *IG* compared to IGs associated with all other shapelets. Such shapelet provides a natural way to divide the original time series into two groups (classes) of segments with qualitatively distinct properties. It is in accordance with the best shapelet that we make the definite classification of segments into sleep and awake in what follows.

But before proceeding, we note that the above procedure could depend on the choice of bin size in our histogram. A histogram bin may be larger or smaller, so to test how appropriate was our choice, we employ the Levene's test (Bland and Altman, 1996; Zimmerman, 2010; NIST, 2017). This test will assess the equality of variances for two groups with respect to bin size. The first group consists of 1%, 2%, 3% grades and the second 10%, 20%, 30% grades. Data in first group and in second group have different variance (p-value 0,029). Next we perform the Levene's test and establish the difference in variance of group with histogram resolutions (1%, 2%, and 3%). In short, we found that the choice of bin size plays little or no role for our analysis. To close this description, we illustrate this entire procedure in a block diagram for easier orientation.

Classification of Time Series via Best Shapelet

To illustrate the classification into sleep and awake via best shapelets we consider the same four subjects as in **Figure 2**. Of course, computation on each of their HRV data leads to a different best shapelet, characteristic for their time series. We obtain the classification as described above explained in more details in **Figure 8** and show the results in **Figure 9** (left panels). Consciousness status determined by our approach is shown vertically (red line) as a function of time during 24 h. The green dashed line denotes the self-reported information. Our method correctly indicates that the subject is sleeping when (most likely) he/she is indeed sleeping, with some exception in **Figure 9A**, where the subject has had somewhat erratic sleep. In contrast, awake status is determined less precisely, since we see many intermittent intervals of sleep stage, which possibly account for subject relaxing or resting with reduces vigilance. Actually, this "conservatism" in establishing wakefulness is desirable in the context of, for example, traffic applications, where one needs an alarm system that goes off at the initial stage of fading vigilance.

To see how our method's output aligns with shapelet distance, we show the distance from the best shapelet for the same four subjects in **Figure 9** (right panels, blue line). Noisy profiles are smoothed for better clarity (black line). Indeed, the first subject seems to have had "shallow" sleep, as his heart activity seems less qualitatively different during sleep. This conclusion comes from observation that even the best shapelet was not discriminatory enough to establish a clear separation in distance statistics, which explains why the method found his sleep to be less stable. However, even in this case, our method identified many (potential) changes of awake status, even if some of them

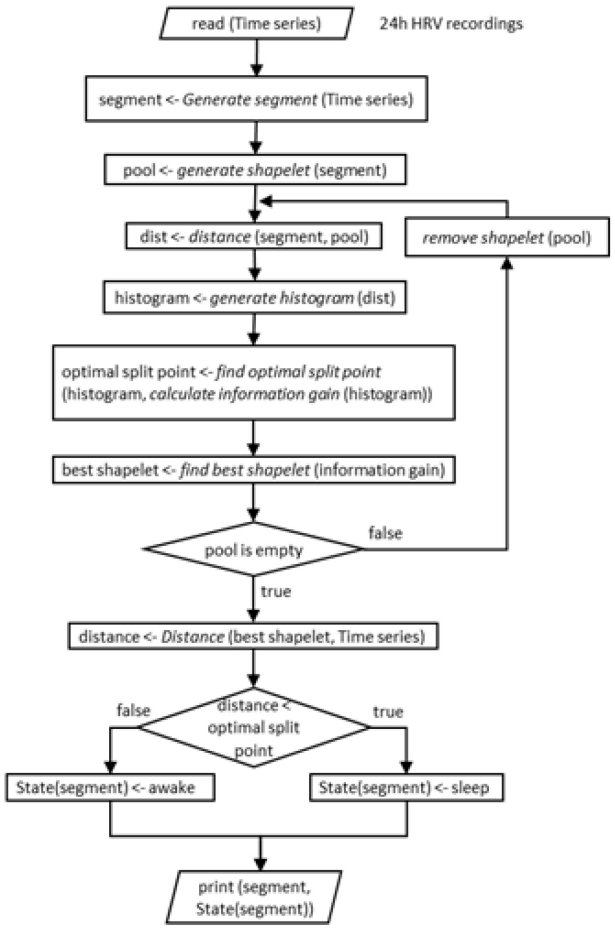

FIGURE 8 | Schematic representation (block diagram) of the entire procedure of our shapelet analysis and identification of best shapelet. It is shown here for easier orientation. Illustration is again done for a shapelet selected from sleep.

are identified incorrectly. Other subjects' sleep was more stable, as correctly found by our method. This confirms that our method is made to indicate awake status only when that status is perfectly clear and that all intermediate stages of subject's consciousness are defaulted as sleep.

Pinpointing and Predicting the Onset of Sleep

The simplest way to put our method to practical use is to make the alarm go off each time the above analysis indicates that the subject is asleep. Since our method robustly predicts wakefulness, we can reliably claim that a subject is indeed awake whenever our method indicates him/her to be awake. In formal terms this means we have many false positives – instances of the method indicating sleep while subject is (most probably) awake. Of course, from the practical viewpoint, false positives are more desirable than false negatives – instances when the method indicates wakefulness while the subject is asleep. Nevertheless, for our method to be of practical use, we need to examine how false positives can be reduced. To this aim we study more closely the performance of our method in the vicinity of the onset of sleep. We report again the data from **Figure 9** but this time zooming to the time window of 2 h around the self-reported time of falling asleep (1 h before and 1 after). The results are shown in **Figure 10**, where we magnify the information from the panels on the left side of **Figure 9**, around the onset of sleep. Recall that this determination of awake status is independent from subject's self-reported information. For the case (a), our method indicates that subject is classified asleep much before he reported to be asleep. While such a conservative determination is in principle desirable for practical purposes, this situation is a false positive that can hinder the operation of the alarm system. On the other hand, our method performs best in case (c), where the subject's status comes out as awake almost entire actual awake time and as sleep almost immediately after the subject (most likely) fell asleep. Cases (b) and (d) are again showing the conservative performance of our method, indicating that subjects are asleep before they (most likely) were actually sleeping. This could be due to them relaxing for the bed time, which is reflected in their cardiorespiratory interaction that gradually becomes more "sleep-like." Nevertheless, in the context of realistic applications of our method, excessive relaxation can lead to fading of vigilance so triggering an alarm in such a situation could be a good strategy.

To further improve the precision of detecting the exact moment of fading vigilance, we note that above results are obtained using *only one* shapelet. And even if this shapelet is the best shapelet, it is likely that classification via other shapelets will also contain useful information. Therefore, it makes sense to average the results obtained via several different shapelets (not necessarily best), expecting that each of them (depending on its size and position) will contribute additional information. To this aim we re-do the analysis from **Figure 10**, but now we average over 50 randomly chosen shapelets. Randomization is done not just via level, but we also introduce a random shift (not just half length as in **Figure 3**), and take shapelets from random location during 24 h. Averaging over all 50 thus obtained classifications, we obtain the results shown in **Figure 11**, where consciousness state is a continuous value ranging between 0 (sleep) and 1 (awake). Lines, colors and time window are as in **Figure 10**.

This insight clearly gives more flexibility in determining the consciousness status. For example, one could adjust the alarm to go off at a prescribed value between 0 and 1, when the vigilance level is deemed too low. Note that pure sleep and awake in these plots mean that almost all 50 shapelets indicate them as such, which offers a more stable classification. But still, confronting with self-reported information (green curve), the actual correlation is weak. This suggests that focusing on the timing of the onset of sleep might not be so useful for practical applications. Perhaps simply quantifying the vigilance might be a better defined and more useful problem to solve. We carried out the same analysis for all 75 subjects in our sample. Findings were similar to the four representative subjects in above two figures. Our method is systematically quick to signals sleep. What is also very clear, is that the heart activity at the onset of sleep strongly

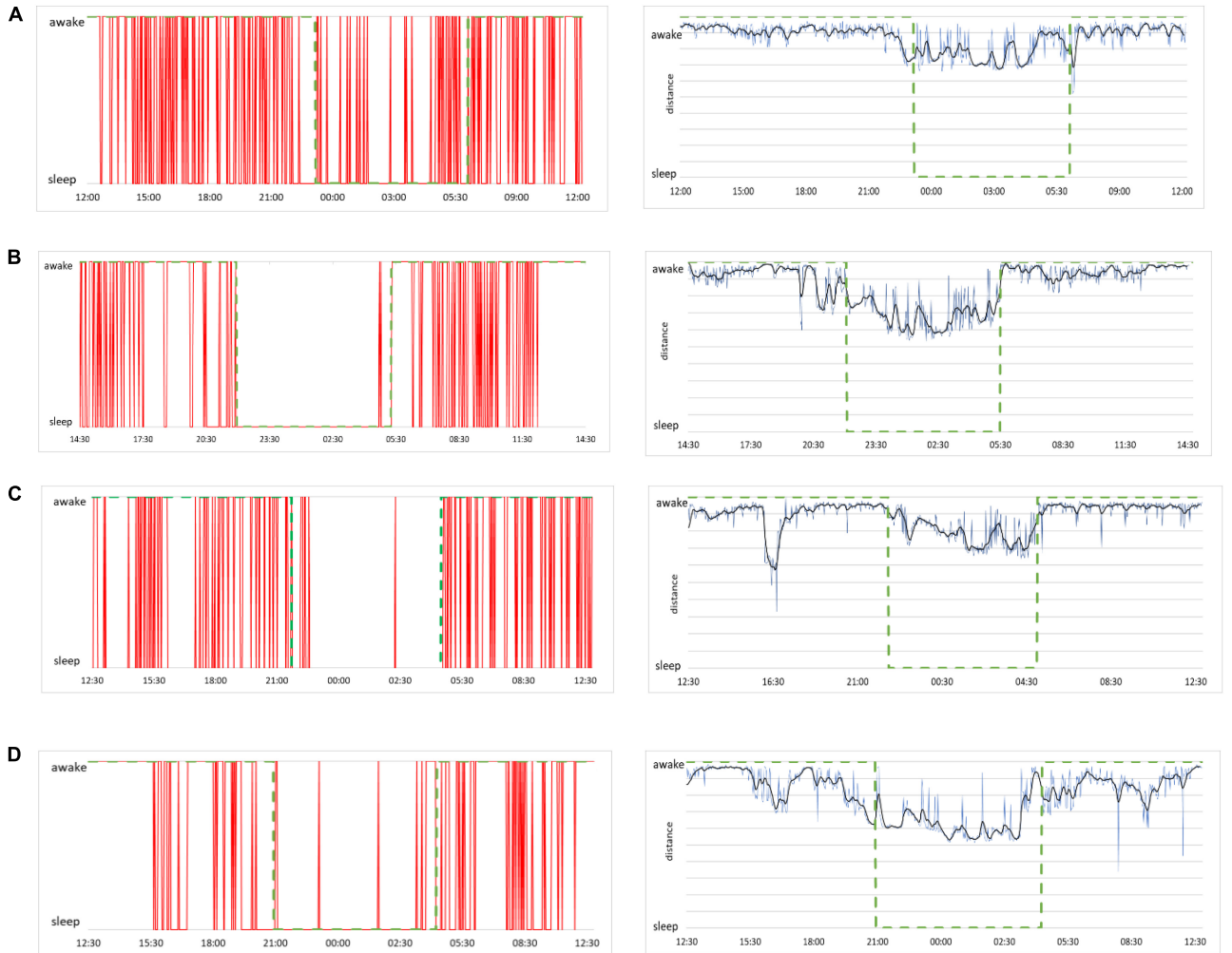

FIGURE 9 | (**A**, left) Sleep and awake stages determined by our method for the case of a male subject, 21 years of age. Red lines indicate consciousness status as a binary value (sleep or awake) as a function of time over 24 h of measurement. (**A**, right) Raw data of distances from the best shapelet as function of time for the same subject (blue line), smoothed via Butterworth filter (black line) for better clarity. Green dashed line shows the self-reported information in both plots. **(B)** The same plots for a female subject, 23 years of age, **(C)** a male subject, 49 years of age, and **(D)** a female subject, 50 years of age.

depends on the particularities of each individual. Universal trends that could be used to standardize our method are very hard to find.

We next examine how good our method is in predicting (anticipating) the moment of a subject falling asleep. It is clear from the previous figure that this is hard, since at the onset of sleep our method indicates frequent transitions between sleep and awake. Yet for practical purposes the first such transition is important, since it suggests that the subject is definitely less vigilant, if not already asleep. Hence, we use our method to approximate the time of falling asleep as follows: We take the self-reported time of falling asleep and search for the nearest continuous interval composed of at least five consecutive segments of sleep (10 min). The beginning of such an interval is taken as the approximation for the time of falling asleep. If subject falls asleep exactly as he/she has indicated, the values will coincide. Now, we scatter plot the self-reported time of falling asleep against the time approximated as just described. The results for men are shown in **Figure 12A** and for women in **Figure 12B**. In most cases our method correctly identifies the transition (almost) immediately after it has occurred or even slightly before. However, in some cases our method is significantly too early or too late in determining the onset of sleep. As already discussed, that is due to large differences in sleeping transition from person to person. Our method (at this stage of development) is not sensitive to it. Yet, the fact that most subjects still lie along the diagonal is a promising sign. Our approach can, at least in principle, establish the onset of sleep for man and woman of any age and confirms that the increase of cardiorespiratory interaction starts before sleep occurs.

To finalize our analysis, we define a measure to quantify the discriminative power of our shapelet-based classification. To this end we consider again the histogram of distances from

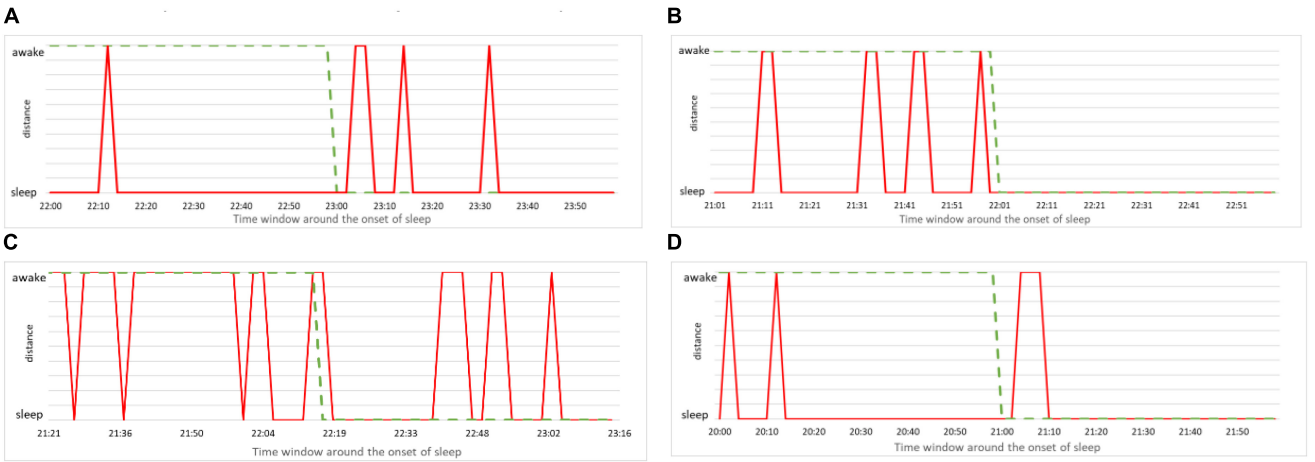

FIGURE 10 | (A) Zoom to the onset of sleep for male subject, 21 years of age. Red line indicates the consciousness status determined by our method as a binary value (sleep or awake) within time window of 1 h prior and 1 h after the self-reported time of falling asleep. Green dashed line is the self-reported information. **(B)** The same for female subject, 23 years of age. **(C)** The same for male subject, 49 years of age. **(D)** The same for female subject, 50 years of age.

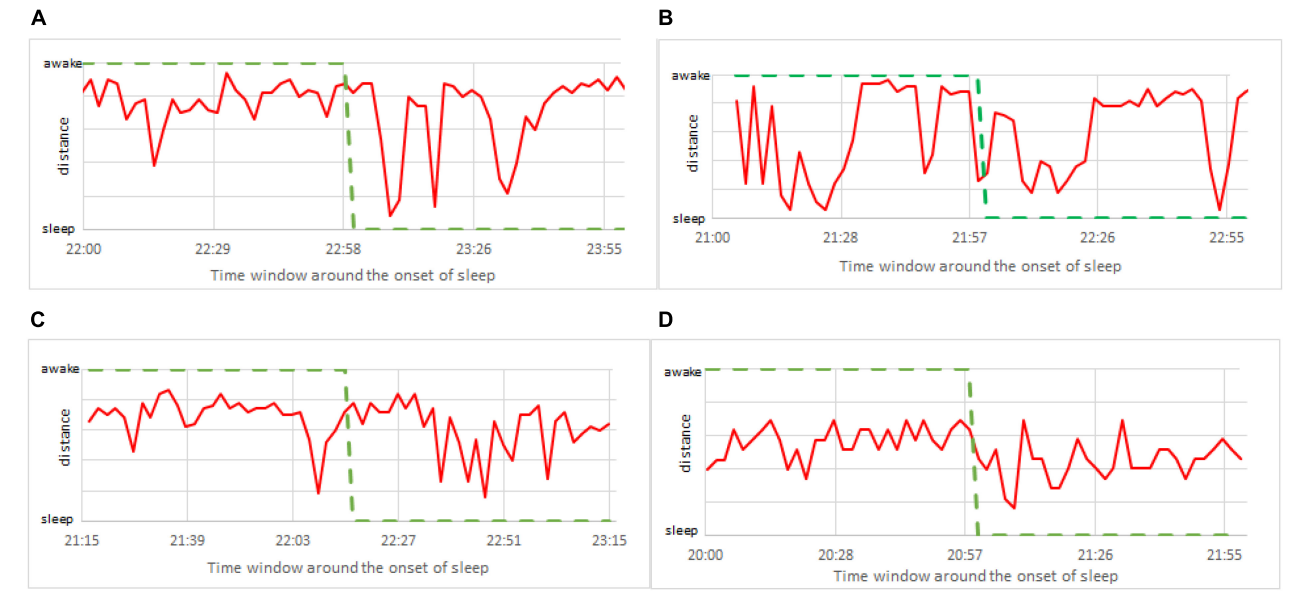

FIGURE 11 | Zoom to the onset of sleep as in **Figure 10**, but this time calculated via 50 randomly chosen shapelets as described in the text (not via single best shapelet). The consciousness status is no longer binary (0 or 1), but a continuous value ranging between sleep (0) and awake (1). **(A)** Male subject, 21 years of age. **(B)** Female subject, 23 years of age. **(C)** Male subject, 49 years of age. **(D)** Female subject, 50 years of age.

best shapelet (as shown earlier). Such histogram has two peaks, corresponding to two consciousness states, separated by the optimal split point. Now, for each subject we calculate the separation between those two peaks. Large separation means that heart activity is very different during sleep as opposed to awake, whereas small separation means the contrary. We scatter plot the values of this separation against the age for all subjects are show the results in (**Figure 13**). As expected, we find a good correlation for men. Interestingly, a negative correlation is significant for men, but not for women. It appears that the discriminatory power of heart activity to differentiate between sleep and awake decreases a lot more with age for men than for women.

DISCUSSION

We proposed a new method for automatically determining the consciousness status (sleep or awake) of a person from heart rate data only. Our method is based on shapelet analysis which looks for self-similarities in the data. By finding the best shapelet – the chunk of time series whose self-similarity properties allow for

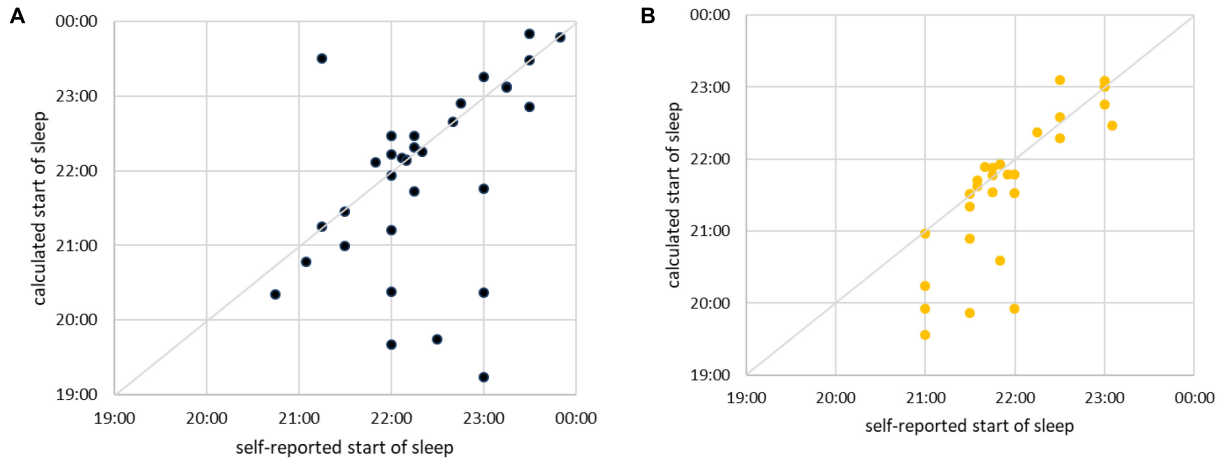

FIGURE 12 | (A) Scatter plot of self-reported time of falling asleep (shown horizontally) vs. time of falling asleep calculated via best shapelet as described in the text (shown vertically) for male subjects. Each subject is shown as one point. The diagonal is marked for easier orientation. For simplicity and easier comparison, we took only subjects who fell asleep between 19:00 and 00:00. **(B)** The same for female subjects.

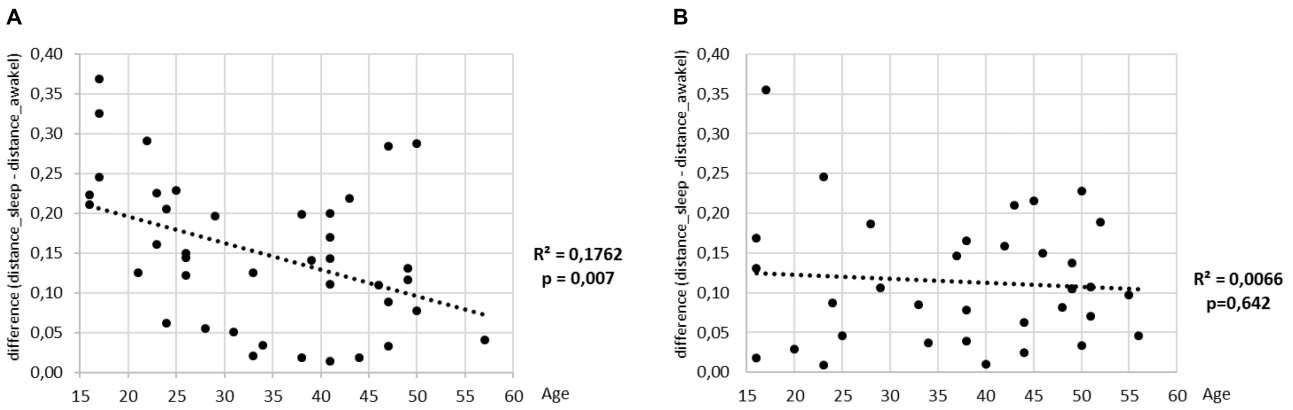

FIGURE 13 | The value of mean distance from the best shapelet for one class minus the mean distance from the best shapelet for the other class (shown on *y*) is scatter plotted against the age (plots **A** for men and **B** for women). Regression lines are indicated in black, along with the respective values of R^2 and *p*-value.

the best split of time series into two classes – we determine the awake and sleep states independently of information provided by the subjects, i.e., relying on HRV data only. The length of the best shapelet for most subjects is close to three lengths of a typical respiration cycle. This was somewhat expected, since RSA (synchronous modulation of heart by respiration rhythms) is known to be a reliable indicator of strong vagal activity and hence a reliable indicator of autonomic state (Moser et al., 2008). The method is developed to offer an individually optimal detection, but it can probably be extended to a longitudinal analysis of patterns, so that changes in behavior can be detected.

One of the applications of the approach is foreseen in public and general safety. Namely, our method can be developed into an alarm system that is triggered in case the system recognizes that the person under observation could be falling asleep. The paramount interest here is to have zero rate of false negatives. Our method seems to have covered this aspect rather well. In contrast, another goal is to minimize the number of false positives, but in this aspect, we encountered several limitations where there is room for improvement.

First, the proper way of calibrating our method would mean to have access to the precise timing of a subject falling asleep ("ground truth"). Note that while self-reported information is useful in narrowing our search, it is really not the ground truth: subjects can only report the time when the wanted to fall asleep, but not the time when they actually did. More complex experiments are needed to establish a reliable ground truth of the onset of sleep. A subject in a sleep laboratory could be simultaneously measured by Holter and by another device capable of independently determining the consciousness status. However, this will inevitably involve equipment that can disturb the sleep itself and the HRV measurements. Also, it is unlikely that any ground truth will be available in any practical (applicative) situation, so the ultimate interest are the methods that operate only with HRV data.

Second, further improvements of our method are possible through novel data analysis approaches. Specifically, note that in this work we used only the best shapelet to compute self-similarities. However, as a side result we found that splitting into just two classes of sleep and awake does not depend heavily on the choice of shapelet. In fact, many other shapelets have similar classification power. This means that one could cumulatively use several shapelets for classification, which would allow classification not as a binary value, but also to classify intermediate stages. Moreover, instead of 2 min segments, one can start with segments of shortened initial length and improve the resolution.

Third, another limitation of our method revolves around using prior data for individual subjects. In commercial applications this might be difficult, since the market might need an alarm system to work immediately and without prior data. This, however, is a very challenging task, especially due to particularities of each individual's heart activity as he/she is falling asleep. On the other hand, having prior data for a period even longer than 24 h would allow for far more precise determination of consciousness status. In fact, this should also enable to predict the onset of sleep minutes ahead, rather than establishing the onset after it had happened.

Fourth, we realize that there are two different way of looking at the problem of determining the consciousness status. One way is to make determination for individuals only based on their prior data. Another is the search for universal patterns in everyone's data and try to extract a universal method from those. Our work has shown that the first approach might be more promising in the short term. For any serious approach to the second approach one would need a far larger and more diverse sample of subjects. However, it is clear that the second way is more promising in terms of applications.

Fifth, we stress that we have focused on just one possible method of determining the onset of sleep from many conceivable methods. Clearly, a pressing issue revolves around comparing such methods and establishing which works best depending on the situation and the available information. Detailed comparison of these methods, while very important, is beyond the scope of this paper. But we note that such comparison might not be simple, since it will involve methods that operate on different foundations, for example, with or without ground truth.

Finally, our work has confirmed that shapelet analysis of cardiorespiratory interactions as present in HRV data is a useful tool. Except for methodological improvements mentioned above, this opens up further research questions. One of them has been mentioned already, namely, sleep phases could be studied via shapelet analysis. Shapelet distance matrices in **Figure 5** reveal distinct patterns within sleep for all subjects, whose more detailed study is warranted.

DATA AVAILABILITY STATEMENT

The datasets generated for this study are available on request to the corresponding author.

ETHICS STATEMENT

Ethical review and approval was not required for the study on human participants in accordance with the local legislation and institutional requirements. The patients/participants provided their written informed consent to participate in this study.

AUTHOR CONTRIBUTIONS

MM, AZ, and ZL envisaged the study. MF and MM arranged for the participation of subjects and collected the data. AZ designed and carried out the data analysis. AZ and MF designed the figures. ZL and AZ wrote, corrected, and carried the manuscript. All authors reviewed the manuscript.

FUNDING

This work was supported by the Slovenian Research Agency via Program P1-0383 and Project J5-8236 and the European Union's Horizon 2020 Research and Innovation Program under the Marie Skłodowska-Curie Grant Agreement No. 642563 (COSMOS).

ACKNOWLEDGMENTS

We most gratefully acknowledge the voluntary participation of subjects. Thanks to colleagues Dietrich von Bonin, Vincent Grote, Helmut Lackner, Dietmar Messerschmidt, Bernhard Puswald, Ljupco Todorovski, Gorazd Drevensek, and the employees of Human Research Institute for their help.

REFERENCES

Aboy, M., Cuesta-Frau, D., Austin, D., and Micó-Tormos, P. (2007). "Characterization of sample entropy in the context of biomedical signal analysis," in *Proceedings of the 29th Annual International Conference of the IEEE Engineering in Medicine and Biology Society*, (Lyon France: IEEE), 5942–5945.

Amani, T. I., Alhady, S. S. N., Ngah, U. K., and Abdullah, A. R. W. (2011). *A Review of ECG Peaks Detection and Classification*. Berlin: Springer-Verlag Berlin Heidelberg.

American Heart Association (2015). *American Heart Association*. Available at: http://www.heart.org/HEARTORG/Conditions/HeartAttack/DiagnosingaHeartAttack/Holter-Monitor_UCM_446437_Article.jsp#.Ww3D3kiFOPr (accessed October 1, 2019).

Barrett, M., Komatireddy, R., Haaser, S., Topol, S., Sheard, J., and Encinas, J. (2014). Comparison of 24-hour holter monitoring with 14-day novel adhesive patch electrocardiographic monitoring. *Am. J. Med.* 1:95.e11-7. doi: 10.1016/j.amjmed.2013.10.003

Bartsch, R., Hennig, T., Heinen, A., Heinrichs, S., and Maass, P. (2005). Statistical analysis of fluctuations in the ECG morphology. *Phys. A Stat. Mech. Appl.* 354, 415–431. doi: 10.1016/j.physa.2005.03.019

Bartsch, R. P., Liu, K. K., Ma, Q. D., and Ivanov, P. C. (2014). Three independent forms of cardio-respiratory coupling: transitions across sleep stages. *Comp. Cardiol.* 41, 781–784.

Bartsch, R. P., Schumann, A. Y., Kantelhardt, J. W., Penzel, T., and Ivanov, P. Ch. (2012). Phase transitions in physiologic coupling. *Proc. Natl. Acad. Sci. U.S.A.* 109, 10181–10186. doi: 10.1073/pnas.1204568109

Batista, G., Wang, X., and Keogh, E. J. (2011). "A complexity-invariant distance measure for time series," in *Proceedings of the 2011 SIAM International Conference on Data Mining* (Mesa: Society for Industrial and Applied Mathematics), 699–710.

Bendat, S. J., and Piersol, A. G. (2010). *Random Data Analysis and Measurement Procedures Fourth Edition*. New York, NY: Wiley.

Bevington, P. R., and Robinson, D. K. (2003). *Data Reduction and Error Analysis for the Physical Sciences Third Edition*. New York, NY: McGraw-Hill.

Billman, G. (2011). Heart rate variability – a historical perspective. *Front. Physiol.* 2:86. doi: 10.3389/fphys.2011.00086

Billman, G. E., Huikuri, H. V., Sacha, J., and Trimmel, K. (2015). An introduction to heart rate variability: methodological considerations and clinical applications. *Front. Physiol.* 6:55. doi: 10.3389/fphys.2015.00055

Bland, J. M., and Altman, D. G. (1996). Statistics notes: measurement error. *BMJ Clin. Res.* 313, 41–42. doi: 10.1136/bmj.313.7059.744

Bonin, D. V., Denjean, B., and Moser, M. (2004). "Therapeutische Sprachgestaltung," in *Onkologie auf Anthroposophischer Grundlage Band 3*, eds V. Fintelmann, and M. Treichler (Frankfurt: Info 3 Verlag).

Canisius, S., and Penzel, T. (2007). Vigilance monitoring–review and practical aspects. (S. Canisius, & T. Penzel, Prev.). *Biomed. Tech.* 1, 77–82. doi: 10.1515/BMT.2007.015

Carmel, D., Farchi, E., Petruschka, Y., and Soffer, A. (2002). "Automatic Query Refinement using Lexical Affinities with maximal information gain," in *SIGIR '02 Proceedings of the 25th Annual International ACM SIGIR Conference on Research and Development in Information Retrieval* (Tampere: ACM), 283–290.

Celebi, E. M., and Aydin, K. (2016). *Unsupervised Learning Algorithms*. Switzerland: Springer International Publishing.

Chouchou, F., and Desseilles, M. (2014). Heart rate variability: a tool to explore the sleeping brain? *Front. Neurosci.* 8:402. doi: 10.3389/fnins.2014.00402

Costa, M., Goldberger, A. L., and Peng, C. K. (2005). Multiscale entropy analysis of biological signals. *Phys. Rev. E* 71:021906. doi: 10.1103/PhysRevE.71.021906

Cover, T. M., and Thomas, J. M. (2006). *Elements of Information Theory*. Hoboken, NJ: John Wiley & Sons.

Daubechies, I. (1992). *Ten Lectures on Wavelets*. Philadelphia: Society for Industrial and Applied Mathematics.

Delgado-Bonal, A., and Martín-Torres, J. (2016). Human vision is determined based on information theory. *Sci. Rep.* 6:36038. doi: 10.1038/srep36038

Denwer, J. W., Reed, S. F., and Porges, S. W. (2007). Methodological issues in the quantification of respiratory sinus arrhythmia. *Biol. Psychol.* 2, 286–294. doi: 10.1016/j.biopsycho.2005.09.005

Deza, M., and Deza, E. (2009). *Encyclopedia of Distances*. Berlin: Springer-Verlag.

Ding, H., Trajcevski, G., Scheuermann, P. I., Wang, X., and Keogh, E. J. (2008). Querying and mining of time series data: experimental comparison of representations and distance measures. *Proc. VLDB Endow.* 1, 1542–1552. doi: 10.14778/1454159.1454226

Dvir, H., Elbaz, I., Havlin, S., Appelbaum, L., Ivanov, P., and Bartsch, R. P. (2018). Neuronal noise as an origin of sleep arousals and its role in sudden infant death syndrome. *Sci. Adv.* 4:eaar6277. doi: 10.1126/sciadv.aar6277

Faloutsos, C., Ranganathan, M., and Manolopoulos, Y. (1994). Fast subsequence matching in time-series databases. *SIGMOD Rec.* 2, 419–429. doi: 10.1145/191843.191925

Ftouni, S., Sletten, T. L., Howard, M., Anderson, C., Lenné, M. G., and Lockley, S. W. (2012). Objective and subjective measures of sleepiness, and their associations with on-road driving events in shift workers. *J. Sleep Res.* 1, 55–69. doi: 10.1111/j.1365-2869.2012.01038.x

Gallasch, E., Moser, M., Kozlovskaya, I. B., Kenner, T., and Noordergraaf, A. (1997). Effects of an eight-day space flight on microvibration and physiological tremor. *AJP Regul. Integr. Comp. Physiol.* 273(1 Pt 2), R86–R92. doi: 10.1152/ajpregu.1997.273.1.R86

Gallasch, E., Rafolt, D., Moser, M., Hindinger, J., Eder, H., and Wiesspeiner, G. (1996). Instrumentation for assessment of tremor, skin vibrations, and cardiovascular variables in MIR space missions. *IEEE Trans. Biomed. Eng.* 3, 328–333. doi: 10.1109/10.486291

Goldin, D. Q., Millstein, T. D., and Kutlu, A. (2004). Bounded similarity querying for time-series data. *Inform. Comput.* 2, 203–241. doi: 10.1016/j.ic.2004.07.001

Grote, V., Levnajic, Z., Puff, H., Ohland, T., Goswami, N., and Frühwirth, M. (2019). Dynamics of vagal activity due to surgery and subsequent rehabilitation. *Front. Neurosci.* 13:1116. doi: 10.3389/fnins.2019.01116

Hills, J., Lines, J., Baranauskas, E., Mapp, J., and Bagnall, A. (2013). Discovery Classification of time series by shapelet transformation. *Data Min. Knowl.* 4, 851–881. doi: 10.1007/s10618-013-0322-1

Hills, J., Lines, J., Mapp, J., Baranauskas, E., and Bagnall, A. (2014). Time-series Classification with Shapelets. *Data Min. Knowl. Discov.* 28, 851–881. doi: 10.1007/s10618-013-0322-1

Horne, J., and Reyner, L. (1995). Sleep related vehicle accidents. *Br. Med. J.* 310, 565–567. doi: 10.1136/bmj.310.6979.565

Hurst, J. W. (1998). Naming of the waves in the ECG, with a brief account of their genesis. *Circulation* 98, 1937–1942. doi: 10.1161/01.CIR.98.18.1937

Iaizzo, P. A. (2005). *Handbook of Cardiac Anatomy, Physiology, and Devices*. Totowa: Humana Press.

James, G., Hastie, T., Tibshirani, R., and Witten, D. (2013). *An Introduction to Statistical Learning with Applications in R*. New York, NY: Springer.

Joysys (2018). *Creating Healthy Choises Joysys*. Available at: https://joysys.at/en/product/chronocord8/ (accessed October 1, 2019).

Kaplan, K. A., Hirshman, J., Hernandez, B., Stefanick, M. L., Hoffman, A. R., and Redline, S. (2017). When a gold standard isn't so golden: lack of prediction of subjective sleep quality from sleep polysomnography. *Byol. Psychol.* 123, 37–46. doi: 10.1016/j.biopsycho.2016.11.010

Kin-Pong, C., and Wai-Chee Fu, A. (1999). *Efficient Time Series Matching by Wavelets. Proceedings of the 15th International Conference on Data Engineering*. Washington: IEEE Computer Society.

Klabunde, R. E. (2012). *Cardiovascular Physiology Concepts*, 2nd Edn, Philadelphia: Wolters Kluwer Health/Lippincott Williams & Wilkins.

Krul, S., Louise, O. N., and Jonas de, J. (2013). *Tachycardia*. Available at: https://www.textbookofcardiology.org (accessed October 1, 2019).

Längkvist, M., Lars, K., and Amy, L. (2014). A review of unsupervised feature learning and deep learning for time-series modeling. *Pattern Recogn. Lett.* 42, 11–24. doi: 10.1016/j.patrec.2014.01.008

Liao, W. T. (2005). Clustering of time series data—a survey. *Pattern Recogn.* 11, 1857–1874. doi: 10.1016/j.patcog.2005.01.025

Lynn, W. D., Omar, J. E., and David, J. M. (2013). Arm and wrist surface potential mapping for wearable ECG rhythm recording devices: a pilot clinical study. *J. Phys. Conf. Ser.* 450:012026. doi: 10.1088/1742-6596/450/1/012026

MacKay, D. J. (2005). *Information Theory, Inference, and Learning Algorithms*. Cambridge: Cambridge University Press.

Medical Training and Simulation LLC (2017). *Practical Clinical Skills*. Available at: https://www.practicalclinicalskills.com (accessed October 1, 2019).

Mitchell, T. M. (1997). *Machine Learning (McGraw-Hill International Editions Computer Science Series)*, 1st Edn, New York, NY: McGraw-Hill.

Moser, M., Frühwirth, M., and Kenner, T. (2008). The symphony of life. *IEEE Eng. Med. Biol. Mag.* 1, 29–37. doi: 10.1109/MEMB.2007.907365

Moser, M., Frühwirth, M., Penter, R., and Winker, R. (2006). Why Life Oscillates - from a topographical towards a functional chronobiology. *Cancer Causes Control* 71, 591–599. doi: 10.1007/s10552-006-0015-9

Moser, M., Lehofer, M., Hildebrandt, G., Voica, M., Egner, S., and Kenner, T. (1995). Phase- and frequency coordination of cardiac and respiratory function. *Biol. Rhythm Res.* 26, 100–111. doi: 10.1080/09291019509360328

Moser, M., Lehofer, M., Sedminek, A., Lux, M., Zapotoczky, H. G., and Kenner, T. (1994). Heart rate variability as a prognostic tool in cardiology. A contribution to the problem from a theoretical point of view. *Circulation* 90, 1078–1082. doi: 10.1161/01.CIR.90.2.1078

National Institute of Neurological Disorders and Stroke (2019). *Neurological and Neurodevelopmental Disorders*. Available at: https://www.ninds.nih.gov/Disorders/Patient-Caregiver-Education/Understanding-Sleep (accessed June 1, 2019).

Niizeki, K., and Saitoh, T. (2018). Association between phase coupling of respiratory sinus arrhythmia and slow wave brain activity during sleep. *Front. Physiol.* 9:1338. doi: 10.3389/fphys.2018.01338

NIST (2017). *Coefficient of Variation*. Available at: https://www.itl.nist.gov/div898/software/dataplot/refman2/auxillar/coefvari.html (accessed October 1, 2019).

Noble, R. J., Stanley, H. J., and Donald, A. R. (1990). "Electrocardiography," in *Clinical Methods: The History, Physical, and Laboratory Examinations*, 3rd Edn, eds V. Walker, W. D. Hall, and J. W. Hurst, (Boston: Butterworth).

Ogilvie, R. D. (2001). The process of falling asleep. *Sleep Med. Rev.* 3, 247–270. doi: 10.1053/smrv.2001.0145

Penzel, T., Kantelhardt, J. W., Bartsch, R. P., Riedl, M., Kraemer, J. F., Wessel, N., et al. (2016). Modulations of heart rate, ECG, and cardio-respiratory coupling observed in polysomnography. *Front. Physiol.* 7:460. doi: 10.3389/fphys.2016.00460

Perski, A., Olsson, G., Landou, C., de Faire, U., Theorell, T., Hamsten, A., et al. (1992). Minimum heart rate and coronary atherosclerosis: independent relations to global severity and rate of progression of angiographic lesions in men with myocardial infarction at a young age. *Am. Heart. J.* 3, 609–616. doi: 10.1016/0002-8703(92)90497-j

Pinnell, J., Simon, T., and Simon, H. (2007). Cardiac muscle physiology. *BJA Educ.* 3, 85–88. doi: 10.1093/bjaceaccp/mkm013

Quintana-Gallego, E., Villa-Gil, M., Carmona-Bernal, C., Botebol-Benhamou, G., Martínez-Martínez, A., Sánchez-Armengol, A., et al. (2004). Home respiratory polygraphy for diagnosis of sleep-disordered. *Eur. Respir. J.* 3, 443–448. doi: 10.1183/09031936.04.00140603

Rakthanmanon, T., and Keogh, E. (2013). "Fast shapelets: a scalable algorithm for discovering time series shapelets," in *Proceedings of the SIAM International Conference on Data Mining*, eds J. Ghosh, Z. Obradovic, D. Jennifer, Z. Zhi-Hua, K. Chandrika, and P. Srinivasan, (Austin: Society for Industrial and Applied Mathematics).

Richman, J. S., and Moorman, J. R. (2000). Physiological time-series analysis using approximate entropy and sample entropy. *Am. J. Physiol. Heart Circ. Physiol.* 278, H2039–H2049. doi: 10.1152/ajpheart.2000.278.6.H2039

Romine, W., Banerjee, T., and Goodman, G. (2019). Toward sensor-based sleep monitoring with electrodermal activity measures. *Sensors* 6, 1–9. doi: 10.3390/s19061417

Royal, D. (2003). *Findings for National Survey of Distracted and Drowsy Driving Attitudes and Behavior: 2002*. Available at: http://www.nhtsa.dot.gov/People/injury/drowsy_driving1/survey-distractive03/index.html (accessed October 1, 2019).

Sadek, I., Biswas, J., and Abdulrazak, B. (2019). Ballistocardiogram signal processing: a review. *Health Inf. Sci. Syst.* 7:10. doi: 10.1007/s13755-019-0071-7

Sarzynski, M. A., Rankinen, T., Earnest, C. P., Leon, A. S., Rao, D. C., Skinner, J. S., et al. (2013). Measured maximal heart rates compared to commonly used age-based prediction equations in the Heritage Family Study. *Am. J. Human Biol.* 5, 695–701. doi: 10.1002/ajhb.22431

Shapiro, L. (2019). *Information Gain Tutorial*. Available at: https://homes.cs.washington.edu/∼shapiro/EE596/notes/InfoGain.pdf (accessed October 1, 2019).

Small, M. (2005). *Applied Nonlinear Time Series Analysis: Applications in Physics, Physiology and Finance*. London: World Scientific Publishing Co.

Sonka, M., Hlavac, V., and Boyle, R. (2015). *Image Processing, Analysis, and Machine Vision Forth Edition*. Boston: Cengage Learning.

Surawicz, B., and Knilans, T. K. (2008). *Chou's Electrocardiography in Clinical Practice: Adult and Pediatric Sixth Edition*. Philadelphia: Saunders.

Uğuz, H. (2011). A two-stage feature selection method for text categorization by using information gain, principal component analysis and genetic algorithm. *Knowl. Based Syst.* 24, 1024–1032. doi: 10.1016/j.knosys.2011.04.014

Xi, X., Keogh, E., Shelton, C., and Wei, L. (2006). "Fast time series classification using numerosity reduction," in *Proceedings of the 23rd International Conference on Machine Learning* (Riverside, CA: University of California), 1033–1040.

Yaffee, R. A., and McGee, M. (2000). *Introduction to Time Series Analysis and Forecasting: With Applications of SAS and SPSS*. Orlando: Academic Press, Inc.

Yasuma, F., and Hayano, J.-I. (2004). Respiratory sinus arrhythmia: why does the heartbeat synchronize with respiratory Rhythm? *CHEST J.* 2, 683–690. doi: 10.1378/chest.125.2.683

Ye, L., and Keogh, E. (2009). "Time series shapelets: a new primitive for data mining," in *Proceedings of the 15th ACM SIGKDD International Conference on Knowledge Discovery and Data Mining*, (Paris: ACM), 947–956.

Yentes, J. M., Hunt, N., Schmid, K. K., Kaipust, J. P., McGrath, D., and Stergiou, N. (2013). The appropriate use of approximate entropy and sample entropy with short data sets. *Ann. Biomed. Eng.* 41, 349–365. doi: 10.1007/s10439-012-0668-3

Zimmerman, D. W. (2010). A note on preliminary tests of equality of variances. *Br. J. Math. Stat. Psychol.* 1, 173–181. doi: 10.1348/000711004849222

Zou, Y., Donner, R. V., Marwan, N., Donges, J. F., and Kurths, J. (2019). Complex network approaches to nonlinear time series analysis. *Phys. Rep.* 787, 1–97. doi: 10.1016/j.physrep.2018.10.005

Conflict of Interest: The authors declare that the research was conducted in the absence of any commercial or financial relationships that could be construed as a potential conflict of interest.

frontiers in Physiology

ORIGINAL RESEARCH
published: 14 February 2020
doi: 10.3389/fphys.2020.00024

Slow 0.1 Hz Breathing and Body Posture Induced Perturbations of RRI and Respiratory Signal Complexity and Cardiorespiratory Coupling

Zoran Matić[1], *Mirjana M. Platiša*[2], *Aleksandar Kalauzi*[3] *and Tijana Bojić*[4]*

[1] Biomedical Engineering and Technology, University of Belgrade, Belgrade, Serbia, [2] Faculty of Medicine, Institute of Biophysics, University of Belgrade, Belgrade, Serbia, [3] Department for Life Sciences, Institute for Multidisciplinary Research, University of Belgrade, Belgrade, Serbia, [4] Laboratory for Radiobiology and Molecular Genetics-080, Institute for Nuclear Sciences Vinča, University of Belgrade, Belgrade, Serbia

Objective: We explored the physiological background of the non-linear operating mode of cardiorespiratory oscillators as the fundamental question of cardiorespiratory homeodynamics and as a prerequisite for the understanding of neurocardiovascular diseases. We investigated 20 healthy human subjects for changes using electrocardiac RR interval (RRI) and respiratory signal (Resp) Detrended Fluctuation Analysis (DFA, α_{1RRI}, α_{2RRI}, α_{1Resp}, α_{2Resp}), Multiple Scaling Entropy (MSE_{RRI1-4}, $MSE_{RRI5-10}$, $MSE_{Resp1-4}$, $MSE_{Resp5-10}$), spectral coherence ($Coh_{RRI-Resp}$), cross DFA (ρ_1 and ρ_2) and cross MSE (X_{MSE1-4} and $X_{MSE5-10}$) indices in four physiological conditions: supine with spontaneous breathing, standing with spontaneous breathing, supine with 0.1 Hz breathing and standing with 0.1 Hz breathing.

Main results: Standing is primarily characterized by the change of RRI parameters, insensitivity to change with respiratory parameters, decrease of $Coh_{RRI-Resp}$ and insensitivity to change of in ρ_1, ρ_2, X_{MSE1-4}, and $X_{MSE5-10}$. Slow breathing in supine position was characterized by the change of the linear and non-linear parameters of both signals, reflecting the dominant vagal RRI modulation and the impact of slow 0.1 Hz breathing on Resp parameters. $Coh_{RRI-Resp}$ did not change with respect to supine position, while ρ_1 increased. Slow breathing in standing reflected the qualitatively specific state of autonomic regulation with striking impact on both cardiac and respiratory parameters, with specific patterns of cardiorespiratory coupling.

Significance: Our results show that cardiac and respiratory short term and long term complexity parameters have different, state dependent patterns. Sympathovagal non-linear interactions are dependent on the pattern of their activation, having different scaling properties when individually activated with respect to the state of their joint activation. All investigated states induced a change of α_1 vs. α_2 relationship, which can be accurately expressed by the proposed measure—inter-fractal angle θ. Short scale (α_1 vs. MSE_{1-4}) and long scale (α_2 vs. MSE_{5-10}) complexity measures had reciprocal interrelation in standing with 0.1 Hz breathing, with specific cardiorespiratory coupling pattern (ρ_1 vs. X_{MSE1-4}). These results support the hypothesis of hierarchical organization

OPEN ACCESS

Edited by:
Luca Faes,
University of Palermo, Italy

Reviewed by:
Mathias Baumert,
University of Adelaide, Australia
Paolo Castiglioni,
Fondazione Don Carlo Gnocchi Onlus (IRCCS), Italy
Marcel Cezary Młynczak,
Warsaw University of Technology, Poland

***Correspondence:**
Tijana Bojić
tijanabojic@vinca.rs;
bojictijana@gmail.com

Specialty section:
This article was submitted to Autonomic Neuroscience, a section of the journal Frontiers in Physiology

Received: *29 September 2019*
Accepted: *14 January 2020*
Published: *14 February 2020*

Citation:
Matić Z, Platiša MM, Kalauzi A and Bojić T (2020) Slow 0.1 Hz Breathing and Body Posture Induced Perturbations of RRI and Respiratory Signal Complexity and Cardiorespiratory Coupling. Front. Physiol. 11:24. doi: 10.3389/fphys.2020.00024

of cardiorespiratory complexity mechanisms and their recruitment in ascendant manner with respect to the increase of behavioral challenge complexity. Specific and comprehensive cardiorespiratory regulation in standing with 0.1 Hz breathing suggests this state as the potentially most beneficial maneuver for cardiorespiratory conditioning.

Keywords: complexity, RR interval variability, respiration rhythm variability, cardiorespiratory coupling, slow breathing, orthostasis

INTRODUCTION

The interaction of cardiac RRI and respiratory signal is a complex, mutually interrelated phenomenon. Related modern research poses questions like: why do RRI and respiratory signal values vary and what generates their complexity when forming a *meaningful, structural richness* (Grassberger, 1991)? Lack/decrease of RRI variability has been observed as a sign of pathology (Task Force Guidelines, 1996; Platiša and Gal, 2010; Valencia et al., 2013; Voss et al., 2013; Platiša et al., 2016a). Complementing homeostatic assumption, the lack of RRI oscillations ("oscillation death," Stankovski et al., 2017) outlines a danger resulting from serious cardiac problems (Task Force Guidelines, 1996; Neves et al., 2012; Platiša et al., 2016b). Classical data on HRV refer to the changes of HRV in the linear domain, while more than 80% of HRV fluctuations belong to non-linear complex patterns (Yamamoto and Hughson, 1994). Although a few studies have pointed to increased complexity in the disease (Buccelletti et al., 2012; Valenza et al., 2017), it seems that the pathogenesis is most often followed by "de-complexification" (an increase of regular patterns in biological rhythm, Buccelletti et al., 2012; Sassi et al., 2015). So, complex and high rhythm variability refers to *homeodynamics* (Ernst, 2014) as a biophysical background of allometric physiological regulation (long term memory and multiscale correlations, West, 2010). Therefore, homeodynamics is a fundamental property of advanced biological sophistication.

Cardiac homeodynamics is a result of multilevel coupling: excitation-contraction coupling in the heart (Bers, 2018); hormonal regulation (Bai et al., 2009); thermoregulation (Fleisher et al., 1996); with autonomic nervous system (ANS) regulation as the dominant factor of this phenomenon. ANS regulation of cardiac homeodynamics is obtained by:

(i) sympathetic and parasympathetic effectors, with prevalently antagonistic, synchronous, synergetic, simultaneous (in-coupled) action on the heart (Zoccoli et al., 2001; Bojić, 2003, 2019; Silvani et al., 2003; Paton et al., 2005; Gierałtowski et al., 2013), and

(ii) coupling of cardiac rhythm with other biological oscillations, especially with the ones generated from breathing (i.e., central coupling of neural oscillators in ventrolateral medulla Porta et al., 2012; Schulz et al., 2013, 2018; Del Negro et al., 2018 and peripheral coupling dominated by the Bainbridge reflex (Bainbridge, 1930; Billman, 2011; Kapidžić et al., 2014).

Cardiopulmonary coupling is an intriguing phenomenon whose principal role, the energetic efficacy of oxygen transport, was recently found to extend to the adaptive capacity of the organism to internal and external challenges (Porges, 2007). This capacity for adaptation is investigated by the measurements of cardiopulmonary complexity by non-linear domain techniques (Goldberger, 2006). In the context of fundamental research, the majority of data on cardiovascular and respiratory autonomic patterns is based on the analysis of parameters of HRV linear domain. On the basis of these results, we deduce the antagonism of autonomic effectors on RRI regulation (change of posture, i.e., supine vs. standing, Montano et al., 1994; Levy and Martin, 1996; Jasson et al., 1997) or their synergism of action (i.e., supine vs. standing with slow breathing, de Paula Vidigal et al., 2016). These interrelated patterns of sympathetic vs. parasympathetic activity on RRI regulation are not confirmed for non-linear domain dynamics (Sassi et al., 2015).

Physiological states as RRI and respiration regulatory patterns include:

Supine position (supin), considered the standard baseline for all cardiopulmonary physiological investigations. It is characterized by sympathetic withdrawal and small parasympathetic dominance on RRI regulation (Levy and Martin, 1996).

Active standing (stand), a typical, well-characterized cardiocirculatory pattern of sympathetic dominance and vagal withdrawal on RRI regulation (Levy and Martin, 1996). The respiration pattern is characterized by increased ventilation and unchanged mean respiratory frequency with respect to supine position (Chang et al., 2005). With respect to supine position, this state is known for its beneficial effects on a number of neurocardiovascular (i.e., heart failure) and respiratory disturbances (Chang et al., 2004a,b; Zafiropoulos et al., 2004). The effect of active standing, to the best of our knowledge, has not been investigated with respect to the parameters of RRI, respiration and cardiopulmonary coupling in the non-linear domain, that could be of critical importance for the evaluation of RRI and respiratory adaptability on internal (i.e., disease state) or external (i.e., microgravity) challenges.

Slow 0.1 Hz breathing, a specific breathing frequency resulting from the maximum effect of respiration on RRI modulation (RSA, Eckberg, 1983; max Total Power of HRV, Cooke et al., 1998). This effect is vagally mediated and most probably obtained by system resonance effects of respiratory oscillatory drive on heart rate regulatory networks modulated by baroreflex (Julien, 2006; Castiglioni and Parati, 2011). This is, to the best of our knowledge, the maximal respiratory mediated physiological vagal drive on the heart. Its functional meaning was primarily attributed to energetic efficiency of the cardiorespiratory system, but also to the adaptability of the

organism to unexpected environmental demands (Porges, 2007). Increased cardiorespiratory synchrony in slow 0.1 Hz breathing supports the energetic efficiency theory (Goldberger, 2006), but until now the question of cardiopulmonary adaptability was not addressed.

Specifically, regarding respiratory complexity, the change of posture and breathing regime are significantly interrelated with the breathing pattern (Mortola et al., 2016; Hernandez et al., 2019; Mortola, 2019). These two conditions, both individually and jointly, could give an insight into the contribution of (a) the peripheral factor for changed respiratory mechanics (horizontal vs. vertical plane) during orthostatic challenge, and (b) the impact of slow, voluntary 0.1 Hz control of breathing to the complexity regimes of the respiratory signal. Variability of the respiratory signal in the non-linear domain is of critical importance for the recovery of intensive care patients on artificial ventilation (Papaioannou et al., 2011). To the best of our knowledge, there are no data on the non-linear dynamics of respiratory signal in the conditions of peripheral respiratory drive change (change of posture) combined with the change of slow 0.1 Hz frequency respiratory drive. This interaction could be one of the critical mechanisms for the beneficial effect of posture change and slow breathing on critical care situations like weaning from artificial ventilation (Stiller, 2013).

Finally, as it goes for the simplest non-linear systems, RRI and respiratory regulation in coupled behavioral states like **supination with slow 0.1 Hz breathing** (**supin01**) and **standing with slow 0.1 Hz** breathing (**stand01**), most probably contravene the principles of proportionality and superposition (Goldberger, 2006). Slow 0.1 Hz breathing in two specific body postures could potentially have completely different effects on cardiorespiratory complexity parameters with respect to the predicted simple summation. Additionally, contrary to the previously investigated pharmacological joint *blockade* of sympathetic and parasympathetic activity on the RRI regulation (Silva et al., 2017a), to the best of our knowledge, cardiopulmonary complexity measures were not investigated in the state of joint physiological *enhancement/synergy* of sympathetic and vagal modulation of RRI (standing with slow 0.1 Hz breathing). This state was identified in the intensive care practice as the state of particular benefit for cardiopulmonary rehabilitation (Cooke et al., 1998; Bruton and Lewith, 2005; Dick et al., 2014; Russo et al., 2017).

Cardiorespiratory Variables as an Insight Into Cardiorespiratory Cross Talk

Several studies have shown DFA exponent α to have a great power for probing complexity, as self-similarity across scale (Peng et al., 1995a,b, 2002; Ivanov et al., 1999; Fadel et al., 2004; Gierałtowski et al., 2013; Kristoufek, 2015; Barbiery et al., 2017). The advantages of fractal scaling exponents α_1 and α_2 over conventional methods like spectral analysis and Hurst exponent include the possibility of detecting long range correlations embedded in non-stationary/non-ergodic time series and of avoiding spurious detection of long range correlations that are the consequence of non-stationarities (Peng et al., 2002; Sassi et al., 2015). This method is validated (Peng et al., 1994) and successfully applied on both RRI (Peng et al., 1995a, 2002; Francis et al., 2002; Castiglioni et al., 2009, 2011) and respiratory interval time series (Peng et al., 2002; Fadel et al., 2004; Papaioannou et al., 2011). It quantifies information self-similarity across scale on both short term (α_1) and long term time scales (α_2).

MSE is another measure of signal complexity (i.e., irregularity) successfully applied on physiological signals (Costa et al., 2003) and in specific RRI (Silva et al., 2016, 2017a,b). It quantifies information irregularity (unpredictability) of sequence structural evolution in signal on both short term (MSE_{1-4}) and long term time scales (MSE_{5-10}).

Measures of self-similarity (DFA) and irregularity (MSE) are critical parameters of cardiovascular and respiratory system adaptability and physiologic plasticity (Goldberger, 2006). Fractal dynamics and irregularity in spontaneous RRI and respiratory signal fluctuations have implications for:

a. Understanding physiological cardiopulmonary regulation
b. Recognition of life-threatening cardiovascular events (i.e., heart failure—Silva et al., 2017a; Huikuri et al., 2000; Goldberger et al., 2002)
c. Recognition of respiratory disturbances (i.e., adaptability of critically ill patients to spontaneous breathing—Papaioannou et al., 2011)
d. Evaluation of detrimental effects of respiratory pathologies on neurocardiovascular physiology (Goulart et al., 2016). This ultimate factor unequivocally speaks in favor of the importance of understanding the cardiopulmonary coupling and its physiological background.

Finally, physiological non-linear signals like RRI (Peng et al., 1995a) and respiratory signal (Peng et al., 2002) couple (Moser et al., 2006; Schulz et al., 2018). The pattern and degree of the coupling can be evaluated both by means of linear and non-linear analytical methods (Podobnik and Stanley, 2008; Horvatic et al., 2011; Podobnik et al., 2011; Zebende, 2011; Blinowska and Zygierewicz, 2012; Kristoufek, 2014, 2015; Kwapien et al., 2015; Sassi et al., 2015). In accordance with that preposition, we applied spectral coherence ($Coh_{RRI-Resp}$, in the linear domain), cross DFA and cross MSE (ρ and X_{MSE} in the non-linear domain, respectively) as the tools for estimating the level of cardiorespiratory coupling in four different physiological states. In order to investigate scale dependent changes of cardiopulmonary coupling of both complexity patterns, we separately analyzed cross DFA and cross MSE for short term and long term time scales (ρ_1, ρ_2 and X_{MSE1-4}, $X_{MSE5-10}$, respectively).

On the basis of the above facts we formulated the following working hypotheses:

a. Individual posture changes and breathing regime changes differently affect RRI and respiratory complexity measures due to different mechanisms of regulation;
b. Slow 0.1 Hz breathing could have posture dependent effect on RRI and respiration complexity measures;

c. Standing with slow 0.1 Hz breathing could be regarded from the standpoint of cardiopulmonary complexity evaluation as a state of particular interest for cardiopulmonary adaptive conditioning;
d. Different forms of cardiopulmonary coupling ($Coh_{RRI-Resp}$, ρ, and X_{MSE}) could have different, state-dependent patterns and these patterns could scale in dependent and mutually interrelated ways.

The scope of this comprehensive analysis was to analytically investigate complex state-specific synergetic and/or antagonistic patterns of RRI regulation, state-specific impact of body plane and breathing regime on respiratory regulation and to provide synthetic conclusions regarding the patterns of cardiopulmonary coupling. The four physiological states were chosen as typical patterns of RRI vegetative effectors' activity and respiratory regulation.

METHODS

Subjects

We conducted the study protocol on 20 healthy adult human subjects (13 males, age 34.4 ± 7.4). The protocol was approved by the Ethical Committee of the Faculty of Medicine, University of Belgrade (No. 2650/IV-24). Criteria for inclusion of subjects into the study were: absence of any health problems and an age between 20 and 45 years. Exclusion criteria were: subjugation to any therapy (acupuncture, medications, etc.); a history of cardiovascular, pulmonar or any other diseases; presence of any health disorders at the time of the assessment or in the time leading up to the performance of the experimental measurements (such as cold, flu, pollen allergy, high temperature, migraines, etc.) and pathological symptoms during the experimental procedures (high blood pressure, arrhythmias, headache, fatigue, etc.). For female participants, an additional criterium of exclusion was the second part of menstrual cycle (because of its substantial and diverse cardiovascular autonomic regulation in females, Bai et al., 2009; Javorka et al., 2018). All participants were advised to refrain from food and drink from about 4 h before the experiment, not to exercise (running, gym, yoga, other), to be restful and alert.

Five participants (out of 25) were excluded because of pathological symptoms discovered during the recordings.

Study Protocol

The study protocol was performed under controlled laboratory conditions at the Laboratory for Biosignals, Institute for Biophysics, Faculty of Medicine, University of Belgrade. It was conducted in a quiet, refreshing environment at a constant temperature (22 ± 1°C) during the experimental procedures for all subjects. Experiments were undertaken between 8 and 12 a.m., in order to control the circadian rhythm variability stemming from autonomic regulation (Bojić, 2003). All subjects were subjected to 10 min of relaxation in a supine position before recording. There was no restriction imposed on the air flow rate. Instead, subjects were advised to adjust the ventilation at the rate that felt most comfortable for them. They were also strictly instructed not to talk during the experimental procedures. The ECG (RRI) and respiration signals were simultaneously recorded in four conditions/sessions: supine and standing positions at spontaneous breathing rates, and in supine and standing positions with the slow paced 0.1 Hz breathing rates (supine, stand, supin01, and stand01, respectively). Session recordings lasted for 20 min, with a 5 min pause between the supine and standing position, in order to meet the criteria for cardiorespiratory complexity analysis (Peng et al., 1995a, 2002) and to obtain the stabilization of autonomic regulation in each state (Bojić, 2003). The sequence of these four sessions was randomly chosen, aiming at avoiding possible sequence influence on the experimental results. Slow breathing with a paced rhythm of 0.1 Hz was dictated by a computer web metronom sound[1]. Subjects adjusted each start of inhalation and exhalation according to the beap sound of the metronome. Thus, inhalation and exhalation in slow breathing sessions had equal durations. Subjects were trained and instructed for slow breathing regime before the recording sessions.

Data Acqusition

ECG and respiration signal acquisition was done by means of Biopac MP100 system (Biopac System, Inc, Santa Barbara, CA, USA; AcqKnowledge 3.91 software). Main ECG lead registration electrodes were attached on the projections of clavicle bones and the grounding on the right ankle. The belt with resistive strain gauge transducer for continuous recording of breathing was placed slightly above the costal line. Both signals were sampled with 1,000 Hz frequency rate. We adjusted filters according to biopack instructions for general measurements: gain setting 10, low pass filter with 10 Hz and without high pass filter (DC-absolute respiratory measurement).

Data Processing

We maintained controlled conditions during the recordings. Subjects were instructed to take a comfortable position which would allow them not to make any movements during the 20 min recording session. By visual analysis we agreed that there was no need for additional filtering of ECG signals. Respiration signal was low pass filtered (4th order Chebyshev filter) in order to erase little jitters physiologicaly appearing in the minimum level of expiration, but unrelated to research results (Kapidžić et al., 2014; **Supplementary Data Sheet 1**). The corresponding cut-off frequency was 1 Hz. RRIs were extracted from the ECG signal using Pick Peak tool in Origin (Microcal, Northampton, MA, USA; missed R peaks we added manually). Since the sample rate of the respiration signal was uniform (1,000 Hz), while RRI values form signals with unequally positioned samples (sampling frequency lower frequency than 1,000 Hz), a resampling of respiration signal was performed, according to the samples of RRIs. It was done using our custom Matlab program (Kapidžić et al., 2014; **Supplementary Data Sheet 1**).

The indices for our examination were: (a) linear measures of heart rate variability: mean value and standard deviation (Task Force Guidelines, 1996) (b) short term exponent α_1 as

[1]https://www.webmetronome.com/

a fractal measure which in heart rate strongly correlates with changes in low and high frequency oscillations (sympathetic and parasympathetic activity) (Weippert et al., 2015; Shiau, 2018); (c) long term exponent α_2 as a fractal measure which in heart rate spectrum corresponds to a very low frequency band (Francis et al., 2002); (d) multiscaling entropy at short time scales (1–4 samples, MSE_{1-4}), related to fast oscillations, respiratory and predominately vagal control (Silva et al., 2016); (e) multiscaling entropy at long time scales (5–10 samples, MSE_{5-10}), related to slow oscillations, predominately of sympathetic control (Silva et al., 2016); (f) spectral coherence ($Coh_{RRI-Resp}$), reflecting the presence (Daoud et al., 2018) and degree (Faes and Nollo, 2011) of linear cardiac and respiratory oscillatory synchronization; (g) short scale and long scale cross DFA (ρ_1 and ρ_2, respectively Podobnik and Stanley, 2008; Horvatic et al., 2011; Podobnik et al., 2011; Zebende, 2011; Kristoufek, 2015; Kwapien et al., 2015 as the parameters of cross correlations of fractal RRI and respiratory variations; and (h) short and long scale cross MSE (X_{MSE1-4} and $X_{MSE5-10}$, respectively) as the measure of cross correlation in MSE domain (Costa et al., 2005). Programs for Cross DFA and cross MSE are available within **Supplementary Data Sheet 1**.

Non-linear indices of RRI and respiration were calculated using Matlab 2007b (Mathworks, Natick, USA). Applying an algorhithm for detrended fluctuation analysis, we obtained two numerical series: one with values of log ($F(n)$), the other for log (n). After ploting log ($F(n)$) vs. log (n), linear fit (regression line) was computed for the first 8 sample points (corresponding to $n = 4$–13). The slope of this regression line is regarded as the short term fractal scaling exponent α_1. The same was done for the rest of the samples (following 16 points—$n > 13$), regarded as the long term fractal scaling exponent α_2 (Peng et al., 1995a; Perakakis et al., 2009; please see Figure 4 in **Appendix II**). The number of points for short term α_1 and long term α_2 are not accidently chosen. They reflect two specific scaling regimes which are usually separated by a specific crossover point (discrete change of slope) in regression line (Peng et al., 1995b; Perakakis et al., 2009). In several subjects, the crossover was not positioned at the 9th point; for some subjects it was at an earlier point, such as the 6th, 7th, 8th, and for other subjects at a later point, such as the 10th and 11th point. Thus, in these cases we considered less points for obtaining α_1 (5, 6, and 7 points, respectively) or later points for α_2 (after 11th, 12th, etc). This occurred especially in sessions with slow breathing. Peng and co-workers noted that not all subjects exhibit crossover (and separation on two scaling regimes, Peng et al., 1995b), just as there were few cases of this kind in our sample. Characteristic crossover patterns are not just a feature of a healthy or diseased state, as Peng and co-workers pointed out (Peng et al., 1995b). Breathing frequency exerts influence on the crossover point as well (Perakakis et al., 2009; Platiša and Gal, 2010).

Moreover, we introduce here one additional measure, *inter-fractal angle* θ which reflects the relationship between two scaling regimes; in other words, it is an angle that short term and long term regression lines form between each other. In order to explain inter-fractal angle θ we conducted an angular analysis (detailed explanation in **Appendix II**). Instead of slopes of regression lines α_1 and α_2, angles that regression lines form with x-axis α_{A1} and α_{A2} were taken into account for the purpose of direct physical and physiological interpretation. Inter-fractal angle θ is directly proportional to the difference between α_{A1} and α_{A2} ($\theta = \alpha_{A1} - \alpha_{A2}$). We defined α_{A1} and α_{A2} as short term fractal angle and long term fractal angle with the abscissa, respectively. Additionally, our analytic tool characterizes the inter-fractal angle θ as a random variable, as well as its changes under the influence of orthostasis and slow breathing, which was analyzed using a probability density estimate procedure (PDE, supplied with Matlab, 2007b). In order to perform this analysis, the choice of inter-fractal angle θ with respect to the α_1/α_2 relation bypassed the possible calculation error for the case where slopes converge to infinite values (see **Appendix II**). Four numerical series (supine, stand, supin01, stand01), with 20 inter-fractal angle values each, were subjected to PDE analysis. Thus, we obtained four PDE profiles for four physiological conditions, in which distributions could be calculated (for detailed description please see Kalauzi et al., 2012). Additionally, we estimated PDE of the fractal angles α_{A1} and α_{A2}. The aim of this was to try to elicit a physiological explanation of inter-fractal angle changes (please see **Appendices II** and **III**).

Multiscale entropies (MSE_{1-4} on short scales and MSE_{5-10} on long scales) were calculated as additional non-linear measures. They are based on the concept of sample entropy which by definition represents a "negative natural logarithm of the conditional probability that two sequences similar for m point intervals remain similar at the next point within a tolerance r" (Richman and Moorman, 2000). MSE algorithm makes estimation of sample entropy for each course-grained time series (averaged values from the data points within non-overlapping windows of increasing length/scale factor, Costa et al., 2005). Input criteria parameters for the sample entropy used had fixed values for all subjects: size of the window (pattern length) $m = 2$, and similarity criterion (standard deviation of a signal sequence) $r = 0.15$. The output of the algorithm consisted of two numerical series; one representing values of sample entropy for each scale factor and the other consisting of scale factor values ($n = 1, \ldots, 20$). MSE_{1-4} was calculated as mean value from 1 to 4th sample points (sample entropy vs. scale factor), and MSE_{5-10} as mean value from 5 to 10th sample points (sample entropy vs. scale factor).

RRI-respiratory coherence ($Coh_{RRI-Resp}$) was calculated using the following procedure: equidistant resampled RRI and respiration signals were imported in OriginPro 8.6 (OriginLab Corporation, Northampton, MA, USA). Within the Origin toolbox Analysis/Signal Processing/FFT/Coherence we made the following parameter settings: mean RRI for sampling interval of signals and Welch method for power spectral density estimation were chosen [decomposition of signal by Hanning window into smaller parts (256 points long), with 50% overlap (128 points)]. After the execution of the algorithm, two numerical rows were generated; one with values of frequency [Hz], the other with values of RRI-respiration cross power (variance) distributed over frequency ranges [s^2/Hz]. Then, we plotted them as x vs. y coordinates, respectively, to get cross power spectrum as a function of frequency (see Figure 7 in **Appendix IV**). Using visual observation and peak pick tool, we determined the

maximum value (peak) on the cross power spectrum diagram ($Coh_{RRI-Resp}$). This usually corresponds with or near the location of breathing frequency (on the x-axis). We considered then that $Coh_{RRI-Resp}$ represented the strength of the linear cardiorespiratory coupling. Values of $Coh_{RRI-Resp}$ over 0.8 were assumed as high level/strong cardiorespiratory coupling. For a more detailed explanation of the application of the mentioned coherence method see **Appendix IV** (and/or Platiša et al., 2016a; Radovanović et al., 2018).

The short term and long term cross DFA (ρ_1 and ρ_2, respectively) parameters were calculated using the procedure described in Podobnik et al. (2011) and Kristoufek (2015) (see **Supplementary Data Sheet 1**). For every scale s, detrended cross-correlation coefficient was given by

$$\rho_{DCCA}(s) = \frac{F^2_{DCCA}(s)}{F_{DFA,x}(s)\,F_{DFA,y}(s)}$$

where $F^2_{DCCA}(s)$ is a detrended covariance between partial sums (profiles) of the two signals, while $F_{DFA,x}(s)$ and $F_{DFA,y}(s)$ are square roots of detrended variances of their partial sums. For each scaling range, both short ($s = 4$–13) and long ($s = 14$–108), this coefficient was averaged within the corresponding limits. Short term and long term scale cross MSE's (X_{MSE1-4} and $X_{MSE5-10}$, respectively) were obtained by applying our custom made MATLAB program for calculating conventional cross sample entropy on signals previously prepared by coarse-graining procedure (Costa et al., 2005) (see **Supplementary Data Sheet 1**). For each scale range, these values were averaged ($n = 1$–4 for X_{MSE1-4} and $n = 5$–10 for $X_{MSE5-10}$).

Statistical Analysis

We stored all calculated results in a dataset crated with SPSS 19 (Statistical Package for the Social Sciences, 14, IBM, New York, USA). Statistical analysis was subsequently done by means of SPSS 19 toolboxes. We applied both visual checking of Gaussian distribution [by means of the frequency distributions (histograms), stem-and-leaf plot, boxplot, P-P plot (probability-probability plot) and Q-Q plot (quantile-quantile plot)] and Shapiro-Wilk normality test. Both visual checking and Shapiro-Wilk normality test of each parameter in 20 subjects confirmed that our data had non-Gaussian distribution. Therefore, we applied the non-parametric Kruskal Wallis test with *post-hoc* Mann Whitney test with Bonferroni's correction for multiple measurements to compare all samples (**Table 2**).

RESULTS

It is obvious even from visual observation (**Figure 1**) that changes of body posture and breathing frequency affect RRI variability. While orthostasis causes a decrease in mean value and linear variability (standard deviation) of RRI, orthostasis with slow breathing results in the decrease of the RRI mean value only

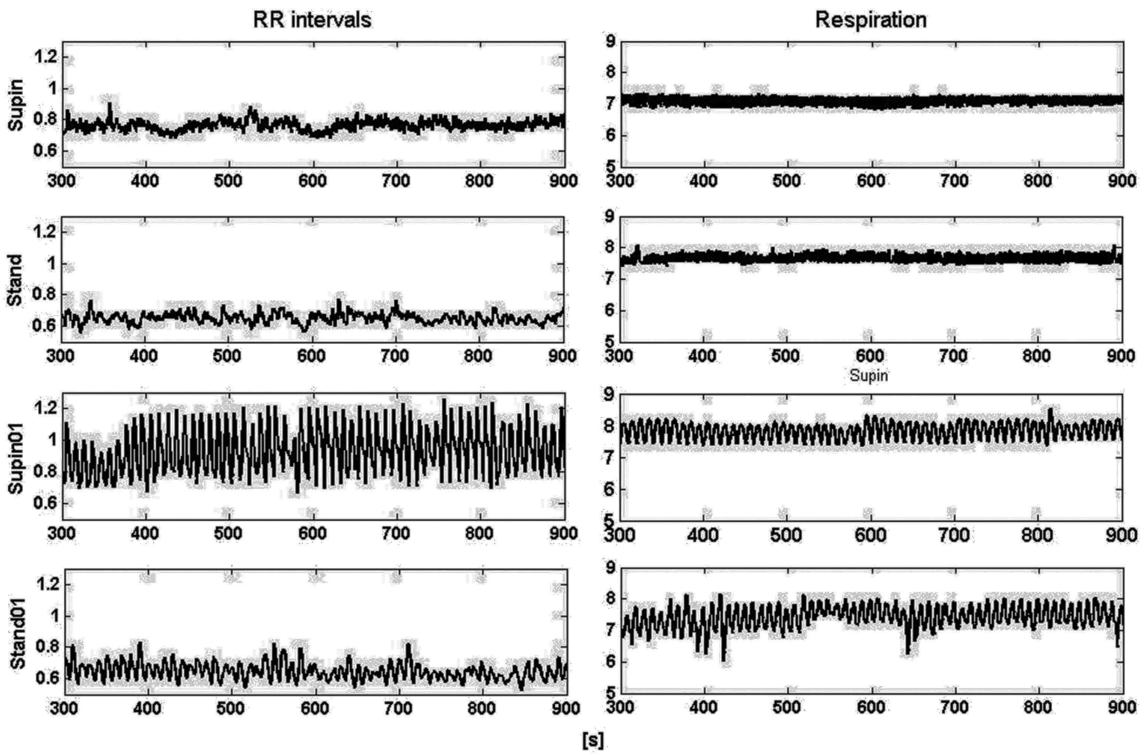

FIGURE 1 | Segments (600 s) of RRI (left) and respiratory (right) signals recorded at supine position and standing with spontaneous (supin and stand, respectively) and 0.1 Hz breathing (supin01 and stand01, respectively).

TABLE 1 | Linear and non-linear parameters (mean, SD) of 20 healthy subjects.

Group	Parameter	Supin	Stand	Supin01	Stand01
Cardiac parameters	mRRI [s]	0.9937 ± 0.1377	0.7263 ± 0.1021	1.0592 ± 0.1257	0.7480 ± 0.0867
	sdRRI [s]	0.0621 ± 0.0237	0.0465 ± 0.0175	0.0905 ± 0.0347	0.0702 ± 0.0225
	α_{1RRI}	0.8975 ± 0.1925	1.3114 ± 0.1379	1.0342 ± 0.1421	1.3408 ± 0.1005
	α_{2RRI}	0.8232 ± 0.1244	0.7874 ± 0.1249	0.6922 ± 0.1647	0.5545 ± 0.1463
	θ_{RRI} [^{0}]	2.2 ± 8.3	14.5 ± 5.6	11.5 ± 8.7	24.6 ± 6.7
	α_{A1RRI} [^{0}]	41.4 ± 5.9	52.5 ± 3	45.7 ± 4	53.2 ± 2.1
	α_{A2RRI} [^{0}]	39.2 ± 4.4	38 ± 4.5	34.2 ± 6.7	28.6 ± 6.3
	MSE_{RRI1-4}	1.7936 ± 0.1783	1.5583 ± 0.2974	1.6713 ± 0.2463	1.4715 ± 0.1784
	MSE_{RR5-10}	1.7706 ± 0.2138	1.8951 ± 0.2391	1.4991 ± 0.1848	1.9123 ± 0.1732
Respiratory parameters	mResp [s]	4.55 ± 1.45	4.56 ± 1.78	10	10
	sdResp	0.89 ± 0.61	1.09 ± 1.35	0	0
	α_{1Resp}	0.3679 ± 0.2603	0.4975 ± 0.2728	0.9268 ± 0.3133	1.1387 ± 0.2357
	α_{2Resp}	0.5848 ± 0.2319	0.6119 ± 0.2132	0.4850 ± 0.2003	0.3759 ± 0.1028
	θ_{Resp} [^{0}]	−10.3 ± 18.8	−5.5 ± 18.5	16 ± 16.1	27.5 ± 7.2
	α_{A1Resp} [^{0}]	19.1 ± 11.4	25.2 ± 11.8	41.3 ± 12.1	47.9 ± 8.2
	α_{A2Resp} [^{0}]	29.4 ± 10.6	30.7 ± 9.3	25.3 ± 10	20.4 ± 5.6
	$MSE_{Resp1-4}$	1.4456 ± 0.2631	1.3185 ± 0.4117	1.3772 ± 0.3074	1.0995 ± 0.2837
	$MSE_{Resp5-10}$	1.1396 ± 0.2532	1.0423 ± 0.3523	1.3040 ± 0.3065	1.3382 ± 0.3132
Cardio-pulmonary coupling	$Coh_{RRI-Resp}$	0.8983 ± 0.0563	0.7397 ± 0.1986	0.8703 ± 0.1137	0.8663 ± 0.1363
	ρ_1	−0.2419 ± 0.1905	−0.2002 ± 0.1916	−0.0096 ± 0.2665	−0.0697 ± 0.2787
	ρ_2	−0.1346 ± 0.1314	−0.0190 ± 0.1234	−0.0232 ± 0.2471	0.0097 ± 0.2429
	X_{MSE1-4}	2.2733 ± 0.20298	2.2719 ± 0.40199	2.1490 ± 0.24829	1.9344 ± 0.21773
	$X_{MSE5-10}$	2.1765 ± 0.21385	2.1253 ± 0.27514	2.3176 ± 0.15034	2.4292 ± 0.46726

Supin, supine position; stand, standing; supin01, supine position with paced 0.1 Hz breathing; stand01, standing with paced 0.1 Hz breathing; mRRI, mean value of RRI signal; sdRRI, standard deviation of RRI signal; α_{1RRI}, short term fractal scaling exponent of RRI signal; α_{2RRI}, long term fractal scaling exponent of RRI signal; θ_{RRI}, inter-fractal angle of RRI signal; α_{A1RRI}, short term fractal angle of RRI signal; α_{A2RRI}, long term fractal angle of RRI signal; MSE_{RRI1-4}, short term multiscaling entropy of RRI signal (for 1–4th sample); $MSE_{RRI5-10}$, long term multiscaling entropy of RRI signal (for 5–10th sample); mResp, mean value of respiration signal; sdResp, standard deviation of respiration signal; α_{1Resp}, short term fractal scaling exponent of respiration signal; α_{2Resp}, long term fractal scaling exponent of respiration signal; θ_{Resp}, inter-fractal angle of respiration signal; α_{A1Resp}, short term fractal angle of respiration signal; α_{A2Resp}, long term fractal angle of respiration signal; $MSE_{Resp1-4}$, short term multiscaling entropy of respiration signal (for 1–4th sample); $MSE_{Resp5-10}$, long term multiscaling entropy of respiration signal (for 5–10th sample); $Coh_{RRI-Resp}$, RRI-respiration coherence; $\rho_{DCCARRI-Resp}$, RRI-respiration detrended cross correlation coefficient; ρ_1, short term scaling RRI-respiration detrended cross correlation coefficient; ρ_2, long term scaling RRI-respiration detrended cross correlation coefficient; X_{MSE1-4}, short term RRI-respiration cross multiscaling entropy; $X_{MSE5-10}$, long term RRI-respiration cross multiscaling entropy.

(**Tables 1**, **2**). Supine position with slow breathing induced the highest values of mean linear RRI variability (sdRRI, **Table 1**).

Mean values and standard deviations of non-linear parameters of RRI and respiratory signal variability are reported in **Table 1**. From the results calculated for 20 subjects, we calculated the horizontal mean value estimation in each sample of the non-linear parameter. Then, we plotted these mean values with their standard deviation as error bars (**Figures 2**, **3**). On these plots we were able to observe changes of inter-fractal angle θ, a new quantity for y_1 vs. y_2 relationship, with superior accuracy with respect to the existing relations of slopes (De Souza et al., 2014, for details see **Appendix II**). Statistical significance of changes induced by body posture and breathing frequency on RRI and respiratory signal linear and non-linear parameters for 20 subjects are reported in **Table 2**.

State dependent changes of the coefficients are reported in **Table 2**. Due to the non-Gaussian distribution of the data confirmed by visual inspection and Shapiro-Wilk normality test, we applied the non-parametric Kruskal Wallis test. The variables that manifested significant state dependent change were compared with supine values (as the baseline) by Mann-Whitney test using the Bonferroni correction of the statistical significance from multiple permuted measurements ($p{\cdot}m < 0.5$, for $m = 3$, where m is the number of comparisons[2]). The mean value of RRI (mRRI) was significantly changed just under the influence of orthostasis and the standard deviation of RRI (sdRRI) was significantly changed in supine with 0.1 Hz breathing. The short term scaling exponent α_1 of RRI signal (α_{1RRI}) was significantly increased under the influence of body posture (supin-stand), slow breathing (supin-supin01) and in the state of standing with 0.1 Hz breathing (supin-stand01). The long term scaling exponent α_2 was significantly decreased in supine with slow breathing and in standing with slow breathing positions, while during orthostasis alone α_2 was not significantly changed. The inter-fractal angle θ_{RRI} significantly increased in all three statistical conditions. This change was a consequence of the individual and joint change of α_{A1RRI} and α_{A2RRI} (**Table 1**, for detailed analysis see **Appendix III**). α_{A1RRI} increases both

[2]https://www.ibm.com/support/pages/post-hoc-comparisons-kruskal-wallis-test

TABLE 2 | Change of linear and non-linear cardiorespiratory parameters in different conditions.

Group	Parameter	Supin-stand	Supin-supin01	Supin-stand01
Cardiac parameters	mRRI	**0.001↓**	0.306	**0.001↑**
	sdRRI	**0.072↓**	**0.021↑**	0.831
	α_{1RRI}	**0.001↑**	**0.030↑**	**0.001↑**
	α_{2RRI}	>0.99	**0.027↓**	**0.001↓**
	θ_{RRI} [^{0}]	**0.001↑**	**0.006↑**	**0.001↑**
	MSE_{RRI1-4}	**0.015↓**	0.471	**0.001↓**
	$MSE_{RRI5-10}$	0.120	**0.001↓**	0.063↑
Respiratory parameter	mResp	>0.99		–
	sdResp	>0.99		–
	α_{1Resp}^*	0.273	**0.001↑**	**0.001↑**
	α_{2Resp}^*	2.775	0.273	**0.001↓**
	θ_{Resp} [^{0}]	0.942	**0.001↑**	**0.001↑**
	$MSE_{Resp1-4}$	>0.99	>0.99	**0.001↓**
	$MSE_{Resp5-10}$	>0.99	0.258	**0.054↑**
Cardio-pulmonary coupling	$Coh_{RRI-Resp}$	**0.018↓**	>0.99	>0.99
	ρ_1	1.194	**0.003↑**	**0.072↑**
	ρ_2	0.015	0.228	0.105
	X_{MSE1-4}	>0.99	0.402	**0.001↓**
	$X_{MSE5-10}$	0.981	0.189	**0.051↑**

*post-hoc Mann-Whitney test for independent samples with Bonferroni corrected p-value ($p \cdot m < 0.5$, for $m = 3$, where m is the number of comparisons) after Kruskal-Wallis test for multiple comparation for 20 healthy subjects;↓-decrease of the change; ↑-increase of the change); supin-stand, supine position (with spontaneous breathing) vs. standing position (with spontaneous breathing); supine-supin01, supine position (with spontaneous breathing) vs. supination with paced 0.1 Hz breathing; supine-stan01, supine position (with spontaneous breathing) vs. standing with paced 0.1 Hz breathing; bolded numbers, results with statistical significance ($p < 0.05$); *Statistical significances of the respective angles were identical; mRRI, mean value of RRI signal; sdRRI, standard deviation of RRI signal; α_{1RRI}, short term fractal scaling exponent of RRI signal; α_{1Resp}, short term fractal scaling exponent of respiratory signal; α_{2RRI}, long term fractal scaling exponent of RRI signal; α_{2Resp}, long term fractal scaling exponent of respiratory signal; MSE_{RRI1-4}, short term multiscaling entropy of RRI signal (for 1–4th sample); $MSE_{RRI5-10}$, long term multiscaling entropy of RRI signal (for 5–10th sample); $MSE_{Resp1-4}$, short term multiscaling entropy of respiratory signal (for 1–4th sample); $MSE_{Resp5-10}$, long term multiscaling entropy of respiratory signal (for 5–10th sample); $Coh_{RRI-Resp}$, RRI-respiration coherence; ρ_1, short term scaling RRI-respiration detrended cross correlation coefficient; ρ_2, long term scaling RRI-respiration detrended cross correlation coefficient X_{MSE1-4}, short term RRI-respiration cross multiscaling entropy, $X_{MSE5-10}$, long term RRI-respiration cross multiscaling entropy; grayshaded variables: variables which were not confirmed by Kruskal Wallis test as state dependent.*

as a consequence of posture change (supin-stand) and a change of breathing regime (supin-supin01). α_{A2RRI} was decreased by slow breathing in two statistical cases (supin-supin01 and supin-stand01). Change of posture alone (supin-stand) did not result with a joint (opposite) change of α_{A1RRI} and α_{A2RRI}, but by increase of α_{A1RRI} only.

Short term multiscaling entropy of RRI (MSE_{RRI1-4}) was significantly decreased under the influence of body posture (supin-stand) and the change of body posture combined with the slow breathing regime (supin01-stand01). The long term multiscaling entropy ($MSE_{RRI5-10}$) was increased by slow breathing in standing position (supin01-stand01, a significance level of $p = 0.063$), and decreased by slow breathing in supine position (supin-supin01). Joint (opposite) changes of MSE_{RRI1-4} and $MSE_{RRI5-10}$ happened in the case of orthostasis with controlled breathing regime (supin01-stand01). The change of breathing regime (supin-supin01) only occurred when there was a change in $MSE_{RRI5-10}$ (decrease). Of particular interest was the result that in stand01 both fractal (α_{1RRI} vs. α_{2RRI}) and irregularity properties of RRI (MSE_{RRI1-4} vs. $MSE_{RRI5-10}$) are reciprocally regulated. The analysis of scale dependent patterns revealed that both short scale (α_{1RRI} vs. MSE_{RRI1-4}) and long scale (α_{2RRI} vs. $MSE_{RRI5-10}$) parameters were also reciprocally regulated (**Table 2**).

In the respiratory signal, mean value and standard deviation (mResp and sdResp) changed only with the change of breathing regime (supin-supin01) and not with the change of posture (supin-stand). We also visually evaluated the respiratory signal DFA plot for the crossover point (**Figure 3A**) and applied the inter-fractal angle θ_{Resp} analysis analogous to the RRI signal analysis (**Tables 1**, **2**). Detailed PDE analysis of the inter-fractal angle θ_{Resp} and its components are presented in **Appendix III**, Figure 6. α_{1Resp} did not change significantly with the posture change (supin-stand), but it increased in the case of controlled breathing regime (supin-supin01). α_{2Resp} did not change significantly either with the change of posture (supin-stand, $p = 0.99$) and in the condition of controlled breathing in supination (supin-supin01, $p = 0.273$). A significant decrease of α_{2Resp} was registered during the condition of standing with controlled breathing regime (supin-stand01). Joint changes of α_{1Resp} and α_{2Resp} were in the opposite direction. The inter-fractal angle θ_{Resp} did not change as a result of body posture change (supin-stand), but only under the controlled breathing regime (supin-supin01, supine-stand01, increase, $p < 0.001$).

The angle α_{A1Resp} did not change as the result of a body posture change (supin-stand), but significantly increased in all conditions with the controlled breathing regime ($p < 0.001$). The angle α_{A2Resp} also did not respond to the posture change (supine-stand) and slow breathing regime in supine position (supine-supin01, $p = 0.273$). α_{A2Resp} significantly decreased in the regime of slow breathing combined with standing (supin-stand01). Joint changes of α_{A1Resp} and α_{A2Resp} (supine-stand01) were in the opposite direction. State dependent, statistically confirmed changes of angles α_{A1Resp} and α_{A2Resp} were identical to the changes of the respective slopes (i.e., $\alpha_{1Resp}$and α_{2Resp}; **Table 2**).

Change of α_{1Resp} ($\Delta\alpha_{1Resp}$, **Table 3**) was positive in all physiological conditions. Change of α_{2Resp} ($\Delta\alpha_{2Resp}$, **Table 3**) was negative only in conditions of slow 0.1 Hz breathing. Change of inter-fractal angle θ ($\Delta\theta_{Resp}$, see **Table 3** and **Appendix II**) was always significant and positive in the conditions of controlled breathing regime (supin-supin01,), while insensitive to posture changes only (supin-stand).

Short term multiscaling entropy ($MSE_{Resp1-4}$) was significantly decreased in conditions of combined standing position with slow breathing (supin-stand01). Long term multiscaling entropy ($MSE_{Resp5-10}$) increased only in the condition of combined standing and slow breathing regime (supin-stand01, significance level of $p = 0.054$). In the condition of joint $MSE_{Resp1-4}$ and $MSE_{Resp5-10}$ change, the parameters changed in opposite directions.

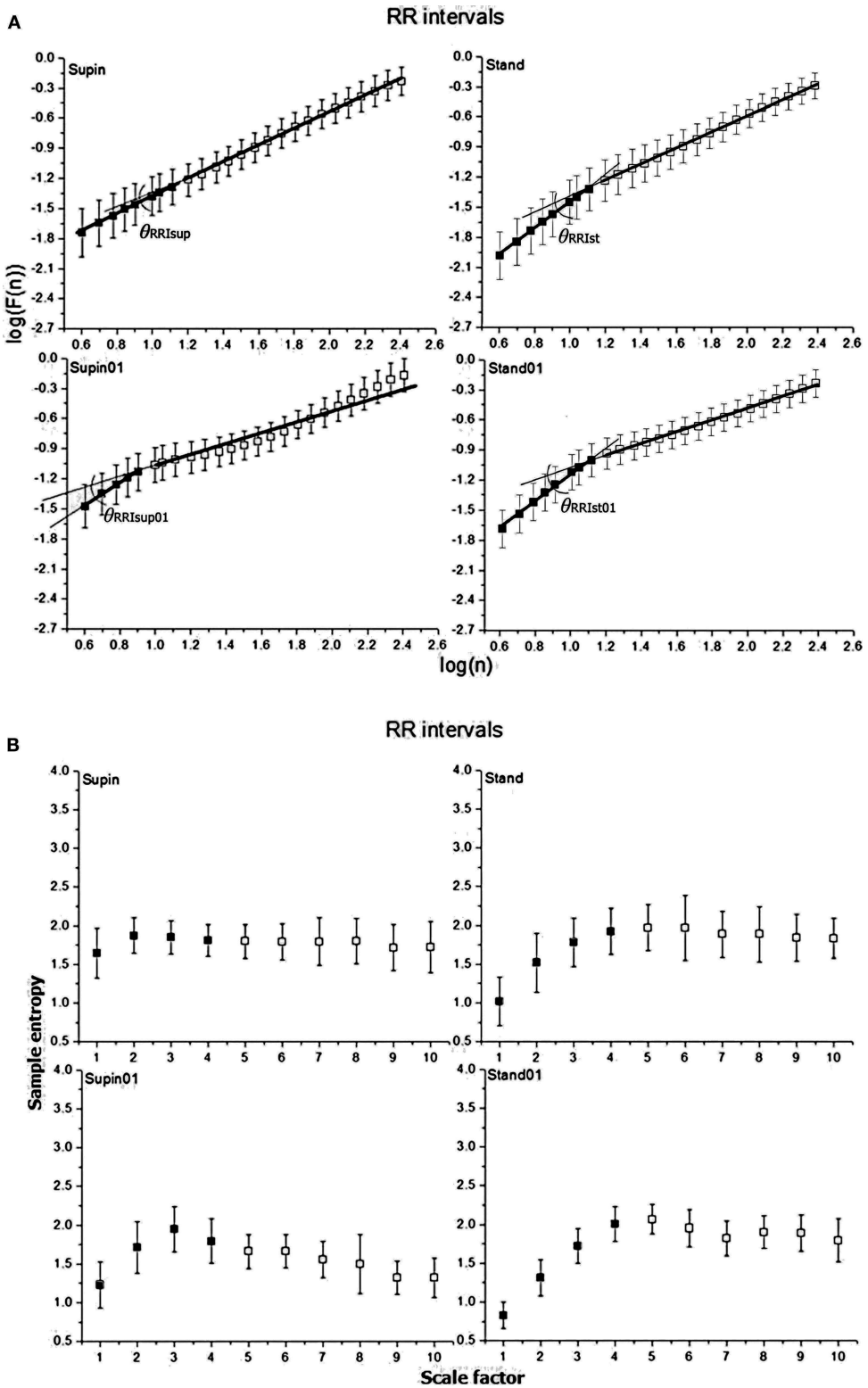

FIGURE 2 | Graphic representation of non-linear properties of RRI variability in 20 healthy subjects expressed through: **(A)** fractal indices: full dark colored squares (dots) represent samples of short term fractal scaling exponent α_1; empty squares represent samples for long term fractal scaling exponent α_2; RRI inter-fractal angles: θ_{RRIsup}, supine position with spontaneous breathing; θ_{RRIst}, standing with spontaneous breathing; $\theta_{RRIsup01}$, supine position with paced 0.1 Hz breathing; $\theta_{RRIst01}$, standing with paced 0.1 Hz breathing; F(n), root-mean-square fluctuations, *n*, window size; **(B)** multiscaling entropy (1–20 samples); mean value of the first four samples (dark colored squares) is short term multiscaling entropy MSE_{1-4}; mean value of 5–10th sample (light colored squares) is long term multiscaling entropy MSE_{5-10}; supin, supine position; stand, standing; supin01, supine position with paced 0.1 Hz breathing; stand01, standing with paced 0.1 Hz breathing.

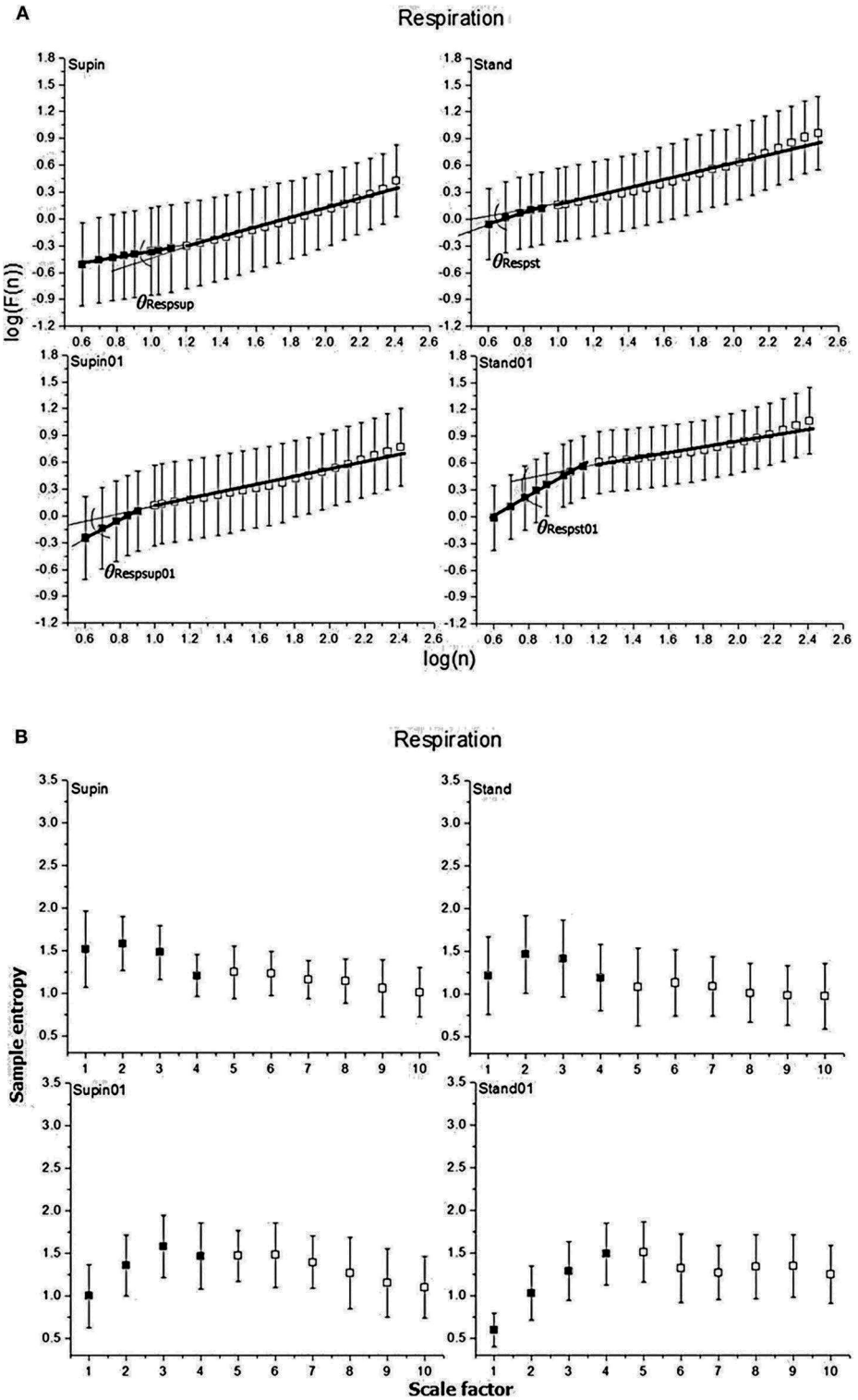

FIGURE 3 | Graphic representation of non-linear properties of respiration signal in 20 healthy subjects expressed through: **(A)** fractal indices; full colored squares (dots) represent samples of short term fractal scaling exponent α_1; empty (uncolored) squares represent samples for long term fractal scaling exponent α_2; RRI inter-fractal angles: θ_{RRIsup}, supine position with spontaneous breathing; θ_{RRIst}, standing with spontaneous breathing; $\theta_{RRIsup01}$, supine position with paced 0.1 Hz breathing; $\theta_{RRIst01}$, standing with paced 0.1 Hz breathing; F(n), root-mean-square fluctuations, *n*, window size; **(B)** multiscaling entropy (1–20 samples); mean value of the first four samples (dark colored squares) is short term multiscaling entropy MSE_{1-4}; mean value of 5–10th sample (light colored squares) is long term multiscaling entropy MSE_{5-10}; supin, supine position; stand, standing; supin01, supine position with paced 0.1 Hz breathing; stand01, standing with paced 0.1 Hz breathing.

TABLE 3 | Change (arithmetic difference) of detrended fluctuation analysis parameters between physiological states.

Parameter	Supin-stand	Supin-supin01	Stand-stand01	Supin01-stand01
$\Delta\alpha_{1RRI}$	0.4139 ± 0.20127	0.1367 ± 0.15330	0.0294 ± 0.12612	0.3066 ± 0.16099
$\Delta\alpha_{2RRI}$	−0.0358 ± 0.16469	−0.1311 ± 0.20205	−0.2329 ± 0.12008	−0.1377 ± 0.19485
$\Delta\theta_{RRI}$ [0]	12.4 ± 10.3	9.3 ± 9.9	10 ± 4.4	13.1 ± 10.8
$\Delta\alpha_{1Resp}$	0.1296 ± 0.21130	0.5588 ± 0.36660	0.6412 ± 0.40181	0.2119 ± 0.39949
$\Delta\alpha_{2Resp}$	0.0271 ± 0.20977	−0.0998 ± 0.19600	−0.2360 ± 0.17368	−0.1091 ± 0.20976
$\Delta\theta_{Resp}$ [0]	4.8 ± 12.4	26.4 ± 20.3	32.9 ± 21.5	11.5 ± 20.8

Supin, supine position; stand, standing; supin01, supine position with paced 0.1 Hz breathing; stand01, standing with paced 0.1 Hz breathing; $\Delta\alpha_{1RRI}$, change of short term fractal exponent α_1 of RRI signal; $\Delta\alpha_{2RRI}$, change of long term fractal exponent α_2 of RRI signal; $\Delta\theta_{RRI}$, change of inter-fractal angle of RRI signal; $\Delta\alpha_{1Resp}$, change of short term fractal exponent α_1 of respiration signal; $\Delta\alpha_{2Resp}$, change of long term fractal exponent α_2 of respiration signal; $\Delta\theta_{Resp}$, change of inter-fractal angle of respiration signal.

We underline the result that in standing with 0.1 Hz breathing both fractal (α_{1Resp} vs. α_{2Resp}) and irregularity properties of respiratory signal ($MSE_{Resp1-4}$ vs. $MSE_{Resp5-10}$) were reciprocally regulated. The analysis of scale dependent patterns revealed that in this state both short scale (α_{1Resp} vs. $MSE_{Resp1-4}$) and long scale (α_{2Resp} vs. $MSE_{Resp5-10}$) parameters were also reciprocally regulated (**Table 2**).

RRI-respiratory coherence ($Coh_{RRI-Resp}$) was decreased under the influence of orthostasis (supin-stand). ρ_1 significantly increased during slow breathing in supine position ($p = 0.003$) and standing with slow 0.1 Hz breathing (significance level of $p = 0.072$). Our statistical approach could not confirm state-dependent ρ_2 changes. X_{MSE1-4} and $X_{MSE5-10}$ decreased and increased, respectively, in the condition of orthostasis combined with slow breathing.

DISCUSSION

In recent years influence of slow breathing on heart rate variability (HRV) has been the focus or research (Russo et al., 2017). An increase of HRV has been recognized as one of the important physiological indicators of positive therapeutic effects of slow breathing techniques on the cardiovascular system (Bruton and Lewith, 2005; Dick et al., 2014; Russo et al., 2017) and the physiological indicator of cardiovagal function (Shields, 2009). Also, the research on the orthostasis effect on HRV has been well-documented (De Souza et al., 2014; Zaidi and Collins, 2016; Valente et al., 2018) and is routinely used as a sensitive test for the evaluation of "physiological adaptive mechanisms" generated by the autonomic nervous system (head up tilt, Zygmunt and Stanczyk, 2010; Hoshi et al., 2019). Most of the studies that evaluate HRV in these physiological conditions (supine position, standing, supine position with 0.1 Hz breathing and standing with 0.1 Hz) focused on linear properties of HRV (Kabir et al., 2011; de Paula Vidigal et al., 2016; Javorka et al., 2018; Jha et al., 2018). However, non-linear properties quantify and explain up to 80% of total RRI variability (Vandeput, 2010) and reflect physiological mechanisms of multiinteracting cardiovascular control, mostly exerted through sympatho-vagal effectors operating in non-linear fashion (de Godoy, 2016). Regarding the respiratory signal, a higher variability and complexity of respiratory rhythm was found in healthy subjects, while complexity decreases in the presence of diseases (Papaioannou et al., 2011; Reulecke et al., 2018). This is the first study which aimed to analyze parallel changes of RRI and respiratory rhythm complexity during individual and combined posture and breathing pattern changes. Ultimately the goal of this approach was to provide an insight into cardiorespiratory coupling in physiological conditions characterized by typical cardiac autonomic patterns, identifying the condition potentially most beneficial for cardiopulmonary adaptability.

As stated above, the actual evaluations of physiological RRI complexity measures were performed in the conditions of selective and total pharmacological *blockade* of sympathetic and parasympathetic system (Castiglioni et al., 2011; Silva et al., 2017a), posture change, mental stress (Castiglioni et al., 2009; Javorka et al., 2018), exercise and aging (Castiglioni et al., 2009). To the best of our knowledge, our approach is the first one to evaluate the physiologic background of RRI complexity measures in the conditions of physiological selective and joint *enhancement* of sympathetic (orthostasis) and parasympathetic (0.1 Hz breathing) activity on RRI regulation.

Changes of posture and slow 0.1 Hz breathing are also significantly interrelated with the breathing pattern (Mortola et al., 2016; Hernandez et al., 2019; Mortola, 2019), and, both individually and jointly, provide an insight into the contribution of (a) the peripheral factor of changed respiratory mechanics (horizontal vs. vertical plane, Mortola, 2019) during orthostatic challenge, and (b) the impact of central, slow 0.1 Hz breathing control on the complexity regimes of the respiratory signal (Papaioannou et al., 2011; Mortola et al., 2016; Reulecke et al., 2018). Finally, parallel evaluation of cardiorespiratory parameters and cardiorespiratory coupling by the RRI-Resp coherence, cross DFA and cross MSE provides an insight into cardiorespiratory integrative mechanisms in these conditions.

In order to verify the reproducibility of an autonomic pattern characteristic for supin, stand, supin01, and stand01 we calculated the following linear parameters: absolute values, changes of mean, and standard deviation of RRI. The absolute values and their changes were in accordance with the literature (Javorka et al., 2018; Valente et al., 2018), where supin was characterized by slight parasympathetic dominance (Levy and Martin, 1996), stand by sympathetic dominance (**Table 1**, decrease of mean RRI and SD with respect to supin, **Table 2**, Sobiech et al., 2017), supin01 with maximized parasympathetic

dominance (**Table 1**, increase of SD with respect to supine, Shields, 2009) and stand01 with combined situation of higher sympathetic tone on mean RRI regulation (decrease of mRRI with respect to supin01, **Table 1**) with variability, most probably parasympathetically mediated, comparable to the supin values (**Table 1**, supin-stand01, **Table 2**, $p = 0.831$).

α_{1RRI}

A change of body posture (**Table 1**, supin-stand, sympathetic domination with parasympathetic withdrawal) determines a change in the α_{1RRI} parameter, from the value characteristic for the presence of long range correlations (supin, $0.5 < \alpha_{1RRI} < 1$, Peng et al., 1995a) toward Brownian noise (stand, $\alpha_{1RRI} \rightarrow 1.5$, Peng et al., 1995a). Changes of breathing pattern (**Table 1**, supin-supin01, parasympathetic domination) affect $\alpha_{1RRI,}$ causing a shift from the value characteristic for long range correlations (supin, $0.5 < \alpha_{1RRI} < 1$, Peng et al., 1995a) toward 1/f noise (supin01, $\alpha_{1RRI} \rightarrow 1$, Peng et al., 1995a). Combined changes of body posture and slow breathing (**Table 1**, supin-stand01, $\alpha_{1RRI} \rightarrow 1.5$, Peng et al., 1995a) further increase α_{1RRI} toward Brownian noise. With respect to supin01, this change was even higher, shifting the quality of correlations from 1/f noise (**Table 1**, supin01, $\alpha_{1RRI} \rightarrow 1$, Peng et al., 1995a) toward Brownian noise (stand01, $\alpha_{1RRI} \rightarrow 1.5$, Peng et al., 1995a). The overall conclusion is that sympathovagal non-linear interactions might be dependent on the pattern of their activation, having different scaling properties when individually activated (i.e., sympathetic activation in stand, $\alpha_{1RRI} \rightarrow 1.5$, Brownian noise, vs. parasympathetic activation on supin01, $\alpha_{1RRI} < 1$, 1/f noise, **Table 2**, $p < 0.05$ and $p < 0.05$, respectively) with respect to the state of their joint activation in stand01, where their non-linear RRI modulation appears to be additive, in the sense of Brownian noise (**Table 2**, $p < 0.001$).

α_{2RRI}

Change of body posture (**Table 1**, supin-stand, sympathetic domination with parasympathetic withdrawal) diminishes α_{2RRI} from the pattern of long range correlations (supin, $0.5 < \alpha_{2RRI} < 1$, Peng et al., 1995a) toward randomness ($\alpha_{2RRI} \rightarrow 0.5$, Peng et al., 1995a). This change was not significant (**Table 2**, $p > 0.05$). Change of α_{2RRI} by the change of breathing pattern (**Table 1**, supin-supin01, parasympathetic domination) significantly affects α_{2RRI} value toward that of a random pattern (**Table 2**). Combined changes of body posture with slow breathing (**Table 1**, stand-stand01) significantly decrease α_{2RRI} value toward randomness (**Table 1**, $\alpha_{2RRI} \rightarrow 0.5$, Peng et al., 1995a; **Table 2**, $p < 0.05$), both with respect to stand and with respect to supin01 (**Table 1**, $\alpha_{2RRI} \rightarrow 0.5$, supin01-stand01, **Table 2**, $p < 0.05$). The overall conclusion is that sympathetic and parasympathetic drive in the state of combined orthostasis and slow breathing (stand01) synergistically contribute to the increase of α_{2RRI} randomness, with greater contribution of parasympathetic drive with respect to sympathetic (**Table 1**, supin-supin01: $p < 0.01$; stand-stand01: $p < 0.001$, regarding the parasympathetic change, and supin-stand: $p > 0.05$; supin01-stand01: $p > 0.05$, regarding the sympathetic change).

$\Delta\alpha_{1RRI}$

Change of α_{1RRI} was always positive in all body and breathing pattern changes with maximal change between supin-stand (**Table 1**, sympathetic dominance with parasympathetic withdrawal) and minimal change between stand-stand01, implying a potential additive effect of sympathetic activation and parasympathetic withdrawal on $\Delta\alpha_{1RRI}$ in the orthostasis on one side, and on the other side, potentially antagonistic action on $\Delta\alpha_{1RRI}$ of joint parasympathetic and sympathetic activation in stand01 condition (**Table 3**).

$\Delta\alpha_{2RRI}$

Change of $\Delta\alpha_{2RRI}$ was always negative with minimum (absolute values) between supin-stand (sympathetic dominance with parasympathetic withdrawal) and maximum between supin01-stand01 (**Table 3**), implying a potential additive effect on $\Delta\alpha_{2RRI}$ of joint parasympathetic and sympathetic activation in stand01 condition.

These results of $\Delta\alpha_{1RRI}$ and $\Delta\alpha_{2RRI}$ (**Table 3**) imply that α_{1RRI} and α_{2RRI} are reciprocally regulated and mutually interdependent. This phenomenon was first noticed by Peng et al. (1995a) as a different α_{1RRI} vs. α_{2RRI} relationship between normal subjects and patients with congestive heart failure. This relationship was quantified as the α_1/α_2 ratio in physiological circumstances (women, change of posture, De Souza et al., 2014) but did not succeed in distinguishing state dependent RRI complexity changes. For this reason, we considered the angular values (θ, **Appendices II** and **III**), as more sensitive to individual and combined changes of the angle rays compared to the change of the α_1/α_2 index.

θ_{RRI}

In order to quantify the observed interdependence, we propose the inter-fractal angle θ_{RRI} between the linear regression lines of α_{1RRI} and α_{2RRI}, with the vertex at the crossover point (**Appendix II**, Figures 2, 4). The angle θ_{RRI} has its minimal value in the supine position (**Table 1**, sympathetic withdrawal with slight domination of parasympathetic drive). θ_{RRI} significantly increased both with the change of body posture (**Table 1**, supin-stand) and breathing pattern (supin-supin01), with a maximum increase in a combined state (supin01-stand01). It is reasonable to deduce that individual and joint physiological enhancements of sympathetic and parasympathetic drive contribute to the increase of the inter-fractal angle θ_{RRI}. We explored in detail the individual behaviors of α_{A1RRI}, α_{A2RRI}, and θ_{RRI} in four physiological conditions by PDE analysis (**Appendix III**). Figure 5A in **Appendix III** supports the view that supine state was characterized by multimodality of α_{A1RRI} generating regimes (three regimes, with dominant one approximately at mean 39°, with the greatest overall standard deviation). Change of posture shifted α_{A1RRI} toward unimodality (mean ∼53° and decrease of overall standard deviation). Voluntary slow breathing induced lighter α_{A1RRI} regime homogenization with respect to the change of posture (shifting from trimodality to bimodality, with dominant regime on ∼47° and with slightly decreased standard deviation). The most distinguished regime of α_{A1RRI} unimodality was in the circumstance of joint orthostasis with

slow breathing (mean value of dominant regime 54°, the lowest value of standard deviation). α_{A2RRI} showed fewer characteristic changes, though bimodality could be observed both in orthostasis and slow breathing (**Appendix III**, Figure 5B) and the dominant regime in stand01 condition. A large θ_{RRI} standard deviation was characteristic of all four conditions. Inter-fractal angle θ_{RRI} reflected the PDE pattern and changes similar to α_{A1RRI} (trimodality in supin and the shift toward unimodality in stand, supin01 and stand01) with the most distinct unimodality in stand and stand01 conditions. These results are in accordance with the results of Castiglioni et al. (2009) that a basic physiologic, healthy regime (supin) was characterized by the spectrum of α_{1RRI} and α_{2RRI} coefficients, the non-linear variables analogous to the angles α_{A1RRI} and α_{A2RRI}, as described by our analysis. To the best of our knowledge this is the first time that the spectrums of α_{1RRI} and α_{2RRI} are described by PDE and that the PDE pattern change was observed in four physiological conditions (supin, stand, supin01, stand01).

MSE_{RRI1-4} and $MSE_{RRI5-10}$ also showed opposite changes in stand01 condition, suggesting that orthostasis with slow 0.1 Hz breathing was the determinant factor of this type of change. The pattern of joint MSE_{RRI1-4} and $MSE_{RRI5-10}$ change was opposite to the pattern of joint α_{1RRI} and α_{2RRI} change (MSE_{RRI1-4} decrease and $MSE_{RRI5-10}$ increase) indicating that these non-linear parameters do not reflect the same, but potentially complementary information on non-linear variability (Costa et al., 2003; Perakakis et al., 2009). Body posture reversed the direction of $MSE_{RRI5-10}$ change induced by slow breathing (decrease for supin-supin01 and increase for supin-stand01, significance level of $p = 0.063$), which was suggestive of the hypothesis that the body posture might be the crucial factor for the direction of change of $MSE_{RRI5-10}$. To the best of our knowledge, these are the first results on individual and joint effects of body posture and breathing regime on MSE_{RRI1-4} and $MSE_{RRI5-10}$.

Regarding the respiratory signal, body posture did not change the linear parameters of breathing pattern (mResp and sdResp), while their change was obvious and expected with the change of breathing frequency. The same pattern, regarding the three statistical cases, was observed for mean values of all non-linear parameters (α_{1Resp}, α_{2Resp}, θ_{Resp}, α_{A1Resp}, α_{A2Resp}, $MSE_{Resp1-4}$, $MSE_{Resp5-10}$; **Table 2**), implying that body posture change by itself cannot provoke the robust changes of mean values of non-linear respiratory parameters. This finding supports the opinion that mechanic changes (horizontal vs. vertical plane) and cardiocirculatory patterns specific for the posture state (supin-stand, **Table 2**) do not influence robustly the breathing pattern in the non-linear domain. Slow breathing in both statistical cases induced significant increases in θ_{Resp}. In the supin-supin01 case, this increase was due only to the significant increase of α_{1Resp}, while in supin-stand01 the change was obtained by the joint, opposite changes of α_{1Resp} (i.e., α_{A1Resp}) and α_{2Resp} (i.e., α_{A2Resp}) (**Table 2**). This result implies that short term (α_{A1Resp}) and long term (α_{A2Resp}) respiratory complexities are influenced in opposite directions by slow 0.1 Hz breathing coupled with a change in posture, making the change of θ_{Resp} more enhanced only with respect to the θ_{Resp} change by orthostasis (supin-stand; **Table 2**). This relationship between α_{1Resp} and α_{2Resp} (θ_{Resp}) could hypothetically represent the result of confluent resonant cortical influences of posture maintenance motor system and slow 0.1 Hz respiration drive on brainstem autonomic respiratory network, considered to be an informational integrator of respiratory system (Feldman and McCrimmon, 2003).

PDE of α_{A1Resp} (**Appendix III**, Figure 6A) reveals two different bimodal distributions which changed the regime dominance pattern by posture change (from unidominant pattern in supin to equally represented bimodal regime in stand). Bimodality was significantly changed by slow 0.1 Hz breathing in the sense of shifting the dominant regime with the mean of ∼11° to the regime with dominant regime at the mean of ∼45°. The dominance of the unimodal pattern was even more enhanced by joint slow breathing in the standing position (mean α_{A1Resp} ∼48°). α_{A2Resp} PDE (**Appendix III**, Figure 6B) was less sensitive on the posture change (multimodal regime pattern with low regime definition and high value of standard deviation). Slow breathing in the supine condition (supin01) defined two regimes of α_{A2Resp}, with the dominant regime at the mean value of 28° and lower standard deviation with respect to the supine condition alone. Joint standing with slow breathing manifested clear regrouping of the two regimes into one, with mean of 22° and lower overall standard deviation. This data reveal that subtle, fine changes on breathing pattern in non-linear domain also happen during the postural change, but it appears that posture plays a role of secondary, enhancing factor of slow breathing impact on respiratory complexity. PDE analysis of inter-fractal angle θ_{Resp} (**Appendix III**, Figure 6C) illustrates the increase in multimodalities of the θ_{Resp} from prevailingly bimodal, with the dominant peak at −19° (supin), to potentially 5-modal regime in orthostasis (stand). Slow 0.1 Hz breathing introduced the shift of dominant pattern toward the regime of θ_{Resp} with mean of ∼18° (supin vs. supin01). Standing with slow breathing induced dramatic regrouping of θ_{Resp} values into one dominant regime with a mean value of 26° and a low value of the standard deviation. The general conclusion is that the individual change of posture increases the number of modalities of all three angle parameters of respiratory complexity, while the individual slow breathing regime restricts this number. The maximal, apparent synergistic reductive effect on multimodalities of Resp angles was registered in the combined (stand01) state. This was in accordance with the fact that demanding posture requirements necessitate more adaptable respiratory patterns, also in non-linear domain, while cortical influences of slow breathing impose the inhibitory effect on the brainstem respiratory neural network chaotic properties and dictate a monomodal pattern of their non-linear operating mode. The state of stand01 could represent a qualitatively specific state, typical for the behavior of non-linear systems (Goldberger, 2006). Multimodality of Resp angles, only specific for the orthostasis in the function of respiratory adaptability to the diversity of expected environmental (i.e., behavioral) challenges, with one and only one imposed behavior (slow 0.1 Hz breathing), could

become a qualitatively changed *enhancer* of 0.1 Hz breathing impact on Resp angles monomodal pattern.

$MSE_{Resp1-4}$ and $MSE_{Resp5-10}$ were parameters less sensitive to the change of breathing frequency, but were jointly modified in the condition supin-stand01.

Also in the case of respiratory signal complexity, in standing with 0.1 Hz breathing, both fractal (α_{1Resp} vs. α_{2Resp}) and irregularity properties of respiration ($MSE_{Resp1-4}$ vs. $MSE_{Resp5-10}$) were reciprocally regulated. The analysis of scale dependent pattern revealed that in this state both short scale (α_{1Resp} vs. $MSE_{Resp1-4}$) and long scale (α_{2Resp} vs. $MSE_{Resp5-10}$) parameters were also reciprocally regulated (**Table 2**). Opposite fractal patterns were evident also for the state supin01 (α_{1RRI} increase, α_{2RRI} decrease, $p < 0.05$; α_{1Resp} increase, α_{2Resp} decrease, not significant), while this state was not characterized by the opposite change of the respective MSE scale pattern. This was also the case of the respective RRI parameters.

These results show that:

a. The result of the scale dependent reciprocal pattern (α_1 vs. MSE_{1-4}) (α_2 vs. MSE_{5-10}) of both RRI and the respiratory signal in stand01 was not the consequence of calculation bias;
b. Mechanisms responsible for the changes of self-similarity and irregularity properties of RRI and respiratory signal are independently regulated in the state supin01;
c. The same RRI and respiratory complexity mechanisms are jointly and reciprocally regulated in the state stand01.

Cardiorespiratory regulation is integrated all along brainstem-hypothalamic axes up to limbic subcortical and cortical structures (Feldman and Ellenberger, 1988; Feldman and McCrimmon, 2003; Dampney, 2015). Behavioral control of breathing, with its specific voluntary component, is a state dependent, hierarchically organized dynamic system (Orem and Kubin, 2005; Kiselev and Karavaev, 2019; Noble and Hochman, 2019) with state dependent impact on cardiovascular regulation (best illustrated by the cardiovascular consequences of sleep apnea, Somers et al., 2008). These fundamental conclusions were drawn from the analysis of linear parameters of cardiorespiratory regulation.

The state specific pattern of both RRI and respiratory complexity regulation support the view that also RRI and respiratory complexity mechanisms are:

a. Hierarchically regulated (loosely coordinated ("dual control," Feldman and Ellenberger, 1988) cardiorespiratory control in individual behavioral tasks stand and supin01, transformed into well-defined and coordinated ("unitary control" Feldman and Ellenberger, 1988) cardiorespiratory response in the state of joined orthostasis with slow 0.1 Hz breathing).
b. That hierarchical recruitment of regulatory complexity mechanisms most probably increases "bottom-up" with respect to the increment of the behavioral challenge (i.e., from medullar level toward higher diencephalo-telencephalic structures). The behaviorally most complex state in our experimental design, stand01, was characterized by reciprocal scale dependent and pattern specific cardiorespiratory response.

Regarding cardiopulmonary coupling, our data report for the first time that these linear and non-linear mechanisms are independently and differently engaged with respect to the behavioral state, where linear coupling ($Coh_{RRI-Resp}$) appears to be sensitive on body posture change, while non-linear coupling (ρ_1, X_{MSE1-4}, and $X_{MSE5-10}$) jointly and most dynamically change in the state of standing with 0.1 Hz breathing.

Cross DFA parameters ρ_1 and ρ_2 register anticross correlation, or 180° phase shift of RRI and respiratory signal in all four physiological states, with the exception of ρ_2 in stand01 (**Table 1**). State dependent change was statistically confirmed only for ρ_1 (**Table 2**). In the supine position, as the baseline state of reference, we registered maximal negative phase shift of RR and respiratory signal both for short and long scales. Minimal negative phase shift of RR and respiratory signal on short scales (ρ_1) was noted in supin01 (**Tables 1**, **2**, $p = 0.003$). This phenomenon was most probably the consequence of increased synchrony of RRI-Resp on short scales, due to the potentially maximal values of RSA in this condition.

Cross MSE parameters X_{MSE1-4} and $X_{MSE5-10}$ report positive cross correlation in all four physiological states. Maximal degree of positive MSE cross correlation both for short and long scales was detected in supination, as the baseline state of reference. X_{MSE1-4} and $X_{MSE5-10}$ were insensitive to individual posture and breathing pattern change, but jointly and oppositely changed in the condition of orthostasis combined with slow breathing (decrease and increase, respectively, **Table 2**) in the state of combined orthostasis and slow breathing. In that state ρ_1 this manifests an increase of borderline significance ($p = 0.072$). A general conclusion might be that (a) ρ_1, ρ_2, X_{MSE1-4} and $X_{MSE5-10}$ are not dependent on the body posture change; (b) cross DFA and cross MSE coupling regimes are most probably independently regulated, referring to different patterns of change with respect to the physiological state (supin01: ρ_1 increase and X_{MSE1-4}, $X_{MSE5-10}$ not significant; stand01: ρ_1 increase and X_{MSE1-4}, $X_{MSE5-10}$ decrease and increase, respectively). The results speak for the ρ_1 positive correlation with the increase of vagal modulation to the heart, while X_{MSE1-4} and $X_{MSE5-10}$ could correlate with synergic slow breathing and posture control.

Even though we are speaking about borderline significances ($p\rho_1 = 0.072$, $pX_{MSE5-10} = 0.051$) and solid statistical confirmation for X_{MSE1-4} ($p < 0.0001$), a general picture of state dependent changes of cardiopulmonary complexity identifies standing with slow 0.1 Hz breathing as the most composite but the best defined state. Regarding cardiopulmonary coupling, this state was characterized by a decrease of short scale irregularity coupling ($\mathbf{X_{MSE1-4}}$) and increase in short scale self-similarity coupling ($\boldsymbol{\rho_1}$). This opposite pattern of short scale cardiopulmonary coupling for ρ_1 and X_{MSE1-4} was statistically confirmed only for the state of joint orthostasis with slow 0.1 Hz breathing, suggesting that only joint enhancement of volitional 0.1 Hz drive with sympathovagal modulation on the RRI could result in specific short scale coupling pattern. This cannot be attributed to vagal modulation only (traditional short scale RRI variability interpretation), but to the action of hierarchically higher structures on the sympatho-vagal pattern that potentiates short scale coupling in self-similarity

and reduces short scale coupling in irregularity. The pattern of short scale cardiopulmonary coupling specific for the state stand01 could be a feedback information of particular importance for the higher order cardiopulmonary network (locus coeruleus, central nucleus of amygdala, paraventricular nucleus of hypothalamus, Noble and Hochman, 2019), dorsomedial hypothalamus and midbrain periaqueductal gray (Dampney, 2015). These structures are of essential importance for the organization of cardiopulmonary response to environmental threatening stimuli, i.e., cardiopulmonary adaptability to the challenges (Dampney, 2015). Long lasting stressful threats inevitably induce pathological plasticity changes at the functional level of integrative networks (Bajić et al., 2010; Dampney, 2015), and these changes are initially observed on the short scale feedback RRI regulatory processes (i.e., impairment of baroreflex function, Bajić et al., 2010; Park et al., 2017). Scale dependent change of cardiopulmonary coupling in different behavioral conditions has not investigated previously, to the best of our knowledge. Still, our results offer a solid basis for the hypothesis that, together with quiet sleep (Zoccoli et al., 2001), the state of combined standing with 0.1 Hz breathing could be (one of?) the state of short scale functional recovering process of the cardiopulmonary pathologic plasticity.

The role and the presence of long range components in this pattern of cardiopulmonary coupling could be followed by statistically discrete increases of $MSE_{RRI5-10}$, $MSE_{Resp5-10}$ and finally their increased coupling ($X_{MSE5-10}$, $p = 0.051$). These results need further evaluation.

Finally, non-linear parameters of cardiorespiratory coupling had different patterns of state dependent change with respect to a linear effect; $Coh_{RRI-Resp}$, suggesting that state dependent cardiopulmonary interaction is a multilevel, dynamically controlled phenomenon.

As a limited view, when speaking about cardiorespiratory coupling, we speak about mutual, bidirectional interaction between cardiac and respiratory oscillations (Porta et al., 2012; Dick et al., 2014; Radovanović et al., 2018). Besides neuro-humoral, there are also physical circumstances involved as a part of indirect cardiorespiratory coupling (Porta et al., 2012). Though it exerts small influence (Billman, 2011; Porta et al., 2012), it should not be completely underestimated. Bearing this in mind, multifactorial physical and neuro-humoral interplay contribute to state dependent heart-lung interrelations as a unique biophysical model of dynamic, coupled oscillators (Dick et al., 2014).

LIMITATION OF THE STUDY

The ratio of spontaneous breathing inspirium vs. expirium duration (i/e) is ∼1:2. In order to obtain sufficiently long RRI and respiratory signals for selected analysis and in physiological steady state of cardiorespiratory regulatory mechanisms, we designed 20 min registration sessions for each physiological state. Controlled 0.1 Hz breathing with i/e 1:2 was too fatiguing for examinees and we were compelled to apply the paced breathing in i/e relation 1:1.

The literature suggests that HF HRV and RSA are greater when breathing with a regime of low compared to high i/e ratio (Strauss-Blasche et al., 2000; Porges, 2007). In a study by Van Diest et al. (2014), where the influence of i/e relation during breathing frequency of 0.1 Hz (frequency of paced breathing) was specifically investigated, both 0.49 and 1.44 i/e ratio resulted in significant increase of RSA and decrease of HR, with respect to the baseline RSA and HR values for spontaneous breathing (Van Diest et al., 2014). This means that in both (extreme) situations of i/e relation we have parasympathetic dominance on HR regulation, the condition that we aimed to achieve. We consider useful to emphasize that our i/e condition (∼1) during 0.1 Hz breathing is lower than the i/e condition of Van Diest et al. (2014) (1.44, an inverse relationship of i/e with respect to the value 1:2, typical for spontaneous breathing) and that consequently the difference between the parasympathetic drives to the heart of the two i/e conditions (0.49 vs. 1) could be negligible. Still, we recognize the potential limitation of this approach for the fine interpretation of respiratory mechanisms and we considered this caveat in the interpretation of the results.

CONCLUSIONS

A major conclusion regarding parameters α_{1RRI} and α_{2RRI} is that they are reciprocally regulated and interdependent in four physiological conditions: supine, standing, supine with 0.1 Hz breathing and standing with 0.1 Hz breathing. That is in agreement with the existing literature (Peng et al., 1995a). This relationship can be described and quantified by the inter-fractal angle θ_{RRI}, which was a sensitive parameter of the change of this relationship in investigated physiological states.

Regarding α_{1RRI}, an orthostatic sympathetic increase contributes to α_{1RRI} in the sense of Brownian noise, while slow breathing parasympathetic increase contributes to the increase of α_{1RRI} in 1/f sense. In stand01 condition we report the maximal similarity of α_{1RRI} to Brownian noise, suggesting that physiological sympathovagal influence on short scale RRI self-similarity properties might be dependent on the pattern of their activation (i.e., individual vs. joint activation) and synergetic in the state stand01.

Regarding α_{2RRI}, individual sympathetic and parasympathetic activation contribute to the increase of α_{2RRI} randomness, with greater contribution of parasympathetic drive with respect to sympathetic. In the state of combined orthostasis and slow breathing (stand01) this contribution appears synergetic.

PDE analysis of α_{A1RRI}, α_{A2RRI}, and θ_{RRI} revealed that baseline physiologic, healthy regime (supin) was characterized by the widest population (group) spectrum of α_{1RRI}, α_{2RRI}, and θ_{RRI} coefficients, which was in accordance with the results of (Castiglioni et al., 2009). PDE of these values is characterized by specific, state dependent changes of non-linear RR operating regimes. Again, the state of standing with 0.1 Hz breathing was the state of the best defined, maximal unimodality of all RRI angular parameters.

Additionally, in stand01 both fractal (α_{1RRI} vs. α_{2RRI}) and irregularity properties of RRI (MSE_{RRI1-4} vs. $MSE_{RRI5-10}$) are reciprocally regulated. The analysis of scale dependent patterns revealed that both short scale (α_{1RRI} vs. MSE_{RRI1-4}) and long scale (α_{2RRI} vs. $MSE_{RRI5-10}$) parameters were also reciprocally regulated (**Table 2**). All the results based on analysis

of RRI complexity measurements speak in favor of stand01 being a qualitatively specific, regulatory well-defined state on multidimensional levels, where we reported the inter-relation of only two levels—horizontal (α_{1RRI} vs. α_{2RRI} and MSE_{RRI1-4} vs. $MSE_{RRI5-10}$ relationships) and vertical (α_{1RRI} vs. MSE_{RRI1-4} and α_{2RRI} vs. $MSE_{RRI5-10}$ relationships).

Non-linear parameters of respiratory signals (α_{1Resp}, α_{2Resp}, θ_{Resp}, α_{A1Resp}, α_{A2Resp}, $MSE_{Resp1-4}$, $MSE_{Resp5-10}$) were robustly sensitive only to breathing regime change, while subtle PDE changes were observed as the result of the posture change. These changes were described mostly as a different number of operating regimes induced both by the change of posture and by the voluntary breathing regime. Demanding posture requirements necessitate more adaptable respiratory patterns, also in the non-linear domain, for the expected environmental (i.e., behavioral) challenges. Only one constant, long lasting and repetitive behavioral task, as was the slow 0.1 Hz breathing, qualitatively changed the feature of multimodality into a dominant monomodal respiratory pattern. Cortical influences of posture maintenance and slow breathing might jointly impose the inhibitory effect on brainstem respiratory neural network complexity properties and dictate monomodal pattern of their non-linear operating mode (Feldman and McCrimmon, 2003).

As a concluding remark, we stress that cardiorespiratory coupling in the non-linear domain is a highly dynamical, complex, interactive, state dependent phenomenon of cross talk between and within the cardiovascular and respiratory systems. This dynamical multilevel cross talk was also scale dependent, with different state dependent response patterns with respect to the patterns of changes in linear domain. The non-linear measures validating cardiopulmonary adaptability identify the state of standing with 0.1 Hz breathing as the most dynamic state, characterized by a specific complexity pattern, potentially beneficial for cardiopulmonary rehabilitation and conditioning. Future studies, on larger statistical samples, should address patterns of cardiopulmonary coupling in these and other states [i.e., exercise (Młynczak and Krysztofiak, 2018), sleep (Zoccoli et al., 2001), microgravity (Migeotte et al., 2003), neurocardiovascular pathologies (Bojić, 2019)] and potential parallel patterns of RR and respiratory variability changes both in linear and non-linear domain.

CLINICAL IMPLICATIONS

One of the major implications of our research was the potential for cardiopulmonary rehabilitation. As we addressed in the Introduction, literature data report beneficial effects of slow 0.1 Hz breathing on cardiopulmonary rehabilitation. The opposite pattern of short scale cardiopulmonary coupling for $\boldsymbol{\rho_1}$ and $\mathbf{X}_{MSE1-4}$, statistically confirmed only for the state of joint orthostasis with slow 0.1 Hz breathing, suggests that only joint enhancement of sympathetic and parasympathetic modulation on the RRI could result in the specific short scale coupling pattern. This pattern can be attributed to the resultant sympatho-vagal pattern that recruits and potentiates short scale cardiopulmonary coupling in self-similarity and reduces short scale coupling in irregularity. Since this was the first time that these results are reported, our statement is hypothetical and needs further evaluation.

Regarding the patients, if this state specific pattern of cardiopulmonary coupling was confirmed as the basis for the beneficial effect of slow breathing in orthostasis, this pattern could gain diagnostic value and become the scope of medical treatments by different approaches. Even though these phenomena were confirmed both for the respiratory system ("short term" and "long term facilitation," Feldman and McCrimmon, 2003) and the cardiovascular system (Platiša et al., 2016b, 2019), a detailed description of the analog phenomena of cardiorespiratory interaction in healthy and patients needs to be addressed.

Finally, evaluation of cardiovascular and respiratory parameters of non-linear operational modes is of critical importance in intensive care unit patients. It was observed that low complexity of respiratory signal was a reliable prognostic sign of unsuccessful weaning of surgical critically ill patients from artificial ventilation (Papaioannou et al., 2011). Our data propose the evaluation of the rehab protocol for conscious artificially ventilated patients in the form of patient's slow voluntary breathing combined with orthostasis. On the basis of our results, hypothetically, this maneuver would potentiate the complexity of respiratory signal, promote the adaptive pattern of cardiopulmonary coupling and improve the odds for a successful weaning from artificial ventilation. This hypothesis necessitates clinical trials. Data obtained on integratory cardiorespiratory mechanisms might be of interest also for understanding the cardiorespiratory consequences of microgravity exposure (Migeotte et al., 2003; Prisk, 2014; Mandsager et al., 2015) and their successful surpassing by cardiorespiratory conditioning before and during the space flights.

DATA AVAILABILITY STATEMENT

The datasets generated for this study are available on request to the corresponding author.

ETHICS STATEMENT

The studies involving human participants were reviewed and approved by Ethical Committee of Faculty of Medicine, University of Belgrade (No. 2650/IV-24). The patients/participants provided their written informed consent to participate in this study.

AUTHOR CONTRIBUTIONS

TB and MP designed the experimental protocol. TB, MP, and ZM recruited the research subjects. ZM performed the experiments and data acquisition. MP supervised the experiments. ZM performed the data analysis under MP, AK, and TB supervision. AK and MP programmed the algorithms. AK and ZM addressed the major computational tasks. ZM and TB did the scientific writing. TB gave the physiological interpretation of the data. All the authors approved the final content of the manuscript.

FUNDING

This work was financed by the Ministry of Education, Science and Technological Development of the Republic of Serbia, projects III 41028 and TR 31020.

ACKNOWLEDGMENTS

We were especially thankful to the volunteers from the Institute of Nuclear Sciences Vinča and the Faculty of Medicine University of Belgrade, as well to other friends and colleagues who supported our study by volunteering as the research subjects. We express sincere thanks to Dr. David Cavanaugh, University of Alabama, for his valuable time dedicated to the linguistic accuracy of the manuscript.

SUPPLEMENTARY MATERIAL

The Supplementary Material for this article can be found online at: https://www.frontiersin.org/articles/10.3389/fphys.2020.00024/full#supplementary-material

REFERENCES

Bai, X., Li, J., Zhou, L., and Li, X. (2009).Influence of the menstrual cycle on nonlinear properties of heart rate variability in young women. *Am. J. Physiol. Heart Circ. Physiol.* 297, H765–H774. doi: 10.1152/ajpheart.01283.2008

Bainbridge, F. A. (1930). The relation between respiration and the pulse-rate. *J. Physiol.* 54, 192–202. doi: 10.1113/jphysiol.1920.sp001918

Bajić, D., Loncar-Turukalo, T., Stojicić, S., Sarenac, O., Bojić, T., Murphy, D., et al. (2010). Temporal analysis of the spontaneous baroreceptor reflex during mild emotional stress in the rat. *Stress* 13, 142–154. doi: 10.3109/10253890903089842

Barbiery, R., Scilingo, E. P., and Valenza, G. (2017). *Complexity and Nonlinearity in Cardiovascular Signals*. Cham: Springer.

Bers, D. M. (2018). "Excitation-contraction coupling," in *Cardiac Electrophysiology: From Cell to Bedside*, *7th Edn.*, eds D. P. Zipes, J. Jalife, and W. G. Stevenson (Philadelphia, PA: Elsevier), 151–159. doi: 10.1016/B978-0-323-44733-1.00016-X

Billman, G. E. (2011). Heart rate variability–a historical perspective. *Front. Physiol.* 2:86. doi: 10.3389/fphys.2011.00086

Blinowska, K. J., and Zygierewicz, J. (2012). *Practical Biomedical Signal Analysis Using MATLAB* (Boca Raton, FL; London; New York, NY: CRC Press; Taylor & Francis Group), 75–99. doi: 10.1201/b11148

Bojić, T. (2003). *Mechanisms of neural control and effects of acoustic stimulation on cardiovascular system during the wake-sleep cycle* (dissertation), Alma Mater Università di Bologna, Bologna, Italy.

Bojić, T. (2019). Editorial: neurocardiovascular diseases: new aspects of the old issues. *Front. Neurosci*.12:1032. doi: 10.3389/fnins.2018.01032

Bruton, A., and Lewith, G. T. (2005). The Buteyko breathing technique for asthma: a review. *Complement. Ther. Med.* 13, 41–46. doi: 10.1016/j.ctim.2005.01.003

Buccelletti, F., Bocci, M. G., Gilardi, E., Fiore, V., Calcinaro, S., Fragnoli, C., et al. (2012). Linear and nonlinear heart rate variability indexes in clinical practice. *Comp. Math. Meth. Med.* 2012:219080. doi: 10.1155/2012/219080

Castiglioni, P., and Parati, G. (2011). Present trends and future directions in the analysis of cardiovascular variability. *J. Hypertens.* 29, 1285–1288. doi: 10.1097/HJH.0b013e3283491d97

Castiglioni, P., Parati, G., Civijian, A., Quintin, L., and Di Rienzo, M. (2009). Local scale exponents of blood pressure and heart rate variability by detrended fluctuation analysis: effects of posture, exercise, and aging. *IEE Trans. Biomed. Eng.* 56, 675–684. doi: 10.1109/TBME.2008.2005949

Castiglioni, P., Parati, G., Di Rienzo, M., Carabalona, R., Cividjian, A., and Quintin, L. (2011). Scale exponents of blood pressure and heart rate during autonomic blockade as assessed by detrended fluctuation analysis. *J. Physiol.* 582, 355–369. doi: 10.1113/jphysiol.2010.196428

Chang, A. T., Boots, R., Hodges, P. W., and Paratz, J. (2004b). Standing with assistance of a tilttable in intensive care: a survey of Australian physiotherapy practice. *Aust. J. Physiother.* 50, 51–54. doi: 10.1016/S0004-9514(14)60249-X

Chang, A. T., Boots, R. J., Brown, M. G., Paratz, J. D., and Hodges, P. W. (2005). Ventilatory changesfollowing head-up tilt and standing in healthy subjects. *Eur. J. Appl. Physiol.* 95, 409–417. doi: 10.1007/s00421-005-0019-2

Chang, A. T., Boots, R. J., Hodges, P. W., Thomas, P. J., and Paratz, J. D. (2004a). Standing with theassistance of a tilt table improves minute ventilation in chronic critically ill patients. *Arch. Phys. Med. Rehabil.* 85, 1972–1976. doi: 10.1016/j.apmr.2004.03.024

Cooke, W. H., Cox, J. F., Diedrich, A. M., Taylor, J. A., Beightol, L. A., Ames, J. E., et al. (1998). Controlled breathing protocols probe human autonomic cardiovascular rhythms. *Am. J. Physiol.* 274, H709–H718. doi: 10.1152/ajpheart.1998.274.2.H709

Costa, M., Goldberger, A. L., and Peng, C. K. (2005). *Multiscale Entropy Analysis (MSE)*, Tutorial from Physionet website. Available online at: https://www.physionet.org/physiotools/mse/tutorial/tutorial.pdf

Costa, M., Peng, C.-K., Goldberger, A. L., and Hausdorff, J. M. (2003). Multiscale entropy analysis of human gaint dynamics. *Phys. A Stat. Mech. Appl.* 330, 53–60, doi: 10.1016/j.physa.2003.08.022

Dampney, R. A. (2015). Central mechanisms regulating coordinated cardiovascular and respiratory function during stress and arousal. *Am. J. Physiol. Regul. Integr. Comp. Physiol.* 309, R429–R443. doi: 10.1152/ajpregu.00051.2015

Daoud, M., Ravier, P., and Buttelli, O. (2018). Use of cardiorespiratory coherence to separate spectral bands of the heart rate variability. *Biomed. Sig. Proc. Contr.* 46, 260–267. doi: 10.1016/j.bspc.2018.08.003

de Godoy, M. F. (2016). Nonlinear analysis of heart rate variability: a comprehensive review. *J. Cardiol. Ther.* 3, 528–533. doi: 10.17554/j.issn.2309-6861.2016.03.101-4

de Paula Vidigal, G. A., Tavares, B. S., Garner, D. M., Porto, A. A., de Abreu, L. C., Ferreira, C., et al. (2016). Slow breathing influences cardiac autonomic responses to postural maneuver: slow breathing and HRV. *Complement. Ther. Clin. Pract.* 23, 14–20. doi: 10.1016/j.ctcp.2015.11.005

De Souza, A. C. A., Cisternas, J. R., de Abreu, L. C., Roque, A. L., Monteiro, C. B. M., Adami, F., et al. (2014). Fractal correlation property of heart rate variability in response to the postural change maneuver in healthy woman. *Int. Arch. Med.* 7:25. doi: 10.1186/1755-7682-7-25

Del Negro, C. A., Funk, G. D., and Feldman, J. L. (2018). Breathing matters. *Nat. Rev. Neurosci.* 19, 351–367. doi: 10.1038/s41583-018-0003-6

Dick, T. E., Hsieh, Y. H., Dhingra, R. R., Baekey, D. M., Galán, R. F., Wehrwein, E., et al. (2014).Cardiorespiratory coupling: common rhythms in cardiac., sympathetic, and respiratory activities. *Prog. Brain. Res.* 209, 191–205. doi: 10.1016/B978-0-444-63274-6.00010-2

Eckberg, D. (1983). Human sinus arrhythmia as an index of vagal cardiac outflow. *J. Appl. Physiol. Respir. Environ. Exerc. Physiol.* 54, 961–966. doi: 10.1152/jappl.1983.54.4.961

Ernst, G. (2014). *Heart Rate Variability*. London: Springer-Verlag, preface p. v.

Fadel, P. J., Barman, S. M., Phillips, S. W., and Gebber, G. L. (2004). Fractal fluctuations in human respiration. *J. Appl. Physiol.* 97, 2056–2064. doi: 10.1152/japplphysiol.00657.2004

Faes, L., and Nollo, G. (2011). "Multivariate frequency domain analysis of causal interactions in physiological time series," in *Biomedical Engineering, Trends in Electronics, Communications and Software*, ed A. N. Laskovski (Rijeka: InTech), 403–428. doi: 10.5772/13065

Feldman, J. L., and Ellenberger, H. H. (1988). Central coordination of respiratory and cardiovascular control in mammals. *Annu. Rev. Physiol.* 50, 593–606. doi: 10.1146/annurev.ph.50.030188.003113

Feldman, J. L., and McCrimmon, D. R. (2003). "Neural control of breathing," in *Fundamental Neuroscience*, eds L. R. Squire, F. E. Bloom, S. K. McConnell,

J. L. Roberts, N. C. Spitzer, and M. J. Zigmond (New York, NY: Academic Press), 967–990.

Fleisher, L. A., Frank, S. M., Sessler, D. I., Cheng, C., Matsukawa, T., and Vannier, C. A. (1996). Thermoregulation and heart rate variability. *Clin. Sci*. 90, 97–103. doi: 10.1042/cs0900097

Francis, D. P., Willson, K., Georgiadou, P., Wensel, R., Davies, L. C., Coats, A., et al. (2002). Physiological basis of fractal complexity properties of heart rate variability in man. *J. Physiol*. 542, 619–629. doi: 10.1113/jphysiol.2001.013389

Gierałtowski, J., Hoyer, D., Tetschke, F., Nowack, S., Schneider, U., Zebrowski, J. (2013). Development of multiscale complexity and multifractality of fetal heart rate variability. *Auton. Neurosci*. 178, 29–36. doi: 10.1016/j.autneu.2013.01.009

Goldberger, A. L. (2006). Complex systems. *Proc. Am. Thorac. Soc*. 3, 467–472. doi: 10.1513/pats.200603-028MS

Goldberger, A. L., Amaral, L. A., Hausdorff, J. M., Ivanov, P. Ch., Peng, C. K., and Stanley, H. E. (2002). Fractal dynamics in physiology: alterations with disease and aging. *Proc. Natl. Acad. Sci. U.S.A*. 99, 2466–2472. doi: 10.1073/pnas.012579499

Goulart, C. L., Simon, J. C., Schneiders, P.de, B., San Martin, E. A., Cabiddu, R., Borghi-Silva, A., et al. (2016). Respiratory muscle strength effect on linear and nonlinear heart rate variability parameters in COPD patients. *Int. J. Chron. Obstruct. Pulmon. Dis*. 11, 1671–1677. doi: 10.2147/COPD.S108860

Grassberger, P. (1991). "Information and complexity measures in dynamical systems," in *Information Dynamics*, eds H. Atmanspacher and H. Scheingraber (New York, NY: Plenum Press), 15–33. doi: 10.1007/978-1-4899-2305-9_2

Hernandez, L., Manning, J., and Zhang, Sh. (2019). Voluntary control of breathing affects center of pressure complexity during static standing in healthy older adults. *Gait Posture* 68, 488–493. doi: 10.1016/j.gaitpost.2018.12.032

Horvatic, D., Stanley, H. E., and Podobnik, B. (2011). Detrended cross-correlation analysis for non-stationary time series with periodic trends. *Europhys. Lett*. 94, 18007-p1–18007-p6. doi: 10.1209/0295-5075/94/18007

Hoshi, R. A., Andreão, R. V., Santos, I. S., Dantas, E. M., Mill, H. G., Lotufo, P. A., et al. (2019). Linear and nonlinear analyses of heart rate variability following orthostatism in subclinical hypothyroidism. *Medicine* 98, 1–7. doi: 10.1097/MD.0000000000014140

Huikuri, H. V., Mäkikallio, T. H., Peng, C. K., Goldberger, A. L., Hintze, U., and Møller, M. (2000).Fractal correlation properties of R-R interval dynamics and mortality in patients with depressed left ventricular function after an acute myocardial infarction. *Circulation* 101, 47–53. doi: 10.1161/01.CIR.101.1.47

Ivanov, P. C., Amaral, L. A., Goldberger, A. L., Havlin, S., Rosenblum, M. G., Struzik, Z. R., et al. (1999). Multifractality in human heartbeat dynamics. *Nature* 399, 461–465. doi: 10.1038/20924

Jasson, S., Médigue, C., Maison-Blanche, P., Montano, N., Meyer, L., and Vermeiren, C. (1997). Instant power spectrum analysis of heart rate variability during orthostatic tilt using a time-/frequency-domain method. *Circulation* 96, 3521–3526. doi: 10.1161/01.CIR.96.10.3521

Javorka, M., El-Hamad, F., Czippelova, B., Turianikova, Z., Krohova, J., Lazarova, Z., et al. (2018). Role of respiration in the cardiovascular response to orthostatic and mental stress. *Am. J. Physiol. Regul. Integr. Comp. Physiol*. 314, R761–R769. doi: 10.1152/ajpregu.00430.2017

Jha, R. K., Acharya, A., and Nepal, O. (2018). Autonomic influence on heart rate for deep breathing and Valsalva maneuver in healthy subjects. *J. Nepal. Med. Assoc*. 56, 670–673. doi: 10.31729/jnma.3618

Julien, C. (2006). The enigma of Mayer waves: facts and models. *Cardiovasc. Res*. 70, 12–21. doi: 10.1016/j.cardiores.2005.11.008

Kabir, M. M., Saint, D. A., Nalivaiko, E., Abbot, D., Voss, A., and Baumert, M. (2011).Quantification of cardiorespiratory interactions based on joint symbolic dynamics. *Ann. Biomed. Eng*. 39, 2604–2614. doi: 10.1007/s10439-011-0332-3

Kalauzi, A., Vučković, A., and Bojić, T. (2012). EEG alpha phase shifts during transition from wakefulness to drowsiness. *Int. J. Psychophysiol*. 86, 195–205. doi: 10.1016/j.ijpsycho.2012.04.012

Kapidžić, A., Platiša, M., Bojić, T., and Kalauzi, A. (2014). RRI respiratory signal waveform modeling in human slow paced and spontaneous breathing. *Respir. Physiol. Neurobiol.* 203, 51–59. doi: 10.1016/j.resp.2014.08.004

Kiselev, A. R., and Karavaev, A. S. (2019). The intensity of oscillations of the photoplethysmographic waveform variability at frequencies 0.04–0.4 Hz is effective marker of hypertension and coronary artery disease in males. *Blood Press* 12, 1–8. doi: 10.1080/08037051.2019.1645586

Kristoufek, L. (2014). Measuring correlations between non-stationary series with DCCA coefficient. *Physica A*. 402, 291–298. doi: 10.1016/j.physa.2014.01.058

Kristoufek, L. (2015). Detrended fluctuation analysis as a regression framework: estimating dependence at different scales. *Phys. Rev. E Stat. Nonlin. Soft. Matter. Phys*. 91:022802. doi: 10.1103/PhysRevE.91.022802

Kwapien, J., Oświecimka, P., and Drozdz, S. (2015). Detrended fluctuation analysis made flexible to detect range of cross-correlated fluctuations. *Phys. Rev. E Stat. Nonlin. Soft. Matter. Phys*. 92:052815. doi: 10.1103/PhysRevE.92.052815

Levy, M. N., and Martin, P. J. (1996). "autonomic control of cardiac conduction and automaticity," in *Nervous Control of the Heart*, eds J. T. Shepherd and S. F. Vatner (Amsterdam: Harwood Academic Publishers), 201–223.

Mandsager, K. T., Robertson, D., and Diedrich, A. (2015). The function of the autonomic nervous system during spaceflight. *Clin. Auton. Res*. 25, 141–151. doi: 10.1007/s10286-015-0285-y

Migeotte, P. F., Prisk, G. K., and Paiva, M. (2003). Microgravity alters respiratory sinus arrhythmia and short-term heart rate variability in humans. *Am. J. Physiol. Heart. Circ. Physiol*. 284, H1995–H2006. doi: 10.1152/ajpheart.00409.2002

Młynczak, M., and Krysztofiak, H. (2018). Discovery of causal paths in cardiorespiratory parameters: a time-independent approach in elite athletes. *Front. Physiol*. 9:1455. doi: 10.3389/fphys.2018.01455

Montano, N., Ruscone, T. G., Porta, A., Lombardi, F., Pagani, M., and Malliani, A. (1994). Power spectrum analysis of heart rate variability to assess the changes in sympathovagal balance during graded orthostatic tilt. *Circulation* 90, 1826–1831. doi: 10.1161/01.CIR.90.4.1826

Mortola, J. P. (2019). How to breathe? Respiratory mechanics and breathing pattern. *Respir. Physiol. Neurobiol*. 261, 48–54. doi: 10.1016/j.resp.2018.12.005

Mortola, J. P., Marqhescu, D., and Sieqrist-Johnstone, R. (2016). Thinking about breathing: effect on respiratory sinus arrhythmia. *Respir. Physiol. Neurobiol*. 223, 28–36. doi: 10.1016/j.resp.2015.12.004

Moser, M., Frühwirth, M., Penter, R., and Winker, R. (2006). Why life oscillates–from a topographical towards a functional chronobiology. *Cancer Causes Control*. 17, 591–599. doi: 10.1007/s10552-006-0015-9

Neves, V. R., Takahashi, A. C., do Santos-Hiss, M. D., Kiviniemi, A. M., Tulppo, M. P., and de Moura, S. C. (2012). Linear and nonlinear analysis of heart rate variability in coronary disease. *Clin. Auton. Res*. 22, 175–183. doi: 10.1007/s10286-012-0160-z

Noble, D. J., and Hochman, S. (2019). Hypothesis: pulmonary afferent activity patterns during slow, deep breathing contribute to the neural induction of physiological relaxation. *Front. Physiol*. 10:1176. doi: 10.3389/fphys.2019.01176

Orem, J., and Kubin, L. (2005). "Respiratory physiology: central neural control," in *Principles and Practice of Sleep Medicine*, *4th Edn.*, eds M. H. Kryger, T. Roth, and W. C. Dement (Philadelphia, PA: Elsevier/Saunders), 213–223. doi: 10.1016/B0-72-160797-7/50024-0

Papaioannou, V. E., Chouvarda, I. G., Maglaveras, N. K., and Pneumatikos, I. A. (2011). Study of multiparameter respiratory pattern complexity in surgical critically ill patientsduring weaning trials. *BMC Physiol*. 11:2. doi: 10.1186/1472-6793-11-2

Park, J., Marvar, P. J., Liao, P., Kankam, M. L., Norrholm, S. D., Downey, R. M., et al. (2017). Baroreflex dysfunction and augmented sympathetic nerve responses during mental stress in veterans with post-traumatic stress disorder. *J Physiol*. 595, 4893–4908. doi: 10.1113/JP274269

Paton, J. F. R., Boscan, P., Pickering, A. E., and Nalivaiko, E. (2005). The Yin and Yang of cardiac autonomic control: vago-sympathetic interactions revisited. *Brain Res. Rev*. 49, 555–565. doi: 10.1016/j.brainresrev.2005.02.005

Peng, C. K., Buldyrev, S. V., Havlin, S., Simons, M., Stanley, H. E., and Goldberger, A. L. (1994). Mosaic orgnization of DNA nucleotides. *Phys. Rev*. 49, 1685–1689. doi: 10.1103/PhysRevE.49.1685

Peng, C. K., Halvin S, Stanley, H. E., and Goldberger, A. L. (1995b). Quantification of scaling exponents and crossover phenomena in nonstationary heartbeat series. *Chaos* 5, 82–87. doi: 10.1063/1.166141

Peng, C. K., Halvin, S., Hausdorff, J. M., Mietus, J. E., Stanley, H. E., and Goldberger, A. l. (1995a). Fractal mechanisms and heart rate dynamics: long-range correlations and their breakedown with disease. *J. Electrocardiol*. 28, 59–65. doi: 10.1016/S0022-0736(95)80017-4

Peng, C. K., Mietus, J. E., Liu, Y., Lee, C., Hausdorff, J. M., and Stanley, H. E. (2002). Quantifying fractal dynamics of human respiration: age and gender effects. *Ann. Biomed. Eng*. 30, 683–692. doi: 10.1114/1.1481053

Perakakis, P., Taylor, M., Martinez-Nieto, E., Revithi, I., and Vila, J. (2009). Breathing frequency bias in fractal analysis of heart rate variability. *Biol. Psychol*. 82, 82–88. doi: 10.1016/j.biopsycho.2009.06.004

Platiša, M., Bojić, T., Pavlović, S., Radovanović, N., and Kalauzi, A. (2016b). Uncoupling of cardiac and respiratory rhythm in atrial fibrillation. *Biomed. Eng. Biomed. Tech*. 61, 657–663. doi: 10.1515/bmt-2016-0057

Platiša, M., and Gal, V. (2010). "Influence of breathing frequency on short term scaling exponent and spectral powers of RR interval series," in *Proceeding of 6th ESCO Conference* (Berlin), 1–3.

Platiša, M. M., Bojić, T., Mazić, S., and Kalauzi, A. (2019). Generalized Poincaré plots analysis of heart period dynamics in different physiological conditions: trained vs.untrained men. *PLoS ONE* 14:e0219281. doi: 10.1371/journal.pone.0219281

Platiša, M. M., Bojić, T., Pavlović, S. U., Radovanović, N. N., and Kalauzi, A. (2016a). Generalized Poincaré plots–a new method for evaluation of regimes in cardiac neural control in atrial fibrillation and healthy subjects. *Front. Neurosci*. 10:38. doi: 10.3389/fnins.2016.00038

Podobnik, B., Jiang, Z. Q., Zhou, W. X., and Stanley, H. E. (2011). Statisctical tests for power-law cross-correlated processes. *Phys. Rev. E Stat. Nonlin. Soft Matter Phys*. 84:066118. doi: 10.1103/PhysRevE.84.066118

Podobnik, B., and Stanley, H. E. (2008). Detrended cross-correlation analysis: a new method for analyzing two nonstationary time series. *Phys. Rev. Lett*. 100:084102. doi: 10.1103/PhysRevLett.100.084102

Porges, S. W. (2007). The polyvagal perspective. *Biol. Psychol*. 74, 116–143. doi: 10.1016/j.biopsycho.2006.06.009

Porta, A., Bassani, T., Bari, V., Tobaldini, E., Takahashi, C. M., Catai, A. M., et al. (2012). Model based assessment of baroreflex and cardiopulmonary couplings during graded head-up tilt. *Comput. Biol. Med*. 42, 298–305. doi: 10.1016/j.compbiomed.2011.04.019

Prisk, G. K. (2014). Microgravity and the respiratory system. *Eur. Respir. J*. 43, 1459–1471. doi: 10.1183/09031936.00001414

Radovanović, N., Pavlović, S., Milašinović, G., Kirćanski, B., and Platiša, M. (2018). Bidirectional cardio-respiratory interactions in heart failure. *Front. Physiol*. 9:165. doi: 10.3389/fphys.2018.00165

Reulecke, S., Charleston-Villalobos, S., Voss, A., Gonzalez-Camarena, R., Gonzalez-Hermosillo, J. A., Gaitan-Gonzalez, M. J., et al. (2018). Temporal analysis of cardiovascular and respiratory complexity by multiscale entropy based on sympolic dynamics. *IEEE. J. Biomed. Health Inform*. 22, 1046–1058. doi: 10.1109/JBHI.2017.2761354

Richman, J. S., and Moorman, J. R. (2000). Physiological time-series analysis using approximate entropy and sample entropy. *Am. J. Physiol. Heart Circ. Physiol*. 278, H2039–H2049. doi: 10.1152/ajpheart.2000.278.6.H2039

Russo, M. A., Santarelli, D. M., and O'Rourke, D. (2017). The physiological effects of slow breathing in the healthy human. *Breathe* 13, 298–309. doi: 10.1183/20734735.009817

Sassi, R., Cerutti, S., Lombardi, F., Malik, M., Hikuri, H., V., et al. (2015). Advances in heart rate variability signal analysis: joint position statement by the e-Cardiology ESC Working Group and the European Heart Rhythm Association co-endorsed by the Asian Pacific Heart Rhythm Society. *Europace* 17, 1341–1353. doi: 10.1093/europace/euv015

Schulz, S., Adochiei, F. C., Edu, I. R., Schroeder, R., Costin, H., Bär, K. J., et al. (2013). Cardiovascular and cardiorespiratory coupling analyses: a review. *Philos. Trans. A Math. Phys. Eng. Sci*. 371:20120191. doi: 10.1098/rsta.2012.0191

Schulz, S., Haueisen, J., Bär, K.-J., and Voss, A. (2018). Multivariate assessment of the central-cardiorespiratory network structure in neuropathological disease. *Physiol. Meas*. 39:07400. doi: 10.1088/1361-6579/aace9b

Shiau, Y.-H. (2018). Can fractal analysis on heart rate variability reflect physiological causes for cardiorespiratory interaction? *Ann. Sleep Med. Res.* 2:1009.

Shields, R. W. (2009). Heart rate variability with deep breathing as a clinical test of cardiovagal function. *Clev. Clin. J. Med*. 76, S37–40. doi: 10.3949/ccjm.76.s2.08

Silva, L. E. V., Lataro, R. M., Castania, J. A., da Silva, C. A., Valencia, J. F., Murta, L., et al. (2016). Multiscale entropy analysis of heart rate variability in heart failure, hypertensive, and sinoaortic-denervated rats: classical and refined approaches. *Am. J. Physiol. Regul. Integr. Comp. Physiol*. 311, R150–R156. doi: 10.1152/ajpregu.00076.2016

Silva, L. E. V., Lataro, R. M., Castania, J. A., Silva, C. A. A., Salgado, H. C., Fazan, R. Jr., et al. (2017a). Nonlinearities of heart rate variability in animal models of impaired cardiac control: contribution of different time scales. *J. Appl. Physiol. (1985)* 123, 344–351. doi: 10.1152/japplphysiol.00059.2017

Silva, L. E. V., Silva, C. A., Salgado, H. C., and Fazan, R. Jr. (2017b). The role of sympathetic and vagal cardiac control on complexity of heart rate dynamics. *Am. J. Physiol. Heart Circ. Physiol*. 312, H469–H477. doi: 10.1152/ajpheart.00507.2016

Silvani, A., Bojić, T., Cianci, T., Franzini, C., Lodi, C. A., Predieri, S., et al. (2003). Effects of acoustic stimulation on cardiovascular regulation during sleep. *Sleep* 26, 201–205. doi: 10.1093/sleep/26.2.201

Sobiech, T., Buchner, T., Krzesinski, P., and Gielerak, G. (2017). Cardiorespiratory coupling in young healthy subjects. *Physiol. Meas*. 38, 2186–2202. doi: 10.1088/1361-6579/aa9693

Somers, V. K., White, D. P., Amin, R., Abraham, W. T., Costa, F., Culebras, A., et al. (2008). Sleep apnea and cardiovascular disease: an American Heart Association/American College Of Cardiology Foundation Scientific Statement from the American Heart Association Council for High Blood Pressure Research Professional Education Committee, Council on Clinical Cardiology, Stroke Council, and Council On Cardiovascular Nursing. In collaboration with the National Heart, Lung, and Blood Institute National Center on Sleep Disorders Research (National Institutes of Health). *Circulation* 118, 1080–1111. doi: 10.1161/CIRCULATIONAHA.107.189420

Stankovski, T., Pereira, T., McClintock, P. V. E., and Stefanovska, A. (2017). Coupling functions universal insights into dynamical interaction mechanisms. *Rev. Mod. Phys.* 89, 045001-1–045001-50. doi: 10.1103/RevModPhys.89.045001

Stiller, K. (2013). Physiotherapy in intensive care: an updated systematic review. *Chest* 144, 825–847. doi: 10.1378/chest.12-2930

Strauss-Blasche, G., Moser, M., Voica, M., McLeod, D. R., Klammer, N., and Marktl, W. (2000). Relative timing of inspiration and expiration affects respiratory sinus arrhythmia. *Clin. Exp. Pharmacol. Physiol*. 27, 601–606. doi: 10.1046/j.1440-1681.2000.03306.x

Task Force Guidelines. (1996). Heart rate variability. Standards of measurement, physiological interpretation, and clinical use. Task Force of The European Society of Cardiology and The North American Society of Pacing and Electrophysiology (Membership of the Task Force listed in the Appendix). *Eur. Heart J*. 17, 354–381. doi: 10.1093/oxfordjournals.eurheartj.a014868

Valencia, J. F., Vallverdú, M., Porta, A., Voss, A., Schroeder, R., and Vázquez, R. (2013). Ischemic risk stratification by means of multivariate analysis of the heart rate variability. *Physiol. Meas*. 34, 325–338. doi: 10.1088/0967-3334/34/3/325

Valente, M., Javorka, M., Porta, A., Bari, V., Krohova, J., Czippelova, B., et al. (2018). Univariate and multivariate conditional entropy measures for the characterization of short-term cardiovascular complexity under physiological stress. *Physiol. Meas*. 39, 1–14. doi: 10.1088/1361-6579/aa9a91

Valenza, G., Citi, L., Garcia, R. G., Taylor, J. N., Toschi, N., and Barbieri, R. (2017). Complexity variability assessment of nonlinear time-varying cardiovascular control. *Sci. Rep*. 7:42779. doi: 10.1038/srep42779

Van Diest, I., Verstappen, K., Aubert, A. E., Widjaja, D., Vansteenwegen, D., and Vlemincx, E. (2014). Inhalation/Exhalation ratio modulates the effect of slow breathing on heart rate variability and relaxation. *Appl. Psychophysiol. Biofeedback* 39, 171–180. doi: 10.1007/s10484-014-9253-x

Vandeput, S. (2010). *Heart rate variability: linear and nonlinear analysis with application in human physiology* (Ph.D. dissertation thesis), Katholieke Universiteit Leuven, Faculty of Electrical Engineering, Leuven, Belgium, 20.

Voss, A., Schroeder, R., Vallverdú, M., Schulz, S., Cygankiewicz, I., and Vázquez, R. (2013). Short-term vs. long-term heart rate variability in ischemic cardiomyopathy risk stratification. *Front. Physiol*. 4:364. doi: 10.3389/fphys.2013.00364

Weippert, M., Behrens, K., Rieger, A., Kumar, M., and Behrens, M. (2015). Effects of breathing patterns and light exercise on linear and nonlinear heart rate variability. *Appl. Physiol. Nutr. Metab*. 40, 1–7. doi: 10.1139/apnm-2014-0493

West, B. C. (2010). Fractal physiology and the fractional calculus: a perspective. *Front. Phys*. 1:12. doi: 10.3389/fphys.2010.00012

Yamamoto, Y., and Hughson, R. L. (1994). On the fractal nature of heart rate variability in humans: effects of data length and beta-adrenergic blockade. *Am. J. Physiol*. 266, R40–R49. doi: 10.1152/ajpregu.1994.266.1.R40

Zafiropoulos, B., Alison, J. A., and McCarren, B. (2004). Physiological responses to the earlymobilisation of the intubated, ventilated abdominal surgery patient. *Aust. J. Physiother*. 50, 95–100. doi: 10.1016/s0004-9514(14)60101-x

Zaidi, S. N., and Collins, S. M. (2016). Orthostatic stress induced changes in heart rate variability, pulse transit time and QRS duration. *J. Bioeng. Biomed. Sci.* 6, 1–6. doi: 10.1016/S0004-9514(14)60101-X

Zebende, G. F. (2011). DCCA cross-correlation coefficient: Quantifying level of cross-correlation. *Phys. A* 390, 614–618. doi: 10.1016/j.physa.2010.10.022

Zoccoli, G., Andreoli, E., Bojić, T., Cianci, T., Franzini, C., Predieri, S., et al. (2001). Central and baroreflex control of heart rate during the wake-sleep cycle in rat. *Sleep* 24, 753–758. doi: 10.1093/sleep/24.7.753

Zygmunt, A., and Stanczyk, J. (2010). Methods of evaluation of autonomic nervous system function. *Arch. Med. Sci.* 6, 11–18. doi: 10.5114/aoms.2010.13500

Conflict of Interest: The authors declare that the research was conducted in the absence of any commercial or financial relationships that could be construed as a potential conflict of interest.

frontiers in Physiology

ORIGINAL RESEARCH
published: 25 February 2020
doi: 10.3389/fphys.2020.00134

A Transfer Entropy Approach for the Assessment of the Impact of Inspiratory Muscle Training on the Cardiorespiratory Coupling of Amateur Cyclists

*Raphael Martins de Abreu[1], Aparecida Maria Catai[1], Beatrice Cairo[2], Patricia Rehder-Santos[1], Claudio Donisete da Silva[1], Étore De Favari Signini[1], Camila Akemi Sakaguchi[1] and Alberto Porta[2,3]**

[1] Department of Physical Therapy, Federal University of São Carlos, São Carlos, Brazil, [2] Department of Biomedical Sciences for Health, University of Milan, Milan, Italy, [3] Department of Cardiothoracic – Vascular Anesthesia and Intensive Care, IRCCS Policlinico San Donato, Milan, Italy

OPEN ACCESS

Edited by:
Andreas Voss,
Institut für Innovative Gesundheitstechnologien (IGHT), Germany

Reviewed by:
Michal Javorka,
Comenius University, Slovakia
Satoshi Iwase,
Aichi Medical University, Japan

***Correspondence:**
Alberto Porta
alberto.porta@unimi.it

Specialty section:
This article was submitted to Autonomic Neuroscience, a section of the journal Frontiers in Physiology

Received: 24 June 2019
Accepted: 07 February 2020
Published: 25 February 2020

Citation:
Abreu RM, Catai AM, Cairo B, Rehder-Santos P, Silva CD, Signini ÉDF, Sakaguchi CA and Porta A (2020) A Transfer Entropy Approach for the Assessment of the Impact of Inspiratory Muscle Training on the Cardiorespiratory Coupling of Amateur Cyclists. Front. Physiol. 11:134. doi: 10.3389/fphys.2020.00134

The strength of cardiorespiratory interactions diminishes with age. Physical exercise can reduce the rate of this trend. Inspiratory muscle training (IMT) is a technique capable of improving cardiorespiratory interactions. This study evaluates the effect of IMT on cardiorespiratory coupling in amateur cyclists. Thirty male young healthy cyclists underwent a sham IMT of very low intensity (SHAM, $n = 9$), an IMT of moderate intensity at 60% of the maximal inspiratory pressure (MIP60, $n = 10$) and an IMT of high intensity at the critical inspiratory pressure (CIP, $n = 11$). Electrocardiogram, non-invasive arterial pressure, and thoracic respiratory movement (RM) were recorded before (PRE) and after (POST) training at rest in supine position (REST) and during active standing (STAND). The beat-to-beat series of heart period (HP) and systolic arterial pressure (SAP) were analyzed with the RM signal via a traditional non-causal approach, such as squared coherence function, and via a causal model-based transfer entropy (TE) approach. Cardiorespiratory coupling was quantified via the HP-RM squared coherence at the respiratory rate (K^2_{HP-RM}), the unconditioned TE from RM to HP ($TE_{RM\rightarrow HP}$) and the TE from RM to HP conditioned on SAP ($TE_{RM\rightarrow HP|SAP}$). In PRE condition we found that STAND led to a decrease of $TE_{RM\rightarrow HP|SAP}$. After SHAM and CIP training this tendency was confirmed, while MIP60 inverted it by empowering cardiorespiratory coupling. This behavior was observed in presence of unvaried SAP mean and with usual responses of the baroreflex control and HP mean to STAND. $TE_{RM\rightarrow HP}$ and K^2_{HP-RM} were not able to detect the post-training increase of cardiorespiratory coupling strength during STAND, thus suggesting that conditioning out SAP is important for the assessment

of cardiorespiratory interactions. Since the usual response of HP mean, SAP mean and baroreflex sensitivity to postural stressor were observed after MIP60 training, we conclude that the post-training increase of cardiorespiratory coupling during STAND in MIP60 group might be the genuine effect of some rearrangements at the level of central respiratory network and its interactions with sympathetic drive and vagal activity.

Keywords: multivariate linear regression model, sport medicine, breathing exercise, heart rate variability, complexity, autonomic nervous system, cardiac control, baroreflex

INTRODUCTION

In the field of the analysis of spontaneous fluctuations of heart period (HP) with the term *cardiorespiratory coupling* (CRC) is intended the set of mechanisms responsible for a variable quote of HP variability (HPV) driven by respiration. For example, respiratory sinus arrhythmia (RSA) (Hirsch and Bishop, 1981) is considered to be, at least partially, the genuine consequence of the activity of respiratory centers modulating vagal motoneuron responsiveness and activity (Eckberg and Karemaker, 2009). The abovementioned definition has two important consequences over CRC assessment: (i) both HPV and respiration need to be acquired, namely at least a bivariate analysis framework should be arranged (Bracic Lotric and Stefanovska, 2000; Bartsch et al., 2007; Porta et al., 2012, 2015; Penzel et al., 2016; Mazzucco et al., 2017); (ii) directionality of the interactions (i.e. from respiration to HPV) must be taken into account, thus restricting signal processing methods suitable to be exploited to those belonging to the causal class (Porta et al., 2012, 2015; Iatsenko et al., 2013; Widjaja et al., 2015).

The computation of the CRC strength (CRCS), namely the degree of association between HP and respiration in the time direction from respiration to HP, is of paramount importance because it decreases with age (Iatsenko et al., 2013; Porta et al., 2014) and this decline provides information complementary to that derived from different autonomic control markers such as RSA (Laitinen et al., 2004; Beckers et al., 2006), cardiac baroreflex sensitivity (Laitinen et al., 1998; Milan-Mattos et al., 2018), cardiac control complexity (Kaplan et al., 1991; Catai et al., 2014) and the gain of the relation from respiration to HP (Saul et al., 1991). The relevance of assessing CRCS is further outlined by the well-known finding that it declines in situations evoking a high sympathetic tone and/or modulation such as during postural challenges (Porta et al., 2012, 2015) and it is altered in pathological conditions (Garcia et al., 2013; Schulz et al., 2013, 2015; Riedl et al., 2014; Penzel et al., 2016). Improving CRCS might be advisable because it would lead to a greater fraction of HPV driven by respiration and, as such, a more powerful and efficient cardiac vagal control might be in place irrespective of the efficiency of the cardiac baroreflex.

Physical exercise might improve CRC. Indeed, a moderate exercise training produces vagal control enhancement (Al-Ani et al., 1996) and it is exploited as a countermeasure to limit the decrease of the HPV magnitude with age (Albinet et al., 2010). Among the possible exercises the inspiratory muscle training (IMT) might be effective in improving CRCS. This position, taken in this study as a working hypothesis, is supported by numerous studies that suggested that IMT is able to improve RSA in both healthy and pathological subjects (Ferreira et al., 2013; Kaminski et al., 2015; Da Luz Goulart et al., 2016; Martins de Abreu et al., 2017; Karsten et al., 2018; Rodrigues et al., 2018). Even though the increase of RSA does not necessary imply an increase of CRCS (Eckberg and Karemaker, 2009; Porta et al., 2012, 2015), the unmodified cardiac baroreflex sensitivity observed after IMT of moderate intensity (DeLucia et al., 2018) prompts for a possible role of an empowered CRC to explain the after training elevation of RSA.

The aim of the study is to assess the effect of IMT training on CRCS in amateur cyclists. This population was chosen because these non-professional sportsmen should have a high vagal basal tone and CRCS that might be improved further with some difficulty, thus stressing more evidently the potential of IMT. The CRCS was measured using a more traditional non-causal technique such as the squared coherence (Saul et al., 1991) and more original causal methods based on the computation of transfer entropy (TE) (Barnett et al., 2009; Porta and Faes, 2016). Both a causal bivariate (Porta et al., 2018) and a causal trivariate (Porta et al., 2015) approach assessing the interactions from respiration to HPV unconditioned and conditioned on systolic arterial pressure (SAP) variability are exploited. This comparison is carried out to better understand the need of accounting for the influence of SAP variability when estimating CRCS to eventually discard the effects of respiration on HPV that are mediated by SAP changes at the respiratory frequency (RF) via the activation of cardiac baroreflex (Baselli et al., 1994; Nollo et al., 2005). CRCS is measured before (PRE) and after (POST) 11 weeks of IMT at rest in supine condition (REST) and during sympathetic activation induced by acting standing (STAND). Baroreflex control is monitored via sequence analysis (Bertinieri et al., 1985; Parati et al., 1988) to better understand its role in explaining the observed findings. Analysis was carried in three groups of amateur cyclists undergoing different IMT intensities.

Abbreviations: μ, mean; σ^2, variance; BRS, baroreflex sensitivity; CIP, IMT at the critical inspiratory pressure; CRC, cardiorespiratory coupling; CRCS, CRC strength; ECG, electrocardiogram; HP, heart period; HPV, HP variability; IMT, inspiratory muscle training; K^2, squared coherence function; MEP, maximal expiratory pressure; MIP, maximal inspiratory pressure; MIP60, IMT against a respiratory resistance set to 60% of MIP; POST, after 11 weeks of IMT; PRE, before 11 weeks of IMT; REST, at rest in supine position; RF, respiratory frequency; RM, respiratory movement signal; RSA, respiratory sinus arrhythmia; SAP, systolic arterial pressure; SEQ%, percentage of HP-SAP pattern of baroreflex origin; SHAM, IMT against an inspiratory resistance of 6 cmH_2O; STAND, active standing; TE, transfer entropy; VO_2, oxygen uptake.

MATERIALS AND METHODS

Characterization of the Population

The full description of the population, justification of the sample size, description of the fitness state, characterization of the IMT and experimental protocol was reported in Martins de Abreu et al. (2019). Briefly, a total of 100 recreational male cyclists were screened for eligibility. Subjects were apparently healthy with age ranging from 20 to 40 years. They practiced cycling for 150 min per week, for at least 6 months. We excluded cyclists with alterations of the cardiac electric and/or respiratory activity as detectable during incremental treadmill exercise and cardiopulmonary tests, obese with body mass index larger than 30 $kg{\cdot}m^{-2}$, subjects with cardiovascular risk factors, smokers or former smokers with less than 1 year of interruption, habitual drinkers, drug abusers or recreational drug users, subjects who used drugs or medicines that could interfere with cardiac control and autonomic function, and who performed any type of IMT during the last 12 months. For the eligibility and the characterization of the population, cyclists underwent traditional anamnesis, conventional 12-lead electrocardiogram (ECG) at rest, treadmill exercise test, cardiopulmonary test for the assessment of peak oxygen uptake (peak VO_2), and the evaluation of maximal inspiratory pressure (MIP) and maximal expiratory pressure (MEP).

The training protocol was registered in the ClinicalTrials.gov (NCT02984189) and the study was approved by the Human Research Ethics Committee of the Federal University of São Carlos (UFSCar) (Protocol: 1.558.731). The study adhered to the principles of the Declaration of Helsinki for research studies involving humans. All participants provided a written informed consent to participate in the study.

IMT Protocol

Only 50 individuals met the eligibility criteria and were randomized into the three groups undergoing different intensities of IMT. Randomization process was based on the creation of groups formed by three subjects (i.e. triplets) with similar age and aerobic functional classification. Random allocation, performed via brown envelops, was carried out over these triplets. One smaller group of two individuals was created because 50 was not a multiple of 3. The three groups were composed by 17, 17 and 16 subjects. The first group performed a sham IMT (SHAM) of very low intensity against an inspiratory resistance of 6 cmH_2O. The second group followed an IMT of moderate intensity against a respiratory resistance set to 60% of MIP (MIP60). The third group was trained at the critical inspiratory pressure (CIP) as determined in Rehder-Santos et al. (2019) and corresponding to an optimized high intensity IMT ranging from 80% to 90% of MIP (CIP). One subject was moved from the CIP group to the MIP60 one to avoid the retreat of this individual during the first session of the training. Therefore, SHAM, MIP60 and CIP groups were formed by 17, 18, and 15 subjects respectively. Some of subjects were excluded mainly because they did not conclude the training, namely 8, 8 and 3 cyclists in the SHAM, MIP60 and CIP groups respectively. Therefore, 9, 10, and 12 subjects concluded the SHAM, MIP60 and CIP training and could undergo the POST session of recording. Unfortunately, in 1 subject belonging to the CIP group the signals were of poor quality, thus allowing the analysis of the recordings of 9, 10, and 11 subjects in the SHAM, MIP60 and CIP groups respectively. The SHAM, MIP60 and CIP groups were similar in terms of age, body mass index, peak VO_2, MIP and MEP as tested via one-way analysis of variance, or Kruskal–Wallis one-way analysis of variance on ranks when appropriate, applied to continuous variables, or χ^2 test applied to aerobic functional classification (Martins de Abreu et al., 2019).

The subjects performed IMT for about 1 h, 3 days per week, for 11 weeks, using a linear inspiratory loading device PowerBreathe (Ironman K5, HaB Ltd, United Kingdom). The protocol was composed of a warm-up phase lasting 5 min during which each participant performed a constant loading protocol at 50% of his training load, followed by 3 consecutive IMT sessions of 15 min. The second and the third IMT sessions were preceded by 1-min recovery. During training, the subjects were instructed to maintain the breathing rate at 12 acts per minute and this rate was reinforced by a verbal command of the physiotherapist. Volunteers who did not complete the 3 weekly IMT sessions or the 11 full weeks of IMT, or modified their physical activities, physical training or lifestyles, or started using any supplement or medication during IMT were excluded.

Experimental Protocol and Data Acquisition

The overall duration of the study was 13 weeks. Evaluation of cardiovascular control markers were carried out during the first and thirteenth weeks, just before and after IMT being the PRE and POST conditions respectively. For cardiovascular control assessment we acquired the ECG (lead MC5) via a bioamplifier (BioAmp FE132, ADInstruments, Australia), non-invasive continuous finger arterial pressure (Finometer Pro, Finapres Medical Systems, Netherlands) and respiratory movement (RM) through a thoracic belt (Marazza, Monza, Italy). Signals were sampled at 1000 Hz (Power Lab 8/35, ADInstruments, Australia). Recording sessions were carried out at the Cardiovascular Physical Therapy Laboratory, Department of Physical Therapy, UFSCar, São Carlos, Brazil according to standardized criteria minimizing individual and environmental factors that might increase the variance of cardiovascular control markers (Milan-Mattos et al., 2018). Subjects were initially maintained at REST for 10 min to stabilize the cardiovascular variables. After this period, signals were recorded for 15 min at REST. Then, the subject was asked to change posture and signals were acquired for additional 15 min during STAND. STAND session followed always REST. Throughout the procedure, subjects were instructed to breathe spontaneously and were not allowed to talk.

Extraction of Beat-to-Beat Variability Series

The HP was determined over the ECG as the temporal distance between two consecutive R-wave peaks. The *i*th SAP was detected

as the maximum of arterial pressure signal within the *i*th HP. The RM signal was sampled at the first R-wave delimiting the onset of the *i*th HP. Delineations of the R-wave peak and arterial pressure maximum were carefully checked to avoid erroneous detections or missed beats. If isolated ectopic beats affected HP and SAP, these measures were linearly interpolated using the closest values unaffected by ectopies. Since we were interested in short-term cardiac control, analyses were carried out over sequences of 256 consecutive HP, SAP and RM values (Task Force, 1996). The sequences were selected in a random position within REST and STAND periods. The random position was decided according to an automatic routine randomly extracting the onset of the segment from a uniform distribution of integers ranging from the session onset to the session offset (minus 256). The operator has no possibility to intervene on the selection. The procedure avoided the selection of the first 3 min of STAND. We computed the mean and variance of HP and SAP series, labeled as μ_{HP}, σ^2_{HP}, μ_{SAP} and σ^2_{SAP} and expressed in ms, ms^2, mmHg and mmHg^2 respectively. With the exception of the means, all the other markers were computed over linearly detrended sequences.

Squared Coherence Analysis

The degree of linear coupling between HP and RM series as a function of the frequency f was computed via squared coherence function $K^2_{HP-RM}(f)$. The $K^2_{HP-RM}(f)$ is defined as the ratio between the square HP-RM cross-spectrum modulus divided by the product of the HP and RM power spectra. $K^2_{HP-RM}(f)$ ranges from 0 to 1, where 0 indicates perfect uncorrelation between HP and RM at the frequency f, while 1 indicates full correlation. The cross-spectrum and power spectra were estimated according to a parametric approach based on the bivariate autoregressive model (Porta et al., 2000). The coefficients of the model were identified via a traditional least squares technique and the order was fixed at 10 (Porta et al., 2000). $K^2_{HP-RM}(f)$ was sampled in correspondence of the weighted average of the central frequency of the RM spectral components in high frequency (HF, from 0.15 to 0.4 Hz) band. This frequency was taken as an estimate of the RF. The sampling of the $K^2_{HP-RM}(f)$ at the RF was referred to as $K^2_{HP-RM}(RF)$ and it is dimensionless.

Model-Based Conditional and Unconditional TE

The degree of association in the temporal direction from a cause signal to an effect one was computed via TE measuring the amount of information transferred from the cause to the effect (Schreiber, 2000). Defined the restricted universe of knowledge as the set formed by the effect and all the possible confounding factors, the TE computes the reduction of information carried by the target signal when the restricted universe of knowledge is completed by including the presumed cause to become the full universe of knowledge. The greater the TE, the higher the association from the cause to the effect, the larger the coupling strength from the cause to the effect.

In this specific application the presumed cause is RM, the effect is HP and the possible confounding factor is SAP. At difference with $K^2_{HP-RM}(f)$ the TE has the inherent advantage to be an asymmetric function, namely the TE from RM to HP is different from the TE from HP to RM. This feature makes TE to be particularly attractive in quantifying CRCS whether the degree of association in the temporal direction from HP to RM is present and larger than that in the reverse temporal direction. Indeed, in this situation $K^2_{HP-RM}(f)$ would be dominated by mechanisms operating in the temporal direction that have nothing to do with CRC. The TE from RM to HP was computed in two different full universes of knowledge Ω_2 = {HP, RM} and Ω_3 = {HP, RM, SAP} respectively. Assigned Ω_2 and Ω_3 we defined $\Omega_2\backslash RM$ = {HP} and $\Omega_3\backslash RM$ = {HP, SAP} as the two restricted universes of knowledge built from Ω_2 and Ω_3 after excluding the presumed cause RM. The TE from RM to HP in Ω_2, termed $TE_{RM\rightarrow HP}$, was computed as a half of the logarithm of the prediction error variance of HP in $\Omega_2\backslash RM$ to that of HP in Ω_2 (Barnett et al., 2009; Porta et al., 2018). The TE from RM to HP in Ω_3 conditioned on SAP, termed $TE_{RM\rightarrow HP|SAP}$, was computed as a half of the logarithm of the prediction error variance of HP in $\Omega_3\backslash RM$ to that of HP in Ω_3 (Barnett et al., 2009; Porta et al., 2015). Both $TE_{RM\rightarrow HP}$ and $TE_{RM\rightarrow HP|SAP}$ were dimensionless.

In this specific application a model-based approach based on multivariate linear regression models, namely the class of the autoregressive model with exogenous input (Baselli et al., 1997), was exploited to fit the series in Ω_2, $\Omega_2\backslash RM$, Ω_3, and $\Omega_3\backslash RM$. After normalizing HP, SAP, and RM series to have zero mean and unit variance by subtracting the mean and by dividing the result by the standard deviation, the coefficients of the models were identified via traditional least squares approach and Cholesky decomposition method (Baselli et al., 1997). In the computation of $TE_{RM\rightarrow HP}$ and $TE_{RM\rightarrow HP|SAP}$ the model order was optimized in the range from 8 to 16 according to the Akaike's figure of merit (Akaike, 1974) computed in Ω_2 and Ω_3 respectively. The prediction error was computed as the difference between the current value of the HP series and its best prediction provided by the model. Immediate effects (i.e. within the current HP) from SAP and RM to HP were considered in agreement with the fastness of the vagal actions characterizing both cardiac baroreflex, namely the link from SAP to HP, and CRC, namely the pathway from RM to HP (Eckberg, 1976; Porta et al., 2013b). All the regressions have the same number of coefficients equal to the optimal model order. The models in $\Omega_2\backslash RM$ and $\Omega_3\backslash RM$ were separately identified using the optimal model order estimated in Ω_2 and Ω_3 respectively (Porta et al., 2015).

Cardiac Baroreflex Evaluation

The sequence technique is one of the most utilized methods for the characterization of cardiac baroreflex from spontaneous HP and SAP variability series (Bertinieri et al., 1985; Parati et al., 1988). We applied the sequence technique as implemented in Porta et al. (2000, 2013a). More specifically, we defined as HP-SAP pattern of baroreflex origin an HP-SAP joint scheme featuring three consecutive and contemporaneous HP and SAP increases or decreases. Therefore, an HP-SAP pattern of baroreflex origin is characterized by same-sign HP and SAP ramps with a delay between them equal to 0 beats, thus focusing on the fast vagal arm of the cardiac baroreflex featuring very short latencies compatible with the measurement convention adopted

in this study (Eckberg, 1976; Milan-Mattos et al., 2018). All the detected HP-SAP patterns of baroreflex origin were retained in this analysis regardless of the magnitude of total, or partial, SAP and HP variations and the strength of the linear association between HP and SAP values (Porta et al., 2013a). The baroreflex sensitivity (BRS) was computed as the mean of the slopes of the regression lines of HP on SAP calculated over all HP-SAP patterns of baroreflex origin. BRS was positive by definition and expressed in ms·mmHg^{-1}. The percentage of the HP-SAP patterns of baroreflex origin with respect to the overall amount of HP-SAP joint schemes (SEQ%) was assessed as well and taken as a measure of the degree of involvement of cardiac baroreflex control. By definition, SEQ% ranged between 0 and 100.

Statistical Analysis

Normality was tested via Shapiro–Wilk test. The assessment of the effect of IMT on time domain, cardiac baroreflex and CRCS indexes was carried out within an assigned group of athletes via two-way repeated measures analysis of variance (Holm–Sidak correction for multiple comparisons). The significance of the effect of training within the same experimental condition (i.e. REST or STAND) and the response to postural challenge within the same period of analysis (i.e. PRE or POST) was tested. Assigned the group of subject, if the null hypothesis of normal distribution of a given variable was rejected in some experimental condition or period of analysis, the values of that variable in all experimental conditions and periods of analysis were log-transformed before performing two-way repeated measures analysis of variance. No formal statistical analysis was carried out among different groups (i.e. SHAM, MIP60 and CIP). Comparison among different groups was qualitative and based on the observation of significances detected by the previously mentioned two-way repeated measures approach. Data are expressed as mean ± standard deviation. Statistical analysis was carried out using a commercial statistical program (Sigmaplot, v.14.0, Systat Software, Inc., Chicago, IL, United States). A $p < 0.05$ was always considered statistically significant.

RESULTS

Time domain markers are summarized in **Table 1**. The effect of STAND was significant over μ_{HP} regardless of the training status (i.e. PRE and POST) and type of training (i.e. SHAM, MIP60, and CIP). SHAM and MIP60 trainings lengthened μ_{HP} at REST respectively, while CIP training shortened μ_{HP} during STAND. σ^2_{HP} and μ_{SAP} were not influenced by experimental condition and training status. This finding held irrespective of the type of training. σ^2_{SAP} did not vary with the training status but it was affected by the postural challenge. Indeed, in both PRE and POST sessions σ^2_{SAP} increased during STAND and this result held only in the MIP60 group. In the SHAM and CIP groups RF was not affected by either experimental condition or training status. A post-training decrease of RF was observed in the MIP60 group at REST, while no effect of training was visible during STAND. In the same group orthostatic challenge did not influence the RF regardless of the training status.

The grouped vertical bar graphs of **Figure 1** show BRS and SEQ% computed over SHAM (**Figures 1A,D**), MIP60 (**Figures 1B,E**), and CIP (**Figures 1C,F**) groups in PRE (black bars) and POST (white bars) sessions as a function of the experimental condition (i.e. REST and STAND). STAND decreased BRS and increased SEQ%. This tendency held regardless of the training condition (i.e. PRE and POST) and was observed in all the groups (i.e. SHAM, MIP60 and CIP). However, the effect of STAND over BRS and SEQ% was more powerful in MIP60 (**Figures 1B,E**) and CIP (**Figures 1C,F**) groups than in the SHAM one (**Figures 1A,D**). IMT did not influence BRS and SEQ% given that no significant PRE-POST difference was observed either at REST or during STAND irrespective of the IMT intensity.

Figure 2 shows an example of the K^2_{HP-RM} and TE analyses performed over series recorded at REST and during STAND in a subject belonging to the SHAM group. The series of HP, RM and SAP acquired at REST and during STAND are shown in **Figures 2A,C,E** and **Figures 2B,D,F** respectively. During STAND μ_{HP} decreases and σ^2_{SAP} increases. The corresponding K^2_{HP-RM} functions are reported in **Figures 2G,H** respectively with the indication of the inferior and superior limit of the HF band (dotted lines) and sampling at the RF (solid circle). The values of the K^2_{HP-RM}(RF), $TE_{RM\rightarrow HP}$, and $TE_{RM\rightarrow HP|SAP}$ are given below the panels representing K^2_{HP-RM}. The values of K^2_{HP-RM}(RF), $TE_{RM\rightarrow HP}$, and $TE_{RM\rightarrow HP|SAP}$ at REST are higher than the correspondent value during STAND, thus indicating a reduced cardiorespiratory coupling with the postural challenge. $TE_{RM\rightarrow HP}$ is larger than $TE_{RM\rightarrow HP|SAP}$, thus suggesting that a portion of the information transferred from RM to HP is mediated by SAP changes.

The grouped vertical bar graphs of **Figure 3** show K^2_{HP-RM}(RF) computed over SHAM (**Figure 3A**), MIP60 (**Figure 3B**), and CIP (**Figure 3C**) groups in PRE (black bars) and POST (white bars) sessions as a function of the experimental condition (i.e. REST and STAND). All the groups responded to the orthostatic challenge by decreasing K^2_{HP-RM}(RF) in both PRE and POST sessions. However, the decrease was significant solely in SHAM (**Figure 3A**) and CIP (**Figure 3C**) groups, while in the MIP60 group the reduction was not significant (**Figure 3B**). Regardless of the IMT intensity no effect of training was visible over K^2_{HP-RM}(RF) both at REST and during STAND.

Figure 4 has the same structure as **Figure 3** but it shows $TE_{RM\rightarrow HP}$. This parameter did not change with either training status (i.e. PRE and POST) or experimental condition (i.e. REST and STAND). This conclusion held regardless of the type of training, namely SHAM (**Figure 4A**), MIP60 (**Figure 4B**), and CIP (**Figure 4C**).

Figure 5 has the same structure as **Figure 3** but it shows $TE_{RM\rightarrow HP|SAP}$. Regardless of the training condition (i.e. PRE or POST) STAND influenced $TE_{RM\rightarrow HP|SAP}$. This consideration held for all the groups. Remarkably, the sign of the $TE_{RM\rightarrow HP|SAP}$ variation induced by STAND depended on the intensity of the IMT training. Indeed, in POST condition, while STAND decreased $TE_{RM\rightarrow HP|SAP}$ in SHAM (**Figure 5A**) and CIP (**Figure 5C**) group, the postural challenge significantly increased $TE_{RM\rightarrow HP|SAP}$ in the MIP60 group

TABLE 1 | Time domain HP and SAP markers and RF during SHAM, MIP60, and CIP trainings.

Index	Experimental condition	SHAM		MIP60		CIP	
		REST	STAND	REST	STAND	REST	STAND
μ_{HP} [ms]	PRE	990 ± 113	810 ± 135*	992 ± 181	815 ± 165*	946 ± 76	791 ± 71*
	POST	1063 ± 133§	876 ± 178*	1106 ± 175§	849 ± 98*	928 ± 109	737 ± 95§*
σ^2_{HP} [ms^2]	PRE	4289 ± 3631	3392 ± 1774	2607 ± 1850	3582 ± 3978	2859 ± 2745	2369 ± 1508
	POST	5190 ± 3647	4695 ± 3980	4149 ± 2658	4000 ± 3821	1856 ± 1390	1650 ± 1388
μ_{SAP} [mmHg]	PRE	111 ± 17	104 ± 16	112 ± 14	116 ± 18	110 ± 9	109 ± 14
	POST	98 ± 38	95 ± 39	112 ± 23	114 ± 24	113 ± 16	115 ± 16
σ^2_{SAP} [mmHg^2]	PRE	32 ± 22	52 ± 20	15 ± 5	41 ± 20*	23 ± 13	29 ± 12
	POST	36 ± 25	38 ± 30	23 ± 13	46 ± 29*	30 ± 16	39 ± 25
RF [apm]	PRE	15.9 ± 3.7	14.0 ± 3.4	18.3 ± 4.5	15.8 ± 4.9	17.0 ± 3.7	15.7 ± 3.2
	POST	16.4 ± 1.8	15.9 ± 3.9	15.2 ± 5.0§	16.4 ± 5.3	18.9 ± 4.2	17.9 ± 3.8

*IMT, inspiratory muscle training; SHAM, sham IMT; MIP60, IMT at 60% of the maximum inspiratory pressure; CIP, IMT training at the critical inspiratory pressure; REST, at rest in supine position; STAND, active standing; HP, heart period; SAP, systolic arterial pressure; μ_{HP}, HP mean; σ^2_{HP}, HP variance; μ_{SAP}, SAP mean; σ^2_{SAP}, SAP variance; RF, respiratory frequency expressed in acts per minute (apm). Data are presented as mean ± standard deviation. The symbol * indicates $p < 0.05$ vs. REST within the same period of analysis (i.e. PRE or POST) assigned the training group. The symbol § indicates $p < 0.05$ versus POST within the same experimental condition (i.e. REST or STAND) assigned the training group.*

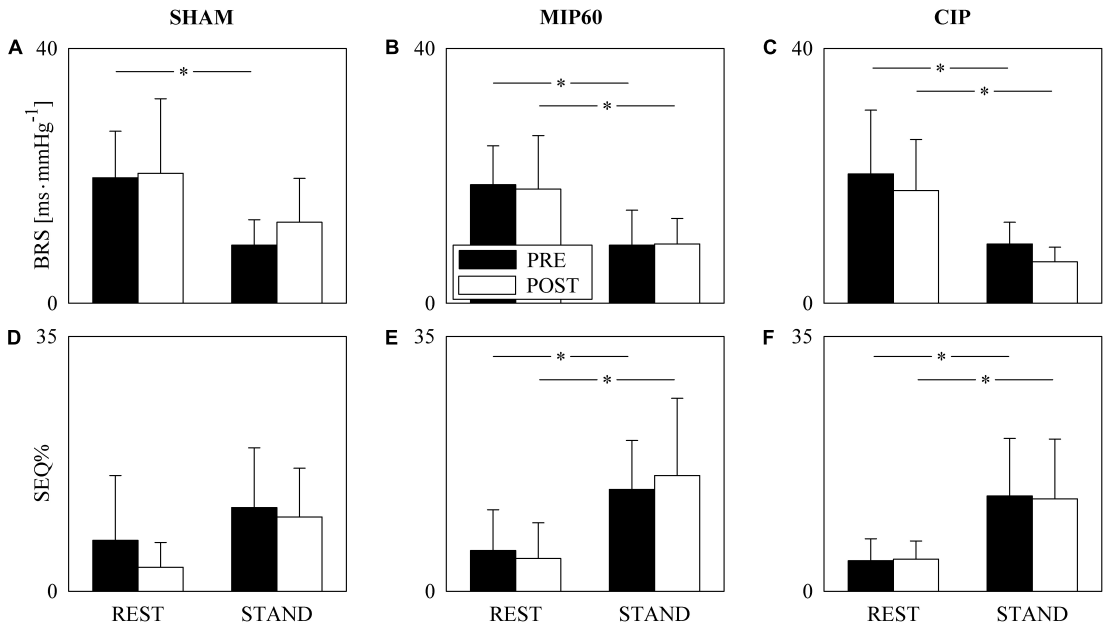

FIGURE 1 | The grouped vertical bar graphs show BRS **(A–C)** and SEQ% **(D–F)** before (PRE, black bars) and after (POST, white bars) training as a function of the experimental condition (i.e. REST and STAND) in the three considered groups, namely SHAM **(A,D)**, MIP60 **(B,E)**, and CIP **(C,F)**. The values are reported as mean plus standard deviation. The symbol * indicates a statistically significant difference versus REST within the same training condition (i.e. PRE or POST) with $p < 0.05$.

(**Figure 5B**). At REST the decrease of $TE_{RM \rightarrow HP|SAP}$ in response to STAND was significant regardless of the group (**Figures 5A–C**). No PRE-POST difference was detected both at REST and during STAND (**Figures 5A–C**) and this result held for all the groups.

DISCUSSION

The main finding of this study can be summarized as follows: (i) in PRE condition sympathetic activation and vagal withdrawal induced by postural challenge reduced CRCS even though the significance of the decrease depends on the CRC marker; (ii) in MIP60 group a causal CRCS marker conditioning SAP out can detect the post-training increase of CRCS during STAND, while more traditional non-causal and simpler causal CRCS indexes cannot; (iii) in MIP60 group the post-training increase of $TE_{RM \rightarrow HP|SAP}$ induced by STAND was observed without significant modifications of μ_{SAP} and RF and in presence of the expected response of μ_{HP} and BRS to STAND; (iv) CIP was not able to prevent the decrease of CRCS in response to STAND.

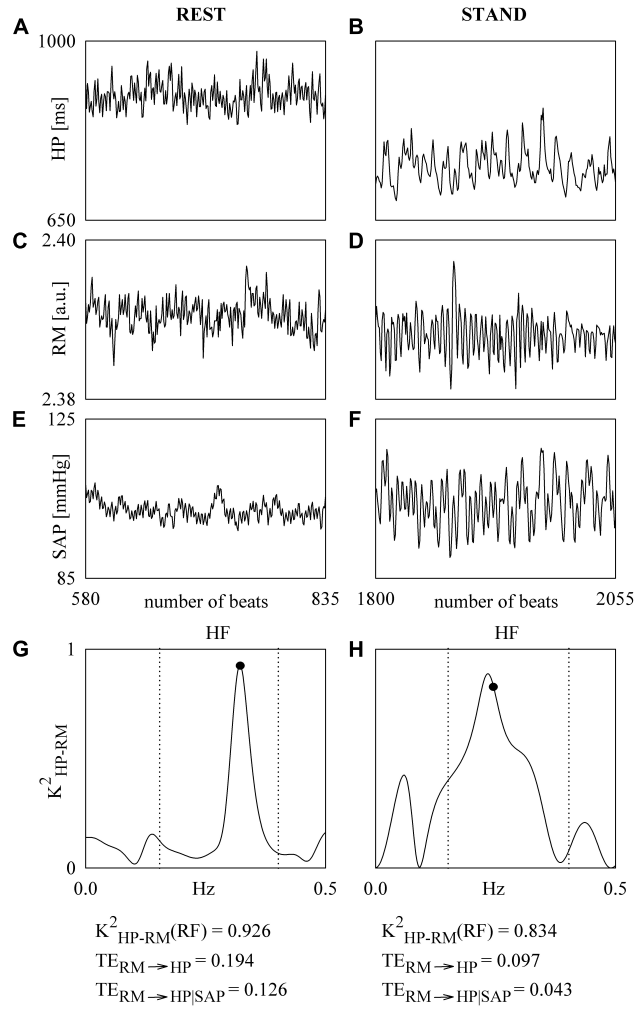

FIGURE 2 | The line plots show the series of HP **(A,B)**, RM **(C,D)**, and SAP **(E,F)**. The series are recorded from a SHAM subject at REST **(A,C,E)** and during STAND **(B,D,F)**. The K^2_{HP-SAP} functions computed over the HP and RM series at REST and during STAND are shown in **(G,H)**. The sampling of the K^2_{HP-SAP} function at the RF is indicated by a solid circle in **(G,H)**. The limits of the HF band are given as dotted lines in **(G,H)**. The values of the K^2_{HP-RM}(RF), $TE_{RM \rightarrow HP}$, and $TE_{RM \rightarrow HP|SAP}$ are reported below the panels representing K^2_{HP-RM}.

On the Need of a Causal Approach Conditioning SAP Variability Out for the Evaluation of CRCS

The quantification of CRCS necessitates the computation of the association between RM and HP dynamics in a specific time direction (i.e. from RM to HP) and the possibility of conditioning out any signal that might act as a confounding factor masking or biasing the considered HP-RM association. Signal processing tools assessing causality are suitable candidates for the evaluation of CRCS because the temporal direction of the dynamical interactions can be accounted for, confounding factors can be easily conditioned out, and the computed metrics might have attracting features such as being dimensionless and bounded (e.g. TE is bounded between 0 and the Shannon entropy of HP series) (Porta and Faes, 2016). In this study we exploited a model-based approach assessing the information transferred from RM to HPV as the reduction of information carried by the HP series resulting from the acquisition of the RM signal in addition to HP and SAP variability series (Barnett et al., 2009; Porta et al., 2015). It can be argued that the possibility of imposing a temporal direction of interactions (i.e. from RM to HP) might be irrelevant in assessing CRC because it is unlikely that modifications of HP could affect respiratory centers because no anatomical feedback from HP to RM does exist. However, given that the hypothesis of open loop relation from RM to HP has been repeatedly rejected in experiment conditions commonly exploited in cardiac autonomic control analysis and with respiratory signals routinely acquired in many laboratories (Yana et al., 1993; Porta et al., 2013b), some caution about the use of non-causal tools such as $K^2_{HP-RM}(f)$ is advisable. An active pathway on the reverse time direction (i.e. from HP to RM) might be the mere consequence of the different rapidity of the recorded variables to respond to respiratory center inputs (Yana et al., 1993; Porta et al., 2013b). The possibility of conditioning out confounding factors is even more important than that of imposing causality. Indeed, it is well-known that the association between RM and HPV might be mediated by cardiac baroreflex (Porta et al., 2012) solicited by SAP fluctuations resulting from modifications of the venous return driven by respiratory-related changes of intrathoracic pressure (Toska and Eriksen, 1993; Caiani et al., 2000). Accounting for baroreflex influences on the HP-RM link might be important in our experimental protocol given that IMT generates remarkable modifications of intrathoracic pressures (Lurie et al., 2002; Convertino et al., 2004b; Vranish and Bailey, 2015), that might have some impact on baroreflex responses (Angell James, 1971), and given that sympathetic activation evoked by STAND is mediated by the baroreflex engagement (Taylor and Eckberg, 1996; Porta et al., 2011, 2012). If these influences were not accounted for, the association between RM and HP dynamics might be biased by the simultaneous action of pathways other than the directed action of RM on HRV. Therefore, it is not surprising to find out that the statistical power of the $TE_{RM \rightarrow HP|SAP}$ is greater than that of a rougher causal marker that does not take into account SAP, such as the $TE_{RM \rightarrow HP}$. Even the modifications of K^2_{HP-RM}(RF) with STAND might be the sole consequence of disregarding SAP dynamics. Indeed, the decrease of K^2_{HP-RM}(RF) during STAND might be the genuine result of the reduction of the cardiac baroreflex sensitivity at the RF in response to the postural stimulus (Cooke et al., 1999; De Maria et al., 2019) limiting the strength of the HP-RM link mediated by SAP changes.

Effect of the Orthostatic Challenge on CRCS in PRE Condition

This study confirms that orthostatic challenge determines a reduction of CRCS. Indeed, in PRE condition all the considered CRCS markers reached the same conclusion, even though with different statistical power. Indeed, the reduction of $TE_{RM \rightarrow HP}$ during STAND was less evident than that of K^2_{HP-RM}(RF)

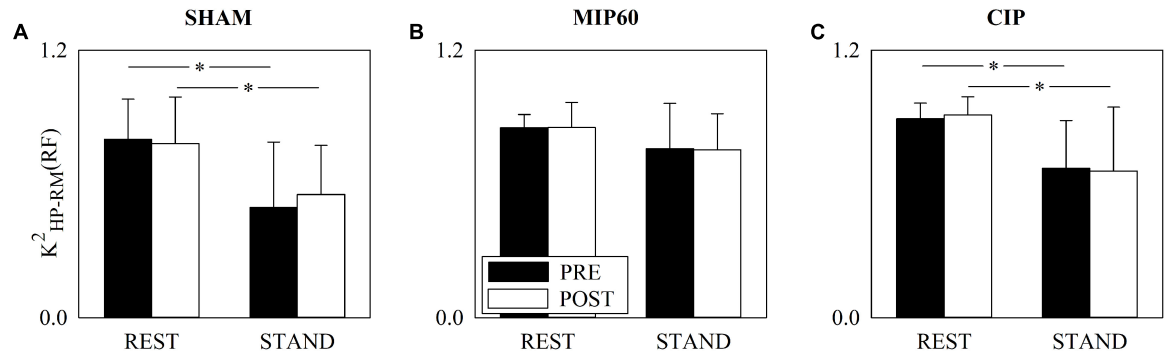

FIGURE 3 | The grouped vertical bar graphs show $K^2_{HP-RM}(RF)$ before (PRE, black bars) and after (POST, white bars) training as a function of the experimental condition (i.e. REST and STAND) in the three considered groups, namely SHAM **(A)**, MIP60 **(B)**, and CIP **(C)**. The values are reported as mean plus standard deviation. The symbol * indicates a statistically significant difference versus REST within the same training condition (i.e. PRE or POST) with $p < 0.05$.

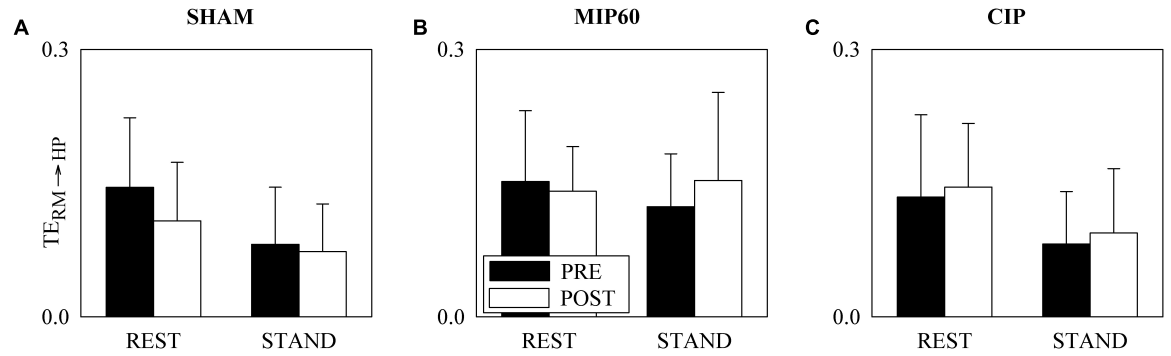

FIGURE 4 | The grouped vertical bar graphs show $TE_{RM \rightarrow HP}$ before (PRE, black bars) and after (POST, white bars) training as a function of the experimental condition (i.e. REST and STAND) in the three considered groups, namely SHAM **(A)**, MIP60 **(B)**, and CIP **(C)**. The values are reported as mean plus standard deviation.

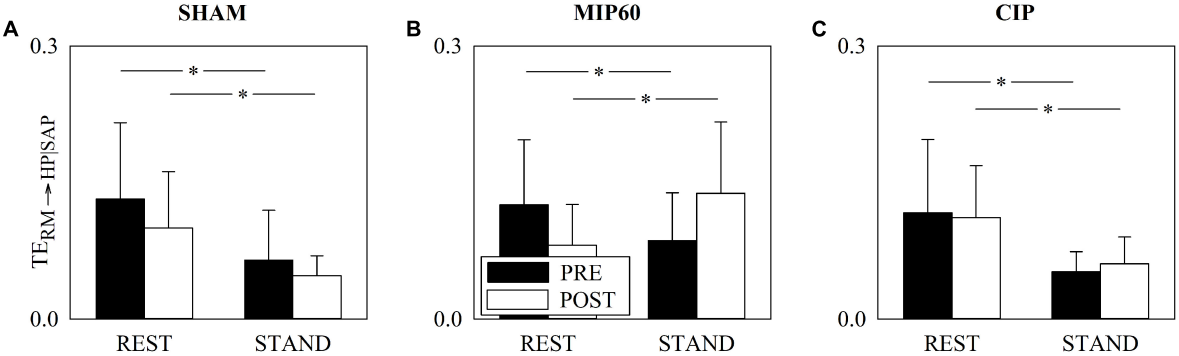

FIGURE 5 | The grouped vertical bar graphs show $TE_{RM \rightarrow HP|SAP}$ before (PRE, black bars) and after (POST, white bars) training as a function of the experimental condition (i.e. REST and STAND) in the three considered groups, namely SHAM **(A)**, MIP60 **(B)**, and CIP **(C)**. The values are reported as mean plus standard deviation. The symbol * indicates a statistically significant difference versus REST within the same training condition (i.e. PRE or POST) with $p < 0.05$.

and $TE_{RM \rightarrow HP|SAP}$. A CRCS decrease, proportional to the magnitude of the postural stimulus (i.e. the tilt table inclination during graded head-up tilt test), was observed via a causal method decomposing the variance of HP series using a multivariate partial power spectral decomposition technique (Porta et al., 2012) and via a model-based conditional TE approach (Porta et al., 2015). The sympathetic activation and vagal withdrawal associated to the orthostatic challenge (Montano et al., 1994; Cooke et al., 1999; Furlan et al., 2000; Marchi A. et al., 2016) is likely to be responsible for the decoupling of the respiratory rhythm modulating vagal drive and HP dynamics. This decoupling is favored by the decrease

of the gain of the HP-RM transfer function (Saul et al., 1991; Yana et al., 1993) and by the reduction of the RSA (Pomeranz et al., 1985) known to occur when cardiac vagal control is limited like during parasympathetic blockade performed via high dose administration of atropine. The reduction of the CRCS is robustly detected in presence of a shift of the sympathovagal balance toward a sympathetic predominance even when this unbalance is not evoked by an orthostatic challenge such as during healthy aging (Iatsenko et al., 2013; Nemati et al., 2013; Porta et al., 2014), thus stressing the inverse relationship between markers of CRC and vagal control and the possibility to use CRCS as a further marker of vagal responsiveness of the sinus node.

Effect of the Orthostatic Challenge on CRCS in POST Condition

The effects of IMT on CRCS seem to be of limited entity both at REST and during STAND. Indeed, no significant difference between PRE and POST was observed and this finding held irrespective of the IMT intensity and type of CRCS marker. However, some influences of IMT became visible when the response to STAND was analyzed in POST condition. Indeed, $TE_{RM\rightarrow HP|SAP}$ decreased during STAND compared to REST in both SHAM and CIP groups, while it increased in the MIP60 group. The post-training increase of CRCS induced by STAND was not detectable via ${K^2}_{HP-RM}$(RF) and $TE_{RM\rightarrow HP}$ likely due to the limited ability of a non-causal index of CRC, such as ${K^2}_{HP-RM}$(RF), and of a simpler causal marker that does not account for confounding factors such as $TE_{RM\rightarrow HP}$. It seems that after MIP60 training amateur cyclists could cope with the postural stressor with an increased CRC in presence of a usual response of sympathetic and vagal sympathetic branches of the autonomic nervous system to the postural stressor as denoted by the decrease of μ_{HP} and increase of ${\sigma^2}_{SAP}$. The mechanism underlying the improvement of CRCS during STAND induced by the MIP60 training is unclear. Breathing through an inspiratory resistance of limited value decreases intrathoracic pressure and increases stroke volume, cardiac output and SAP (Lurie et al., 2002; Convertino et al., 2004b). Given the rhythmical nature of respiration, modifications of intrathoracic pressure and, consequently, of stroke volume (Toska and Eriksen, 1993; Caiani et al., 2000), periodically solicit the stretch-sensitive areas of barosensory vessels located in thorax (Angell James, 1971) and this dynamical stimulation might be responsible for producing post-training beneficial effects in terms of augmented vessel elasticity and reduced mechanical stiffness. This mechanism was advocated to explain the improved baroreflex control after IMT of light-to-moderate intensity in patients suffering for orthostatic hypotension as a consequence of spinal cord injury (Aslan et al., 2016). However, this baroreflex-mediated mechanism cannot explain the complexity of our results and findings present in literature. Indeed, if an IMT of moderate intensity was able to empower baroreflex, we would expect a greater after-training BRS. Conversely, no PRE-POST variation of BRS was observed and the usual trend of baroreflex markers with STAND was detected after MIP60 training. The lack of influences on the baroreflex regulation is in agreement with data derived during a session of breathing through an inspiratory resistance of small value (Convertino et al., 2004a) and with the long-term effects of an IMT training of moderate intensity (DeLucia et al., 2018). We suggest that the post-training changes of CRCS detected by $TE_{RM\rightarrow HP|SAP}$ during STAND in MIP60 group are due to mechanisms unrelated to baroreflex. Also modifications of RF cannot explain this finding given that RF did not change in MIP60 group during STAND. We speculate that the MIP60 training might have promoted central respiratory network modifications (Spyer, 1995; Eckberg, 2003) through the solicitation of the afferent pulmonary and atrial stretch-activated neural circuits during training (Seals et al., 1990; Taha et al., 1995; Eckberg and Karemaker, 2009; Crystal and Salem, 2012). Remarkably, the post-training increase of CRCS was detected only by $TE_{RM\rightarrow HP|SAP}$ likely because the unvaried action of baroreflex might act as a confounding factor for the direct relation from RM to HP. Moreover, since this effect of the MIP60 training was visible solely during the sympathetic activation induced by the orthostatic stimulus, we speculate that this IMT might not produce exclusively modifications of the interactions between respiratory centers and vagal activity but also with central sympathetic drive. Remarkably, the post-training increase of CRCS during STAND observed in the MIP60 group was not detected in SHAM and CIP groups likely because the intensity of the SHAM training was too low to produce any post-training modifications of the cardiac control, while the CIP training might be ineffective. The ineffectiveness of CIP training might be related to the inability, compared to MIP60, to produce really important transmural pressures, namely the difference between intramural atrial pressure and extramural intrathoracic pressure being the net stimulus for the low pressure receptors in the atria. We conjecture that this inability prevents the generation of empowered variations of the afferent neural activity during the CIP training and, consequently, the possibility to stimulate some rearrangements at the level of central respiratory network. This supposition needs to be corroborated by the observation of additional variables during CIP session such venous return, atrial and intrathoracic pressure and stroke volume.

Limitations of the Study and Future Developments

We remark the exploratory value of this study and recommend taking conclusions as hypotheses that should be tested over groups of larger size. With the results of the present work in mind future studies should be focused on a single type of IMT to concentrate the experimental effort on a single group of individuals. It is worth noting that at REST the MIP60 training was able to evoke a significant bradycardia in presence of an unvaried SAP. This finding is in contrast with some studies suggesting that IMT of moderate intensity could lower arterial pressure while leaving unmodified HP values in both normotensive (Vranish and Bailey, 2015; DeLucia et al., 2018) and hypertensive (Ferreira et al., 2013) subjects. Even the improvement of arterial pressure regulation, reported in subjects with orthostatic hypotension such as those after spinal cord

injury (Aslan et al., 2016), it is not evident in our study given that the baroreflex control is not affected by IMT. These considerations suggest that, although belonging to the class of IMT, our modality of IMT might lead to long-term effects different from those reported in literature and/or long-term consequences depending on the trained population, thus stressing the need of standardization of the IMT to better control its chronic effects according to the type of treated subjects. This standardization appears to be mandatory especially whether IMT of moderate intensity is to be proposed as a standard practice in physiotherapy and sports medicine.

CONCLUSION

This study suggests that an IMT of moderate intensity, such as MIP60, improves cardiac autonomic control by acting on CRC and this improvement is visible using a causal tool conditioning SAP out and only under a sympathetic stressor such as STAND. This improvement appears to be independent of cardiac baroreflex because the usual trends of BRS with STAND are detected after the MIP60 training. The present result indicates that the long-term effects of IMT of moderate intensity might be not limited to lower arterial pressure and vascular resistance (DeLucia et al., 2018) but they might be even wider through the possible involvement of regulatory centers in the brain stem that are not specifically devoted to arterial pressure control. This improvement is associated exclusively with an IMT training of moderate intensity. We suggest that the favorable effects of IMT of moderate intensity observed in patients featuring a high sympathetic drive (Ferreira et al., 2013; Da Luz Goulart et al., 2016; Martins de Abreu et al., 2017) and in healthy old subjects (Rodrigues et al., 2018) could be related to an improved CRC more evident under sympathetic stressor. The exploration of the mechanisms underlying the effects of MIP60 training might favor its specific application as a countermeasure of the progressive increase of sympathetic drive contributing to the decrease of CRCS in physiological and pathological situations.

DATA AVAILABILITY STATEMENT

The datasets generated for this study are available on request to the corresponding author.

ETHICS STATEMENT

The studies involving human participants were reviewed and approved by the Human Research Ethics Committee of the Federal University of São Carlos (UFSCar) under the protocol 1.558.731. The patients/participants provided their written informed consent to participate in this study.

AUTHOR CONTRIBUTIONS

AP conceived and designed the study. RA, PR-S, CDS, ÉS, and CAS performed the experiments. RA and BC analyzed the data. RA and AP drafted the manuscript and prepared the figures. RA, AC, BC, PR-S, CDS, ÉS, CAS, and AP interpreted the results, edited and revised the manuscript, and approved the final version of the manuscript.

FUNDING

This work was supported by the Fundação de Amparo à Pesquisa do Estado de São Paulo, Brazil (FAPESP, grants: 2016/22215-7; 2017/13402-0; and 2018/11123-0), Coordenação de Aperfeiçoamento de Pessoal de Nível Superior, Brazil (CAPES, Postgraduate Program in Physiotherapy, grant: 001), and Conselho Nacional de Desenvolvimento Científico e Tecnológico-CNPq (grant 3121938/2013-2).

REFERENCES

Akaike, H. (1974). A new look at the statistical novel identification. *IEEE Trans. Autom. Control* 19, 716–723. doi: 10.1109/tac.1974.1100705

Al-Ani, M., Munir, S. M., White, M., Townend, J., and Coote, J. H. (1996). Changes in R-R variability before and after endurance training measured by power spectral analysis and by the effect of isometric muscle contraction. *Eur. J. Appl. Physiol.* 74, 397–403. doi: 10.1007/bf02337719

Albinet, C. T., Boucard, G., Bouquet, C. A., and Audiffren, M. (2010). Increased heart rate variability and executive performance after aerobic training in the elderly. *Eur. J. Appl. Physiol.* 109, 617–624. doi: 10.1007/s00421-010-1393-y

Angell James, J. E. (1971). The effects of changes of extramural, intrathoracic, pressure on aortic arch baroreceptors. *J. Physiol.* 214, 89–103. doi: 10.1113/jphysiol.1971.sp009420

Aslan, S. C., Randall, D. C., Krassioukov, A. V., Phillips, A., and Ovechkin, A. V. (2016). Respiratory training improves blood pressure regulation in individuals with chronic spinal cord injury. *Arch. Phys. Med. Rehabil.* 97, 964–973. doi: 10.1016/j.apmr.2015.11.018

Barnett, L., Barrett, A. B., and Seth, A. K. (2009). Granger causality and transfer entropy are equivalent for Gaussian variables. *Phys. Rev. Lett.* 103:238701.

Bartsch, R., Kartelhardt, J. W., Penzel, T., and Havlin, S. (2007). Experimental evidence for phase synchronization transitions in the human cardiorespiratory system. *Phys. Rev. Lett.* 98:054102.

Baselli, G., Cerutti, S., Badilini, F., Biancardi, L., Porta, A., Pagani, M., et al. (1994). Model for the assessment of heart period and arterial pressure variability interactions and of respiration influences. *Med. Biol. Eng. Comput.* 32, 143–152. doi: 10.1007/bf02518911

Baselli, G., Porta, A., Rimoldi, O., Pagani, M., and Cerutti, S. (1997). Spectral decomposition in multichannel recordings based on multivariate parametric identification. *IEEE Trans. Biomed. Eng.* 44, 1092–1101. doi: 10.1109/10.641336

Beckers, F., Verheyden, B., and Aubert, A. E. (2006). Aging and nonlinear heart rate control in a healthy population. *Am. J. Physiol.* 290, H2560–H2570.

Bertinieri, G., di Rienzo, M., Cavallazzi, A., Ferrari, A. U., Pedotti, A., and Mancia, G. (1985). A new approach to analysis of the arterial baroreflex. *J. Hypertens Suppl.* 3, S79–S81.

Bracic Lotric, M., and Stefanovska, A. (2000). Synchronization and modulation in the human cardiorespiratory system. *Physica A* 283, 451–461. doi: 10.1016/s0378-4371(00)00204-1

Caiani, E. G., Turiel, M., Muzzupappa, S., Porta, A., Baselli, G., Pagani, M., et al. (2000). Evaluation of respiratory influences on left ventricular function parameters extracted from echocardiographic acoustic quantification. *Physiol. Meas.* 21, 175–186. doi: 10.1088/0967-3334/21/1/321

Catai, A. M., Takahashi, A. C. M., Perseguini, N. M., Milan, J., Minatel, V., Rehder-Santos, P., et al. (2014). Effect of the postural challenge on the dependence of the cardiovascular control complexity on age. *Entropy* 16, 6686–6704. doi: 10.3390/e16126686

Convertino, V. A., Ratliff, D. A., Ryan, K. L., Cooke, W. H., Doerr, D. F., Ludwig, D. A., et al. (2004a). Effects of inspiratory impedance on the carotid-cardiac baroreflex response in humans. *Clin. Auton. Res.* 14, 240–248.

Convertino, V. A., Ratliff, D. A., Ryan, K. L., Doerr, D. F., Ludwid, D. A., Muniz, G. W., et al. (2004b). Hemodynamics associated with breathing through an inspiratory impedance threshold device in human volunteers. *Crit. Care Med.* 32, S381–S386.

Cooke, W. H., Hoag, J. B., Crossman, A. A., Kuusela, T. A., Tahvanainen, K. U. O., and Eckberg, D. L. (1999). Human responses to upright tilt: a window on central autonomic integration. *J. Physiol.* 517, 617–628. doi: 10.1111/j.1469-7793.1999.0617t.x

Crystal, G. J., and Salem, M. R. (2012). The Bainbridge and the "reverse" Bainbridge reflexes: history, physiology, and clinical relevance. *Anesth. Analg.* 114, 520–532. doi: 10.1213/ANE.0b013e3182312e21

Da Luz Goulart, C., Simon, J. C., De Borba Schneiders, P., San Martin, E. A., Cabiddu, R., Borghi-Silva, A., et al. (2016). Respiratory muscle strength effect on linear and nonlinear heart rate variability parameters in COPD patients. *Int. J. Chron. Obstruct. Pulmon. Dis.* 11, 1671–1677. doi: 10.2147/COPD.S108860

De Maria, B., Bari, V., Cairo, B., Vaini, E., Esler, M., Lambert, E., et al. (2019). Characterization of the asymmetry of the cardiac and sympathetic arms of the baroreflex from spontaneous variability during incremental head-up tilt. *Front. Physiol.* 10:342. doi: 10.3389/fphys.2019.00342

DeLucia, C. M., De Asis, R. M., and Bailey, E. F. (2018). Daily inspiratory muscle training lowers blood pressure and vascular resistance in healthy men and women. *Exp. Physiol.* 103, 201–211. doi: 10.1113/EP086641

Eckberg, D. L. (1976). Temporal response patterns of the human sinus node to brief carotid baroreceptor stimuli. *J. Physiol.* 258, 769–782. doi: 10.1113/jphysiol.1976.sp011445

Eckberg, D. L. (2003). The human respiratory gate. *J. Physiol.* 548, 339–352. doi: 10.1111/j.1469-7793.2003.00339.x

Eckberg, D. L., and Karemaker, J. M. (2009). Point:counterpoint: respiratory sinus arrhythmia is due to a central mechanism vs. respiratory sinus arrhythmia is due to the baroreflex mechanism. *J. Appl. Physiol.* 106, 1740–1744.

Ferreira, J. B., Plentz, R. D., Stein, C., Casali, K. R., Arena, R., and Lago, P. D. (2013). Inspiratory muscle training reduces blood pressure and sympathetic activity in hypertensive patients: a randomized controlled trial. *Int. J. Cardiol.* 166, 61–67. doi: 10.1016/j.ijcard.2011.09.069

Furlan, R., Porta, A., Costa, F., Tank, J., Baker, L., Schiavi, R., et al. (2000). Oscillatory patterns in sympathetic neural discharge and cardiovascular variables during orthostatic stimulus. *Circulation* 101, 886–892. doi: 10.1161/01.cir.101.8.886

Garcia, A. J., Koschnitzky, J. E., Dashevskiy, T., and Ramirez, J.-M. (2013). Cardiorespiratory coupling in health and disease. *Auton. Neurosci.* 175, 26–37. doi: 10.1016/j.autneu.2013.02.006

Hirsch, J. A., and Bishop, B. (1981). Respiratory sinus arrhythmia in humans: how breathing pattern modulates heart rate. *Am. J. Physiol.* 241, H620–H629.

Iatsenko, D., Bernjak, A., Stankovski, T., Shiogai, Y., Owen-Lynch, P. J., Clarkson, P. B. M., et al. (2013). A. Evolution of cardiorespiratory interactions with age. *Phil. Trans. R. Soc. A* 371:20110622. doi: 10.1098/rsta.2011.0622

Kaminski, D. M., Schaan, B. D., da Silva, A. M., Soares, P. P., and Lago, P. D. (2015). Inspiratory muscle training in patients with diabetic autonomic neuropathy: a randomized clinical trial. *Clin. Auton. Res.* 25, 263–266. doi: 10.1007/s10286-015-0291-0

Kaplan, D. T., Furman, I., Pincus, S. M., Ryan, S. M., and Lipsitz, L. A. (1991). Aging and the complexity of cardiovascular dynamics. *Biophys. J.* 59, 945–949. doi: 10.1016/s0006-3495(91)82309-8

Karsten, M., Ribeiro, G. S., Esquivel, M. S., and Matte, D. L. (2018). The effects of inspiratory muscle training with linear workload devices on the sports performance and cardiopulmonary function of athletes: a systematic review and meta-analysis. *Phys. Ther. Sport* 34, 92–104. doi: 10.1016/j.ptsp.2018.09.004

Laitinen, T., Hartikainen, J., Vanninen, E., Niskanen, L., Geelen, G., and Länsimies, E. (1998). Age and sex dependency of baroreflex sensitivity in healthy subjects. *J. Appl. Physiol.* 84, 576–583. doi: 10.1152/jappl.1998.84.2.576

Laitinen, T., Niskamen, L., Geelen, G., Lansimies, E., and Hartikainen, J. (2004). Age dependency of cardiovascular autonomic responses to head-up tilt in healthy subjects. *J. Appl. Physiol.* 96, 2333–2340. doi: 10.1152/japplphysiol.00444.2003

Lurie, K. G., Zielinski, T., Voelckel, W., McKnite, S., and Plaisance, P. (2002). Augmentation of ventricular preload during treatment of cardiovascular collapse and cardiac arrest. *Crit. Care Med.* 30, S162–S165.

Marchi, A., Bari, V., De Maria, B., Esler, M., Lambert, E., Baumert, M., et al. (2016). Calibrated variability of muscle sympathetic nerve activity during graded head-up tilt in humans and its link with noradrenaline data and cardiovascular rhythms. *Am. J. Physiol.* 310, R1134–R1143. doi: 10.1152/ajpregu.00541.2015

Martins de Abreu, R., Porta, A., Rehder-Santos, P., Cairo, B., Donisete da Silva, C., and De Favari Signini, E. (2019). Effects of inspiratory muscle training intensity on cardiovascular control in amateur cyclists. *Am. J. Physiol.* 317, R891–R902. doi: 10.1152/ajpregu.00167.2019

Martins de Abreu, R., Rehder-Santos, P., Minatel, V., Dos Santos, G. L., and Catai, A. M. (2017). Effects of inspiratory muscle training on cardiovascular autonomic control: a systematic review. *Auton. Neurosci.* 208, 29–35. doi: 10.1016/j.autneu.2017.09.002

Mazzucco, C. E., Marchi, A., Bari, V., De Maria, B., Guzzetti, S., Raimondi, F., et al. (2017). Mechanical ventilatory modes and cardioventilatory phase synchronization in acute respiratory failure patients. *Physiol. Meas.* 38, 895–911. doi: 10.1088/1361-6579/aa56ae

Milan-Mattos, J. C., Porta, A., Perseguini, N. M., Minatel, V., Rehder-Santos, P., Takahashi, A. C. M., et al. (2018). Influence of age and gender on the phase and strength of the relation between heart period and systolic blood pressure spontaneous fluctuations. *J. Appl. Physiol.* 124, 791–804. doi: 10.1152/japplphysiol.00903.2017

Montano, N., Gnecchi-Ruscone, T., Porta, A., Lombardi, F., Pagani, M., and Malliani, A. (1994). Power spectrum analysis of heart rate variability to assess changes in sympatho-vagal balance during graded orthostatic tilt. *Circulation* 90, 1826–1831. doi: 10.1161/01.cir.90.4.1826

Nemati, S., Edwards, B. A., Lee, J., Pittman-Polletta, B., Butler, J. P., and Malhotra, A. (2013). Respiration and heart rate complexity: effects of age and gender assessed by band-limited transfer entropy. *Resp. Physiol. Neurobi.* 189, 27–33. doi: 10.1016/j.resp.2013.06.016

Nollo, G., Faes, L., Porta, A., Antolini, R., and Ravelli, F. (2005). Exploring directionality in spontaneous heart period and systolic pressure variability interactions in humans: implications in the evaluation of baroreflex gain. *Am. J. Physiol.* 288, H1777–H1785.

Parati, G., di Rienzo, M., Bertinieri, G., Pomidossi, G., Casadei, R., Groppelli, A., et al. (1988). Evaluation of the baroreceptor-heart rate reflex by 24-hour intra-arterial blood pressure monitoring in humans. *Hypertension* 12, 214–222. doi: 10.1161/01.hyp.12.2.214

Penzel, T., Kantelhardt, J. W., Bartsch, R. P., Riedl, M., Kramer, J., Wessel, N., et al. (2016). Modulations of heart rate, ECG, and cardio-respiratory coupling observed in polysomnography. *Front. Physiol.* 7:460. doi: 10.3389/fphys.2016.00460

Pomeranz, B., Macaulay, R. J. B., Caudill, M. A., Kutz, I., Adam, D., Gordon, D., et al. (1985). Assessment of autonomic function in humans by heart-rate spectral-analysis. *Am. J. Physiol.* 248, H151–H153.

Porta, A., Baselli, G., Rimoldi, O., Malliani, A., and Pagani, M. (2000). Assessing baroreflex gain from spontaneous variability in conscious dogs: role of causality and respiration. *Am. J. Physiol.* 279, H2558–H2567.

Porta, A., Bari, V., Bassani, T., Marchi, A., Pistuddi, V., and Ranucci, M. (2013a). Model-based causal closed loop approach to the estimate of baroreflex sensitivity during propofol anesthesia in patients undergoing coronary artery bypass graft. *J. Appl. Physiol.* 115, 1032–1042. doi: 10.1152/japplphysiol.00537.2013

Porta, A., Bassani, T., Bari, V., Tobaldini, E., Takahashi, A. C. M., Catai, A. M., et al. (2012). Model-based assessment of baroreflex and cardiopulmonary couplings during graded head-up tilt. *Comput. Biol. Med.* 42, 298–305.2015. doi: 10.1016/j.compbiomed.2011.04.019

Porta, A., Castiglioni, P., Di Rienzo, M., Bassani, T., Bari, V., Faes, L., et al. (2013b). Cardiovascular control and time domain Granger causality: insights

from selective autonomic blockade. *Phil. Trans. R. Soc. A* 371:20120161. doi: 10.1098/rsta.2012.0161

Porta, A., Catai, A. M., Takahashi, A. C. M., Magagnin, V., Bassani, T., Tobaldini, E., et al. (2011). Causal relationships between heart period and systolic arterial pressure during graded head-up tilt. *Am. J. Physiol.* 300, R378–R386. doi: 10.1152/ajpregu.00553.2010

Porta, A., and Faes, L. (2016). Wiener-Granger causality in network physiology with applications to cardiovascular control and neuroscience. *Proc. IEEE* 104, 282–309. doi: 10.1109/jproc.2015.2476824

Porta, A., Faes, L., Bari, V., Marchi, A., Bassani, T., Nollo, G., et al. (2014). Effect of age on complexity and causality of the cardiovascular control: comparison between model-based and model-free approaches. *PLoS One* 9:e89463. doi: 10.1371/journal.pone.0089463

Porta, A., Faes, L., Nollo, G., Bari, V., Marchi, A., De Maria, B., et al. (2015). Conditional self-entropy and conditional joint transfer entropy in heart period variability during graded postural challenge. *PLoS One* 10:e0132851. doi: 10.1371/journal.pone.0132851

Porta, A., Maestri, R., Bari, V., De Maria, B., Cairo, B., Vaini, E., et al. (2018). Paced breathing increases the redundancy of cardiorespiratory control in healthy individuals and chronic heart failure patients. *Entropy* 20:949. doi: 10.3390/e20120949

Rehder-Santos, P., Minatel, V., Milan-Mattos, J. C., De Favari Signini, E., Abreu, R. M., Dato, C. C., et al. (2019). Critical inspiratory pressure – a new methodology for evaluating and training the inspiratory musculature for recreational cyclists: study protocol for a randomized controlled trial. *Trials* 20:258. doi: 10.1186/s13063-019-3353-0

Riedl, M., Muller, A., Kraemer, J. F., Penzel, T., Kurths, J., and Wessel, N. (2014). Cardio-respiratory coordination increases during sleep apnea. *PLoS One* 9:e93866. doi: 10.1371/journal.pone.0093866

Rodrigues, G. D., Gurgel, J. L., Gonçalves, T. R., and da Silva Soares, P. P. (2018). Inspiratory muscle training improves physical performance and cardiac autonomic modulation in older women. *Eur. J. Appl. Physiol.* 118, 1143–1152. doi: 10.1007/s00421-018-3844-9

Saul, J. P., Berger, R. D., Albrecht, P., Stein, S. P., Chen, M. H., and Cohen, R. J. (1991). Transfer function analysis of the circulation: unique insights into cardiovascular regulation. *Am. J. Physiol.* 261, H1231–H1245.

Schreiber, T. (2000). Measuring information transfer. *Phys. Rev. Lett.* 85, 461–464. doi: 10.1103/physrevlett.85.461

Schulz, S., Adochiei, F.-C., Edu, I.-R., Schroeder, R., Costin, H., Bär, K.-J., et al. (2013). Cardiovascular and cardiorespiratory coupling analyses: a review. *Phil. Trans. R. Soc. A* 371:20120191. doi: 10.1098/rsta.2012.0191

Schulz, S., Bär, K.-J., and Voss, A. (2015). Analyses of heart rate, respiration and cardiorespiratory coupling in patients with schizophrenia. *Entropy* 17, 483–501. doi: 10.3390/e17020483

Seals, D. R., Suwarno, N. O., and Dempsey, J. A. (1990). Influence of lung volume on sympathetic nerve discharge in normal subjects. *Circ. Res.* 67, 130–141. doi: 10.1161/01.res.67.1.130

Spyer, K. M. (1995). Central nervous mechanisms responsible for cardio-respiratory homeostasis. *Adv. Exp. Med. Biol.* 381, 73–79. doi: 10.1007/978-1-4615-1895-2_8

Taha, B. H., Simon, P. M., Dempsey, J. A., Skatrud, J. B., and Iber, C. (1995). Respiratory sinus arrhythmia in humans: an obligatory role for vagal feedback from the lungs. *J. Appl. Physiol.* 78, 638–645. doi: 10.1152/jappl.1995.78.2.638

Task Force (1996). Heart rate variability: standards of measurement, physiological interpretation, and clinical use. Task force of the european society of cardiology and the north american society of pacing and electrophysiology. *Eur. Heart J.* 17, 354–381.

Taylor, J. A., and Eckberg, D. L. (1996). Fundamental relations between short-term RR interval and arterial pressure oscillations in humans. *Circulation* 93, 1527–1532. doi: 10.1161/01.cir.93.8.1527

Toska, K., and Eriksen, M. (1993). Respiration-synchronous fluctuations in stroke volume, heart rate and arterial pressure in humans. *J. Physiol.* 472, 501–512. doi: 10.1113/jphysiol.1993.sp019958

Vranish, J. R., and Bailey, E. F. (2015). Daily respiratory training with large intrathoracic pressures, but not large lung volumes, lowers blood pressure in normotensive adults. *Respir. Physiol. Neurobiol.* 216, 63–69. doi: 10.1016/j.resp.2015.06.002

Widjaja, D., Montalto, A., Vlemincx, E., Marinazzo, D., Van Huffel, S., and Faes, L. (2015). Cardiorespiratory information dynamics during mental arithmetic and sustained attention. *PLoS One* 10:e0129112. doi: 10.1371/journal.pone.0129112

Yana, K., Saul, J. P., Berger, R. D., Perrott, M. H., and Cohen, R. J. (1993). A time domain approach for the fluctuation analysis of heart rate related to instantaneous lung volume. *IEEE Trans. Biomed. Eng.* 40, 74–81. doi: 10.1109/10.204773

Conflict of Interest: The authors declare that the research was conducted in the absence of any commercial or financial relationships that could be construed as a potential conflict of interest.

The reviewer MJ declared a past collaboration with one of the authors AP to the handling Editor.

frontiers in Neuroscience

ORIGINAL RESEARCH
published: 11 March 2020
doi: 10.3389/fnins.2020.00204

Respiratory Sinus Arrhythmia Mechanisms in Young Obese Subjects

Michal Javorka[1], Jana Krohova[1], Barbora Czippelova[1], Zuzana Turianikova[1], Nikoleta Mazgutova[1], Radovan Wiszt[1], Miriam Ciljakova[2,3], Dana Cernochova[2,3], Riccardo Pernice[4], Alessandro Busacca[4] and Luca Faes[4]*

[1] Department of Physiology and Biomedical Center Martin, Jessenius Faculty of Medicine, Comenius University, Martin, Slovakia, [2] Department of Pediatrics, National Institute of Diabetes and Endocrinology, Lubochna, Slovakia, [3] Department of Pediatrics, Jessenius Faculty of Medicine, Comenius University and University Hospital, Martin, Slovakia, [4] Department of Engineering, University of Palermo, Palermo, Italy

OPEN ACCESS

Edited by:
Andreas Voss, Institut für Innovative Gesundheitstechnologien (IGHT), Germany

Reviewed by:
Niels Wessel, Humboldt University of Berlin, Germany
Luiz Carlos Marques Vanderlei, São Paulo State University, Brazil

***Correspondence:**
Jana Krohova
jana.krohova@uniba.sk

Specialty section:
This article was submitted to Autonomic Neuroscience, a section of the journal Frontiers in Neuroscience

Received: *01 January 2020*
Accepted: *24 February 2020*
Published: *11 March 2020*

Citation:
Javorka M, Krohova J, Czippelova B, Turianikova Z, Mazgutova N, Wiszt R, Ciljakova M, Cernochova D, Pernice R, Busacca A and Faes L (2020) Respiratory Sinus Arrhythmia Mechanisms in Young Obese Subjects. Front. Neurosci. 14:204. doi: 10.3389/fnins.2020.00204

Autonomic nervous system (ANS) activity and imbalance between its sympathetic and parasympathetic components are important factors contributing to the initiation and progression of many cardiovascular disorders related to obesity. The results on respiratory sinus arrhythmia (RSA) magnitude changes as a parasympathetic index were not straightforward in previous studies on young obese subjects. Considering the potentially unbalanced ANS regulation with impaired parasympathetic control in obese patients, the aim of this study was to compare the relative contribution of baroreflex and non-baroreflex (central) mechanisms to the origin of RSA in obese vs. control subjects. To this end, we applied a recently proposed information-theoretic methodology – partial information decomposition (PID) – to the time series of heart rate variability (HRV, computed from RR intervals in the ECG), systolic blood pressure (SBP) variability, and respiration (RESP) pattern measured in 29 obese and 29 age- and gender-matched non-obese adolescents and young adults monitored in the resting supine position and during postural and cognitive stress evoked by head-up tilt and mental arithmetic. PID was used to quantify the so-called unique information transferred from RESP to HRV and from SBP to HRV, reflecting, respectively, non-baroreflex and RESP-unrelated baroreflex HRV mechanisms, and the redundant information transferred from (RESP, SBP) to HRV, reflecting RESP-related baroreflex RSA mechanisms. Our results suggest that obesity is associated: (i) with blunted involvement of non-baroreflex RSA mechanisms, documented by the lower unique information transferred from RESP to HRV at rest; and (ii) with a reduced response to postural stress (but not to mental stress), documented by the lack of changes in the unique information transferred from RESP and SBP to HRV in obese subjects moving from supine to upright, and by a decreased redundant information transfer in obese compared to controls in the upright position. These findings were observed in the presence of an unchanged RSA

magnitude measured as the high frequency (HF) power of HRV, thus suggesting that the changes in ANS imbalance related to obesity in adolescents and young adults are subtle and can be revealed by dissecting RSA mechanisms into its components during various challenges.

Keywords: respiratory sinus arrhythmia, obesity, autonomic nervous system, information decomposition, multiscale analysis

INTRODUCTION

Obesity is a complex, multifactorial chronic disease associated with many adverse health consequences (Laederach-Hofmann et al., 2000; De Lorenzo et al., 2019). The prevalence of obesity in adults but also in children and adolescents prominently increased during last decades (World Health Organization [WHO], 2012). In the European Union, over 20% of school-age children (around 12 million children) suffer from overweight or obesity (Bagchi and Preuss, 2012). This results in an increasing occurrence of obesity-related complications (dyslipidemia, atherosclerotic changes, hypertension, impaired glucose tolerance, type 2 diabetes mellitus, etc.) even in childhood and adolescence (Vanderlei et al., 2010; Juonala et al., 2011; Cote et al., 2013; McCrindle, 2015; Ortega et al., 2016; Urbina et al., 2019).

Many cardiovascular disorders – including coronary artery disease, ventricular arrhythmia, arterial hypertension, left ventricular hypertrophy, and cardiomyopathy – are associated with obesity (Karason et al., 1999; Poirier et al., 2006). Autonomic nervous system (ANS) activity and imbalance between its two main components (parasympathetic and sympathetic nervous control) are important factors contributing to the initiation and progression of many cardiovascular disorders related to obesity (Ito et al., 2001; Cote et al., 2013; McCrindle, 2015; Ortega et al., 2016; Urbina et al., 2019).

To assess cardiovascular autonomic control changes in obese children and adolescents, heart rate variability (HRV) analysis in frequency domain was traditionally performed. High frequency (HF) HRV spectral power corresponding to the magnitude of respiratory-related heart rate oscillations – respiratory sinus arrhythmia (RSA) – was often analyzed due to its straightforward interpretation as an index of phasic parasympathetic activity, while the interpretation of slower oscillations in terms of sympathetic activity is more equivocal (Eckberg, 2000). Several studies demonstrated lower parasympathetic activity (lower HF HRV power) in obese children and adolescents (Paschoal et al., 2009; Thayer et al., 2010; Liao et al., 2014). In contrast, no significant differences in the HF power of HRV were observed in other studies between young obese subjects and healthy age- and gender-matched controls (Paschoal et al., 2009; Vanderlei et al., 2010; Javorka et al., 2016). Previous studies also demonstrated an impairment of arterial baroreflex (lower baroreflex sensitivity expressed as heart rate changes related to arterial blood pressure change) in obese children and adolescents, illustrating an impairment of reflex parasympathetic control (Honzikova et al., 2006; Krontoradova et al., 2008; Lazarova et al., 2009; Honzikova and Zavodna, 2016).

In order to shed light on the physiological mechanisms related to the controversial results reported above, this work undertakes a different approach than frequency domain analysis. Our motivation is the known fact that RSA results in humans from two principal pathways, reflecting a central mechanism (i.e., the connection of respiratory and cardiac control centers) and peripheral mechanisms (with a dominant role of high-pressure baroreflex mechanism). Although both these pathways are involved in the origin of RSA, their relative contribution varies with physiological conditions (Krohova et al., 2018). In this study, considering the potentially impaired parasympathetic control in young obese patients, our goal was to compare the relative contribution of baroreflex and non-baroreflex mechanisms in the origin of RSA in obese vs. control non-obese adolescents and young adults. To get insight into these mechanisms, we applied a recently developed information-theoretic approach to dissect causal interactions in multivariate time series, i.e., multiscale PID (Williams and Beer, 2010; Faes et al., 2017, 2018), computing the related measures on the cardiovascular and respiratory oscillations obtained at rest and during the application of two physiological stressors (i.e., orthostasis and cognitive load).

MATERIALS AND METHODS

The study group consisted of 58 adolescents and young adults, including 29 obese (O group) participants (14 female, age range: 12.4–22.7 years; median age: 15.4 years) and 29 age- and gender-matched healthy control (C group) subjects (age range: 12.5–22.1 years, median age: 15.8 years). The division to the O and C groups was based on the Cole's chart (Cole et al., 2000), which takes age into account when the body mass index (BMI) is used to diagnose overweight or obesity. The majority of obese subjects (25 out of 29 participants) were in the range of BMI 29–38 kg/m^2 corresponding to obesity classes I and II. The sample of subjects was recruited as a part of larger project focused on the study of obesity-related cardiovascular complications (e.g., see Czippelova et al., 2019). All measurements took place in the morning hours (from 8 am to 11 am), in a quiet examination room with temperature ranging between 22 and 25°C. All subjects must not suffer from any current or previous infectious disease (at least three weeks prior to the examination date), cardiovascular disease including hypertension (diagnosed using 24-h ambulatory blood pressure monitoring following examination), diabetes mellitus, psychiatric disorders, and hypothyroidism. All probands were instructed not to use substances influencing ANS or cardiovascular system activity during 24 h and not to perform strenuous physical

activity during 48 h prior to examination. Fourteen female subjects in each group were examined in the proliferative phase (6th–13th day) of their menstrual cycle. All subjects or their legal representatives (in participants under 18 years of age) provided written informed consent to participate in the study. The study was approved by the Ethics Committee of Jessenius Faculty of Medicine, Comenius University. Detailed characteristics of obese and control groups are shown in **Table 1**.

In this work we used a subset of continuous recordings of ECG (horizontal bipolar thoracic lead; CardioFax ECG-9620, NihonKohden, Japan), finger arterial blood pressure (volume-clamp photoplethysmography method; Finometer Pro, FMS, Netherlands) and respiratory volume (respiratory inductive plethysmography; RespiTrace, NIMS, United States) measured during four phases of the study protocol: supine rest (15 min), head-up tilt (HUT) to 45 degrees for 8 min to evoke mild orthostatic stress, supine recovery (10 min) and non-verbal mental arithmetics (MA) in the supine position (6 min). As the next step, the 300 beats lasing segments of RR interval, the systolic blood pressure (SBP), and respiration volume signal (RESP) were extracted from the continuous recordings. For more detailed information about the protocol and time series extraction see Javorka et al. (2017) and Krohova et al. (2019).

Data Analysis

As a first step, we calculated the spectral power of HRV in the HF band (0.15–0.4 Hz) using fast Fourier transform. The procedure started with resampling (cubic spline, 2 Hz) of the HRV time series to obtain an equidistant time series. Then, slower oscillations and trends were removed using the detrending procedure of Tarvainen et al. (2002). Subsequently, the mean power spectrum of the analyzed segment was computed and spectral power in the HF band was obtained by integration.

As a second step, we applied a recently proposed method, framed in information theory, to dissect causal interactions in multivariate time series according to the so-called PID (Williams and Beer, 2010; Faes et al., 2017, 2018; Krohova et al., 2019). PID was used in order to dissect the information transferred from SBP and RESP, considered as the sources of causal interactions, to the RR interval considered as the target, into contributions related to the information provided about the target individually by each source (interactions SBP → RR and RESP → RR) and the information provided as a result of the interaction between the two sources (interaction RESP → SBP → RR). Specifically, PID decomposes the joint transfer entropy (TE) from (RESP, SBP) to RR evidencing the unique TEs representing information flowing from one source to the target that is not affected by the other source (measures $U_{RESP\rightarrow RR}$ and $U_{SBP\rightarrow RR}$), and the redundant TE (measure $R_{RESP,SBP\rightarrow RR}$) representing the amount of overlapped information from the two sources. PID enables also to separate redundant TE from the synergistic TE ($S_{RESP,SBP\rightarrow RR}$, related to the excess of information that two sources transfer to the target when they are considered together compared to the sum of the information transferred by both sources separately) – in this study analysis of synergy was not included in the results. The computation of these measures is based on a linear parametric modeling of the three time series which is described in detail elsewhere (Williams and Beer, 2010; Faes et al., 2017, 2018; Krohova et al., 2019).

From a physiological point of view, these measures represent various phenomena: the unique TE $U_{SBP\rightarrow RR}$ can be thought as reflecting the strength of the effects of SBP on RR unrelated to RESP occurring along the cardiac chronotropic baroreflex arm, while the unique TE $U_{RESP\rightarrow RR}$ represents the baroreflex-independent effect of RESP on RR [i.e., the non-baroreflex (mostly central) mechanism of RSA]. The redundant TE $R_{RESP,SBP\rightarrow RR}$ reflects the information transferred from RESP to RR through SBP (along the indirect pathway RESP → SBP → RR), thus describing baroreflex-mediated respiratory effects on heart rate.

Although in its original formulation PID analyzes the "raw" original time series measured from ECG, arterial pressure, and RESP signals, a recent development based on filtering the time series in order to eliminate the short temporal scales allows to compute the PID measures with reference to the slower oscillations (long time scales) contained in the observed processes (Williams and Beer, 2010; Faes et al., 2017, 2018; Krohova et al., 2019). Thus, while interactions between cardiovascular and respiratory time series are dominantly reflected at the short time scales (Faes et al., 2012; Javorka et al., 2017) included in the raw unfiltered time series, the advantage of multiscale PID is that all the above mentioned information measures could be calculated at any assigned time scale τ. In this study, in addition to raw time series analyzed at a time scale $\tau_1 = 1$ which includes all oscillations, we calculated PID measures also for a longer scale – τ_2 determined – for each subject and experimental condition – as the time scale which removes the oscillations in the HF band and thus evidences slower oscillations [we refer to Krohova et al. (2019) for more detailed information].

TABLE 1 | The main characteristics of participants.

	Control group	Obese group	*P*-value
Age (years)	16.5 (2.6)	16.4 (2.7)	0.898
Height (cm)	170 (12)	171 (9)	0.881
Weight (kg)	61.3 (12.1)	96.7 (15.1)	<0.001
Body mass index (kg/m^2)	21.0 (2.3)	33.2 (4.4)	<0.001
Fat mass (%)	18.7 (7.2)	38.7 (7.3)	<0.001
Skeletal muscle mass (kg)	27.81 (6.9)	33.31 (7.0)	0.004
Waist circumference (cm)	72 (7)	99 (12)	<0.001
Waist to hip ratio (–)	0.76 (0.05)	0.84 (0.09)	<0.001

Values are expressed as mean (SD). The fat mass and skeletal muscle mass were evaluated using the InBody J10 device (Biospace, South Korea) which uses the direct segmental multi-frequency bioelectrical impedance analysis method (DSM-BIA). The differences between the groups of obese and healthy adolescents and young adults were evaluated by Mann–Whitney U-test, in addition to assessing the difference in body mass index that was evaluated using a t-test (with respect to data normality).

Statistical Analysis

Due to the non-normal distribution of the data the statistical comparison of a given measure (in both information and frequency domains) across conditions (supine rest, HUT, supine

recovery, MA) for both time scales was performed using the non-parametric Friedman test with two *post hoc* pairwise comparisons using the Conover test: supine rest vs. HUT, and supine recovery vs. MA. The differences between the groups of obese and healthy adolescents and young adults were evaluated by means of the Mann–Whitney test for each measure of information decomposition on a scale representing original data (τ_1) and slower oscillations (τ_2), as well as for the spectral power of RR interval computed in the HF band. The results were considered statistically significant for *P*-values < 0.05. Results are reported in terms of *P*-values and effect sizes. Effect sizes were quantified by: Kendall's coefficient of concordance *W* (comparison of supine rest vs. HUT, and supine recovery vs. MA) and by dividing the absolute (positive) standardized test statistic *Z* by the square root of the number of pairs ($n = 58$) (between group difference). According to Cohen's classification of effect sizes, the value 0.1 represents small effect, 0.3 moderate effect, and 0.5 and above large effect.

RESULTS

Respiratory Sinus Arrhythmia Magnitude

Figure 1 reports the estimated magnitude of RSA, expressed as the distribution of the spectral power of HRV in the HF band computed in the two groups during the four phases of the experimental protocol. Both HUT and MA were accompanied by a significant decrease in the HF power of HRV ($P < 0.001$ for HUT and MA in O and C groups, effect size: 0.524–1). During the whole protocol we did not observe any significant difference in the RR interval spectral power between the two groups ($0.460 \leq P \leq 0.692$, effect size: 0.052–0.097).

Effects of Stress Condition on the Interconnections Between Cardiovascular and Respiratory Signals

The distribution across subjects of the three considered PID measures computed on the raw data (without filtering, scale $\tau_1 = 1$) during the four phases of the protocol (supine rest, HUT, supine recovery, and MA) are shown in **Figure 2** for both obese and control groups (O and C, respectively).

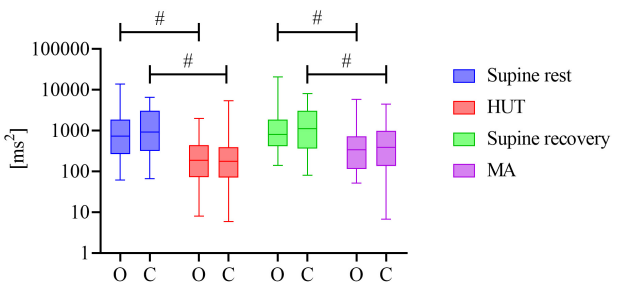

FIGURE 1 | Distribution of HRV spectral power values in the HF band (*y*-axis with a logarithmic scale) over four phases (supine rest, HUT, supine recovery, and MA) for the groups of obese (O) and healthy (C) adolescents and young adults. The distributions are shown as box plots. # represents a statistically significant difference between preceding rest phase and physiological stress (orthostasis or mental arithmetic task).

As the first step, we compared the impact of two types of physiological stress (supine rest vs. HUT, and supine recovery vs. MA) on the PID measures. For the C group, the transition from rest to HUT was associated with a significantly higher unique TE from SBP to RR (**Figure 2A**; $P < 0.001$, effect size: 0.655) and a significantly lower unique TE from RESP to RR (**Figure 2B**; $P < 0.001$, effect size: 0.596), while no significant changes were observed comparing MA with the previous rest period ($U_{SBP \rightarrow RR}$: $P = 0.252$, effect size: 0.029; $U_{RESP \rightarrow RR}$: $P = 0.599$, effect size: 0.001). For the O group, no significant changes across conditions were observed for either $U_{SBP \rightarrow RR}$ or $U_{RESP \rightarrow RR}$. On the other hand, the redundant TE $R_{RESP,SBP \rightarrow RR}$ was significantly higher during orthostasis in both groups (**Figure 2C**; $P \leq 0.001$, effect size: 0.524–0.629).

As the second step, we evaluated the differences in the PID measures observed between the groups of obese and healthy subjects. The unique TE from SBP to RR was significantly higher in the O group compared to healthy controls (C group) at rest (**Figure 2A**; $P = 0.004$, effect size: 0.374). In contrast, the unique TE from RESP to RR was significantly lower in the obese group during both resting conditions (**Figure 2B**; $P \leq 0.049$, effect size: 0.259–0.340). The redundant TE from RESP and SBP to RR was significantly lower during HUT in O group compared to controls (**Figure 2C**; $P = 0.036$, effect size: 0.275).

No significant between groups differences in PID measures were observed when only slower oscillations (τ_2) were analyzed ($P \geq 0.179$, effect size: 0.011–0.177, results not shown).

DISCUSSION

The major findings of our study include: (i) the observation of a well preserved parasympathetic nervous activity, expressed by RSA magnitude, and its responsiveness to stressors in young obese patients; (ii) the ability of PID to detect subtle abnormalities in RSA-related indexes in young obese patients compared to healthy controls, documented by reduced non-baroreflex respiratory effects on HRV (unique information transfer RESP → RR) in the resting condition and reduced baroreflex respiratory effects on HRV (redundant information transfer RESP → SBP → RR) during postural stress; and (iii) the ability of PID to reveal a reduced response to postural stress in young obese patients, documented by the lack of tilt-induced alterations of the cardiovascular and respiratory effects on HRV (unique information transfer RESP → RR and SBP → RR) compared with healthy controls.

The ANS plays an important role in the pathogenesis of cardiovascular disorders associated with obesity (Alam et al., 2009). The ANS is a very important control mechanism influencing energy balance and metabolic rate. Its activity is under the control of hypothalamic structures closely connected with the appetite control centers. Changes in the ANS activity and a dysbalance of its components can contribute to the obesity development but it is assumed that they are rather

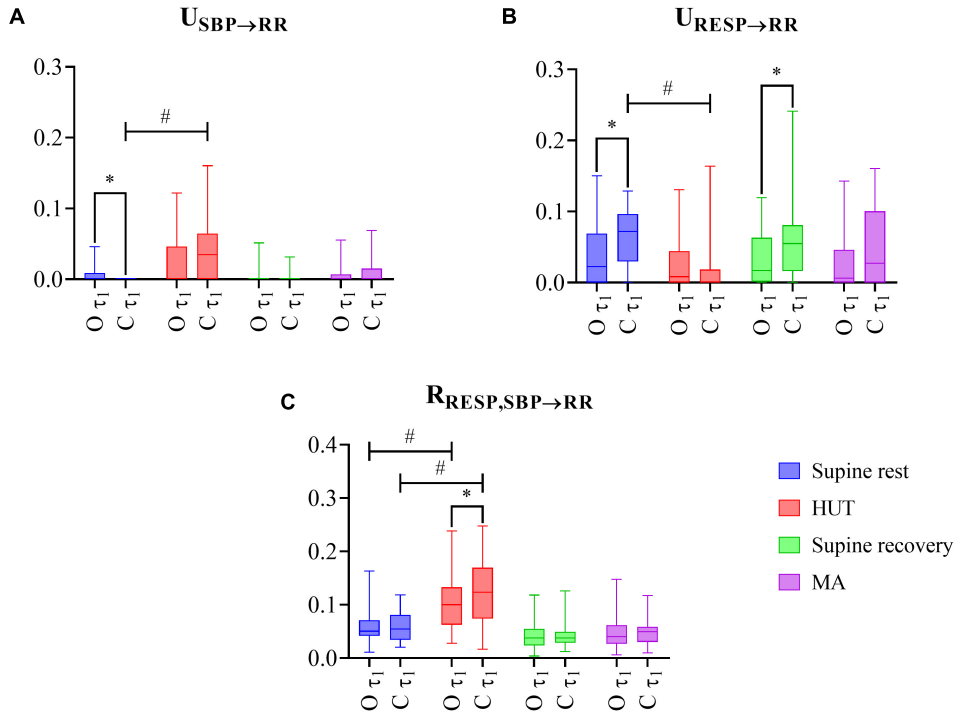

FIGURE 2 | The results of multiscale information decomposition during four phases (rest, HUT, supine recovery, and MA) calculated for the raw (non-filtered) data (τ_1) for the group of obese (O) and healthy non-obese control (C) adolescents and young adults. Graphs represent distribution of values in box plots for: **(A)** unique transfer entropy from SBP to RR ($U_{SBP\rightarrow RR}$) and **(B)** from RESP to RR ($U_{RESP\rightarrow RR}$), and **(C)** redundant transfer entropy ($R_{RESP,SBP\rightarrow RR}$) * indicates a statistically significant difference between the group of obese and healthy subjects and # represents a statistically significant difference between preceding rest phase and physiological stress (orthostasis or mental arithmetics task).

its consequence (Karason et al., 1999; Nagai and Moritani, 2004). A shift in cardiovascular autonomic control balance toward sympathetic nervous system dominance could contribute to the progression of serious cardiovascular complications in obese patients and significantly increase the risks of ventricular arrhythmia and sudden cardiac death in this population (Grassi et al., 1995; Muscelli et al., 1998). In previous studies, autonomic cardiovascular dysregulation in young obese patients was analyzed using linear and non-linear HRV analysis but the results of these studies were not consistent.

In accordance with several previous studies (Paschoal et al., 2009; Vanderlei et al., 2010; Javorka et al., 2016), no significant differences between young obese patients and controls were observed in this work in the RSA magnitude expressed as HRV HF power – an index reflexing the phasic cardiac parasympathetic activity. Our results extend the previous observations by the demonstration that HF power changes as a response to an application of two stressors (orthostatic test, MA) were similar in young obese patients and healthy controls. This finding indicates a well preserved parasympathetic nervous system reactivity in young obese subjects.

Applying PID analysis on the raw measured cardiovascular and respiratory time series, the orthostatic stress induced by HUT (but not the cognitive load induced by MA) resulted in an increased involvement of the high-pressure baroreflex as expressed by an increase in unique TE from SBP to RR in control group. This observation is in concert with the results of previous studies where the effect of orthostasis on the strength of the cardiac chronotropic baroreflex arm was analyzed in the frequency domain (Nollo et al., 2005) and using information-theoretic methods (Faes et al., 2013; Javorka et al., 2017). Higher baroreflex influence on heart rate was demonstrated also in both groups during orthostasis by an increase of the redundancy between respiratory and arterial pressure effects on HRV, indicating an increased importance of the indirect pathway RESP → SBP → RR during the unloading of baroreceptors associated with HUT. Moreover, considering the non-baroreflex mechanisms in the generation of RR intervals oscillations, their importance decreased during parasympathetic inhibition associated with orthostasis (decreased unique TE from RESP to RR during HUT in controls).

Although HF HRV power including its reactivity to physiological stressors was not able to distinguish between obese subjects and controls, the results of PID focused on disentangling basic mechanisms of RSA revealed some subtle between group differences. We applied multiscale PID to non-invasively assess the contribution of baroreflex (SBP → RR connection) and non-baroreflex (mostly central; RESP → RR connection) mechanisms to RSA. In our previous study, the relative contribution of these mechanisms was analyzed in young healthy subjects. At rest – both supine rest phase before HUT and recovery supine rest phase preceding MA – a lower

contribution of non-baroreflex RSA mechanisms was found in the obese group, as reflected by the decreased unique TE from RESP to RR ($U_{RESP \rightarrow RR}$) in comparison with controls. This was accompanied by a slightly higher baroreflex contribution to RSA ($U_{SBP \rightarrow RR}$) at rest. This novel observation reveals the shift in the relative contribution of RSA mechanisms associated with obesity. Interestingly, this shift in RSA mechanisms is in the same direction as the shift observed during HUT (Krohova et al., 2018), probably mirroring a shift of the sympathovagal balance toward sympathetic activation and vagal withdrawal.

In response to the physical stress, another between-groups difference was detected: the orthostatic load was connected with a significantly lower redundancy between influences of RESP and SBP on RR in obesity. This finding indicates that the indirect connection between RESP and HRV – cascade RESP → SBP → RR – is partially suppressed in obese group compared to controls. It could reflect the initial impairment of cardiac chronotropic baroreflex function in this group – the observation found in previous studies by a decreased baroreflex sensitivity (Honzikova et al., 2006; Lazarova et al., 2009).

The observed differences in $U_{RESP \rightarrow RR}$ could be also related to ventilatory pattern differences (Javorka et al., 2018). Therefore, we also measured tidal volume and respiratory rate from a calibrated RESP signal. Significantly higher tidal volume ($P \leq 0.036$) and no significant differences in respiratory rate ($P \geq 0.129$) were found in the obese patients compared to the control group. These differences – being mostly in favor of stronger respiratory influence on HRV – cannot be responsible for the observed between-group differences in the unique TE from RESP to RR. It should be noted that tidal volume reflects the amplitude of the respiratory input while information transfer reflects the involvement of the RSA-related mechanisms; therefore, the increased tidal volume (stronger input) together with the decreased information transfer (weaker link) could balance each other, possibly contributing to explain the preserved RSA magnitude found in obese patients across all experimental conditions. Taken together, our results indicate a slightly decreased parasympathetic HRV influence in young obese patients at rest. The results of the present study are summarized in the causal interaction models of RSA mechanisms during supine rest, HUT, and MA separately for healthy and obese adolescents and young adults (**Figure 3**).

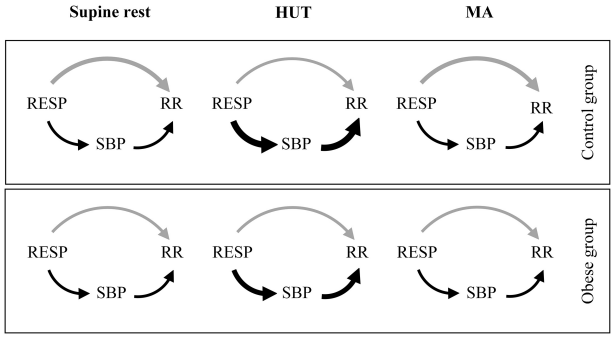

FIGURE 3 | Proposed causal interaction models of RSA mechanisms during supine rest, HUT, and MA. The arrow thickness reflects the strength of the causal coupling in the given direction, with changes in thickness corresponding to statistically significant variations between groups or conditions. The gray arrow represents the direct effects of RESP on RR ($U_{RESP \rightarrow RR}$; strength of non-baroreflex RSA mechanisms) and the black arrows represent the effects of RESP on RR mediated through SBP ($R_{RESP,SBP \rightarrow RR}$; strength of baroreflex RSA mechanism).

Importantly, between-groups differences in PID parameters were not detectable when HF oscillations were removed and we analyzed the cardiovascular and respiratory time series on scale τ_2 representing oscillations slower than those contained in the HF band. This indicates that observed subtle differences between groups reflected RESP-related oscillations.

From the clinical point of view, the results of our study point toward three important conclusions. Firstly, it is important to stress that while RSA magnitude (HF HRV) was not influenced by obesity, novel measures of the coupling strength between signals revealed subtle differences. We suggest that the coupling measures focused on the more detailed analysis of RSA mechanisms could be used in future for a detection of the subjects with impaired autonomic control not only associated with obesity. Secondly, significant differences between groups (obese vs. controls) were revealed mostly at stress conditions (orthostasis) pointing toward an importance of ANS testing during different physiological states (not only at rest). Lastly, we suggest that the analysis of interconnections between physiological signals can improve our understanding of the mechanisms underlying the oscillations. In our case, HF HRV (RSA) oscillations origin included both baroreflex and non-baroreflex mechanisms. The better understanding of the HRV mechanisms can improve the interpretability of the HRV analysis results.

CONCLUSION

We conclude that the RSA magnitude and its responsiveness to physical and cognitive stress are well preserved in young obese subjects. However, the information domain analysis of cardiovascular and cardiorespiratory interactions contributing to the origin of RSA revealed subtle differences mostly during orthostasis pointing toward evidence of an initial parasympathetic nervous system impairment.

DATA AVAILABILITY STATEMENT

The datasets generated for this study are available on written request to the corresponding author JK (jana.krohova@uniba.sk).

ETHICS STATEMENT

The studies involving human participants were reviewed and approved by the Ethics Committee of Jessenius Faculty of Medicine, Comenius University. Written informed consent to

participate in this study was provided by the participants' legal guardian/next of kin.

AUTHOR CONTRIBUTIONS

MJ, MC, and LF designed the study. MC and DC arranged for the probands participation. ZT, BC, NM, JK, and RW performed the measurements. JK and BC analyzed the data. MJ, JK, and LF wrote the manuscript. MJ, JK, LF, and RP contributed to the interpretation of the results. AB and MC helped supervise the project. All authors reviewed the manuscript.

FUNDING

This work was supported by the grants APVV-0235-12, VEGA 1/0117/17, VEGA 1/0199/19, VEGA 1/0200/19, project "Biomedical Center Martin" ITMS code: 26220220187, "Center of Excellence for Research in Personalized Therapy (CEVYPET)", ITMS: 26220120053, co-funded from the EU sources and European Regional Development Fund, "PRIN 2017 PRJ-0167, "Stochastic forecasting in complex systems", and PON R&I 2014-2020 AIM project no. AIM1851228-2, University of Palermo, Italy.

REFERENCES

Alam, I., Lewis, M. J., Lewis, K. E., Stephens, J. W., and Baxter, J. N. (2009). Influence of bariatric surgery on indices of cardiac autonomic control. *Auton. Neurosci.* 151, 168–173. doi: 10.1016/j.autneu.2009.08.007

Bagchi, D., and Preuss, H. G. (2012). *Obesity: Epidemiology, Pathophysiology, and Prevention*, 2nd Edn, Milton Park: Taylor & Francis.

Cole, T. J., Bellizzi, M. C., Flegal, K. M., and Dietz, W. H. (2000). Establishing a standard definition for child overweight and obesity worldwide: international survey. *BMJ* 320:1240. doi: 10.1136/bmj.320.7244.1240

Cote, A. T., Harris, K. C., Panagiotopoulos, C., Sandor, G. G., and Devlin, A. M. (2013). Childhood obesity and cardiovascular dysfunction. *J. Am. Coll. Cardiol.* 62, 1309–1319. doi: 10.1016/j.jacc.2013.07.042

Czippelova, B., Turianikova, Z., Krohova, J., Wiszt, R., Lazarova, Z., Pozorciakova, K., et al. (2019). Arterial stiffness and endothelial function in young obese patients - vascular resistance matters. *J. Atheroscler. Thromb.* 26, 1015–1025. doi: 10.5551/jat.47530

De Lorenzo, A., Gratteri, S., Gualtieri, P., Cammarano, A., Bertucci, P., and Di Renzo, L. (2019). Why primary obesity is a disease? *J. Transl. Med.* 17:169. doi: 10.1186/s12967-019-1919-y

Eckberg, D. L. (2000). Physiological basis for human autonomic rhythms. *Ann. Med.* 32, 341–349. doi: 10.3109/07853890008995937

Faes, L., Bari, V., Ranucci, M., and Porta, A. (2018). Multiscale decomposition of cardiovascular and cardiorespiratory information transfer under general Anesthesia. *Conf. Proc. IEEE Eng. Med. Biol. Soc.* 2018, 4607–4610. doi: 10.1109/EMBC.2018.8513191

Faes, L., Marinazzo, D., and Stramaglia, S. (2017). Multiscale information decomposition: exact computation for multivariate gaussian processes. *Entropy* 19:408. doi: 10.3390/E19080408

Faes, L., Nollo, G., and Porta, A. (2012). Non-uniform multivariate embedding to assess the information transfer in cardiovascular and cardiorespiratory variability series. *Comput. Biol. Med.* 42, 290–297. doi: 10.1016/j.compbiomed.2011.02.007

Faes, L., Nollo, G., and Porta, A. (2013). Mechanisms of causal interaction between short-term RR interval and systolic arterial pressure oscillations during orthostatic challenge. *J. Appl. Physiol.* 114, 1657–1667. doi: 10.1152/japplphysiol.01172.2012

Grassi, G., Seravalle, G., Cattaneo, B. M., Bolla, G. B., Lanfranchi, A., Colombo, M., et al. (1995). Sympathetic activation in obese normotensive subjects. *Hypertension* 25(4 Pt 1), 560–563. doi: 10.1161/01.hyp.25.4.560

Honzikova, N., Novakova, Z., Zavodna, E., Paderova, J., Lokaj, P., Fiser, B., et al. (2006). Baroreflex sensitivity in children, adolescents, and young adults with essential and white-coat hypertension. *Klin. Padiatr.* 218, 237–242. doi: 10.1055/s-2005-836596

Honzikova, N., and Zavodna, E. (2016). Baroreflex sensitivity in children and adolescents: physiology, hypertension, obesity, diabetes mellitus. *Physiol. Res.* 65, 879–889.

Ito, H., Ohshima, A., Tsuzuki, M., Ohto, N., Yanagawa, M., Maruyama, T., et al. (2001). Effects of increased physical activity and mild calorie restriction on heart rate variability in obese women. *Jpn. Heart J.* 42, 459–469. doi: 10.1536/jhj.42.459

Javorka, M., El-Hamad, F., Czippelova, B., Turianikova, Z., Krohova, J., Lazarova, Z., et al. (2018). Role of respiration in the cardiovascular response to orthostatic and mental stress. *Am. J. Physiol. Regul. Integr. Comp. Physiol.* 314, R761–R769. doi: 10.1152/ajpregu.00430.2017

Javorka, M., Krohova, J., Czippelova, B., Turianikova, Z., Lazarova, Z., Javorka, K., et al. (2017). Basic cardiovascular variability signals: mutual directed interactions explored in the information domain. *Physiol. Meas.* 38, 877–894. doi: 10.1088/1361-6579/aa5b77

Javorka, M., Turianikova, Z., Tonhajzerova, I., Lazarova, Z., Czippelova, B., and Javorka, K. (2016). Heart rate and blood pressure control in obesity - how to detect early dysregulation? *Clin. Physiol. Funct. Imaging* 36, 337–345. doi: 10.1111/cpf.12234

Juonala, M., Magnussen, C. G., Berenson, G. S., Venn, A., Burns, T. L., Sabin, M. A., et al. (2011). Childhood adiposity, adult adiposity, and cardiovascular risk factors. *N. Engl. J. Med.* 365, 1876–1885. doi: 10.1056/NEJMoa1010112

Karason, K., Molgaard, H., Wikstrand, J., and Sjostrom, L. (1999). Heart rate variability in obesity and the effect of weight loss. *Am. J. Cardiol.* 83, 1242–1247. doi: 10.1016/s0002-9149(99)00066-61

Krohova, J., Czippelova, B., Turianikova, Z., Lazarova, Z., Wiszt, R., Javorka, M., et al. (2018). Information domain analysis of respiratory sinus arrhythmia mechanisms. *Physiol. Res.* 67(Suppl. 4), S611–S618.

Krohova, J., Faes, L., Czippelova, B., Turianikova, Z., Mazgutova, N., Pernice, R., et al. (2019). Multiscale information decomposition dissects control mechanisms of heart rate variability at rest and during physiological stress. *Entropy* 21:526. doi: 10.3390/E21050526

Krontoradova, K., Honzikova, N., Fiser, B., Novakova, Z., Zavodna, E., Hrstkova, H., et al. (2008). Overweight and decreased baroreflex sensitivity as independent risk factors for hypertension in children, adolescents, and young adults. *Physiol. Res.* 57, 385–391.

Laederach-Hofmann, K., Mussgay, L., and Ruddel, H. (2000). Autonomic cardiovascular regulation in obesity. *J. Endocrinol.* 164, 59–66. doi: 10.1677/joe.0.1640059

Lazarova, Z., Tonhajzerova, I., Trunkvalterova, Z., Brozmanova, A., Honzikova, N., Javorka, K., et al. (2009). Baroreflex sensitivity is reduced in obese normotensive children and adolescents. *Can. J. Physiol. Pharmacol.* 87, 565–571. doi: 10.1139/y09-041

Liao, D., Rodriguez-Colon, S. M., He, F., and Bixler, E. O. (2014). Childhood obesity and autonomic dysfunction: risk for cardiac morbidity and mortality. *Curr. Treat Options Cardiovasc. Med.* 16:342. doi: 10.1007/s11936-014-0342-341

McCrindle, B. W. (2015). Cardiovascular consequences of childhood obesity. *Can. J. Cardiol.* 31, 124–130. doi: 10.1016/j.cjca.2014.08.017

Muscelli, E., Emdin, M., Natali, A., Pratali, L., Camastra, S., Gastaldelli, A., et al. (1998). Autonomic and hemodynamic responses to insulin in lean and obese humans. *J. Clin. Endocrinol. Metab.* 83, 2084–2090. doi: 10.1210/jcem.83.6.4878

Nagai, N., and Moritani, T. (2004). Effect of physical activity on autonomic nervous system function in lean and obese children. *Int. J. Obes. Relat. Metab. Disord.* 28, 27–33. doi: 10.1038/sj.ijo.0802470

Nollo, G., Faes, L., Porta, A., Antolini, R., and Ravelli, F. (2005). Exploring directionality in spontaneous heart period and systolic pressure variability

interactions in humans: implications in the evaluation of baroreflex gain. *Am. J. Physiol. Heart Circ. Physiol.* 288, H1777–H1785. doi: 10.1152/ajpheart.00594.2004

Ortega, F. B., Lavie, C. J., and Blair, S. N. (2016). Obesity and cardiovascular disease. *Circ. Res.* 118, 1752–1770. doi: 10.1161/CIRCRESAHA.115.306883

Paschoal, M. A., Trevizan, P. F., and Scodeler, N. F. (2009). Heart rate variability, blood lipids and physical capacity of obese and non-obese children. *Arq. Bras. Cardiol.* 93, 239–246. doi: 10.1590/s0066-782x2009000900007

Poirier, P., Giles, T. D., Bray, G. A., Hong, Y., Stern, J. S., Pi-Sunyer, F. X., et al. (2006). Obesity and cardiovascular disease: pathophysiology, evaluation, and effect of weight loss: an update of the 1997 american heart association scientific statement on obesity and heart disease from the obesity committee of the council on nutrition, physical activity, and metabolism. *Circulation* 113, 898–918. doi: 10.1161/CIRCULATIONAHA.106.171016

Tarvainen, M. P., Ranta-Aho, P. O., and Karjalainen, P. A. (2002). An advanced detrending method with application to HRV analysis. *IEEE Trans. Biomed. Eng.* 49, 172–175. doi: 10.1109/10.979357

Thayer, J. F., Yamamoto, S. S., and Brosschot, J. F. (2010). The relationship of autonomic imbalance, heart rate variability and cardiovascular disease risk factors. *Int. J. Cardiol.* 141, 122–131. doi: 10.1016/j.ijcard.2009.09.543

Urbina, E. M., Khoury, P. R., Bazzano, L., Burns, T. L., Daniels, S., Dwyer, T., et al. (2019). Relation of blood pressure in childhood to self-reported hypertension in adulthood. *Hypertension* 73, 1224–1230. doi: 10.1161/HYPERTENSIONAHA.118.12334

Vanderlei, L. C., Pastre, C. M., Freitas Junior, I. F., and Godoy, M. F. (2010). Analysis of cardiac autonomic modulation in obese and eutrophic children. *Clinics* 65, 789–792. doi: 10.1590/s1807-59322010000800008

Williams, P. L., and Beer, R. D. (2010). Nonnegative decomposition of multivariate information. *arXiv* [Preprint], doi: 10.1109/TSMCB.2010.2044788

World Health Organization [WHO], (2012). *Population-Based Approaches to Childhood Obesity Prevention*. Geneva: World Health Organization.

Conflict of Interest: The authors declare that the research was conducted in the absence of any commercial or financial relationships that could be construed as a potential conflict of interest.

frontiers in Physiology

ORIGINAL RESEARCH
published: 28 April 2020
doi: 10.3389/fphys.2020.00341

Time Window Determination for Inference of Time-Varying Dynamics: Application to Cardiorespiratory Interaction

Dushko Lukarski[1,2], *Margarita Ginovska*[3], *Hristina Spasevska*[3] *and Tomislav Stankovski*[1,4]*

[1] Faculty of Medicine, Ss. Cyril and Methodius University, Skopje, Macedonia, [2] University Clinic for Radiotherapy and Oncology, Skopje, Macedonia, [3] Faculty of Electrical Engineering and Information Technologies, Ss. Cyril and Methodius University, Skopje, Macedonia, [4] Department of Physics, Lancaster University, Lancaster, United Kingdom

OPEN ACCESS

Edited by:
Andreas Voss,
Institut für Innovative Gesundheitstechnologien (IGHT), Germany

Reviewed by:
Mathias Baumert,
University of Adelaide, Australia
Dirk Cysarz,
Witten/Herdecke University, Germany

***Correspondence:**
Tomislav Stankovski
t.stankovski@ukim.edu.mk

Specialty section:
This article was submitted to Autonomic Neuroscience, a section of the journal Frontiers in Physiology

Received: 10 December 2019
Accepted: 24 March 2020
Published: 28 April 2020

Citation:
Lukarski D, Ginovska M, Spasevska H and Stankovski T (2020) Time Window Determination for Inference of Time-Varying Dynamics: Application to Cardiorespiratory Interaction. Front. Physiol. 11:341. doi: 10.3389/fphys.2020.00341

Interacting dynamical systems abound in nature, with examples ranging from biology and population dynamics, through physics and chemistry, to communications and climate. Often their states, parameters and functions are time-varying, because such systems interact with other systems and the environment, exchanging information and matter. A common problem when analysing time-series data from dynamical systems is how to determine the length of the time window for the analysis. When one needs to follow the time-variability of the dynamics, or the dynamical parameters and functions, the time window needs to be resolved first. We tackled this problem by introducing a method for adaptive determination of the time window for interacting oscillators, as modeled and scaled for the cardiorespiratory interaction. By investigating a system of coupled phase oscillators and utilizing the Dynamical Bayesian Inference method, we propose a procedure to determine the time window and the propagation parameter of the covariance matrix. The optimal values are determined so that the inferred parameters follow the dynamics of the actual ones and at the same time the error of the inference represented by the covariance matrix is minimal. The effectiveness of the methodology is presented on a system of coupled limit-cycle oscillators and on the cardiorespiratory interaction. Three cases of cardiorespiratory interaction were considered—measurement with spontaneous free breathing, one with periodic sine breathing and one with a-periodic time-varying breathing. The results showed that the cardiorespiratory coupling strength and similarity of form of coupling functions have greater values for slower breathing, and this variability follows continuously the change of the breathing frequency. The method can be applied effectively to other time-varying oscillatory interactions and carries important implications for analysis of general dynamical systems.

Keywords: time-series analysis, dynamical systems, dynamical Bayesian inference, coupled oscillators, coupling functions

1. INTRODUCTION

Dynamical systems are widespread in nature, with examples including biological, chemical, climatological and social systems. Often they interact with other systems and the environment, exchanging information and matter (Winfree, 1980; Haken, 1983; Kuramoto, 1984; Pikovsky et al., 2001; Strogatz, 2001). This makes their states, parameters and functions time-varying (Kloeden and Rasmussen, 2011; Stankovski, 2013; Suprunenko et al., 2013; Lehnertz et al., 2014).

Biological dynamical systems form an important group of such systems. They are the central focus to medicine and biomedicine. Different physiological systems reflect the function of human bodily organs and processes, directly linked to various states and diseases (Peskin, 1981; Levy et al., 2006). Understanding and being able to detect certain physiological characteristics of such systems and functions is thus of great importance and relevance to science with direct implications for the human well-being.

Such biological systems are usually not isolated, but interact between each other (Bashan et al., 2012). The cardiorespiratory interaction, as central mechanism of the cardiovascular system, has been studied extensively in relation to different states and diseases (Schäfer et al., 1998; Stefanovska et al., 2000; Stankovski et al., 2012; Iatsenko et al., 2013; Kralemann et al., 2013a; Schulz et al., 2018; Grote et al., 2019). The cardiac and the respiration signals can be acquired by non-invasive measurements, making the investigations of cardiorespiratory interaction easily accessible. Both systems have periodic oscillatory dynamics, which makes them also very convenient for modeling in terms of their phase dynamics (Rosenblum et al., 2002; Stankovski et al., 2012; Kralemann et al., 2013a; Ticcinelli et al., 2017). Similarly to the other open biological systems, the dynamics of the cardiorespiratory system can also be time-varying, including a situation where the frequency, the coupling strength or the coupling function are varying in time—which adds a challenging complexity when analysing such data.

Different aspects of the cardiorespiratory interaction have been studied, including phase synchronization, coupling strength/directionality and the coupling functions (Rosenblum et al., 2002; Paluš and Stefanovska, 2003; Voss et al., 2008; Stankovski et al., 2012; Kralemann et al., 2013a; Hagos et al., 2019). The latter describe the functional mechanism of how the interactions occur and develop (Stankovski et al., 2017). As such, the coupling functions have attracted much attention recently, with many publications describing novel aspects of interaction mechanisms of the cardiorespiratory and other interactions across different scientific fields (Kiss et al., 2007; Ranganathan et al., 2014; Stankovski et al., 2014b; Ashwin et al., 2019; Moon and Wettlaufer, 2019; Rosenblum et al., 2019). The main focus of the current paper will be also on coupling functions and how to infer optimally their time-variability.

Even though physiological dynamical systems, including the all-important cardiorespiratory interaction, are of great value and importance, when analysing their data, inevitable, one faces a *problem of how to determine the length of the time window*. Namely, when analysing the time-series data one needs to be able to follow the time-variability of the dynamics, i.e., the dynamical parameters and functions, but in order to do so, one needs to determine first the length of the time window. Then the data are usually analyzed through consecutive time windows, i.e., data portions of the time-series. Here, the length of the window will determine the time-resolution of the resulting parameters and functions. The main requirement for the window length is usually a tradeoff between (i) long enough time window to have the required amount of data for the methods to work correctly and (ii) short enough time window to get as good as possible time-resolution of the resulting parameters and functions. These conflicting requirements, (i) and (ii), make the choice for the window length very difficult and ambiguous, hence, usually, the time window length is a free parameter and it is chosen based on the subjective experience and intuition of the expert analyst.

In this paper, we developed a procedure for determination of the time window based on data analyses, as opposed to the previous practice of arbitrary choice. We extend a method for Dynamical Bayesian Inference of time-varying dynamics in the presence of noise, to utilize the inferred covariance matrix in order to determine the best choice of the time window. The choice is based on the inferred results as a tradeoff between low parameter error and low noise strength error. The method is tested and demonstrated on numerical phase and limit-cycle oscillators and on time-varying cardiorespiratory interactions.

2. METHODS AND MODELING RESULTS

2.1. Dynamical Bayesian Inference

In the context of the method of interest, the dynamical inference refers to a model inference that will describe the solution of a system of differential equations via time series analysis. When two oscillators interact sufficiently weakly, their motion is effectively approximated with their phase dynamics (Kuramoto, 1984; Nakao et al., 2014). If we describe the system phase as a generic monotonic change of the variables, the dynamical process can be presented as:

$$\dot{\varphi}_i = \omega_i + q_i(\varphi_i, \varphi_j) + \xi_i, \tag{1}$$

where φ_i is the phase of the i-th oscillator, ω_i is its phase velocity, q_i is the coupling function between the two oscillators, and ξ_i is the noise. It is assumed that the noise is white Gaussian $\xi_i(t)\xi_j(\tau) = \delta(t-\tau)E_{ij}$, where the symmetric matrix E_{ij} incorporates the information about the correlation between the noises of the different oscillators.

The periodic behavior of the system indicates that the coupling function can be represented by a Fourier decomposition:

$$q_i(\varphi_i, \varphi_j) = \sum_{k=1}^{\infty}\sum_{s=1}^{\infty} c_{i;k,s} e^{i2\pi k\varphi_i} e^{i2\pi s\varphi_j} \tag{2}$$

Usually, the dynamics will be well-described by a finite number K of Fourier terms, hence Equation (1) can be written as:

$$\dot{\varphi}_i = \sum_{k=-K}^{K} {c_k}^i \Phi_{i,k}(\varphi_i, \varphi_j) + \xi_i(t), \tag{3}$$

where $i = \{1, 2\}, \Phi_{1,0} = \Phi_{2,0} = 1, {c_0}^i = \omega_i$ and the rest $\Phi_{i,k}$ and ${c_k}^i$ are the K most important Fourier components (in this work we used $K = 2$). If a white Gaussian noise is assumed $\langle \xi_i(t)\xi_j(\tau)\rangle = \delta(t-\tau)E_{ij}$, the task is than reduced to inference of the unknown parameters of the model:

$$M = \left\{{c_k}^i, E_{ij}\right\}. \tag{4}$$

For a given time series of observed phases $\chi = \left\{\varphi_{i,n} \equiv \varphi_i(t_n)\right\}, (t_n = nh, i = 1, 2)$, the Bayesian statistics allows us to determine the posterior density, using the prior density $p_{prior}(M)$ as well as a likelihood function $l(\chi|M)$:

$$p_\chi(M|\chi) = \frac{l(\chi|M)p_{prior}(M)}{\int l(\chi|M)p_{prior}(M)dM}. \tag{5}$$

In the Dynamical Bayesian Inference (Smelyanskiy et al., 2005; Duggento et al., 2012; Stankovski et al., 2012, 2014a) one makes certain initial assumptions about the parameters of the model that describes the observed time series. Then, the Bayesian theorem is successively applied in a recursive stepwise manner and in each following step of the inference, the inferred model parameters are getting closer to their real value. With each step of the inference, one obtains the value of the concentration matrix Ξ (which is the inverse of the covariance matrix $\Xi = \Sigma^{-1}$).

2.1.1. The Challenge of the Time Window and the Propagation Parameter

When using the aforementioned method, the time series of the phases of the oscillators are acquired by measurements followed by signal processing. The time series can be considered as time sequences of blocks of samples. Each block incorporates the samples in a certain time interval, hence the duration of the block determines the time window t_w. The Bayesian inference is performed for each block and values for the parameters of the model and the couplings of the oscillators are obtained. The output values of the previous block are used as input values for the inference of the current block.

The method comprises a dynamical inference, so it needs to follow the time evolution of the set of parameters c and at the same time to enable separation of the dynamical effects from the noise. To achieve such separation, in the propagation sequence of the method, the input covariance matrix for the following block $\Sigma_{prior}^{(n+1)}$ is not taken as simply equal to the output covariance matrix of the current block Σ_{post}^{n}, but it is modified by the diffusion matrix Σ_{diff}. The diffusion matrix is defined by the normal diffusion of each of the parameters. Hence, the input covariance matrix for the following block is a convolution of the two current normal distributions $\Sigma_{prior}^{(n+1)} = \Sigma_{post}^{n} + \Sigma_{diff}$ (Duggento et al., 2012; Stankovski et al., 2012). The covariance matrix Σ_{diff} describes which part of the dynamical field defined by the oscillators is changed and the intensity of those changes. The elements of this matrix are given by $(\Sigma_{diff})_{(i,j)} = \rho_{ij}\sigma_i\sigma_j$, where σ_i is the standard deviation of the diffusion of the parameter c_i, after time window t_w from the previous to the next block of samples, and $\rho_{(i,j)}$ gives the correlation between the changes of the parameters c_i and c_j. A special case is investigated, when there is no correlation between the parameters, i.e., $\rho_{(i,j)} = 0$, for $i \neq j$ and each standard deviation σ_i is a known fraction of the corresponding parameter c_i: $\sigma_i = p_w c_i$, where p_w, called the propagation parameter, is a constant parameter. The index w in p_w emphasizes that the propagation parameter is determined for a time window of length t_w. In this way the propagation parameter defines how much variability should the method search for and infer. Being an input in the covariance matrix Σ_{diff} it expresses our belief about which part of the dynamics has changed, and the extent of that change. This is a tradeoff between inferring correctly the time-varying parameters and not inferring too much random noise perturbations. In the earlier works, this propagation parameter p_w was a free parameter chosen arbitrarily.

In the method of Dynamical Bayesian Inference (Duggento et al., 2012; Stankovski et al., 2012) the time window and the propagation parameter are free parameters and they are arbitrarily selected. The purpose of this research is to propose a method to determine the values of these two parameter in order to optimize the inference of the parameters and the noise.

As an indicator of quality of the inference the covariance matrix Σ is used. By definition, this is a matrix whose element in the (i, j) position is the covariance between the i-th and j-th element of a multidimensional random vector. The elements on the main diagonal of the covariance matrix are the variances of the variables, i.e., the covariance of each element with itself. Since the square of the variance is the standard deviation, by minimizing the sum of squares of the elements of the covariance matrix we are minimizing the standard deviations of the inferred model parameters. Therefore, we use the sum of squares of all the elements of the covariance matrix $Q_\Sigma = Sum_{i,j}({\Sigma_{i,j}}^2)$, called quadrature covariance matrix, as an indicator of deviations of the inferred parameters from the real intrinsic parameters.

2.2. Determination of the Time Window

In order to developed and present the procedure for determination of the time window we investigate first two coupled phase oscillators in presence of noise:

$$\begin{aligned} \dot{\varphi}_1 &= \omega_1(t) + a_1 sin(\varphi_1) + a_3(t) sin(\varphi_2) + \sqrt{E_{11}}\xi_{11}(t) \\ \dot{\varphi}_2 &= \omega_2 + a_2 sin(\varphi_1) + a_4 sin(\varphi_2) + \sqrt{E_{22}}\xi_{22}(t). \end{aligned} \tag{6}$$

Here, ω_1 and ω_2 are parameters for the angular frequency of the corresponding oscillators, a_1 and a_4 are the parameters of their own dynamics, and a_2 and a_3 are the coupling parameters for the direct influence from the other oscillator. Two of the parameters are varied periodically in time, the frequency $\omega_1(t)$ and the coupling parameter $a_3(t)$. Uncorrelated Gaussian white noises are used. In this way the true values of the parameters of the oscillatory systems are known in advance.

From these oscillatory systems we generate numerical signals which we then introduce as input data for the Dynamical Bayesian Inference. As a result we obtain the inferred values of the parameters and the noise, as well as the quadrature matrix Q_Σ for each block of the inference. Apart from Q_Σ, we evaluate the error difference between the inferred parameters c_i and their true values $\tilde{c}_i$: $\Delta c_i = c_i - \tilde{c}_i$, and the same was done with the noise strengths $\Delta E_i = E_i - \tilde{E}_i$. We investigate the dependance of Q_Σ, Δc_i and ΔE_i on the time window t_w, for different values of the propagation parameter p_w.

For the system of two coupled phase oscillators (Equation 6) we simulated multiple time series of 2,000 s each, with sampling step $h = 0.01$, corresponding to a 10 ms step. These time series are the input data for the Dynamical Bayesian Inference. In the study the parameters a_1, a_2, and a_4 are constant: $a_1 = 0.8, a_2 = 0$, and $a_4 = 0.6$. The frequency ω_2 was varied in the interval from 0.785 to 31.4. The time-varying parameters are given by:

$$\begin{aligned} \omega_1 &= \omega_{1,const} - 0.5 sin 2\pi f_1 t \\ a_3 &= a_{3,const} - 0.3 sin(2\pi f_3 t + \pi/2), \end{aligned} \tag{7}$$

where $a_{3,const}$ was either 0.8 or 1.3, $\omega_{1,const}$ was varied in the interval 0.785–62.8, and the oscillator frequencies f_1 and f_2 were changed in the interval 0.001–0.02. For the noise (E_{11}, E_{22}) values in the interval (0.01, 10) were taken. For these values we investigated the dependence of Q_Σ, Δc_i and ΔE_i on the time window t_w and the propagation parameter p_w.

The typical look of the dependance of Q_Σ on the time window t_w and the propagation parameter p_w is given in **Figure 1A**. The function of the quadrature matrix Q_Σ on the time window t_w shows a maximum that depends on the value of the propagation parameter p_w. We have determined that the maximum is obtained for the value of the time window $t_{w,max} = 1/p_w$. As the relationship shows, with decreasing value of p_w, the maximum is shifted to greater values of t_w (as shown on **Figure 1B**).

The performed analysis showed that for all combinations of t_w and p_w that place the inference on the left of the maximum ($t_w < t_{w,max}$) of the corresponding curve $Q_\Sigma(t_w)$, the inference does not follow the time change of the parameters—shown on **Figure 1C**. It appears that such combinations of t_w and p_w do not allow the inference to reach the amplitude of change of the time-varying parameter. We will call this behavior as the delayed-inference regime.

For $t_w > t_{w,max}$, the value of Q_Σ steadily decreases (as shown in **Figure 1**) and the deviations of the inferred parameters from their true values also decrease. However, values for the time window that are too large also prevent appropriate inference of the time changes of the parameters simply because there are too few blocks for their representation.

Based on these results we conclude that the time window should have a value as high as possible, in order for Q_Σ to be as low as possible, but at the same time a value that is still low enough to be able to accurately represent the dynamic of the parameter that is changing with the highest frequency. Therefore, in the analysis, we performed an initial estimation of the time change of the parameters of the model by using a small arbitrary value for the time window and an initial value of the propagation parameter $p_w = 0.2$. We use small time window in order for inferred parameters to be able to describe the fast changes of their true values. Then we performed a fast Fourier transform on the initial estimation of the parameters from which we determined the highest frequency of the time-varying change of the parameters. We denote this frequency as f_{max} and the corresponding period as $T_{min} = 1/f_{max}$. From our analysis of the time-varying ability we concluded that the minimal number of blocks needed to accurately describe this fastest changing

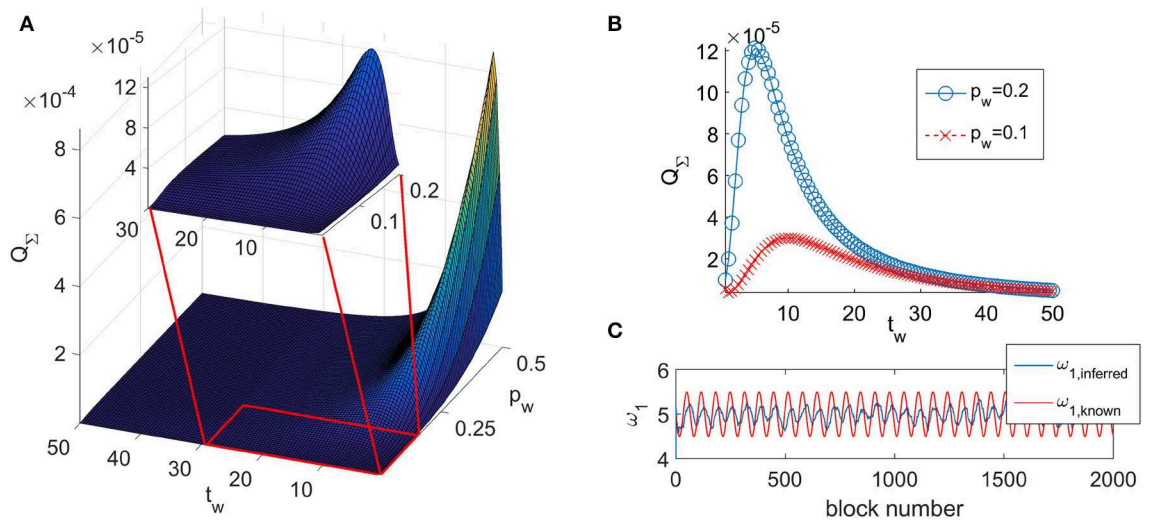

FIGURE 1 | (A) Typical look of the dependance of Q_Σ on the time window t_w and the propagation parameter p_w for coupled phase oscillators (Equation 6). **(B)** Q_Σ as a function of the time window t_w for two different values of the propagation parameter p_w. **(C)** The inferred value of a parameter $\omega_{1,inferred}$ and the known value of the same parameter $\omega_{1,known}$.

parameter is eight blocks, i.e., the time window should be taken as $t_{w,opt} = \frac{T_{min}}{8} = \frac{1}{8f_{max}}$. That will give a resolution of eight points to describe the fastest oscillating inferred parameter. For all the other parameters there will be more points describing their oscillations.

2.3. Determination of the Propagation Parameter

From the numerical analysis we determined that the inferred covariance matrix Q_Σ increases with the increase of the propagation parameter p_w up to saturation for very big values of p_w ($p_w > 7$ in our simulations). Hence, in order to get the best possible inference, we should use the smallest possible propagation parameter. However, as we have shown in **Figure 1**, for small propagation parameter, smaller than $p_{w,min} = 1/t_{w,max}$ the inference does not follow the time change of the parameters and is in the delayed-inference regime.

To determine the optimal value of the propagation parameter we have investigated the difference between the inferred parameters and their known value. We have evaluated this difference in two different ways.

One was to look at the graphs like the one shown in **Figure 1C** for different values of the time window t_w and by evaluating the difference between the inferred parameter and its known value to determine the minimal value for t_w for which the inferred parameter starts to follow the change of the known parameter. This will be the t_w value when the Δc_i stops manifesting periodic changes in time.

The second way was to calculate the mean square error (MSE) between the time series of the inferred parameter and the time series of its known value (excluding the first two blocks of the inference). The mean square error was calculated for different values of the propagation parameter and a graph $MSE = f(p_w)$ was constructed for different $t_w = t_{w,opt}$ values. These graphs showed a minimum that gives the p_w value for which the correspondence between the inferred and the known value of the parameters is the best.

We have performed this evaluation for different frequencies of change of the parameters of the model and for different noises. The time window values used in these simulations were the optimal values ($t_{w,opt}$). From these analysis we have found that the optimal value for the propagation parameter depends both on the frequencies of the changes of the parameters (i.e., on the optimal time window) and on the noise. Further, we have found that the optimal value of the propagation parameter is approximately linearly dependent on the frequency of the fastest changing parameter f_{max} (**Figure 2A**). The slope and the intercept of the linear function were found to depend on the noise. This dependence can approximately be described by inverse power law (**Figure 2A**).

From the numerical analysis we have determined that we can relate the optimal propagation parameter, $p_{w,opt}$, to the optimal time window, $t_{w,opt}$. As a rule, the optimal propagation parameter needs to be greater than the reciprocal optimal time window $p_{w,opt} > 1/t_{w,opt}$. Further more, in the interval of frequencies and noises that we investigated, which are of interest and corresponds to cardiorespiratory interactions, the propagation parameter in the Dynamical Bayesian Inference can be selected as follows. For slow dynamics, when the optimal time window is >40 s, one can use the value $p_{w,opt} = 0.1$ as optimal propagation parameter. For optimal time windows in the interval $t_{w,opt} \in (10s, 40s)$, one can use the value $p_{w,opt} = 0.2$ as optimal propagation parameter. For fast dynamics, when the optimal time window is <10 s, the optimal propagation parameter should be calculated as $p_{w,opt} = 2/t_{w,opt}$. We emphasize that these values can be used

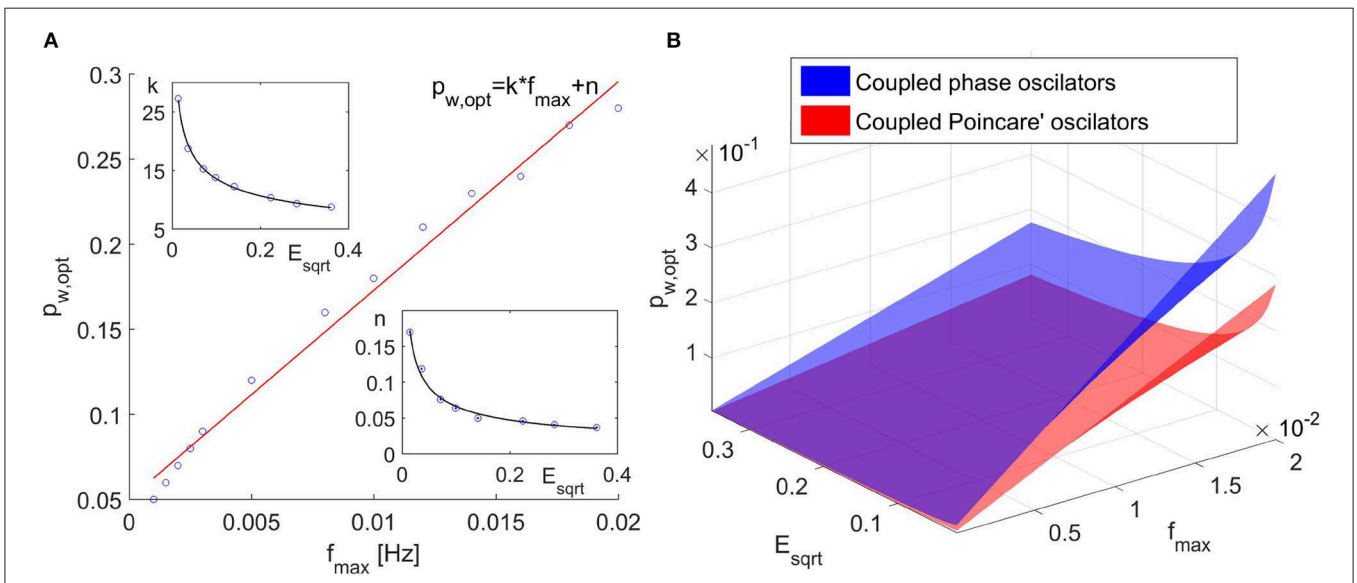

FIGURE 2 | (A) Optimal propagation parameter $p_{w,opt}$ as a function on the maximal frequency of the parameter change. **(B)** Optimal propagation parameter as a function of the maximal frequency of parameter change and the noise for coupled phase oscillators and coupled Poincaré oscillators.

for cardiorespiratory interactions when the noise is not too small. With decreasing noise, one needs to take increasingly higher values for the optimal propagation parameter.

2.4. Algorithm for the Optimization of Time Window and Propagation Parameter Values

Based on the results obtained in sections 2.2 and 2.3 we propose the following algorithm for determining of the optimal time window $t_{w,opt}$ and propagation parameter $p_{w,opt}$.

Using a small arbitrary value for the time window and an initial value for the propagation parameter of $p_w = 0.2$ we perform an initial inference. The arbitrary value for the time window can be the smallest value at which the method gives an output. For values smaller than this arbitrary value of t_w the Bayesian inference will not work (the execution of the code will give a "Singular matrix error", because the concentration matrix will be too small). In this way we will obtain the initial inferred parameters c_{ij} and noises E_{ij} that describe the model. This inference will have the best information on the parameter dynamics in terms of time-variation, but the parameter noise will be quite large. Then we perform a fast Fourier transform of the inferred parameters c_{ij}. By observing both the dynamic of each of the parameters and their fast Fourier transform, we are able to determine what the highest frequency of change of the parameters is. We denote this frequency as f_{max}. The corresponding period is $T_{min} = 1/f_{max}$. By assuming the minimal number of blocks needed to accurately describe this fastest changing parameter, the time window should be taken as $t_{w,opt} = T_{min}/8 = 1/8f_{max}$. This will give a resolution of eight points to describe the fastest oscillating inferred parameter. For all the other parameters there will be more points describing their oscillations.

Based on the value of the optimal time window, for the case scaled around the frequencies in the cardiorespiratory range, when the noise is not too small, we can determine the optimal propagation parameter as:

$$p_{w,opt} = \begin{cases} 0.1, & t_{w,opt} > 40 \\ 0.2, & t_{w,opt} \in [10, 40] \\ \frac{2}{t_{w,opt}}, & t_{w,opt} < 10. \end{cases} \quad (8)$$

With these values for $t_{w,opt}$ and $p_{w,opt}$ we perform a second, optimized inference. In this inference the covariance matrix will have smaller value, thus resulting in an improved inference.

2.5. Analysis of Coupled Limit-Cycle Oscillators

To test the proposed algorithm for determination of the time window and the propagation parameter, we investigate a system of two coupled limit-cycle oscillators – Poincaré oscillators

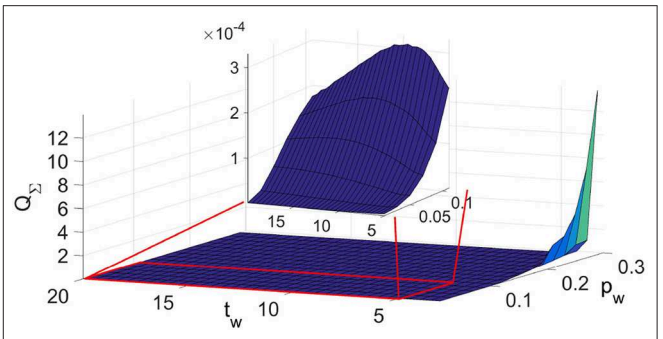

FIGURE 3 | Typical look of the dependance of quadrature matrix Q_Σ on the time window t_w and the propagation parameter p_w for coupled Poincaré oscillators.

subject to white noise:

$$\begin{aligned} \dot{x}_1 &= -\left(\sqrt{x_1^2 + y_1^2} - 1\right)x_1 - \omega_1(t)y_1 + \varepsilon_1(x_2 - x_1) + \xi_1(t) \\ \dot{y}_1 &= -\left(\sqrt{x_1^2 + y_1^2} - 1\right)y_1 + \omega_1(t)x_1 + \varepsilon_1(y_2 - y_1) + \xi_2(t) \\ \dot{x}_2 &= -\left(\sqrt{x_2^2 + y_2^2} - 1\right)x_2 - \omega_2 y_2 + \varepsilon_2(t)(x_1 - x_2) + \xi_3(t) \\ \dot{y}_2 &= -\left(\sqrt{x_2^2 + y_2^2} - 1\right)y_2 + \omega_2 x_2 + \varepsilon_2(t)(y_1 - y_2) + \xi_4(t), \end{aligned} \quad (9)$$

where periodic time-variability is introduced in the frequency of the first oscillator $\omega_1(t) = 1 - 0.4sin(2\pi f_1 t)$ and in the coupling parameter from the first to the second oscillator $\varepsilon_2(t) = 0.2 - 0.1sin(2\pi f_2 t)$. The noises are again white and Gaussian, with no correlations between them and were changed in the interval $E_i \in [0.005, 0.05], i = \{1, 2, 3, 4\}$. The other parameters are $\omega_2 = 4.91$ and $\varepsilon_1 = 0.05$. The frequency of the time-variability was changed in the interval $f_i \in [0.0015, 0.02], i = \{1, 2\}$.

In **Figure 3** we show the quadrature covariance matrix as a function of the time window and the propagation parameter.

As in the case of the coupled phase oscillators, here as well we see a maximum in the function of the quadrature covariance matrix Q_Σ on the time window t_w that depends on the value of the propagation parameter as $t_{w,max} = 1/p_w$. Again, the performed analysis showed that for values of t_w smaller than the value for the maximum of the curve, $t_{w,max}$, regardless of the value of the propagation parameter, the inference does not follow the time change of the parameters.

The results for the propagation parameter also showed increase in the inferred quadrature matrix Q_Σ with the increase of the propagation parameter p_w and by implementing the same analysis as in the case of coupled phase oscillators, we found that the optimal propagation parameter increases linearly with the increase of the maximal frequency change of the parameters. Again the slope and the intercept of the line $p_{w,opt} = k * f_{max} + n$ showed decrease with increasing noise and the decrease can be approximated with inverse power law. As expected, we

determined different values for the coefficients of the inverse power laws. However, these coefficients always yielded values for the propagation parameter $p_{w,opt}$ smaller than the one for the coupled phase oscillators, as shown in **Figure 2B**, hence the determination of the propagation parameter according to the Equation (8) will give satisfactory results.

3. APPLICATION TO CARDIORESPIRATORY INTERACTION

It is well-appreciated that the cardiac and respiration dynamics are oscillating, while being part of the multi-system body they are not isolated, but they are open systems where their parameters and functions are time-varying (Glass, 2001; Stankovski et al., 2012; Kralemann et al., 2013b; Rosenblum et al., 2019). The oscillatory nature makes them suitable to be represented with the phase dynamics (Kuramoto, 1984; Nakao, 2016). These two aspect of the cardiorespiratory dynamics, the oscillatory phase dynamics and their time-variability, make the proposed method of dynamical Bayesian inference with adaptive time window very good fit for such analysis.

In order to demonstrate the potential of the method on experimental data, we analyzed cardiorespiratory measurements conducted on one male subject, age 35, non-smoker without cardiovascular health issues. The study was reviewed and approved by Ethical Committee, Faculty of Medicine, Saints Cyril and Methodius, Skopje, Macedonia and the participant provided written informed consent that the collected data might be used and published for research purposes. The respiration followed a predetermined pattern by following a visual and audio computer simulation in which a ball was moved along a sine line on a computer screen. The frequency of the movement of the ball, together with the sine line, was changing according to the law that we wanted the respiration to follow. When the ball was reaching the maximum and minimum of the sine line, a short sound beep was also generated. The measurements were performed using Biopac equipment with the subject in supine position. The respiration was measured by placing a respiratory transducer on the chest of the subject measuring the changes in the chest circumference, while the cardiac function was recorded by performing a three-lead ECG measurement.

Three different patterns of respiration were studied and compared: spontaneous free breathing, time-varying breathing following a sine wave and time-varying breathing following a-periodic signal. The average respiratory rates of the investigated respiratory patterns were 14.7 BrPM (Breaths per Minute) for the spontaneous free breathing, 15.5 BrPM for the respiration following a sine law and 17.0 BrPM for the breathing following the aperiodic signal. These average respiratory rates correspond to average respiratory frequencies of 0.245, 0.258, and 0.283 Hz, respectively. The corresponding average heart rates were found to be 68.3 BPM (Beats per Minute), 69.0 and 77.4 BPM for the spontaneous free breathing, periodic and aperiodic respiration, respectively.

In **Figure 4** we show first in detail the cardiorespiratory measurements for a time varying respiration following a simple sine law. The frequency of respiration is varied according to the law $f = 0.3 + 0.2sin(2\pi t/560)$, [Hz]. The time-varying perturbed respiration signal is shown in **Figure 4A** and its wavelet transform is given in **Figure 4B**. On **Figure 4C** we give the corresponding ECG signal and on **Figure 4D** the wavelet transform of the cardiac signal.

In **Figure 5** we show the signals and their wavelet transforms for the three different patterns of respiration that the subject followed: (a) respiration signal recorded during free breathing, (b) time-frequency wavelet transform of the free breathing respiration, (c) wavelet transform of time varying respiration following a simple sine law (the same as depicted in **Figure 4B** for comparison), (d) wavelet transform of time varying respiration following an a-periodic behavior and the signal itself (e). The a-periodic signal was taken to be the z-component of a chaotic Lorenz system (Lorenz, 1963).

After the wavelet power inspection of the measurements we performed the phase extraction procedure. For robust phase extraction, the oscillating intervals were estimated by standard digital filtering procedures, including a FIR filter followed by a zero-phase filtering procedure (filtfilt) to ensure that no time or phase lags were introduced by the filtering. The boundary of the interval for the respiration signal was r = 0.145–0.6 Hz; and boundary of the interval for the heart activity from the ECG signal was h = 0.6–2 Hz (Kralemann et al., 2008; Shiogai et al., 2010; Stankovski et al., 2016). The phases of the filtered signals were estimated by use of the Hilbert transform, and the protophase-to-phase transformation Kralemann et al. (2008) was then applied to the resultant protophases to obtain invariant observable-independent phases.

In the case of free breathing, as can be seen in **Figure 5B**, there was no single frequency dominating the time variance of the parameters. Therefore, when we did the first inference of our algorithm, higher frequencies emerged in the variance of the parameters and in their Fast Fourier Transform. Since we wanted to include the higher frequencies in the consequent investigation we had to use smaller time windows, as our algorithm suggests ($t_{w,opt} = 9s$). This increased the covariance matrix, but at the same time faster changes were included in the inference and we were able to follow better the time evolution of the parameter change and of the coupling functions. In the case of time varying respiration according to the sine law, as is the case of **Figure 4**, the frequency of change of the respiration dominated the first inference. This led to higher optimal time window ($t_{w,opt} = 62s$) and to a second inference with reduced covariance matrix. In the case of time varying respiration according to a-periodic law, as is the case of **Figures 5D,E**, again the algorithm gave smaller values for the optimal time window ($t_{w,opt} = 15.6s$), that enabled inclusion of different frequencies of change of the parameters at the cost of increased covariance matrix.

Finally we present the application results of our method for the cardiorespiratory coupling. Once we have determined the optimal values for the time window and the propagation parameter we can proceed with the inference of the parameters of the model c_i, from which we can calculate the coupling quantities and characteristics. We evaluated the coupling functions on a $2\pi \times 2\pi$ grid using the relevant base functions, i.e., Fourier

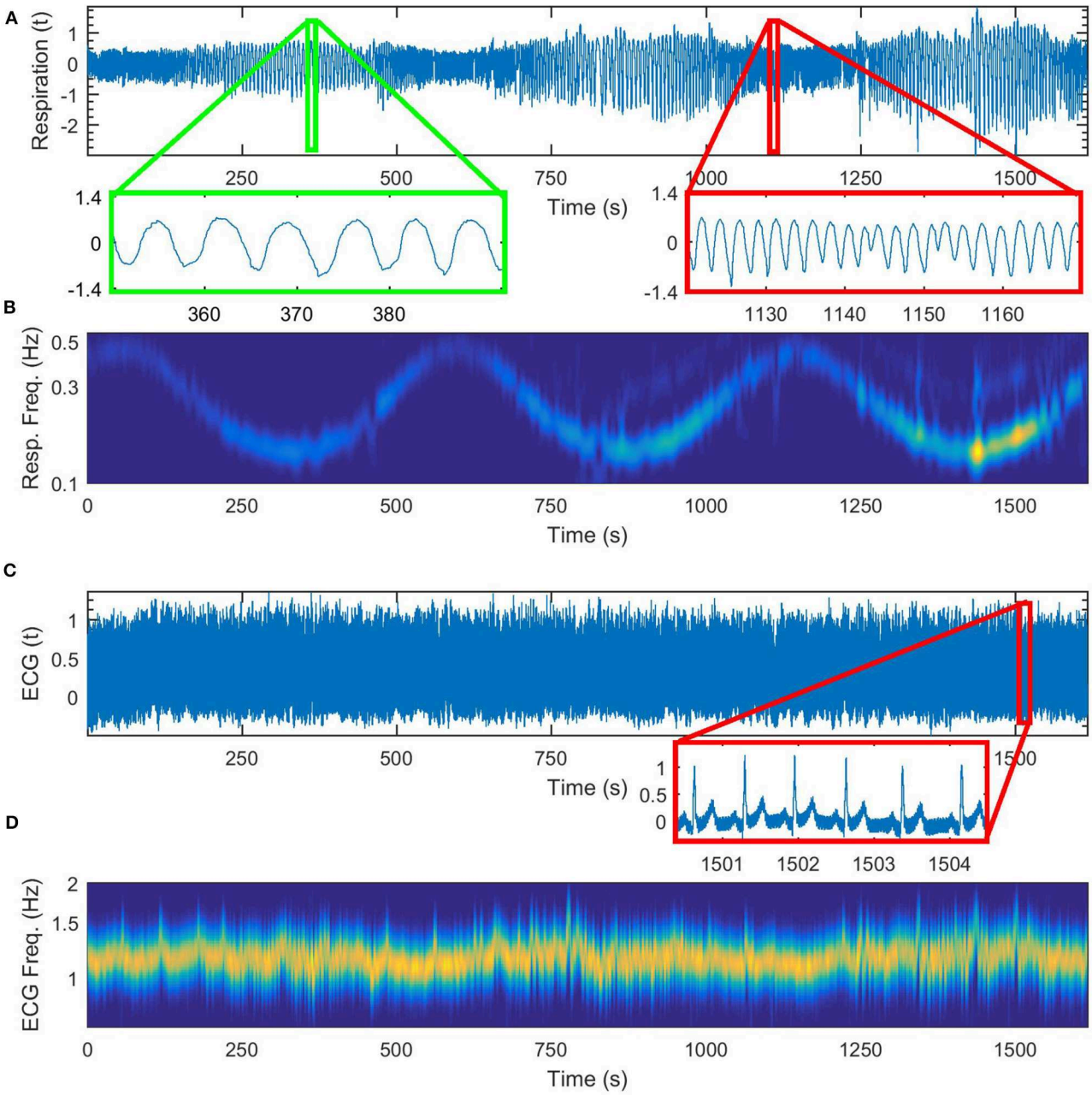

FIGURE 4 | Cardiorespiratory measurements for a time-varying respiration following a sine law, **(A)** respiration signal, **(B)** wavelet transform of the respiration signal, **(C)** ECG signal, **(D)** wavelet transform of the ECG signal.

components scaled by their inferred coupling parameters. We calculated the coupling strength $CPL_i(t)$ as the Euclidian norm of the inferred parameters for a particular coupling. Importantly, we also calculated the index for similarity of coupling functions $\rho(t)$ which quantifies the similarity of the forms of two coupling functions irrespectively of their coupling strength amplitudes. The similarity index is unique measure of coupling functions and it is calculated as correlation index between the vectors c_i of two coupling functions (Kralemann et al., 2013a; Ticcinelli et al., 2017). It is important to note that the coupling strength and the similarity index present two different dimensions of a coupling function (Stankovski, 2017). In our analysis we calculated the similarity index between the time-average coupling function and every coupling function calculated from each time window—in this way we got the time-variability of the form of the coupling function as compared to the average coupling function.

In **Figures 6A–D** we present the results for the cardiorespiratory interaction when the respiration varies

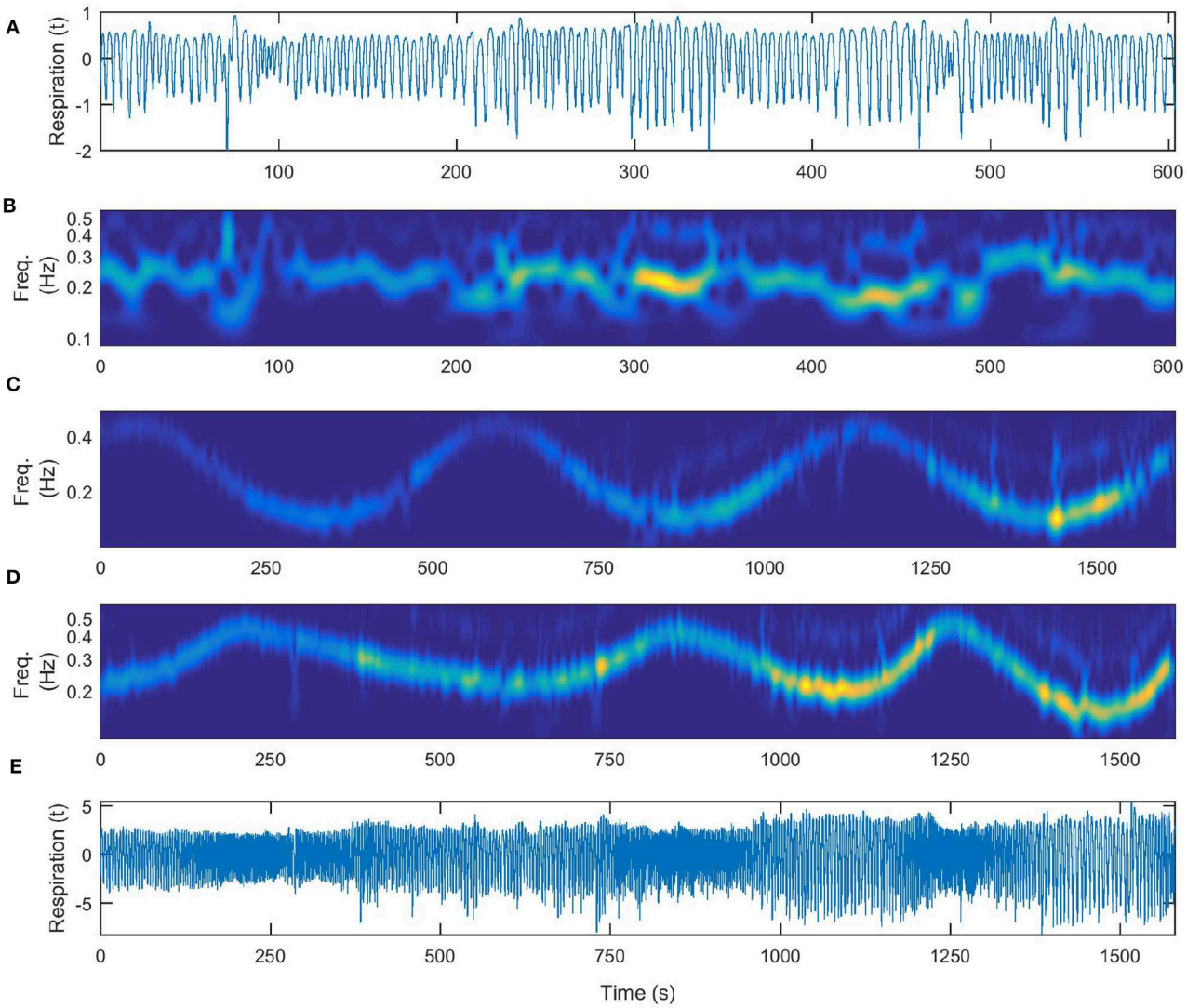

FIGURE 5 | Time-varying nature of the respiration measurements. **(A)** Respiratory signal recorded during free breathing. **(B)** Wavelet transform of the free breathing respiration. **(C)** Wavelet transform of time-varying respiration following a simple sine law (for comparison the same as depicted in **Figure 4B**). **(D)** Wavelet transform of time-varying respiration following an a-periodic behavior, **(E)** the same recorded signal of time-varying respiration following an a-periodic behavior.

according to sine law. In **Figure 6A** we give the wavelet transform of the respiration for comparison. In **Figure 6B** the time-variation of the coupling strength from the first oscillator (the respiratory system) to the second one (cardiac system) is presented. We can see here that the coupling strength has a minimum where the frequency of respiration is maximal and a maximum where the frequency of the respiration is minimal, i.e., the time-variability of the coupling strength resembles an inverse of the sine wave respiration. This confirms known results that the cardiorespiratory coupling strength is higher on slower breathing (Stankovski et al., 2012, 2013). In **Figure 6C** we present the time-variation of the index for similarity of form of coupling functions, which again follows the inverse of the sine wave respiration. This demonstrates that the form of the coupling function, and thus the underlaying cardiorespiratory mechanism, is time-varying and is following the deterministic perturbation we induced on the respiration. Again the higher similarity is associated with lower respiration frequencies and slower breathing. In **Figure 6D** we give the coupling functions at specific time points that correspond to maximal and minimal frequencies of respiration. Here we can also follow the time evolution of the coupling function close to the minimal frequency of respiration. The qualitative 3D representation of the coupling functions in **Figure 6D** shows visually consistent values of the coupling strength amplitude and similarity of the form of the functions as compared to the quantitative values presented in **Figures 6B,C**.

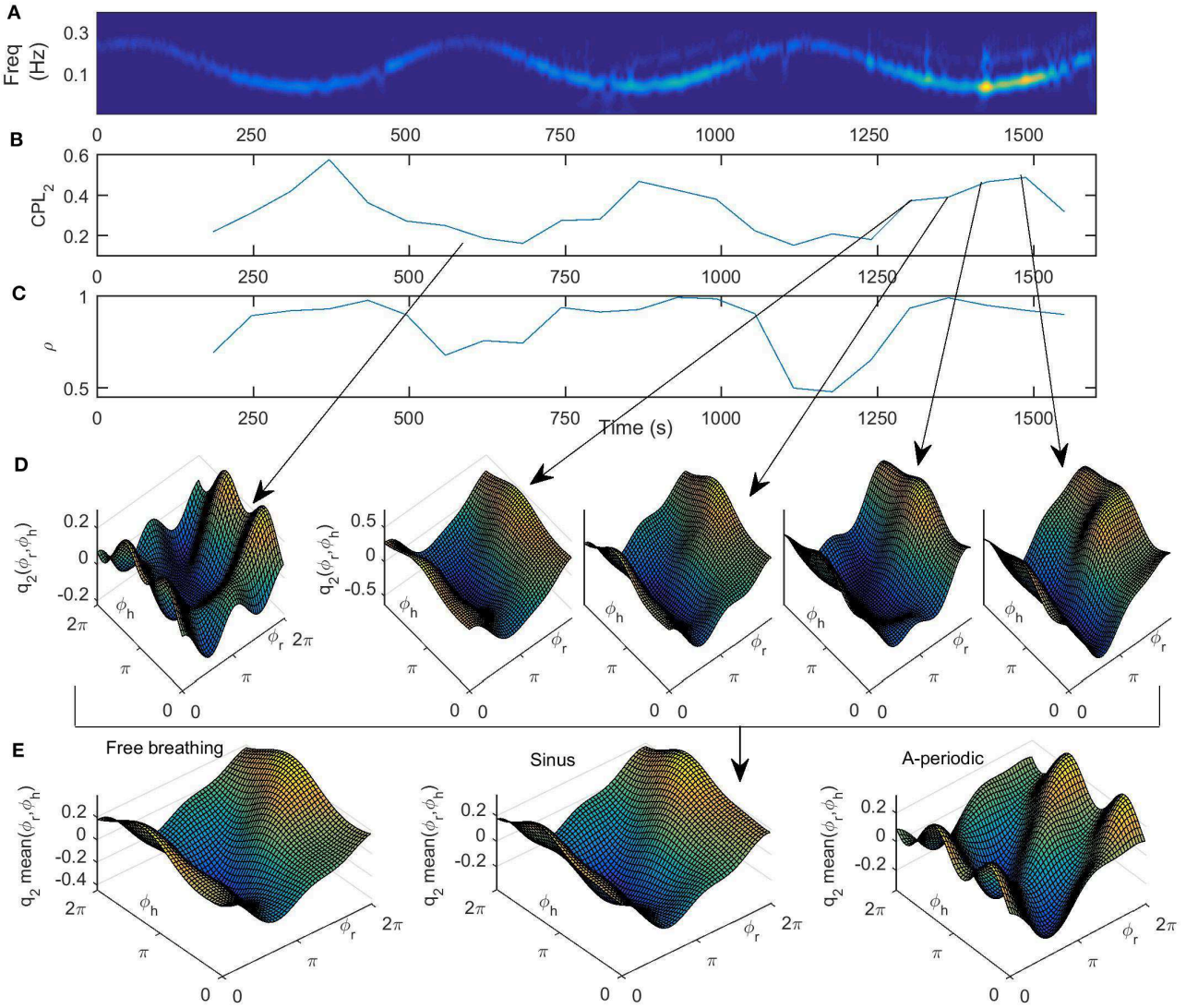

FIGURE 6 | (A) Wavelet transform of time-varying respiration following a simple sine law, **(B)** the time variation of the coupling strength $CPL_2(t)$ from the first oscillator (the respiratory system) to the second one (cardiac system), **(C)** time variation of similarity of form of coupling functions $\rho(t)$, **(D)** coupling functions $q_2(\phi_r, \phi_h)$ at specific time points, indicated by the gray arrows, that correspond to maximal and minimal frequency of respiration, and **(E)** the mean, i.e., time-averaged coupling functions for all three breathing patterns under investigation.

Finally, in **Figure 6E** we present the form of the time-averaged coupling function for all three breathing patterns under investigation. By comparison, we see that the form of the three functions is qualitatively similar, with larger deviations for the a-periodic breathing in comparison to the free and sine breathing. From **Figure 6** we can see that the reconstructed cardiorespiratory coupling functions are described by complex functions whose form changes quantitatively over time and with the change of frequency of respiration. This implies that the interactions of the cardiorespiratory system can themselves be time-varying processes. In particular, the form of the coupling function indicates that when it is high for the respiration phase between $3\pi/2$ and $\pi/2$ (**Figure 6E**), then the respiration accelerates the cardiac oscillations. Similarly, when the coupling function is low for respiration phase between $\pi/2$ and $3\pi/2$ (**Figure 6E**), then the respiration decelerates the cardiac oscillations. These inferred coupling functions describe in detail the cardiorespiratory interaction mechanism.

4. DISCUSSION AND CONCLUSION

In this study we have tackled the longstanding problem of choosing the right size of time window when analyzing dynamical time-series. We proposed new methodology for determination of the time window and the propagation parameter within the framework of the Dynamical Bayesian

Inference method. We tested the method first on the case of coupled phase oscillators and then for the case of coupled limit-cycle oscillators. We then applied the methodology on cardiorespiratory interaction for three cases of respiration—free breathing, controlled breathing following sine law and controlled breathing following an a-periodic time-variation. We obtained the coupling functions and confirmed their complex form that changes quantitatively over time.

To some extent the problem of time window determination is an ill-posed question, especially in experimental analysis, because in theory it is very hard to find a general solution. There can be very different systems, with very different types of time-variabilities acting on different parts of the systems. Nevertheless, the reality is that often there is time-variability and one needs not to ignore, but to do something about it. For this reasons, the solution we proposed is modeled and scaled to an important, albeit specific and not general, problem of cardiorespiratory interaction. In particular we took the systems to be oscillatory, hence we used the phase dynamics representation, and we assumed that the time-variation are slowly changing in respect to the oscillating frequencies. This allowed us to model a dynamic situation often encountered in the cardiorespiratory interaction. Additionally, by using second order Fourier expansion for the model base functions, we encountered limitations in inferring highly non-linear dynamics and very slow trends.

On the analysis of a predefined interacting phase oscillators we developed detailed conditions for the time window determination. These could not be determined exactly in an unknown system of coupled limit-cycle oscillators (like the example of the Poincaré oscillators in section 2.5), however, based on the phase oscillator acting as a limiting model, the analysis showed that one can find the boundaries and inequalities from which the time window can be determine in these cases. The use of the inferred covariance matrix as an indicator of the goodness of fit may become too strict and imprecise if there are large variations arising from the noise. In such case one should apply other stochastic methods in combination with this method to determine the effect of the noise and to ascertain the role of the covariance for determination of the time window. When dealing with biological open oscillatory systems, one might encounter a case where there is time-variability of the time-variability. In such case, the presented methodology may be applied recursively, for the different levels of time-variability observed.

The application to the cardiorespiratory interaction lead to some novel results, some were extended, and some results were consistent with previous findings. Namely the change of the coupling strength with slower breathing is known, and now we extended this to show that this variations appear continuously and were following the sine perturbation. A new insight is that the index for similarity of cardiorespiratory coupling functions is also higher with slower breathing and was following continuously the sine perturbation. In fact, in this analysis set up of the cardiorespiratory interaction, it was found that both the coupling strength and the similarity index were changing similarly, and in accordance with the perturbation (which is not the case in general). The inferred form of the cardiorespiratory coupling function, in the three types of breathing observed, was found to be consistent with what has been observed in previous studies. Interestingly, even though the window length determined for the three different types of breathing was quite different in length (free $t_{w,opt} = 9s$, sine $t_{w,opt} = 62s$ and a-periodic $t_{w,opt} = 15.6s$), the form of the coupling functions (**Figure 6E**) were qualitatively very similar.

During slower breathing, the form of the coupling functions changes predominantly along the respiration phase axis and is relatively constant along cardiac phase axis. The latter suggests that this coupling is predominately determined by the direct influence of respiration on the heart. This is most visible on the coupling function during low frequency parts of the breathing following sine law (**Figure 6D**) and not so visible for the aperiodic breathing which is at higher respiration frequencies. In physiology, this influence of the respiration frequency to the variability of the heart rate has been attributed to Respiratory Sinus Arrythmia (RSA) (Hirsch and Bishop, 1981), and various studies have linked the cardio-respiratory coupling with RSA (Iatsenko et al., 2013; Schulz et al., 2013; Kralemann et al., 2013a). Recent physiological studies discussed that the main function of the RSA is to improve cardiac efficiency while maintaining physiological levels of arterial CO_2 (Elstad et al., 2018). Our findings confirm these previous findings that RSA is more pronounced during slow deep breathing (Hirsch and Bishop, 1981).

Needles to say, even though this study was presented for oscillatory interactions and in particular for cardiorespiratory interaction, its implications span much widely. Some of the solutions proposed with this methodology for time window determination are relevant and can be used for other oscillatory interactions, for other methods of time-series analysis, and for other dynamical systems with time-variability, more generally.

DATA AVAILABILITY STATEMENT

The datasets generated for this study are available on request to the corresponding author.

ETHICS STATEMENT

The studies involving human participants were reviewed and approved by Ethical committee, Faculty of Medicine, Saints Cyril and Methodius, Skopje, Macedonia. The patients/participants provided their written informed consent to participate in this study.

AUTHOR CONTRIBUTIONS

DL and TS conceived and planned the research and wrote the first draft of the manuscript. DL designed the methodological procedure and completed the analysis with advice and supervision from TS, HS, and MG. All authors discussed the results and contributed to the editing of the manuscript.

FUNDING

The work was supported by the Faculty of Medicine research project TYROCARES grant MEDF1805 and by the Department of Medical Physics.

ACKNOWLEDGMENTS

We acknowledge valuable support and access to facilities from the Institute of Pathophysiology Nuclear Medicine, at Faculty of Medicine Skopje, Macedonia.

REFERENCES

Ashwin, P., Bick, C., and Poignard, C. (2019). State-dependent effective interactions in oscillator networks through coupling functions with dead zones. *arXiv* 1904.00626. doi: 10.1098/rsta.2019.0042

Bashan, A., Bartsch, R. P., Kantelhardt, J. W., Havlin, S., and Ivanov, P. C. (2012). Network physiology reveals relations between network topology and physiological function. *Nat. Commun.* 3:702. doi: 10.1038/ncomms1705

Duggento, A., Stankovski, T., McClintock, P. V. E., and Stefanovska, A. (2012). Dynamical Bayesian inference of time-evolving interactions: from a pair of coupled oscillators to networks of oscillators. *Phys. Rev. E* 86:061126. doi: 10.1103/PhysRevE.86.061126

Elstad, M., O'Callaghan, E. L., Smith, A. J., Ben-Tal, A., and Ramchandra, R. (2018). Cardiorespiratory interactions in humans and animals: rhythms for life. *Am. J. Physiol. Heart Circ. Physiol.* 315, H6–H17. doi: 10.1152/ajpheart.00701.2017

Glass, L. (2001). Synchronization and rhythmic processes in physiology. *Nature* 410, 277–284. doi: 10.1038/35065745

Grote, V., Levnajic, Z., Puff, H., Ohland, T., Goswami, N., Frühwirth, M., et al. (2019). Dynamics of vagal activity due to surgery and subsequent rehabilitation. *Front. Neurosci.* 13:1116. doi: 10.3389/fnins.2019.01116

Hagos, Z., Stankovski, T., Newman, J., Pereira, T., McClintock, P. V., and Stefanovska, A. (2019). Synchronization transitions caused by time-varying coupling functions. *Philos. Trans. R. Soc. A* 377:20190275. doi: 10.1098/rsta.2019.0275

Haken, H. (1983). *Synergetics, An Introduction*. Berlin: Springer.

Hirsch, J. A., and Bishop, B. (1981). Respiratory sinus arrhythmia in humans—how breathing pattern modulates heart rate. *Am. J. Physiol.* 241, H620–H629. doi: 10.1152/ajpheart.1981.241.4.H620

Iatsenko, D., Bernjak, A., Stankovski, T., Shiogai, Y., Owen-Lynch, P. J., Clarkson, P. B. M., et al. (2013). Evolution of cardio-respiratory interactions with age. *Phil. Trans. R. Soc. Lond. A* 371:20110622. doi: 10.1098/rsta.2011.0622

Kiss, I. Z., Rusin, C. G., Kori, H., and Hudson, J. L. (2007). Engineering complex dynamical structures: sequential patterns and desynchronization. *Science* 316, 1886–1889. doi: 10.1126/science.1140858

Kloeden, P. E., and Rasmussen, M. (2011). *Nonautonomous Dynamical Systems*. New York, NY: AMS Mathematical Surveys and Monographs.

Kralemann, B., Cimponeriu, L., Rosenblum, M., Pikovsky, A., and Mrowka, R. (2008). Phase dynamics of coupled oscillators reconstructed from data. *Phys. Rev. E* 77:066205. doi: 10.1103/PhysRevE.77.066205

Kralemann, B., Frühwirth, M., Pikovsky, A., Rosenblum, M., Kenner, T., Schaefer, J., et al. (2013a). *In vivo* cardiac phase response curve elucidates human respiratory heart rate variability. *Nat. Commun.* 4:2418. doi: 10.1038/ncomms3418

Kralemann, B., Pikovsky, A., and Rosenblum, M. (2013b). Detecting triplet locking by triplet synchronization indices. *Phys. Rev. E* 87:052904. doi: 10.1103/PhysRevE.87.052904

Kuramoto, Y. (1984). *Chemical Oscillations, Waves, and Turbulence*. Berlin: Springer-Verlag.

Lehnertz, K., Ansmann, G., Bialonski, S., Dickten, H., Geier, C., and Porz, S. (2014). Evolving networks in the human epileptic brain. *Phys. D* 267, 7–15. doi: 10.1016/j.physd.2013.06.009

Levy, M., Stanton, B., and Koeppen, B. (2006). *Berne & Levy Principles of Physiology*. St. Louis, MO: Elsevier Mosby.

Lorenz, E. N. (1963). Deterministic non-periodic flow. *J. Atmos. Sci.* 20, 130–141.

Moon, W., and Wettlaufer, J. S. (2019). Coupling functions in climate. *Philos. Trans. R. Soc. A* 377:20190006. doi: 10.1098/rsta.2019.0006

Nakao, H. (2016). Phase reduction approach to synchronisation of nonlinear oscillators. *Contemp. Phys.* 57, 188–214. doi: 10.1080/00107514.2015.1094987

Nakao, H., Yanagita, T., and Kawamura, Y. (2014). Phase-reduction approach to synchronization of spatiotemporal rhythms in reaction-diffusion systems. *Phys. Rev. X* 4:021032. doi: 10.1103/PhysRevX.4.021032

Paluš, M., and Stefanovska, A. (2003). Direction of coupling from phases of interacting oscillators: An information-theoretic approach. *Phys. Rev. E* 67:055201. doi: 10.1103/PhysRevE.67.055201

Peskin, C. S. (1981). *Lectures on Mathematical Aspects of Physiology, Vol. 19*. Providence, RI: American Mathematical Society, 1–107.

Pikovsky, A., Rosenblum, M., and Kurths, J. (2001). *Synchronization—A Universal Concept in Nonlinear Sciences*. Cambridge: Cambridge University Press.

Ranganathan, S., Spaiser, V., Mann, R. P., and Sumpter, D. J. T. (2014). Bayesian dynamical systems modelling in the social sciences. *PLoS ONE* 9:e86468. doi: 10.1371/journal.pone.0086468

Rosenblum, M., Frühwirth, M., Moser, M., and Pikovsky, A. (2019). Dynamical disentanglement in an analysis of oscillatory systems: an application to respiratory sinus arrhythmia. *Philos. Trans. R. Soc. A* 377:20190045. doi: 10.1098/rsta.2019.0045

Rosenblum, M. G., Cimponeriu, L., Bezerianos, A., Patzak, A., and Mrowka, R. (2002). Identification of coupling direction: application to cardiorespiratory interaction. *Phys. Rev. E.* 65:041909. doi: 10.1103/PhysRevE.65.041909

Schäfer, C., Rosenblum, M. G., Kurths, J., and Abel, H. H. (1998). Heartbeat synchronised with ventilation. *Nature* 392, 239–240. doi: 10.1038/32567

Schulz, S., Adochiei, F.-C., Edu, I.-R., Schroeder, R., Costin, H., Bär, K.-J., et al. (2013). Cardiovascular and cardiorespiratory coupling analyses: a review. *Philos. Trans. R. Soc. Math. Phys. Eng. Sci.* 371:20120191. doi: 10.1098/rsta.2012.0191

Schulz, S., Haueisen, J., Bär, K.-J., and Voss, A. (2018). Multivariate assessment of the central-cardiorespiratory network structure in neuropathological disease. *Physiol. Meas.* 39:074004. doi: 10.1088/1361-6579/aace9b

Shiogai, Y., Stefanovska, A., and McClintock, P. V. E. (2010). Nonlinear dynamics of cardiovascular ageing. *Phys. Rep.* 488, 51–110. doi: 10.1016/j.physrep.2009.12.003

Smelyanskiy, V. N., Luchinsky, D. G., Stefanovska, A., and McClintock, P. V. E. (2005). Inference of a nonlinear stochastic model of the cardiorespiratory interaction. *Phys. Rev. Lett.* 94:098101. doi: 10.1103/PhysRevLett.94.098101

Stankovski, T. (2013). *Tackling the Inverse Problem for Non-Autonomous Systems: Application to the Life Sciences*. Berlin: Springer.

Stankovski, T. (2017). Time-varying coupling functions: dynamical inference and cause of synchronization transitions. *Phys. Rev. E* 95:022206. doi: 10.1103/PhysRevE.95.022206

Stankovski, T., Cooke, W. H., Rudas, L., Stefanovska, A., and Eckberg, D. L. (2013). Time-frequency methods and voluntary ramped-frequency breathing: a powerful combination for exploration of human neurophysiological mechanisms. *J. Appl. Physiol.* 115, 1806–1821. doi: 10.1152/japplphysiol.00802.2013

Stankovski, T., Duggento, A., McClintock, P. V. E., and Stefanovska, A. (2012). Inference of time-evolving coupled dynamical systems in the presence of noise. *Phys. Rev. Lett.* 109:024101. doi: 10.1103/PhysRevLett.109.024101

Stankovski, T., Duggento, A., McClintock, P. V. E., and Stefanovska, A. (2014a). A tutorial on time-evolving dynamical Bayesian inference. *Eur. Phys. J. Spec. Top.* 223, 2685–2703. doi: 10.1140/epjst/e2014-02286-7

Stankovski, T., McClintock, P. V. E., and Stefanovska, A. (2014b). Coupling functions enable secure communications. *Phys. Rev. X* 4:011026. doi: 10.1103/PhysRevX.4.011026

Stankovski, T., Pereira, T., McClintock, P. V. E., and Stefanovska, A. (2017). Coupling functions: universal insights into dynamical interaction mechanisms. *Rev. Mod. Phys.* 89:045001. doi: 10.1103/RevModPhys.89.045001

Stankovski, T., Petkoski, S., Raeder, J., Smith, A. F., McClintock, P. V. E., and Stefanovska, A. (2016). Alterations in the coupling functions between cortical and cardio-respiratory oscillations due to anaesthesia with propofol and sevoflurane. *Phil. Trans. R. Soc. A* 374:20150186. doi: 10.1098/rsta.2015.0186

Stefanovska, A., Haken, H., McClintock, P. V. E., Hožič, M., Bajrović, F., and Ribarič, S. (2000). Reversible transitions between synchronization states of the cardiorespiratory system. *Phys. Rev. Lett.* 85, 4831–4834. doi: 10.1103/PhysRevLett.85.4831

Strogatz, S. (2001). *Nonlinear Dynamics And Chaos*. Boulder, CO: Westview Press.

Suprunenko, Y. F., Clemson, P. T., and Stefanovska, A. (2013). Chronotaxic systems: a new class of self-sustained nonautonomous oscillators. *Phys. Rev. Lett.* 111:024101. doi: 10.1103/PhysRevLett.111.024101

Ticcinelli, V., Stankovski, T., Iatsenko, D., Bernjak, A., Bradbury, A., Gallagher, A., et al. (2017). Coherence and coupling functions reveal microvascular impairment in treated hypertension. *Front. Physiol.* 8:749. doi: 10.3389/fphys.2017.00749

Voss, A., Schulz, S., Schroeder, R., Baumert, M., and Caminal, P. (2008). Methods derived from nonlinear dynamics for analysing heart rate variability. *Philos. Trans. R. Soc. A Math. Phys. Eng. Sci.* 367, 277–296. doi: 10.1098/rsta.2008.0232

Winfree, A. T. (1980). *The Geometry of Biological Time*. New York, NY: Springer-Verlag.

Conflict of Interest: The authors declare that the research was conducted in the absence of any commercial or financial relationships that could be construed as a potential conflict of interest.

frontiers in Neuroscience

ORIGINAL RESEARCH
published: 16 June 2020
doi: 10.3389/fnins.2020.00617

The Cardiorespiratory Network in Healthy First-Degree Relatives of Schizophrenic Patients

*Steffen Schulz[1], Jens Haueisen[2], Karl-Jürgen Bär[3] and Andreas Voss[1]**

[1] Institute of Innovative Health Technologies (IGHT), University of Applied Sciences, Jena, Germany, [2] Institute of Biomedical Engineering and Informatics, Ilmenau University of Technology, Ilmenau, Germany, [3] Department of Psychosomatic Medicine and Psychotherapy, Jena University Hospital, Jena, Germany

Impaired heart rate- and respiratory regulatory processes as a sign of an autonomic dysfunction seems to be obviously present in patients suffering from schizophrenia. Since the linear and non-linear couplings within the cardiorespiratory system with respiration as an important homeostatic control mechanism are only partially investigated so far for those subjects, we aimed to characterize instantaneous cardiorespiratory couplings by quantifying the casual interaction between heart rate (HR) and respiration (RESP). Therefore, we investigated causal linear and non-linear cardiorespiratory couplings of 23 patients suffering from schizophrenia (SZO), 20 healthy first-degree relatives (REL) and 23 healthy subjects, who were age-gender matched (CON). From all participants' heart rate (HR) and respirations (respiratory frequency, RESP) were investigated for 30 min under resting conditions. The results revealed highly significant increased HR, reduced HR variability, increased respiration rates and impaired cardiorespiratory couplings in SZO in comparison to CON. SZO were revealed bidirectional couplings, with respiration as the driver (RESP → HR), and with weaker linear and non-linear coupling strengths when RESP influencing HR (RESP → HR) and with stronger linear and non-linear coupling strengths when HR influencing RESP (HR → RESP). For REL we found only significant increased HR and only slightly reduced cardiorespiratory couplings compared to CON. These findings clearly pointing to an underlying disease-inherent genetic component of the cardiac system for SZO and REL, and those respiratory alterations are only clearly present in SZO seem to be connected to their mental emotional states.

Keywords: cardiorespiratory coupling, Network Physiology, partial directed coherence, transfer entropy, schizophrenia, relatives

OPEN ACCESS

Edited by:
Vitor Engracia Valenti,
São Paulo State University, Brazil

Reviewed by:
Carolina Varon,
Delft University of Technology, Netherlands
Tomislav Stankovski,
Ss. Cyril and Methodius University in Skopje, North Macedonia
Ahsan H. Khandoker,
Khalifa University, United Arab Emirates

****Correspondence:***
Andreas Voss
andreas.voss@eah-jena.de

Specialty section:
This article was submitted to Autonomic Neuroscience, a section of the journal Frontiers in Neuroscience

Received: *19 December 2019*
Accepted: *19 May 2020*
Published: *16 June 2020*

Citation:
Schulz S, Haueisen J, Bär K-J and Voss A (2020) The Cardiorespiratory Network in Healthy First-Degree Relatives of Schizophrenic Patients. Front. Neurosci. 14:617. doi: 10.3389/fnins.2020.00617

INTRODUCTION

Schizophrenia represents a mental disorder along with increased cardiovascular mortality rate, shorter life expectancy, higher risk of developing cardiovascular disease (CVD) in proportion to the general population (Hennekens et al., 2005; McGrath et al., 2008; Laursen et al., 2014). One reason in schizophrenia, besides others (Straus et al., 2004; Hennekens et al., 2005; Ringen et al., 2014), seems to be an unbalanced autonomic nervous system (ANS) during the acute psychosis state quantified by analyses heart rate variability (HRV) and respiratory variability (RESPV).

Different studies suggested as a major contributing factor the unbalanced sympathovagal balance for schizophrenic patients, as well as for their healthy first-degree relatives (Valkonen-Korhonen et al., 2003; Bär et al., 2005, 2007; Chang et al., 2009; Schulz et al., 2013c). However, investigations of respiration and cardiorespiratory couplings is becoming more of interest in medicine and research (Peupelmann et al., 2009; Bär et al., 2012; Schulz et al., 2012a,b, 2013b, 2014, 2018) for schizophrenia since respiration plays a major part homeostatic regulatory control processes. As far as we know there exist only a few investigations dealing with causal couplings quantifying the coupling strengths and coupling directions in these patients. The field of Network Physiology aiming to identify and quantify the dynamics within the (patho)physiological network with their different sub-networks and their interactions between them (Bashan et al., 2012) but seems to be a promising multivariate concept to describe the cardiorespiratory system. Moreover, Network Physiology quantifies healthy and diseased states investigating the coupling between systems and sub-systems by determining structural, dynamical and regulatory changes. These new concepts allow getting a better understanding of the complexity of physiological as well as pathophysiological processes in health and disease by linking genetic and subcellular levels with intercellular coupling pathways between integrated systems and subsystems (Ivanov et al., 2016).

Studies investigating HRV generally showed an altered sympathovagal balance pointing to dysregulation of heart rate for schizophrenic patients and partially their first-degree healthy relatives (Toichi et al., 1999; Valkonen-Korhonen et al., 2003; Bär et al., 2005, 2007, 2010; Castro et al., 2009; Chang et al., 2009; Voss et al., 2010). The pattern of an unbalanced ANS (heart rate) in schizophrenic patients and their relatives seem to hallmark a disease-inherent genetic feature of this disease. Busjahn et al. (1998) highlighted that there exist a genetic dependency of HRV indices. Studies analyzing respiration and cardiorespiratory couplings in schizophrenia are exclusive (Peupelmann et al., 2009; Bär et al., 2012; Schulz et al., 2012a,b, 2013b, 2015b, 2018) and demonstrated significantly altered dynamic and variability of respiration as well as impaired cardiorespiratory couplings for schizophrenic patients but not for their healthy first-degree relatives. Respiration is regulated in the brain stem primarily for metabolic and homeostatic purposes, it also constantly reacts to changes in emotions (Homma and Masaoka, 2008). It seems that the altered psychotic states of schizophrenic patients compared to healthy subjects have a great influence on their cardiorespiratory system characterized by an interplay of different linear and non-linear subsystems (Voss et al., 2009). The respiratory sinus arrhythmia (RSA) occupies an important part of cardiorespiratory couplings. RSA describes the rhythmic fluctuation of heart rate in proportion to respiration. Under normal physiological conditions RSA characterizes changes between inspiratory heart rate acceleration and expiratory heart rate deceleration (Eckberg, 2003). Studies have actually shown that the coupling between cardiovascular system and respiration is strongly non-linear (Novak et al., 1993). For the analysis of the cardiorespiratory system as a complex physiological regulatory network, a variety of methods have been proposed (Schulz et al., 2013a; Bartsch et al., 2015; Faes et al., 2015; Liu et al., 2015; Ivanov et al., 2016) basing on Granger causality, phase synchronization, entropies, non-linear prediction, symbolization, and time delay stability (TDS) (Schulz et al., 2018).

Investigating the coupling between heart rate and respiration could provide potential clinically insights into (patho)physiological autonomic processes in schizophrenia and their relatives. In contrast to our preliminary work in this field, we have applied a pool of different coupling methods from the time and frequency domain that can quantify both linear and non-linear causal couplings. This will allow us to gain more insight into the regulatory processes of the cardiorespiratory system, which will provide a better understanding of how individual systems interact with each other in a healthy and explored state. This study aimed to quantify instantaneous cardiorespiratory couplings in schizophrenic patients and their healthy first-degree relatives. Therefore, multivariate linear and non-linear causal coupling approaches [normalized short time partial directed coherence, multivariate transfer entropy, cross conditional entropy, and respiratory sinus arrhythmia (peak-to-valley)] were applied determining causal coupling strengths and directions. We speculate that these new findings are important for a full understanding of (patho)physiological regulatory processes and possibly may help to improve treatment strategies in schizophrenia and identify those patients at increased risk for cardiovascular disease accompanied by ANS dysfunction.

MATERIALS AND METHODS

Subjects

Twenty-three untreated patients suffering from paranoid schizophrenia (SZO), 20 healthy first-degree relatives (REL) and 23 healthy controls subjects (CON) (age–gender matched) (**Table 1**) were enrolled in this pilot study. Patients were included only when they had not taken any medication for at least 8 weeks. From all participants the serum drug levels were checked for legal drugs (e.g., antipsychotics, antidepressants, and benzodiazepines) and illegal drugs (e.g., cannabis). In accordance with the inclusion criteria, only subjects with negative results were included in the

TABLE 1 | Clinical and demographic data of the study population.

Data	Healthy controls subjects (CON)	Healthy first-degree relatives (REL)	Schizophrenic patients (SZO)
Number of participants	23	20	23
Gender (male/female)	13/10	12/8	12/11
Age (mean ± std in years)	30.3 ± 9.5	31.7 ± 10.7	30.4 ± 10.3
PANSS, mean (min-max)	n.a.	n.a.	85.7 (43–124)
SANS, mean (min-max)	n.a.	n.a.	49.6 (14–81)
SAPS, mean (min-max)	n.a.	n.a.	60.9 (6–108)

Psychotic symptoms for acute schizophrenia were quantified using the Scale for the Assessment of Positive Symptoms (SAPS) and negative symptoms (SANS) and positive and negative syndrome scales (PANSS); n.a., not applicable.

study. Paranoid schizophrenia was diagnosed when patients fulfilled DSM-IV criteria [Diagnostic and statistical manual of mental disorders, 4th edition. Psychotic symptoms (positive and negative) were quantified using the Positive and Negative Syndrome Scale (PANSS (Kay et al., 1987)]. The semi-structured clinical interview SCID-1 was used for patients to approve the clinical diagnosis. Control subjects were recruited from hospital staff, medical students and the local community. From all healthy control subjects and relatives interview and clinical investigation were performed to rule out any psychiatric or other disease or disruptive medication. Additionally for all controls the Structured Clinical Interview SCID II and a personality inventory (Freiburger Persönlichkeitsinventar) were applied to detect personality traits or disorders that could affect autonomic function (LeBlanc et al., 2004), and if present they were not included in this study.

The written informed consent to a protocol approved by the local ethics committee of the Jena University Hospital (ethics committee number: 1190-09/03) was provided by all participants. This study complies with the Declaration of Helsinki.

Data Recordings and Pre-processing

A short-term ECG (1,000 Hz) and synchronized calibrated respiratory inductive plethysmography signal (Bär et al., 2012) (LifeShirt®, VivoMetrics, Inc., Ventura, CA, United States) were recorded for 30 min under resting conditions [between 3 and 6 p.m. in a quiet room which was kept comfortably warm (22–24°C)] after 10 min rest in supine position. Subjects were asked not to talk, to relax and to breathe normally during the recording. For the further analyses from the raw data.

- Time series of successive beat-to-beat intervals (BBI, msec) and
- Time series of respiratory frequency (RESP, sec) as the time intervals between consecutive breathing cycles were automatically extracted.

These time series were afterward adaptively filtered (Wessel et al., 2000) to exclude and interpolate ventricular premature events and/or artifacts to obtain normal-to-normal beat time series (NN). Linear interpolation procedure was applied to filtered time series (BBI, RESP) for synchronization and resampling (2 Hz).

Basic Data From the Heart Rate and Respiration

Basic indices from heart rate and respiration were determined as:

- meanNN: mean value of the NN intervals of BBI (msec), and RESP (sec) as respiratory cycle length;
- sdNN: standard deviation of the NN intervals of BBI (msec), and RESP (sec);
- HR: basic heart rate as the number of heart beats per minute (1/min), and
- BF: breathing frequency as the number of breaths per minute (1/min).

Coupling Analyses

Different approaches can be used for the quantification of linear and non-linear cardiorespiratory couplings (Schulz et al., 2013a). In this study, we analyzed the coupling between BBI and RESP applying the linear normalized short-time partial directed coherence (NSTPDC) (Adochiei et al., 2013), the linear/non-linear multivariate Transfer Entropy (MuTE) (Montalto et al., 2014) and the non-linear cross conditional entropy (CCE) (Porta et al., 1999) approaches as well as the respiratory sinus arrhythmia (RSA).

Normalized Short-Time Partial Directed Coherence

NSTPDC represents an enhancement of the traditional partial directed coherence (PDC) (Baccala and Sameshima, 2001) approach assessing linear Granger causality in the frequency domain quantifying direct and indirect couplings within a set of multivariate time series. The fundamental basis of the NSTPDC is the time-variant partial directed coherence approach [tvPDC, $\pi_{xy}(f,n)$] is allowing to determine causal short-term couplings between non-stationary time series at certain frequency f applying a window function (n is the number of windows) (Milde et al., 2011). An m-dimensional autoregressive (AR) model is used to calculate NSTPDC indices. The optimal model order p_{opt} was determined by the stepwise least squares algorithm (Neumaier and Schneider, 2001) and the Schwarz's Bayesian Criterion (SBC) (Schneider and Neumaier, 2001). The coupling direction between two time series, x and y, (e.g., BBI and RESP) was determined by a coupling factor (CF) which is determined by the quotient of $\pi_{xy}(f,n)$ and $\pi_{yx}(f,n)$.

$$\mathrm{CF} = \frac{\frac{1}{n}\sum \pi_{xy}(f,n)}{\frac{1}{n}\sum \pi_{yx}(f,n)} \tag{1}$$

$$\bar{a} = \frac{1}{n}\sum \pi_{xy}(f,n)$$

$$\bar{b} = \frac{1}{n}\sum \pi_{yx}(f,n)$$

The results of CF were normalized and result in the normalized factor (NF), which characterizes the coupling direction.

$$\max(\bar{a},\bar{b})$$

$$\mathrm{NF} = \left\{ \begin{array}{c} 2,\ if\ \left(max = \bar{a}\ \&\frac{\bar{a}}{\bar{b}} > 5\right) \\ 1,\ if\ (max = \bar{a}\ \&\ 2 < \frac{\bar{a}}{\bar{b}} \le 5) \\ 0,\ if\ (max = \bar{a}\ \&\ 0 \le \frac{\bar{a}}{\bar{b}} \le 2) \end{array} \right\} \text{ and}$$

$$\mathrm{NF} = \left\{ \begin{array}{c} -2,\ if\ \left(max = \bar{b}\ \&\frac{\bar{b}}{\bar{a}} > 5\right) \\ -1,\ if\ (max = \bar{b}\ \&\ 2 < \frac{\bar{b}}{\bar{a}} \le 5) \\ 0,\ if (max = \bar{b}\ \&\ 0 \le \frac{\bar{b}}{\bar{a}} \le 2) \end{array} \right\} \tag{2}$$

Thereby, NF (NF = {−2, −1, 0, 1, 2}) determinates the causal coupling direction between the two time series (x_{BBI} and y_{RESP}) as a function of frequency f.

Coupling direction:

- NF = {−2| 2} (where −2 denotes y_{RESP} as driver, +2 denotes x_{BBI} as driver): Strong unidirectional coupling;
- NF = {−1.5– < −2} or NF = {1.5–<2}: Weak unidirectional coupling;
- NF = {−1| 1} (−1 denotes y_{RESP} as driver, +1 denotes x_{BBI} as driver): Strong bidirectional coupling;
- NF = {−0.5– < −1} or NF = {0.5–<1}: Weak bidirectional coupling, and
- NF = 0: Equal influence in both directions and/or no coupling with respect to coupling strengths (If both area indices have equal values greater than zero, there is equal influence in both directions; if both area indices have equal values but are zero, there is no coupling).

Coupling strength:

In each window (f = 0–2 Hz) an area is made up of CF allowing to assess the coupling strength. For x_{BBI} and y_{RESP} these areas are:$A_{BBI\rightarrow RESP}$ and $A_{RESP\rightarrow BBI}$ [a.u.]. The values of these area indices ranges between 0 and 1 [0,1]. Thereby, 1 points to that from x all information is transferred (→) toward y ($A_{x\rightarrow y}$ = 1). Hamming window with a length of 120 samples and a shift of 30 samples per each iteration step was applied. To ensure scale-invariance all time series were normalized to zero mean and unit variance (Schulz et al., 2015a).

Multivariate Transfer Entropy

Transfer Entropy (TE) introduced by Schreiber (Schreiber, 2000) is able to quantify linear as well as non-linear information transfer between time series, to detect driver-response-relationships, and to assess asymmetries between information transfers. TE has the big advantage that it is "model-free" approach (Schulz et al., 2013a) making TE very sensitive to any types of dynamical information transfer. Montalto et al. (2014) introduced the Multivariate Transfer Entropy (MuTE) as a MATLAB toolbox with different entropy estimators to transfer the classical TE from a bivariate approach into a multivariate approach. The coupling strength of a multivariate set of time series can be determined as:

$$\mathrm{MuTE}_{X\rightarrow Y} \tag{3}$$

with information transfer from X toward (→) Y, or vice versa. In this study we wanted to quantify non-linear couplings within the cardiorespiratory system with high specificity and sensitivity, therefore, we applied the non-uniform embedding (NN NUE) technique with the nearest neighbor estimator shown to be most suitable to detect non-linearities with high specificity and sensitivity (Montalto et al., 2014).

Cross Conditional Entropy

Porta et al. (1999) introduced the cross conditional entropy ($CE_{x/y}$) based on the conditional entropy (CE). Thereby, $CE_{x/y}$ determines the level of coupling between the two time series x and y,

$$CE_{x|y} = -\sum_{L-1} p\left(y_{L-1}\right) \sum_{t|L-1} p\left(\frac{x\left(t\right)}{y_{L-1}}\right) \log p(x(t)/y_{L-1}) \tag{4}$$

with the pattern length L, the joint probability $p(y_{L-1})$ of the pattern $y_{L-1}(t)$ and the conditional probability $p(x(t)/y_{L-1})$ of the sample $x(t)$, given that the pattern y_{L-1}. $CE_{x/y}$ assesses the amount of information contained in the sample $x(t)$ in the case that the pattern of $L-1$ samples of $y_{L-1}(t)$ is existing. Moreover, $CE_{x/y}$ quantifies causality by determining direct couplings regarding to cross-prediction approaches.

Finally, an uncoupling function $\overline{UF}$ can be estimated that determines the information content that is transferred between two time series (Porta et al., 1999). Here, we calculated the $\overline{UF}_{x,y}$ between HR and BF as $\overline{UF}_{HR,BF}$. The larger $\overline{UF}$, the more decoupled the two time series are ($\overline{UF} = 1$, HR und BF are completely independent from each other).

Respiratory Sinus Arrhythmia

Respiratory Sinus Arrhythmia (RSA) is used as an index of cardiac parasympathetic activity derived by heart rate changes (BBI) which correspond to inspiration and expiration (Grossman et al., 1990a). RSA is characterized by the shortening of heart rate intervals (BBI) during inspiration and the lengthening of heart rate intervals during expiration. In this study, we assess RSA in the time domain applying the peak-to-valley approach (RSA_{P2V}, msec). The LifeShirt® automatically estimated RSA using the peak-to-valley approach for each breathing cycle (Grossman et al., 1990b).

Surrogate Data

To evaluate the significance of the cardiorespiratory couplings between CON and SZO as well as REL a surrogate data approach was applied (Schreiber and Schmitz, 2000). Here, from all original time series 20 independent surrogates were derived for each schizophrenic patient (SZOs), each relative (RELs), and each healthy control (CONs). The temporal structure within the original time series was destroyed by randomly permuting each sample to derived new surrogate time series. Afterward, we tested if significant couplings between the original time series were confirmed by the surrogate data. Therefore, a statistical defined coupling threshold level t_s (defined as the mean + 2*SD of the resultant distribution derived from all surrogates SZOs, RELs, and CONs) was introduced. Significant valid couplings were present if no significant differences between two surrogate groups exist and if couplings (original data) were higher than t_{su}.

In addition, a second surrogate approach was applied by generating random phase surrogates to test for non-linearity in the data. This surrogate approach is known as phase randomization and preserves linear behavior (i.e., the power spectrum/autocorrelation) but destroys any non-linear behavior. Preserving the power spectrum while randomizing the Fourier phases of the data providing surrogates in which any non-linear structure is destroyed (Lancaster et al., 2018).

Statistics

For the statistical evaluation of the results between SZO, REL and CON first the Kruskal–Wallis test followed by the *post hoc* non-parametric exact two-tailed Mann–Whitney U-test in combination with the Kolmogorov–Smirnov test (check for equal distributions) (SPPS 21.0) were applied. The significance

level was set to $p < 0.01$, and for highly significant different to $p < 0.004$ (Bonferroni–Holm adjustment). In order to check, if effects size have a relevant influence, effect sizes based on Cohen's d were applied to describe the magnitude of the differences between the groups. The most popular effect size measure is Cohen's d (Cohen, 1988).

Results were expressed in median and 25 and 75% percentiles.

RESULTS

The Kruskal–Wallis test revealed for all indices, with the exception of $sdNN_{\_RESP}$, significant differences ($p < 0.01$) between all three groups.

Patients Suffering From Schizophrenia vs. Healthy Subjects

Basic data from HR analysis revealed highly significant differences between SZO and CON. SZO showed shortened mean value of the NN intervals ($meanNN_{\_BBI}$) and reduced variability ($sdNN_{\_BBI}$) and higher HR (**Table 2**).

Variability analyses of RESP showed a reduced (significant) mean respiratory cycle length ($meanNN_{\_RESP}$) and consequently an increased breathing frequency (BF) in SZO compared to CON (**Table 2**).

Cardiorespiratory analysis revealed significant differences between the couplings in SZO than CON (**Table 2**).

NSTPDC analyses revealed a highly significant NF (CON: NF = -1.9 ± 0.2; SZO: NF = -1.0 ± 0.8) between SZO and CON. For CON, the NF was approximately -2, suggesting a strong unidirectional information transfer from RESP → BBI. For SZO the NF was approximately -1 pointing to a strong bidirectional information transfer with RESP as the driver (RESP → BBI). The coupling strengths were significantly different for both area indices ($A_{\mathrm{BBI} \rightarrow \mathrm{RESP}}$, $A_{\mathrm{RESP} \rightarrow \mathrm{BBI}}$) between both groups. In the case that BBI influenced RESP ($A_{\mathrm{BBI} \rightarrow \mathrm{RESP}}$), SZO demonstrated a higher coupling strength in comparison to CON. In the case that RESP influenced BBI ($A_{\mathrm{RESP} \rightarrow \mathrm{BBI}}$) we found a lower coupling strength for SZO compared to CON (**Figures 1**, **2**).

MuTE showed similar results as NSTPDC, but with non-linear components, that in the case that BBI influenced RESP ($\mathrm{MuTE}_{\mathrm{BBI} \rightarrow \mathrm{RESP}}$) higher coupling strength with non-linear components was present for SZO, and in the case that RESP influenced BBI ($\mathrm{MuTE}_{\mathrm{RESP} \rightarrow \mathrm{BBI}}$) lower coupling strength with non-linear components was found for SZO in comparison to CON.

The uncoupling function quantifying the information transfer between HR and BF revealed an increased value for SZO in comparison to CON, pointing to stronger decoupling of the cardiac and respiratory system in SZO.

Highly significantly lower RSA values ($\mathrm{RSA}_{\mathrm{P2V}}$) were found for SZO in compassion to CON.

All significant couplings were confirmed by surrogate analysis. No significant differences in linear and non-linear coupling indices were found between the groups for surrogate time series.

The results from phase randomization surrogate analysis revealed highly significant differences in all three NSTPDC

TABLE 2 | Results of heart rate- and respiratory variability and cardiorespiratory coupling analyses to differentiate between patients suffering from paranoid schizophrenia (SZO), healthy first-degree relatives (REL), and healthy control subjects (CON).

	Index	CON vs. SZO	Cohen's *d*	CON vs. REL	Cohen's *d*	SZO vs. REL	Cohen's *d*	CON			REL			SZO		
								Median	[25–75]		Median	[25–75]		Median	[25–75]	
Cardiac	HR	***	†††	***	†††	n.s	†††	62.4	56.7	70.8	72.8	69.8	80.0	80.9	71.5	88.6
	$meanNN_{\_BBI}$	***	†††	***	†††	n.s	†††	962.1	847.9	1058.2	824.2	750.2	859.2	741.4	677.4	839.1
	$sdNN_{\_BBI}$	***	†††	n.s	†††	n.s	††	66.2	49.4	75.3	47.5	35.1	55.1	43.7	27.9	57.4
Respiratoy	BF	***	†††	n.s	†††	n.s	†††	14.9	13.2	16.8	16.0	14.2	18.7	20.3	15.5	23.2
	$meanNN_{\_RESP}$	***	†††	n.s	††	n.s	†††	4.0	3.6	4.5	3.8	3.2	4.2	2.9	2.6	3.9
	$sdNN_{\_RESP}$	n.s	–	n.s	–	n.s	–	0.78	0.56	1.23	0.49	0.42	0.87	0.70	0.38	1.27
Couplings	NF	***	†††	n.s	†††	***	†††	−1.9	−2.0	−1.9	−1.8	−1.9	−1.6	−1.3	−1.7	−0.8
	$A_{\mathrm{BBI} \rightarrow \mathrm{RESP}}$	***	†††	n.s	†††	n.s	†††	0.04	0.03	0.06	0.06	0.04	0.08	0.07	0.06	0.10
	$A_{\mathrm{RESP} \rightarrow \mathrm{BBI}}$	***	†††	n.s	††	***	†††	0.46	0.35	0.53	0.39	0.33	0.46	0.27	0.19	0.35
	$\mathrm{MuTE}_{\mathrm{BBI} \rightarrow \mathrm{RESP}}$	**	†††	n.s	††	n.s	††	0.000	0.000	0.011	0.005	0.000	0.015	0.012	0.000	0.018
	$\mathrm{MuTE}_{\mathrm{RESP} \rightarrow \mathrm{BBI}}$	***	†††	n.s	††	n.s	†††	0.047	0.033	0.061	0.043	0.011	0.049	0.011	0.000	0.026
	$\overline{\mathrm{U}}\,\tilde{\mathrm{F}}_{X,Y}$	***	†††	n.s	†	***	†††	0.10	0.08	0.13	0.09	0.07	0.14	0.14	0.11	0.19
	$\mathrm{RSA}_{\mathrm{P2V}}$	***	†††	**	††	**	†††	123.0	58.8	201.9	58.9	31.6	98.3	30.8	14.8	51.4

*BBI, beat-to-beat intervals; RESP, time intervals between consecutive breathing cycles; HR, heart rate; BF, breathing frequency; A, area from NSTPDC for identifying the coupling strength; MuTE, multivariate Transfer Entropy; $\overline{\mathrm{U}}\tilde{\mathrm{F}}_{HR,BF}$, RSA, respiratory sinus arrhythmia; $_{P2V}$, peak-to-valley; p, univariate significance level: **<0.01, ***<0.004; n.s., not significant; Cohen's d: †0.1—0.3: small effect, ††0.3—0.5: medium effect, †††0.5 and higher: strong effect).*

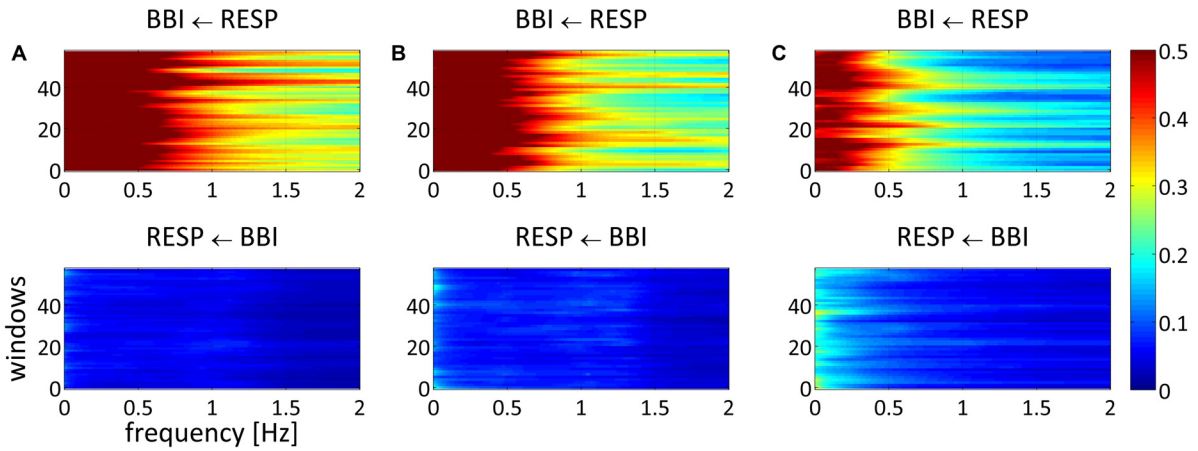

FIGURE 1 | Averaged NSTPDC plots for cardiorespiratory coupling analyses for **(A)** healthy subjects, **(B)** healthy first-degree relatives, and **(C)** schizophrenic patients. Arrows indicating the causal coupling direction from one time series to another, e.g., RESP ← BBI, indicating the causal information transfer from BBI to RESP. Coupling strength ranges from blue (no coupling) to red (maximum coupling). BBI, beat-to-beat intervals; RESP, time intervals between consecutive breathing cycles.

indices whereas MuTE only showed significant $\mathrm{MuTE}_{\mathrm{BBI} \rightarrow \mathrm{RESP}}$ (**Table 3**) comparing CON with SZO.

Healthy First-Degree Relatives of Schizophrenic Patients vs. Healthy Subjects

Indices from cardiac variability demonstrated only a significant increased HR in REL compared to CON and consequently shortened mean value of the NN intervals ($\mathrm{meanNN}_{\_BBI}$).

Respiratory variability analyses did not demonstrate significant differences between REL and CON.

Results for cardiorespiratory couplings showed only significant different for RSA analyses with decreased RSA values ($\mathrm{RSA}_{\mathrm{P2V}}$) for REL compared to CON (**Table 2** and **Figure 2**).

All significant couplings were confirmed by surrogate analysis. No significant differences in linear and non-linear coupling indices were found between the groups for surrogate time series.

Phase randomization surrogate analysis showed significance for $A_{\mathrm{BBI} \rightarrow \mathrm{RESP}}$ comparing CON and REL (**Table 3**).

Patients Suffering From Schizophrenia vs. Their Healthy First-Degree Relatives

Basic indices from HR and respiration did not contribute to a differentiation of these groups.

Results for cardiorespiratory couplings revealed highly significant differences for NSTPDC, CCE, and RSA analyses.

NSTPDC results demonstrated a highly significant NF value and $A_{\mathrm{RESP} \rightarrow \mathrm{BBI}}$ value between REL and SZO. Thereby, REL showed −1.7 indicating to a weak unidirectional coupling with RESP as the driver and BBI as the target variable. The coupling strength ($A_{\mathrm{RESP} \rightarrow \mathit{BBI}}$) was highly significant increased in REL compared to SZO (**Figures 1**, **2**).

The uncoupling function revealed highly significant decreased value for REL in comparison to SZO, pointing to weaker decoupling (=stronger coupling) between the cardiac and respiratory system in comparison to SZO.

Significant higher RSA values ($\mathrm{RSA}_{\mathrm{P2V}}$) for REL were found for REL compared to SZO (**Table 2** and **Figure 2**).

All significant couplings were confirmed by surrogate analysis. No significant differences in linear and non-linear coupling indices were found between the groups for surrogate time series.

Phase randomization surrogate analysis for NSTPDC demonstrated a highly significant NF value and $A_{\mathrm{RESP} \rightarrow \mathrm{BBI}}$ value between REL and SZO (**Table 3**).

DISCUSSION AND CONCLUSION

In our study, we found highly significant increased HR, reduced HRV, higher BF, and impaired cardiorespiratory couplings for schizophrenic patients compared to healthy control subjects. For SZO these couplings were characterized as bidirectional ones, with a driver-responder relationship from RESP → BBI, with weaker linear and non-linear coupling strengths when respiration influencing heart rate and with stronger linear and non-linear coupling strengths when HR influencing respiration. For the healthy first-degree relatives we found only significant increased HR and impaired RSA compared to healthy subjects (**Figures 2**, **3**).

The variability analyses of basic heart rate indices are consistent with different studies that have shown an impaired sympathovagal tone in untreated schizophrenic patients (Mujica-Parodi et al., 2005; Boettger et al., 2006; Bär et al., 2007; Chang et al., 2010; Schulz et al., 2013c, 2015a). These results suggest an impairment of the ANS shown by a reduced HRV ($\mathrm{sdNN}_{\_BBI}\downarrow$, $\mathrm{meanNN}_{\_BBI}\downarrow$) expressed by a higher sympathovagal activation of the ANS. Furthermore, a predominant sympathetic activation for SZO (2.94 ± 2.28) was additionally confirmed by significantly increased LF/HF compared to CON (1.74 ± 1.57) and to REL (1.78 ± 1.15). Impaired cardiac regulation, which is one

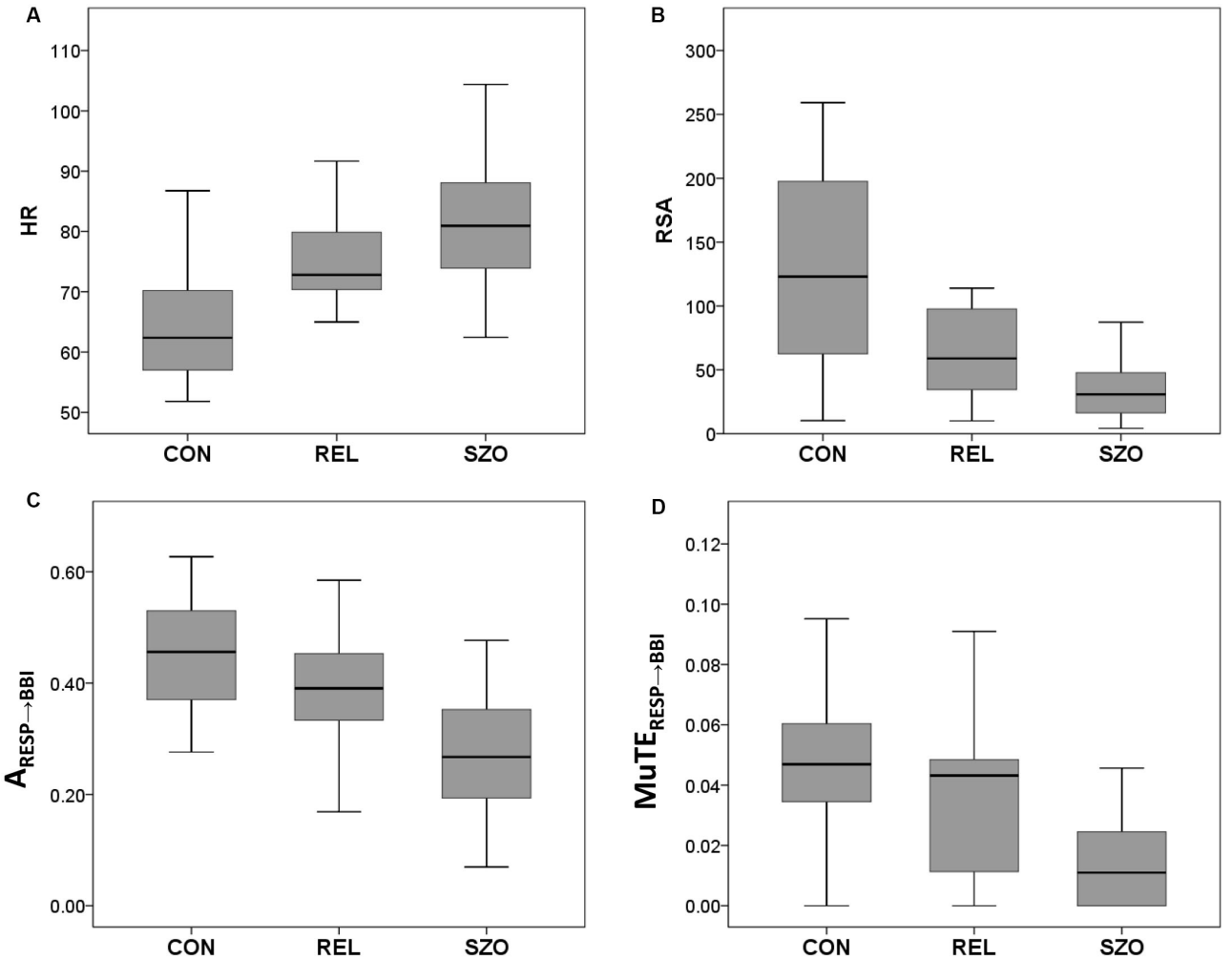

FIGURE 2 | Box plots of significant cardiorespiratory indices from healthy subjects (CON), healthy first-degree relatives (REL), and schizophrenic patients (SZO) for **(A)** heart rate (HR), **(B)** respiratory sinus arrhythmia (RSA), **(C)** the coupling strength from normalized short-time partial directed coherence (NSTPDC) analysis from RESP to BBI, and **(D)** the coupling strength from multivariate transfer entropy (MuTE) analysis from RESP to BBI (BBI, beat-to-beat intervals; RESP, time intervals between consecutive breathing cycles). Boxes indicate data between 25th and 75th percentile with the horizontal bar reflecting the median.

TABLE 3 | Results of phase randomization surrogate analyses for cardiorespiratory couplings between patients suffering from paranoid schizophrenia (SZO), healthy first-degree relatives (REL), and healthy control subjects (CON).

	Index	CON vs. SZO	CON vs. REL	SZO vs. REL	CON			REL			SZO		
					Median	[25–75]		Median	[25–75]		Median	[25–75]	
Couplings	NF	***	n.s	***	−2.0	−2.0	−1.8	−1.8	−1.9	−1.5	−0.9	−1.5	−0.2
	$A_{BBI \rightarrow RESP}$	***	*	n.s	0.03	0.02	0.04	0.05	0.04	0.06	0.06	0.04	0.07
	$A_{RESP \rightarrow BBI}$	***	n.s	***	0.34	0.24	0.40	0.26	0.21	0.33	0.14	0.09	0.21
	$MuTE_{BBI \rightarrow RESP}$	**	n.s	n.s	0.002	0.000	0.008	0.005	0.002	0.012	0.008	0.003	0.016
	$MuTE_{RESP \rightarrow BBI}$	n.s	n.s	n.s	0.004	0.002	0.006	0.006	0.003	0.008	0.007	0.004	0.011

*BB, beat-to-beat intervals; RESP, time intervals between consecutive breathing cycles; A, area from NSTPDC for identifying the coupling strength; MuTE, multivariate Transfer Entropy; p, univariate significance level: *<0.05, **<0.01, ***<0.004; n.s., not significant.*

of the major contributors to changed sympathovagal balance, represented by higher basic HR in the first episode and during untreated conditions could clearly be demonstrated by several studies and seems to be a hallmark in schizophrenic patients. Bär et al. (2007) speculated that reduced HR seems to be highlighting that the cardiac system is not able to adapt to the different demands arising from posture or exertion, and moreover, that patients are at higher risk of developing

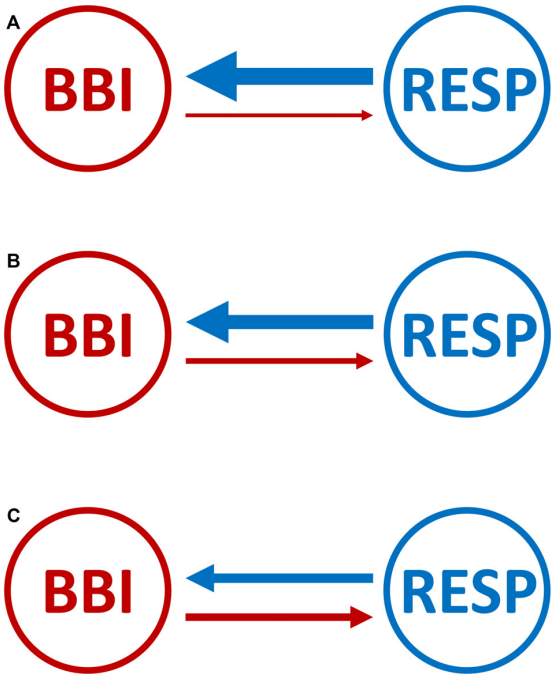

FIGURE 3 | Graphical representation of the cardiorespiratory network structure with causal coupling strength and direction between the cardiac- and the respiratory system for **(A)** healthy subjects, **(B)** healthy first-degree relatives, and **(C)** schizophrenic patients. Arrows indicating the causal coupling direction from one time series to another. The thickness of the lines and arrows indicating the coupling strength and the direction between the two variables. The thicker the line the stronger the coupling strength (BBI, beat-to-beat intervals; RESP, time intervals between consecutive breathing cycles).

arrhythmias. Valkonen-Korhonen et al. (2003) also demonstrated significantly reduced RMSSD and HF performance in psychotic patients and unchanged HRV in mental tasks than in healthy controls. They concluded that patients could not adjust HRV according to the task load. One could assume that acute psychosis state in these subjects leads to a restricted ability of the ANS to respond to external demands. Voss et al. (2011) also demonstrated reduced linear and non-linear HRV pointing to a higher sympathovagal activity in schizophrenic patients and their relatives. Moreover, the impairment of cardiac activity (complexity) confirms the assumption of an changed sympathovagal HR regulation in schizophrenia (Voss et al., 2009). Healthy first-degree relatives of patients showed only increased HR supported by other studies (Bär et al., 2010; Berger et al., 2010; Bär et al., 2012; Abhishekh et al., 2014).

Basic respiratory indices variability analysis showed significantly increased BF in SZO compared to CON supporting other findings dealing with untreated patients (Peupelmann et al., 2009; Bär et al., 2012; Schulz et al., 2012a). Here, it was shown that schizophrenia is accompanied by significantly shorter inspiration and expiration times and a higher BF. For healthy first-degree relatives we found no significant differences in respiratory activity compared to healthy subjects. This is in accordance to the findings of Bär et al. (2012), who only observed alterations in respiration for schizophrenia but not for relatives. They speculated that these findings could be a sign of excitement in critically diseased patients. In other study (Schulz et al., 2012a) we found significantly impaired respiratory variability and respiratory dynamics in schizophrenic patients, but neither for healthy first-degree relatives. This is a noteworthy fact that for schizophrenic patients and their first-degree healthy relatives comparable alterations in HRV (reduced) are present (Castro et al., 2009; Bär et al., 2010, 2012; Voss et al., 2010). These findings further leads to the assumption that an underlying disease-related genetic susceptibility of cardiac regulatory activity is obviously present in schizophrenia and relatives.

However, the entire cardiorespiratory system seems not to be affected, and that the dysfunction of the ANS appears to have a cardiac genetic basis. For example, it could also be shown that a genetic dependency of HRV was evident in healthy twins (Busjahn et al., 1998). In another study (Voss et al., 1996) HRV in the time- and non-linear dynamics domains found significant alterations between twin- and non-twin pairs (62, twin pairs: 30 monozygotic, and 32 dizygotic) leading to the assumption that there exists a genetic component in cardiac system in the generation of heart rate and its variability. Wang et al. (2009) investigated the heritability of HRV under stress and at rest and its dependency on ethnicity and gender (in 427 European and 308 African American twins). They found the same genes influenced HRV under stress and at rest independent of ethnicity and gender. Meda et al. (2014) investigated the genetic background of schizophrenia and its relatives studying the brain's default mode network (DMN) of 296 schizophrenic patients (SZO), 179 unaffected first-degree relatives of SZO (SZREL) and 324 healthy subjects. They showed changes of functional connectivity in SZO and that these changes in DMN were selective only for SZREL familial, with genes regulating specific neurodevelopmental and transmission processes primarily mediating DMN discontinuity.

Personality anxiety has been shown to be associated with altered breathing alterations and BF (Masaoka and Homma, 1997, 1999). The authors found that a higher BF was not associated with metabolic factors and is coordinated with the limbic system and the respiratory drive (Masaoka and Homma, 2001). Boiten et al. (1994) found that alterations in breathing reflect the state a of emotional reaction connected with the requirements to react to emotional situations. Furthermore, symptoms of panic attacks and pulmonary patients overlap that panic anxiety highlights a cardiopulmonary disorder and that shortness of breath highlights an underlying anxiety disorder (Smoller et al., 1996). Respiratory changes may be explained by the fact that excitation disturbances in prefrontal are of the amygdala as assumed in paranoid schizophrenia could be responsible for the connection between psychopathology and alterations of respiration (Bär et al., 2012; Schulz et al., 2018, 2019). Therefore, chronic changes in HR and respiration in schizophrenia appear to be associated with cardiac dysfunction and not just a simple stress-related anxiety disorder (Schulz et al., 2015a).

Linear cardiorespiratory coupling analysis revealed a bidirectionally pronounced coupling direction (NF: −1.0) with

respiration as the driver toward cardiac activity (RESP → BBI) in SZO vs. CON who demonstrating a more pronounced RSA regulation. The linear coupling from heart to respiration BBI → RESP (significantly increased in SZO) is supposed to be an RSA complementary biomarker as a reciprocal part of the cardiorespiratory interrelationship (Dick et al., 2014). Dick et al. (2014) stated that the joint interrelationship between the airways and the ANS as a function of gas exchange is emphasized by the fact that the ANS transmits information to the respiratory tract, which generates beat-to-beat changes, while the information transfer from respiration to the ANS is pronounced as a part of the RSA control loop.

Results from phase randomization surrogate analysis confirmed in general the underlying linear coupling structure for the directions BBI → RESP and RESP → BBI when considering NSTPDC results. But there was one exception, in the case when CON was compared with REL; we found in phase randomization surrogates a significant difference for $A_{BBI \rightarrow RESP}$ that was not present in the original time series. This can be a consequence of the low absolute values for the coupling strength.

For cardiorespiratory couplings with non-linear components significantly lower coupling strength was found in the direction RESP → BBI suggesting impaired non-linear regulatory pathways within the RSA-loop.

Phase randomization surrogates showed also significant differences between CON and SZO in the case of that BBI influenced RESP ($MuTE_{BBI \rightarrow RESP}$) as already found in the original time series. This means that the found difference in the coupling between CON and SZO (original time series) for the direction BBI → RESP was of linear nature without non-linear components. On the other side, we found no significant difference in coupling for the direction RESP → BBI in phase randomization surrogates (but in the original time series) pointing to a strong non-linear coupling behavior when RESP influenced BBI in the original time series.

In the study of Peupelmann et al. (2009), they found that the severity of schizophrenia is connected to alterations in breathing, and speculated that the vagal control within the brainstem does not work properly and leads to these findings. In the case that respiration transfers information toward the heart (RESP → BBI) is related to central respiratory driving mechanisms is respect to responses of the cardiac system (Faes et al., 2011). These impaired central respiratory driving mechanisms are assumed to be the cause of the impairments in the cardiac system in SZO (Schulz et al., 2015a, 2019). Bär et al. (2012) investigated cardiorespiratory couplings in control subjects compared to schizophrenic patients and their relatives. They observed impaired cardiorespiratory coupling, which was characterized by increased decoupling function (CCE) and complexity of cardiorespiratory couplings in schizophrenic patients. Williams et al. (2004) stated "that dissociation of amygdala prefrontal circuits and excitation leads to inhibition of signal processing of threat-related signals in SZO. In particular, dysregulation in the normal cycle of mutual feedback between amygdala work processes and autonomic regulatory activities is characterized by reduced amygdala activity and excessive excitation in these patients." In addition, our results demonstrated that RSA is inhibited supported by other studies (Bär et al., 2012; Schulz et al., 2015a) which showed altered cardiorespiratory interactions and restricted RSA in untreated SZO. Thus, we speculate that impaired vagal control in the brain stem or restricted control pathways of higher centers is responsible for these results. In other study, we found that fractal structures of RSA were strengthened in SZO leading to the assumption that the rhythmic components of the RSA time series did fluctuated more randomly supporting the assumption that cardiac control in heart rate regulation agrees less with respiration in SZO leading to reduced RSA_{P2V} in SZO (Schulz et al., 2015a). We speculated that the impairment of cardiac regulation is not a stress-related excitation but more chronic and significant alterations in hear rate and breathing regulation (Schulz et al., 2015a). The significant alterations within the cardiorespiratory system seem clearly pointing to a disease-related hallmark in SZO and could reflect responses of the ANS during psychosis in acute schizophrenic patients. Due to, that relatives are not in the same "emotional and psychotic state" as patients it seems to be that the alterations within the cardiorespiratory system are closely connected to the emotions in SZO (Suess et al., 1980; Masaoka et al., 2001; Dimitriev et al., 2014; Jerath et al., 2015) and occur mainly only in this disease (Schulz et al., 2015b).

The novelty of this study, in contrast to our previous studies, is that in this study we were able to use a variety of methods from different domains, such as time domain, Granger causality and entropy domain. Especially, the application of two different causality approaches allowed us to assess coupling strength and the direction of the cardiorespiratory couplings. These features were not investigated and were possible so far. By determining causal relationships, it is now possible to understand how the cardiorespiratory system works in these patients. Schulz et al. (2015b), we applied and tested the introduced high-resolution joint symbolic dynamics approach to determine if with this approach a differentiation of the three groups is possible and to assess short-term non-causal couplings. We found a significantly altered heart rate pattern, respiratory pattern and cardiorespiratory couplings in SZO and only marginal alterations for REL group comparison to CON. Here, in this study, we are able to determine the causality of regulatory systems (heart and respiration) for these participants giving new insides of autonomic control.

For schizophrenia, this question has not yet been clarified as to what the defined working mechanisms are that are responsible for the obvious dysregulation of the ANS, since the number of brain areas (cortical, subcortical, and brain stem) is involved in autonomous regulatory processes. To sum up, we demonstrated a significantly impaired heart- and respiratory regulation expressed in their variability and dynamics and an impaired cardiorespiratory interactions in schizophrenic patients, and only a significantly altered heart rate regulation in healthy first-degree relatives. These results are consistent with previous studies, which also showed reduced HRV in schizophrenia and its first-degree healthy relatives, which clearly indicate underlying disease-related genetic vulnerability of the cardiovascular system

(particularly within the cardiac subsystem). In schizophrenia, the results might be a result of lower vagal control within the brain stem, impaired communication between the brain stem and higher centers, or panic and anxiety-related alterations in the brain stem during the acute psychosis state in SZO (Schulz et al., 2018, 2019). Moreover, relatives do not seem to be in the same emotional and psychotic state as their sick schizophrenic relatives. As a result of the fact that in relatives only the cardiac system seems to be affected, it explains that the cardiorespiratory couplings are not significantly altered compared to the sick relatives (schizophrenia). Therefore, it seems that the alterations within the cardiorespiratory system and the linkages between the related subsystems that are apparent in schizophrenia are closely related to psychotic emotions that are evident during the acute phase of this disease (Schulz et al., 2015b), highlighted by alterations within the cardiac- and the respiratory systems. The interrelationship between the autonomous nerves system (cardiovascular and cardiorespiratory) in neuropathological diseases and the associated central control mechanisms are still not fully addressed in research.

DATA AVAILABILITY STATEMENT

The raw data supporting the conclusions of this article will be made available by the authors, without undue reservation, to any qualified researcher.

ETHICS STATEMENT

The studies involving human participants were reviewed and approved by the local ethics committee of the Jena University Hospital. The patients/participants provided their written informed consent to participate in this study.

AUTHOR CONTRIBUTIONS

SS analyzed and interpreted the data, wrote the article, and final approval of the version to be published. K-JB conceived and designed the study, collected and assembled the data, interpreted the data, critically revised the article for significant intellectual content, and reread the final version prior to its publication. AV interpreted the data, did a critical revision of the article for its significant intellectual content, and reread the final version prior to its publication. JH did a critical revision of the article for its significant intellectual content, and reread the final version prior to its publication.

FUNDING

This work was supported by grants from the German Federal Ministry for Economic Affairs and Energy (BMWI) (ZF4485201SB7).

REFERENCES

Abhishekh, H. A., Kumar, N. C., Thirthalli, J., Chandrashekar, H., Gangadhar, B. N., and Sathyaprabha, T. N. (2014). Prolonged reaction to mental arithmetic stress in first-degree relatives of schizophrenia patients. *Clin. Schizophr. Relat. Psychoses.* 8, 137–142. doi: 10.3371/csrp.abku.022213

Adochiei, F., Schulz, S., Edu, I., Costin, H., and Voss, A. (2013). A new normalised short time PDC for dynamic coupling analyses. *Biomed. Tech.* 58.

Baccala, L. A., and Sameshima, K. (2001). Partial directed coherence: a new concept in neural structure determination. *Biol. Cybern.* 84, 463–474. doi: 10.1007/pl00007990

Bär, K. J., Berger, S., Metzner, M., Boettger, M. K., Schulz, S., Ramachandraiah, C. T., et al. (2010). Autonomic dysfunction in unaffected first-degree relatives of patients suffering from schizophrenia. *Schizophr. Bull.* 36, 1050–1058. doi: 10.1093/schbul/sbp024

Bär, K. J., Boettger, M. K., Koschke, M., Schulz, S., Chokka, P., Yeragani, V. K., et al. (2007). Non-linear complexity measures of heart rate variability in acute schizophrenia. *Clin. Neurophysiol.* 118, 2009–2015. doi: 10.1016/j.clinph.2007.06.012

Bär, K. J., Letzsch, A., Jochum, T., Wagner, G., Greiner, W., and Sauer, H. (2005). Loss of efferent vagal activity in acute schizophrenia. *J. Psychiatr. Res.* 39, 519–527. doi: 10.1016/j.jpsychires.2004.12.007

Bär, K. J., Rachow, T., Schulz, S., Bassarab, K., Haufe, S., Berger, S., et al. (2012). The phrenic component of acute schizophrenia–a name and its physiological reality. *PLoS One* 7:e33459. doi: 10.1371/journal.pone.0033459

Bartsch, R. P., Liu, K. K., Bashan, A., and Ivanov, P. C. (2015). Network physiology: how organ systems dynamically interact. *PLoS One* 10:e0142143. doi: 10.1371/journal.pone.00142143

Bashan, A., Bartsch, R. P., Kantelhardt, J. W., Havlin, S., and Ivanov, P. (2012). Network physiology reveals relations between network topology and physiological function. *Nat. Commun.* 3:702.

Berger, S., Boettger, M. K., Tancer, M., Guinjoan, S. M., Yeragani, V. K., and Bar, K. J. (2010). Reduced cardio-respiratory coupling indicates suppression of vagal activity in healthy relatives of patients with schizophrenia. *Prog. Neuropsychopharmacol. Biol. Psychiatry* 34, 406–411. doi: 10.1016/j.pnpbp.2010.01.009

Boettger, S., Hoyer, D., Falkenhahn, K., Kaatz, M., Yeragani, V. K., and Bar, K. J. (2006). Altered diurnal autonomic variation and reduced vagal information flow in acute schizophrenia. *Clin. Neurophysiol.* 117, 2715–2722. doi: 10.1016/j.clinph.2006.08.009

Boiten, F. A., Frijda, N. H., and Wientjes, C. J. (1994). Emotions and respiratory patterns: review and critical analysis. *Int. J. Psychophysiol.* 17, 103–128. doi: 10.1016/0167-8760(94)90027-2

Busjahn, A., Voss, A., Knoblauch, H., Knoblauch, M., Jeschke, E., Wessel, N., et al. (1998). Angiotensin-converting enzyme and angiotensinogen gene polymorphisms and heart rate variability in twins. *Am. J. Cardiol.* 81, 755–760.

Castro, M. N., Vigo, D. E., Chu, E. M., Fahrer, R. D., De Achaval, D., Costanzo, E. Y., et al. (2009). Heart rate variability response to mental arithmetic stress is abnormal in first-degree relatives of individuals with schizophrenia. *Schizophr. Res.* 109, 134–140. doi: 10.1016/j.schres.2008.12.026

Chang, J. S., Yoo, C. S., Yi, S. H., Hong, K. H., Lee, Y. S., Oh, H. S., et al. (2010). Changes in heart rate dynamics of patients with schizophrenia treated with risperidone. *Prog. Neuropsychopharmacol. Biol. Psychiatry* 34, 924–929. doi: 10.1016/j.pnpbp.2010.04.017

Chang, J. S., Yoo, C. S., Yi, S. H., Hong, K. H., Oh, H. S., Hwang, J. Y., et al. (2009). Differential pattern of heart rate variability in patients with schizophrenia. *Prog. Neuropsychopharmacol. Biol. Psychiatry* 33, 991–995. doi: 10.1016/j.pnpbp.2009.05.004

Cohen, J. (1988). *Statistical Power Analysis for the Behavioral Sciences*. New Jersey: L. Erlbaum Associates.

Dick, T. E., Hsieh, Y. H., Dhingra, R. R., Baekey, D. M., Galan, R. F., Wehrwein, E., et al. (2014). Cardiorespiratory coupling: common rhythms in cardiac, sympathetic, and respiratory activities. *Prog. Brain Res.* 209, 191–205.

Dimitriev, D. A., Saperova, E. V., Dimitriev, A. D., and Karpenko, Y. D. (2014). Effect of anxiety on the function of the cardiorespiratory system. *Hum. Physiol.* 40, 433–439. doi: 10.1134/s0362119714040069

Eckberg, D. L. (2003). The human respiratory gate. *J. Physiol.* 548, 339–352. doi: 10.1111/j.1469-7793.2003.00339.x

Faes, L., Marinazzo, D., Jurysta, F., and Nollo, G. (2015). Linear and non-linear brain-heart and brain-brain interactions during sleep. *Physiol. Meas.* 36, 683–698. doi: 10.1088/0967-3334/36/4/683

Faes, L., Nollo, G., and Porta, A. (2011). Information domain approach to the investigation of cardio-vascular, cardio-pulmonary, and vasculo-pulmonary causal couplings. *Front. Physiol.* 2:80. doi: 10.3389/fphys.2011.00080

Grossman, P., Stemmler, G., and Meinhardt, E. (1990a). Paced respiratory sinus arrhythmia as an index of cardiac parasympathetic tone during varying behavioral tasks. *Psychophysiology* 27, 404–416. doi: 10.1111/j.1469-8986.1990.tb02335.x

Grossman, P., Van Beek, J., and Wientjes, C. (1990b). A comparison of three quantification methods for estimation of respiratory sinus arrhythmia. *Psychophysiology* 27, 702–714. doi: 10.1111/j.1469-8986.1990.tb03198.x

Hennekens, C. H., Hennekens, A. R., Hollar, D., and Casey, D. E. (2005). schizophrenia and increased risks of cardiovascular disease. *Am. Heart J.* 150, 1115–1121. doi: 10.1016/j.ahj.2005.02.007

Homma, I., and Masaoka, Y. (2008). Breathing rhythms and emotions. *Exp. Physiol.* 93, 1011–1021. doi: 10.1113/expphysiol.2008.042424

Ivanov, P. C., Liu, K. K., and Bartsch, R. P. (2016). Focus on the emerging new fields of network physiology and network medicine. *New J. Phys.* 18:100201. doi: 10.1088/1367-2630/18/10/100201

Jerath, R., Crawford, M. W., Barnes, V. A., and Harden, K. (2015). Self-regulation of breathing as a primary treatment for anxiety. *Appl. Psychophysiol. Biofeedb.* 40, 107–115. doi: 10.1007/s10484-015-9279-8

Kay, S. R., Fiszbein, A., and Opler, L. A. (1987). The positive and negative syndrome scale (PANSS) for schizophrenia. *Schizophr. Bull.* 13, 261–276. doi: 10.1093/schbul/13.2.261

Lancaster, G., Iatsenko, D., Pidde, A., Ticcinelli, V., and Stefanovska, A. (2018). Surrogate data for hypothesis testing of physical systems. *Phys. Rep.* 748, 1–60. doi: 10.1016/j.physrep.2018.06.001

Laursen, T. M., Nordentoft, M., and Mortensen, P. B. (2014). Excess early mortality in schizophrenia. *Annu. Rev. Clin. Psychol.* 10, 425–448. doi: 10.1146/annurev-clinpsy-032813-153657

LeBlanc, J., Ducharme, M. B., and Thompson, M. (2004). Study on the correlation of the autonomic nervous system responses to a stressor of high discomfort with personality traits. *Physiol. Behav.* 82, 647–652. doi: 10.1016/j.physbeh.2004.05.014

Liu, K. K., Bartsch, R. P., Lin, A., Mantegna, R. N., and Ivanov, P. (2015). Plasticity of brain wave network interactions and evolution across physiologic states. *Front. Neural Circ.* 9:62. doi: 10.3389/fphys.2011.00062

Masaoka, Y., and Homma, I. (1997). Anxiety and respiratory patterns: their relationship during mental stress and physical load. *Int. J. Psychophysiol.* 27, 153–159. doi: 10.1016/s0167-8760(97)00052-4

Masaoka, Y., and Homma, I. (1999). Expiratory time determined by individual anxiety levels in humans. *J. Appl. Physiol.* 86, 1329–1336. doi: 10.1152/jappl.1999.86.4.1329

Masaoka, Y., and Homma, I. (2001). The effect of anticipatory anxiety on breathing and metabolism in humans. *Respir. Physiol.* 128, 171–177. doi: 10.1016/s0034-5687(01)00278-x

Masaoka, Y., Kanamaru, A., and Homma, I. (2001). *Anxiety and Respiration*. Berlin: Springer.

McGrath, J., Saha, S., Chant, D., and Welham, J. (2008). Schizophrenia: a concise overview of incidence, prevalence, and mortality. *Epidemiol. Rev.* 30, 67–76. doi: 10.1093/epirev/mxn001

Meda, S. A., Ruano, G., Windemuth, A., O'neil, K., Berwise, C., Dunn, S. M., et al. (2014). Multivariate analysis reveals genetic associations of the resting default mode network in psychotic bipolar disorder and schizophrenia. *Proc. Natl. Acad. Sci. U.S.A.* 111, E2066–E2075.

Milde, T., Schwab, K., Walther, M., Eiselt, M., Schelenz, C., Voss, A., et al. (2011). Time-variant partial directed coherence in analysis of the cardiovascular system. A methodological study. *Physiol. Measur.* 32, 1787–1805. doi: 10.1088/0967-3334/32/11/s06

Montalto, A., Faes, L., and Marinazzo, D. (2014). MuTE: a MATLAB toolbox to compare established and novel estimators of the multivariate transfer entropy. *PLoS One* 9:e109462. doi: 10.1371/journal.pone.00109462

Mujica-Parodi, L. R., Yeragani, V., and Malaspina, D. (2005). Nonlinear complexity and spectral analyses of heart rate variability in medicated and unmedicated patients with schizophrenia. *Neuropsychobiology* 51, 10–15. doi: 10.1159/000082850

Neumaier, A., and Schneider, T. (2001). Estimation of parameters and eigenmodes of multivariate autoregressive models. *ACM Trans. Math. Softw.* 27, 27–57. doi: 10.1145/382043.382304

Novak, V., Novak, P., De Champlain, J., Le Blanc, A. R., Martin, R., and Nadeau, R. (1993). Influence of respiration on heart rate and blood pressure fluctuations. *J. Appl. Physiol.* 74, 617–626. doi: 10.1152/jappl.1993.74.2.617

Peupelmann, J., Boettger, M. K., Ruhland, C., Berger, S., Ramachandraiah, C. T., Yeragani, V. K., et al. (2009). Cardio-respiratory coupling indicates suppression of vagal activity in acute schizophrenia. *Schizophr. Res.* 112, 153–157. doi: 10.1016/j.schres.2009.03.042

Porta, A., Baselli, G., Lombardi, F., Montano, N., Malliani, A., and Cerutti, S. (1999). Conditional entropy approach for the evaluation of the coupling strength. *Biol. Cybern.* 81, 119–129. doi: 10.1007/s004220050549

Ringen, P. A., Engh, J. A., Birkenaes, A. B., Dieset, I., and Andreassen, O. A. (2014). Increased mortality in schizophrenia due to cardiovascular disease - a non-systematic review of epidemiology, possible causes, and interventions. *Front. Psychiatry* 5:137. doi: 10.3389/fphys.2011.000137

Schneider, T., and Neumaier, A. (2001). Algorithm 808: ARFIT—a matlab package for the estimation of parameters and eigenmodes of multivariate autoregressive models. *ACM Trans. Math. Softw.* 27, 58–65. doi: 10.1145/382043.382316

Schreiber, T. (2000). Measuring information transfer. *Phys. Rev. Lett.* 85, 461–464. doi: 10.1103/physrevlett.85.461

Schreiber, T., and Schmitz, A. (2000). Surrogate time series. *Phys. D* 142, 346–382.

Schulz, S., Adochiei, F. C., Edu, I. R., Schroeder, R., Costin, H., Bar, K. J., et al. (2013a). Cardiovascular and cardiorespiratory coupling analyses: a review. *Philos. Trans. A Math. Phys. Eng. Sci.* 371:20120191. doi: 10.1098/rsta.2012.0191

Schulz, S., Bar, K. J., and Voss, A. (2012b). Respiratory variability and cardiorespiratory coupling analyses in patients suffering from schizophrenia and their healthy first-degree relatives. *Biomed. Tech.* 57.

Schulz, S., Bär, K. J., and Voss, A. (2012a). "Cardiovascular and cardiorespiratory coupling in unmedicated schizophrenic patients in comparison to healthy subjects," in *Proceedings of the 2012 Annual International Conference of the IEEE Engineering in Medicine and Biology Society*, San Diego, CA.

Schulz, S., Bär, K. J., and Voss, A. (2015a). Analyses of heart rate, respiration and cardiorespiratory coupling in patients with schizophrenia. *Entropy* 17, 483–501. doi: 10.3390/e17020483

Schulz, S., Haueisen, J., Bär, K. J., and Voss, A. (2013b). Quantification of cardiorespiratory coupling in acute schizophrenia applying high resolution joint symbolic dynamics. *Comput. Cardiol. Conf.* 2013, 101–104.

Schulz, S., Haueisen, J., Bär, K.-J., and Andreas, V. (2015b). High-resolution joint symbolic analysis to enhance classification of the cardiorespiratory system in patients with schizophrenia and their relatives. *Philos. Trans. A Math. Phys. Eng. Sci.* 373:20140098. doi: 10.1098/rsta.2014.0098

Schulz, S., Haueisen, J., Bär, K. J., and Voss, A. (2014). Changed cardiorespiratory phase-coupling pattern in patients suffering from schizophrenia. *Biomed. Tech.* 59.

Schulz, S., Haueisen, J., Bar, K. J., and Voss, A. (2018). Multivariate assessment of the central-cardiorespiratory network structure in neuropathological disease. *Physiol. Measur.* 39:074004. doi: 10.1088/1361-6579/aace9b

Schulz, S., Haueisen, J., Bär, K.-J., and Voss, A. (2019). Altered causal coupling pathways within the central-autonomic-network in patients suffering from schizophrenia. *Entropy* 21:733. doi: 10.3390/e21080733

Schulz, S., Tupaika, N., Berger, S., Haueisen, J., Bär, K. J., and Voss, A. (2013c). Cardiovascular coupling analysis with high-resolution joint symbolic dynamics in patients suffering from acute schizophrenia. *Physiol. Measur.* 34, 883–901. doi: 10.1088/0967-3334/34/8/883

Smoller, J. W., Pollack, M. H., Otto, M. W., Rosenbaum, J. F., and Kradin, R. L. (1996). Panic anxiety, dyspnea, and respiratory disease. Theoretical and clinical considerations. *Am. J. Respir. Crit. Care Med.* 154, 6–17. doi: 10.1164/ajrccm.154.1.8680700

Straus, S. M., Bleumink, G. S., Dieleman, J. P., Van Der Lei, J., Jong, G. W., Kingma, J. H., et al. (2004). Antipsychotics and the risk of sudden cardiac death. *Arch. Intern. Med.* 164, 1293–1297.

Suess, W. M., Alexander, A. B., Smith, D. D., Sweeney, H. W., and Marion, R. J. (1980). The effects of psychological stress on respiration: a preliminary study of anxiety and hyperventilation. *Psychophysiology* 17, 535–540. doi: 10.1111/j.1469-8986.1980.tb02293.x

Toichi, M., Kubota, Y., Murai, T., Kamio, Y., Sakihama, M., Toriuchi, T., et al. (1999). The influence of psychotic states on the autonomic nervous system in schizophrenia. *Int. J. Psychophysiol.* 31, 147–154. doi: 10.1016/s0167-8760(98)00047-6

Valkonen-Korhonen, M., Tarvainen, M. P., Ranta-Aho, P., Karjalainen, P. A., Partanen, J., Karhu, J., et al. (2003). Heart rate variability in acute psychosis. *Psychophysiology* 40, 716–726. doi: 10.1111/1469-8986.00072

Voss, A., Busjahn, A., Wessel, N., Schurath, R., Faulhaber, H. D., Luft, F. C., et al. (1996). Familial and genetic influences on heart rate variability. *J. Electrocardiol.* 29(Suppl.), 154–160. doi: 10.1016/s0022-0736(96)80045-8

Voss, A., Schulz, S., and Baer, K. J. (2010). Linear and nonlinear analysis of autonomic regulation of heart rate variability in healthy first-degree relatives of patients with schizophrenia. *Conf. Proc. IEEE Eng. Med. Biol. Soc.* 2010, 5395–5398.

Voss, A., Schulz, S., and Schroder, R. (2011). "Analysis of cardiovascular oscillations using nonlinear dynamics methods for an enhanced diagnosis of heart and neurological diseases and for risk stratification," in *Proceedings of the E-Health and Bioengineering Conference (EHB), 2011*, Iasi.

Voss, A., Schulz, S., Schroeder, R., Baumert, M., and Caminal, P. (2009). Methods derived from nonlinear dynamics for analysing heart rate variability. *Philos. Trans. A Math. Phys. Eng. Sci.* 367, 277–296. doi: 10.1098/rsta.2008.0232

Wang, X., Ding, X., Su, S., Li, Z., Riese, H., Thayer, J. F., et al. (2009). Genetic influences on heart rate variability at rest and during stress. *Psychophysiology* 46, 458–465. doi: 10.1111/j.1469-8986.2009.00793.x

Wessel, N., Voss, A., Malberg, H., Ziehmann, C., Voss, H., Schirdewan, A., et al. (2000). Nonlinear analysis of complex phenomena in cardiological data. *Z. Herzschr. Elektrophys.* 11, 159–173. doi: 10.1007/s003990070035

Williams, L. M., Das, P., Harris, A. W., Liddell, B. B., Brammer, M. J., Olivieri, G., et al. (2004). Dysregulation of arousal and amygdala-prefrontal systems in paranoid schizophrenia. *Am. J. Psychiatry* 161, 480–489. doi: 10.1176/appi.ajp.161.3.480

Conflict of Interest: The authors declare that the research was conducted in the absence of any commercial or financial relationships that could be construed as a potential conflict of interest.

frontiers in Neuroscience

BRIEF RESEARCH REPORT
published: 17 June 2020
doi: 10.3389/fnins.2020.00568

Complex Visceral Coupling During Central Sleep Apnea in Cats

*Alexandra V. Limanskaya[1,2], Irina I. Busygina[3], Ekaterina V. Levichkina[1,4] and Ivan N. Pigarev[1]**

[1] Institute for Information Transmission Problems (Kharkevich Institute), Russian Academy of Sciences, Moscow, Russia, [2] Department of Higher Nervous Activity, Faculty of Biology, Lomonosov Moscow State University, Moscow, Russia, [3] Pavlov Institute of Physiology, Russian Academy of Sciences, Saint Petersburg, Russia, [4] Department of Optometry and Vision Sciences, The University of Melbourne, Parkville, VIC, Australia

Central sleep apnea is a sudden arrest of breathing during sleep caused by the central commands to the thoracoabdominal muscles. It is a widespread phenomenon in both healthy and diseased people, as well as in some animals. However, there is an ongoing debate whether it can be considered as a pathological deviation of the respiratory function or an adaptive mechanism of an unclear function. We performed chronic recordings from six behaving cats over multiple sleep/wake cycles, which included electroencephalogram, ECG, eye movements, air flow, and thoracic respiratory muscle movements, and in four cats combined that with the registration of myoelectric activity of the stomach and the duodenum. In these experiments, we observed frequent central cessations of breathing (for 5–13 s) during sleep. Each of the sleep apnea episodes was accompanied by a stereotypical complex of somatic and visceral effects. The heart rate increased 3–5 s before the respiration arrest and strongly decreased during the absence of respiration. The myoelectric activity of the stomach and the duodenum also often demonstrated a strong suppression during the apnea episodes. The general composition of the visceral effects was stable during all periods of observation (up to 3 years in one cat). We hypothesize that the stereotypic coupling of activities in various visceral systems during episodes of central sleep apnea most likely reflects a complex adaptive behavior rather than an isolated respiratory pathology and discuss the probable function of this phenomenon.

Keywords: central sleep apnea, heart rate, respiration, stomach motility, duodenal motility, visceral theory of sleep

OPEN ACCESS

Edited by:
Tijana Bojić, University of Belgrade, Serbia

Reviewed by:
Steffen Schulz, Institut für Innovative Gesundheitstechnologien (IGHT), Germany
Arcady A. Putilov, Federal Research Center of Fundamental and Translational Medicine, Russia

****Correspondence:***
Ivan N. Pigarev
pigarev@iitp.ru

Specialty section:
This article was submitted to Autonomic Neuroscience, a section of the journal Frontiers in Neuroscience

Received: *30 December 2019*
Accepted: *08 May 2020*
Published: *17 June 2020*

Citation:
Limanskaya AV, Busygina II, Levichkina EV and Pigarev IN (2020) Complex Visceral Coupling During Central Sleep Apnea in Cats. Front. Neurosci. 14:568. doi: 10.3389/fnins.2020.00568

INTRODUCTION

Sleep-related breathing disorders, including central sleep apnea in humans, currently are at the focus of attention of many sleep studies. Generally, central apnea manifests as a short absence or reduction of breathing during sleep (9–14-s in length) caused by the cessation or the attenuation of the central respiratory drive from the breathing control center to the thoracoabdominal muscles. This phenomenon, or rather a group of phenomena, has a complex manifestation. Apnea can occur as an isolated disorder or as one of the numerous symptoms accompanying other illnesses (e.g., congenital heart failure and obstructive sleep apnea), or it can even be an intrinsic feature of the normal breathing system of a healthy organism, for instance, in high-altitude conditions or in early infancy (Hernandez and Patil, 2016; Baillieul et al., 2019).

Although recent advances in sleep research provided valuable descriptions of the various aspects of this phenomenon and of its manifestation types (Eckert et al., 2007; Javaheri et al., 2017), there is still no agreement regarding the possible functional role of central sleep apnea. The noticed link between central sleep apnea and the malfunction of the cardio-respiratory system led some researchers to an assumption that central apnea represents a pathological phenomenon related to a failure in breathing control and therefore requires specific treatment, while others proposed that it may have an important adaptive purpose (see e.g., Gay, 2008; Malhotra et al., 2008; Cowie, 2017). Similar effects with common features to those described in human subjects were also observed in kittens (McGinty et al., 1979), as well as in rodent models (e.g., Sato et al., 1990; Nakamura et al., 2003; Davis and O'Donnell, 2013).

During a series of studies not focused on apnea but devoted to the exploration of cortical representations of the visceral system in wakefulness and in sleep (Pigarev et al., 2013, 2016), which required a prolonged collection of somnographic data over multiple sleep/wake cycles, we, to our surprise, realized that central apnea is a frequent event of sleep in cats. Moreover, we noted a correlation between changes of the multiple parameters of visceral functioning surrounding the apnea episodes. In this paper, we describe these patterns of co-occurrence of visceral disturbances and discuss their possible adaptive function. These results were partly presented in abstract form (Limanskaya, 2019).

MATERIALS AND METHODS

In this study, we retrospectively analyzed recordings obtained in the course of four different previous projects, and therefore we had an opportunity to analyze data from six healthy adult cats.

All experiments with these cats were performed using our modification of the painless head fixation approach (Noda et al., 1971; Pigarev et al., 2009), necessary to record stable polysomnography from animals during a long period of time, up to 8 h a day. The recordings used for further analysis covered periods of both wakefulness and sleep. The number of experimental sessions analyzed in a single cat varied from 20 to 78.

Surgery and day-to-day treatment of the animals were carried out in accordance with the ethical principles for the maintenance and use of animals in neuroscience research (Zimmermann, 1987), the NIH Guidelines for the Care and Use of Animals, and the Declaration of Helsinki on Ethical Principles for Medical Research. Current Russian laws do not bind scientific institutes to have special ethic committees; the assessment of research proposals is instead conducted by the institutional scientific councils in the course of their discussion concerning providing financial support to a particular study. According to the rules of the foundations that distribute grants for scientific research in Russia, ethics evaluation is done by the council of reviewers prior to making a decision regarding the financial support of a particular study. Both councils are guided by the recommendations of the above-mentioned documents.

The preparation of the animals for the experiments included an acclimatization of each animal to the laboratory environment and either one (in two cats) or two separate surgeries (in four cats), with recovery intervals after each of them. The general approach to chronic studies conducted in behaving animals such as cats is to purchase an animal of a reasonably young age (∼1 year) and acclimatize it to the laboratory environment and to the investigators involved in the experiments. This "shaping" process was based on positive reinforcement techniques and usually took a couple of weeks before any surgery was performed.

Both surgeries were conducted under deep anesthesia (premedication with xylazine, 0.15 ml/kg; for the main anesthesia, we used zoletil, 6 mg/kg, for the first injection, and additional doses of 5 mg periodically with intervals of about 20 min to keep the appropriate level of animal sedation.

During the first surgery, a pre-fabricated halo frame for subsequent painless head fixation during the recording session was attached to the skull. The frame was manufactured using a thin steel wire as a base, with acrylic dental cement as filling and cover, and attached to the skull with eight 2.5-mm surgical-grade steel screws. The skin and soft tissues were removed from the top of the cranium (from the area inside the frame), and the surface of the skull was covered with a thin layer of acrylic dental cement [for a detailed description, see Pigarev et al. (2009)]. At this stage, two electrodes manufactured from thin (0.5 mm) Elgiloy wire for electroencephalogram (EEG) monitoring were implanted epidurally over the frontal and the occipital cortices.

After a complete recovery (at least 4 weeks), the animal was trained to stay for a prolonged time with its head fixed to ensure stable recordings over sleep/wake cycles. The duration of this training depended on the individual behavior of an animal. Usually within a couple of weeks, an animal gets acclimatized to head fixation and begins sleeping with its head fixed. After that, the second surgery can be performed. During the second surgery, intramural bipolar electrodes were implanted, allowing the recording of myoelectrical activity from the stomach and the duodenum. Intramural electrodes were implanted into the walls of these organs using the method proposed by Papasova and Milenov (1965) and Papasova et al. (1966b). The details of this procedure were previously described in Pigarev et al. (2013) as well. The same type of anesthesia was used for this procedure.

For the ECG recording, we used one lead from the stomach wall, and the second was from the ground screw inserted in the bone at the top of the skull. Since the recordings necessary to investigate central sleep apnea were mainly done in sleep, when the animal does not move, mostly there were no motion artifacts, and the QRS complexes in ECG and the R maxima of the QRS were automatically identified by Spike 2 built-in algorithms for spike sorting by shape. In rare cases when intense muscle jerks occurred during rapid eye movement (REM) sleep and resulted in artifacts, the corresponding correction was done after a visual inspection. Moments of R pick maxima were used to calculate the heart rate mean over time. For this procedure, we also used Spike 2 built-in algorithm, which replaced each event with Gaussian kernel (exponential time constant of 3 s).

The experiments were conducted during daytime in a diffusely illuminated room, with permanent video monitoring of the animal.

All standard polysomnographic parameters were recorded: cortical EEG, ECG, respiratory movements (using a thoracoabdominal belt with a piezoelectric sensor), air flow (with thermo-sensors placed in front of the nose), eye movements, and opening/closing of the eyelids (with an infrared oculometer). In addition to that, in four animals, we recorded the myoelectrical activity of the stomach and the duodenum.

All these signals were amplified with NeuroBioLab amplifiers stored on a hard drive using LabChart system (ADInstrument, Australia) and analyzed offline using LabChart and Spike 2 (CED, GB) programs. The ECG and duodenum myoelectric signals were recorded with 1 kHz sampling rate. For all other parameters, the sampling rate was 200 Hz.

DATA ANALYSIS

Polysomnograms and video recordings were visually examined for the presence of respiratory cessation in sleep (apnea and cessation of movements of the thoracoabdominal muscles longer than 5 s), and the durations of respiratory arrests were estimated.

The separation of the states of vigilance was based on a visual inspection of the polysomnograms and on video recordings. As signs of slow wave (SW) sleep, we used the increase of delta wave amplitudes in EEG, slowing of respiration, general decrease of the animal's motor activity, slow gaze drifts replacing saccadic eye movements, and closing of the eyelids. After selecting the intervals of SW sleep and wakefulness using these criteria, we performed a quantitative comparison of the power spectral density between these two conditions.

The EEG of the assumed SW sleep and wakefulness periods was broken into 10-s intervals, and the EEG spectra were calculated (Chronux data analysis toolbox for Matlab[1]). We analyzed the EEG spectra within frequency ranges known to depend on the state of vigilance: delta, sleep spindle, and gamma ranges. We found that, in all recordings, the delta and the spindle range power spectral density values in EEG were significantly higher in SW sleep while power in gamma range was always higher in wakefulness (Wilcoxon rank sum test $p < 0.001$). These criteria commonly characterize sleep—wake differences (Contreras and Steriade, 1996; Destexhe et al., 1999). Periods of REM sleep could be easily determined as occurring just after intervals of SW sleep desynchronization of the general EEG—the presence of eye and lid movements and very typical jerks of facial muscles as observed on video.

The myoelectrical activities of the stomach and the duodenum were analyzed only for estimation of the reduction of their motility-related features during apnea episodes. For stomach activity, this manifested as an absence or a reduction of high-amplitude myoelectrical waves during periods of respiratory cessations (**Figure 1**, channel 2). For the duodenum, this manifested as the absence of high-frequency spike potentials, as can be seen in **Figure 1** (channel 3). For a detailed description of the relationships between the myoelectrical activity of the stomach and the duodenum and their motility, see Papasova et al. (1966a), Costa and Furness (1982), Sarna (1989), and Martinez-de-Juan et al. (2000).

[1]http://chronux.org

RESULTS

The presented results were obtained from a retrospective analysis of the polysomnograms recorded in six cats, which were used in four different projects devoted to the investigation of various aspects of sleep in chronic experiments.

In all six animals, episodes of central sleep apnea were found in most of the analyzed experiments.

Figure 1 presents typical examples of central sleep apnea episodes as recorded in the four cats. All of them were registered in the transitional period from REM to SW sleep. Two vertical lines mark the borders of each apnea episode. Respiration arrest is seen in channels 4 and 6. Channel 4 represents nasal airflow and channel 6 represents the movements of the thoracic cage.

The heart rate increased 3–5 s before the cessation of breathing in all the observed sleep apnea episodes in all six cats. By the onset of the apnea episodes, the heart rate always decreased and remained at a low level until the first breath. During the apnea episodes, the intervals between two sequential heartbeats could sometimes be twice longer than during periods before the respiration arrest (e.g., **Figure 1**, cat 4, channel 7).

An example of heart palpitations can be seen in the ECG (channel 7) as well as in the heart rate curve (channel 8). During the recorded sleep apnea episodes (e.g., 115 of 293 in one cat), even the ones that happened during REM sleep, the eyes and the eyelids remained practically immobile (channel 5).

Channels 2 and 3 demonstrate the myoelectrical activity recorded from the walls of the stomach and the duodenum correspondingly. It is seen that, at the time of apnea onset, the myoelectric stomach activity (channel 2) gradually disappeared. The periodic myoelectrical duodenal activity (channel 3) persists. However, these periodic slow waves reflect the electrical activity of the enteric nervous system and not the peristaltic intestinal movements. Intestinal motility is more related to the higher-frequency spike potentials superimposed on these slow waves (Papasova et al., 1966a; Costa and Furness, 1982; Sarna, 1989; Martinez-de-Juan et al., 2000). Such spike potentials are seen in **Figure 1**, just before the apnea episodes in cats 1 and 2. However, the spike potentials were usually absent during respiratory arrests. Thus, it seems that duodenal and stomach motility might be decreased or absent during central sleep apnea.

In two cats (cats 1 and 2 in **Figure 1**), the results of all 78 daily experiment sessions (from 2 to 8 h in length) conducted during 1 year (67 on the first and 11 on the second animal) were analyzed for the presence of central sleep apnea episodes. These episodes were detected in 59 out of 78 experiments on the first cat (293 apnea episodes detected) and in 10 out of 11 experiments on the second cat (71 episodes). In these two cats, the cardio-respiratory activity and the activity of the stomach and the duodenum were recorded. For one of these two cats, with 78 daily

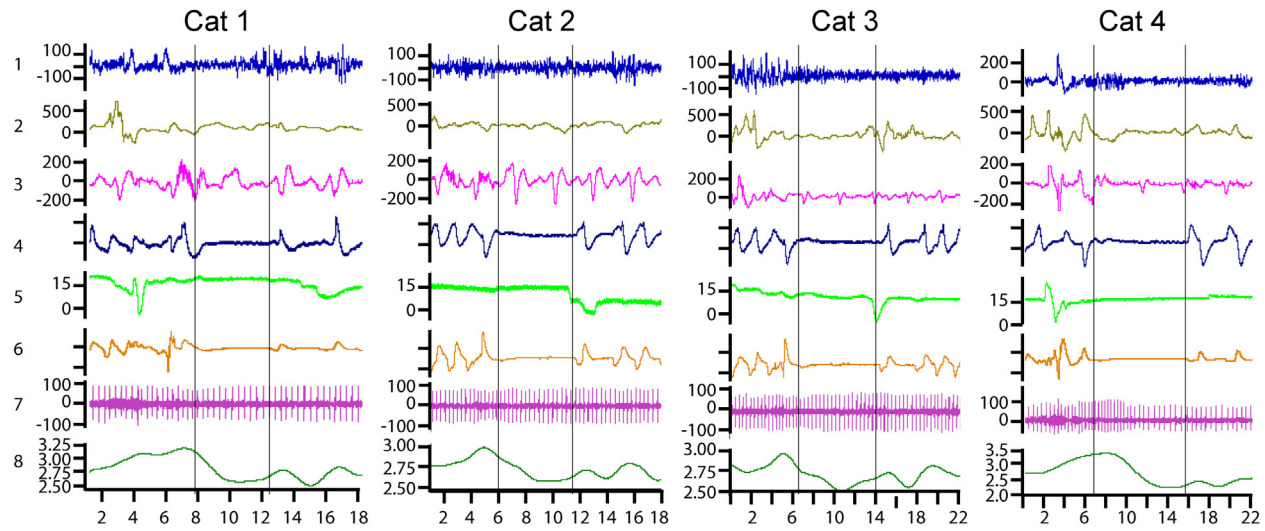

FIGURE 1 | Examples of central sleep apnea episodes recorded in four cats. Channel 1—cortical electroencephalograph (EEG), μV; channel 2—myoelectric activity of the stomach, μV; channel 3—myoelectric activity of the duodenum, μV; channel 4—nasal air flow in arbitrary units; channel 5—vertical eye movements, degrees of the visual angle; channel 6—movements of the thoracoabdominal respiratory muscles in arbitrary units; channel 7—ECG in μV; and channel 8—heart rate curve, heart beats per second. The horizontal axis shows the time scale in seconds.

TABLE 1 | Description of central sleep apnea episodes recorded in one cat during 1 year.

	Slow wave sleep (SWS)/rapid eye movement (REM) transition	REM sleep	Slow wave sleep	Total
Number of apnea episodes	183 (62.4%)	63 (21.5%)	47 (16%)	293 (100%)
Mean duration of apnea episode (s)	9.8 ± 2.26	9 ± 2.58	9.9 ± 2.49	9.7 ± 2.37
Number of episodes with the absence of eye movements	105 (57%)	37 (59%)	33 (70%)	175 (58%)
Number of apnea episodes with the reduction in myoelectric activity of the stomach and/or the intestine	115 (63%)	33 (52%)	34 (72%)	182 (62%)
Mean (±SEM) interval between episodes (min)	13.1 ± 10.4	15.97 ± 14.4	16 ± 9.3	14.3 ± 10.1

experiments and 293 apnea episodes, the descriptive statistics of the various aspects of central sleep apnea episodes distribution over sleep–wake cycle are presented in **Table 1**. The common features of central apnea episodes demonstrated in **Figure 1** were first identified and examined in these two animals.

In two cats (3 and 4 in **Figure 1**), the recorded visceral parameters also included heart rate, respiration, and activity of the stomach and the duodenum. In the remaining two cats (5 and 6), the visceral parameters included only the activity of the heart and respiration. In these four cats (3, 4, 5, and 6), we analyzed only quasi randomly selected experiments (20 in each cat) that were uniformly distributed across the periods from the beginning to the end of these studies (1–3 years). The goal of this analysis was to determine whether central sleep apnea episodes and their typical pattern were present in all animals during the entire intervals of these studies.

Table 1 summarizes the numbers and the durations of apnea episodes per sleep state and the frequencies of the effects co-occurring with the apnea episodes for one cat's recordings performed during 1 year.

The table shows that the largest number of respiratory arrests was observed during the transition periods between SW and REM sleep (the direction of the transition period was not taken into account and the data were pooled together). The durations of apnea episodes obviously did not differ for the different phases of sleep.

We noticed only one episode of central sleep apnea during the transition from wakefulness to SW sleep.

DISCUSSION

Central apnea episodes during sleep were observed in all six cats during natural sleep. This corresponds to the numerous descriptions of these effects given in previous animal studies on kittens, rats, and mice (McGinty et al., 1979; Sato et al., 1990; Nakamura et al., 2003; Davis and O'Donnell, 2013). The novel element of this study was the observation of cardio-respiratory coupling in all observed apnea episodes. In addition, in a substantial fraction of registered sleep apnea episodes, we also noted stabilization of the eyes and eyelid movements, and the changes of stomach and intestinal myoelectric activity suggested a decrease in their motility.

The co-occurrence of the changes in heart rate, the myoelectric activity of the duodenum and the stomach, and ocular motions with the breathing arrests, the stereotypical pattern of these visceral changes in sleep, and the absence of such organized changes in wakefulness seem indicative of the existence of some coordinated central neural program that controls central apneas specifically during sleep. A central apnea episode therefore represents a complex effect involving multiple visceral systems rather than an isolated one, happening only in the respiratory system.

An obvious limitation of this study was in the number of simultaneously recorded visceral parameters. It would be important to enlarge this list in the future in order to see whether other visceral systems also can be engaged in this coordinated process. The other omission is the inability to correlate these events to the activity of the brain structures closely involved in the regulation of these parameters and thus to find the origin of such stereotypically orchestrated changes of the visceral parameters.

In a cat observed for 3 years, the pattern of apnea episodes remained constant during this prolonged period. The age of the cats used in our study varied from 1 to 5 years, and episodes of central apnea were noted at all ages. These animals passed veterinary examinations and there were no indications on any pathological deviations in their health.

The recorded episodes of central sleep apnea had a characteristic pattern of coordinated changes occurring in several visceral systems. Namely, cardiac changes preceded the ones in breathing, and changes in breathing were frequently accompanied by stereotypical changes of gastrointestinal activity. What could be the functional role of such coordinated complex which exists only in sleep?

Our previous studies demonstrated that, during sleep, multiple cortical areas, which processed various exteroceptive signals during wakefulness, switch to processing of the interoceptive information [see, e.g., Pigarev (1994), Pigarev et al. (2013)]. Thus, the cerebral cortex becomes substantially visceral during sleep. We proposed that, during sleep, the cerebral cortex is engaged in a diagnostic of the visceral state of an organism and the restoration of the detected defects in various visceral systems. For that reason, the cerebral cortex receives and processes interoceptive signals during sleep (Pigarev, 2014; Pigarev and Pigareva, 2014, 2015).

Note that the observed complex activity during central apnea always starts from an increase of the heart rate. Together with simultaneous deep respiratory movements, the increased heart rate provides all tissues, first of all the brain, with a sufficient amount of oxygen. Only after that, respiration stops and the heart rate decreases, and the gastrointestinal motility slows down as well. We hypothesize that such simultaneous visceral "dying down" is necessary to synchronize the analysis of incoming visceral information in the brain, the information that normally represents organs of different rhythmicity. This mechanism can presumably achieve a similar result to the one existing in the visual system, namely, the saccadic suppression, when information processing is severely diminished during saccadic eye movements in order to achieve stability of visual perception (Benedetto and Morrone, 2017). A similar idea is used in stroboscopic methods of investigation of moving objects, e.g., in MRI investigations of the heart's structure, when scanning moments are synchronized with a particular phase of the heart cycle. In the case of central apnea, the heart strongly reduces its frequency in order to increase the time interval when it would be possible to get a reading of information from stable heart and respiratory systems. Other visceral systems, if necessary, join this process of total stabilization. The stabilization of the eyes also indicates a reduction of activity in the oculomotor cortical areas which, in line with the visceral theory of sleep (Pigarev, 2014), are also involved in the processing of visceral information during sleep and potentially capable of sending viscero-motor commands.

Our observations suggest that the selective elimination of sleep apnea might lead to health problems, potentially starting with the cardio-respiratory function but not limited to it. A strong increase of the heart rate before respiratory arrest potentially allows testing this assumption in a relatively simple experiment. Using a permanent automatic monitoring of the heart rate, it seems possible to detect increasing heart rate frequency and deliver some alarming stimulation to interrupt sleep and, consequently, respiratory arrest. A similar approach to heart rate monitoring is used in some automatic devices designed for vagus nerve stimulation because the heart rate was found to be increased before epileptic seizures in many cases. In epileptic patients, modern vagal stimulation devices detect increasing heart rate during sleep and switch on a stimulation of the vagus nerve to prevent the development of convulsive activity [see, e.g., Dibue-Adjei et al. (2019)]. Elimination of the entire visceral complexes accompanying the apnea episodes would allow assessing the possible consequences of this action for the health of the animals. However, considering that frequent awakening might have a negative effect by itself, it would be necessary to have a group of control animals that get the same alarming signals irrespective of the presence of apnea in their sleep. This approach is similar to the one successfully used in the disk-over-water experimental devices for a sleep deprivation research in the classical experiments conducted in the laboratory of Allan Rechtschaffen (Bergmann et al., 1989).

Within the frame of the proposed functional role of central sleep apnea, the increased number of these events may indicate potential health problems related to cardio-respiratory function. Attempts to eliminate central apneas by some artificial manipulations may lead to aggravation of the existing problems. In fact, the use of adaptive servo-ventilation to eliminate the respiratory influences of central apnea was found to be harmful rather than helpful in some cases, leading to increased mortality—mainly of sudden death related to arrhythmic events (Cowie et al., 2015), and a specific adaptive role of central apnea was suggested (Cowie, 2017). The increased number of sleep apnea episodes at high altitudes in healthy subjects (Mees and de la Chaux, 2009) also fits well to the assumption of the regulatory role of central apnea. The same logic explains the increased number of central sleep apnea episodes in the case of obesity or smoking (Block et al., 1979). We suggest that, during unexpected alteration of cardio-respiratory function, the brain needs information concerning the states of various organs in

order to develop a strategy for survival, and this can be realized during periods of central sleep apnea.

DATA AVAILABILITY STATEMENT

The datasets generated for this study are available on request to the corresponding author.

ETHICS STATEMENT

Ethical review and approval was not required for the animal study because surgery and day-to-day treatment of the animals were carried out in accordance with the ethical principles for the maintenance and use of animals in neuroscience research (Zimmermann, 1987), NIH guidelines for the care and use of animals and Declaration of Helsinki on Ethical Principles for Medical Research. Current Russian lows do not bind scientific institutes to have special ethic committees; instead, assessment of the research proposals is conducted by the Institutional Scientific Councils in the course of their discussion concerning providing financial support to a particular study. In foundations, distributing grants for scientific researches, ethic evaluation is done by Council of reviewers before a decision concerning financial support of a study. Both these councils in general are guided by the recommendations of the above-mentioned documents.

AUTHOR CONTRIBUTIONS

AL and IP contributed conception and design of the study, and collected the data. IB, AL, and IP performed operations. All authors analyzed the data, contributed to manuscript revision, and read and approved the submitted version. AL, IP, and EL wrote the first draft of the manuscript.

FUNDING

This study was partly supported by the Russian Foundation for Basic Research (grant no. 19-04-00215).

REFERENCES

Baillieul, S., Revol, B., Jullian-Desayes, I., Joyeux-Faure, M., Tamisier, R., and Pépin, J.-L. (2019). Diagnosis and management of central sleep apnea syndrome. *Expert Rev. Respir. Med.* 6, 545–557. doi: 10.1080/17476348.2019.104226

Benedetto, A., and Morrone, M. C. (2017). Saccadic suppression is embedded within extended oscillatory modulation of sensitivity. *J. Neurosci.* 37, 3661–3670. doi: 10.1523/jneurosci.2390-16.2016

Bergmann, B. M., Kushida, C. A., Everson, C. A., Gilliland, M. A., Obermeyer, W., and Rechtschaffen, A. (1989). Sleep deprivation in the rat: II. Methodology. *Sleep* 12, 5–12. doi: 10.1093/sleep/12.1.5

Block, A. J., Boysen, P. G., Wynne, J. W., and Hunt, L. A. (1979). Sleep apnea, hypopnea and oxygen desaturation in normal subjects — a strong male predominance. *N. Engl. J. Med.* 300, 513–517. doi: 10.1056/NEJM197903083001001

Contreras, D., and Steriade, M. (1996). Spindle oscillation in cats: the role of corticothalamic feedback in a thalamically generated rhythm. *J. Physiol.* 490, 159–179. doi: 10.1113/jphysiol.1996.sp021133

Costa, M., and Furness, J. B. (1982). "Nervous control of intestinal motility," in *Mediators and Drugs in Gastrointestinal Motility I. Handbook of Experimental Pharmacology (Contribution of Handbuch der Experimentallen Pharakologie*, ed. G. Bertaccini (Berlin: Springer), 279–382. doi: 10.1007/978-3-642-68437-1_10

Cowie, M. R. (2017). Sleep apnea: state of the art. *Trends Cardiovasc. Med.* 27, 280–289. doi: 10.1016/j.tcm.2016.12.005

Cowie, M. R., Woehrle, H., Wegscheider, K., Angermann, C., d'Ortho, M. P., Erdmann, E., et al. (2015). Adaptive servo-ventilation for central sleep apnea in systolic heart failure. *N. Engl. J. Med.* 2015, 1095–1105. doi: 10.1056/nejmoa1506459

Davis, E. M., and O'Donnell, C. P. (2013). Rodent models of sleep apnea. *Respir. Physiol. Neurobiol.* 188, 355–361. doi: 10.1016/j.resp.2013.05.022

Destexhe, A., Contreras, D., and Steriade, M. (1999). Cortically-induced coherence of a thalamic-generated oscilation. *Neuroscience* 92, 427–443. doi: 10.1016/s0306-4522(99)00024-x

Dibue-Adjei, M., Brigo, F., Yamamoto, T., Vonck, K., and Trinka, E. (2019). Vagus nerve stimulation in refractory and super-refractory status epilepticus -a systematic review. *Brain Stimul.* 12, 1101–1110. doi: 10.1016/j.brs.2019.05.011

Eckert, D. J., Jordan, A. S., Merchia, P., and Malhotra, A. (2007). Central sleep apnea: pathophysiology and treatment. *Chest* 131, 595–607.

Gay, P. C. (2008). Complex sleep apnea: it really is a disease. *J. Clin. Sleep Med.* 4, 403–405. doi: 10.5664/jcsm.27272

Hernandez, A. B., and Patil, S. P. (2016). Pathophysiology of central sleep apneas. *Sleep Breath.* 20, 467–482. doi: 10.1007/s11325-015-1290-z

Javaheri, S., Barbe, F., Campos-Rodriguez, F., Dempsey, J. A., Khayat, R., Javaheri, S., et al. (2017). Sleep apnea types, mechanisms, and clinical cardiovascular consequences. *J. Am. Coll. Cardiol.* 69, 841–858. doi: 10.1016/j.jacc.2016.11.069

Limanskaya, A. V. (2019). Visceral complex of central sleep apnea in cats. *Sleep Med.* 64:S227.

Malhotra, A., Bertisch, S., and Wellman, A. (2008). Complex sleep apnea: it isn't really a disease. *J Clin. Sleep Med.* 4, 406–408. doi: 10.5664/jcsm.27273

Martinez-de-Juan, J. L., Saiz, J., Meseguer, M., and Ponce, J. L. (2000). Small bowel motility: relationship between smooth muscle contraction and electroenterogram signal. *Med. Eng. Phys.* 22, 189–199. doi: 10.1016/s1350-4533(00)00032-1

McGinty, D. J., London, M. S., Baker, T. L., Stevenson, M., Hoppenbrouwers, T., Harper, R. M., et al. (1979). Sleep apnea in normal kittens. *Sleep* 1, 393–412.

Mees, K., and de la Chaux, R. (2009). Polygraphy of sleep at altitudes between 5300 m and 7500 m during an expedition to Mt. Everest (MedEx 2006). *Wilderness Environ. Med.* 20, 161–165. doi: 10.1580/08-weme-br-187r2.1

Nakamura, A., Fukuda, Y., and Kuwaki, T. (2003). Sleep apnea and effect of chemostimulation on breathing instability in mice. *J. Appl. Physiol.* 94, 525–532. doi: 10.1152/japplphysiol.00226.2002

Noda, H., Freeman, R. B., Gies, B., and Creutzfeldt, O. D. (1971). Neural responses in the visual cortex of awake cats to stationary and moving targets. *Exp. Brain Res.* 12, 389–405. doi: 10.1007/bf00234494

Papasova, M., Boev, K., Milenov, K., and Atanasova, E. (1966b). Mechanical and bio-electrical activity of the stomach wall. *Izv. Inst. Fiziol.* 10, 15–24.

Papasova, M., Boev, K., Milenov, K., and Atanasova, E. (1966a). Dependence between the appearence of spike-potentials in the electrogastrogram and the intensity of the contraction wave of the gastric wall. *Comptes Rend Acad. Bulg. Sci.* 19, 241–250.

Papasova, M., and Milenov, K. (1965). Method for biopotential recordings from stomach muscles of cats with chronically implanted electrodes. *Izv. Inst. Phisiol. BAN* 9, 187–195.

Pigarev, I. N. (1994). Neurons of visual cortex respond to visceral stimulation during slow wave sleep. *Neuroscience* 62, 1237–1243. doi: 10.1016/0306-4522(94)90355-7

Pigarev, I. N. (2014). The visceral theory of sleep. *Neurosci. Behav. Physiol.* 44, 421–434. doi: 10.1007/s11055-014-9928-z

Pigarev, I. N., Bagaev, V. A., Levichkina, E. V., Fedorov, G. O., and Busigina, I. I. (2013). Cortical visual areas process intestinal information during slow-wave sleep. *Neurogastroenterol. Motil.* 25, 268–275. doi: 10.1111/nmo.12052

Pigarev, I. N., Bibikov, N. G., and Busygina, I. I. (2016). Changes in the intragastric environment during sleep affect the statistical characteristics of neuron activity in the cerebral cortex. *Neurosci. Behav. Physiol.* 46, 64–72. doi: 10.1007/s11055-015-0199-0

Pigarev, I. N., and Pigareva, M. L. (2014). Partial sleep in the context of augmentation of brain function. *Front. Syst. Neurosci.* 8:75. doi: 10.3389/fnsys.2014.00075

Pigarev, I. N., and Pigareva, M. L. (2015). The state of sleep and the current brain paradigm. *Front. Syst. Neurosci.* 9:139. doi: 10.3389/fnsys.2015.00139

Pigarev, I. N., Saalmann, Y. B., and Vidyasagar, T. R. (2009). A minimally invasive and reversible system for chronic recordings from multiple brain sites in macaque monkeys. *J. Neurosci. Methods* 181, 151–158. doi: 10.1016/j.jneumeth.2009.04.024

Sarna, S. K. (1989). "In vivo myoelectric activity: methods, analysis, and interpretation," in *Supplement 16: Handbook of Physiology, The Gastrointestinal System, Motility and Cyrculation*, eds S. G. Schultz and J. D. Wood (Oxford: Oxford University Press), 817–834.

Sato, T., Saito, H., Seto, K., and Takatsuji, H. (1990). Sleep apneas and cardiac arrhythmias in freely moving rats. *Am. J. Physiol.* 259, R282–R287.

Zimmermann, M. (1987). Ethical Principles for maintenance and use of animals in neuroscience research. *Neurosci. Lett.* 73:1. doi: 10.1016/0304-3940(87)90020-6

Conflict of Interest: The authors declare that the research was conducted in the absence of any commercial or financial relationships that could be construed as a potential conflict of interest.

frontiers in Physiology

BRIEF RESEARCH REPORT
published: 30 June 2020
doi: 10.3389/fphys.2020.00630

Effect of Acute Hypoxia on Cardiorespiratory Coherence in Male Runners

Dmitriy Yu Uryumtsev, Valentina V. Gultyaeva, Margarita I. Zinchenko, Victor I. Baranov, Vladimir N. Melnikov, Natalia V. Balioz and Sergey G. Krivoschekov*

Laboratory of Functional Reserves of Organism, Scientific Research Institute of Physiology and Basic Medicine, Novosibirsk, Russia

Understanding the mechanisms of oxygen supply regulation, which involves the respiratory and cardiovascular systems, during human adaptation to intense physical activity, accompanied by hypoxemia, is important for the management of a training process. The objectives of this study were to investigate the cardiorespiratory coherence (CRC) changes in the low-frequency band in response to hypoxic exposure and to verify a dependence of these changes upon sports qualification level in athletes. Twenty male runners aged 17–25 years were exposed to acute normobaric hypoxia (10% O_2) for 10 min. Respiration, gas exchange, and heart rate were measured at baseline, during hypoxia, and after the exposure. To evaluate cardiorespiratory coupling, squared coherence was calculated based on 5-s averaged time series of heart and respiratory rhythms. Based on sports qualification level achieved over 4 years after the experimental testing, athletes were retrospectively divided into two groups, one high level (HLG, n = 10) and the other middle level (MLG, n = 10). No differences in anthropometric traits were observed between the groups. In the pooled group, acute hypoxia significantly increased CRC at frequencies 0.030–0.045 Hz and 0.075 Hz. In response to hypoxia, oxygen consumption decreased in HLG, and carbon dioxide production and ventilation increased in MLG. At 0.070–0.080 Hz frequencies in hypoxia, the CRC in HLG was higher than in MLG. Thus, highly qualified athletes enhance intersystem integration in response to hypoxia. This finding can be a physiological sign for the prognosis of qualification level in runners.

Keywords: athletes, hypoxia, cardiorespiratory coupling, squared coherence, cross-spectral analysis, heart rate, training

OPEN ACCESS

Edited by:
Tijana Bojić,
University of Belgrade, Serbia

Reviewed by:
Andreas Voss,
Institut für Innovative Gesundheitstechnologien (IGHT), Germany
Maximilian Moser,
Medical University of Graz, Austria

****Correspondence:***
Valentina V. Gultyaeva
gultyaevavv@physiol.ru

Specialty section:
This article was submitted to Autonomic Neuroscience, a section of the journal Frontiers in Physiology

Received: *26 December 2019*
Accepted: *18 May 2020*
Published: *30 June 2020*

Citation:
Uryumtsev DY, Gultyaeva VV, Zinchenko MI, Baranov VI, Melnikov VN, Balioz NV and Krivoschekov SG (2020) Effect of Acute Hypoxia on Cardiorespiratory Coherence in Male Runners. Front. Physiol. 11:630. doi: 10.3389/fphys.2020.00630

INTRODUCTION

At rest and during sleep, the coupling of the cardiovascular and respiratory systems manifests as respiratory sinus arrhythmia (RSA) and cardiorespiratory phase synchronization (clustering of heartbeats within each respiratory cycle) (Moser et al., 1995; Kralemann et al., 2013; Bartsch et al., 2014). When metabolic demand increases, the phase regulatory system is inhibited (review:

Hayano and Yuda, 2019). Stress tests from a battery of Ewing tests (handgrip static load and tilt test) have been shown to lead to the disappearance of intersystem phase synchronization (Sobiech et al., 2017). However, while moderate hypoxia does not change RSA, hypercapnic stress increases RSA amplitude in line with heart rate (HR) (Tzeng et al., 2007; Brown et al., 2014) and declines with increasing hypoxia in dogs (Yasuma and Hayano, 2000). Other work suggests that orthostatic challenge and cognitive load enhance the role of the baroreflex-mediated cardiorespiratory interaction (Krohova et al., 2018). Since the effect of baroreflex is demonstrated in the low-frequency (LF) band, it seems reasonable to suspect that stress induces a rise in cardiorespiratory coupling in a lower frequency range rather than in the range characterizing vagal tone.

Early data suggest that physical training changes patterns of cardiorespiratory interaction. Mlynczak and Krysztofiak (2019) used a Granger causality framework that parameterized cardiorespiratory causal link structures and directions to distinguish athletes from non-athletes at rest with 83% accuracy. Increased cardiorespiratory coordination after training has also been shown (Balagué et al., 2016). Training leads to a decrease in the number of principal components in cardiorespiratory response to acute physical exercise. For example, cardiovascular and respiratory responses to incremental cycling testing, which in most healthy individuals have two components, are simplified to one component after 6 weeks of aerobic and resistance training in more than half of the subjects (Balagué et al., 2016). *Prima facie* then, training appears to increase coordination among systems.

Since the integrating factor for the respiratory and cardiovascular anatomical systems is the oxygen supply, acute hypoxia provides an appropriate paradigm within which to assess how the integration between systems changes across physical training. We have previously demonstrated that the magnitude of the relationship between the hypoxic responses of the systems depends on the kind of sport and the athlete's qualification level (Divert et al., 2015, 2017). In contrast to less experienced swimmers, for example, high-level swimmers show high intra-group correlations between cardiorespiratory indices in response to acute hypoxia and hypercapnia (Divert et al., 2017). Similarly, among ski racers, the highest results are achieved in the case of highly correlating chemoreflex responses of the respiratory and heart systems, assessed in hypoxic and hypercapnic tests (Divert et al., 2015). Limiting these data is the fact that findings were obtained by calculating correlations among time-averaged values. Temporal coupling of heart and respiratory waves under hypoxic stress in athletes with different qualification levels remains unknown.

In many high-performance sports contexts, results depend substantially upon oxygen supply and its regulation. Good coordination between the cardiovascular and respiratory systems under conditions of hypoxia can increase the physical capacity and physiological reserves of energy exchange. In particular, improvements in the mechanisms underlying the complex regulation of gas exchange, manifested in greater cardiorespiratory coherence (CRC) in the LF band, can be expected in high-level athletes. Commensurately, the objectives of the present study were to investigate CRC LF changes in response to hypoxic exposure and to verify a dependence of these changes upon sports qualification level in athletes.

MATERIALS AND METHODS

Subjects

The study sample included 20 non-smoking middle-distance male runners aged 18–25 years. To complete the first objective, we analyzed the pooled group of athletes (n = 20). Based on sports qualification level achieved over 4 years after the hypoxic experimental testing, athletes were retrospectively divided into two groups, one high level (HLG, n = 10) and the other middle level (MLG, n = 10). We assigned those runners who had achieved the level of being a candidate for a master's degree to HLG, according to the Russian sports classification scale, and those who had not to the MLG. Anthropometric characteristics did not differ between the groups (**Table 1**). To complete the second objective, we analyzed the dependence of the coherence changes in response to hypoxic exposure taking into account the HLG and MLG classification. All subjects provided written informed consent prior to participation. The study was approved by the Ethics Committee of the Scientific Research Institute of Physiology and Basic Medicine (Protocol No. 1 of 21.01.2016) and performed in accordance with the Declaration of Helsinki.

Procedure

All investigations were performed in the morning by the same research assistant at an air temperature of 25°C in three functional states: at rest (baseline), during 10 min of breathing a hypoxic mixture with 10% O_2 content through a face mask, and during the 10 min of breathing the ambient air (recovery). The specific duration of stages varied depending on the physical well-being of the subjects (range 8–10 min). The testing was conducted in a sitting position. The hypoxic mixture was prepared using an Armed 7F-3L (Russia) oxygen concentrator.

Data Recording

A spiroergometric system, Oxycon Pro (Erich Jaeger, Germany), was used for recording the following respiratory parameters: breath rate (BR), carbon dioxide production (VCO2), oxygen consumption (VO2), and minute ventilation (VE). HR and blood oxygen saturation (SpO2) data were recorded by Pulse Oximeter BCI 3304 Autocorr (Smiths Medical, United States) and then automatically transferred to the Oxycon Pro. The Oxycon Pro software averaged data from the respiratory system and heartbeats and presented them at a maximum frequency of 0.2 Hz (period, 5 s).

TABLE 1 | Anthropometric characteristics of the subjects, Mean (SD).

Group	Height (cm)	Body weight (kg)	BMI (kg/m^2)
Pooled	180.7 (5.7)	68.7 (8.0)	21.1 (1.6)
HLG	179.4 (6.7)	68.8 (8.9)	21.5 (1.8)
MLG	181.9 (4.6)	68.5 (7.5)	20.6 (1.4)

Data Analysis

Data analysis was performed using the STATISTICA10 software package (StatSoft). To meet the criterion of stationarity, we visually identified non-stationary areas occurring just after the onset of hypoxia and recovery period (1.5–2 min) and removed these parts from the analysis. We marked the corresponding items "remove trend" and "subtract the mean from the input series" in the STATISTICA10 software settings. To evaluate cardiorespiratory interaction, squared coherence was calculated based on Time Series Bivariate Fourier (Cross Spectrum) analysis of heart and respiratory rhythms (hereafter referred to as coherence). To estimate the spectral density of HR and BR, a Hamming window with a width of 5 points was used. Missing data (4.9%) were replaced by averaging nearby time points. For the group analysis, individual coherence values were superimposed on the frequency grid in 0.005 Hz increments by linear interpolation.

To analyze the effect of the hypoxia on dependent variables (SpO2, HR, BR, VCO2, VO2, VE, coherence values at different frequencies), two-way Repeated Measures Analysis of Variance (ANOVA) was conducted. The between-subjects factor was Group (two categories, HLG and MLG), and the within-subject factor was State (baseline/hypoxia). The main effects and interaction between factors (Group and State) were tested, and Fisher LSD *post hoc* tests were employed. The inter-group differences in anthropometric indices were assessed by the Student *t*-test. For conclusions, p-values < 0.05 were accepted to reject null hypotheses. However, $p < 0.1$ is also indicated to show a tendency of statistical difference. The calculated data are presented in figures as means and standard errors (Mean, SE) and in the tables as means and standard deviations (Mean, SD).

RESULTS

Hypoxic Responses of Mean Values for Respiratory, Cardiac, and Gas Exchange Parameters

Overall, during hypoxia, oxygen saturation decreased by 21% and HR increased by 31%, but BR did not change significantly. Two-way repeated-measures ANOVA showed neither an effect of Group nor of Group × State on these parameters (**Table 2**). The reaction of gas exchange and pulmonary ventilation to hypoxia differed between groups. Oxygen consumption decreased only in HLG, and carbon dioxide production and minute ventilation increased only in MLG.

Cross-Spectral Analysis in the Pooled Group

At baseline, in the frequency range 0.025–0.045 Hz, a plateau zone is observed with a minimum coherence of approximately 0.23 and significantly higher coherence values at frequencies 0.050–0.070 Hz, with a group maximum value of 0.43 at a frequency of 0.060 Hz (LSD *post hoc*, $p < 0.001$). In hypoxia, the coherence values do not differ at all from the frequencies studied and are close to the above-mentioned maximum baseline level (**Figure 1**). At recovery, the coherence values are in an intermediate position between baseline and hypoxic values. Thus,

TABLE 2 | Respiratory, cardiac, and gas exchange parameters at baseline and during hypoxia.

		Baseline		Hypoxia		ANOVA, *p*		
Parameter	**Group**	**Mean**	**SD**	**Mean**	**SD**	**Group**	**State**	**Group × State**
SpO_2 (%)	Pooled	97.5	(1.1)	76.8	(6.1)		0.000	
	HLG	97.3	(0.9)	74.9	(7.6)	NS	0.000	NS
	MLG	97.8	(1.2)	78.7	(3.4)			
HR (beats × min^{-1})	Pooled	65.3	(9.0)	85.4	(11.4)		0.000	
	HLG	61.3	(8.9)	83.4	(15.2)	NS	0.000	NS
	MLG	69.2	(7.7)	87.4	(5.8)			
BR (breaths × min^{-1})	Pooled	13.5	(4.0)	14.0	(5.1)		NS	
	HLG	13.3	(4.1)	12.8	(3.4)	NS	NS	NS
	MLG	13.8	(4.1)	15.2	(6.2)			
VCO_2 (mL × min^{-1})	Pooled	236.2	(40.2)	266.5	(76.4)		0.044	
	HLG	243.6	(43.5)	244.9	(83.9)	NS	0.028	0.034
	MLG	228.8	(37.4)	288.1	(65.0)*			
VO_2 (mL × min^{-1})	Pooled	255.1	(35.8)	211.7	(59.0)		0.000	
	HLG	259.4	(35.2)	199.1	(68.7)*	NS	0.000	0.082
	MLG	250.8	(37.9)	224.3	(47.7)			
VE (L × min^{-1})	Pooled	10.3	(1.8)	12.2	(4.2)		0.026	
	HLG	10.4	(2,3)	10.8	(2.7)	NS	0.018	0.066
	MLG	10.2	(1,4)	13.6	(5.0)*			

*SpO_2, blood oxygen saturation; HR, heart rate; BR, breath rate; VCO_2, carbon dioxide production; VO_2, oxygen consumption; VE, ventilation; NS, non-significant; *significant difference between states at $p < 0.01$ (LSD post hoc) for the given group only.*

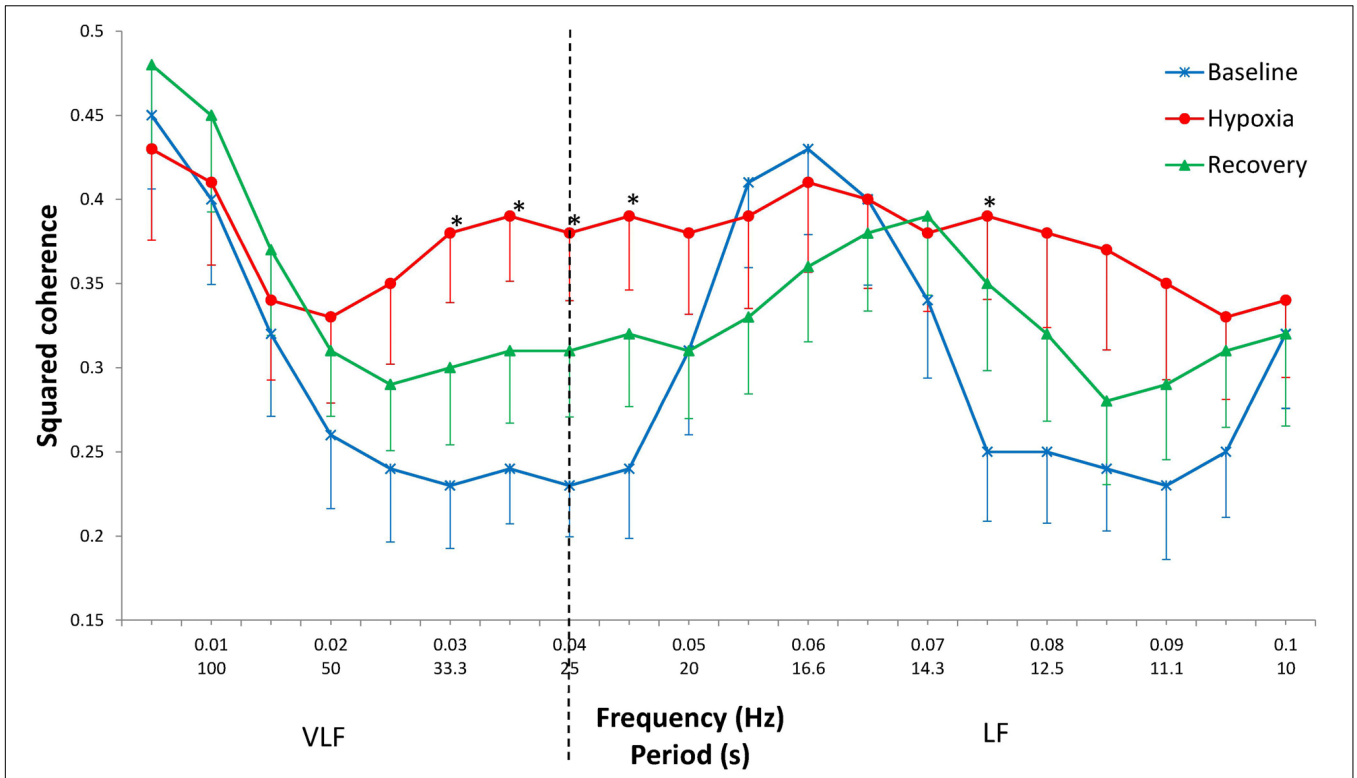

FIGURE 1 | Squared coherence between cardiac and respiratory rhythms by frequency at baseline, during hypoxia, and after hypoxia (recovery). Mean ± SE. *Significant difference between baseline and hypoxia ($p < 0.050$).

the subsequent statistical analysis was performed for two states only (baseline and hypoxia).

The increase in coherence during hypoxia in comparison with the baseline values is mostly evident at frequencies 0.030–0.045 Hz ($p < 0.050$) and at a frequency of 0.075 Hz ($p = 0.029$). In the range 0.080–0.090 Hz, the coherence tended to increase ($p = 0.053$–0.066).

Cross-Spectral Analysis in HLG and MLG

In response to hypoxia, the CRC in the 0.075–0.085 Hz range increases only in the HLG (interaction "Group × State," $p = 0.010$–0.021) (**Figure 2**). In the range of 0.070–0.080 Hz during hypoxia, coherence was significantly higher in HLG than in MLG ($p = 0.008$–0.023). At frequencies of 0.030–0.045 Hz, the coherence gain during hypoxia does not differ significantly between groups (State distinct effect $p = 0.001$–0.016; Group effect and Group × State interaction effect did not reach a borderline level of significance). No effects were established for State, Group, or their interaction effects over frequencies 0.015–0.025 Hz and 0.050–0.065 Hz.

DISCUSSION

The present study establishes two novel facts. First, at rest, the peak CRC in the low–very LF band is around 0.060 Hz; hypoxia enhances the coupling at frequencies 0.030–0.045 Hz and 0.075 Hz. The second fact concerns differences related to the degree of sports training (and by inference, fitness): the hypoxic coherence at 0.070–0.080 Hz frequencies in high-level runners is significantly higher than in middle-level athletes.

The difference between highly trained versus moderately trained runners in response to hypoxia was also expressed in different dynamics of gas exchange and ventilation. In HLG, oxygen consumption decreased, but minute ventilation and carbon dioxide production did not change. In MLG, ventilation and CO_2 production increased, whereas oxygen consumption did not change. Therefore, one can potentially conclude that high-level runners are characterized by reduced sensitivity to hypoxia. This allows them not to increase energy expenditure for the work of respiratory muscles. In the moderately trained group, however, there was an increase in ventilation, suggesting that the work of the muscles increased and, as a consequence, carbon dioxide production increased without total changes in oxygen consumption. It can be concluded that in more highly trained runners, there is a more economical mode of operation during hypoxia at physical rest. Increased CRC under hypoxic conditions probably plays a similar role: «Tuning and synchronization of rhythms saves energy» (Moser et al., 2006).

It has been shown previously that acute hypoxia causes an increase in sympathetic activity and an increase in sympatho-respiratory coupling in rodents (Dick et al., 2014). The enhanced

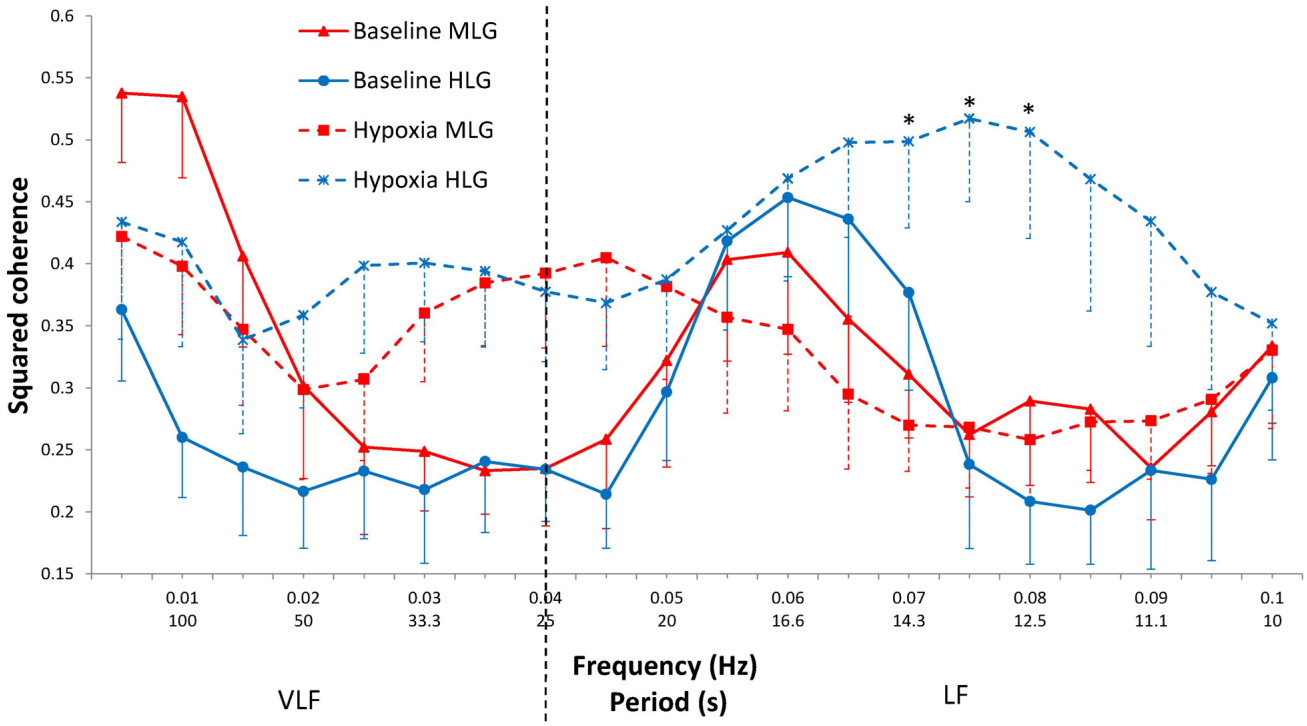

FIGURE 2 | Squared coherence between cardiac and respiratory rhythms by frequency at baseline (solid lines) and during hypoxia (dashed lines) in MLG (red) and HLG (blue). Mean ± SE. *significant difference between groups for the hypoxic state ($p < 0.030$).

respiratory-sympathetic coupling under these conditions is a result of synchronized activation of respiratory and sympathetic medullar neurons (Zoccal, 2015; Lindsey et al., 2018). In the present study, the growth of CRC at rest in normobaric hypoxia in humans is shown for the first time, and the prevailing frequencies at which it occurs were highlighted. The frequency component of HR variability, close to 0.076 Hz, is related to the baroreflex control of blood pressure (Kuusela et al., 2003). One can assume that an increase in CRC at this frequency is associated with an increase in the influence of baroreflex tuning in the heart and respiratory rhythms under the influence of hypoxia.

A physiological network is known to undergo topological transitions associated with rapid reorganization of interactions on time scales of several minutes (Bashan et al., 2012). It seems likely that higher coherence values during hypoxic stress in the more highly trained group are associated with a higher rate of network rearrangement. The 10-min hypoxia was sufficient for the athletes from this group to form new between-systems interactions, in contrast to less highly trained runners. Otherwise, one can assume that higher-level runners have developed more precisely coordinated responses to the exposure.

Mlynczak and Krysztofiak (2018, 2019) have studied cardiorespiratory links in sportsmen in normoxic conditions at rest by various mathematical non-linear methods. In the latest research, the authors were able to distinguish athletes from non-athletes with an accuracy of 83% on average. Platiša et al. (2019) have demonstrated modified neural control of heart-rate behavior in athletes compared with untrained subjects. In our study, runners differ in normoxia only in the qualification level, but we were able to demonstrate differences between moderately and highly trained runners in different reactions to hypoxic stress, reflected in greater coherence at frequencies of 0.07–0.08 Hz. It may be that greater training is reflected not only in changes in the mean values of cardiorespiratory parameters but also in alterations to the mechanisms that provide optimal (precise) settings of chemoreceptor reactions to developing hypoxemia. The less highly trained athletes may have cardiovascular and respiratory values similar to those in higher-skilled athletes at baseline, but the former may demonstrate less cardiorespiratory coupling at certain frequencies under conditions of hypoxia.

It has been shown earlier in our laboratory (Divert et al., 2015) that cardiorespiratory reactions to hypoxic and hypercapnic tests divide athletes into the clusters depending on the type of sports performance they are specialized in. This finding has initiated subsequent studies that led to the conclusion of a close, mutually substitutional relationship between respiratory and cardiovascular systems under hypoxic conditions (Melnikov et al., 2017). For example, it has been shown that the parameters of the training process and the features of the respiration pattern that appear as a consequence of training modulate the sensitivity of brain structures to hypoxia as reflected in changes in the EEG α-rhythm under conditions of hypoxia (Balioz and Krivoshchekov, 2012).

The results of the present study suggest that progressive training in sports performance improves the mechanisms of cardiorespiratory integration, which results in the optimization of response to changes in blood oxygen saturation. It seems likely that there are optimal zones of these interactions for each particular kind of sport. These zones can serve to identify athletes with prospects for a high qualification level.

Limitations

Since these are our first results showing the effect of acute hypoxia on CRC in humans, we cannot conclude definitely whether the associations observed are specific features of the runners or are peculiar to sportsmen of other types. The next limitation is associated with the low time resolution of the measured parameters and the possible transient nature of the investigated phenomena.

Further Considerations

In the future, we consider it appropriate to confirm these findings in more numerous groups and to investigate the effect of hypoxia on cardiorespiratory coupling in other sports types.

CONCLUSION

Highly qualified runners have improved mechanisms of intersystem integration through an increase in the accuracy of cardiorespiratory regulation. In hypoxia, the improvement manifests itself in the strengthening of CRC at frequencies 0.07–0.08 Hz. Strengthening cross-system integration provides optimal responses to hypoxic exposure and reflects the adaptive adjustment of the cardio-respiratory system in athletes during intense aerobic training. Such an increase in coupling between two systems, synergistically working on one function, can serve as an additional sign for the prognosis of qualification level in runners.

DATA AVAILABILITY STATEMENT

The datasets generated for this study are available on request to the corresponding author.

ETHICS STATEMENT

The studies involving human participants were reviewed and approved by the Ethics Committee of the Scientific Research Institute of Physiology and Basic Medicine. The patients/participants provided their written informed consent to participate in this study.

AUTHOR CONTRIBUTIONS

DU and SK conceptualized the research question and study design and supervised the entire project. DU and VB performed the data analysis. All authors interpreted the results. MZ and VG drafted the manuscript. VM edited the English text. VG, VM, NB, and DU critically reviewed and significantly contributed to the manuscript. All authors contributed to the article and approved the submitted version.

FUNDING

The study was supported by the Budgetary funding for basic scientific research (theme No. AAAA-A16-116021010227-3).

ACKNOWLEDGMENTS

We would like to thank Nathan Consedine (Auckland, New Zealand) for support in the translation of the manuscript.

REFERENCES

Balagué, N., González, J., Javierre, C., Hristovski, R., Aragonés, D., Álamo, J., et al. (2016). Cardiorespiratory coordination after training and detraining. A principal component analysis approach. *Front. Physiol.* 7:35. doi: 10.3389/fphys.2016.00035

Balioz, N. V., and Krivoshchekov, S. G. (2012). Individual typological features in the EEG of athletes after acute hypoxic treatment. *Hum. Physiol.* 38, 470–477. doi: 10.1134/S0362119712050027

Bartsch, R. P., Liu, K. K., Ma, Q. D., and Ivanov, P. C. (2014). Three independent forms of cardio-respiratory coupling: transitions across sleep stages. *Comput. Cardiol.* 41, 781–784.

Bashan, A., Bartsch, R. P., Kantelhardt, J. W., Havlin, S., and Ivanov, P. Ch (2012). Network physiology reveals relations between network topology and physiological function. *Nat. Commun.* 3:702. doi: 10.1038/ncomms1705

Brown, S. J., Barnes, M. J., and Mündel, T. (2014). Effects of hypoxia and hypercapnia on human HRV and respiratory sinus arrhythmia. *Acta Physiol. Hung.* 101, 263–272. doi: 10.1556/APhysiol.101.2014.3.1

Dick, T. E., Hsieh, Y. H., Dhingra, R. R., Baekey, D. M., Galan, R. F., Wehrwein, E., et al. (2014). Cardiorespiratory coupling: common rhythms in cardiac, sympathetic, and respiratory activities. *Prog. Brain Res.* 209, 191–205. doi: 10.1016/B978-0-444-63274-6.00010-2

Divert, V. E., Komlyagina, T. G., Krasnikova, N. V., Martynov, A. B., Timofeev, S. I., and Krivoschekov, S. G. (2017). Cardiorespiratory responses of swimmers to hypoxia and hypercapnia. *Novosibirsk State Pedagog. Univ. Bul.* 7, 207–224. doi: 10.15293/2226-3365.1705.14

Divert, V. E., Krivoshchekov, S. G., and Vodyanitsky, S. N. (2015). Individual-typological assessment of cardiorespiratory responses to hypoxia and hypercapnia in young healthy men. *Hum. Physiol.* 41, 166–174. doi: 10.3389/fphys.2019.0004510.1134/S036211971502005X

Hayano, J., and Yuda, E. (2019). Pitfalls of assessment of autonomic function by heart rate variability. *J. Physiol. Anthropol.* 38:3. doi: 10.1186/s40101-019-0193-2

Kralemann, B., Frühwirth, M., Pikovsky, A., Rosenblum, M., Kenner, T., Schaefer, J., et al. (2013). In vivo cardiac phase response curve elucidates human respiratory heart rate variability. *Nat. Commun.* 4:2418. doi: 10.1038/ncomms3418

Krohova, J., Czippelova, B., Turianikova, Z., Lazarova, Z., Wiszt, R., Javorka, M., et al. (2018). Information domain analysis of respiratory sinus arrhythmia mechanisms. *Physiol. Res.* 67(Suppl. 4), S611–S618. doi: 10.33549/physiolres.934049

Kuusela, T. A., Kaila, T. J., and Kähönen, M. (2003). Fine structure of the low-frequency spectra of heart rate and blood pressure. *BMC Physiol.* 3:11. doi: 10.1186/1472-6793-3-11

Lindsey, B. G., Nuding, S. C., Segers, L. S., and Morris, K. F. (2018). Carotid bodies and the integrated cardiorespiratory response to hypoxia. *Physiology* 33, 281–297. doi: 10.1152/physiol.00014.2018

Melnikov, V. N., Krivoschekov, S. G., Divert, V. E., Komlyagina, T. G., and Consedine, N. S. (2017). Baseline values of cardiovascular and respiratory parameters predict response to acute hypoxia in young healthy men. *Physiol. Res.* 66, 467–479. doi: 10.33549/physiolres.933328

Mlynczak, M., and Krysztofiak, H. (2018). Discovery of causal paths in cardiorespiratory parameters: a time-independent approach in elite athletes. *Front. Physiol.* 9:1455. doi: 10.3389/fphys.2018.01455

Mlynczak, M., and Krysztofiak, H. (2019). Cardiorespiratory temporal causal links and the differences by sport or lack thereof. *Front. Physiol.* 10:45. doi: 10.3389/fphys.2019.00045

Moser, M., Frühwirth, M., Penter, R., and Winker, R. (2006). Why life oscillates – from a topographical towards a functional chronobiology. *Cancer Causes Control* 17, 591–599. doi: 10.1007/s10552-006-0015-9

Moser, M., Lehofer, M., Hildebrandt, G., Voica, M., Egner, S., and Kenner, T. (1995). Phase and frequency coordination of cardiac and respiratory function. *Biol. Rhythm Res.* 26, 100–111. doi: 10.1080/09291019509360328

Platiša, M. M., Bojić, T., Mazić, S., and Kalauzi, A. (2019). Generalized Poincaré plots analysis of heart period dynamics in different physiological conditions: trained vs. untrained men. *PLoS One* 14:e0219281. doi: 10.1371/journal.pone.0219281

Sobiech, T., Buchner, T., Krzesinski, P., and Gielerak, G. (2017). Cardiorespiratory coupling in young healthy subjects. *Physiol. Meas.* 38:2186. doi: 10.1088/1361-6579/aa9693

Tzeng, Y. C., Larsen, P. D., and Galletly, D. C. (2007). Effects of hypercapnia and hypoxia on respiratory sinus arrhythmia in conscious humans during spontaneous respiration. *Am. J. Physiol. Heart Circ. Physiol.* 292, H2397–H2407. doi: 10.1152/ajpheart.00817.2006

Yasuma, F., and Hayano, J. (2000). Impact of acute hypoxia on heart rate and blood pressure variability in conscious dogs. *Am. J. Physiol. Heart. Circ. Physiol.* 279, H2344–H2349. doi: 10.1152/ajpheart.2000.279.5.H2344

Zoccal, D. B. (2015). Peripheral chemoreceptors and cardiorespiratory coupling: a link to sympatho-excitation. *Exp. Physiol.* 100, 143–148. doi: 10.1113/expphysiol.2014.079558

Conflict of Interest: The authors declare that the research was conducted in the absence of any commercial or financial relationships that could be construed as a potential conflict of interest.

frontiers in Neuroscience

BRIEF RESEARCH REPORT
published: 14 July 2020
doi: 10.3389/fnins.2020.00740

Vitamin B_{12} Supplementation and NT-proBNP Levels in COPD Patients: A Secondary Analysis of a Randomized and Controlled Study in Rehabilitation

*Fernanda Viana Paulin, Leandro Steinhorst Goelzer and Paulo de Tarso Müller**

Laboratory of Respiratory Pathophysiology, Respiratory Division, Department of Medicine, Federal University of Mato Grosso do Sul, Campo Grande, Brazil

Purpose: There is evidence of complex interaction between vitamin B_{12} (vB_{12}) level, hyperhomocysteinemia (HyCy), and natriuretic peptide secretion. Exercise training could also modulate such interaction. In this secondary analysis of a Randomized Clinical Trial performed in a chronic obstructive pulmonary disease (COPD) rehabilitation setting, our primary objective was to investigate the interaction between vB_{12} supplementation, exercise training, and changes in NT-proBNP levels after 8 weeks of intervention. Secondary objectives were to explore the correlations between acute changes in NT-proBNP levels with (i) acute exercise and (ii) oxygen uptake ($V'O_2$) kinetics during rest-to-exercise transition.

Methods: Thirty-two subjects with COPD were randomized into four groups: Rehabilitation+vB_{12} (n = 8), Rehabilitation (n = 8), vB_{12} (n = 8), or Maltodextrin(n = 8). They were evaluated at baseline and after 8 weeks, during resting and immediately after maximal exercise constant work-rate tests (CWTs, Tlim), for NT-proBNP plasmatic levels.

Results: After interaction analysis, the supplementation with vB_{12} significantly changed the time course of NT-proBNP responses during treatment (p = 0.048). However, the final analysis could not support a significant change in NT-proBNP levels owing to high-intensity constant work-rate exercise (p-value $>$ 0.05). There was a statistically significant correlation between $V'O_2$ time constant and ΔNT-proBNP values (Tlim – rest) at baseline (p = 0.049) and 2 months later (p = 0.015), considering all subjects (n = 32).

Conclusion: We conclude that vB_{12} supplementation could modulate NT-proBNP secretion. Moreover, possibly, the slower the initial $V'O_2$ adjustments toward a steady-state during rest-to-exercise transitions, the more severe the ventricular chamber volume/pressure stress recruitment, expressed through higher NT-proBNP secretion in subjects with larger $V'O_2$ time constants, despite unchanged final acute exercise-induced neurohormone secretion.

Keywords: COPD, exercise training, hyperhomocysteinemia, natriuretic peptides, vitamin B_{12}

OPEN ACCESS

Edited by:
Tijana Bojić,
University of Belgrade, Serbia

Reviewed by:
Moacir Fernandes Godoy,
Faculty of Medicine of São José do Rio Preto, Brazil
Vlasta Bari,
IRCCS Policlinico San Donato, Italy

***Correspondence:**
Paulo de Tarso Müller
paulo.muller@ufms.br

Specialty section:
This article was submitted to Autonomic Neuroscience, a section of the journal Frontiers in Neuroscience

Received: *09 January 2020*
Accepted: *23 June 2020*
Published: *14 July 2020*

Citation:
Paulin FV, Goelzer LS and Müller PT (2020) Vitamin B_{12} Supplementation and NT-proBNP Levels in COPD Patients: A Secondary Analysis of a Randomized and Controlled Study in Rehabilitation. Front. Neurosci. 14:740. doi: 10.3389/fnins.2020.00740

INTRODUCTION

In a recent Randomized Controlled Trial (RCT), we showed a slight but significant increase in maximal exercise tolerance (*T*lim) in patients with chronic obstructive pulmonary disease (COPD) supplemented with vitamin B_{12} during physical training, but without effects on oxygen uptake ($V'O_2$) kinetics beyond training alone (Paulin et al., 2017). Individuals with COPD are at risk of vitamin B_{12} deficiency (Solomon, 2016) and hyperhomocysteinemia (HyCy) (Seemungal et al., 2007; Fimognari et al., 2009). Accordingly, HyCy is linked to numerous cardiovascular alteration (Ganguly and Alam, 2015) including histological changes in the heart (Piquereau et al., 2017), impaired global and segmental cardiac contractility (Kaya et al., 2014), or increased N-terminal-pro-B-type natriuretic peptide (NT-proBNP) secretion (Herrmann et al., 2007; Guéant Rodriguez et al., 2013). This prepropeptide is synthesized and stored as a high molecular weight mass propeptide from both the atria and ventricles, and released mainly under pressure/volume overload of the cardiac chambers, after cleavage of the active form of BNP, inducing natriuresis and vasodilatation (Calzetta et al., 2016). However, NT-proBNP has a longer plasma half-life and attains larger concentrations, besides being described as a significant marker of prognosis in heart failure (HF) (Cipriano et al., 2014). Moreover, vitamin B_{12} or folic acid supplementation reduced NT-proBNP levels after 2 months of supplementation in subjects with NT-proBNP > 40 pg/mL (Herrmann et al., 2007), mitigated HyCy-induced cardiac dysfunction (Jeremic et al., 2018), and proved to be protective for mitochondrial function and cardiac contractile properties in a murine model, with lessening of upregulated atrial brain natriuretic peptide (ANP) (Piquereau et al., 2017). In contrast, an experimental study was negative for cardiac morphological alterations during HyCy induction (Taban-Shomal et al., 2009).

It is recognized that physical training causes a reduction in cardiac natriuretic peptides in HF (Cipriano et al., 2014) as well as which, a beneficial interaction between physical training and vitamin B_{12} or folate supplementation in reducing HyCy has been suggested (König et al., 2003; Tyagi and Joshua, 2014). Of note, there is evidence of increased secretion of BNP associated with increased pulmonary vascular resistance during acute exercise in COPD (Fujii et al., 1999); a mechanism which demonstrates potential for attenuation through physical training. Thus, this secondary analysis aims primarily to explore the interaction between vitamin B_{12} supplementation, physical training, and resting/exercise levels for NT-proBNP in a stable population of COPD patients. In addition, we sought to analyze possible associations between acute changes in NT-proBNP levels during exercise with *T*lim, delivered power (watts, w), and oxygen uptake kinetics ($V'O_2$ time constant) on an ergometer, in order to explore the determinants of these possible changes.The central hypothesis was that there would be attenuation of neurohormone alterations with supplementation alone or combined with physical training.

MATERIALS AND METHODS

As this is a secondary study of an already published RCT, the entire methodology has been previously described in detail (Paulin et al., 2017). Similarly, ethical considerations and consent details are published and recorded in the Brasilian Clinical Trials Registry (ReBEC number RBR-55f97c/2014). Additional unpublished methods will be considered in this exploratory study.

Participants and Study Design

In the final analysis, 32 stable COPD patients were consecutively randomized to four groups: (1) 8-weeks physical rehabilitation (REHA) group, (2) 8-weeks physical rehabilitation group with daily vitamin B_{12} supplementation of 500 mg (REHA+B_{12}), (3) supplementation group as stand-alone with daily vitamin B_{12} supplementation of 500 mg (B_{12}), and (4) placebo group (maltodextrin 500 mg) (P). All groups continued with their usual optimized pharmacological treatment for COPD. Among the subjects who completed the study, 28/32 were already being followed up at the specialized COPD clinic and had an echocardiogram performed within the previous 6 months. Mild mitral or aortic reflux and ventricular hypertrophy were accepted in the inclusion criteria. Patient history and further detailed physical examinations did not show signs of associated heart disease in the remaining subjects recruited without echocardiography.

Standard Doppler Echocardiography

All transthoracic echocardiography followed standard guidelines (Lang et al., 2005). Measurements of the cardiac cavities, interventricular septum, and left ventricular posterior wall thickness were collected by M-mode and two-dimensional analysis. Left atrial volume used the biplane Simpson method and was indexed by body surface. The ejection fraction was measured by the Teichholz method. The tricuspid reflux velocity was obtained by continuous Doppler in the right ventricle inlet, and the sPAP value was calculated by adding 10 mmHg of pressure in the right atrium.

Cardiopulmonary Exercise Testing (CPET)

All subjects were invited to perform an incremental cardiopulmonary exercise testing (CPET) and two equal constant work-rate tests (CWTs, 75% of the maximum incremental CPET load) to calculate time constants (*tau*, τ) for $V'O_2$ during the rest-to-exercise transition. Detailed CWT methods and oxygen uptake kinetics analysis were previously published (Paulin et al., 2017; Müller et al., 2019). Blood samples were collected at rest and *T*lim during the first CWT, before and after 8 weeks, for NT-proBNP plasmatic level analysis (**Figure 1**).

NT-proBNP Analysis

After a suitable rest period, before the CWT, a polyurethane 22G catheter (Injex-Cath, Ourinhos, Brazil) was inserted on the back of the patient's right hand for venous blood sample

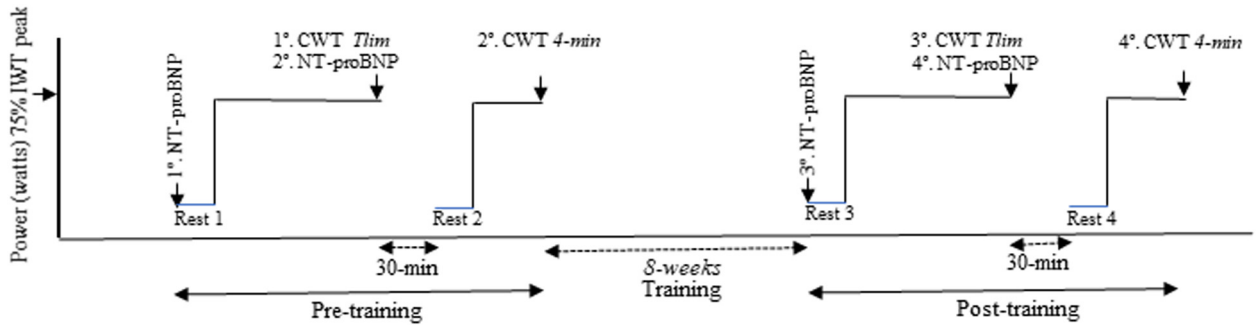

FIGURE 1 | Exercise protocol during constant work test (CWT) before and after 8 weeks.

TABLE 1 | Selected baseline clinical and physiological characteristic of the four groups of COPD patients.

	REHA+B_{12}	REHA+P	B_{12}	P	*p*-value
Subjects, n	8	8	8	8	1.000
Antropometry					
Age (years)	56.5 ± 5.0	65.2 ± 6.0	63.4 ± 5.2	58.1 ± 10.3	0.156
Gender (M/F)	3/5	3/5	5/3	5/3	0.289
BMI (kg/m^2)	24.5 ± 2.9	25.1 ± 6.0	24.5 ± 4.0	28.3 ± 5.5	0.332
Lung function					
FVC, % pred	65.2 ± 16.0	72.2 ± 10.0	66.0 ± 13.0	73.0 ± 13.1	0.534
FEV_1, % pred	34.0 ± 11.0	39.2 ± 6.8	32.8 ± 7.6	41.7 ± 12.3	0.235
FEV_1/FVC, %	40.7 ± 10.4	43.5±9.2	41.2±11.4	44.9±6.8	0.695
PaO_2, mmHg, rest	66.2 ± 9.3	73.8 ± 9.1	76.4 ± 16.0	75.5 ± 7.6	0.348
CPET data					
$V'O_{2peak}$, % pred	50.5 ± 16.1	65.1 ± 17.7	68.8 ± 18.2	64.7 ± 18.2	0.191
W_{peak}, % pred	43.6 ± 12.4	46.8 ± 13.1	34.7 ± 12.0	43.1 ± 15.2	0.324
T_{lim}, s	410 ± 311	314 ± 230	259 ± 110*	436 ± 143	**0.041**
τ, s	65 ± 37	84 ± 39	69 ± 22	69 ± 25	0.617
k, 10^{-3}/*s*	17.7 ± 7.1	13.1 ± 6.2	14.3 ± 4.5	15.7 ± 4.4	0.443
Blood analysis					
Vitamin B12 (pre), pg/mL	385 ± 207	454 ± 309	451 ± 215	467 ± 114	0.877
Vitamin B12 (post), pg/mL	567 ± 227†	358 ± 177	544 ± 145	442 ± 204	0.148
ΔVitamin B12, pg/mL	182 ± 206	−71 ± 175	93 ± 262	−16 ± 103	0.060
Vitamin B12 < 300 pg/mL, *n*	3	4	3	1	0.340
Creatinine, mg%	0.8 ± 0.2	0.9 ± 0.2	0.8 ± 0.1	0.8 ± 0.1	0.314
Hematocrit, %	47 ± 3	46 ± 4	43 ± 5	43 ± 3	0.118
Hemoglobin, g %	15 ± 1	15 ± 1	14 ± 2	14 ± 1	0.102
Echocardiography					
LVM, g/m^2	156 ± 22	132 ± 21	108 ± 17	122 ± 35	0.332
EF, %	70 ± 3.8	66 ± 2.1	69 ± 4.8	65 ± 4.2	0.126
LA, mm	36 ± 1.4	37 ± 4.5	30 ± 1.2	31 ± 2.4	0.201
LVDD, mm	46 ± 2.1	49 ± 1.9	45 ± 2.1	44 ± 2.9	0.133
PAP, mmHg	32 ± 2.1	29 ± 1.7	32 ± 1.9	29 ± 2.3	0.070

*Abbreviations: BMI, body mass index; FVC, forced vital capacity; FEV_1, forced expiratory volume in 1 s; DL_{co}, carbon monoxide diffusion capacity; PaO_2, partial pressure of oxygen in arterial blood; $V'O_{2peak}$, peak oxygen consumption; T_{lim}, maximal tolerance exercise time; τ, time constant (tau); TD, time delay; k, rate of $V'O_2$ increase toward steady-state; LVM, left ventricular mass; EF, ejection fraction; LA, left atrium; LVDD, left ventricular diastolic diameter; PAP, pulmonary arterial pressure. *p < 0.05 B_{12} vs P; †p < 0.05 B_{12} pre vs B_{12} post (Group REHA+B_{12}). The Bold is only to highlight significant values, i.e, p-value < 0.05.*

collections at rest and during exercise. The material was collected in tubes containing a mixture of plasma-lithium, as recommended by the manufacturer, and incubated at -20°C for 30 min. The electrochemiluminescence sandwich immunoassay by COBAS e602® system (Roche Diagnostics, Germany) measurement method was used, with a measurement range of 5–35,000 pg/mL and predicted coefficient of variation < 3.1%.

Data Analysis and Statistics

Data are expressed as mean ± standard deviation (SD) or median (IQR), mirroring, respectively, Gaussian or non-Gaussian distribution after the Shapiro–Wilk test. As τ (time constant, *tau*)—representing the time to attain 63% of the steady-state $V'O_2$ during a CWT—demonstrates marked skewness, we performed a reciprocal transformation and used k ($k = 1/\tau$) instead of τ. In exponential growth, k is equal to the reciprocal of the time constant *tau*, i.e., $k = 1/\tau$ and *represents the rate of increase in* $V'O_2$ *toward a steady-state plateau. Hence, the faster the rate of adjustment (k) of* $V'O_2$ *toward the steady-state during rest-to-exercise constant work-rate exercise transitions, the lower the time constant tau*. Thus, we chose to perform Pearson product-moment coefficients for correlations using k, as k generates a more robust Gaussian distribution (Bland and Altman, 1996) and *would imply similarly to a plausible physiological significance, as we recently suggested* (Müller et al., 2019). The slopes of linear regression for pre- and post-training moments were compared with Univariate ANCOVA. In the temporal analysis of the effects of training and supplementation, we performed three-way repeated measures (RM) ANOVA with two between-subjects factors (training and supplementation) and four within-subjects RM (NT-proBNP level at rest/*T*lim at baseline and rest/*T*lim after 2 months), taking into account the sphericity standard and the Greenhouse-Geisser correction. In addition, one-way ANOVA for groups was performed for comparison of baseline characteristics and one-way RM ANOVA for time-dependent within-group NT-proBNP level changes. The calculated study power > 0.8, with an alpha risk of 0.05 (two-tailed), was calculated from the placebo Group with their respective SD differences. Thus, we considered the average within-subjects SD difference of 1 pg/mL for NT-proBNP and, two between-subjects factors, B_{12} and exercise, with measured SD of the difference of 103 pg/mL and 100 s, respectively, in a three-way RM ANOVA design. We defined a p-value < 0.05 as statistically significant. The statistical program

TABLE 2 | NT-proBNP levels during acute exercise (rest and *T*lim) evaluated at baseline and after 2 months of intervention.

Group	Test time				One-way RM ANOVA[1] *p*-value	Three-way RM ANOVA *p*-value
	Baseline		2 Months			
	Rest	*T*lim	Rest	*T*lim		
REHA+B_{12}	41.1 (25.8–77.1)	42.7 (23.7–82.3)	50.1 (30.1–64.1)	51.0 (30.2–69.4)	0.958	0.075
REHA+P	95.0 (43.9–140.4)	100.3 (45.2–146.8)	49.5 (21.8–157.1)	50.5 (25.9–157.0)	0.204	0.917
B_{12}	55.9 (41.1–121.8)	60.9 (43.7–126.8)	72.9 (40.8–134.7)	75.7 (47.6–133.2)	0.639	**0.048**
P	20.7 (18.8–111.6)	22.1 (20.1–118.2)	74.4 (21.9–175.1)	75.3 (25.2–177.6)	0.120	0.525
Average (min-max)	49.5 (27.9–123.3)	51.0 (24.2–130.4)	64.0 (27.8–99.4)	68.9 (29.7–105.0)	–	–
One-wayANOVA[2] *p*-value	0.090	0.127	0.400	0.372		

Abbreviations: REHA, rehabilitation; B_{12}, vitamin B_{12}; P, placebo; Tlim, time for maximal exercise tolerance. [1]within-subjects one-way RM ANOVA; [2]between-subjects one-way RM ANOVA. The Bold is only to highlight significant values, i.e, p-value < 0.05.

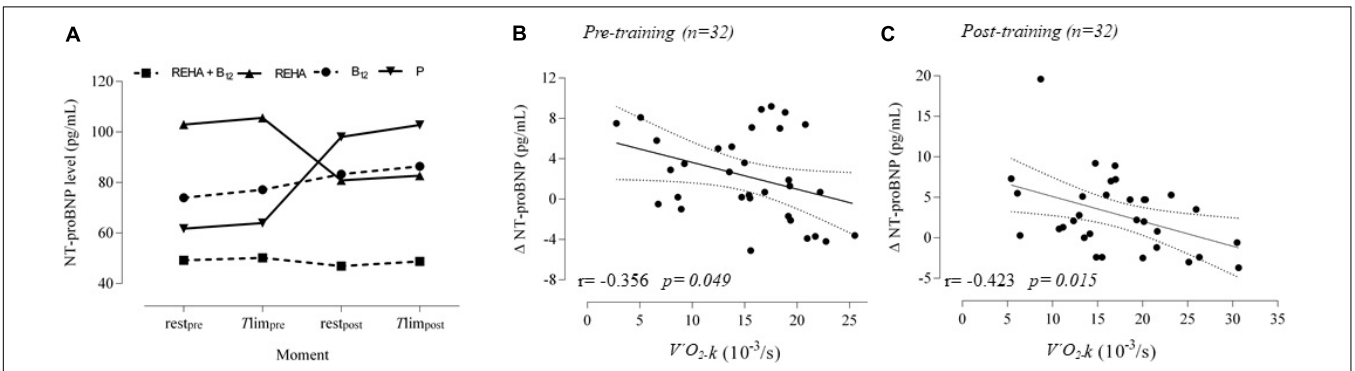

FIGURE 2 | NT-proBNP levels at rest and *T*lim, before and after 2 months. The time course is depicted in **(A)** (interrupted lines were constructed only to show the time course of NT-proBNP level under vitamin B12 influence compared to control groups). Correlations for acute responses (*T*lim – rest, Δ) *vs* individual time constant for $V'O_2$ (*k or 1/tau*) at baseline and 2 months later are represented in **(B)** and **(C)**. During the rest-to-exercise transition following constant work-rate exercise, there is an oxygen deficit that is inversely related to the rate of increase in$V'O_2$ (*k*) toward the steady-state condition.

SPSS 20.0 was used for all statistical analysis (SPSS, IBM Corp, United States, 2011).

RESULTS

Selected baseline characteristics are described in **Table 1** and detailed data have been previously published (Paulin et al., 2017). The groups were relatively balanced, with a significant difference only for *T*lim at baseline ($p = 0.041$, **Table 1**). Despite a similar baseline PaO_2, the groups as a whole ($n = 32$) presented significantly reduced hemoglobin saturation through peripheral oximetry post-exercise ($p < 0.0001$). After interaction analysis, the supplementation with vitamin B_{12} significantly changed the time course of NT-proBNP level during treatment ($p = 0.048$, **Table 2** and **Figure 2A**). In addition, the final analysis did not support a significant change in NT-proBNP levels owing to high-intensity constant work-rate exercise (three-way RM ANOVA analysis and one-way RM ANOVA analysis with *p*-value > 0.05 for both, **Table 2**). A statistically significant correlation was observed only between $V'O_2$ time constant and ΔNT-proBNP level (*T*lim – rest) at baseline ($p = 0.049$, **Figure 2B**) and 2 months later ($p = 0.015$, **Figure 2C**), considering all subjects ($n = 32$), with an absence of significant correlations between ΔNT-proBNP level and *T*lim or delivered Power on the cycle ergometer ($p > 0.05$ for both). The pre- and post-training slopes representing the correlation between the $V'O_2$ time constant and ΔNT-proBNP (**Figures 2B,C**) were not significantly different for the groups as a whole ($p = 0.259$).

DISCUSSION

This exploratory study suggests that B_{12} measurements and/or supplementation should be considered in future studies on cardiovascular morbidity in COPD subjects. This is in line with the overall pathophysiology of cardiovascular morbidity in COPD which has not yet been totally unraveled. In addition, we did not detect acute changes in plasma levels for NT-proBNP during high-intensity constant work-rate exercise. However, during the rest-to-exercise transition, patients with slower $V'O_2$ adjustments toward a steady-state appeared to secrete higher NT-proBNP levels.

Normal levels of vitamin B_{12} do not rule out the possibility of cobalamin deficiency, and *low-normal* levels (200–300 pg/mL), when associated with risk factors for increased oxidative stress, demonstrate metabolic evidence of deficiency, with high levels of HyCy or methylmalonic acid (MMA), since this vitamin is inactivated by oxidation (Solomon, 2016). Our study population contained at least three subjects in each group with levels < 300 pg/mL of vitamin B_{12} and supplementation significantly increased their levels after 8 weeks for the REHA+B_{12} group and not significantly for the B_{12} group (Paulin et al., 2017).

Several previously cited animal and human studies have described a relationship between vitamin B_{12} or folic acid level, HyCy, and NT-proBNP levels. Although preliminary, our study points to an attenuating effect on NT-proBNP secretion with vitamin B12 supplementation, in agreement with previous studies (Herrmann et al., 2007; Guéant Rodriguez et al., 2013), despite weak evidence. In monitoring the evolution of HF, attenuated or stable levels of NT-proBNP secretion were associated with fewer total cardiovascular events (Franke et al., 2011). Although the mechanisms underpinning this small but significant effect are largely unexplored, downregulation of natriuretic peptide production by reducing homocysteine and MMA accumulation under certain conditions is possible (Piquereau et al., 2017).

Two important secondary findings were described. Although we did not find an acute change in NT-proBNP owing to acute exercise during high-intensity CWT, there was a small but significant relationship between an acute change in this neurohormone (Δ) and oxygen uptake kinetics. Our study differs from a previous study, which showed increased secretion of BNP after exercise in a population similar to ours during CWT (Fujii et al., 1999). These contradictory results occurred despite both presenting significant hemoglobin desaturation during exercise. Arterial hypoxemia is a known trigger for natriuretic peptide secretion (Fujii et al., 1999). Surprisingly, our study agrees with another study for NT-proBNP also under CWT in mild-to-moderate COPD (Wang et al., 2011). Differences may reflect other factors, such as the secretion-to-metabolization ratio of natriuretic peptides and differences in exercise protocol. Our data suggest that much of the secretion of natriuretic peptides during CWT occurs at the time of initial adjustment during rest-to-exercise transitions, where the sudden change in the cardiac chamber pressure/volume condition is additionally stressed by the direct effect of transmural pressure, due to the abrupt increase in intrathoracic respiratory pressure swings, following the kinetics of the increase in pulmonary arterial pressure during the first minute and posterior decay during exercise (Lonsdorfer-Wolf et al., 2004). In this sense, our study is in agreement with a previous study that showed a direct relationship between BNP secretion and oxygen deficit during constant work-rate exercise in HF (Brunner-La Rocca et al., 1999).

As a limitation of this study, we cite the small number of individuals, notwithstanding this being partially tempered by the strong study design. In addition, we did not measure homocysteine and MMA levels. Four subjects were not evaluated by echocardiography; however, clinical data, NT-proBNP levels, and CPET analysis were not compatible with major heart disease.

CONCLUSION

We suggest that vitamin B_{12} supplementation could modulate NT-proBNP secretion, but the effects are small and further studies are needed. Moreover, we did not find an increase in neurohormone level caused by acute exercise *per se*; however, there was an association with slower $V'O_2$ adjustment during the rest-to-exercise transition. The significance of this neurohormone dynamic warrants more detailed studies, considering different modalities of exercise training,

e.g., high-intensity 1-min bouts, with unexplored cardiac neurohormone signaling and unknown cardiovascular consequences.

DATA AVAILABILITY STATEMENT

The datasets generated for this study are available on request to the corresponding author.

ETHICS STATEMENT

The studies involving human participants were reviewed and approved by the Human Research Ethics Committee, affiliated to Brazilian Clinical Trial Registry and Federal University of Mato Grosso Do Sul. The patients/participants provided their written informed consent to participate in this study.

AUTHOR CONTRIBUTIONS

PM contributed to study design, literature search, data collection, analysis of data, and manuscript preparation and review. FP contributed to literature search, data collection, analysis of data, and manuscript preparation and review. LG contributed to study design, literature search, data collection, analysis of data, and manuscript review. All authors contributed to the article and approved the submitted version.

FUNDING

This study was supported by Post-Graduate Program on Health and Development in West Central Region at Federal University of Mato Grosso do Sul (Brazil) and was financed in part by the Coordenação de Aperfeiçoamento de Pessoal de Nível Superior (CAPES), Brazil—Finance Code 001.

ACKNOWLEDGMENTS

The authors would like to thank the technical support team for their help during collection and processing of blood analysis for NT-proBNP.

REFERENCES

Bland, J. M., and Altman, D. G. (1996). Transforming data. *B.M.J.* 312:770.

Brunner-La Rocca, H. P., Weilenmann, D., Follath, F., Schlumpf, M., Rickli, H., Schalcher, C., et al. (1999). Oxygen uptake kinetics during low level exercise in patients with heart failure: relation to neurohormones, peak oxygen consumption, and clinical findings. *Heart* 81, 121–127. doi: 10.1136/hrt.81.2.121

Calzetta, L., Orlandi, A., Page, C., Paola, R., Barbara, R., Giuseppe, R., et al. (2016). Brain natriuretic peptide: much more than a biomarker. *Int. J. Cardiol.* 221, 1031–1038. doi: 10.1016/j.ijcard.2016.07.109

Cipriano, G., Cipriano, V. T., da Silva, V. Z., Cipriano, G. F., Chiappa, G. R., de Lima, A. C., et al. (2014). Aerobic exercise effect on prognostic markers for systolic heart failure patients: a systematic review and meta-analysis. *Heart Fail. Rev.* 19, 655–667. doi: 10.1007/s10741-013-9407-6

Fimognari, F. L., Loffredo, L., Di Simone, S., Sampietro, F., Pastorelli, R., Monaldo, M., et al. (2009). Hyperhomocysteinaemia and poor vitamin B status in chronic obstructive pulmonary disease. *Nutr. Metab. Cardiovasc. Dis.* 19, 654–659. doi: 10.1016/j.numecd.2008.12.006

Franke, J., Frankenstein, L., Schellberg, D., Bajrovic, A., Wolter, J. S., Ehlermann, P., et al. (2011). Is there an additional benefit of serial NT-proBNP measurements in patients with stable chronic heart failure receiving individually optimized therapy? *Clin. Res. Cardiol.* 100, 1059–1067. doi: 10.1007/s00392-011-0340-1

Fujii, T., Otsuka, T., Tanaka, S., Kanazawa, H., Hirata, K., Kohno, M., et al. (1999). Plasma endothelin-1 level in chronic obstructive pulmonary disease: relationship with natriuretic peptide. *Respiration* 66, 212–219. doi: 10.1159/000029380

Ganguly, P., and Alam, S. F. (2015). Role of homocysteine in the development of cardiovascular disease. *Nutr. J.* 14:6. doi: 10.1186/1475-2891-14-6

Guéant Rodriguez, R. M., Spada, R., Pooya, S., Jeannesson, E., Moreno Garcia, M. A., Anello, G., et al. (2013). Homocysteine predicts increased NT-pro-BNP through impaired fatty acid oxidation. *Int. J. Cardiol.* 167, 768–775. doi: 10.1016/j.ijcard.2012.03.047

Herrmann, M., Stanger, O., Paulweber, B., Hufnagl, C., and Herrmann, W. (2007). Effect of folate supplementation on N-terminal pro-brain natriuretic peptide. *Int. J. Cardiol.* 118, 267–269. doi: 10.1016/j.ijcard.2006.07.034

Jeremic, J., Nikolic Turnic, T., Zivkovic, V., Jeremic, N., Milosavljevic, I., Srejovic, I., et al. (2018). Vitamin B complex mitigates cardiac dysfunction in high-methionine diet-induced hyperhomocysteinemia. *Clin. Exp. Pharmacol. Physiol.* 45, 683–693. doi: 10.1111/1440-1681.12930

Kaya, Z., Bicer, A., Yalcin, F., Er, A., Camuzcuoglu, A., Korkmaz, N., et al. (2014). Impaired global and segmental myocardial deformation assessed by two-dimensional speckle tracking echocardiography in patients with vitamin B12 deficiency. *Cardiol. J.* 21, 60–66. doi: 10.5603/CJ.a2013.0059

König, D., Bissé, E., Deibert, P., Müller, H. M., Wieland, H., and Berg, A. (2003). Influence of training volume and acute physical exercise on the homocysteine levels in endurance-trained men: interactions with plasma folate and vitamin B12. *Ann. Nutr. Metab.* 47, 114–118. doi: 10.1159/000070032

Lang, R. M., Bierig, M., Devereux, R. B., Flachskampf, F. A., Foster, E., Pellikka, P. A., et al. (2005). Recommendations for chamber quantification: a report from the American Society of Echocardiography's Guidelines and Standards Committee and the Chamber Quantification Writing Group, developed in conjunction with the European Association of Echocardiography, a branch of the European Society of Cardiology. *J. Am. Soc. Echocardiogr.* 18, 1440–1463. doi: 10.1016/j.echo.2005.10.005

Lonsdorfer-Wolf, E., Bougault, V., Doutreleau, S., Charloux, A., Lonsdorfer, J., and Oswald-Mammosser, M. (2004). Intermittent exercise test in chronic obstructive pulmonary disease patients: how do the pulmonary hemodynamics adapt? *Med. Sci. Sports Exerc.* 36, 2032–2039. doi: 10.1249/01.mss.0000147631.59070.7d

Müller, P. T., Nogueira, J. Z., Augusto, T. R., and Chiappa, G. R. (2019). Faster oxygen uptake, heart rate and ventilatory kinetics in Stepping compared to cycle ergometry in COPD patients during moderate intensity exercise. *Appl. Physiol. Nutr. Metab.* 44, 879–885. doi: 10.1139/apnm-2018-0662

Paulin, F. V., Zagatto, A. M., Chiappa, G. R., and Müller, P. T. (2017). Addition of vitamin B12 to exercise training improves cycle ergometer endurance in advanced COPD patients: a randomized and controlled study. *Respir. Med.* 122, 23–29. doi: 10.1016/j.rmed.2016.11.015

Piquereau, J., Moulin, M., Zurlo, G., Mateo, P., Gressette, M., Paul, J. L., et al. (2017). Cobalamin and folate protect mitochondrial and contractile functions in a murine model of cardiac pressure overload. *J. Mol. Cell Cardiol.* 102, 34–44. doi: 10.1016/j.yjmcc.2016.11.010

Seemungal, T. A., Lun, J. C., Davis, G., Neblett, C., Chinyepi, N., Dookhan, C., et al. (2007). Plasma homocysteine is elevated in COPD patients and is related to COPD severity. *Int. J. Chron. Obstruct. Pulmon. Dis.* 2, 313–321. doi: 10.2147/copd.s2147

Solomon, L. R. (2016). Low cobalamin levels as predictors of cobalamin deficiency: importance of comorbidities associated with increased oxidative stress. *Am. J. Med.* 129, 115.e9–115.e16. doi: 10.1016/j.amjmed.2015.07.017

Taban-Shomal, O., Kilter, H., Wagner, A., Schorr, H., Umanskaya, N., Hübner, U., et al. (2009). The cardiac effects of prolonged vitamin B12 and folate deficiency in rats. *Cardiovasc. Toxicol.* 9, 95–102. doi: 10.1007/s12012-009-9038-2

Tyagi, S. C., and Joshua, I. G. (2014). Exercise and nutrition in myocardial matrix metabolism, remodeling, regeneration, epigenetics, microcirculation, and muscle. *Can. J. Physiol. Pharmacol.* 92, 521–523. doi: 10.1139/cjpp-2014-0197

Wang, H. Y., Xu, Q. F., Xiao, Y., Zhang, J., and Sperry, A. (2011). Cardiac response and N-terminal-pro-brain natriuretic peptide kinetics during exercise in patients with COPD. *Respir. Care* 56, 796–799. doi: 10.4187/respcare.00935a

Conflict of Interest: The authors declare that the research was conducted in the absence of any commercial or financial relationships that could be construed as a potential conflict of interest.

frontiers in Physiology

METHODS
published: 05 August 2020
doi: 10.3389/fphys.2020.00867

Cardiopulmonary Resonance Function and Indices—A Quantitative Measurement for Respiratory Sinus Arrhythmia

Jiajia Cui[1], *Zhipei Huang*[1]*, *Jiankang Wu*[1,2] *and Hong Jiang*[3]

[1] Sensor Networks and Application Research Center, School of Electronic, Electrical and Communication Engineering, University of Chinese Academy of Sciences, Beijing, China, [2] CAS Institute of Healthcare Technologies, Nanjing, China, [3] Department of Cardiology, Integrated Chinese and Western Medicine, China-Japan Friendship Hospital, Beijing, China

Respiratory sinus arrhythmia (RSA) represents a physiological phenomenon of cardiopulmonary interaction. It is known as a measure of efficiency of the circulation system, as well as a biomarker of cardiac vagal and well-being. In this article, RSA is modeled as modulation of heart rate by respiration in an interactive cardiopulmonary system with the most effective system state of resonance. By mathematically modeling of this modulation, we propose a quantitative measurement for RSA referred to as "Cardiopulmonary Resonance Function (CRF) and Cardiopulmonary Resonance Indices (CRI)," which are derived by disentanglement of the RR-intervals series into respiratory-modulation component, R-HRV, and the rest, NR-HRV using spectral G-causality. Evaluation of CRI performance in quantifying RSA has been conducted in the scenarios of paced breathing and in the different sleep stages. The preliminary experimental results have shown superior representation ability of CRF and CRI compared to Heart Rate Variability (HRV) and Cardiopulmonary Coupling index (CPC).

Keywords: heart rate variability, respiratory sinus arrhythmia, spectral G-causality, cardiopulmonary interaction, coupled resonance

OPEN ACCESS

Edited by:
Andreas Voss, Institut für Innovative Gesundheitstechnologien (IGHT), Germany

Reviewed by:
Antonio Roberto Zamunér, Catholic University of Maule, Chile
Valdo Jose Dias Da Silva, Universidade Federal do Triângulo Mineiro, Brazil

***Correspondence:**
Zhipei Huang
Zhphuang@ucas.ac.cn

Specialty section:
This article was submitted to Autonomic Neuroscience, a section of the journal Frontiers in Physiology

Received: *13 August 2019*
Accepted: *26 June 2020*
Published: *05 August 2020*

Citation:
Cui J, Huang Z, Wu J and Jiang H (2020) Cardiopulmonary Resonance Function and Indices—A Quantitative Measurement for Respiratory Sinus Arrhythmia. Front. Physiol. 11:867. doi: 10.3389/fphys.2020.00867

INTRODUCTION

There is an urgent need for quantitative assessment of autonomic nervous function. Heart rate variability (HRV) is widely used as a non-invasive method. Particularly, low-frequency (LF, 0.04–0.15 Hz) and high-frequency (HF, 0.15–0.4 Hz) spectral components of HRV are used as the separate metrics of sympathetic and vagal(parasympathetic) functions (Appel et al., 1989). But as a simplified framework, HRV lacks solid physiological foundation, is not able to accommodate varieties of clinical cases (Hayano and Yuda, 2019). For example, HRV measures will change significantly in different physiologic states such as wake and sleep, exercise and rest, circadian rhythms, as well as with pathologic conditions (Task Force of the European Society of Cardiology the North American Society of Pacing Electrophysiology, 1996).

Cardiopulmonary interaction plays important role in the circulation system, and physiologically presents as respiratory sinus arrhythmia (RSA) phenomenon. RSA is regarded as a non-invasive measure of parasympathetic cardiac control (Katona and Jih, 1975; Topcu et al., 2018). The vagal origin of RSA can be found in the vagal synapses, which are faster than the sympathetic ones and are therefore able to translate central respiratory oscillations present in the brainstem to changes of cardiac sinus node discharge rate, which is not capable for slow sympathetic synapses.

Tracking the autonomic regulation in RSA using the electrocardiogram and respiratory measurements is a feasible and important approach to gain our knowledge toward autonomic nervous system and its clinical applications.

The quantitative study of RSA has profound significance in physiology and pathology, as well as extensive clinical applications. Some studies have shown that RSA reaches a relatively stable state in deep sleep (Bernston et al., 1997) and a study of the hibernation of 37 polar bears in the University of Minnesota found that RSA reached their peak during the hibernation. At the same time, as a vagal inflammatory reflex was discovered (Tracey, 2002), quantification of the HRV components, which are not directly related to respiration, is important for the analysis of long-range and scaling properties of the cardiac dynamics (Ivanov et al., 1999; Schmitt and Ivanov, 2007). Examples of application of RSA analysis include clinical psychology (Wielgus et al., 2016), treatment of substance use disorder (Price and Crowell, 2016), prediction of the course of depression (Panaite et al., 2016), quantification of cardiac vagal tone and its relation to evolutionary and behavioral functions (Grossman and Taylor, 2007), quantification of vagal activity during stress in infants (Ritz et al., 2012), and even in cancer patients (Moser et al., 2006), to name just a few.

A variety of data analysis techniques quantifying RSA have been proposed in the literature, for a discussion of commonly used metrics and their advantages and drawbacks see, e.g. (Lewis et al., 2012). The techniques quantifying RSA can be divided into two categories, the time domain and the frequency domain. In time domain, continuous wavelet transform (WTC) is used for its advantage to analyze transient and non-linear signals. This method demonstrates the dynamic behavior of respiration sinus arrhythmia through the analysis of the WTC between heart rate and respiration signals (Jan et al., 2019). Phase analysis technique could help to disentangling respiratory sinus in heart rate variability records, but the final HRV index obtained by this technique is complex to calculate in time domain, and its physiological significance is not clear (Topcu et al., 2018). There are works which use respiratory and RR sequences to calculate G-causality and system gain as the measure of RSA. Much further work is needed to make these produced measures useful in clinical research and applications (Fonseca et al., 2013). In the frequency domain, HF of HRV indicators quantifies RSA on specific frequency bands, while Cardiopulmonary Coupling (CPC) measures the correlation between RR interval and respiratory sequence in the frequency domain. Both are empirical, without solid theoretical foundation and systematic design, therefore serious clinical applications are not seen so far (Thomas et al., 2005).

In the rest of this article, our contributions in developing quantitative measures for RSA are described as follows:

In section Cardiopulmonary Resonance Model (CRM), we model RSA as modulation of heart rate by respiration in an interactive cardiopulmonary system with the most effective system state of resonance. Mathematically, it is described by bivariate autoregressive model of respiration series and RR intervals, and quantitatively it is assessed by Granger causality function. The whole model is referred to as Cardiopulmonary Resonance Model (CRM).

In section Cardiopulmonary Resonance Indices (CRI), based on the cardiopulmonary resonance concept, and Granger causality function which is referred to as cardiopulmonary resonance function (CRF) after, a set of quantitative measures for RSA is proposed, and named as Cardiopulmonary Resonance Indices (CRI).

In section Applications Scenarios, to show the effectiveness of CRM and CRI, two application scenarios, paced breathing and sleep stage discrimination, are studied. It has been shown that CRF and CRI provide ideal visual interpretation and numerical measures for cardiopulmonary interactions toward resonance state in paced breathing scenario as the paced breathing rate coming down to 0.1 Hz. The same is true as the sleep stage moves to deep sleep.

CARDIOPULMONARY RESONANCE MODEL (CRM)

We are committed to building a cardiopulmonary resonance model for the purpose of quantitative assessment of RSA with hypothesis that cardiopulmonary interaction is important in circulation system to ensure efficient delivery of oxygen and nutrient, and that the efficiency is optimized at the state of cardiopulmonary resonance. Mathematically, we present a bivariate autoregressive model of respiration series and RR intervals, calculate respiratory and non-respiratory related component on RR intervals in the frequency domain using Granger-causality.

Bivariate Autoregressive Model of Respiration Series and RR Intervals

The cardiopulmonary interaction can be interpreted as functional connectivity analysis such as synchrony (Engel and Singer, 2001) and phase coherence (Nunez et al., 2001) and so on. Our model takes direct central respiratory modulation of the parasympathetic cardiac signal as the main mechanism for RSA. A powerful technique for extracting directed functional connectivity from data is Granger causality (G-causality) (Granger, 1969). According to G-causality, X_2causes X_1 if the inclusion of past observations of X_2 reduces the prediction error of X_1 in a linear regression model of X_1 and X_2, as compared to a model which includes only previous observations of X_1.

The change process of RR can be regarded as a Markov process, ignoring other factors affecting heart rate in short term, we described the RR intervals($X_1(t)$) and respiration signal($X_2(t)$) (both of length T) by a bivariate auto-regressive model:

$$X_1(t) = \sum_{j=1}^{p} A_{11,j} X_1(t-j) + \sum_{j=1}^{p} A_{12,j} X_2(t-j) + \xi_1(t)$$
$$X_2(t) = \sum_{j=1}^{p} A_{21,j} X_1(t-j) + \sum_{j=1}^{p} A_{22,j} X_2(t-j) + \xi_2(t)$$

where p is the maximum number of lagged observations included in the model (the model order, $p < \mathrm{T}$). A contains the coefficients of the model, and ξ_1, ξ_2 are the residuals for each time series.

In order to ensure RR intervals in the normal range and without a mutation, we use interpolation as a substitute for points that do not meet the following conditions:

$$|RRI_i - \overline{RRI}| < 1.5 * Std(RRI)$$
$$0.7 * RRI_{i-1} < RRI_i < 1.3 * RRI_{i-1}$$

where RRI is the RR intervals, $RRI_{i-1}$and RRI_i are adjacent intervals.

For each record around 120 s, under the assumption of stationary property of signals, and for efficiency of computation, we normalize the RR intervals and respiration series to zero-mean and unit variance. The magnitude of RSA can be measured by the log ratio of the prediction error variances for the restricted (R) and unrestricted (U) models:

$$G_{2\to 1} = \ln \frac{\mathrm{var}(\xi_{1R(12)})}{\mathrm{var}(\xi_{1U})}$$

where $\xi_{1R(12)}$ is derived from the model omitting the $A_{12,j}$(for all j) coefficients in the first equation and $\xi_{1U}$is derived from the full model.

The estimation of the model of each record requires as a parameter the number of time-lags (p) to include, i.e., the model order. A principle means to specify the model order is to minimize a criterion that balances the variance accounted for by the model, against the number of coefficients to be estimated. We chose the Akaike information criterion (Akaike, 1974) for n variables in which the $\sum$ denotes the noise covariance matrix:

$$AIC(p) = \ln(\det(\sum)) + \frac{2pn^2}{T}$$

Spectral G-causality of Respiration Series and RR Intervals

For the dynamics of the cardiopulmonary system are easier to understand and interpret in the frequency domain, we calculate the Spectral G-causality of respiration series and RR intervals.

The Fourier transform of the bivariate auto-regressive model in time domain gives:

$$\begin{pmatrix} A_{11}(f) & A_{12}(f) \\ A_{21}(f) & A_{22}(f) \end{pmatrix} \begin{pmatrix} X_1(f) \\ X_2(f) \end{pmatrix} = \begin{pmatrix} E_1(f) \\ E_2(f) \end{pmatrix}$$

in which the components of A are

$$A_{lm}(f) = \delta_{lm} - \sum_{j=1}^{p} A_{lm}(j) e^{(-i2\pi fj)},$$
$$\delta_{lm} = 0(l = m), \delta_{lm} = 1(l \neq m)$$

E is the Fourier transform of the residual matrix.

For the sake of calculation, we rewrite it as

$$\begin{pmatrix} X_1(f) \\ X_2(f) \end{pmatrix} = \begin{pmatrix} H_{11}(f) & H_{12}(f) \\ H_{21}(f) & H_{22}(f) \end{pmatrix} \begin{pmatrix} E_1(f) \\ E_2(f) \end{pmatrix}$$

where H is the transfer matrix. The spectral matrix S can now be derived as

$$S(f) = \langle X(f)X^*(f) \rangle = \left\langle H(f) \sum H^*(f) \right\rangle$$

in which the $\sum$ denotes the noise covariance matrix.

A split of U into sub-processes X and Y includes a decomposition

$$S(f) = \begin{pmatrix} S_{xx}(f) & S_{xy}(f) \\ S_{yx}(f) & S_{yy}(f) \end{pmatrix}$$

of the cross-power spectral density and a similar decomposition for the transfer function $H(f)$.
Then $S_{xx}(f)$ is the spectral density of X, which is given by

$$S_{xx}(f) = H_{xx}(f) \sum {}_{xx} H^*_{xx}(f) + 2\,\mathrm{Re}\{H_{xx}(f) \sum {}_{xy} H^*_{xy}(f)\} + H_{\mathrm{xy}}(f) \sum {}_{yy} H^*_{xy}(f)$$

Thus, we can get the Spectral G-causality of respiration series and RR intervals:

$$G_{Y\to X}(f) = \ln \left(\frac{|S_{xx}(f)|}{|S_{xx}(f) - H_{xy}(f) \sum {}_{y|x} H_{xy}(f)^*|} \right)$$

$$\sum {}_{y|x} \equiv \sum {}_{yy} - \sum {}_{yx} \sum {}^{-1}_{xx} \sum {}_{xy}$$

where $\sum$ denotes the residual covariance matrix.

For the non-respiratory components, we get:

$$G_{N-RESP}(f) = 1\text{-}G_{Y\to X}(f)$$

Now we have both the measurement of respiratory and the non-respiratory components effects on RR intervals in the frequency domain, R-HRV and NR-HRV, respectively. Here we focus on the spectral G-causality of respiration series and RR intervals, $G_{Y\to X}(f)$. For convenience, we simply write it as $G(f)$, and rename it as Cardiopulmonary Resonance Function (CRF) in the rest of this article.

CARDIOPULMONARY RESONANCE INDICES (CRI)

With cardiopulmonary resonance function (CRF), we are now able to establish a quantitative measurement for RSA, referred

to as Cardiopulmonary Resonance Indices (CRI), with the hope that it will be able to play a role in quantifying cardiopulmonary system efficiency, and as a biomarker for cardiac vagal tone and well-being, on the basis of CRF and key concept of cardiopulmonary resonance.

Figure 1A shows the power spectral curves of RR interval series and respiration series, as well as the corresponding cardiopulmonary resonance function, *G(f)*. *G(f)* represent the strength of RSA, the modulation of respiration to heart rate. *G(f)* is a monotonic function of frequency f with single peak around the main respiration frequency, can be considered as the spectral energy distribution function of cardiopulmonary resonance system. The cardiopulmonary resonance indices (CRI) consists of the following numerical measure:

A) Cardiopulmonary Resonance Amplitude (CRA) is defined as the maximum of Cardiopulmonary resonance function *G(f)*:

$$CRA \equiv MaxCRF$$

Refer to **Figure 1B**, in consideration of the main frequency bands of heart rate variability and respiration rate, *G(f)* is plotted in the frequency range of 0.0033–0.5 Hz. Denote the frequency where the maxima of *G(f)* appears as cardiopulmonary resonance frequency f_A. CRF is around main respiration rate.

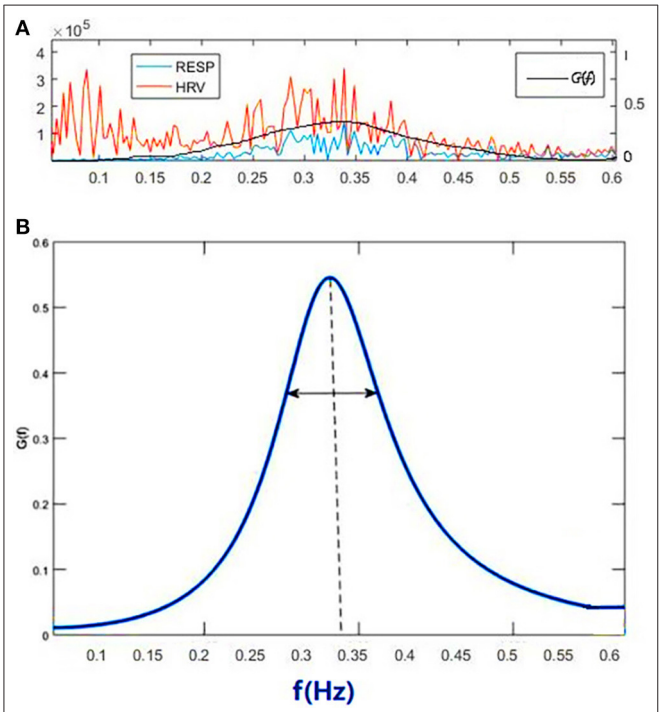

FIGURE 1 | Illustration of Cardiopulmonary Resonance Function (CRF) and Cardiopulmonary Resonance Indices (CRI). **(A)** the power spectral curves of RR interval series and respiration series, as well as the corresponding cardiopulmonary resonance function, *G(f)*. **(B)** the schematic diagram of CRA and CRW. CRA is taken from the maximum point of *G(f)* (CRF); CRW, the bandwidth of CRF as indicated by the bi-directional arrow line.

In free breathing, respiration rate is around 0.20–0.30 Hz, in the range of HRV high frequency. That is the point of consistence between HRV_HF measure and RSA strength in representing the regal level. As we will see in the next section paced breathing experiments, as paced breathing frequency down to 0.1 Hz, both RSA energy and HRV energy shall move and focus around 0.1 Hz as well. In this case, the hypothesis of HRV_HF representing regal activity may not hold.

B) Cardiopulmonary Resonance bandWidth (CRW). As shown in **Figure 1B**, CRW is defined as the CRF bandwidth, the degree of RSA energy concentration. CRA and CRW are related. While CRW is narrow, CRA is big.

C) Cardiopulmonary Resonance Quality factor (CRQ). CRQ is defined to measure the merit of the cardiopulmonary resonance system by adopting the quality factor measure for inductor, capacitor, and resistor LCR oscillator where interaction between lung and heart resemble the energy flow between inductor and capacitor, while non-respiration factors are equivalent to resistor, damping the resonance. Mathematically, CRQ is defined as

$$CRQ = \frac{f_A}{CRW}$$

Considering the physiological functions, RSA serves to minimize the energy expenditure of the heart while keeping arterial CO_2 levels at physiological tensions. CRQ measures the energy conversion of the system. The lower the dissipation energy, the higher the quality factor and metabolic efficiency. High CRQ indicates high efficiency of cardiopulmonary metabolic system and relatively healthy physiological and psychological state.

APPLICATIONS SCENARIOS

In this section, two application scenarios are presented to demonstrate the descriptive power of CRF and CRI, as well as the application potentials.

Paced Breathing

Experiment Design

HRV biofeedback has been used for the treatment of depression and other autonomic related problems. HRV biofeedback uses

TABLE 1 | Baseline Demographic Characteristics of 30 Participants and *p*-value between 15 men and 15 women.

Characteristics	Men(15)	Women(15)	*p*
Age (y)	24.40 ± 2.830	23.50 ± 2.134	0.631
Height (cm)	175.53 ± 4.872	163.31 ± 4.457	0.035
Weight (kg)	68.33 ± 8.205	57.81 ± 6.304	0.025
SBP (mm Hg)	110.50 ± 9.375	109.90 ± 6.845	0.302
DBP (mm Hg)	68.30 ± 6.521	64.40 ± 8.347	0.413

Data presented as mean ± standard deviation.

HRV measures, mainly time domain and frequency domain, as feedback cues to guide the subject performing slow paced breathing in order to reach resonance state. The objectives of paced breathing in HRV biofeedback is to gain level of parasympathetic nerves activity and improve the autonomic balance. As such, the measures of current status of the subject play most important role in biofeedback process. So far in the HRV biofeedback HRV measures are used, while HRV measures have problems in representing autonomic regulation status (Vaschillo et al., 2006).

The essential physiological phenomenon of the slow and deep paced breathing in HRV biofeedback is respiration sinus arrhythmia (RSA). The level of RSA should be the natural measure as biofeedback cues. As the quantitative measure of RSA, CRF and CRI provide the best visual cue and numerical cues for biofeedback.

During the paced breathing, Cardiopulmonary Resonance Amplitude (CRA) could help us find the optimal respiratory rate for individuals which is usually around 0.1 Hz. The process of training is the process of making CRA keep approaching 1. As we go from the resting state to paced breathing rate coming down to 0.1 Hz, with the frequency decreases, CRA gets bigger and the bandWidth CRW gets smaller. The frequency of obtaining the maximum value of CRA is the personalized resonance frequency of the subject and also the frequency of biofeedback. As an indicator of cardiopulmonary system metabolism, cardiopulmonary resonance quality factor (CRQ) indicates efficiency of cardiopulmonary metabolic system and relatively healthy physiological and psychological state.

This study was carried out in accordance with the recommendations of guidelines of ethical review of clinical research ethics committee of China-Japanese Friendship Hospital. The number is 2019-GZR-138. The protocol was approved by the clinical research ethics committee of Beijing China-Japanese Friendship Hospital. All participants signed informed consent forms. We collected data from 30 healthy adults in ages of 20–30. The baseline demographic characteristics of 30 participants are shown in **Table 1**. The subjects' age, height, weight, and mean systolic and diastolic blood pressure were counted and presented as mean ± standard deviation. The paired *t*-test showed there were no significant differences in age, systolic and diastolic blood pressure between the male and female groups.

The data is collected using one intelligent hardware, worn on the wrist (**Figure 2**). We collected one-lead ECG and respiratory signals of everyone from resting to biofeedback status. The whole process is recorded. During the process of paced breathing rate down to about 0.1 Hz, we use our method to find the individual resonant frequency for every trainee: Starting from the resting state of the subjects, the breathing rate was gradually reduced at 0.01 Hz intervals guided by voice and image on the computer. Each breathing rate was maintained for at least 1 min. It can be seen that Cardiopulmonary Resonance Amplitude (CRA) gradually increases as the respiratory rate decreases

FIGURE 2 | The wearable hardware device used to collect ECG and respiration signals.

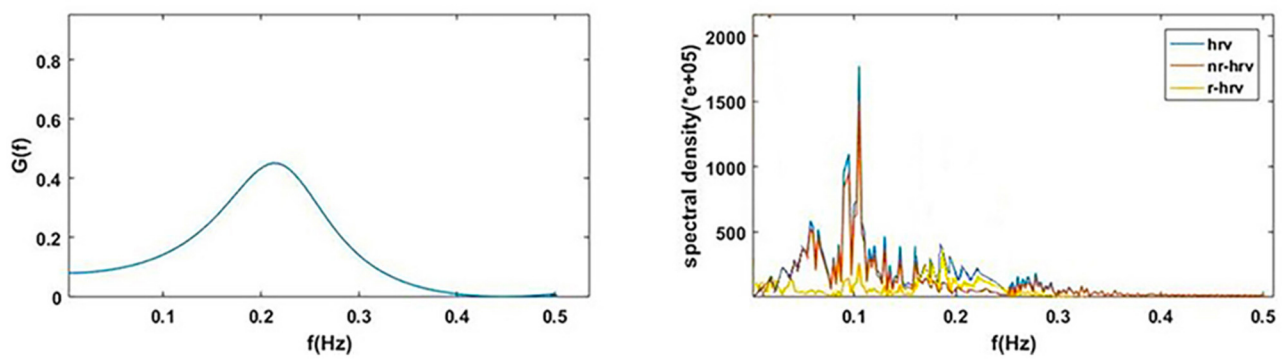

FIGURE 3 | *G(f)* (CRF) and corresponding HRV, R-HRV, and NR-HRV in frequency domain.

and reaches its maximum value around 0.1 Hz. The frequency of obtaining the maximum value of CRA is the personalized resonance frequency of the subject and also the frequency of biofeedback.

Statistical Analysis

To demonstrate the advantage of CRI in paced breathing compared to HRV, we calculated the Cardiopulmonary Resonance Indices (CRI) and HRV in different statues. In order to represent CRF and CRA visually, we draw the CRF curves in the frequency domain with HRV in four status of paced breathing from resting status to biofeedback status. The repeated one-way ANOVA, followed by Dunnett's *post hoc* test was used to represent the significant difference from resting state to biofeedback state of CRI in the breathing training.

CRF and CRI in Paced Breathing

CRF measures the effect of respiration on current heart rate changes in the frequency domain. CRF and corresponding HRV, R-HRV, and NR-HRV in the frequency domain are shown in **Figure 3**.

Respiratory effects in different physiological states have different effects on heart rate. These effects can be directly seen from the power spectrum calculated by spectral G-causality, which is closely related to the current breathing rate of the subjects. CRF expresses the cardiopulmonary interaction at the current time in the frequency domain.

To demonstrate the advantage of CRI in paced breathing compared to HRV, the CRF, HRV, and respiratory power spectral density of one subject of the 30 participants in the experiment from resting to biofeedback status are illustrated in **Figure 4**. The blue lines show respiratory power spectral

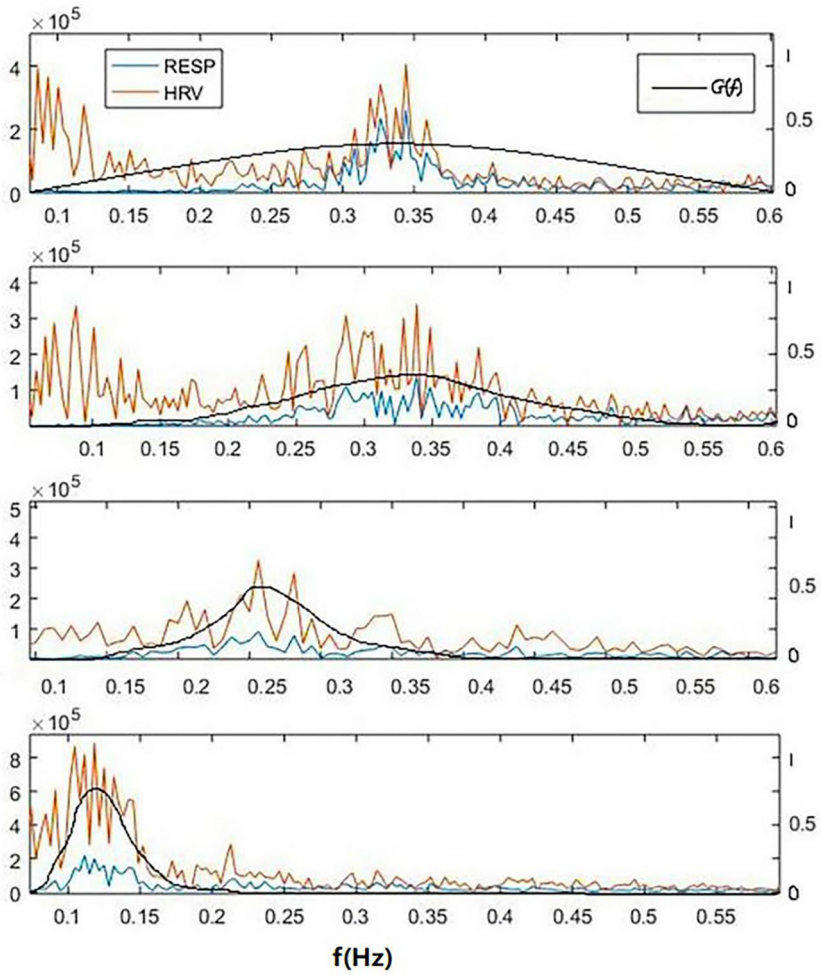

FIGURE 4 | A typical power spectral density curves of respiratory, HRV and corresponding cardiopulmonary resonance function CRF in the frequency domain of a subject for 4 cases of breathing at resting state. From the top: free breathing, paced breathing at frequency of 0.33, 0.26, and 0.12 Hz. It can be seen that paced breathing increases the strength of RSA, and that as the frequency of paced breathing coming down toward, the cardiopulmonary resonance phenomenon becomes stronger, which is very well-captured by the cardiopulmonary resonance function. It can also seen that as the paced breathing frequency approaches 0.1 Hz, around which there is an optimal resonance state for the subject, where HRV_HF is small. That is to say that CRI do represent level of parasympathetic nervus activity at various cases, while HRV do not.

density, orange lines show HRV and black lines show CRF. From the top: free breathing, paced breathing at frequency of 0.33, 0.26, and 0.12 Hz. It can be seen that paced breathing increases the strength of RSA, and that as the frequency of paced breathing coming down toward, the cardiopulmonary resonance phenomenon becomes stronger, which is very well-captured by the cardiopulmonary resonance function. We can also see that as the paced breathing frequency approaches 0.1 Hz, around which there is an optimal resonance state for the subject, where HRV HF is small. That is to say that CRI do represent level of parasympathetic nervus activity at various cases, while HRV do not.

The higher degree of cardiopulmonary coupling during paced breathing, the respiration accounts for a higher proportion of HRV. In the resting state, HRV produced by breathing is weak, then NR-HRV can reflect the influence of other physiological activities on heart rate through autonomic nervous activity.

As can be seen from the figure, with the change of respiratory rate, the distribution of CRF and HRV both shift in the corresponding frequency bands. The distribution of the frequency band of HRV is closely related to the change of respiratory frequency, so the degree of biofeedback can be observed from respiration frequency shift (Vaschillo et al., 2006). However, there is no quantitative measure between the peak value of HRV and the respiratory frequency within HRV biofeedback to describe the intensity and depth of cardiopulmonary interaction. Meanwhile, HRV cannot be used as a measure of RSA due to its low repeatability and large individual differences.

On contrary, CRF show a clear trend in paced breathing. Generally, we calculated CRI in four different states from resting to biofeedback status (from 1 to 4) in **Table 2**. The repeated one-way ANOVA was used to test the differences of CRI in the four states ($p < 0.05$). In **Table 2**, the p-values of CRA, CRW and $f_A$are smaller than 0.05, and the p-value of CRQ is bigger than 0.05. The results showed that CRA, CRW and f_A have significant differences in the four status. CRQ is defined to measure the merit of the cardiopulmonary resonance system, and did not change significantly at different respiratory rates. In order to confirm the significance and stability of the differences between CRA and CRW in the four states further, we performed Dunnett's *post hoc* test shown in **Table 3**. As we can see, CRA increases and CRB decreases during the training. In the most of the pairwise comparisons of state 1, 2, 3, and 4, CRA and CRW show significant differences. These two indicators together represent the intensity of a person's cardiopulmonary interaction and reflect the activity and regulatory capacity of the human vagus nerve with repeatability and stability.

We can see that CRF and CRI could provide ideal visual interpretation and numerical measures for cardiopulmonary interactions toward resonance state in paced breathing scenario. CRF can be used to analyze the human body in different physiological states, get cardiopulmonary coupling value accurately, and analyze the regulation process of human sympathetic and parasympathetic nerves.

TABLE 2 | Cardiopulmonary Resonance Indices for the 4 cases of breathing: free breathing and 3 paced breathing at frequency of 0.33, 0.26, and 0.12Hz.

	1	2	3	4	p
CRA	0.640 ± 0.004	0.710 ± 0.003	0.810 ± 0.005	0.991 ± 0.004	0.003
CRW	0.250 ± 0.030	0.170 ± 0.021	0.130 ± 0.020	0.075 ± 0.021	0.004
f_A	0.360 ± 0.030	0.301 ± 0.030	0.201 ± 0.021	0.110 ± 0.020	0.002
CRQ	1.440 ± 0.375	1.760 ± 0.313	1.541 ± 0.240	1.470 ± 0.304	0.146

The p-value represents the result of the a repeated measures one-way ANOVA. P values show that there is a significant difference between the groups in CRA, CRW and f_A ($P < 0.05$).

TABLE 3 | Dunnett's *post-hoc* test of CRA and CRW for the 4 cases of breathing: free breathing (1), and 3 paced breathing at frequency of 0.33 Hz (2), 0.26 Hz (3), and 0.12 Hz (4).

Comparative group	CRA		CRW	
	Difference of the mean	LSR ($p = 0.05$)	Difference of the mean	LSR($p = 0.05$)
4 and 1	0.351	0.097	0.175	0.047
4 and 2	0.281	0.096	0.095	0.045
4 and 3	0.181	0.096	0.055	0.045
3 and 1	0.170	0.095	0.120	0.042
3 and 2	0.100	0.095	0.040	0.040
2 and 1	0.070	0.095	0.080	0.040

If the value of Difference of the mean > LSR, there is a significant difference between the groups being compared ($p < 0.05$).

Sleep Stage Discrimination

Experiment Design

Cardiopulmonary Coupling index (CPC) was proposed by Thomas et al. (2005) in 2005, which measures the spectral correlation between heart rate sequence and respiratory signal. Therefore, CPC can be a candidate providing measures for RSA. CPC is defined as the product of the average cross-spectral power divided by the average power of each signal as below.

$$CPC(\mathrm{f}_n) = \left|\Gamma_n(R,E)\right|^2 \Lambda_n$$

$$\Lambda_n = \frac{\langle \Gamma_n(R,E)\rangle^2}{\left\langle \hat{R}_n^2 \right\rangle \left\langle \hat{E}_n^2 \right\rangle}$$

in which $\Gamma_n(R,E)$ denotes the cross spectrum of RR intervals and respiratory signals. CPC reflects the degree of sleep and respiratory rhythm disorder through the high frequency, low frequency and very low-frequency parts with a different energy. It overcomes the shortcomings and defects of the HRV method used in the analysis alone. At present, this method has been widely used in the field of evaluating sleep quality and judging sleep and breathing disorders (Yang et al., 2011).

In sleep stage discrimination, we used data from the MIT-BIH database (Ichimaru and Moody, 1999) which has sleep stage labels from polysomnography (PSG). CRI in different sleep stage was calculated and a comparative study was conducted by using Cardiopulmonary Coupling index (CPC) in sleep stage classification. Except for the heart rate, HRV, and respiratory rate, CRA, CRW, and f_A extracted from CRF, meanwhile LF, HF, and LF/HF extracted from CPC are, respectively, used in the classification task to test sleep stage of the subject.

In the experiment, the classifier needs to identify four different sleep stages, including awake, REM, light sleep, and deep sleep. SVM is not able to solve multi-category classification problems directly, but the combination of SVM and decision tree (called DTB-SVM) can be used to solve multi-class classification problems. Based on the structural characteristics of the sleep cycle and the physiological features used in sleep classification, we used three SVM models to classify the sleep stages. As shown in **Figure 5**, firstly, a classifier is used to separate the awake phase and the sleep phase, and then within the sleep phase, the REM phase and the NREM phase are separated, and finally the light sleep and deep sleep are separated by the last classifier. RBF kernel was used in the model. In order to prevent over-fitting, we selected the optimal parameters in the way of K-fold cross-validation and grid search. For the features of CPC and CRI, classifiers of same structure were used to classify the sleep stages.

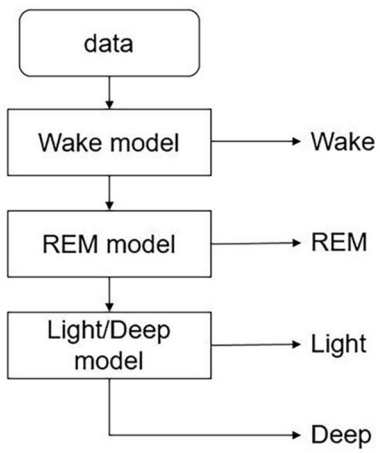

FIGURE 5 | DTB-SVM model for classifying the sleep stages. First, a classifier is used to separate the awake phase and the sleep phase, and then within the sleep phase, the REM phase and the NREM phase are separated, and finally the light sleep and deep sleep are separated by the last classifier.

Statistical Analysis

The confusion matrix was used to explain the accuracy of sleep classification results and to compare the performance of CRI and CPC in classification tasks. Each row of the matrix represents the prediction category, and the total number of each row represents the number of data predicted for that category. Each column

TABLE 4 | Cardiopulmonary Resonance Indices of one subject in different sleep stages of a whole night.

	Wake	REM	Light	Deep
CRA	0.648 ± 0.004	0.674 ± 0.004	0.734 ± 0.003	0.993 ± 0.004
CRW	0.280 ± 0.011	0.231 ± 0.011	0.163 ± 0.010	0.053 ± 0.013
f_A	0.300 ± 0.020	0.290 ± 0.017	0.25 ± 0.016	0.230 ± 0.010
CRQ	1.071 ± 0.230	1.255 ± 0.227	1.534 ± 0.161	4.340 ± 0.102

Data presented as mean ± standard deviation.

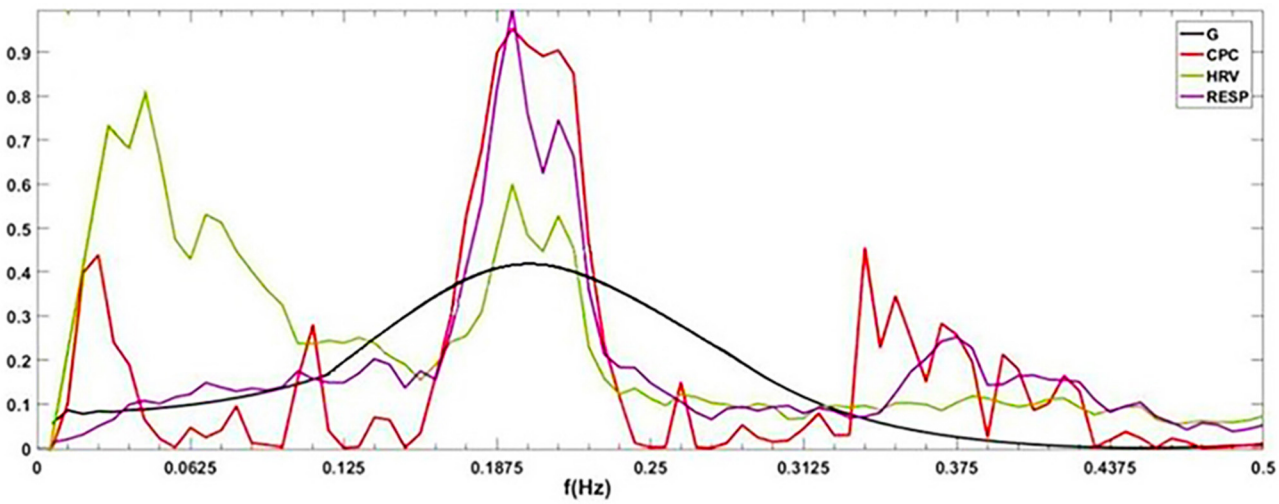

FIGURE 6 | *G(f)* (CRF), CPC, power spectral density of HRV and respiration. By definition, cardiopulmonary resonance function CRF, reflects the strength of RSA, with the peak near the mean of the respiration rate, while CPC is the correlation between HRV and respiration with respect to their power spectrum, having multiple peaks. As the name indicated, CRF well capture the resonance nature of cardiopulmonary system.

represents the true category to which the data belongs, and the total number of data in each column represents the number of data instances in that category.

The effectiveness of the features was measured by the ratio of intra-class divergence and inter-class divergence. The ratio between intra-class divergence and inter-class divergence is defined and calculated as follows (Zhou et al., 2010):

Let $(X, y)\epsilon(R^n \times y)$ be a sample, where R^n is an n-dimensional feature space and $y = \{1,2,....,s\}$ is the label set. L_i is the number of samples in the ith class, and l is the total number of samples. Let X_{ij} denote the jth sample in the ith class, m_i the sample mean of the ith class, and m the sample in the ith class, m_i the sample mean of the ith class, and m the sample mean of all class. The within-class scatter matrix S_W, between-class scatter matrix S_B are defined as

$$S_w = \sum_{i=1}^{s} \sum_{j=1}^{l_i} (X_{ij} - m_i)(X_{ij} - m_i)^T$$

$$S_B = \sum_{i=1}^{s} l_i (m_i - m)(m_i - m)^T$$

Large class separability means small within-class scattering and large between-class scattering. A combination of two of them can be used as a measure, $|S_W|/|S_B|$, where $|\cdot|$ denote the determinant of a matrix. The smaller the ratio, the better the effect of the feature on classification.

In order to demonstrate the good performance of CRI in sleep classification task, we compared the confusion matrix of CRI and CPC classification results. Then, in order to express the role of features further, we conducted the divergence analysis on the features of CRI and CPC. The results showed that CRI was more effective than CPC in sleep classification task, especially in the deep sleep recognition.

CRI in Different Sleep Stages Compared to CPC

To visually compare the difference between CRI and CPC, **Figure 6** shows the CPC, HRV, and CRF of one subject. It contains HRV (0.14 Hz as the demarcation line between high frequency and low frequency), respiration power spectral density, CPC index and *G(f)*, which are all discussed in the frequency domain.

CPC represents the correlation of RR intervals and respiratory signal. It shows that CPC has multiple peaks in the full frequency band. In low-frequency band, for HRV analysis, people usually think sympathetic nerve and parasympathetic nerve interact together, and CPC also shows a spike which indicates a high correlation between respiration and RR intervals, such as blood pressure, etc. It is difficult to find an exact indicator representing the cardiopulmonary coupling state from CPC. Physiologically, RSA, the strength of respiration modulation of heart rate should appear as CRF, cannot be multiple peaks as CPC.

The indices of one subject in four different sleep stage of one night are shown in **Table 4**. It shows that our indices could express the cardiopulmonary interaction phenomenon and the degree of cardiopulmonary coupling resonance in different sleep stages. **Table 5** shows the performance of CRI indicators and CPC indicators on the whole data set in the classification task. CRW, CRA, $f_A$are smaller than LF_CPC and HF_CPC. The results

TABLE 5 | The divergence analysis of the features of CPC and CRI in the sleep classification task.

	LF_CPC	HF_CPC	CRW	CRA	f_A_CRI
$\|S_B\|/\|S_W\|$	7.290	5.365	0.302	1.930	2.311

LF_CPC and HF_CPC are the LF and HF features of CPC, CRW, CRA, and fA_CRI are the features of CRI.

TABLE 7 | The divergence analysis of the features of CPC and CRI in the deep sleep and light sleep.

	LF_CPC	HF_CPC	CRW	CRA	f_A_CRI
$\|S_B\|/\|S_W\|$	8.312	5.432	0.530	1.106	2.867

LF_CPC and HF_CPC are the LF and HF features of CPC, CRW, CRA, and f_A_CRI are the features of CRI.

TABLE 6 | Confusion matrix of sleep stage classification using CPC and CRI.

Actual predicted	Wake		REM		Light		Deep	
	CPC	CRI	CPC	CRI	CPC	CRI	CPC	CRI
Wake	1557	1561	44	44	305	307	50	25
REM	27	30	356	355	97	100	8	12
Light	219	220	88	89	3994	4034	115	87
Deep	13	5	5	5	77	32	259	308
Total	1816	1816	493	493	4473	4473	432	432
Accuracy	85.74%	85.96%	72.21%	72.01%	89.29%	90.19%	59.95%	71.30%

Each value in the table represents the number of samples. At each position in the obfuscation matrix, the values on the left represent the results of CPC, and the values on the right represent the results of CRI. CRI shows superiority in identifying deep sleep, more than 11% higher than CPC.

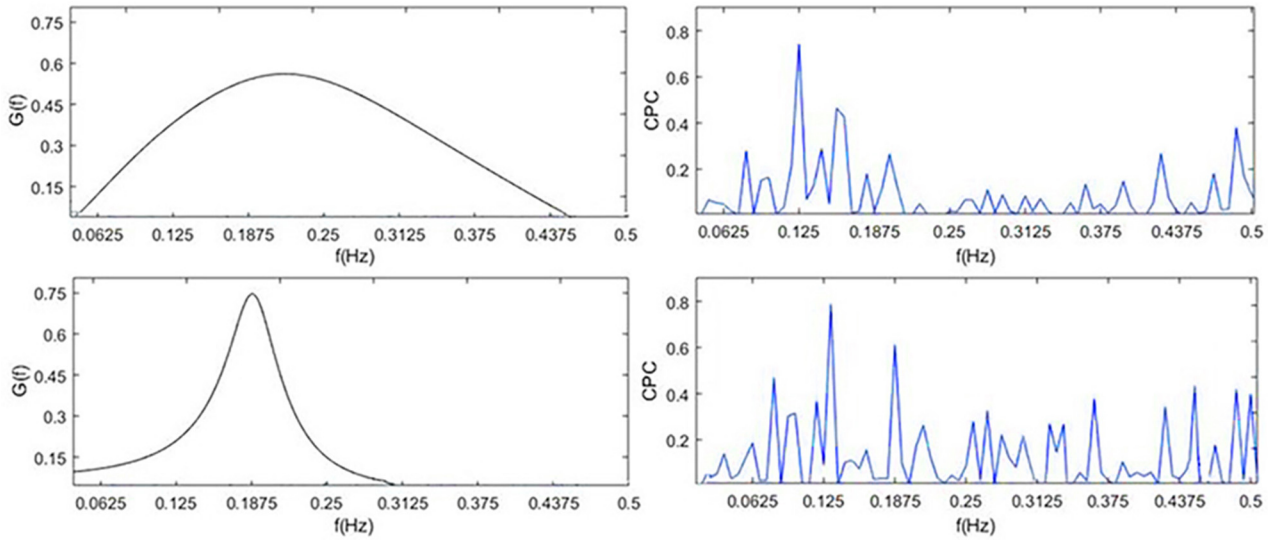

FIGURE 7 | *G(f)* (CRF) and CPC in light sleep (top) and deep sleep (bottom).

show that the CRI features including CRW, CRA, f_A performed better than CPC features including LF_CPC and HF_CPC in the classification task.

The classification results of CRI and CPC were statistically analyzed, respectively, in **Table 6**. It shows that CRI shows superior in distinguishing deep sleep stage than CPC. The overall accuracy of the classification went up 1.28%. Particularly shown in **Table 6**, great progress has been made in distinguishing between deep sleep and light sleep, and the recognition rate of deep sleep has been increased by 11.35%. It shows that CRF performances better than CPC, especially in the distinction between light sleep (NREM_1 and NREM _2) and deep sleep (NREM_3 and NREM _4).

The performance of CPC and CRF in deep sleep and light sleep is shown in **Figure 7**. In the deep sleep stage, CRF shows more concentrated and indicators we proposed are good indications of this phenomenon. It provides meaningful features for the distinguishing of the two. To illustrate the role of CRI in deep sleep recognition, divergence analysis of the features of CPC and CRI in the deep sleep and light sleep was performed in **Table 7**. It shows the performance of CRI indicators and CPC indicators for distinguishing the deep sleep stage. CRW, CRA, f_A are much smaller than LF_CPC and HF_CPC. It shows that CRI features CRW, CRA, f_A performed much better than CPC features LF_CPC and HF_CPC. In the deep sleep, the cardiopulmonary system has the highest metabolic efficiency and the smallest dissipated energy, and the body and mind of the human body can fully rest and recover. This suggests that CRI is a good indicator for different sleep status especially the deep sleep of human body.

The shortcomings of the CPC are obvious. CPC calculates the correlation between RR interval and respiratory signal, with the shape of multiple peaks. Physiologically, RSA, the strength of respiration modulation of heart rate should appear as CRF, cannot be multiple peaks as CPC. Through the study of CRI and Cardiopulmonary Coupling (CPC) in distinguishing deep sleep stage, we got the conclusion that CRI does capture physiologically meaningful characteristics of RSA, therefore, well reflect autonomic status in sleep stages. CRI represents the degree of cardiopulmonary resonance, and reflects parasympathetic nerve activity level well.

CONCLUSION

Respiratory sinus arrhythmia (RSA) represents a physiological phenomenon of cardiopulmonary interaction. It is known as a measure of efficiency of the circulation system, and a biomarker of cardiac vagal and well-being. In this article, we model RSA as modulation of heart rate by respiration in an interactive cardiopulmonary system with the most effective system state of resonance. Mathematically, it is described by bivariate autoregressive model of respiration series and RR intervals, and quantitatively it is assessed by Granger causality function. The whole model is referred to as Cardiopulmonary Resonance Model (CRM). This method has significant physiological significance in the frequency domain and is convenient for us to explain the experimental results. We suggest using this approach as a universal prepossessing technique which allows a researcher to concentrate on particular properties of the HRV data. Then based on the cardiopulmonary resonance concept, and Granger causality function which is referred to as cardiopulmonary resonance function (CRF) here after, a set of quantitative measures for RSA is proposed, and referred to as Cardiopulmonary Resonance Indices (CRI).

To show the effectiveness of CRM and CRI, two application scenarios, paced breathing and sleep stage discrimination, are studied. It is shown that CRF and CRI provide ideal visual interpretation and numerical measures for cardiopulmonary interactions toward resonance in paced breathing scenario as the paced breathing rate coming down to biofeedback status, and as the sleep stage moves to deep sleep. We draw the conclusion that CRI well represents the degree of cardiopulmonary resonance, and reflects parasympathetic nerve activity level. We think it's a good explanation of the physiological function of RSA and it is also good way to quantify the well-being of human body.

This study has certain limitations. As a measure of RSA under static conditions, CRI was not compared with sympathetic and parasympathetic activity indexes obtained by tilt experiment, nor was it tested under different pathological conditions. We plan to carry out relevant research in the future. In addition, we plan to explore the clinical significance of CRQ and the effects of other physiological activities on heart rate based on NR-HRV data in time and frequency domain. We will gradually accurately analyze the regulatory effects of the autonomic nervous system on various physiological organs and activities through the regulation activities of the autonomic nervous system. It is of great significance for us to understand and monitor the regulation process of the autonomic nervous system in different physiological states.

DATA AVAILABILITY STATEMENT

All datasets generated for this study are included in the article/supplementary material.

AUTHOR CONTRIBUTIONS

JC, JW, and ZH designed the study and performed the research. JC analyzed the data and wrote the paper. ZH and JW reviewed and edited the manuscript. HJ designed and assisted the experiment. All authors read and approved the manuscript.

FUNDING

School of Electronic, Electrical and Communication Engineering, University of Chinese Academy of Sciences provided financial support for the experimenters. This research was partially supported by National Natural Science Foundation of China, contract 61431017. CAS Institute of Healthcare Technologies provided the equipment of this research.

ACKNOWLEDGMENTS

Thanks are due to Digital Health Research Institute of Zhong Ke (Nanjing) for provision of laboratory equipment and to Xiang'ao Meng and Zhongdi Liu for the assistance with the experiments.

REFERENCES

Akaike, H. (1974). A new look at the statistical model identification. *IEEE Trans. Autom. Control* 19, 716–723. doi: 10.1007/978-1-4612-1694-0_16

Appel, M. L., Berger, R. D., Saul, J. P., Smith, J. M., and Cohen, R. J. (1989). Beat to beat variability in cardiovascular variables: noise or music? *J. Am. Coll. Cardiol.* 14, 1139–1148. doi: 10.1016/0735-1097(89)90408-7

Bernston, G. G., Bigger, J. T., Eckberg, D. L., Grossman, P., Kaufmann, P. G., Malik, M., et al. (1997). Heart rate variability: origins, methods, and interpretative caveats. *Psychopathy* 34, 623–648. doi: 10.1111/j.1469-8986.1997.tb02140.x

Engel, A., and Singer, W. (2001). Temporal binding and the neural correlates of sensory awareness. *Trends Cogn. Sci.* 5, 16–25. doi: 10.1016/S1364-6613(00)01568-0

Fonseca, D. S., Beda, A., Miranda de, S. Á., Antonio, M. F. L., and Simpson, D. M. (2013). Gain and coherence estimates between respiration and heart-rate: differences between inspiration and expiration. *Auton. Neurosci.* 178, 89–95. doi: 10.1016/j.autneu.2013.03.015

Granger, C. (1969). Investigating causal relations by econometric models and cross-spectral methods. *Econometrica* 37, 424–438. doi: 10.2307/1912791

Grossman, P., and Taylor, E. W. (2007). Toward understanding respiratory sinus arrhythmia: relations to cardiac vagal tone, evolution and biobehavioral functions. *Biol. Psychol.* 74, 263–285. doi: 10.1016/j.biopsycho.2005.11.014

Hayano, J., and Yuda, E. (2019). Pitfalls of assessment of autonomic function by heart rate variability. *J. Physiol. Anthropol.* 38:3. doi: 10.1186/s40101-019-0193-2

Ichimaru, Y., and Moody, G. B. (1999). Development of the polysomnographic database on CD-ROM. *Psychiatry Clin. Neurosci.* 53, 175–177. doi: 10.1046/j.1440-1819.1999.00527.x

Ivanov, P. C., Amaral, L. A. N., Goldberger, A. L., Havlin, S., Rosenblum, M. G., Struzik, Z., et al. (1999). Multifractality in human heartbeat dynamics. *Nature* 399, 461–465. doi: 10.1038/20924

Jan, H. Y., Chen, M. F., Fu, T. C., Lin, W. C., Tsai, C. L., and Lin, K. P. (2019). Evaluation of coherence between ECG and PPG derived parameters on heart rate variability and respiration in healthy Volunteers With/Without Controlled Breathing. *J. Med. Biol. Eng.* 39, 783–795. doi: 10.1007/s40846-019-00468-9

Katona, P. G., and Jih, F. (1975). Respiratory sinus arrhythmia: a noninvasive measure of parasympathetic cardiac control. *J. Appl. Physiol.* 39, 801–805. doi: 10.1152/jappl.1975.39.5.801

Lewis, G. F., Furman, S. A., McCool, M. F., and Porges, S. W. (2012). Statistical strategies to quantify respiratory sinus arrhythmia: are commonly used metrics equivalent? *Biol. Psychol.* 89:349364. doi: 10.1016/j.biopsycho.2011.11.009

Moser, M., Fruhwirth, M., Peter, R., and Winker, R. (2006). Why life oscillates - from a topographical towards functional chronobiology. *Cancer Causes Cont.* 17, 591–599. doi: 10.1007/s10552-006-0015-9

Nunez, P. L., Wingeier, B. M., and Silberstein, R. B. (2001). Spatial-temporal structures of human alpha rhythms: theory, microcurrent sources, multiscale measurements, and global binding of local networks. *Hum. Brain Mapp.* 13, 125–164. doi: 10.1002/hbm.1030

Panaite, V., Hindash, A. C., Bylsma, L. M., Small, B. J., Salomon, K., and Rottenberg, J. (2016). Respiratory sinus arrhythmia reactivity to a sad film predicts depression symptom improvement and symptomatic trajectory. *Int. J. Psychophysiol.* 99, 108–113. doi: 10.1016/j.ijpsycho.2015.12.002

Price, C. J., and Crowell, S. E. (2016). Respiratory sinus arrhythmia as a potential measure in substance use treatment-outcome studies. *Addiction* 111, 615–625. doi: 10.1111/add.13232

Ritz, T., Bosquet Enlow, M., Schulz, S. M., Kitts, R., Staudenmaier, J., and Wright, R. J. (2012). Respiratory sinus arrhythmia as an index of vagal activity during stress in infants: respiratory influences and their control. *PLoS ONE* 7:e52729. doi: 10.1371/journal.pone.0052729

Schmitt, D. T., and Ivanov, P. C. (2007). Fractal scale-invariant and nonlinear properties of cardiac dynamics remain stable with advanced age: a new mechanistic picture of cardiac control in healthy elderly. *Am. J. Physi. Regul. Integr. Comp. Physiol.* 293, R1923–R1937. doi: 10.1152/ajpregu.00372.2007

Task Force of the European Society of Cardiology and the North American Society of Pacing and Electrophysiology. (1996). Heart rate variability. *Circulation* 93, 1043–1065.

Thomas, R. J., Mietus, J. E., Peng, C. K., and Goldberger, K. L. (2005). An electrocardiogram-based technique to assess cardiopulmonary coupling during sleep. *Sleep* 28, 1151–1161. doi: 10.1093/sleep/28.9.1151

Topcu, C., Fruehwirth, M., Moser, M., Rosenblum, M., and Pikovsky, A. S. (2018). Disentangling respiratory sinus arrhythmia in heart rate variability records. *Physiol. Meas.* 39:054002. doi: 10.1088/1361-6579/aabea4

Tracey, K. J. (2002). The inflammatory reflex. *Nature* 420, 853–859. doi: 10.1038/nature01321

Vaschillo, E. G., Vaschillo, B., and Lehrer, P. M. (2006). Characteristics of resonance in heart rate variability stimulated by biofeedback. *Appl. Psychophysiol. Biofeedback* 31, 129–142. doi: 10.1007/s10484-006-9009-3

Wielgus, M. D., Aldrich, J. T., Mezulis, A. H., and Crowell, S. E. (2016). Respiratory sinus arrhythmia as a predictor of self-injurious thoughts and behaviors among adolescents. *Int. J Psychophysiol*. 106, 127–134. doi: 10.1016/j.ijpsycho.2016.05.005

Yang, A. C., Yang, C. H., Hong, C. J., Tsai, J., Kuo, C. H., Peng, C. K., et al. (2011). Sleep state instabilities in major depressive disorder: detection and quantification with electrocardiogram-based cardiopulmonary coupling analysis. *Psychophysiolog* 48, 285–291. doi: 10.1111/j.1469-8986.2010.01060.x

Zhou, L., Wang, L., and Shen, C. (2010). Feature selection with redundancy-constrained class separability. *IEEE Transac. Neural Netw*. 21, 853–858. doi: 10.1109/TNN.2010.2044189

Conflict of Interest: The authors declare that the research was conducted in the absence of any commercial or financial relationships that could be construed as a potential conflict of interest.

frontiers in Physiology

ORIGINAL RESEARCH
published: 08 September 2020
doi: 10.3389/fphys.2020.00762

Heart Rate Variability Synchronizes When Non-experts Vocalize Together

Sebastian Ruiz-Blais[1]*, *Michele Orini*[2] and *Elaine Chew*[3†]

[1] School of Electronic Engineering and Computer Science, Queen Mary University of London, London, United Kingdom,
[2] Department of Clinical Science, Institute of Cardiovascular Science, University College London, London, United Kingdom,
[3] CNRS – UMR9912/STMS (IRCAM), Paris, France

Singing and chanting are ubiquitous across World cultures. It has been theorized that such practices are an adaptive advantage for humans because they facilitate bonding and cohesion between group members. Investigations into the effects of singing together have so far focused on the physiological effects, such as the synchronization of heart rate variability (HRV), of experienced choir singers. Here, we study whether HRV synchronizes for pairs of non-experts in different vocalizing conditions. Using time-frequency coherence (TFC) analysis, we find that HRV becomes more coupled when people make long ($>$ 10 s) sounds synchronously compared to short sounds ($<$ 1 s) and baseline measurements ($p < 0.01$). Furthermore, we find that, although most of the effect can be attributed to respiratory sinus arrhythmia, some HRV synchronization persists when the effect of respiration is removed: long notes show higher partial TFC than baseline and breathing ($p < 0.05$). In addition, we observe that, for most dyads, the frequency of the vocalization onsets matches that of the peaks in the TFC spectra, even though these frequencies are above the typical range of 0.04–0.4 Hz. A clear correspondence between high HRV coupling and the subjective experience of "togetherness" was not found. These results suggest that since autonomic physiological entrainment is observed for non-expert singing, it may be exploited as part of interventions in music therapy or social prescription programs for the general population.

Keywords: HRV, singing, togetherness, coherence, synchronization

OPEN ACCESS

Edited by:
Tijana Boji,
University of Belgrade, Serbia

Reviewed by:
Karin Schiecke,
Friedrich Schiller University Jena, Germany
Dirk Cysarz,
Witten/Herdecke University, Germany

***Correspondence:**
Sebastian Ruiz-Blais
ruizble@gmail.com

†Present address:
Elaine Chew,
Faculty of Natural and Mathematical Sciences, Kings College London, London, United Kingdom

Specialty section:
This article was submitted to Autonomic Neuroscience, a section of the journal Frontiers in Physiology

Received: *20 March 2020*
Accepted: *11 June 2020*
Published: *08 September 2020*

Citation:
Ruiz-Blais S, Orini M and Chew E (2020) Heart Rate Variability Synchronizes When Non-experts Vocalize Together. Front. Physiol. 11:762. doi: 10.3389/fphys.2020.00762

1. INTRODUCTION

There is increasing interest in the effect of music on people's well-being and health. Specifically, a number of studies have shown the benefit of regular choral singing practice (Clift and Hancox, 2010; Dingle et al., 2013; Judd and Pooley, 2014; Pearce et al., 2015). Clift and Hancox (2010) identified possible factors contributing to the health and well-being benefit of choir participation, such as gaining more positive affects, focused attention, deeper breathing, social support, cognitive stimulation, and regular commitment. Dingle et al. (2013) determined three major outcomes of singing: personal (e.g., emotion regulation and spiritual experience), social (e.g., connectedness with other choir members), and functional (e.g., health benefits) outcomes. It has also been proposed that vocalizing together offers an efficient way to create bonds, which was likely an important adaptive trait for our human ancestors (Dunbar, 2017). Singing can occur in a variety of social contexts, such as amongst sport fans and within military and religious organizations. The effects of singing can be appreciated in objective health and behavioral outcomes but also in terms

of the subjective qualities associated with it. Specifically, a subjective experience of togetherness is often reported in ensemble music performance and improvization (Nachmanovitch, 1990), particularly for singing (Hayward, 2014). Such experience has been described as a blurring between the self-other boundaries (Nachmanovitch, 1990), which has been linked to social bonding (Tarr et al., 2014).

Subjective experiences of togetherness have been previously studied in the context of dance (Himberg et al., 2018) and synchronized movement (Noy et al., 2015). These studies point out that interpersonal movement synchrony plays an important role in subjective experiences and aesthetic appreciation. A plausible framework through which to understand togetherness is the concept of interpersonal entrainment, which is a commonly studied phenomenon in music. Entrainment involves independent systems that become synchronized (Clayton, 2012). Four levels of interpersonal entrainment have been proposed for music (Trost et al., 2017): perceptual (the synchronization that occurs between people attending to the same stimulus), autonomic physiological [phase-locking in the activity of the autonomic nervous system (ANS)], motor (the coupling of physical actions), and social (the synchronization of social behavior). For the specific case of singing, interpersonal synchronization can occur at all the above levels: a motor (making the same vocal actions using breath and vocal chords), perceptual (listening to the same vocal sounds), autonomic physiological (the relationship between breathing and autonomic nervous system functions), and social (the communicative aspects of using the voice).

The ANS relates to emotion and behavior by means of the sympathetic and parasympathetic systems, which prepare the organism for action and regulate responses (Porges, 2001). Among relevant actions for individuals are those relating to social interaction, such as facial and vocal expressions, which are ubiquitous in singing interactions. One common way of assessing ANS activity is by analyzing the patterns of heart rate variability (HRV), which is "the degree to which the time interval between successive heart beats fluctuates" (Christou-Champi et al., 2015). HRV has a high frequency (HF) component between 0.15 and 0.4 Hz, which is linked to the vagal parasympathetic activity, and a low frequency (LF) component between 0.04 and 0.15 Hz, which is related to both sympathetic and parasympathetic influences (Saul, 1990). Respiration has an important effect on HRV, called respiratory sinus arrhythmia (RSA), with instantaneous heart rate increasing during inhalation and decreasing during exhalation (Song and Lehrer, 2003; Grossman and Taylor, 2007; Sin et al., 2010). Furthermore, the magnitude of the effect depends on respiration frequency, with lower frequencies showing greater RSA, with a maximum at four breaths per minute (Song and Lehrer, 2003).

It has been proposed that to understand the complexities of social interaction it is necessary to study the behavioral and physiological dynamics of various individuals (De Jaegher et al., 2010). For example, when tapping to a beat, participants adapt one to another, which is an emergent property of dyadic interactions and cannot be studied by looking at individuals separately (Konvalinka et al., 2010; Spiro and Himberg, 2012). Indeed, there is an increasing interest in studying interpersonal autonomic physiology and connecting it with behavioral and psycho-social constructs (Palumbo et al., 2017). In particular, Noy et al. (2015) studied the relationship between dyadic joint hand movements, physiological signals, and subjectively reported *togetherness* by using a mirror game inspired by theater practice (Noy et al., 2011). They found that periods of the interaction when both participants reported high togetherness where associated with increased cardiovascular activity and with high correlation between the heart rate time series of both participants (Noy et al., 2015). Their findings support the hypothesis that subjective togetherness is linked to the coupling between instantaneous heart rates of dyads, although the authors cautioned that the coupling could be a by-product of motion synchronization, for the specific task they used.

The significance of the autonomic nervous system (ANS) entrainment in group singing has been shown by Müller and Lindenberger (2011) and Vickhoff et al. (2013). Müller and Lindenberger (2011) provided the first evidence that heart rate variability (HRV) synchronizes between choir members and their conductor and that the effect is greater when singing in unison. Vickhoff et al. (2013) showed that HRV is coupled between choral singers and is dependent on musical structure, which constrains the respiration patterns. These studies suggest that HRV synchronization between choir members occurs due to RSA. However, given the link between entrainment and affective responses (Trost et al., 2017) and the socio-biological bonding responses to singing (Kreutz, 2014), it is possible that mechanisms other than RSA play a role in the HRV coupling occurring in singing interactions.

By comparing heart and respiration activity on various vocalization and breathing tasks, this study tests whether there is a mechanism beyond RSA mediating HRV coupling in dyads. HRV coupling between participants can be studied using a time-frequency coherence (TFC) analysis, which describes the amount of coupling between two signals over different frequencies (Orini et al., 2012b, 2017a). Furthermore, partial time-frequency coherence (pTFC) provides a means to study the coupling between two signals after removing the effects of a third signal (Orini et al., 2012a,b; Widjaja et al., 2013). We use pTFC to study the coupling between the HRV of dyads beyond the effects of respiration. We expect that, by removing the effect of respiration, there will be no differences in pTFC between baseline and breathing conditions. We propose that some differences might remain between breathing and vocalization conditions, due to influences beyond RSA. Furthermore, this study explores whether HRV synchronization relates to the subjective experience of togetherness, by using continuous subjective ratings of togetherness (Noy et al., 2015). The differences between making short and long vocalizations and making them in-sync or out-of-sync are also explored. We thus attempt to provide insight into the physiological effects of specific characteristics of vocalization, i.e., length and degree of synchrony between people, which shape more complex forms of vocalization such as choir singing. While choir singing involves more elements than this specific case of dyadic vocalization, this experimental design allows the study to isolate some aspects

of singing (e.g., length and synchrony) while preserving the singing experience to some extent (e.g., by giving participants some freedom in the choice of their notes). Finally, HRV synchronization has not been demonstrated for people without singing experience. We aim to reproduce this phenomenon in a non-expert population in order to contribute to research on the use of singing in music therapy contexts.

2. METHODOLOGY

The study received ethical approval by the Research Ethics Committee of Queen Mary University of London.

2.1. Participants

Twenty participants (10 male and 10 female) aged 20–43 were paired in 10 dyads for a vocal interaction experiment. We recruited participants who identified themselves as non-expert singers to extend previous results to people without regular choir or singing practice. Participants were given an information sheet and provided written informed consent. Among the group of 20 participants, one dyad dropped out of the analysis because the participants laughed intermittently, hence affecting the physiological measurements. In addition, continuous subjective ratings from two participants were lost due to technical issues. We thus used data from 18 participants (nine dyads) for the physiological analyses and data from 16 participants for the subjective ratings analyses.

2.2. Procedure

Each dyad was guided through the following phases: briefing, physiological sensors set-up, a warm-up phase, four tasks of vocal interaction, a continuous subjective rating phase, a questionnaire, and an interview. We performed baseline recordings for 1 min before and 1 min after the interactive tasks. The whole procedure lasted about 70 min and participants were compensated with £10 for their time. During the briefing, participants completed the consent forms, and the experiment was explained.

For both the warm-up and the four interactive tasks, participants sat on chairs about 1 m apart and both facing a common central point. This configuration was chosen in part due to the size constraints of the room and to encourage participants to use their peripheral vision for the interaction while not facing each other directly. Participants could thus choose whether or not to make eye contact when interacting. For the subjective ratings, questionnaire, and interviews, participants were each in a different room.

The warm-up phase was designed to give participants awareness of their own voice by exploring different sound parameters, such as pitch, intensity, and duration. Participants were guided through the warm-up one at the time. The experimenter prompted the participants with vocal sounds that they had to imitate immediately after hearing the sounds. The warmup started with a short, mid-range tone, progressing gradually to higher pitches followed by lower pitches. Next, high and low intensities were presented following a similar pattern. Finally, the participants heard and mimicked two long notes; this was to make sure the participants could control their breathing effectively. In all the vocalized tasks participants were encouraged to explore different pitches and intensities freely to give a greater sense of agency, showing in the different choices made by different dyads. Furthermore, while participants were asked to make short notes of about 0.5 s and long notes as long as their breath, they had some freedom in their choices, both to provide a sense of agency and simplify the task. Each task lasted between 90 and 120 s. A short explanation was given before each task, and participants were asked to return to normal breathing at the end of the task.

In the first task (Br), participants were asked to synchronize their breathing without previously agreeing on any strategy. The second task (SNsync) consisted of synchronizing short duration notes. Participants were asked to achieve synchronization without explicitly agreeing to any kind of strategy. In the third task (LN), participants were asked to make synchronized notes of long duration, paying attention to both the beginnings and ends of the notes. Participants were asked to vocalize pitched sounds for the duration of the respiration and to prioritize synchronization over note length, meaning that if a participant would run out of air the other would have to stop as well. In the fourth task (SNasync), participants produced out-of-phase short notes with the constraint of not vocalizing at the same time, but they were otherwise free to choose the timings of their vocalizations.

2.3. Data Recording

2.3.1. Audio and Video

Audio was recorded using a ZOOM H4 recorder at a standard 44,100 Hz sampling rate, and video was recorded with the in-built camera of a MacBook Air using the Photobooth application. A frame where both participants were visible was chosen. Both audio and video recordings were started a few seconds after the beginning of the breathing task and were stopped a few seconds after the end of the asynchronous notes task. Audio and video signals were synchronized using MATLAB's "finddelay" function with a maximum delay of 20 s.

2.3.2. Togetherness Continuous Subjective Ratings

Participants were asked to report the degree of togetherness they experienced with their partner throughout the four interactive tasks, as in previous studies (Noy et al., 2015). Togetherness was defined to the participants as "the extent to which you feel close or connected to your partner." Immediately after the experimental tasks, participants were taken to separate rooms and shown the video recording of the interaction. They were asked to report how much togetherness they experienced during the tasks, using continuous subjective ratings. A rating dial and a visual interface were provided, and they recorded numeric values between 0 and 255 and then normalized to the 0–1 range during the analysis. Participants were instructed to turn the dial to the left side to register low togetherness values and to the right side to register high values. The interface provided visual feedback on the level of togetherness that was reported. The interface was created using Arduino hardware and Processing software. The software included timestamps to allow

synchronization between the video and physiological data. See **Figure 1** for an example of continuous togetherness ratings for one of the dyads.

2.3.3. Physiological Data

Physiological data was continuously recorded for each participant, during the four interactive tasks and baselines, using the BIOPAC MP150 system and software AcqKnowledge. ECG was recorded using three leads (BN-EL30-LEAD3) and a standard configuration with the white active electrode on the right upper chest, the black ground electrode on the left upper chest, and a red active electrode on the left lower chest. Respiration depth was recorded using the BIONOMADIX respiration belt. Signals from both participants were simultaneously recorded using a sampling rate of 1,000 Hz. Timestamps were used to synchronize the physiological data with audio, video, and continuous subjective ratings. See **Figure 1** for an example of the respiration and ECG signals.

We recorded baseline physiological data for 1 min before and after the block of four tasks, during which the participants were asked to breathe normally and relax. For each measure, we computed the average between the initial and final baselines to get single baseline measures (Bs). We also recorded about 20–25 s of data between the tasks allowing the physiological signals to return to baseline.

2.4. Analysis

2.4.1. Physiological Measures

Respiration signals were re-sampled at 4 Hz and a band-pass filter within [0.04–1] Hz was applied to reduce noise introduced by the equipment. For each participant, the RR intervals were obtained from the ECG data using a semi-automated MATLAB GUI as in previous studies (Orini et al., 2017b), which allows for revision and manual correction. Ectopic beats and artifacts were rare, and they were interpolated when present. The RR interval series was re-sampled at 4 Hz and the heart rate variability signal was obtained by high-pass filtering these series with a cut-off frequency of 0.03 Hz.

We computed the mean heart rate (HR) and the Root Mean Square of Successive Differences (RMSSD) between adjacent RR intervals for each participant and each condition (baseline, breathing in synchrony, short notes in synchrony, long notes in synchrony, and asynchronous short notes). HR is a measure of cardiovascular activity, and RMSSD is as common measure of HRV revealing how much the RR intervals fluctuate (Christou-Champi et al., 2015).

We applied the same methodology used in Orini et al. (2012b) to obtain the time-frequency coherence between two signals, which gives the correlation between two signals at different frequencies. The time-frequency coherence is defined as follows:

$$\gamma_{xy}(t,f) = \frac{|S_{xy}(t,f)|}{\sqrt{S_{xx}(t,f)S_{yy}(t,f)}}, \tag{1}$$

where $S_{xy}(t,f)$ is the cross-power spectral density of signals $x(t)$ and $y(t)$, which in this study represent HRV or respiration signals from each one of the participants, and is computed over time:

$$S_{xy}(t,f) = F\{E[x(t+\frac{\tau}{2})y^*(t-\frac{\tau}{2})]\}, \tag{2}$$

and $F\{\cdot\}$ and $E[\cdot]$ are the Fourier transform and the expectation operators, respectively (Orini et al., 2012b).

Although the frequencies of interest to analyze HRV are typically in the range 0.03–0.4 Hz, we were also interested in potential effects of short and fast vocalizations (up to one note per second) and performed the analysis in the range of 0.03–1 Hz.

In order to test the effect of respiration on HRV coupling, we computed the arithmetic mean of the TFC in the respiratory band, using the average of the respiratory frequency of both participants. The respiration frequency was determined for each participant as the peak frequency of the time-frequency spectrum of respiration. The respiratory band was defined by a window around the frequency of the respiration signal, with a width twice the frequency resolution of the time-frequency coherence analysis (0.078 Hz), as in previous studies (Orini et al., 2012c). The band was restricted to the [0.04–1] Hz range. An arithmetic mean was then obtained over time for each condition separately. This provided a coherence index for each condition for each dyad.

We additionally computed a partial time-frequency coherence (pTFC), which assesses the coupling of two signals after removing the effects of a third signal (Orini et al., 2012a; Widjaja et al., 2013). In this case, it was used to determine whether there was coupling beyond the effects of respiration. The pTFC function is defined as follows:

$$\gamma_{xy/z}(t,f) = \frac{|S_{xy/z}(t,f)|}{\sqrt{S_{xx/z}(t,f)S_{yy/z}(t,f)}}, \tag{3}$$

and $S_{xy/z}(t,f)$ is the partial cross-power spectral density, obtained as follows:

$$S_{xy/z}(t,f) = S_{xy}(t,f) - \frac{S_{xz}(t,f)S_{zy}(t,f)}{S_{zz}(t,f)}. \tag{4}$$

For our purposes, the third signal $z(t)$ was the respiration data from one of the participants. Because the respiration signal from either participant could be used to obtain the pTFC, we computed a pTFC using respiration signals from each participant and then averaged the two pTFCs. We averaged the pTFC over frequencies, although in this case we used the full range ($0.03 - 1$ Hz) rather than the respiratory band. Then, as for the TFC, we averaged the results over time to obtain one coherence index per condition.

2.4.2. Statistical Analyses

The measures we used in the statistical analyses were HR, RMSSD of HRV, and average togetherness ratings for individuals and TFC and pTFC for dyads. The Kolgomorov-Smirnov test for normality showed that the distributions were not normal. We thus used the non-parametric Wilcoxon sign rank tests for all analyses, allowing for paired comparisons. We used the Holm-Bonferroni method for multiple comparison correction (Holm, 1979). This consists of ordering the p-values from lowest

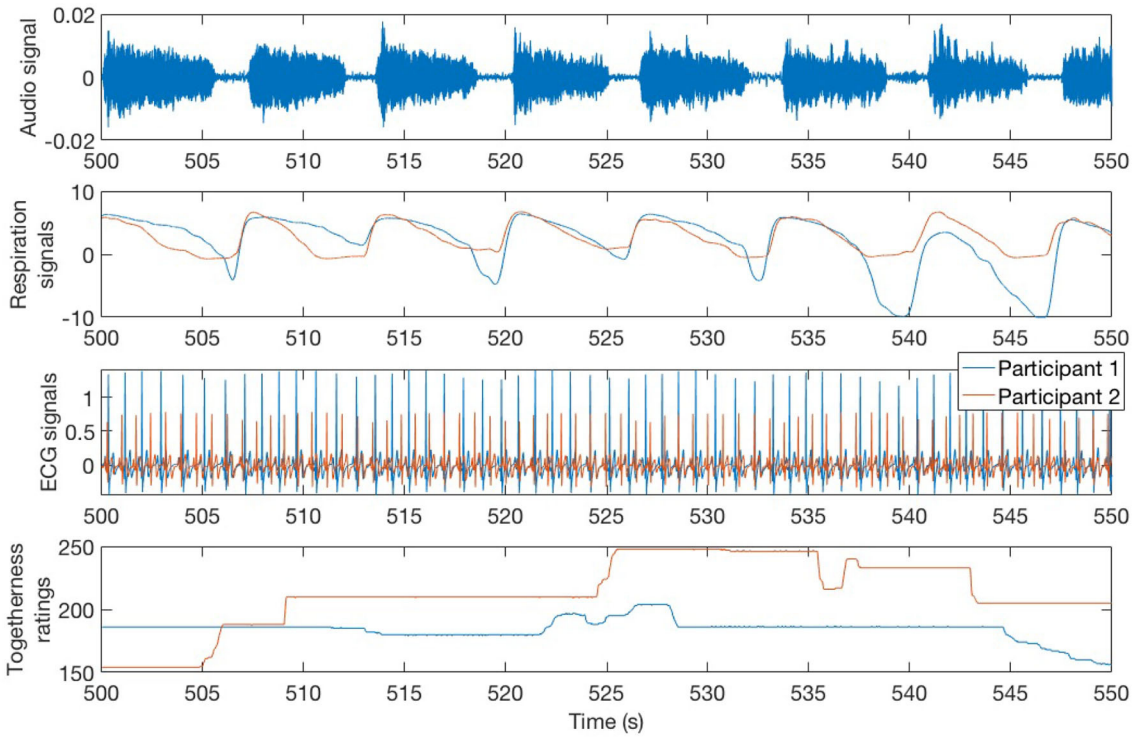

FIGURE 1 | A sample of the synchronized audio, respiration, and ECG signals and togetherness ratings for both participants in dyad 1 during the synchronized Long Notes condition.

to highest (p_k, with $k = 1:M$, where M is the number of comparisons), and then rejecting the null hypothesis for comparisons for which $p_k < 0.05/(M - k + 1)$. Once a null hypothesis is rejected the procedure is stopped. For HR, RMSSD, TFC of respiration, and TFC of HRV we were interested in seven comparisons:

(a) between baseline (Bs) and each condition (Br, SNsync, LN, and SNasync) to test each condition relative to the control;
(b) between Br and LN to test the effect of voice;
(c) between SNsync and LN to test the effect of the length of the vocalizations; and
(d) between SNsync and SNasync to test the synchrony of the vocalizations.

For pTFC, we were only interested in the effect of voice, and performed only three comparisons: LN with Br, LN with Bs, and Br and Bs. The latter allowed us to ensure that there was no coupling for the breathing condition. For the subjective ratings of togetherness, we performed three comparisons: Br and LN, SNsync and LN, and SNsync and SNasync.

2.5. Interviews and Questionnaire

Interviews were conducted to determine the strategies used by the participants to accomplish the tasks and to better understand the way people understand the concept of togetherness. During the interviews, participants were asked to report the aspects that made the tasks engaging, the differences between the tasks regarding their experience of pleasure, engagement, and connection with the other, and the aspects of the interaction contributing to the experience of togetherness. A questionnaire was also used to collect some information such as how challenging the task was for the participants (on a scale from 1 to 10) and to what extent they knew each other.

3. RESULTS

Table 1 shows the mean and standard deviation for HR, RMSSD, respiration frequency, TFC of respiration, and HRV signals averaged in the respiration band, partial TFC of HRV, and subjective togetherness values.

3.1. Heart Rate and RMSSD of HRV

Results for heart rate and RMSSD of HRV are summarized in **Table 2** and **Figure 2**. There was no difference in the averaged HR between conditions (Br, SNsync, LN, and SNasync). We found that RMSSD was greater for Br ($p = 0.0016$), SNsync ($p = 0.011$), LN ($p = 0.0002$), and SNasync ($p = 0.0074$) compared to Baseline, for LN compared to Br ($p = 0.0006$), and for LN compared to SNsync ($p = 0.0002$).

3.2. TFC of Respiration

The results of the TFC between respiration signals are shown in **Table 2**. The TFC of respiration for Br and LN was significantly higher than for Bs ($p = 0.0078$) and for LN than SNsync

TABLE 1 | Means and standard deviations of heart rate (bpm), RMSSD of heart rate variability (ms), average respiratory frequency (Hz), time-frequency coherence of respiration signals averaged in the respiration band, time-frequency coherence of HRV averaged in the respiratory band, partial TFC average, and subjective togetherness for each experimental condition.

	HR	RMSSD	Resp. freq.	Resp TFC	HRV TFC	pTFC	Together.
Baseline	76.4(7.9)	7.2(3.1)	0.63(0.27)	0.58(0.21)	0.32(0.10)	0.12(0.03)	N/A
Breathing	75.8(9.4)	10.6(4.0)	0.25(0.08)	0.91(0.05)	0.86(0.06)	0.13(0.04)	0.52(0.24)
SNsync	76.4(8.9)	8.8(3.1)	0.36(0.20)	0.53(0.18)	0.52(0.13)	0.12(0.04)	0.66(0.14)
LN	74.8(7.3)	14.5(4.7)	0.11(0.04)	0.88(0.06)	0.87(0.09)	0.21(0.07)	0.70(0.14)
SNasync	78.4(9.0)	8.8(2.8)	0.17(0.08)	0.50(0.13)	0.53(0.07)	0.12(0.03)	0.67(0.20)

Togetherness values are normalized to the 0–1 range.

TABLE 2 | Comparisons between conditions for heart rate, RMSSD of heart rate variability, time-frequency coherence of respiration signals averaged in the respiration band, time-frequency coherence of HRV averaged in the respiratory band, partial TFC average and subjective togetherness values.

Comparison	HR *p*-value	RMSSD *p*-value	Resp TFC *p*-value	HRV TFC *p*-value	pTFC *p*-value	Togeth. *p*-value
Bs and Br	0.9133	0.0016*	0.0078*	0.0039*	0.5703	N/A
Bs and SNsync	0.8107	0.0108*	0.4961	0.0117*	N/A	N/A
Bs and LN	0.1701	0.0002*	0.0078*	0.0039*	0.0117*	N/A
Bs and SNasync	0.0778	0.0074*	0.3594	0.0039*	N/A	N/A
Br and LN	0.4204	0.0006*	0.1641	0.4258	0.0078*	0.0174
LN and SNsync	0.2668	0.0002*	0.0039*	0.0039*	N/A	0.1961
SNsync and SNasync	0.0778	0.8107	0.3008	1	N/A	0.3794
Number of comparisons	**7**	**7**	**7**	**7**	**3**	**3**

**Indicates statistical significance using Holm-Bonferroni correction.*

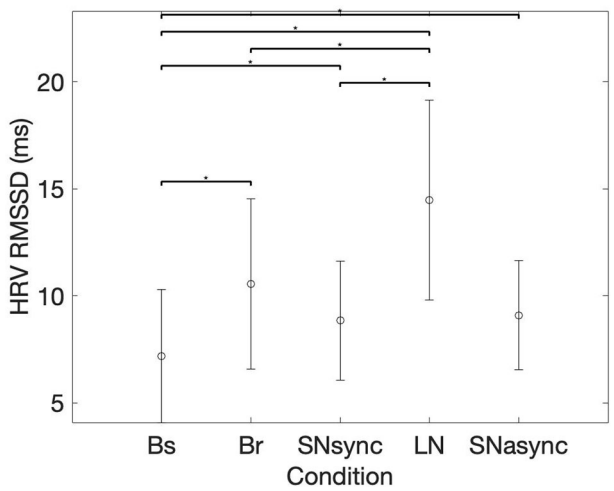

FIGURE 2 | Mean (circles) and SD (bars) for the RMSSD of Heart Rate Variability. *Represents statistically significant differences, using Holm-Bonferroni correction.

($p = 0.0039$). Respiration signals were not more synchronized for SNsync or SNasync compared to Bs.

3.3. HRV Coherence in Respiratory Band

Figure 3 shows the time-frequency coherence between HRV for dyad 1. It can be appreciated that there is an increase in coherence in Br and LN conditions for a range of frequencies, with peaks around 0.3 and 0.1 Hz and harmonic components at multiple frequencies. The average coherence in the respiratory band was greater for Br, LN, and SNasync than Bs ($p = 0.0039$), for SNsync than Bs ($p = 0.0117$), and for LN than SNsync ($p = 0.0039$). All results are summarized in **Table 2** and **Figure 4**.

A stable component at very high frequency (between 0.4 and 0.9 Hz) was present in the time-frequency coherence between HRV for most dyads. To investigate this in more detail we examined the relationship between the peak frequencies in the time-frequency coherence between HRV and the frequency of the vocal bursts (the inverse of the time between the beginnings of successive bursts). Moving average was applied to the audio signals to determine the onsets of the vocal bursts and thus their frequency. In the SNsync condition, participants produced notes every 1.6 s on average (range of 1–2.5 s), corresponding to 0.64 Hz. For seven out of nine dyads, the average frequency of vocal bursts matched either the first or second peak in the corresponding HRV coherence spectra averaged over time for the SN and LN conditions (see **Figure 5**). This effect is even clearer for LN, with 9 out of 9 dyads showing a correspondence between the first peak in the HRV coupling and the frequency between bursts. Because the vocal pattern imposes a respiratory rhythm, we conclude that for SNsync and LN there is an effect of breathing on HRV.

There was no significant difference between the TFC of HRV of LN and Br. Additionally, when analyzing the time

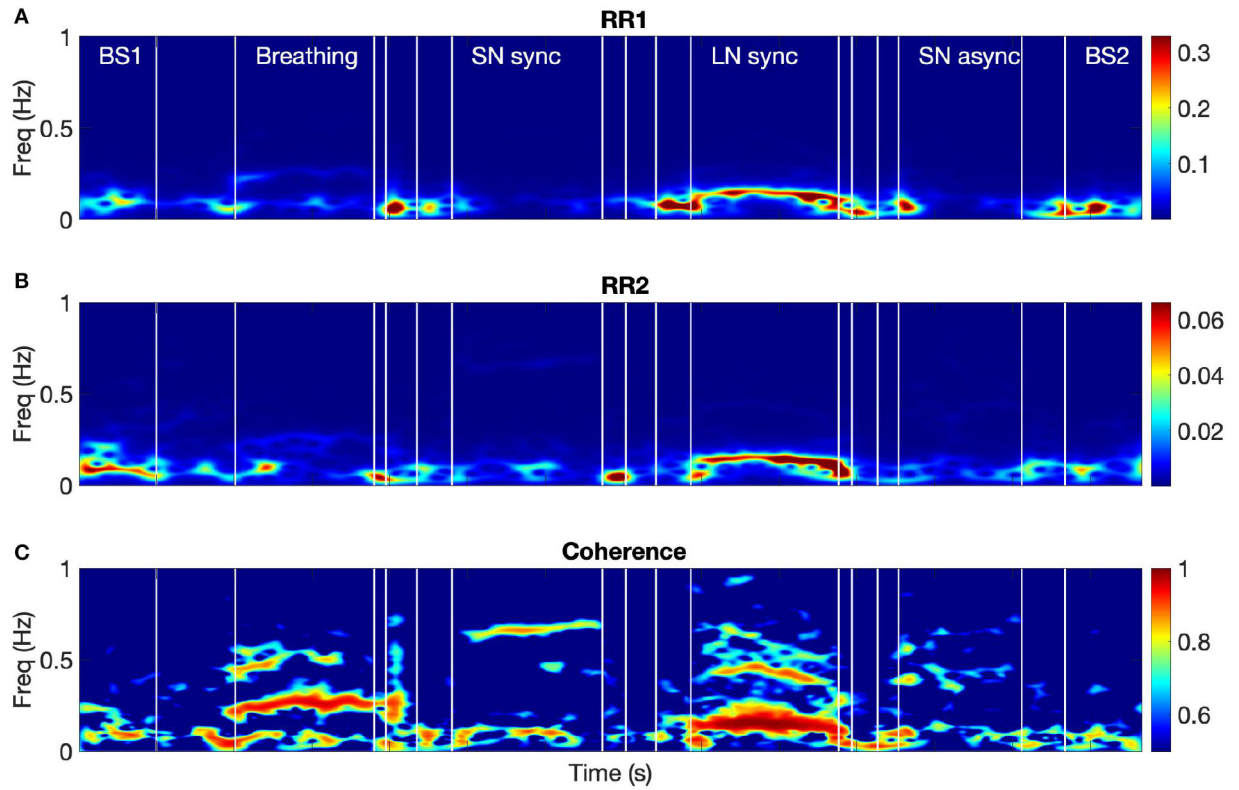

FIGURE 3 | The spectra of the RR intervals for both participants from dyad 1 **(A,B)** and their coherence spectrum **(C)**. BS1 and BS2 refer to the 60-s baselines before and after the tasks, respectively. Breathing refers to the breathing condition and LN to the long notes condition. SNsync and SNasync refer to the conditions with synchronous and asynchronous short notes, respectively.

intervals between successive exhalations using the respiration signals for both conditions, we found that, on average, the period of respiration for the Br condition was of 2.8 s (range of 3.5–5.5 s) vs. an average of 9.1 s (range of 5–22 s) for the LN condition. Participants were thus having longer breathing cycles for LN than for Br, which we discuss in section 4.

3.4. HRV Partial Coherence

In order to determine changes in HRV coherence not related to RSA, we computed the pTFC, which removes the respiratory component from the TFC of the dyad's HRVs (see **Figure 6**). We hypothesized that a significant difference between the long notes and breathing conditions after removing the respiration component would indicate the presence of another mechanism beyond RSA. Results are summarized in **Table 2** and **Figure 7**. Partial TFC was higher during LN than Bs ($p = 0.0117$) and Br ($p = 0.0078$), suggesting that for long notes coupling between HRV in the two participants occurred beyond the effect of breathing. We also found no differences in pTFC during Br vs. Bs conditions, which was expected since these conditions only differ in the breathing pattern and partial coherence removes the effect of breathing. For LN, the average of the TFC on the 0–1 Hz range decreased from 0.87 to 0.21 when removing the effects of respiration (see **Table 1**), suggesting the effect of RSA predominantly mediates the HRV coupling.

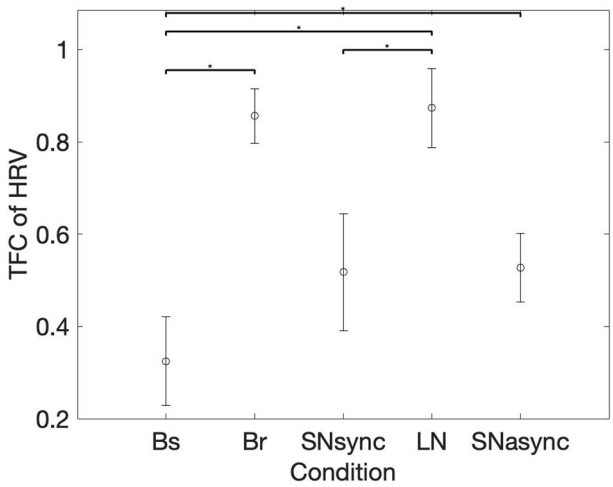

FIGURE 4 | Mean and SD for the TFC average on respiration band. *Represents statistically significant differences using Holm-Bonferroni correction.

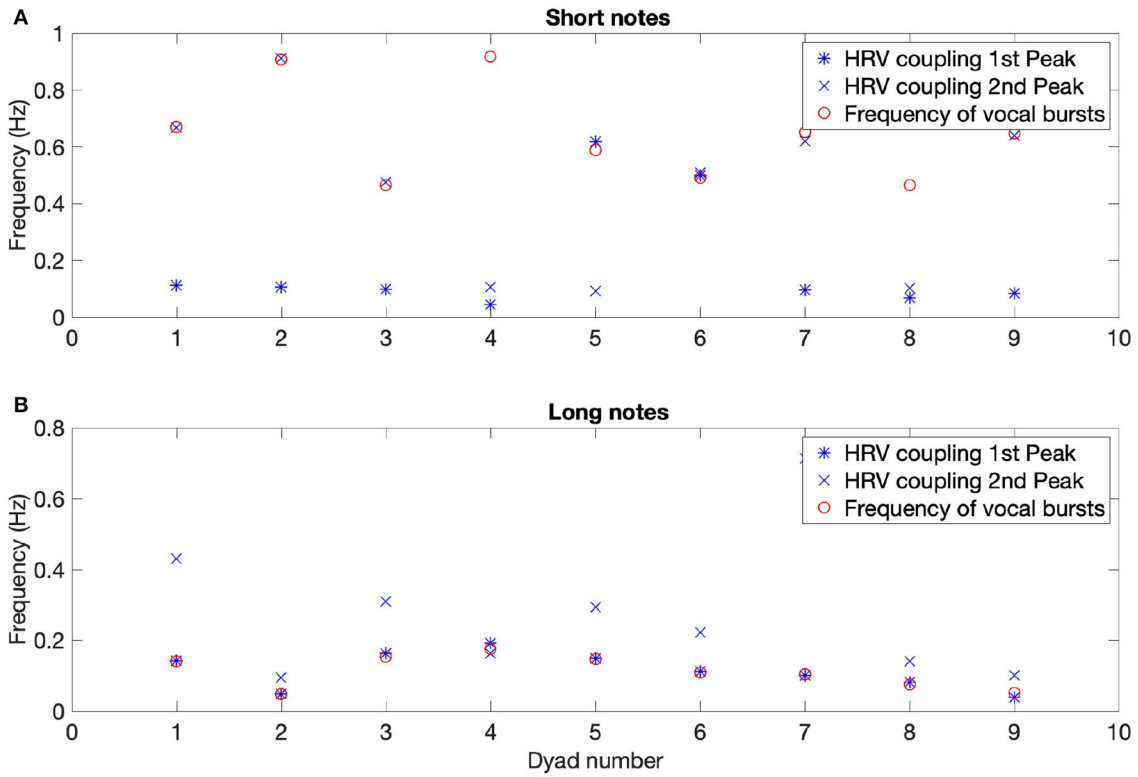

FIGURE 5 | Mean frequency of HRV coherence peaks and of vocal bursts for each dyad, for synchronous short **(A)** and long notes **(B)**. The correspondence between the frequency of vocal bursts and the first peak in the HRV coherence is striking for long vocalizations **(B)**. For short vocalizations, there is a correspondence between the frequency of onsets and one of the first two peaks in the HRV coherence for seven out of nine dyads **(A)**.

3.5. Togetherness

We compared the mean values of togetherness' subjective ratings between Br and LN, SNsync and LN, and SNsync and SNasync. We found no that subjective togetherness was only greater for LN compared to Br ($p = 0.017$), although this remains a trend as results were not significant after correcting for multiple comparisons. The other comparisons were not statistically significant. Participants generally agreed regarding the preferred conditions, indicated by a higher mean in the reported togetherness. LN had the highest mean for nine participants, SNasync was preferred by five participants, SNsync was preferred by two, and Br was preferred by none. The differences between LN and Br suggest that the presence of voice has an important effect on the subjective experience of togetherness. The lack of a statistically significant result might be due both to sample size and the noisy nature of these subjective reports. Interestingly, the SNasync condition was the second preferred condition, suggesting factors other than synchrony are relevant for participants when rating togetherness.

Three kinds of togetherness experiences emerged from the interviews. First, some participants referred to the experience with words such as "existential" or "meditative" and reported it was an "intimate experience" allowing to have a joint expression with someone else. For instance, some people reported having felt more connected than they would by means of conversation. Second, particularly with regards to the asynchronous condition, some participants were engaged by the fact that the interaction was "playful," and that they could come up with ideas more freely than in the synchronous ones. The possibility of responding to each other asynchronously allowed for a call and response game and hence appraised as more interactive. Third, participants found that having a common goal and pursuing it as a team contributed to their experience of togetherness. Some participants reported that they experienced less togetherness in more chaotic parts of the interaction, while more "harmonic" parts gave rise to more togetherness. We speculate that more chaotic interactions could be interpreted as an absence of a common goal by some participants. The previous themes indicate that the construct of togetherness can be divided into at least three different components, which we introduce here as the *existential*, *playful*, and *common-goal* togetherness.

We were also interested in exploring how the self-reported challenge level of the tasks could relate to the experienced togetherness. We found no significant differences in how the participants rated the challenge level of each task and the correlation between the subjectively reported challenge level and the average togetherness was very weak ($r = 0.19$).

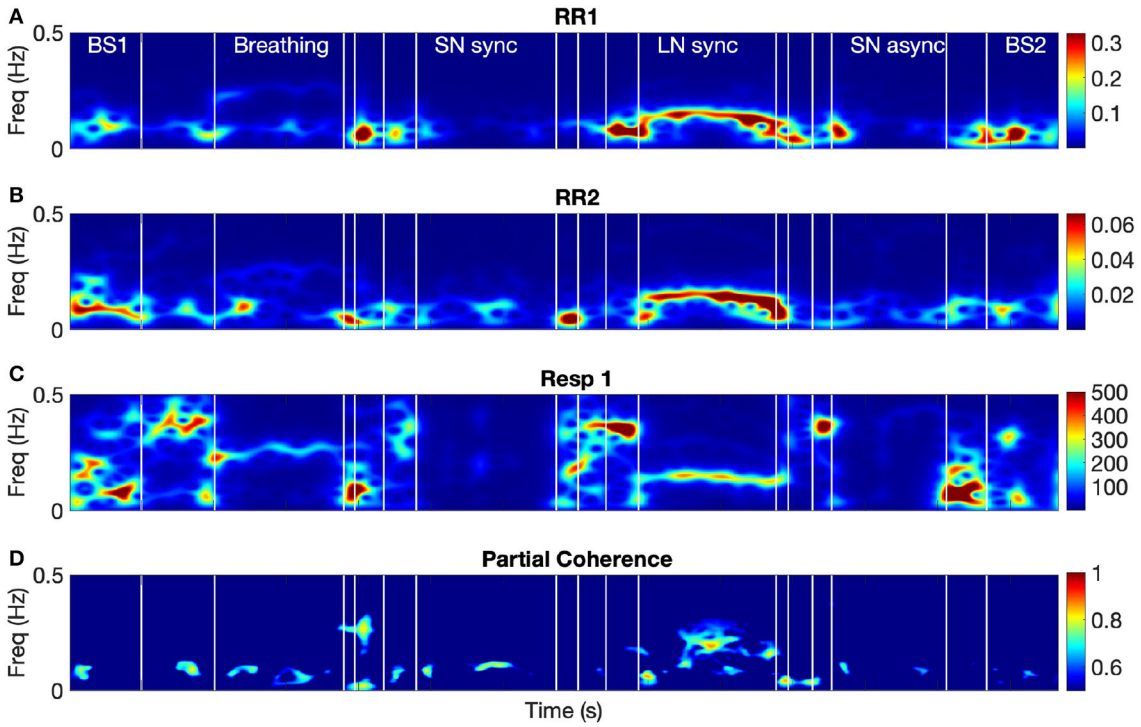

FIGURE 6 | The spectra of the RR intervals for both participants from dyad 1 **(A,B)**, the respiration signal from participant 1 **(C)**, and their partial time-frequency coherence **(D)**. Name of the conditions is the same as in **Figure 3**.

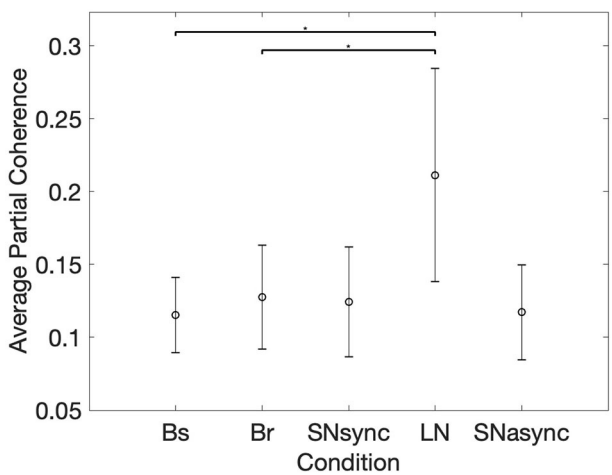

FIGURE 7 | Mean and standard deviation of the average of time-frequency coherence after removing the respiration component. *Represents statistically significant differences using Holm-Bonferroni correction.

4. DISCUSSION

This study shows that synchronization of respiration mediates HRV coupling when non-experts vocalize together, expanding upon previous results (Müller and Lindenberger, 2011; Vickhoff et al., 2013). By comparing the strength of the coupling before and after removing the respiration signal, we conclude that RSA accounts for a significant part of the effect. The finding that HRV coupling was higher after analytically removing the respiration component from the TFC for synchronized long notes but not for synchronized breathing suggests that a mechanism other than RSA also contributes to HRV coupling when vocalizing together. The main difference between LN and Br is the presence of voice, suggesting that either synchronization of vocal muscular action or perception of voice might mediate HRV coupling. Since the vagus nerve links the vocal chords, facial expressions, and heart rate (Porges, 2001), it may be possible that the voice affects HRV by means of the ANS.

The analysis of the audio recordings shows that the frequency of vocal bursts and HRV peaks matched for both synchronized, short, and long note conditions. Differences between synchronized short and long vocalizations can be due to various reasons, such as different physiological mechanisms operating at different frequencies. For the specific tasks that were used, when making long notes, people synchronized both the beginnings and ends of the vocalizations; for short notes, however, people inhaled at different times. In addition, very short notes, made every 1 or 2 s, are likely to have a frequency that is close to the heart rate, and hence are less likely to appear in the spectral analysis due to the heart rate being the natural sampling frequency. Our results show that although frequencies above 0.4 Hz are typically not considered in the HRV

analyses, some coupling persists even at higher frequencies, and the respiratory spectral band should be adjusted to respiration (Orini et al., 2012c). An implication of these results is the possibility to make vocal interventions targeting HRV coupling at specific frequencies.

The time-frequency coherence of respiration and of HRV do not match for SNsync and SNasync (see **Table 2**), suggesting respiration synchrony does not mediate the observed HRV entrainment for short notes. However, in the context of the tasks that were used in this study, the breathing patterns were not controlled and hence the quality of the respiration signals might have been different for short and long notes. While for LN and Br conditions, participants made deeper and more synchronized breaths that fluctuated between two values, for the short notes conditions (SNsync and SNasync), they had freedom to inhale between each pair of vocalizations or to take longer breaths, inhaling only occasionally. Furthermore, the fact that TFC of HRVs was higher during SNasync than during Bs may indicate that participants' vocalizations were coupled, even if they were explicitly asked to perform their notes at different times. We observed that for most dyads and in the SNasync condition, participants timed their short notes in response to their partners (as in the call and response dynamic noted earlier), hence producing some degree of synchrony in the TFC analyses, which yields high values for phase-delayed signals.

Musical entrainment usually refers to the entrainment to a musical beat, which is only possible for frequencies above 0.5 Hz, with a period between beats lower than 2 s (Repp and Doggett, 2007). In our study, only the synchronized short notes condition allowed for such entrainment. Because we found a stronger HRV coupling for vocalizations of longer duration, we conclude that HRV entrainment is primarily due to RSA and is independent of beat entrainment. This is consistent with the four levels of entrainment proposed by Trost et al. (2017) and stresses that aspects other than those related to musical tempo entrain during music interaction and might play a role in affective states. This makes a case for studying music with weak or no sense of beat, as is found in many segments of traditional music and some types of contemporary music, such as drone, ambient, and soundscape genres.

HRV is affected by emotional arousal and valence (Orini et al., 2010, 2019) and is considered a "biomarker of successful emotional regulation," which is the capacity of an individual to maintain positive emotions despite unfavorable contexts (Christou-Champi et al., 2015). Individuals regulate their emotions using slow paced breathing (Song and Lehrer, 2003) presumably by imposing a rhythm on the heart activity patterns, affecting the rest of the body and the brain. The heart-brain connection is being increasingly studied (Dunn et al., 2010; Mather and Thayer, 2018) and RSA has been effectively exploited to affect psychological states (Lehrer and Gevirtz, 2014). One of the possible implications of HRV entrainment between people is a potential role in bonding, by simultaneously affecting the psycho-physiological state (Bernardi et al., 2017) or by facilitating coordination by means of synchronizing inner rhythms (Vickhoff et al., 2013). These are yet to be supported by research.

Contrary to our initial hypothesis, we did not find a strong correlation/interaction between dyadic HRV coupling and a subjective experience of togetherness. In fact, the subjective experience of togetherness is a complex construct and unlikely to be reducible to a physiological marker. We speculate that at least three factors contribute to the subjective experience of togetherness: having a common-goal, playfulness, and existential togetherness. The common-goal factor likely operates at a more abstract level, involving cognitive appraisals of joint success in the task. We assume that this component is not related to autonomic physiological synchrony, because all participants can simultaneously have different appraisals of the same situation. The playful aspect seems to be closely linked to language in the sense that it relates to a call and response interaction. It was mostly reported with regards to the asynchronous condition, where HRV coupling was not significant. The playfulness component is therefore also unlikely to be related to autonomic physiological synchronization. Lastly, the existential aspect of togetherness involves a sense of sameness, which may arise when people are doing the same action ["we-agency", as in Vickhoff et al. (2013)]. This is associated with "oneness" and "spiritual" experiences, typical of many singing contexts (Dingle et al., 2013). We speculate that if HRV coupling is related to a togetherness experience, the existential component of togetherness would be the most relevant. Further research is required to establish whether more specific subjective reports of existential togetherness consistently correlate with autonomic physiological synchrony.

5. CONCLUSION

This study shows that HRV of non-expert singing together shows a higher level of coupling than during baseline. We found that making synchronous long vocalizations produced greater coupling in the respiration band of the heart rate variability coherence compared to making short vocalizations. In addition, for synchronized long vocalizations but not for synchronized breathing, HRV coupling was greater than baseline after removing the effect of respiration. These results suggest that while HRV coupling was mainly driven by a synchronization of the respiratory activity, joint vocalization also contributes to HRV coupling beyond the effect of respiration.

Subjectively experienced togetherness did not show correlations with physiological synchrony, likely due to the complexity of the togetherness construct. Detailed interviews identified three main components to subjective togetherness, which we introduce here as the *existential*, *playful*, and *common-goal* togetherness. Future research is needed to assess the interaction between these components and autonomic physiological synchrony and the potential benefit of interventions resulting in HRV entrainment between people.

DATA AVAILABILITY STATEMENT

The raw data supporting the conclusions of this article will be made available by the authors, without undue reservation.

ETHICS STATEMENT

The studies involving human participants were reviewed and approved by Queen Mary Ethics of Research Committee. The participants provided their written informed consent to participate in this study.

AUTHOR CONTRIBUTIONS

SR-B, EC, and MO contributed conception and design of the study. SR-B performed the statistical analysis and wrote the manuscript. MO provided the analysis tools. All authors contributed to discussion and manuscript revision and read and approved the submitted version.

FUNDING

This result is part of a project that has received funding from the European Research Council (ERC) under the European Union's Horizon 2020 research and innovation program (Grant agreement No. 788960). SR-B has also received support as a doctoral student in the Engineering and Physical Sciences Research Council (EPSRC) and the Arts and Humanities Research Council (AHRC) Centre for Doctoral Training in Media and Arts Technology at Queen Mary University of London (EP/L01632x/1).

ACKNOWLEDGMENTS

We wish to thank the QMUL Experimental Psychology Department for the use of their physiology equipment and facilities.

REFERENCES

Bernardi, N. F., Codrons, E., Di Leo, R., Vandoni, M., Cavallaro, F., Vita, G., et al. (2017). Increase in synchronization of autonomic rhythms between individuals when listening to music. *Front. Physiol.* 8:785. doi: 10.3389/fphys.2017.00785

Christou-Champi, S., Farrow, T. F., and Webb, T. L. (2015). Automatic control of negative emotions: evidence that structured practice increases the efficiency of emotion regulation. *Cogn. Emot.* 29, 319–331. doi: 10.1080/02699931.2014.901213

Clayton, M. (2012). What is entrainment? definition and applications in musical research. *Empir. Musicol. Rev.* 7, 49–56. doi: 10.18061/1811/52979

Clift, S., and Hancox, G. (2010). The significance of choral singing for sustaining psychological wellbeing: findings from a survey of choristers in England, Australia and Germany. *Music Perform. Res.* 3, 79–96. doi: 10.1386/jaah.1.1.19/1

De Jaegher, H., Di Paolo, E., and Gallagher, S. (2010). Can social interaction constitute social cognition? *Trends Cogn. Sci.* 14, 441–447. doi: 10.1016/j.tics.2010.06.009

Dingle, G. A., Brander, C., Ballantyne, J., and Baker, F. A. (2013). To be heard: the social and mental health benefits of choir singing for disadvantaged adults. *Psychol. Music* 41, 405–421. doi: 10.1177/0305735611430081

Dunbar, R. (2017). Group size, vocal grooming and the origins of language. *Psychon. Bull. Rev.* 24, 209–212. doi: 10.3758/s13423-016-1122-6

Dunn, B. D., Galton, H. C., Morgan, R., Evans, D., Oliver, C., Meyer, M., et al. (2010). Listening to your heart: how interoception shapes emotion experience and intuitive decision making. *Psychol. Sci.* 21, 1835–1844. doi: 10.1177/0956797610389191

Grossman, P., and Taylor, E. W. (2007). Toward understanding respiratory sinus arrhythmia: relations to cardiac vagal tone, evolution and biobehavioral functions. *Biol. Psychol.* 74, 263–285. doi: 10.1016/j.biopsycho.2005.11.014

Hayward, G. (2014). *Singing as one: community in synchrony* (Ph.D. thesis). Cambridge University, Cambridge, United Kingdom.

Himberg, T., Laroche, J., Bigé, R., Buchkowski, M., and Bachrach, A. (2018). Coordinated interpersonal behaviour in collective dance improvisation: the aesthetics of kinaesthetic togetherness. *Behav. Sci.* 8:23. doi: 10.3390/bs8020023

Holm, S. (1979). A simple sequentially rejective multiple test procedure. *Scand. J. Stat.* 6, 65–70.

Judd, M., and Pooley, J. A. (2014). The psychological benefits of participating in group singing for members of the general public. *Psychol. Music* 42, 269–283. doi: 10.1177/0305735612471237

Konvalinka, I., Vuust, P., Roepstorff, A., and Frith, C. D. (2010). Follow you, follow me: continuous mutual prediction and adaptation in joint tapping. *Q. J. Exp. Psychol.* 63, 2220–2230. doi: 10.1080/17470218.2010.497843

Kreutz, G. (2014). Does singing facilitate social bonding. *Music Med.* 6, 51–60.

Lehrer, P. M., and Gevirtz, R. (2014). Heart rate variability biofeedback: how and why does it work? *Front. Psychol.* 5:756. doi: 10.3389/fpsyg.2014.00756

Mather, M., and Thayer, J. F. (2018). How heart rate variability affects emotion regulation brain networks. *Curr. Opin. Behav. Sci.* 19, 98–104. doi: 10.1016/j.cobeha.2017.12.017

Müller, V., and Lindenberger, U. (2011). Cardiac and respiratory patterns synchronize between persons during choir singing. *PLoS ONE* 6:e24893. doi: 10.1371/journal.pone.0024893

Nachmanovitch, S. (1990). *Free Play: Improvisation in Life and Art*. New York, NY: Putnam.

Noy, L., Dekel, E., and Alon, U. (2011). The mirror game as a paradigm for studying the dynamics of two people improvising motion together. *Proc. Natl. Acad. Sci. U.S.A.* 108, 20947–20952. doi: 10.1073/pnas.1108155108

Noy, L., Levit-Binun, N., and Golland, Y. (2015). Being in the zone: physiological markers of togetherness in joint improvisation. *Front. Hum. Neurosci.* 9:187. doi: 10.3389/fnhum.2015.00187

Orini, M., Al-Amodi, F., Koelsch, S., and Bailón, R. (2019). The effect of emotional valence on ventricular repolarization dynamics is mediated by heart rate variability: a study of QT variability and music-induced emotions. *Front. Physiol.* 10:1465. doi: 10.3389/fphys.2019.01465

Orini, M., Bailón, R., Enk, R., Koelsch, S., Mainardi, L., and Laguna, P. (2010). A method for continuously assessing the autonomic response to music-induced emotions through HRV analysis. *Med. Biol. Eng. Comput.* 48, 423–433. doi: 10.1007/s11517-010-0592-3

Orini, M., Bailón, R., Laguna, P., Mainardi, L. T., and Barbieri, R. (2012a). A multivariate time-frequency method to characterize the influence of respiration over heart period and arterial pressure. *EURASIP J. Adv. Signal Process.* 214:214. doi: 10.1186/1687-6180-2012-214

Orini, M., Bailon, R., Mainardi, L. T., Laguna, P., and Flandrin, P. (2012b). Characterization of dynamic interactions between cardiovascular signals by time-frequency coherence. *IEEE Trans. Biomed. Eng.* 59, 663–673. doi: 10.1109/TBME.2011.2171959

Orini, M., Laguna, P., Mainardi, L., and Bailón, R. (2012c). Assessment of the dynamic interactions between heart rate and arterial pressure by the cross time–frequency analysis. *Physiol. Meas.* 33:315. doi: 10.1088/0967-3334/33/3/315

Orini, M., Pueyo, E., Laguna, P., and Bailón, R. (2017a). A time-varying nonparametric methodology for assessing changes in QT variability unrelated to heart rate variability. *IEEE Trans. Biomed. Eng.* 65, 1443–1451. doi: 10.1109/TBME.2017.2758925

Orini, M., Tinker, A., Munroe, P. B., and Lambiase, P. D. (2017b). Long-term intra-individual reproducibility of heart rate dynamics during exercise and recovery in the UK biobank cohort. *PLoS ONE* 12:e0183732. doi: 10.1371/journal.pone.0183732

Palumbo, R. V., Marraccini, M. E., Weyandt, L. L., Wilder-Smith, O., McGee, H. A., Liu, S., et al. (2017). Interpersonal autonomic physiology: a systematic review of the literature. *Pers. Soc. Psychol. Rev.* 21, 99–141. doi: 10.1177/1088868316628405

Pearce, E., Launay, J., and Dunbar, R. I. (2015). The ice-breaker effect: singing mediates fast social bonding. *Open Sci.* 2:150221. doi: 10.1098/rsos.150221

Porges, S. W. (2001). The polyvagal theory: phylogenetic substrates of a social nervous system. *Int. J. Psychophysiol.* 42, 123–146. doi: 10.1016/S0167-8760(01)00162-3

Repp, B. H., and Doggett, R. (2007). Tapping to a very slow beat: a comparison of musicians and nonmusicians. *Music Percept.* 24, 367–376. doi: 10.1525/mp.2007.24.4.367

Saul, J. P. (1990). Beat-to-beat variations of heart rate reflect modulation of cardiac autonomic outflow. *Physiology* 5, 32–37. doi: 10.1152/physiologyonline.1990.5.1.32

Sin, P. Y., Galletly, D. C., and Tzeng, Y. (2010). Influence of breathing frequency on the pattern of respiratory sinus arrhythmia and blood pressure: old questions revisited. *Am. J. Physiol. Heart Circ. Physiol.* 298, H1588–H1599. doi: 10.1152/ajpheart.00036.2010

Song, H.-S., and Lehrer, P. M. (2003). The effects of specific respiratory rates on heart rate and heart rate variability. *Appl. Psychophysiol. Biofeedback* 28, 13–23. doi: 10.1023/A:1022312815649

Spiro, N., and Himberg, T. (2012). "Musicians and non-musicians adapting to tempo differences in cooperative tapping tasks," in *Proceedings of the 12th International Conference on Music perception and Cognition and the 8th Triennial Conference of the European Society for the Cognitive Sciences of Music* (Thessaloniki), 950–955.

Tarr, B., Launay, J., and Dunbar, R. I. M. (2014). Music and social bonding: "self-other" merging and neurohormonal mechanisms. *Front. Psychol.* 5:1096. doi: 10.3389/fpsyg.2014.01096

Trost, W., Labbé, C., and Grandjean, D. (2017). Rhythmic entrainment as a musical affect induction mechanism. *Neuropsychologia* 96, 96–110. doi: 10.1016/j.neuropsychologia.2017.01.004

Vickhoff, B., Malmgren, H., Åström, R., Nyberg, G., Ekström, S.-R., Engwall, M., et al. (2013). Music structure determines heart rate variability of singers. *Front. Psychol.* 4:334. doi: 10.3389/fpsyg.2013.00334

Widjaja, D., Orini, M., Vlemincx, E., and Van Huffel, S. (2013). Cardiorespiratory dynamic response to mental stress: a multivariate time-frequency analysis. *Comput. Math. Methods Med.* 2013:451857. doi: 10.1155/2013/451857

Conflict of Interest: The authors declare that the research was conducted in the absence of any commercial or financial relationships that could be construed as a potential conflict of interest.

frontiers in Physiology

BRIEF RESEARCH REPORT
published: 18 September 2020
doi: 10.3389/fphys.2020.542183

Effect of Hyperventilation on Periodic Repolarization Dynamics

Dominik Schüttler[1,2,3], Lukas von Stülpnagel[1,4], Konstantinos D. Rizas[1,2], Axel Bauer[2,4], Stefan Brunner[1†] and Wolfgang Hamm[1,2†]*

[1]Medizinische Klinik und Poliklinik I, University Hospital Munich, Ludwig-Maximilians University Munich (LMU), Munich, Germany, [2]DZHK (German Centre for Cardiovascular Research), Partner Site Munich, Munich Heart Alliance (MHA), Munich, Germany, [3]Walter Brendel Centre of Experimental Medicine, Ludwig-Maximilians University Munich (LMU), Munich, Germany, [4]University Hospital for Internal Medicine III, Medical University Innsbruck, Innsbruck, Austria

Heart and lung functions are closely connected, and the interaction is mediated by the autonomic nervous system. Hyperventilation has been demonstrated to especially activate its sympathetic branch. However, there is still a lack of methods to assess autonomic activity within this cardiorespiratory coupling. Periodic repolarization dynamics (PRD) is an ECG-based biomarker mirroring the effect of efferent cardiac sympathetic activity on the ventricular myocardium. Its calculation is based on beat-to-beat variations of the T wave vector ($dT°$). In the present study, we investigated the effects of a standardized hyperventilation maneuver on changes of PRD and its underlying $dT°$ signal in 11 healthy subjects. In response to hyperventilation, $dT°$ revealed a characteristic pattern and normalized $dT°$ values increased significantly compared to baseline [0.063 (IQR 0.032) vs. 0.376 (IQR 0.093), $p < 0.001$] and recovery [0.082 (IQR 0.029) vs. 0.376 (IQR 0.093), $p < 0.001$]. During recovery, $dT°$ remained on a higher level compared to baseline ($p = 0.019$). When calculating PRD, we found significantly increased PRD values after hyperventilation compared to baseline [3.30 (IQR 2.29) deg^2 vs. 2.76 (IQR 1.43) deg^2, $p = 0.018$]. Linear regression analysis revealed that the increase in PRD level was independent of heart rate ($p = 0.63$). Our pilot data provide further insights in the effect of hyperventilation on sympathetic activity associated repolarization instability.

Keywords: hyperventilation, autonomic function, sympathetic nervous system, repolarization instability, T wave vector, periodic repolarization dynamics

OPEN ACCESS

Edited by:
Tijana Bojić,
University of Belgrade, Serbia

Reviewed by:
Michele Orini,
University College London, United Kingdom
Evan L. Matthews,
Montclair State University, United States

****Correspondence:***
Stefan Brunner
stefan.brunner@med.uni-muenchen.de

[†]These authors have contributed equally to this work

Specialty section:
This article was submitted to Autonomic Neuroscience, a section of the journal Frontiers in Physiology

Received: *11 March 2020*
Accepted: *27 August 2020*
Published: *18 September 2020*

Citation:
Schüttler D, von Stülpnagel L, Rizas KD, Bauer A, Brunner S and Hamm W (2020) Effect of Hyperventilation on Periodic Repolarization Dynamics. Front. Physiol. 11:542183. doi: 10.3389/fphys.2020.542183

INTRODUCTION

Our breathing and heart rate as well as heart function are linked and controlled by the autonomic nervous system. This close connection has been described earlier with heart rates slowing during expiration and a relative tachycardia evolving during inspiration due to vagolytic effects, the so called respiratory sinus arrhythmia (RSA; Yasuma and Hayano, 2004). It is hypothesized that the RSA facilitates efficient respiratory gas exchanges and decreases the workload of the heart while maintaining blood gases in physiological levels (Ben-Tal et al., 2012).

Respiratory dysfunction can influence cardiovascular health, and cardiovascular diseases are often associated with respiratory diseases (Garcia et al., 2013). Breathing disorders and pulmonary diseases are tightly linked to autonomic dysfunction (van Gestel and Steier, 2010; Milagro et al., 2019). On the other hand, it has been demonstrated that the maintenance of correct cardiorespiratory coupling exerts beneficial cardiovascular effects in patients with an attenuated RSA (Ben-Tal et al., 2012).

Hyperventilation especially activates the sympathetic nervous system and results in physiological changes of the cardiovascular system: it increases heart rate and blood pressure most likely due to attenuated baroreceptor sensitivity (Alexopoulos et al., 1995; Van De Borne et al., 2000). Concomitant loss of arterial carbon dioxide levels has been connected to various diseases including cerebral and cardiorespiratory disorders (Laffey and Kavanagh, 2002). Additionally, hyperventilation has been demonstrated to affect the repolarization phase of the cardiac cycle by inducing repolarization abnormalities including ST depression and T wave inversion (Alexopoulos et al., 1996).

Respiratory changes exert influences on autonomic nervous activity and thus controlled breathing maneuvers have been used to evaluate autonomic activity and detect dysfunctional states in cardiovascular diseases (Badra et al., 2001). Hawkins et al. (2019), for example, found significantly reduced responses of heart rate in patients with heart failure and coronary heart disease during hyperventilation compared to a healthy cohort.

To non-invasively assess autonomic function, different heart rate and ECG-based biomarkers have been established so far. Here, especially parameters derived from beat-to-beat alterations of the T wave such as microvolt T wave alternans and periodic repolarization dynamics (PRD) have been of increasing interest as especially the repolarization phase is modulated by the sympathetic nervous system and these parameters have been shown to predict the risk for the development of malignant arrhythmias and mortality (Kaufman et al., 2006; Salerno-Uriarte et al., 2007; Verrier et al., 2011; Rizas et al., 2014, 2017; Aro et al., 2016; Bauer et al., 2019). PRD is an ECG-based biomarker which most probably reflects the effect of sympathetic nervous activity on the ventricular myocardium. Its calculation is based on the quantification of low-frequency oscillations (≤0.1 Hz) of cardiac repolarization. In a first step, the angle between successive repolarization vectors ($dT°$) is determined. Subsequently, low-frequency components are assessed using wavelet analysis (Rizas et al., 2014). It is known that increased PRD is associated with increased mortality and cardiovascular mortality in patients with ischemic as well as non-ischemic cardiomyopathy (Rizas et al., 2014, 2017; Bauer et al., 2019).

In this manuscript, we sought to investigate the effect of a standardized hyperventilation maneuver on PRD in a cohort comprised of healthy individuals.

MATERIALS AND METHODS

In the present study, we included 11 healthy adults (nine men, two women, and mean age 31.0 years in a range of 25–49 years). We performed a standardized hyperventilation maneuver that has been described in different studies before (Guensch et al., 2014; Fischer et al., 2016; Roubille et al., 2017): in brief, after a resting phase in a seated position for 10 min, volunteers performed hyperventilation at a respiratory rate of 30/min for 1 min followed by an apnea phase as long as tolerated. Afterward, study participants stayed in seated rest until the end of the study. During the entire study time of 20 min, we tracked the spatiotemporal properties of cardiac repolarization on a beat-to-beat basis *via* a high-resolution ECG (Schiller medilog AR4 plus, 1,000 Hz) in orthogonal Frank-lead configuration. Standardized ECG filter settings (high-pass 0.1 Hz; low-pass 100 Hz) were used. The ECG-signals were analyzed using MATLAB with established algorithms for calculation of PRD. In particular, for the assessment of $dT°$, the spatiotemporal information of each T wave has been firstly integrated into a single vector $T°$. The instantaneous degree of repolarization instability was subsequently calculated by means of the angle $dT°$ between two successive $T°$ vectors and plotted over time (Rizas et al., 2014). PRD is calculated by the use of wavelet analysis in the low-frequency spectrum (≤0.1 Hz). PRD was calculated out of 5 min ECG intervals: PRD before hyperventilation (baseline) was computed between 5 and 10 min. PRD after hyperventilation was calculated within the 5-min interval directly following the apnea phase of each volunteer. The PRD calculation was performed as previously described (Rizas et al., 2014).

Normalization of the $dT°$ signal and illustration of data were performed using R-software. Additionally, we recorded high-resolution ECGs (1,000 Hz) in Frank-lead configuration during spirometry-controlled ventilation at breathing rates of 10 and 20/min with constant and normal minute ventilation (tidal volume: 6–8 ml/kg; estimated dead space for adjustment at different breathing rates: 2 ml/kg) in 10 volunteers to check influences of breathing rates on $dT°$ and PRD levels. Furthermore, we performed an isometric handgrip (IHG) test in 10 individuals. The maximal voluntary contraction of the dominant forearm was estimated from three 3-s attempts by the use of a digital dynamometer (Takei Digital Hand Grip Dynamometer). After a 5-min baseline period, subjects had to perform a 2-min period of IHG at 30% of maximal voluntary contraction using their dominant forearm. This was followed by a 5-min recovery period. Throughout the test, we continuously recorded high-resolution ECGs (1,000 Hz) in Frank-lead configuration and calculated PRD from the 5-min segments before and directly after the isometric exercise.

Values show median and interquartile ranges. Mann-Whitney-Wilcoxon test was used to reveal statistical differences between $dT°$ values before, during, and after hyperventilation as well as PRD values before and after hyperventilation. Significance was indicated by two-sided values of $p < 0.05$. Spearman analyses were used to detect the correlation between $dT°$ and heart rate as well as PRD and heart rate before and after hyperventilation. Linear regression analysis was performed to test the association between PRD and change in heart rate (dependent variable: PRD after hyperventilation; independent

variables: PRD at baseline before hyperventilation and differences in heart rate before and after hyperventilation).

RESULTS

Figure 1 visualizes the principle of $dT°$ assessment from orthogonal ECG-leads. $dT°$ signals showed a characteristic pattern in response to hyperventilation: after start of the breathing maneuver, $dT°$ signals increased markedly with a noticeable delay. $dT°$ signals peaked at the end or slightly after termination of hyperventilation. **Figure 1** (lower panel) shows a schematic illustration of the $dT°$ signal during our experimental setting. **Figure 2A** shows normalized $dT°$ data for all 11 study participants. During hyperventilation, normalized $dT°$ signals significantly increased compared to baseline [0.376 (IQR 0.093) vs. 0.063 (IQR 0.032), $p < 0.001$] and recovery [0.376 (IQR 0.093) vs. 0.082 (IQR 0.029), $p < 0.001$].

During recovery, $dT°$ signals remained significantly elevated compared to levels detected in the resting phase before hyperventilation ($p = 0.019$). Mean heart rate (MHR) changed concordantly to the increased $dT°$ signals: MHR increased significantly during hyperventilation [91.1 (IQR 10.2) bpm] compared to resting phase [73.2 (IQR 5.7) bpm; $p < 0.001$] and decreased in the recovery phase [72.6 (IQR 7.2) bpm; $p < 0.001$ for hyperventilation vs. recovery]. The recorded $dT°$ signal was further used to assess PRD in order to investigate sympathetic activity associated repolarization instability.

We detected significantly increased values of PRD after hyperventilation compared to baseline levels [3.30 (IQR 2.29) deg^2 vs. 2.76 (IQR 1.43) deg^2; $p = 0.018$; **Figure 3**]. Moreover, there was no association between the difference of mean $dT°$ and the differences of MHRs ($R = 0.17$, $p = 0.61$; Spearman correlation) as well as between the difference of mean PRD and the difference of MHRs before and after hyperventilation ($R = -0.032$; $p = 0.93$; Spearman correlation). Furthermore, we found no correlation between absolute levels of $dT°$ and heart rate before ($R = -0.33$, $p = 0.33$; Spearman correlation) or after hyperventilation ($R = -0.23$, $p = 0.5$; Spearman correlation). Similar results were found for absolute levels of PRD and heart rate before ($R = 0.036$, $p = 0.92$; Spearman correlation) and after hyperventilation ($R = 0.39$, $p = 0.24$; Spearman correlation).

Of note, $dT°$ signals remained stable when comparing respiratory rates of 10 and 20/min with constant minute ventilation in an additional experiment [7.16 (IQR 1.749) vs. 6.86 (IQR 2.50), $p = 0.32$]. **Figure 2B** shows an exemplary $dT°$ signal of one study participant. Also, PRD levels during controlled breathing (10 vs. 20/min) with constant minute ventilation revealed no statistically significant difference [$PRD_{10/min} = 3.17$ (IQR 0.30) vs. $PRD_{20/min} = 3.08$ (IQR 0.36), $p = 0.275$, $n = 10$].

To further exclude heart rate changes as a confounding factor, we performed linear regression analysis. The level of PRD after hyperventilation was not associated with baseline levels of PRD and change of heart rate before and after hyperventilation ($p = 0.63$).

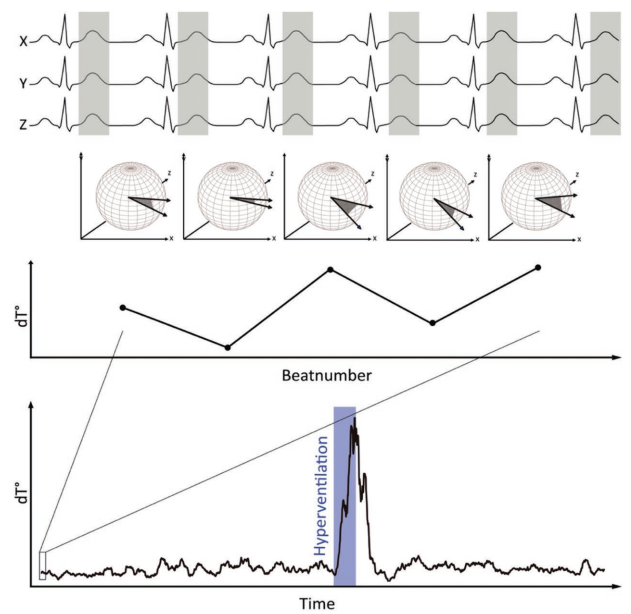

FIGURE 1 | Principle of $dT°$ calculation: spatiotemporal information of each T wave is integrated into a single vector $T°$. The instantaneous degree of repolarization instability is calculated by the angle $dT°$ between two successive $T°$ vectors and plotted over time. During hyperventilation, $dT°$ shows a characteristic pattern.

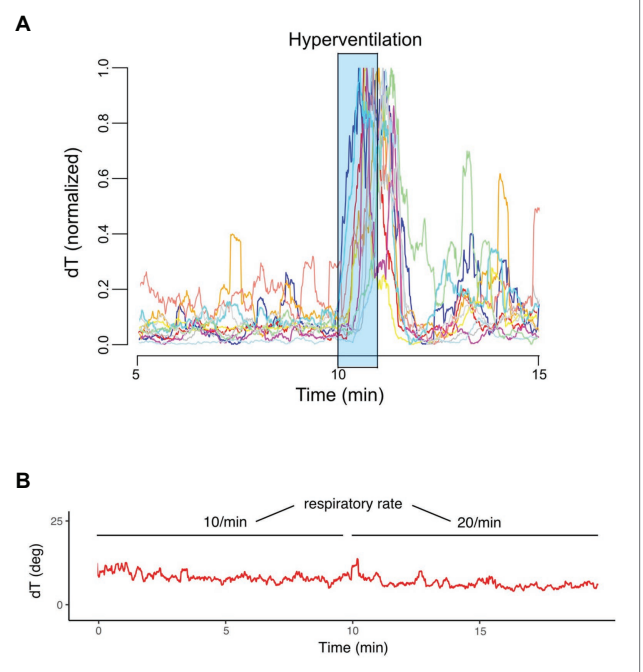

FIGURE 2 | Normalized $dT°$ signals of each study participant ($n = 11$). **(A)** $dT°$ signal at two different respiratory rates (10 and 20/min) and normal minute ventilation **(B)**.

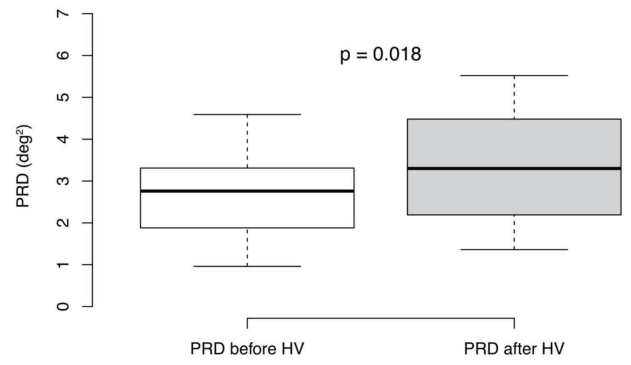

FIGURE 3 | Periodic repolarization dynamics (PRD) levels before and after hyperventilation (HV). Mann-Whitney-Wilcoxon test ($p < 0.05$ estimated as statistically significant), $n = 11$. Boxplots show medians + interquartile ranges.

Isometric handgrip tests at 30% of maximal voluntary contraction showed no significant difference between PRD levels before (2.82, IQR 1.74) and after (3.17, IQR 1.77) contraction ($p = 0.541$).

DISCUSSION

In the present study, we were able to detect a characteristic repolarization pattern in a cohort of healthy young adults during a standardized hyperventilation test. PRD levels were significantly higher after the breathing maneuver. Hyperventilation thus seems to represent a non-invasive method to induce efferent sympathetic activity on the ventricular myocardium.

T wave signals can be affected by breathing patterns *per se* due to a shift in electrical axis. Nevertheless, we saw increased $dT°$ signals with a delay after the onset of hyperventilation with the peak of $dT°$ close to the end of hyperventilation. Additionally, spirometry-controlled changes of breathing rates with constant minute ventilation had no influence on $dT°$ and PRD levels. Moreover, PRD explicitly quantifies low-frequency patterns of repolarization components ($\leq$0.1 Hz). High-frequency components, as those observed because of electrical axis shift during hyperventilation are actively filtered out during calculation of PRD. This effect has been shown using cross-spectral analysis between PRD and respiratory rate in a swine model (Rizas et al., 2014).

In the present study, there was no correlation between heart rate changes and $dT°$ as well as PRD changes. Previous studies showed that an increase of heart rate by means of fixed atrial pacing had no relevant effect on $dT°$ and PRD levels (Rizas et al., 2014; Hamm et al., 2019). Furthermore, linear regression analysis excluded heart rate as a confounding factor for increased sympathetic activity associated repolarization instability. Nevertheless, efferent cardiac sympathetic activity remained elevated when calculating PRD after hyperventilation compared to baseline levels. Our findings are in line with a recent study, where increased muscle sympathetic nerve activity (MSNA) could be measured during the apnea phase following a short phase of hyperventilation (Eckberg et al., 2016). We additionally performed an IHG test as this maneuver has been demonstrated to increase sympathetic activity (Ray and Carrasco, 2000). Here, we were not able to detect significant changes of PRD levels, indicating no influence on sympathetic activity mediated repolarization instability. Activation of the sympathetic nervous system *via* IHG has been demonstrated by the use of microelectrodes into the peroneal nerve (Victor et al., 1988; Ray and Carrasco, 2000) or pupil dilation responses (Nielsen and Mather, 2015). However, it should be noted, that measurements of sympathetic arousal of the skeletal muscle might not be representative of efferent cardiac sympathetic activity. In our experiments, we were not able to detect changed PRD levels after IHG but after hyperventilation indicating differences between those two provocation tests regarding sympathetic activation.

Our pilot data provide further insights in the effect of hyperventilation on sympathetic activity associated repolarization instability. This simple and easily reproducible test could be useful to detect underlying autonomic dysfunctions in patients with cardiovascular or pulmonary/breathing disorders such as heart failure or sleep apnea.

DATA AVAILABILITY STATEMENT

The datasets generated for this study are available on request to the corresponding author.

ETHICS STATEMENT

The studies involving human participants were reviewed and approved by Ethikkommission der Medizinischen Fakultät der LMU München. The patients/participants provided their written informed consent to participate in this study.

AUTHOR CONTRIBUTIONS

DS performed the experiments and prepared the manuscript. LS, KR, and AB revised the manuscript. SB had the idea for the study and was responsible for conducting the study. WH performed the experiments, designed the figure, and performed statistical analyzes. All authors contributed to the article and approved the submitted version.

FUNDING

DS is supported by the Clinician Scientist Program In Vascular Medicine (PRIME, MA 2186/14-1). Funders had no role in study design, data collection and analysis, decision to publish, or preparation of the manuscript. All data sets can be obtained from the corresponding author by request.

REFERENCES

Alexopoulos, D., Christodoulou, J., Toulgaridis, T., Sitafidis, G., Klinaki, A., and Vagenakis, A. G. (1995). Hemodynamic response to hyperventilation test in healthy volunteers. *Clin. Cardiol.* 18, 636–641. doi: 10.1002/clc.4960181109

Alexopoulos, D., Christodoulou, J., Toulgaridis, T., Sitafidis, G., Manias, O., Hahalis, G., et al. (1996). Repolarization abnormalities with prolonged hyperventilation in apparently healthy subjects: incidence, mechanisms and affecting factors. *Eur. Heart J.* 17, 1432–1437. doi: 10.1093/oxfordjournals.eurheartj.a015079

Aro, A. L., Kentta, T. V., and Huikuri, H. V. (2016). Microvolt T-wave alternans: where are we now? *Arrhythmia Electrophysiol. Rev.* 5, 37–40. doi: 10.15420/aer.2015.28.1

Badra, L. J., Cooke, W. H., Hoag, J. B., Crossman, A. A., Kuusela, T. A., Tahvanainen, K. U., et al. (2001). Respiratory modulation of human autonomic rhythms. *Am. J. Physiol. Heart Circ. Physiol.* 280, H2674–H2688. doi: 10.1152/ajpheart.2001.280.6.H2674

Bauer, A., Klemm, M., Rizas, K. D., Hamm, W., Von Stulpnagel, L., Dommasch, M., et al. (2019). Prediction of mortality benefit based on periodic repolarisation dynamics in patients undergoing prophylactic implantation of a defibrillator: a prospective, controlled, multicentre cohort study. *Lancet* 394, 1344–1351. doi: 10.1016/S0140-6736(19)31996-8

Ben-Tal, A., Shamailov, S. S., and Paton, J. F. (2012). Evaluating the physiological significance of respiratory sinus arrhythmia: looking beyond ventilation-perfusion efficiency. *J. Physiol.* 590, 1989–2008. doi: 10.1113/jphysiol.2011.222422

Eckberg, D. L., Cooke, W. H., Diedrich, A., Biaggioni, I., Buckey, J. C. Jr., Pawelczyk, J. A., et al. (2016). Respiratory modulation of human autonomic function on Earth. *J. Physiol.* 594, 5611–5627. doi: 10.1113/JP271654

Fischer, K., Guensch, D. P., Shie, N., Lebel, J., and Friedrich, M. G. (2016). Breathing maneuvers as a vasoactive stimulus for detecting inducible myocardial ischemia—an experimental cardiovascular magnetic resonance study. *PLoS One* 11:e0164524. doi: 10.1371/journal.pone.0164524

Garcia, A. J. 3rd, Koschnitzky, J. E., Dashevskiy, T., and Ramirez, J. M. (2013). Cardiorespiratory coupling in health and disease. *Auton. Neurosci.* 175, 26–37. doi: 10.1016/j.autneu.2013.02.006

Guensch, D. P., Fischer, K., Flewitt, J. A., Yu, J., Lukic, R., Friedrich, J. A., et al. (2014). Breathing manoeuvre-dependent changes in myocardial oxygenation in healthy humans. *Eur. Heart J. Cardiovasc. Imaging* 15, 409–414. doi: 10.1093/ehjci/jet171

Hamm, W., Von Stülpnagel, L., Rizas, K. D., Vdovin, N., Klemm, M., Bauer, A., et al. (2019). Dynamic changes of cardiac repolarization instability during exercise testing. *Med. Sci. Sports Exerc.* 51, 1517–1522. doi: 10.1249/MSS.0000000000001912

Hawkins, S. M., Guensch, D. P., Friedrich, M. G., Vinco, G., Nadeshalingham, G., White, M., et al. (2019). Hyperventilation-induced heart rate response as a potential marker for cardiovascular disease. *Sci. Rep.* 9:17887. doi: 10.1038/s41598-019-54375-9

Kaufman, E. S., Bloomfield, D. M., Steinman, R. C., Namerow, P. B., Costantini, O., Cohen, R. J., et al. (2006). "Indeterminate" microvolt T-wave alternans tests predict high risk of death or sustained ventricular arrhythmias in patients with left ventricular dysfunction. *J. Am. Coll. Cardiol.* 48, 1399–1404. doi: 10.1016/j.jacc.2006.06.044

Laffey, J. G., and Kavanagh, B. P. (2002). Hypocapnia. *N. Engl. J. Med.* 347, 43–53. doi: 10.1056/NEJMra012457

Milagro, J., Deviaene, M., Gil, E., Lazaro, J., Buyse, B., Testelmans, D., et al. (2019). Autonomic dysfunction increases cardiovascular risk in the presence of sleep apnea. *Front. Physiol.* 10:620. doi: 10.3389/fphys.2019.00620

Nielsen, S. E., and Mather, M. (2015). Comparison of two isometric handgrip protocols on sympathetic arousal in women. *Physiol. Behav.* 142, 5–13. doi: 10.1016/j.physbeh.2015.01.031

Ray, C. A., and Carrasco, D. I. (2000). Isometric handgrip training reduces arterial pressure at rest without changes in sympathetic nerve activity. *Am. J. Physiol. Heart Circ. Physiol.* 279, H245–H249. doi: 10.1152/ajpheart.2000.279.1.H245

Rizas, K. D., Mcnitt, S., Hamm, W., Massberg, S., Kaab, S., Zareba, W., et al. (2017). Prediction of sudden and non-sudden cardiac death in post-infarction patients with reduced left ventricular ejection fraction by periodic repolarization dynamics: MADIT-II substudy. *Eur. Heart J.* 38, 2110–2118. doi: 10.1093/eurheartj/ehx161

Rizas, K. D., Nieminen, T., Barthel, P., Zurn, C. S., Kahonen, M., Viik, J., et al. (2014). Sympathetic activity-associated periodic repolarization dynamics predict mortality following myocardial infarction. *J. Clin. Invest.* 124, 1770–1780. doi: 10.1172/JCI70085

Roubille, F., Fischer, K., Guensch, D. P., Tardif, J. C., and Friedrich, M. G. (2017). Impact of hyperventilation and apnea on myocardial oxygenation in patients with obstructive sleep apnea—an oxygenation-sensitive CMR study. *J. Cardiol.* 69, 489–494. doi: 10.1016/j.jjcc.2016.03.011

Salerno-Uriarte, J. A., De Ferrari, G. M., Klersy, C., Pedretti, R. F., Tritto, M., Sallusti, L., et al. (2007). Prognostic value of T-wave alternans in patients with heart failure due to nonischemic cardiomyopathy: results of the ALPHA study. *J. Am. Coll. Cardiol.* 50, 1896–1904. doi: 10.1016/j.jacc.2007.09.004

Van De Borne, P., Mezzetti, S., Montano, N., Narkiewicz, K., Degaute, J. P., and Somers, V. K. (2000). Hyperventilation alters arterial baroreflex control of heart rate and muscle sympathetic nerve activity. *Am. J. Physiol. Heart Circ. Physiol.* 279, H536–H541. doi: 10.1152/ajpheart.2000.279.2.H536

van Gestel, A. J., and Steier, J. (2010). Autonomic dysfunction in patients with chronic obstructive pulmonary disease (COPD). *J. Thorac. Dis.* 2, 215–222. doi: 10.3978/j.issn.2072-1439.2010.02.04.5

Verrier, R. L., Klingenheben, T., Malik, M., El-Sherif, N., Exner, D. V., Hohnloser, S. H., et al. (2011). Microvolt T-wave alternans physiological basis, methods of measurement, and clinical utility—consensus guideline by International Society for Holter and Noninvasive Electrocardiology. *J. Am. Coll. Cardiol.* 58, 1309–1324. doi: 10.1016/j.jacc.2011.06.029

Victor, R. G., Bertocci, L. A., Pryor, S. L., and Nunnally, R. L. (1988). Sympathetic nerve discharge is coupled to muscle cell pH during exercise in humans. *J. Clin. Invest.* 82, 1301–1305. doi: 10.1172/JCI113730

Yasuma, F., and Hayano, J. (2004). Respiratory sinus arrhythmia: why does the heartbeat synchronize with respiratory rhythm? *Chest* 125, 683–690. doi: 10.1378/chest.125.2.683

Conflict of Interest: The authors declare that the research was conducted in the absence of any commercial or financial relationships that could be construed as a potential conflict of interest.

frontiers in Neuroscience

ORIGINAL RESEARCH
published: 24 September 2020
doi: 10.3389/fnins.2020.547433

Instantaneous Cardiac Baroreflex Sensitivity: xBRS Method Quantifies Heart Rate Blood Pressure Variability Ratio at Rest and During Slow Breathing

Niels Wessel[1], Andrej Gapelyuk[1], Jonas Weiß[2], Martin Schmidt[2], Jan F. Kraemer[1], Karsten Berg[1], Hagen Malberg[2], Holger Stepan[3] and Jürgen Kurths[1,4,5]*

[1] Department of Physics, Humboldt-Universität zu Berlin, Berlin, Germany, [2] Institute of Biomedical Engineering, Technische Universität Dresden, Dresden, Germany, [3] Division of Obstetrics, Universitätsklinikum Leipzig, Leipzig, Germany, [4] Potsdam Institute for Climate Impact Research, Potsdam, Germany, [5] Department of Human and Animal Physiology, Saratov State University, Saratov, Russia

Spontaneous baroreflex sensitivity (BRS) is a widely used tool for the quantification of the cardiovascular regulation. Numerous groups use the xBRS method, which calculates the cross-correlation between the systolic beat-to-beat blood pressure and the R-R interval (resampled at 1 Hz) in a 10 s sliding window, with 0–5 s delays for the interval. The delay with the highest correlation is selected and, if significant, the quotient of the standard deviations of the R-R intervals and the systolic blood pressures is recorded as the corresponding xBRS value. In this paper we test the hypothesis that the xBRS method quantifies the causal interactions of spontaneous BRS from non-invasive measurements at rest. We use the term spontaneous BRS in the sense of the sensitivity curve is calculated from non-interventional, i.e., spontaneous, baroreceptor activity. This study includes retrospective analysis of 1828 measurements containing ECG as well as continues blood pressure under resting conditions. Our results show a high correlation between the heart rate – systolic blood pressure variability (HRV/BPV) quotient and the xBRS ($r = 0.94$, $p < 0.001$). For a deeper understanding we conducted two surrogate analyses by substituting the systolic blood pressure by its reversed time series. These showed that the xBRS method was not able to quantify causal relationships between the two signals. It was not possible to distinguish between random and baroreflex controlled sequences. It appears xBRS rather determines the HRV/BPV quotient. We conclude that the xBRS method has a potentially large bias in characterizing the capacity of the arterial baroreflex under resting conditions. During slow breathing, estimates for xBRS are significantly increased, which clearly shows that measurements at rest only involve limited baroreflex activity, but does neither challenge, nor show the full range of the arterial baroreflex regulatory capacity. We show that xBRS is exclusively dominated by the heart rate to systolic blood pressure ratio ($r = 0.965$, $p < 0.001$). Further investigations should focus on additional autonomous testing procedures such as slow breathing or orthostatic testing to provide a basis for a non-invasive evaluation of baroreflex sensitivity.

Keywords: barorecepter reflex sensitivity, heart rate variability, blood pressure variability, slow breathing, rest

OPEN ACCESS

Edited by:
Andreas Voss, Institut für Innovative Gesundheitstechnologien (IGHT), Germany

Reviewed by:
Lauro C. Vianna, University of Brasilia, Brazil
Claudia Lerma, Instituto Nacional de Cardiologia
Ignacio Chavez, Mexico

****Correspondence:***
Niels Wessel
niels.wessel@physik.hu-berlin.de

Specialty section:
This article was submitted to Autonomic Neuroscience, a section of the journal Frontiers in Neuroscience

Received: *31 March 2020*
Accepted: *04 September 2020*
Published: *24 September 2020*

Citation:
Wessel N, Gapelyuk A, Weiß J, Schmidt M, Kraemer JF, Berg K, Malberg H, Stepan H and Kurths J (2020) Instantaneous Cardiac Baroreflex Sensitivity: xBRS Method Quantifies Heart Rate Blood Pressure Variability Ratio at Rest and During Slow Breathing. Front. Neurosci. 14:547433. doi: 10.3389/fnins.2020.547433

INTRODUCTION

The baroreflex is an important component of cardiovascular regulation to maintain homeostasis. The idea of spontaneous baroreflex sensitivity is to estimate the concomitant effect of respiration on heart period and blood pressure based on non-invasive and non-pharmacological driven measurements. Originally, BRS has been assessed by the Oxford method, based on analysis of heart rate response to drug-induced blood pressure variations (Smyth et al., 1969). This method is still the gold standard for assessing baroreflex control. This method has, however, not found wide application in clinical practice due to its laboriousness. It is invasive and requires the administration of vasoactive substances, which is potentially unsafe and costly. Furthermore, undesirable effects of medications on the state of the ANS cannot be excluded. To overcome these drawbacks, numerous methods for non-invasive assessment of BRS have been developed, based on the analysis of spontaneous fluctuations in systolic blood pressure (SAP) and the RR interval (RR). Despite the fact that the idea of using spontaneous heart rate and pressure variations to assess baroreflex may seems desirable, several problems are emerging: In addition to arterial baroreflex itself there are many other sources for pressure and heart rate variations and it is almost impossible to discern baroreflex-driven variations from this mixture. There is no known possibility to isolate specific sets of stimuli and their corresponding reactions. As blood pressure fluctuations during rest in equilibrium are tiny, the effects contributed to the baroreflex seem to be extremely challenging (Lipman et al., 2003) and drastically reducing the signal-to-noise ratio. The synchronous fluctuations of heart rate with respiration, known as respiratory sinus arrhythmia (RSA), are a consequence of the rapid fluctuations of parasympathetic nerve activity toward the sinus node (Blaber and Hughson, 1996). The origin of RSA is known to have various mechanisms (Blaber and Hughson, 1996), including arterial baroreflex and cardiopulmonary baroreceptor responses due to fluctuations of cardiac stroke volume, a direct influence of medullary respiratory neurons on the vagal motor nucleus, and pulmonary stretch receptor response to lung inflation.

Fluctuations in blood pressure and heart period can be of clinical importance as risk markers for cardiovascular morbidity and mortality (Bertinieri et al., 1985; Rothlisberger et al., 2003; La Rovere et al., 2011). However, Lipman et al. (2003) show that spontaneous baroreflex indices do not clearly reflect arterial baroreflex gain. They mainly quantify vagal-mediated heart period oscillations induced by cardiac output fluctuations, and do not reflect barosensory vessel distensibility. Without a clear and consistent relationship the baroreflex gain itself, one can only conclude that spontaneous baroreflex sensitivity cannot be used as proxy for baroreflex gain. Nevertheless, the quantification of this reflex is of great relevance for understanding the cardiovascular system and for risk stratification (Bertinieri et al., 1985; Rothlisberger et al., 2003; La Rovere et al., 2011). Recently (Wessel et al., 2020) we were able to show that the spontaneous sensitivity of the arterial baroreflex (BRS) under resting conditions cannot be estimated by the sequence method (SME), which only quantifies the quotient of heart rate and systolic blood pressure variability. In this paper we test whether the xBRS method (Westerhof et al., 2004; Wesseling et al., 2017) is suitable to quantify the baroreflex sensitivity from non-invasive, non-interventional measurements under resting conditions. Therefore, two surrogate analyses were performed in which, due to the design, no causal relationships between blood pressure and heart rate signal can be present. Furthermore, SME and xBRS were calculated from data collected not only under resting conditions but also under controlled breathing.

DATA

To allow comparison to the results in Wessel et al. (2020), we reanalyzed the same data from 5 different studies in obstetrics, genetics, cardiology and heart surgery (Faber et al., 2004; Barantke et al., 2008; Retzlaff et al., 2009; Boyé et al., 2011; Retzlaff et al., 2011) in a similar manner. Demographic data of all sub-studies were given in Wessel et al. (2020): "All patients gave written, informed consent, and all studies were approved by the respective local ethics committees. From obstetrics (Faber et al., 2004) 915 measurements of 304 pregnant women were included (mean age 28.4 $\pm$ 5.4 years). The data contain 398 recordings of healthy women, 120 from patients with chronic hypertension, 38 from gestational hypertension, 152 from women who later developed pre-eclampsia, 88 from pre-existing hypertension with pre-eclampsia, 12 with other hypertensive disease and 78 from women with intrauterine growth restriction. From genetics (Barantke et al., 2008) we considered measurements from 367 subjects with an age of 10 to 88 years (45.0 $\pm$ 16.3 years), 157 were male (43%). From cardiology (Boyé et al., 2011) we used the measurements from 75 patients with chronic cardiac diseases referred for primary preventive implantable cardioverter-defibrillator implantation following Multicenter Automatic Defibrillator Implantation Trial study criteria, mean age 70.9 $\pm$ 10.1 years, body mass index 27.0 $\pm$ 3.5. From Retzlaff et al. (2009) 302 measurements from patients before and after aortic (AV) or mitral valve (MV) surgery were included for analysis. The mean age of the AV patients and MV patients was 62 $\pm$ 13 years and 59 $\pm$ 2 years, respectively. From Retzlaff et al. (2011) 169 measurements from 58 consecutive patients undergoing either trans-catheter aortic valve implantation (TAVI) or surgical aortic valve replacement (SAVR) with the heart-lung machine and being in stable sinus rhythm were enrolled. Thirty four of them underwent SAVR and 24 of them TAVI, 28 males, mean age 64.6 $\pm$ 13.8 in the SAVR group and 80.5 $\pm$ 7.3 in TAVI.

All measurements of the considered studies were performed under supine resting position for 30 min using the Task Force Monitor (CNSystems, Graz) or the PortaPres device (Finapres Medical Systems, Enschede). In total we gathered 1,828 time series containing the beat-to-beat values of heart rate (HR) as well as systolic blood pressure (SBP). Exclusion criteria were atrial fibrillation, pacemaker activity, technical artifacts, as well as ectopy time greater than 10%, reducing the number of time

TABLE 1 | Basic characteristics of considered parameters in the final data set (Mean ± *SD*: mean value ± standard deviation) and the correlation coefficient r to xBRS (*R* to xBRS, $p < 0.001$ for all coefficients).

	Mean ± *SD*	R to xBRS
xBRS [ms/mmHg]	8.4 ± 5.3	1
$xBRS_{S1}$ [ms/mmHg]	8.4 ± 5.2	0.99
$xBRS_{S2}$ [ms/mmHg]	7.9 ± 4.7	0.97
meanNN [ms]	761 ± 146	0.54
meanBP [mmHg]	129 ± 22.4	−0.2
sdNN [ms]	42.5 ± 18.6	0.67
sdBP [mmHg]	8.1 ± 2.9	−0.25
RMSSD [ms]	25.6 ± 14.7	0.84
$RMSSD_{SBP}$ [mmHg]	2.9 ± 1	−0.21
$RMSSD_{RATIO}$ [ms/mmHg]	9.5 ± 6.1	0.94

$xBRS_{S1}$, surrogate 1 of xBRS; $xBRS_{S2}$, surrogate 2 of xBRS; meanNN, mean beat-to-beat-interval of HR; meanBP, mean blood pressure of SBP; sdNN, standard deviation of HR; sdBP, standard deviation of SBP; RMSSD, root mean square of successive differences of HR; $RMSSD_{SBP}$, root mean square of successive differences of SBP; $RMSSD_{RATIO}$, Ratio of rmssd and rmssd_sbp.

series to 1,576 – careful visual inspection for further technical and physiological artifacts reduced the subjects for reanalysis to 1,439.

In addition to this comprehensive data set of rest measurements, recordings with certain autonomous testing procedures were analyzed in this paper. We used 245 measurements of 44 healthy pregnant women, mean age 30 ± 5.4 years, from the Fetal Autonomic Cardiovascular rEgulation (FACE) study which is currently in progress at the University of Leipzig Medical Center in cooperation with the TU Dresden and the Humboldt-Universität zu Berlin. The study was approved by the committee of ethics of the University of Leipzig Medical Center (357/17-ek). One aim of this study was to characterize the reaction of fetal autonomic regulation to maternal paced breathing based on a context dependent biosignal analysis. The measurements were performed under supine resting position using the PortaPres device (Finapres Medical Systems, Enschede), the fetal ECG signal was recorded from the abdomen of the pregnant woman. Our measurement protocol included 10 min of measurement at rest in supine position, 5 min of paced slow respiration (period 7.5 s – 8 respiration cycles per min), and 5 min of fast respiration (period 3 s – 20 cycles per min). Between both paced respiration conditions was one break of 5 min at rest. Exclusion criteria were rhythm disturbances (many of ventricular or supraventricular ectopic beats), technical artifacts, and incomplete study protocols. The data underwent a careful visual inspection for further artifacts by experts which reduced the analyzed data set to 184 records.

MATERIALS AND METHODS

Originally, BRS was measured by injecting vasoconstrictive agents to raise blood pressure, i.e., quantifying the reflex-like increased beat-to-beat intervals in the electrocardiogram

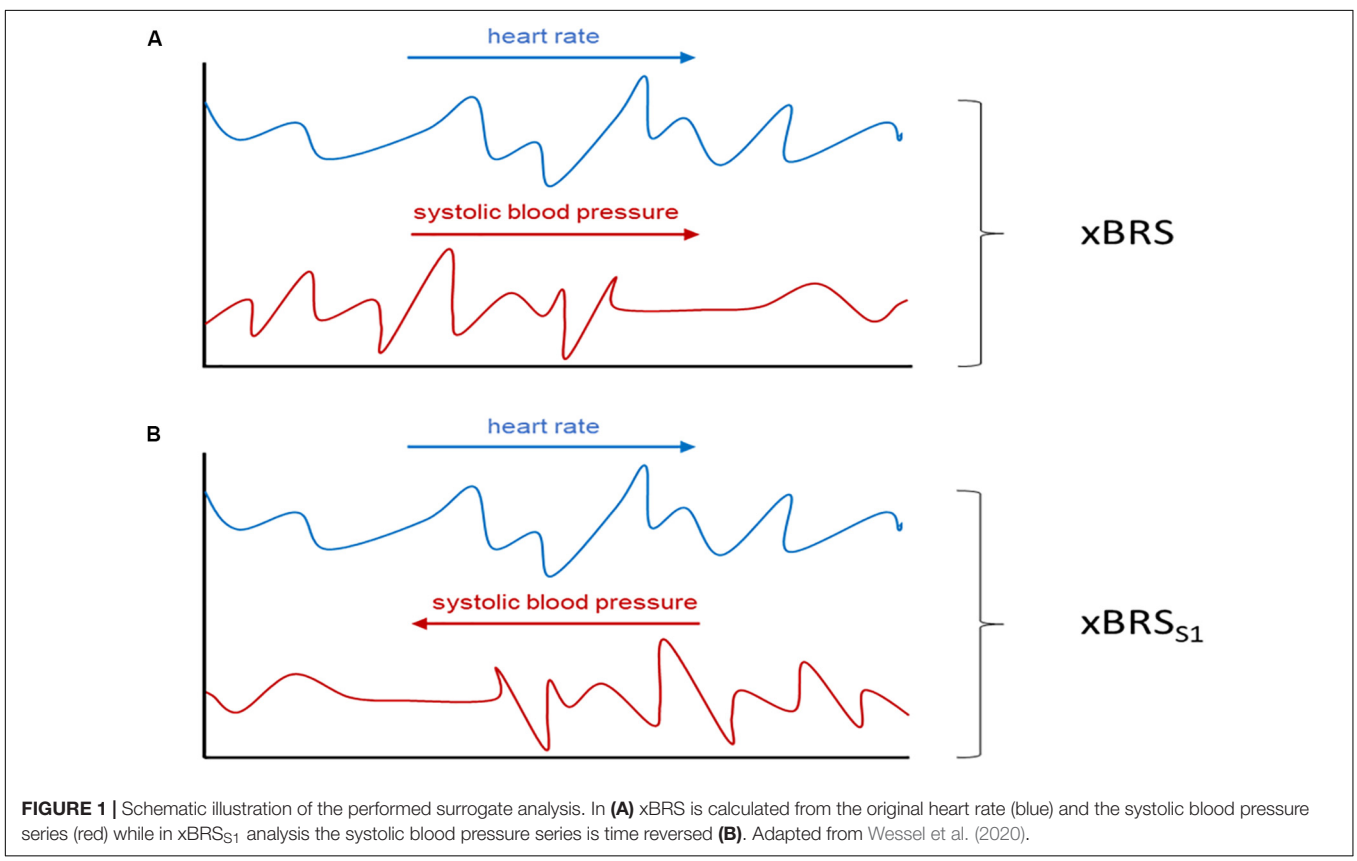

FIGURE 1 | Schematic illustration of the performed surrogate analysis. In **(A)** xBRS is calculated from the original heart rate (blue) and the systolic blood pressure series (red) while in $xBRS_{S1}$ analysis the systolic blood pressure series is time reversed **(B)**. Adapted from Wessel et al. (2020).

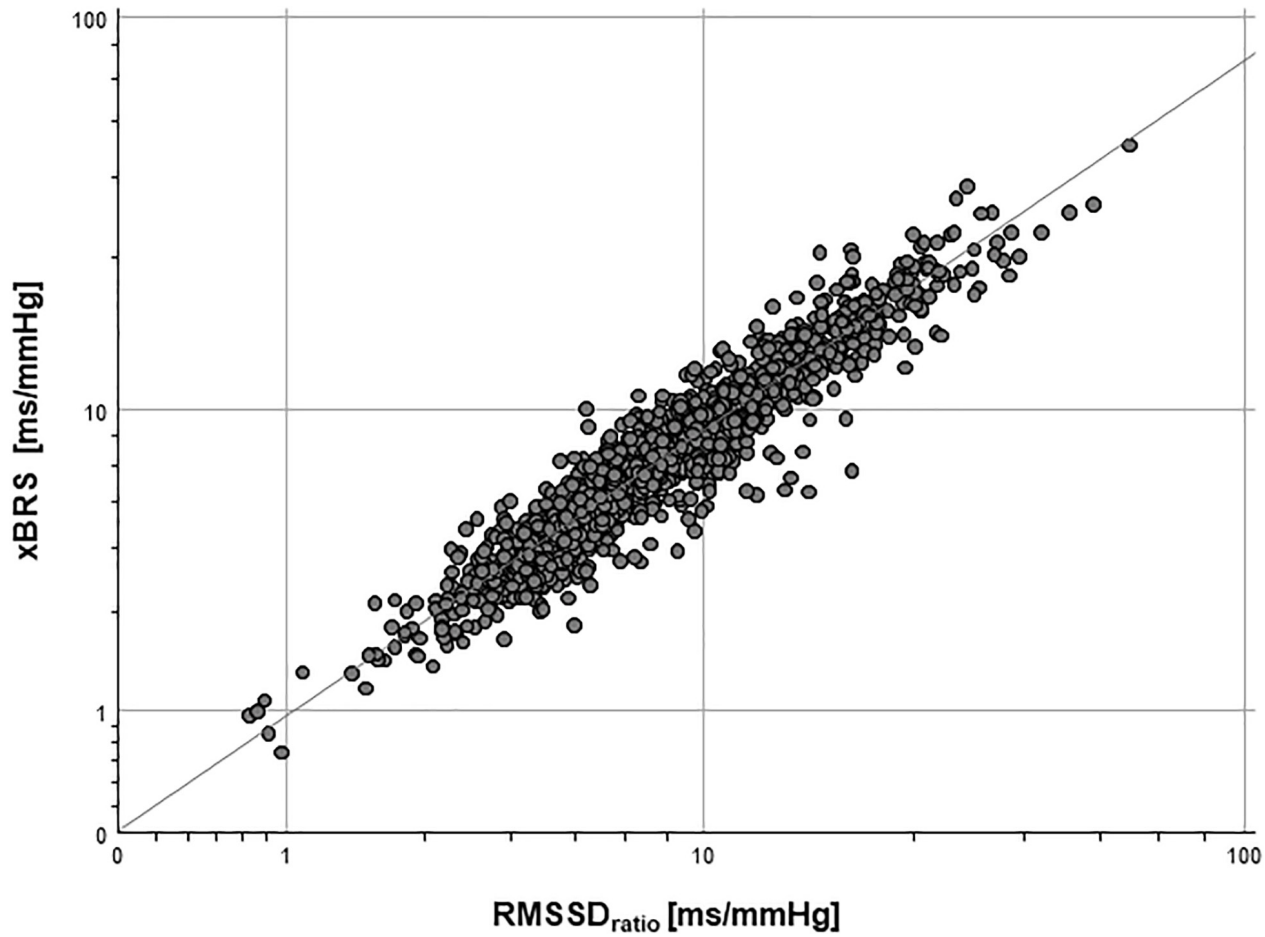

FIGURE 2 | Log-log-plot of xBRS and $RMSSD_{RATIO}$: $R^2 = 0.898$, $p < 0.001$.

(ECG). Later, attempts have been made to determine baroreflex sensitivity non-invasively, most often using spontaneous heart rate variability (HRV) and blood pressure variability (BPV) obtained from continuous finger pressure measurement (Bertinieri et al., 1985; Rothlisberger et al., 2003). The underlying hypothesis is that there is always some spontaneous variability in blood pressure that should allow an estimate of BRS. In this paper, the BRS estimation method under consideration was the xBRS method (Westerhof et al., 2004; Wesseling et al., 2017).

xBRS is a time domain method designed for estimation of BRS from non-invasively obtained SBP and beat-to-beat-interval (BBI) data. The original time series is resampled to obtain evenly sampled data at 1 Hz. Instead of sequences, xBRS uses sliding windows with a fixed length of 10 seconds. For every SBP window, there should exist at least one corresponding BBI window (in a lag range of 0–5) with positive and significant cross correlation ($p < 0.05$, two sided test for zero correlation). The BBI window with highest cross correlation is then selected. xBRS has two advantages: (a) it gives more valid "sequences" for the same time series compared to SME and (b) it allows to observe slow regulation circuits that are presumably arising from sympathetic control. Usually, the resulting number of valid "sequences" in the time series is large enough to enable the calculation of an "instant" measure for xBRS. The xBRS method was developed by Westerhof et al. (2004) and initially it set strict constrains on p-value of the cross correlation ($p < 0.01$). In the last revision (Wesseling et al., 2017), the threshold for the p-value was increased to 0.05, it doubles the percentage of necessary valid windows. Once sequences are selected, the ratio between the standard deviations of BBI and of SBP is used as a measure of baroreflex sensitivity. The reasoning for this decision was that the measure based on ratios of standard deviations does not differ significantly from the slopes of the regressions but is computationally more efficient. In our article we implemented the last revision of the xBRS method; the geometric mean of the instant xBRS values was used as BRS estimate per study period reflecting the approximately log-normal distribution of xBRS values (Wesseling et al., 2017).

Furthermore, different parameters from the time domain were calculated to quantify short term HRV and BPV in this large data set (Wessel et al., 2020, cf. **Table 1**). The $RMSSD_{RATIO}$ defined as $RMSSD_{HRV}$ divided by $RMSSD_{SBP}$ showed the highest

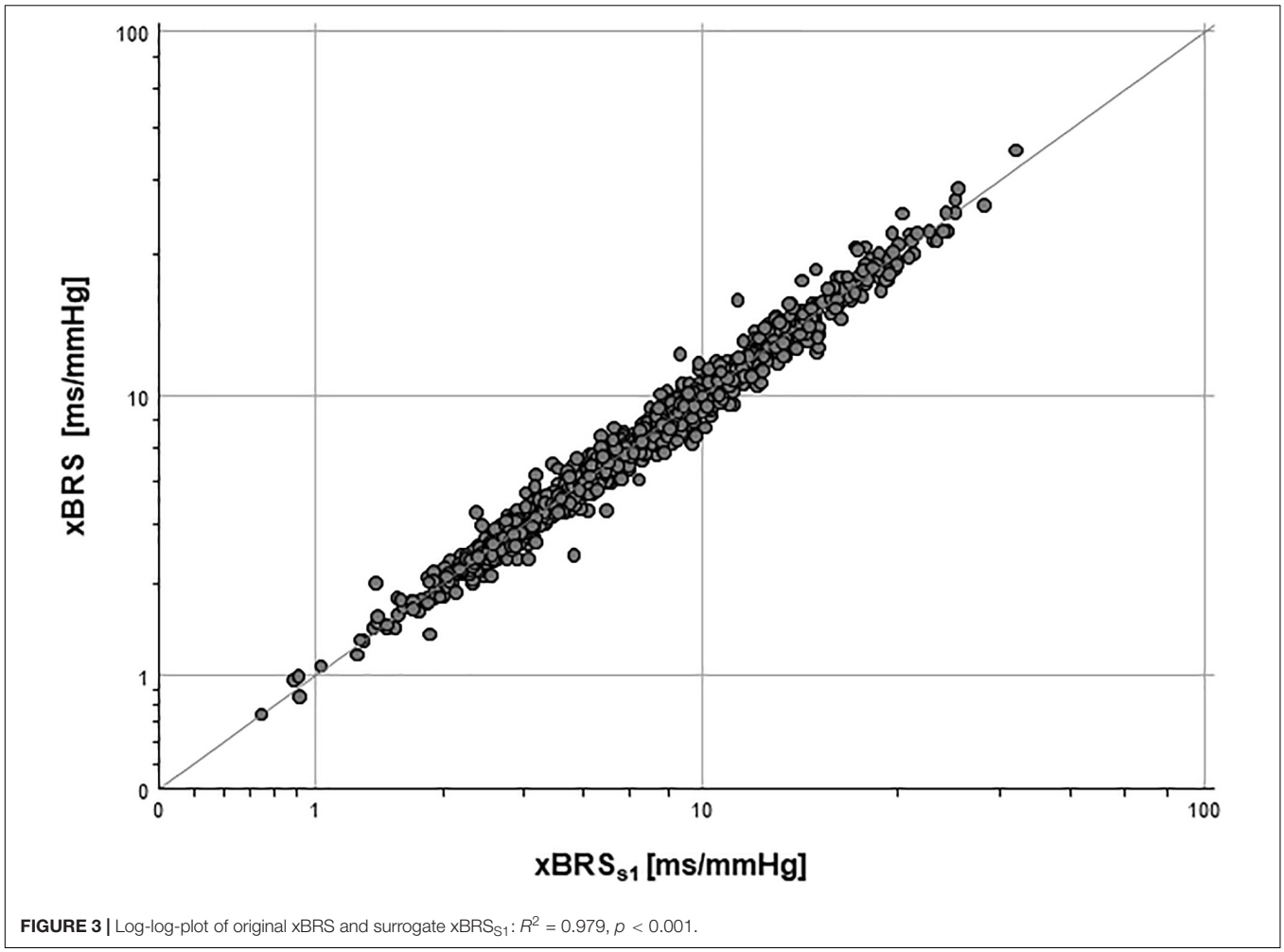

FIGURE 3 | Log-log-plot of original xBRS and surrogate $xBRS_{S1}$: $R^2 = 0.979$, $p < 0.001$.

correlation to the sequence method for BRS estimation there (Wessel et al., 2020).

Analogous to (Wessel et al., 2020) we performed two surrogate analyses in order to ascertain whether xBRS can quantify causal relationships between heart rate and blood pressure and thusly spontaneous BRS:

(a) Systolic blood pressure time-series were analyzed in reversed order, i.e., the first blood pressure value is now the last, the second now the second last etc. This results in surrogate data with the same distribution as the original data since the values of each point are the same, just in a different time position. However, any causal relationship between heart rate and blood pressure has been removed by this procedure (cf. **Figure 1**).
(b) Beat-to-beat-intervals were shuffled using the IAFFT approach (Schreiber and Schmitz, 1996). By applying this procedure causal relationship between heart rate and blood pressure has, again, been removed ($xBRS_{S2}$).

Both surrogate tests are used to test the following hypothesis: "xBRS does quantify causal relationships between heart rate and blood pressure."

Statistical analysis was performed using IBM SPSS Statistics version 24. To quantify significant relations between the parameters used in this study we applied Pearson's correlation as a measure of the linear relationship between two continuous random variables. This measure does not assume normality, but assumes finite variance as well as covariance - properties which were assumed for our data sets.

RESULTS

Table 1 shows the results of the correlation analysis between xBRS and further HRV and BPV parameters in the final data set (n = 1,439). The highest correlation coefficient r was found between xBRS and short-term variability parameters RMSSD ($r = 0.84$, $p < 0.001$). A more precise estimate yields the highest correlation coefficient for $RMSSD_{RATIO}$ ($r = 0.94$, $p < 0.001$, cf. **Figure 2**).

Surrogate analysis (a) between $xBRS_{S1}$ and $RMSSD_{HRV}$ showed high correlation coefficient ($r = 0.84$, $p < 0.001$), i.e., reversing one time series does not affect the results of xBRS. Moreover, the correlation coefficient between $xBRS_{S1}$ and

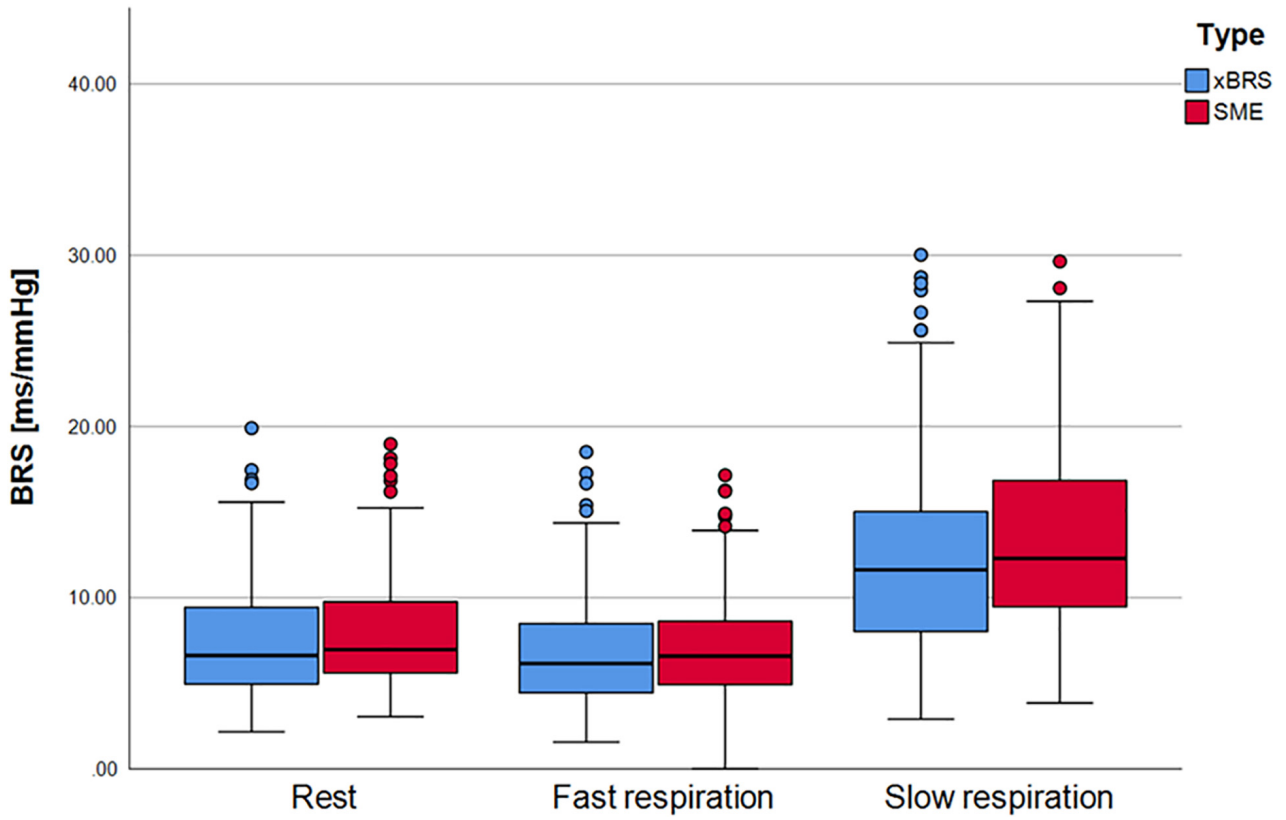

FIGURE 4 | xBRS and SME as BRS estimates for the FACE study. During rest and fast respiration procedure there are only small differences. xBRS and SME values for slow respiration, however, are statistically significant higher as for resting and fast respiration.

$RMSSD_{RATIO}$ was equally high with $r = 0.94$, $p < 0.001$. Finally, the correlation coefficient between original xBRS and surrogate $xBRS_{S1}$ was extremely high with $r = 0.99$, $p < 0.001$ (cf. **Table 1** and **Figure 3**).

In the surrogate analysis (b) the correlation coefficient between $xBRS_{S2}$ and $RMSSD_{HRV}$ was $r = 0.84$, $p < 0.001$. Moreover, the correlation coefficient between $xBRS_{S2}$ and $RMSSD_{RATIO}$ was equally high with $r = 0.93$, $p < 0.001$. Finally, the correlation coefficient between the original xBRS and surrogate $xBRS_{S2}$ again was extremely high with $r = 0.97$, $p < 0.001$ (cf. **Table 1**).

To overcome concerns for bias due to the presence of multiple measurements per subjects, we repeated our procedures on a reduced data set with only the first measurement per subject ($n = 733$) and got similar correlations (xBRS vs. RMSSD: 0.83, xBRS vs. $RMSSD_{RATIO}$: 0.93, $xBRS_{S1}$ vs. RMSSD: 0.83, $xBRS_{S1}$ vs. $RMSSD_{RATIO}$: 0.93, xBRS vs. $xBRS_{S1}$: 0.98). We conclude that the comparison of time series with different time bases has no influence on the results of xBRS. xBRS as an estimate for the spontaneous BRS shows a potentially large methodological bias. This contradicts the hypothesis that xBRS at rest quantifies causal relationships between heart rate and blood pressure.

In order to investigate whether any causal relationship could be quantified by xBRS under slow breathing conditions, we analyzed the data from the FACE study. **Figure 4** shows the xBRS and the SME values under rest conditions, under rapid breathing as well as under slow breathing. There is a, clearly significant, increase in xBRS and SME with slow breathing ($p < 0.001$), showing that measurements at rest only involves certain range baroreflex activation, but not the full capacity of the arterial baroreflex. However, these estimates are, again, exclusively dominated by the heart rate - systolic blood pressure ratio ($r = 0.965$, $p < 0.001$). Moreover, after performing the surrogate analyzes described above, the xBRS estimates do not change between original and surrogate data: The correlation coefficient at rest: xBRS to $xBRS_{S1}$ $r = 0.98$, to $xBRS_{S2}$ $r = 0.96$; 3 s (fast) breathing: xBRS to $xBRS_{S1}$ $r = 0.98$, to $xBRS_{S2}$ $r = 0.94$; slow respiration: xBRS to $xBRS_{S1}$ $r = 0.99$, to $xBRS_{S2}$ $r = 0.97$.

In summary, we found that, even under controlled breathing conditions, no causal relationship between beat-to-beat intervals and the systolic blood pressures could be quantified by xBRS.

Nevertheless, **Figure 5** shows that significantly more, as well as more consistent, results are obtained under controlled slow breathing compared to normal resting measurements. While under resting conditions only 31% of all calculated correlations are significant for this example and are included in the calculation of the xBRS, during slow breathing, the percentage of valid xBRS windows increases to 98%. Furthermore, the mean correlation between heart rate and systolic blood pressure windows is significantly higher during slow breathing. Taken together, these

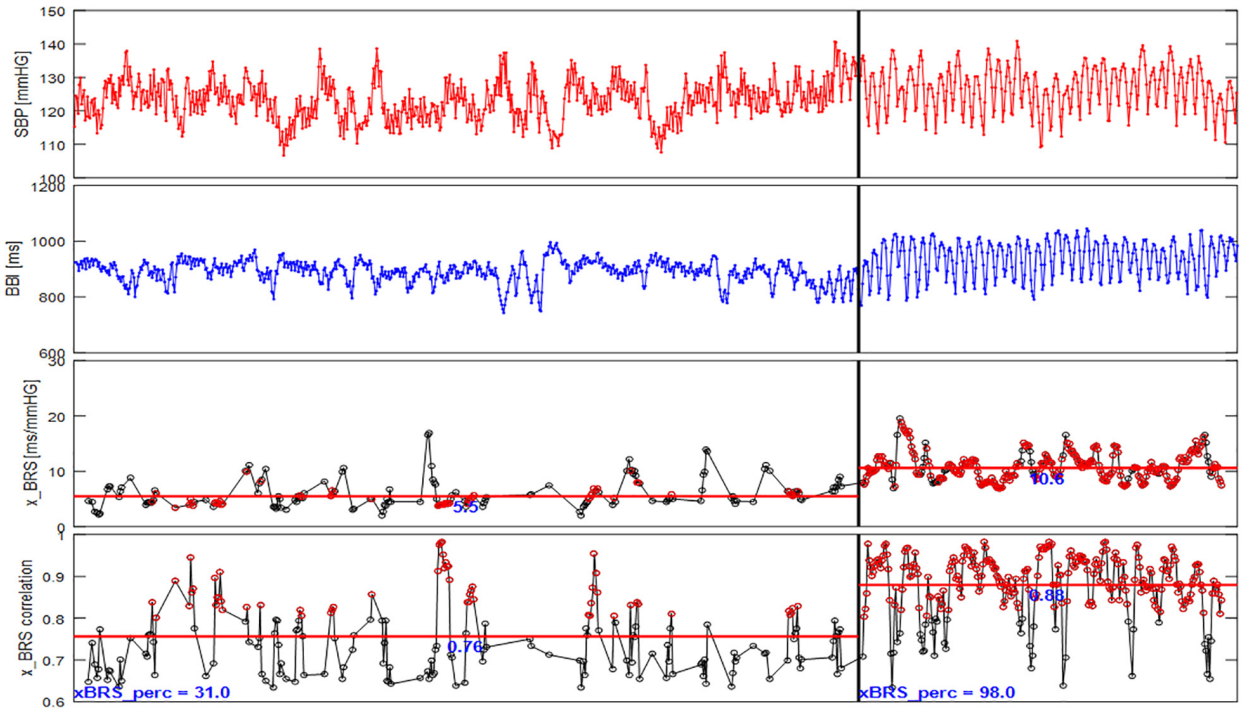

FIGURE 5 | xBRS results for one subject of the FACE study (SBP, systolic blood pressure; BBI, beat-to-beat intervals; x_BRS; x_BRS correlation, the correlation coefficient at valid epochs). During rest (left panel) xBRS value is on average 5.5 ms/mmHg, the average correlation at valid epochs is 0.76, the percentage of valid epochs is 31% only. The xBRS values for slow respiration (right panel) is on average 10.6 ms/mmHg, however, the average correlation at valid epochs is 0.88 and the percentage of valid epochs is 98%. The red markers in the lower panels mark cross correlation values higher than 0.8.

values support the hypothesis that the xBRS values at slow breathing are more consistent with the BRS. A higher BRS implies a higher regulatory capacity, meaning large blood pressure fluctuations can be balanced well by BBI changes which in turn supports maintenance of homeostasis. However, a low baroreflex sensitivity can lead to deviations from homeostasis and thus to events such as a hypertensive crises or fainting spells due to low blood pressure.

DISCUSSION

In this paper we test the hypothesis that the xBRS method quantifies the causal interactions of spontaneous BRS from non-invasive, non-interventional measurements at rest. For the surrogate analysis we substituted the systolic blood pressure by its reversed time series and thusly removed their causal relationship. Our analysis showed that xBRS remains unchanged. Therefore, we conclude that xBRS is not able to estimate causal relationship between heart rate and systolic blood pressure. Our results of the surrogate analysis show, that xBRS can be mostly explained by the short-term HRV, quantified by the RMSSD. Minor deviations of this univariate model are adequately explained by the simple bivariate model $RMSSD_{RATIO}$ which is also based on non-causal interactions.

In contrast, La Rovere et al. (1998) was able to show that low values of pharmacologically determined baroreflex sensitivity (pBRS $<$ 3 ms per mmHg) carry a significant risk of cardiac mortality after myocardial infarction. This indicates a difference between the xBRS estimation at rest and an invasive pBRS, which not only refers to respiration-induced fluctuations, but also includes carotid extensibility (La Rovere et al., 2011). We suspect that the estimation of baroreflex sensitivity is unreliable in cases of relatively shallow breathing. In these cases, there is also only a small respiratory induced blood pressure variation, which leads to only small baroreceptor activation and thus to a low HRV. Even then, in cases where any BRS estimation would result in a spurious low result, the baroreflex could still be fully functional and its sensitivity in the normal range. The BRS could just be impossible to estimate using the currently dominant protocol, i.e., relaxed respiration in resting supine position (Lipman et al., 2003). Goldstein et al. (1982) and Lipman et al. (2003) show that baroreflex sensitivity varies greatly from patient to patient and that different mechanical (neck chamber) and pharmacological techniques for measuring baroreflex sensitivity are likely to measure different aspects of baroreflex function. This contradicts the idea of spontaneous baroreflex sensitivity in the sense that the sensitivity should not be affected by the way it is being measured. Recently developed sophisticated methods for BRS estimation disentangle the effects of respiration from heart period and blood pressure (Pinna et al., 2015; Maestri et al., 2017; Bari et al., 2019), however, all methods fail to be reliable estimates of BRS. An increase in SME values during slow

breathing lead Tzeng et al. (2009) to systematically review the baroreflex function. His hypothesis was that controlled slow breathing, which causes higher blood pressure fluctuations, increases cardiovagal baroreflex gain in young healthy subjects. Baroreflex enhancement was investigated using both the classical pBRS and the non-invasive SME method. Compared to breathing at rest, slow breathing was associated with a significant increase in the SME index, while the pBRS remained unchanged. The SME values for slow breathing are higher than the pBRS values in the study, which could be a result of overestimation or a systematic error in the pBRS determination. However, Arica et al. (2011) showed that pBRS values can be predicted from non-pharmacological indices acquired during slow breathing. From both studies we derive the opinion that autonomic testing should allow a reliable, non-invasive, non-pharmacological driven quantification of the baroreflex gain. This will require large scale medical studies, where the BRS is measured invasively according to the state of the art [modified Oxford method (Ebert and Cowley, 1992)] and additional runs of autonomous tests are performed.

To investigate whether a causal relationship between heart rate and blood pressure exist under controlled breathing conditions, we analyzed the data from the FACE study. We found a clearly significant increase in xBRS and SME under slow breathing conditions compared to rest or fast breathing, showing that the latter ones involve only limited baroreflex activity. However, for all conditions these estimates are exclusively dominated by the heart rate – systolic blood pressure ratio. Moreover, after performing the surrogate analyzes, the xBRS does not vary between original and surrogate data. Thus, even under controlled breathing conditions, no causal relationship between beat-to-beat intervals and the systolic blood pressures could be found.

In conclusion, we demonstrated for all short measurements, under resting conditions and controlled breathing, that $RMSSD_{RATIO}$ carries similar vagally mediated information as xBRS. However, we found, under controlled breathing, a potentially large methodological bias in xBRS and SME as estimates for the baroreflex sensitivity. During slow breathing estimates for SME and xBRS are significantly increasing, which clearly shows that measurements at rest are only accompanied by limited baroreflex activity, but not to the full capacity of the arterial baroreflex. Further investigations should focus on additional autonomic testing procedures (e.g., orthostatic test, carotid occlusion, neck suction) to provide a better empirical foundation of non-invasive assessment of the baroreflex sensitivity.

DATA AVAILABILITY STATEMENT

The data that support the finding of this study are fully available to the authors but cannot be shared publicly due to risk of violating privacy. Requests to access results datasets should be directed to NW.

ETHICS STATEMENT

The studies involving human participants were reviewed and approved by the University of Leipzig Medical Center (357/17-ek). The patients/participants provided their written informed consent to participate in this study.

AUTHOR CONTRIBUTIONS

NW, AG, KB, JKr, and JKu contributed conception and design of the study. NW, HM, and HS organized the database. AG performed the statistical analysis. NW wrote the first draft of the manuscript. All authors contributed to manuscript revision, read and approved the submitted version.

FUNDING

NW, AG, and KB were supported by the DFG grant WE 2834/11-1. HM and JW were supported by the DFG grant MA 2294/8-1. HS was supported by the DFG grant STE 952/12-1. JKu was supported by the project RF Government Grant 075-15-2019-1885. JKr and KB were supported by the BMBF grant 13GW0278E. We acknowledge further support by the DFG for the Open Access Publication Fund of Humboldt-Universität zu Berlin.

ACKNOWLEDGMENTS

We thank Hendrik Bonnemeiner, Robert Bauernschmitt, Andreas Voss, Alexander Schirdewan, and Ludmila Sidorenko for long standing cooperation and providing the data.

REFERENCES

Arica, S., Ince, N. F., Bozkurt, A., Tewfik, A. H., and Birand, A. (2011). Prediction of pharmacologically induced baroreflex sensitivity from local time and frequency domain indices of R-R interval and systolic blood pressure signals obtained during deep breathing. *Comput. Biol. Med.* 41, 442–448. doi: 10.1016/j.compbiomed.2011.04.006

Barantke, M., Krauss, T., Ortak, J., Lieb, W., Reppel, M., Burgdorf, C., et al. (2008). Effects of gender and aging on differential autonomic responses to orthostatic maneuvers. *J. Cardiovasc. Electrophysiol.* 19, 1296–1303. doi: 10.1111/j.1540-8167.2008.01257.x

Bari, V., Vaini, E., Pistuddi, V., et al. (2019). Comparison of causal and non-causal strategies for the assessment of baroreflex sensitivity in predicting acute kidney dysfunction after coronary artery bypass grafting. *Front. Physiol.* 10:1319. doi: 10.3389/fphys.2019.01319

Bertinieri, G., di Rienzo, M., Cavallazzi, A., Ferrari, A. U., Pedotti, A., and Mancia, G. (1985). A new approach to analysis of the arterial baroreflex. *J. Hypertens. Suppl.* 3, S79–S81.

Blaber, A. P., and Hughson, R. L. (1996). Cardiorespiratory interactions during fixed-pace resistive breathing. *J. Appl. Physiol.* 80, 1618–1626. doi: 10.1152/jappl.1996.80.5.1618

Boyé, P., Hassan, A. A., Zacharzowsky, U., Bohl, S., Schwenke, C., van der Geest, R. J., et al. (2011). Prediction of life-threatening arrhythmic events

in patients with chronic myocardial infarction by contrast-enhanced CMR. *JACC Cardiovasc. Imaging* 4:871. doi: 10.1016/j.jcmg.2011.04.014

Ebert, T. J., and Cowley, A. W. Jr. (1992). Baroreflex modulation of sympathetic outflow during physiological increases of vasopressin in humans. *Am. J. Physiol.* 262, H1372–H1378.

Faber, R., Baumert, M., Stepan, H., Wessel, N., Voss, A., and Walther, T. (2004). Baroreflex sensitivity, heart rate and blood pressure variability in hypertensive pregnancy disorders. *J. Hum. Hypertens.* 18, 707–712. doi: 10.1038/sj.jhh.1001730

Goldstein, D. S., Horwitz, D., and Keiser, H. R. (1982). Comparison of techniques for measuring baroreflex sensitivity in man. *Circulation* 66, 432–439. doi: 10.1161/01.cir.66.2.432

La Rovere, M. T., Bigger, Jr., Jt, Marcus, F. I., Mortara, A., and Schwartz, P. J. (1998). Baroreflex sensitivity and heart-rate variability in prediction of total cardiac mortality after myocardial infarction. *Lancet* 351, 478–484. doi: 10.1016/s0140-6736(97)11144-8

La Rovere, M. T., Maestri, R., and Pinna, G. D. (2011). Baroreflex sensitivity assessment – latest advances and strategies. *Eur. Cardiol. Rev.* 7:89. doi: 10.15420/ecr.2011.7.2.89

Lipman, R. D., Salisbury, J. K., and Taylor, J. A. (2003). spontaneous indices are inconsistent with arterial baroreflex gain. *Hypertension* 42, 481–487. doi: 10.1161/01.hyp.0000091370.83602.e6

Maestri, R., La Rovere, M. T., Raczak, G., Danilowicz-Szymanowicz, L., and Pinna, G. D. (2017). Estimation of baroreflex sensitivity by the bivariate phase rectified signal averaging method: a comparison with the phenylephrine method. *Physiol. Meas.* 38, 1874–1884. doi: 10.1088/1361-6579/aa8b5a

Pinna, G. D., Maestri, R., and La Rovere, M. T. (2015). Assessment of baroreflex sensitivity from spontaneous oscillations of blood pressure and heart rate: proven clinical value? *Physiol. Meas.* 36, 741–753. doi: 10.1088/0967-3334/36/4/741

Retzlaff, B., Bauernschmitt, R., Malberg, H., Brockmann, G., Uhl, C., Lange, R., et al. (2009). Depression of cardiovascular autonomic function is more pronounced after mitral valve surgery: evidence for direct trauma. *Philos. Transact. A Math. Phys. Eng. Sci.* 367, 1251–1263. doi: 10.1098/rsta.2008.0272

Retzlaff, B., Wessel, N., Riedl, M., Gapelyuk, A., Malberg, H., Bauernschmitt, N., et al. (2011). Preserved autonomic regulation in patients undergoing transcatheter aortic valve implantation (TAVI) - a prospective, comparative study. *Biomed. Tech.* 56, 185–193. doi: 10.1515/bmt.2011.017

Rothlisberger, B. W., Badra, L. J., Hoag, J. B., Cooke, W. H., Kuusela, T. A., Tahvanainen, K. U., et al. (2003). Spontaneous 'baroreflex sequences' occur as deterministic functions of breathing phase. *Clin. Physiol. Funct. Imaging* 23, 307–313. doi: 10.1046/j.1475-0961.2003.00489.x

Schreiber, T., and Schmitz, A. (1996). Improved surrogate data for nonlinearity tests. *Phys. Rev. Lett.* 77, 635–638. doi: 10.1103/physrevlett.77.635

Smyth, H. S., Sleight, P., and Pickering, G. W. (1969). Reflex regulation of arterial pressure during sleep in man. A quantitative method of assessing baroreflex sensitivity. *Circ. Res.* 24, 109–121. doi: 10.1161/01.res.24.1.109

Tzeng, Y. C., Sin, P. Y. W., Lucas, S. J. E., and Ainslie, P. N. (2009). Respiratory modulation of cardiac baroreflex sensitivity. *J. Appl. Physiol.* 107, 718–724. doi: 10.1152/japplphysiol.00548.2009

Wessel, N., Gapelyuk, A., Kraemer, J. F., Berg, K., and Kurths, J. (2020). Spontaneous baroreflex sensitivity: sequence method at rest does not quantify causal interactions but rather determines the heart rate to blood pressure variability ratio. *Physiol. Meas.* 41:03LT01. doi: 10.1088/1361-6579/ab7edc

Wesseling, K. H., Karemaker, J. M., Castiglioni, P., Toader, E., Cividjian, A., Settels, J. J., et al. (2017). Validity and variability of xBRS: instantaneous cardiac baroreflex sensitivity. *Physiol. Rep.* 5:e13509. doi: 10.14814/phy2.13509

Westerhof, B. E., Gisolf, J., Stok, W. J., Wesseling, K. H., and Karemaker, J. M. (2004). Time-domain cross-correlation baroreflex sensitivity: performance on the EUROBAVAR data set. *J. Hypertens.* 22, 1371–1380. doi: 10.1097/01.hjh.0000125439.28861.ed

Conflict of Interest: The authors declare that the research was conducted in the absence of any commercial or financial relationships that could be construed as a potential conflict of interest.

Advantages of publishing in Frontiers

OPEN ACCESS
Articles are free to read for greatest visibility and readership

FAST PUBLICATION
Around 90 days from submission to decision

HIGH QUALITY PEER-REVIEW
Rigorous, collaborative, and constructive peer-review

TRANSPARENT PEER-REVIEW
Editors and reviewers acknowledged by name on published articles

Frontiers
Avenue du Tribunal-Fédéral 34
1005 Lausanne | Switzerland

Visit us: www.frontiersin.org
Contact us: frontiersin.org/about/contact

REPRODUCIBILITY OF RESEARCH
Support open data and methods to enhance research reproducibility

DIGITAL PUBLISHING
Articles designed for optimal readership across devices

FOLLOW US
@frontiersin

IMPACT METRICS
Advanced article metrics track visibility across digital media

EXTENSIVE PROMOTION
Marketing and promotion of impactful research

LOOP RESEARCH NETWORK
Our network increases your article's readership